SYSTEMS GENETICS OF GLUTATHIONE METABOLISM AND ITS EFFECTS ON HEALTH

by

REBECCA LIZABETH GOULD

(Under the Direction of Robert Pazdro)

ABSTRACT

Glutathione is an abundant tripeptide that protects cells from oxidative stress, xenobiotics, and other stressors. It is found primarily in its reduced form, GSH, and is oxidized to its dimer, glutathione disulfide GSSG, during reduction-oxidation reactions. In general, higher concentrations of GSH and GSH/GSSG protect the cell from injury and disease, whereas an altered intracellular GSH/GSSG balance renders the cell susceptible to oxidative stress and activates pro-inflammatory signaling pathways. As a result, perturbations in GSH homeostasis have been linked with the onset and progression of chronic diseases. Recent evidence from rodents and humans has suggested that genes and loci outside of the canonical GSH synthesis and recycling systems may be responsible for regulation of glutathione, and that glutathione levels are heritable throughout aging. Yet to date, no genetic mapping study has been conducted on glutathione traits in a genetically diverse population. Therefore, the objective of this dissertation was to investigate the genetic regulation of the glutathione redox system and identify the effect of glutathione variation on liver health outcomes in an outbred animal model – the Diversity Outbred (DO) mouse – which reflects the genetic diversity of humans. Chapter 3 quantified the natural variation in hepatic glutathione traits and demonstrates that novel loci are responsible for regulating hepatic

GSH/GSSG. Chapter 4 presents the impact of the hepatic glutathione variation on functional outcomes of liver health and suggests that loci responsible for hepatic steatosis progression overlap with that of hepatic GSSG and total glutathione. Chapter 5 demonstrates that hepatic and renal glutathione phenotypes vary to a similar degree and have both shared and tissue-specific loci associated with their glutathione status. In total, the studies of this dissertation redefine our knowledge of redox biochemistry regulation and conclude that glutathione is regulated by novel loci external to the basic glutathione synthesis and recycling systems at a tissue-specific level. These results support additional work into the impact of these candidate genes on modulation of glutathione metabolism, oxidative stress, and disease, to better inform therapeutic approaches attempting to rescue and restore GSH levels.

INDEX WORDS: Glutathione, Systems genetics, Genetic mapping, Liver redox, NAFLD, Kidney redox

SYSTEMS GENETICS OF GLUTATHIONE METABOLISM AND ITS EFFECTS ON HEALTH

by

REBECCA LIZABETH GOULD

BS, University of Florida, 2017

A Dissertation Submitted to the Graduate Faculty of The University of Georgia in Partial Fulfillment of the Requirements for the Degree

DOCTOR OF PHILOSOPHY

ATHENS, GEORGIA

2021

SYSTEMS GENETICS OF GLUTATHIONE METABOLISM AND ITS EFFECTS ON HEALTH

by

REBECCA LIZABETH GOULD

Major Professor:	Robert Pazdro
Committee:	Claire de La Serre
	Chad Paton
	Hea Jin Park
	Woo Kim

Electronic Version Approved:

Ron Walcott
Vice Provost for Graduate Education and Dean of the Graduate School
The University of Georgia
May 2021

DEDICATION

I would like to dedicate this dissertation to so many. To my fiancé Jeff, thank you for your endless love and support these past few years, and for taking care of our dog, Lacey, when I was working non-stop. To my friends Christine Krebs, Allie Lindke, Jennifer Coalson, Julia Sumkin, Hilary Hilgers, Bekah Washington, Jordan Dewitt, Sam Sego, Sam Buck, and my Athens Church small group, thank you for believing in me, giving me guidance, and being with me as I navigated both my best and toughest seasons of life. To my mom, stepdad, father, and stepmother, thank you for always being only a phone call away. To my brother Jon, thank you for the endless laughs. Without all of you, this dissertation would not have been possible.

I wish to also dedicate this dissertation to my mentors at the University of Florida for believing in me and inspiring me to pursue a PhD and Dietetic Internship at the University of Georgia: Drs. Beth Gankofskie, Anne Mathews, and Charlotte Emerson.

ACKNOWLEDGEMENTS

It is overwhelming to think about how many people helped in the completion of this work. First and foremost, I wish to acknowledge my labmate Steven Craig who was a constant source of knowledge and cared about this research as much as I did. I wish to also acknowledge my other labmates Abigail Starcher, Olivia Delgado, Jessica Strosahl, and Kristen Peissig, as well as my undergraduate researchers Mallory Johns, Kylah Chase, Madeleine Williams, Aida Rassam, Tina Heydari, Dana Thiesfeldt, Darian Williams, Jessica Flynt, and Lynsey Young. These people were there day in and day out to assist with experiments, data collection, harvest days, and this project could not have been completed without their tireless help and flexibility. To my major professor, Dr. Robert Pazdro, thank you for challenging and supporting me, and for always offering analogies that provided perspective and reminded me of the bigger picture. And to Dr. Barbara Grossman, thank you for believing in me and for always checking in on me – you really made Athens and the FDN department feel like "home".

I also wish to acknowledge my committee for their advice, encouragement, and for their challenging questions that ultimately made this work stronger: Dr. Woo Kim, Dr. Hea Jin Park, Dr. Chad Paton, and Dr. Claire de La Serre.

Lastly, I want to acknowledge those outside of my lab that were vital in completing this work through their instruction, advice, equipment, and support: Sue McClatchy, Belinda Cornes, Dr. Greg Keele, Dr. Gary Churchill, Dr. James Stanton, and Dr. Kim Love.

TABLE OF CONTENTS

Page

LIST OF TABLES

Page

LIST OF FIGURES

Page

CHAPTER 1

INTRODUCTION

This dissertation has been prepared in manuscript format. Chapter 2 serves as a literature review and adapts work from two published manuscripts to lend background and rationale for the dissertation research. Chapters 3, 4, and 5 reflect the primary research associated with this dissertation, and Chapter 6 draws conclusions from the combined body of research presented in this dissertation.

CHAPTER 2

LITERATURE REVIEW

Introduction

Glutathione is an abundant tripeptide that provides cells with essential protection against oxidative stress, xenobiotics, and other stressors. Within the cell, GSH is mostly maintained in its reduced active form GSH and is oxidized to the dimer GSSG via a wide array of reduction-oxidation (redox) reactions. In general, higher levels of GSH and GSH/GSSG ratios are associated with protection against disease, whereas higher levels of GSSG and lower GSH/GSSG ratios render a cell susceptible to oxidative stress and disease onset. Given the relevance of glutathione to human health, researchers have investigated the effect of polymorphisms in genes related to glutathione synthesis and recycling to identify their effect on disease development. Yet to date, no studies have mapped the loci and genes that control GSH levels in tissues. Consequently, candidate genes studies in human populations have been restricted to genes with established functions in GSH metabolism. Both animal and clinical studies have concluded that genetic background dictates a proportion of variation in glutathione status and that glutathione traits are indeed heritable, with recent research suggesting that novel genes and alleles may be responsible for the variation in a tissue-specific manner. The studies outlined in this dissertation are the first to perform comprehensive genetic mapping on hepatic and renal glutathione phenotypes and assess the biological relevance of glutathione variation on functional outcomes of hepatic and renal health.

Free radicals, reactive oxygen and nitrogen species, and oxidative stress

Background: A free radical is an atom, molecule, or ion that contains one or more unpaired electrons [1, 2]. Specifically, these electrons are found on the outermost orbital shell associated with the atom or molecule – the valence shell [3]. The valence electrons are the highest energy electrons and therefore, the most reactive, forming chemical bonds as they are gained, lost, or shared with other valence electrons [3, 4]. Because of this chemical structure, most free radicals are short-lived, unstable, and highly reactive, behaving as oxidants or reductants [3, 5]. The first documentation of a free radical reaction was described by Henry John Horstman Fenton in 1894 where he described the oxidation of hydrogen peroxide with iron sulphate [6]. Six years later, Moses Gomberg reported the first organic free radical compound – the triphenylmethyl radical – in 1900 [7]. The first incidence of free radicals observed in a biological system occurred in 1954 through the hemolytic dissociation of water with ionizing radiation [8]. Shortly after in 1956, D. Harman proposed that free radicals could be playing a role in aging of mammals [9], and in 1977, Mittal and Murad demonstrated that an oxygen-derived radical stimulated the action of cellular enzyme guanylate cyclase, indicating that free radicals serve a role in cell signaling [10].

Formation of free radicals: Free radicals can be formed through homolysis of covalent bonds or through the gain or loss of an electron from a neutral atom as energy is supplied, typically in the form of heat, ultraviolet light, or ionizing radiation [2]. These compounds have an unpaired electron and are considered electrophilic, attacking sites with increased electron density, such as carbon-carbon double bonds [2, 11]. When documenting a free radical, the unpaired electron is represented by a superscript dot (•) [10]. The exchange of electrons between in chemical reactions are referred to as reduction-oxidation reactions, or "redox" reactions, which the reducing agent

referring to the atom or molecule donating the electron, and the oxidizing agent accepting the electron [10].

In biological systems, free radical reactions have been divided into three distinct processes: initiation, propagation, and termination [11]. Initiation reactions refers to the formation of free radicals from neutral atoms, or from reactions of free radicals with stable species that results in formation of additional free radicals [11]. Propagation describes a chain reaction where newly generated free radicals react with stable molecules to form new free radical [11]. In turn, that new free radical reacts with other stable molecules or cellular structures [10]. This chain reaction continues until the free radical is neutralized through the process of termination [10]. Termination reactions refer to a net decrease in free radical numbers, such as when two free radicals react to form a stable species [11]. The most biologically significant free radicals are reactive oxygen species (ROS) and reactive nitrogen species (RNS) which are radical and non-radical derivatives of oxygen and nitrogen, respectively [5, 11]. ROS include superoxide anion ($O_2^{\bullet -}$), hydroxyl radical ($^{\bullet}OH$), and hydrogen peroxide (H_2O_2) (Figure 2.1) [2, 11, 12]. Though hydrogen peroxide is not technically a free radical as it contains no unpaired electrons [13, 14], it is considered a ROS as it is unstable and generates highly reactive hydroxyl radicals when interacting with transition metals [14-16]. Furthermore, hydrogen peroxide resembles water's molecular structure and is able to diffuse within and between cells whereas oxygen-derived radicals cannot [17]. RNS include nitric acid ($NO^{\bullet}$), peroxynitrite ($ONOO^-$), peroxynitrous acid (ONOOH), and nitrogen dioxide radical ($^{\bullet}NO_2$) [11, 18].

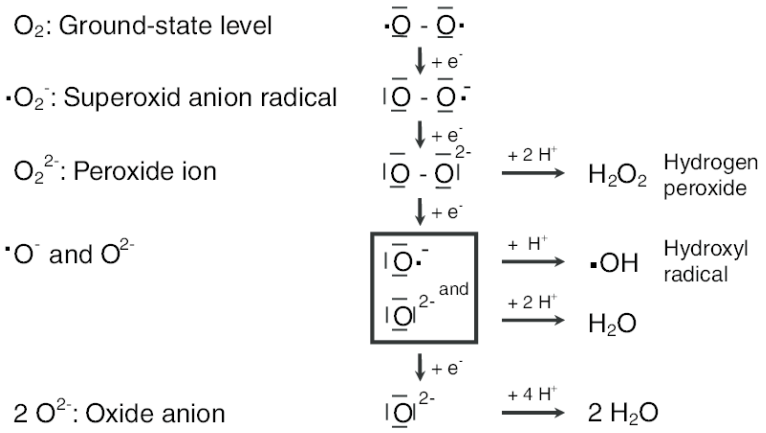

Figure 2.1. Oxidation forms of oxygen. Adapted from Henkel (2010) [19].

Sources of ROS and RNS in biological systems: Free radicals can be generated both exogenously and endogenously. Exogenous sources of free radicals include air pollutants, ultraviolet light, ionizing radiation, pesticides, drugs, tobacco smoke, alcohol, and heavy metals [3]. Endogenous contributors to free radical production include activation of immune cells such as neutrophils, cancer, inflammation, infection, and excessive exercise [12]. Non-enzymatic reactions contributing to free radical production include oxidation of transition metals (i.e., the Fenton reaction and Haber-Weiss reaction; Figure 2.2), autooxidation of thiols [3, 12], and the ETC [3, 20].

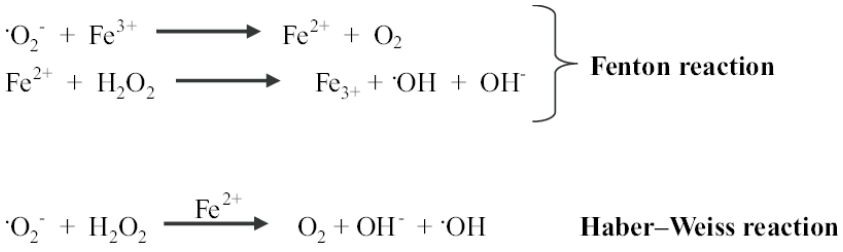

Figure 2.2. Fenton and Haber-Weiss reaction. Figure from Henkel (2010) [19].

The majority of intracellular ROS are produced in the mitochondria where superoxide radicals are produced in mitochondrial respiration at complex I and complex III (Figure 2.3) [3, 20]. Complex I is the entry point for electrons into the respiratory chain by dihydronicotinamide adenine dinucleotide (NADH) donation which allows for protons to be pumped from the mitochondrial matrix to the intermembrane space through Complex I [21]. From there, the electrons are accepted by flavin mononucleotide (FMN) and then passed through a series of iron-sulfur centers to the Coenzyme-Q (CoQ) reduction site [22]. Here, CoQ is reduced to ubiquinol [22]. Electrons are also donated by $FADH_2$ to Complex II which passes them to CoQ through iron-sulfur clusters in Complex II [21, 22]. Electrons are then passed from Complex II to Complex III via ubiquinol which continues to form the proton gradient [22]. Complex III is responsible for funneling electrons from the CoQ pool to mitochondria cytochrome *c* [21]. From there, electrons are passed to Complex IV and continue the proton gradient [22]. Complex IV then passes its electrons to the final electron acceptor: molecular oxygen, creating two H_2O molecules [22]. Superoxide is predominantly produced from the premature leak of electrons from the complexes [22]. As electrons leak from the electron transfer system, they are captured by molecular oxygen to form superoxide [22, 23]. In addition, the FMN cofactor of Complex I reacts with molecular oxygen to generate superoxide [22]. Complex I also generates superoxide through reverse electron transport (RET). RET occurs when the CoQ pool is reduced and electrons are subsequently passed back against the redox potential gradient to Complex I [22]. Superoxide is generated at the CoQ binding site of Complex I, though mechanisms are not fully understood [22]. Complex III generates superoxide through its ubiquinol oxidation center [22, 24]. Before electrons are passed to cytochrome *c*, they are transferred from ubiquinol to the iron-sulfur center of Complex III where they form an unstable intermediate ubisemiquinone ($Q^{\bullet -}$) [22]. This reactive radical reacts with

molecular oxygen to form superoxide [22]. Complex II is not a major source of superoxide, and its generation of superoxide is not well understood [22]. The flux of superoxide from the mitochondria is related to concentration of electron donors and concentration of molecular oxygen (O_2) [21]. Early studies originally estimated that 1-2% of molecular oxygen (O_2) expended during respiration is converted to superoxide [25], through recent evidence suggests that this value is likely lower *in vivo* [22]. This non-enzymatic formation of superoxide is equivalent to the metabolic rate, with a higher metabolic rate resulting in a greater superoxide production [20]. Superoxide produced in the mitochondria can dismutate to form hydroxyl radical, peroxynitrite, and other reactive radicals [10, 12].

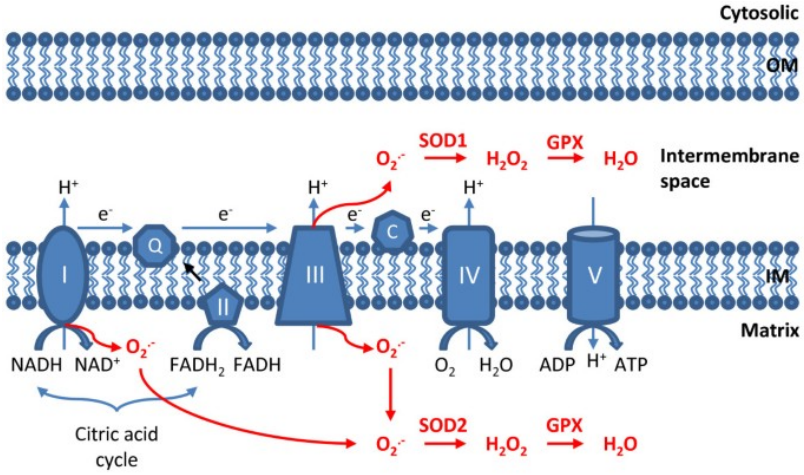

Figure 2.3. Mitochondrial ROS production. Figure from Li et al. (2013) [26].

The endoplasmic reticulum (ER) is a membrane-bound organelle responsible for folding and post-translational modification of membrane and secreted proteins [27]. Oxidative protein folding allows for cysteine residues of substrate peptides to form disulfide bonds, stabilizing the tertiary and quaternary structures [27]. This process is catalyzed by two ER oxidoreductases: protein disulfide isomerase (PDI) and ER oxidoreductin (ERO) [28]. The driving force behind this

is a redox reaction where the substrate peptides are oxidized, forming a sulfur-sulfur bridge [27]. Hydrogen peroxide is then produced as PDI and ERO transfer the electrons from protein thiols to molecular oxygen (Figure 2.4) [27].

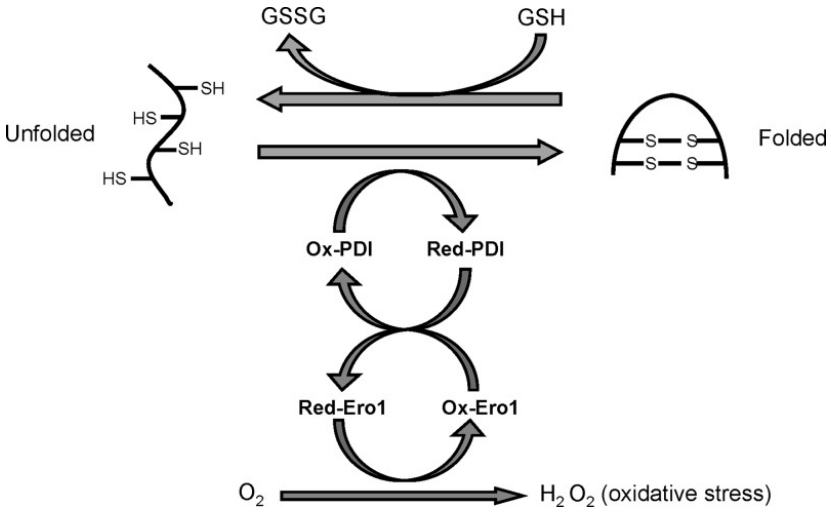

Figure 2.4. Oxidative protein folding in the ER. Figure from Cao and Kaufman (2014) [27].

Alternatively, enzymatic production of ROS is important in several physiological processes including immunity, cell growth, and cell signaling (Figure 2.5) [29]. Xanthine oxidase participates in purine metabolism catalyzing the conversion of hypoxanthine to xanthine and xanthine to uric acid and produces superoxide as a waste product [30, 31]. Nitric oxide synthase (NOS) catalyzes oxidation of arginine to citrulline, producing nitric oxide as a byproduct [32]. Nitric oxide is a free radical and weak oxidant, serving as a critical gaso-transmitter, particularly in cardiovascular contractility and vascular tone as it suppresses cell inflammation and adhesion to promote blood flow and inhibit thrombosis [32]. However, nitric oxide rapidly reacts with superoxide to yield peroxynitrite, which is highly reactive and can form peroxynitrous acid through protonation. This reaction initiates the decay if peroxynitrous acid into a hydroxyl radical and

nitrogen dioxide radical, both of which are highly reactive and lead to the uncoupling of NOS by oxidizing its cysteine residues [33, 34].

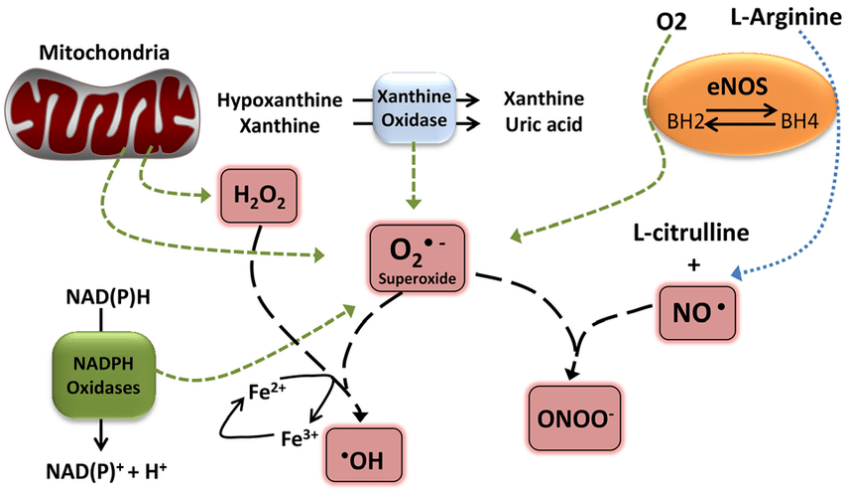

Figure 2.5. ROS generation pathways. Figure from Assari (2006) [31].

As part of the inflammatory response, neutrophils and macrophages produce superoxide to attack and kill pathogens through the action of dihydronicotinamide adenine dinucleotide phosphate (NADPH) oxidases (NOX) (Figures 2.5 and 2.6) [18]. NOX communicate during host responses to viral and bacterial stimuli [29]. In blood vessels, NOX are activated by cytokines and generate superoxide which acts as a second messenger in cell signaling cascades and reacts with other ROS to generate hydrogen peroxide and hypochlorous acid which participate in pathogen killing [31]. Moreover, NADPH-mediated ROS release serves as an inflammatory mediator in its action against the invading pathogens and leads to the recruitment and action of additional macrophages and neutrophils (Figure 2.6) [35].

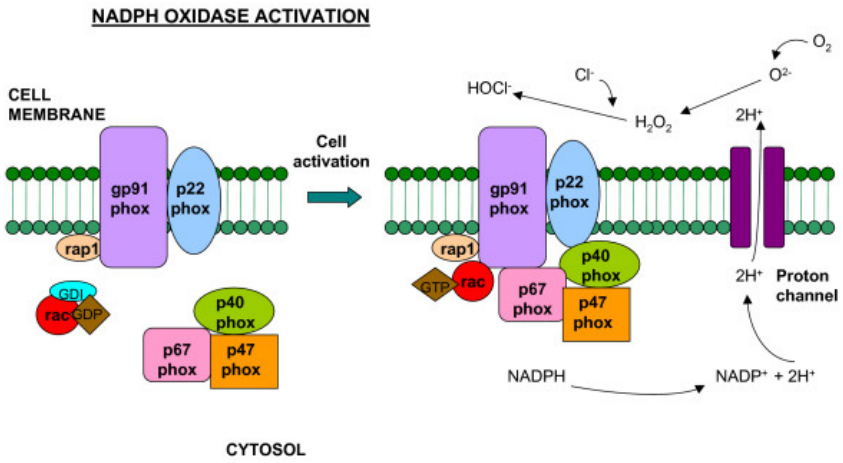

Figure 2.6. Schematic representation of the NOX enzyme in a phagocyte membrane. Figure from Assari (2006) [31].

Lastly, cytochromes P450 are heme-thiolate enzymes that are involved in oxidative metabolism [36]. These monooxygenases produce ROS through their action in drug and xenobiotic metabolism, as well as through biosynthesis of sterols, fatty acids, eicosanoids, and vitamins [37] (Figure 2.7). Inhibition of ROS generation causes cell-cycle arrest and inhibition of cell proliferation, indicating that ROS balance is required for cell growth [38].

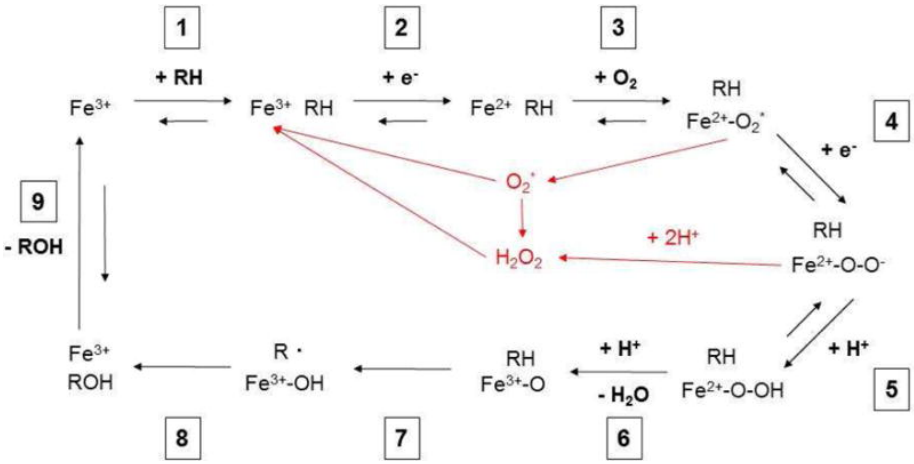

Figure 2.7. Generalized cytochrome reaction mechanism. Figure from Veith and Moorthy (2018) [37].

Molecular targets of free radicals, ROS, and RNS: Due to the highly reactive nature of ROS and RNS, they have the capability of damaging cellular biomolecules with sites of increased electron density in the nucleus, ER, mitochondria, and membranes of cells [2, 11], including ribonucleic acid (RNA), deoxyribonucleic acid (DNA), lipids, carbohydrates, and proteins [39].

Free radicals react with all components of DNA – the purine and pyrimidine bases and the deoxyribose sugar backbone – which causes DNA damage through physical or chemical changes to cellular DNA (Figure 2.8) [3]. These changes affect the way DNA is transcribed and translated [40]. Free radicals react with nucleobases in cellular DNA and these insults renders DNA susceptible to DNA single and double strand breaks [41, 42]. These insults are highly deleterious and interfere with transcription and replication, as well as induce chromosomal rearrangements [43]. If not repaired, these insults result in disrupted gene transcription leading to hybrid proteins, inappropriate gene activation, and ultimately, mutagenesis and carcinogenesis [43]. Promoter regions of genes containing transcription factor-binding sites are particularly susceptible to ROS attacks as they are rich in guanine-cytosine sequences which have a particularly low redox potential and are most prone to oxidation [44, 45]. Alteration in promoter sequences disrupts the transcription factor binding sites, modifying the binding of transcription factors, and thus changing the expression of their target sequences [45]. This modulates not only gene expression and chromatin organization, but DNA repair activity [45]. ROS attack RNA in the same manner, only RNA is especially prone to oxidative damage given that they are single stranded and lack active repair mechanisms [3, 46]. Cytoplasmic RNA is in close proximity to the mitochondria which actively produces ROS through the ETC, rendering it susceptible to ROS attack [3]. For the same reason, mitochondrial DNA is vulnerable to ROS attack [3]. Common biomarkers of nucleic acid oxidation include RNA oxidative damage products, notably 7,8-dihydro-8-oxo-guanosine (8-

oxoG), as well as oxidized nucleotides, such as 8-hydroxydeoxyguanosine (8-OHdG), and single and double stranded breaks in DNA [47].

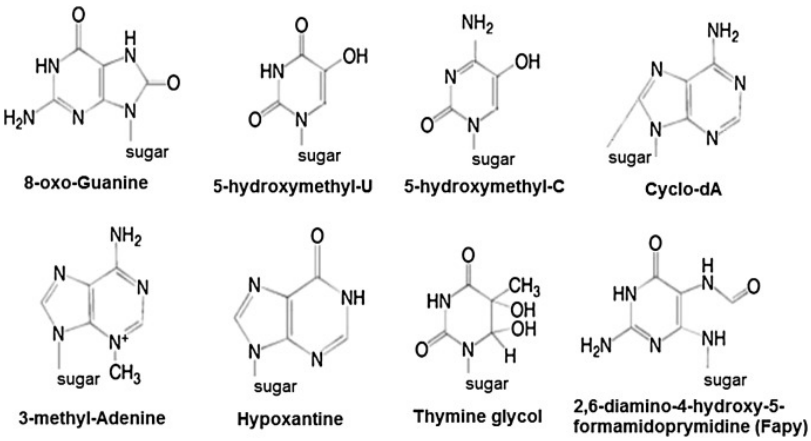

Figure 2.8. Base modifications by ROS. Figure from Birben et al. (2012) [45].

Polyunsaturated fatty acids (PUFA), especially those found within the bilayer of cellular membranes, are prone to oxidative attack [3, 48]. Lipid peroxidation is a process where ROS remove electrons from lipids and produce reactive intermediates [49]. Biomembranes undergo lipid peroxidation through enzymatic and non-enzymatic pathways [49]. Enzymatic lipid peroxidation occurs through the action of lipoxygenase (LOX) and cyclooxygenase (COX) [49]. LOX and COX catalyze the oxygenation of PUFAs, particularly arachidonic and linoleic acid, with molecular oxygen to form lipid hydroperoxide [49]. These enzymatic lipid peroxidation pathways allow for production of lipid signaling mediators, including lipoxins, leukotrienes, and prostaglandins, which are essential participants in intracellular signaling and act as signal transduction molecules [50]. Alternatively, nonenzymatic lipid peroxidation involves the spontaneous oxidation – autooxidation – of lipids (Figure 2.9) [49]. Autooxidation involves the three stages of free radical attack: initiation, propagation, and termination [49]. Free radicals attack the hydrogen on the methylene groups in fatty acids, resulting in the formation of a lipid radical

(L•) [3]. That lipid radical then propagates and reacts with molecular oxygen, forming a lipid peroxyl radical (LOO•) [3]. Alternatively, that lipid radical can react with a hydrogen molecule and form lipid hydroperoxide (LOOH) [49]. During the process of Fenton chemistry, lipid hydroperoxide undergoes reductive cleavage and produces alkoxyl radicals (LO•) [49]. In addition, lipid peroxyl radicals react with neighboring lipid molecules to further the peroxidation process through propagation (Figure 2.10) [3]. Lipid peroxidation causes an interruption in lipid asymmetry which reduces the hydrophobicity of the membrane and leads to depolarization, resulting in a loss of membrane integrity [51]. As a result, there is a loss of membrane functioning, chain breakage, and increased fluidity and permeability [3, 50]. Furthermore, the products of lipid peroxidation induce protein cross-linkages as a result of conjugated Schiff bases between protein amino groups and lipid peroxidation products, inducing carbonyl stress and inactivating membrane-bound proteins and receptors [45, 50, 52]. Lastly, lipid hydroperoxide reacts with lipid structures, including sterols and triacylglycerols, disrupting their function in signaling and energy storage, respectively [50].

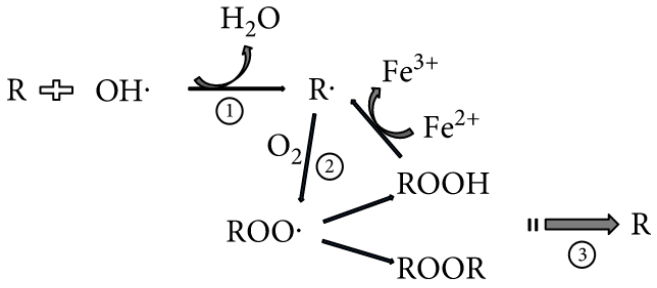

Figure 2.9. Nonenzymatic autoxidation of PUFAs. Figure from Su et al. (2019) [49].
R is polyunsaturated fatty acids containing phospholipids; R· is an alkoxyl radical; ROO· is a peroxyl radical (ROO·); ROOH is a lipid hydroperoxide (ROOH); ROOR is PL-OO· to the bis-allylic position of another PL to form PL-OO-PL· dimers; ① means initiation stage; ② means propagation stage; ③ means termination stage.

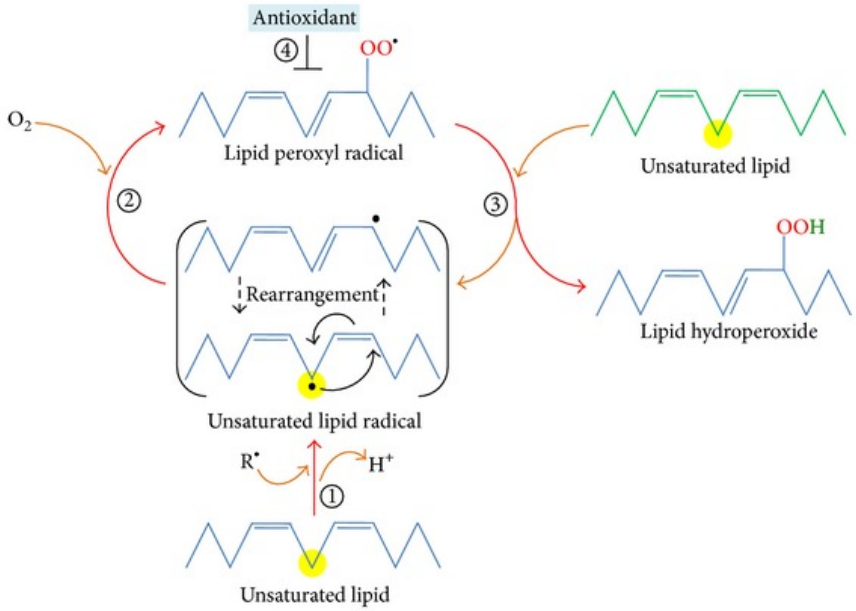

Figure 2.10. Lipid peroxidation process. Figure from Figure from Ayala, Muñoz, and Argüelles (2014) [50].

Lipid peroxyl radicals undergo rearrangement to form endoperoxides and then ultimately electrophilic species malondialdehyde (MDA), isoprostanes, and 4-hydroxylnonenal (4-HNE) – toxic compounds that damage DNA, lipids, peptides, and proteins through adduct formation (Figure 2.11) [3, 49, 51, 53]. These reactive aldehydes react with amino groups in DNA bases and generate pro-mutagenic exocyclic DNA adducts which can induce epigenetic changes and modulate the inflammatory process [54]. When lipid peroxidation products covalently react with cellular proteins, they form adducts with proteins that induce protein crosslinking, disrupts cellular signaling, and stimulates apoptosis [51, 52].

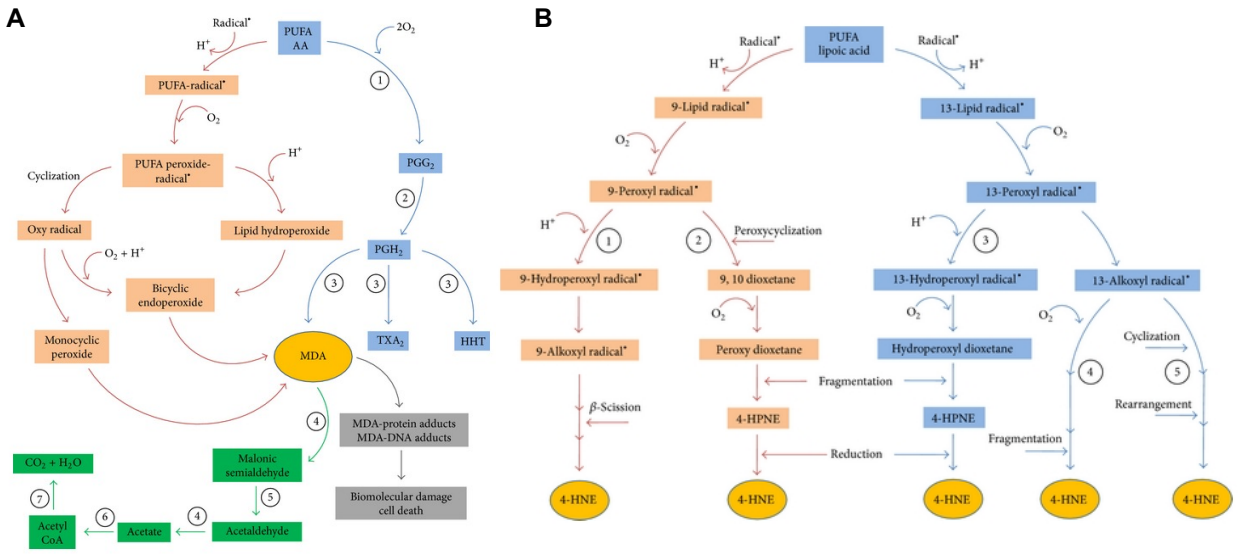

Figure 2.11. Lipid peroxidation fragmentation products. Figure from Ayala, Muñoz, and Argüelles (2014) [50].
A. MDA formation and metabolism and **B.** Nonenzymatic 4-HNE production.

Moreover, these lipid peroxidation-derived aldehydes are particularly toxic as it act as signaling molecules and are involved in regulation of cell proliferation and differentiation, survival, autophagy, apoptosis, necrosis, through regulation of several transcription factors including nuclear factor erythroid 2-related factor 2 (Nrf2), activating protein-1 (AP-1), nuclear factor-kappa B (NF-κB), and peroxisome-proliferator-activated receptors (PPAR) (Figure 2.12) [50].

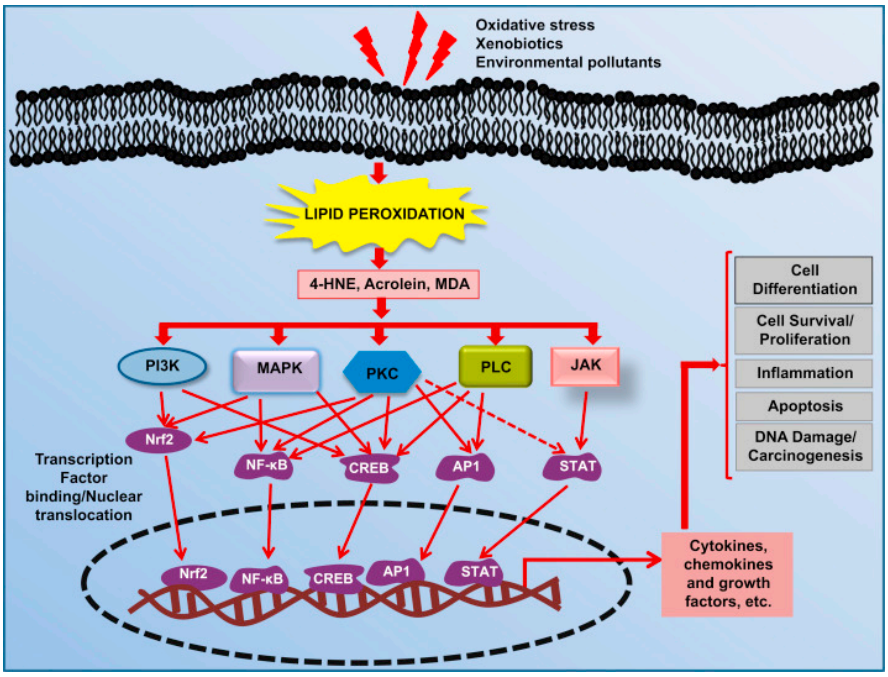

Figure 2.12. Transcription factors modulation by lipid peroxidation-derived aldehydes. Figure from Saxena, Sonowal, and Ramana (2019) [55].

In the presence of oxygen, glucose can undergo spontaneous auto-oxidation [56]. Auto-oxidation of glucose and other sugars yields reactive ketoaldehydes as well as intensifies glycation of proteins, forming glycated protein products including glycated antioxidative enzymes [57, 58]. Glycation is a nonenzymatic-mediated reaction where the sulfhydryl linkages of proteins are replaced by glucose, rendering the protein impaired [56]. In the case of glycated antioxidants, the glycation of these antioxidants limits their ability to detoxify ROS and RNS, further increasing ROS production [58]. The glycation reaction produces a Schiff base, Amadori product, additional ROS, and glycosylation end products (Figure 2.13) [59]. Advanced glycation occurs when the reactive carbonyl of a sugar (such as glucose) reacts nonenzymatically with the N-terminal and lysine groups in proteins, lipoproteins, and nucleic acids [60]. This reaction produces early glycation products which then undergo rearrangement and form reactive intermediate carbonyl products [60]. The generated carbonyls then react with the amino groups of cellular proteins to

form advanced glycation end products (AGEs) [60]. A primary receptor for AGEs is the receptor for AGE (RAGE) [60]. RAGE functions in the innate immune response and activates multiple signal transduction cascades including $p21^{ras}$, p38, ERK1/2 (p44/p42), SAPK/JNK MAP kinases, the Janus kinase/signal transducers, rho-GTPases, and the protein kinase C pathway [60]. Paradoxically, activation of these signaling pathways results downstream consequences, including the generation of more ROS through activation of NOX and the mitochondrial ETC, as well as activation of NF-κB, which then leads to the up-regulation of RAGE production [60].

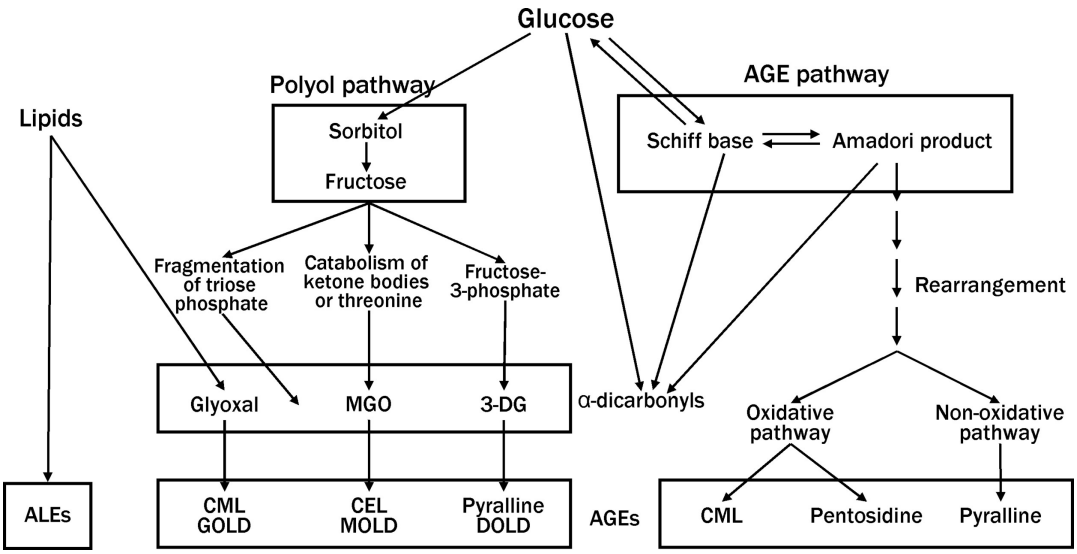

Figure 2.13. Possible pathways for AGE formation. Figure from Tan, Forbes, and Cooper (2007) [60].

Lastly, protein oxidation is induced by reactions with free radicals which renders proteins nonfunctional or denatured as a result of protein-protein cross linkages or loss of enzyme activity [61]. Free radicals attack on amino acids and produce carbon-centered radicals which causes peptide chain fragmentation, aggregation of cross-linked reaction products, altered electric charge, enzyme inactivation, and increased susceptibility of proteins to proteolysis, and ultimately, leads to an inflammatory response [62, 63]. Certain amino acids, such as methionine and cysteine, are

more susceptible to ROS oxidation as they have a high nucleophilic thiol group [64, 65]. ROS attack on amino acid residues produces carbonyl derivatives, and therefore protein carbonyls are considered a biomarker of protein oxidation [66]. Oxidative stress is also closely tied to ER stress where ROS are generated through action of PDI and ERO [28]. Accumulation of unfolded and misfolded proteins in the ER leads to ER stress and release of Ca^{2+} into the cytosol, further increasing ROS formation by the mitochondria through stimulation of mitochondrial oxidative phosphorylation [28].

Impact of oxidative stress on cellular signaling and functioning: ROS and RNS are derived from normal essential metabolic processes, but accumulation of these reactive compounds lead to oxidative and nitrosative stress [12]. This phenomenon is observed in cells and tissues and describes an imbalance between the buildup of ROS and RNS and the ability of the biological system to detoxify these products [12]. An increase in oxidative stress can either occur because of an overproduction and formation of ROS and RNS, or because of an impaired ability to neutralize them, such as insufficient antioxidant status, or both [5].

ROS are essential messengers, indispensable for normal cell signaling and regulation [67]. Low to moderate levels of ROS supports normal extracellular signaling pathways to occur and regulatory systems that control gene expression to be activated [68]. For example, low levels of ROS activate MAP protein kinase signaling pathways which ultimately activate transcription factors AP-1, activating transcription factor (ATF), and NF-κB (Figure 2.14) which supports cell survival and growth [68]. However, accumulation of ROS and RNS render vital biomolecules, including lipids, proteins, and DNA susceptible to oxidation, which leads the cell to either repair the damage or activate signaling pathways to induce cell death [25, 69]. The paradox between ROS and RNS serving as regulators of cellular functions versus as toxic by-products of metabolism are

related to the balance of their concentrations [67]. To combat the increase in ROS or RNS and subsequent damage to biomolecules, intracellular mechanisms initiate the activation of a variety of signaling molecules and transcription factors to encourage resistance to oxidative stress [68].

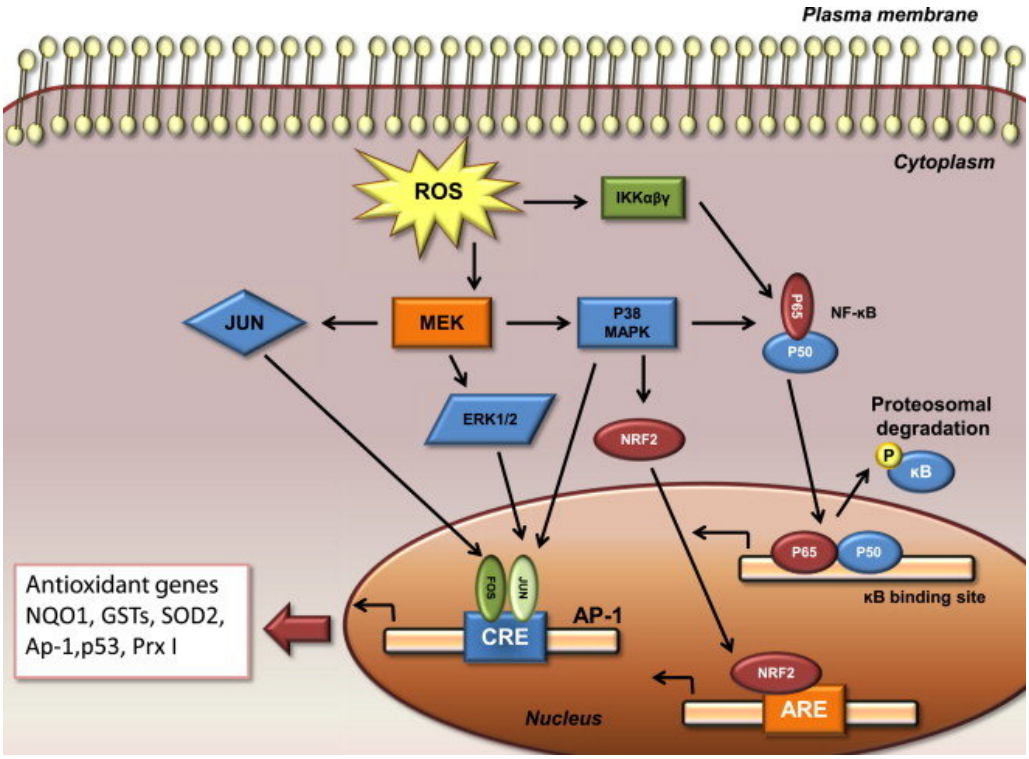

Figure 2.14. Induction of antioxidant responses by ROS. Figure from Espinosa et al. (2015) [70].

Forkhead box (FoxO) 1 transcription factors upregulate gene expression of proteins that will assist in ROS scavenging and repair of the damaged macromolecules [68]. FoxO targets include genes that code for intra- and extracellular antioxidant proteins [71]. Activity of FoxO is modulated by posttranslational modifications, subcellular localization, interaction with coregulators, *FOXO* gene expression, and FoxO protein synthesis and stability [71]. Posttranslational modifications of FoxO are initiated by changes in ROS and regulate FoxO antioxidant activity through ubiquitination, phosphorylation, and acetylation, which then affect FoxO activity and stability (Figure 2.15) [71]. Stress-activated kinase JNK phosphorylates FoxO

which leads to its activation and nuclear translocation, whereas the acetyltransferase CBP/p300 is activated by ROS and results in FoxO acetylation [72] Conversely, SIRT1 deacetylates FoxO [72]. Acetylation of FoxO can activate and inhibit its transcriptional activity depending on the target gene [72].

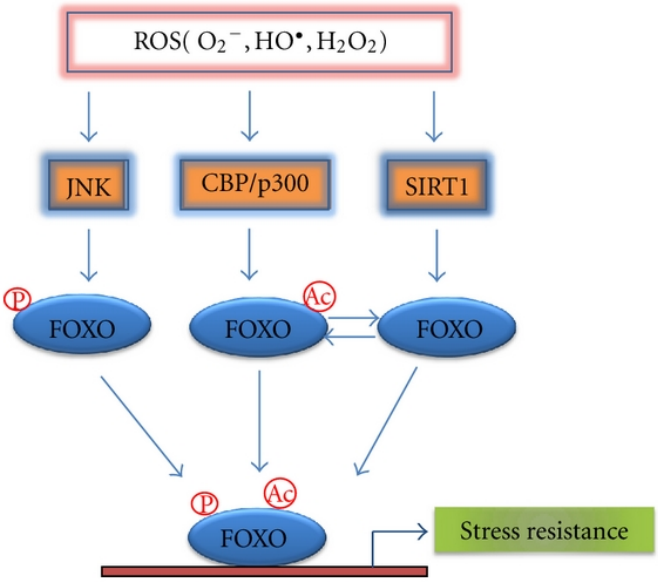

Figure 2.15. Model of FOXO regulation during ROS-induced oxidative stress. Figure from Ponugoti, Dong, and Graves (2012) [72].

Nrf2, deemed the master regulator of anti-oxidative responses [73], is stabilized in conditions of oxidative stress, rendering it active and able to induce the expression of antioxidants and other cytoprotective genes, thus promoting a decrease in oxidative stress and an anti-inflammatory expression profile [73]. The expression of Nrf2 is tightly regulated and after translation, Nrf2 is bound to a Keap1 homodimer which allows the binding of the Cul3/Rbx1 E3 ubiquitin ligase complex and results in the proteasomal degradation of Nrf2 (Figure 2.16) [73]. Under conditions of oxidative stress, ROS modify the cysteine thiol of Keap1, inducing release of Keap1 and activation of Nrf2, allowing Nrf2 to translocate to the nucleus and form a heterodimer

with musculoaponeurotic fibrosarcoma (Maf) transcription factors to induce expression of the cytoprotective genes, including antioxidant response element (ARE) [74, 75], and inhibit expression of pro-inflammatory genes [73, 76]. ARE is located in the promoter region of many cytoprotective genes and is a *cis*-regulatory element found in the promoter region of cytoprotective and antioxidant genes. BTB and CNC homology1 (Bach1) represses ARE by binding to Maf protein and inhibiting Nrf2 binding to ARE [75]. In response to Nrf2 activation, Bach1 is exported from the nucleus and subsequently degraded by proteasomes [75]. Following gene induction, Nrf2 is phosphorylated within the nucleus and either exported into the cytosol for degradation or ubiquinated and degraded within the nucleus [76].

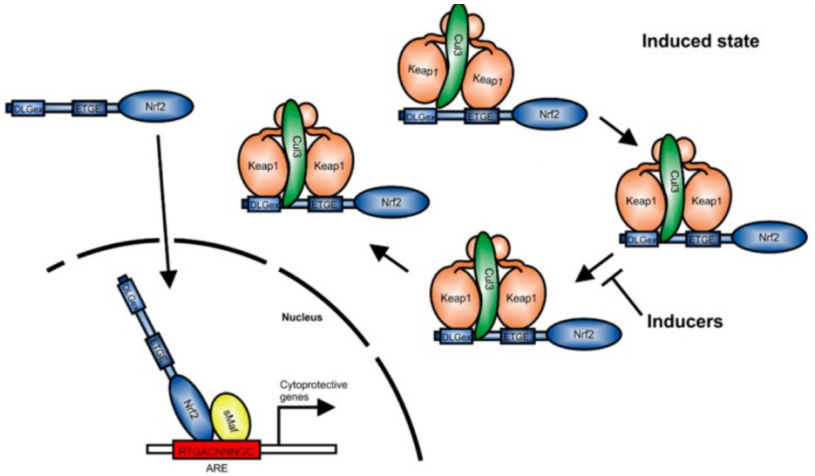

Figure 2.16. Regulation of Nrf2 expression. Figure from Ma (2013) [76].

In addition, ROS and RNS alter the regulation of the phosphatidylinositol 3-kinase (PI3K) pathway, which involves AKT serine threonine protein kinase, TSC2, and mammalian target of rapamycin (mTOR) complexes (Figure 2.17) [5, 77, 78]. AKT supports cell growth, survival, and proliferation by through its inhibition of FoxO and the activation of mTOR [77]. mTOR signaling is responsible for regulating protein synthesis, cell growth, survival and proliferation [79]. mTOR is a component of two functionally distinct components: mTOR complex 1 (mTORC1) and mTOR

complex (mTORC2) [78]. mTORC1 regulates translation, autophagy, growth, mitochondria and ribosome biogenesis, and lipid biosynthesis, while mTORC2 regulates cell survival and proliferation [78]. mTORC1 is a key suppressor of mitochondrial oxidative stress [79] and regulates cellular homeostasis and stress responses through phosphorylation of regulatory associated protein of mTOR (RAPTOR) [80]. Oxidative stress both suppresses and stimulates mTORC1 through upstream signaling pathways (Figure 2.17) [80], and the activation of mTORC1 has downstream effects which induce Nrf2 expression, as well as promote Nrf2 translocation into the nucleus (Figure 2.18) [81]. Activation of mTORC1 also leads to the activation of NF-κB and results in pro-inflammatory phenotype and reduces Ca^{2+}-ATPase activity in the sarcoplasmic and ER [5].

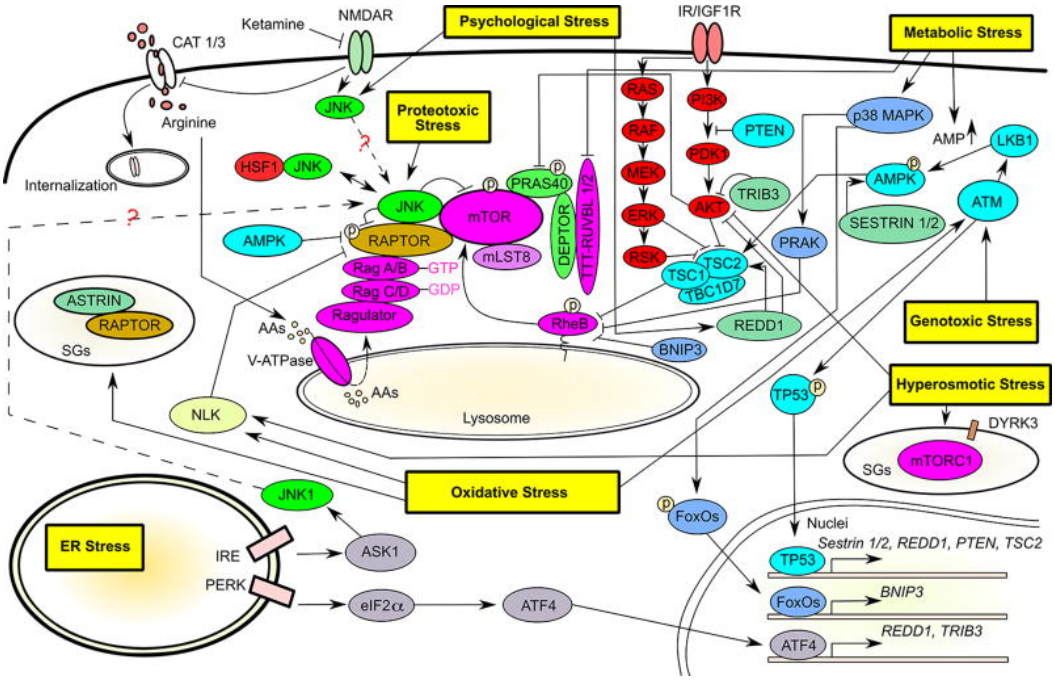

Figure 2.17. mTORC1 senses diverse stresses. Figure from Su and Dai (2017) [80].

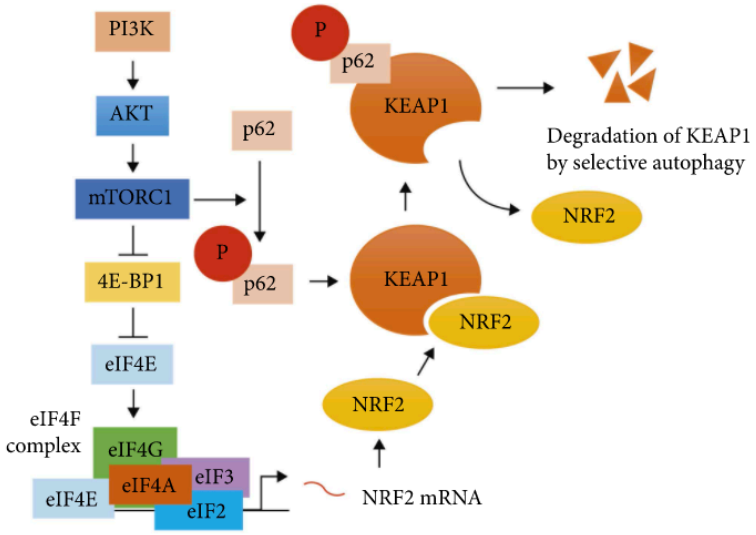

Figure 2.18. The effect of mTORC1 on Nrf2 expression and activation. Figure from Woo et al (2019) [81].

Oxidative stress results in a pro-inflammatory environment [82]. In response to ROS, expression of peroxiredoxin (Prx) is upregulated to clear peroxide, and Prx acts as an inflammatory signal by activating macrophages to release TNF-α [83]. NF-κB is a transcription factor that regulates gene expression and is a pivotal mediatory of inflammatory responses [84]. Activation of NF-κB in response to oxidative stress results in a pro-inflammatory state [84]. NF-κB consists of five proteins: the REL subfamily (p65/RELA, RELB, and c-REL), and the NF-κB subfamily proteins (p50 and p52, along with their precursors p105 and p100, respectively) [82]. The canonical pathway includes p50 in conjunction with RelA and it is activated by cytokine receptors and recognition receptors, including toll like receptors [82]. Alternatively, the non-canonical pathway is where p52 and RelB are in conjunction with one another and are triggered by receptors including CD40 [82]. NF-κB is localized in the cytoplasm with most being in the form of p50/p65 (RelA) [82]. IκB proteins mask the active DNA binding domain of NF-κB to inhibit them from translocating into the nucleus [82]. In response to inflammatory signals, including tumor necrosis factor alpha (TNF-α) and lipopolysaccharide (LPS), IκB is phosphorylated by upstream kinases

(IKK), resulting in the ubiquitination and proteasomal degradation of IκB. Active NF-κB can then translocate to the nucleus and promote the expression of pro-inflammatory cytokines and chemokines (Figure 2.19) [82, 84]. In concert to NF-κB-dependent transcriptional activation, cell inflammasomes can be activated by cytokines signaling which facilitate the proteolytic maturation of interleukins 1β and 18 [85]. ROS have also been shown to act as signaling molecules and mediate inflammasome assembly and activation, though the mechanisms of how ROS facilitate this are not fully understood [86].

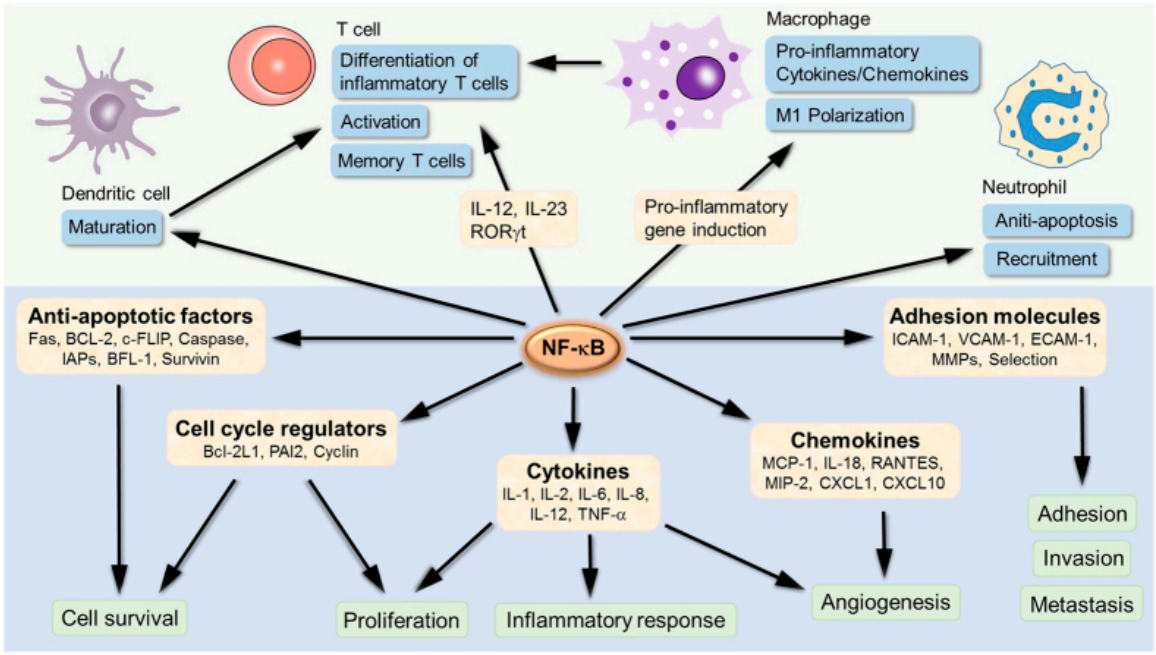

Figure 2.19. NF-κB target genes involved in inflammation development and progression. Figure from Liu et al. (2017) [84].

Alternatively, oxidative stress can inhibit the NF-κB pathway (Figure 2.20) [82]. Though ROS can activate phosphorylation of IKK, they can also oxidize the IKK cysteine residues and inhibit the release of NF-κB [82]. Similarly, ROS can oxidize the cysteine residue within p50, inhibiting the action of NF-κB [82]. Lastly, separately from NF-κB's role in production of pro-inflammatory cytokines and chemokines, NF-κB plays a protective role by decreasing ROS accumulation

through the modulation of Nrf2 activity to encourage expression of cytoprotectants and antioxidant enzymes [82].

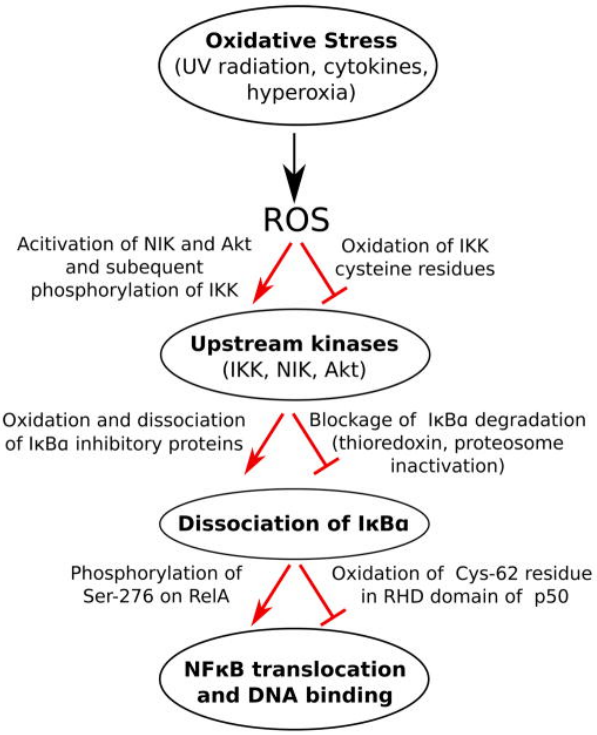

Figure 2.20. Effect of increased stress on NF-κB pathway. Figure from Lingappan (2018) [82].

Both oxidative stress and inflammation mediate cell death [25, 87]. Cell death is caused by both non-physiological (necrotic) and regulated (apoptotic) pathways [69]. Inflammation primarily triggers regulated necrosis – necroptosis – which results in organelle and cellular swelling, disruption of the plasma membrane, and loss of cellular content [87]. When cytokines such as TNF-α bind to cell receptors, it initiates a signaling cascade which ultimately activates receptor-interacting protein kinase (RIP) and initiates a pro-necrotic complex resulting in the inhibition of NF-κB, lysosomal membrane polarization, plasma membrane permeabilization, and overproduction of ROS by the mitochondria, resulting in "oxidative burst" [87]. Necrosis leads to further inflammation as the loss of intracellular content serve as signals to neighboring cells to

trigger additional inflammatory reactions [87]. Alternatively, apoptosis is a tightly regulated process of cell death where the cell undergoes self-destruction [88]. It is triggered by death receptors at the cell surface, or within the mitochondria and ER [89], and regulated through receptor activation, caspase activation, B-cell-lymphoma protein 2 (Bcl-2) family proteins, and mitochondrial dysfunction [69]. In the case of excessive mitochondria-generated ROS, the ROS cause the release of pro-apoptotic proteins, including cytochrome *c*, which trigger caspase activation and apoptosis (Figure 2.21) [25]. Normally, cytochrome *c* is bound to the inner mitochondrial membrane with cardiolipin, but when cardiolipin is oxidized by excessive ROS, it decreases its affinity for cytochrome *c*, breaching the association between itself and the mitochondrial membrane [25]. Cytochrome *c* then leaves the mitochondria and triggers caspase activation [25]. Caspases are initially synthesized inactive, but in response to apoptotic stimuli, such as cytochrome *c*, they become rapidly cleaved and induce the cleavage of downstream caspases, as well as nuclear, plasma membrane, and mitochondrial proteins, causing cell death [90].

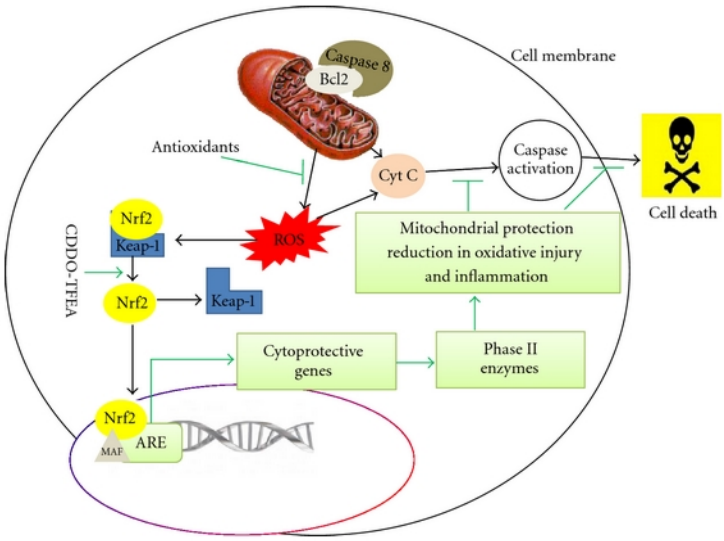

Figure 2.21. Nrf2/ARE and caspase activation. Figure from Petri, Körner, and Kiaei (2012) [74].

Apoptosis is also caused by ROS-mediated damage to nuclear genetic material [25]. The critical tumor suppressor p53 regulates cell-cycle arrest, apoptosis, or differentiation in response to cellular stresses through its action as a transcription factor [91]. This "guardian of the genome" senses DNA damage and triggers protective responses to repair DNA and stop cells from dividing with damaged DNA [92]. Much like Nrf2, p53 is tightly regulated by posttranslational ubiquitination, phosphorylation, acetylation, methylation, and sumoylation [91]. In the absence of cellular stressors, p53 is inactive due to its interaction with Mdm2/MdmX, as they ubiquinate p53 for proteasomal degradation [91]. However, as ROS accumulate, p53 is post-translationally modified and activated (Figure 2.22) [91].

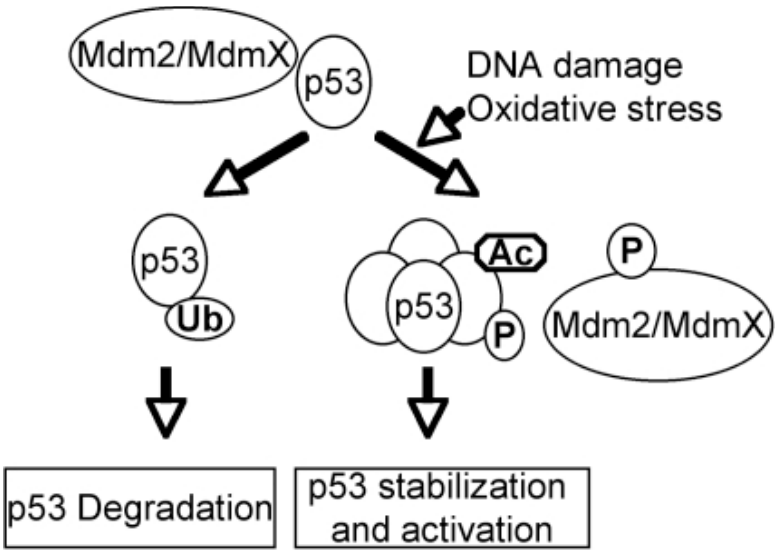

Figure 2.22. Activation of p53 in response to DNA damage and oxidative stresses. Figure from Liu and Xu (2011) [91].

During low levels of oxidative stress, p53 activates the expression of cytoprotectants to decrease ROS accumulation and ensure cell survival [91]. p53 upregulates expression of antioxidant enzymes, as well as TIGAR (Tp53-induced glycolysis and apoptosis regulator) which inhibits glycolysis and increases intracellular NADPH and GSH concentrations to protect against

ROS and cell death [25]. However, under high levels of oxidative stress, p53 upregulates the expression of prooxidative genes to increase cellular stress and ROS levels, ultimately causing cell death (Figure 2.23) [91]. In the case of DNA damage by ROS, p53 protein is activated and transmits a variety of stress-induced signals to activate antiproliferative responses, including apoptosis, autophagy, and cellular senescence [93]. Moreover, the increase in p53 activity triggers pro-apoptotic Bcl-2 protein expression which target the outer mitochondrial membrane and cause the release of cytochrome *c*, triggering caspase-mediated apoptosis [25, 89].

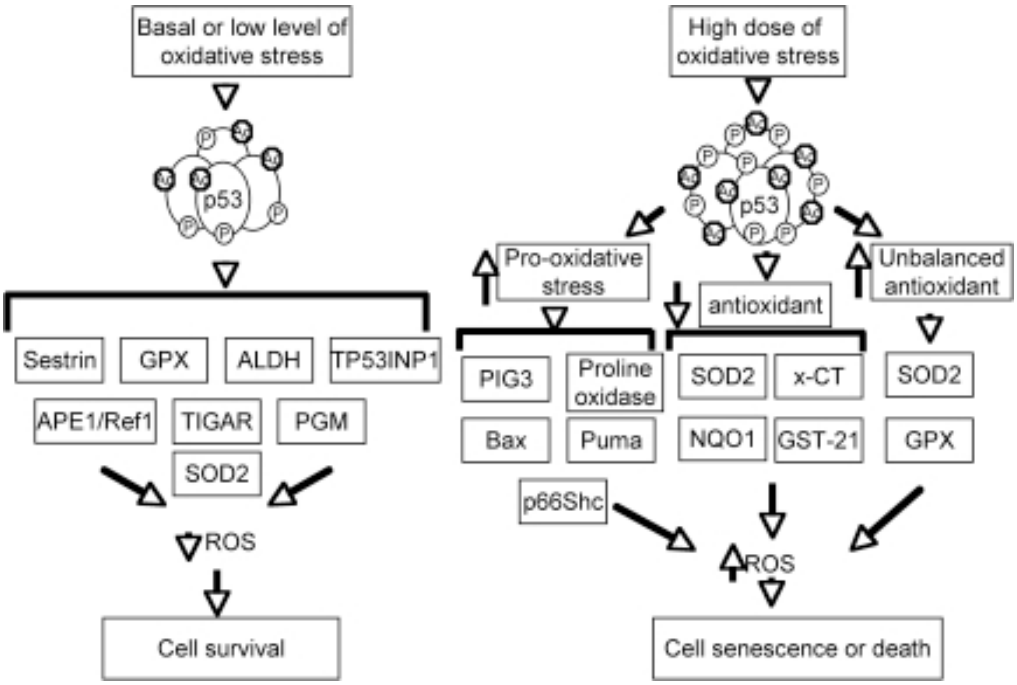

Figure 2.23. Context-dependent roles of p53 in cellular responses to oxidative stresses by turning on distinct target genes. Figure from Liu and Xu (2011) [91].

Oxidative stress induces cellular senescence - the state of permanent cell cycle arrest - by affecting the regulation of important senescence and survival pathways, including the p53 pathway [5]. Cellular senescence is a tumor constraining mechanism to halt cell proliferation as a result of DNA damage [94]. Accumulation of senescent cells within a tissue high levels results in

senescence-associated secretory phenotype [94]. SASP involves secretions of interleukins, chemokines, and growth factors, as well as degradative enzymes such as matrix mellanoproteases (MMPs) and insoluble protein components [5]. These secretions behave in a paracrine fashion to affect neighboring cells and promote tumor formation [94]. Morphologically, senescent cells are observed to have increased cell volume and organelle size, as well as appearance of vacuoles in the cytoplasm and ER and presence of cytoplasmic microfilaments [94]. SASP is associated with promoting an increased production of ROS, primarily through increased mitochondrial ROS generation [94, 95]. Thus, ROS-induced SASP promotes a positive feedback look which further amplifies the senescence signals (Figure 2.24) [94]. Downstream effects of SASP include tumorigenesis, immunomodulation, senescence amplification, and transformation of tissue microenvironment [94].

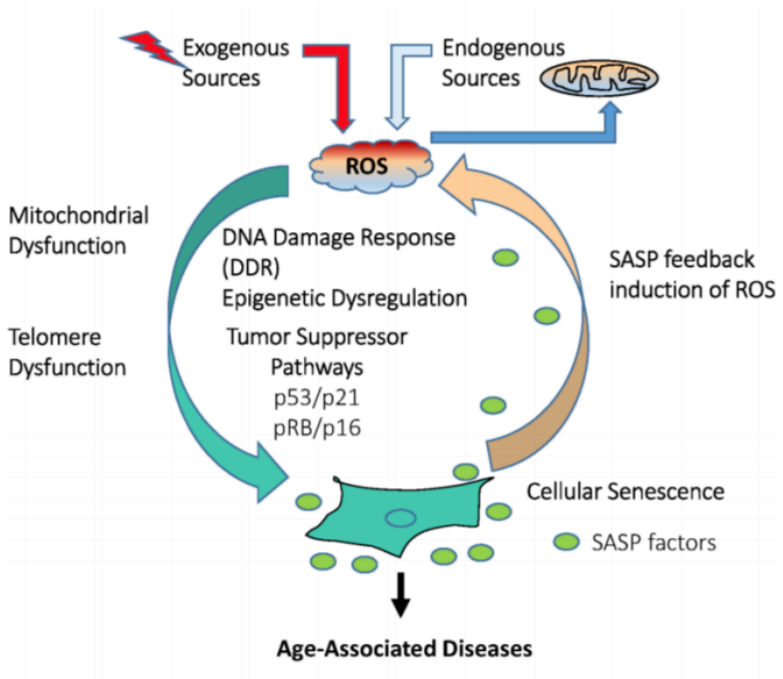

Figure 2.24. ROS induces cellular senescence. Figure from Pole, Dimri, and Dimri (2016) [96].

ROS are also implicated in necrotic cell death in a c-Jun N-terminal kinase (JNK)- and poly(ADP–ribose) polymerase (PARP–1)-dependent manner [97]. Unlike apoptotic cell death, necrotically dying cells will initiate a pro-inflammatory state and lead to damage to neighboring cells [98, 99]. The PARP-1 enzyme is activated by DNA damage and binds to fragmented DNA, consuming NAD^+ in the process [100]. It participates in automodification by binding to the fragmented DNA and unwinding DNA from the histone, releasing PAR [100]. Therefore, excessive DNA damage results in NAD^+ depletion and accumulation of PAR [100]. PARP-1 also functions as a transcription coactivator and corepressor in inflammation and increases accessibility to promoter DNA for pro-inflammatory cytokines through histone ADP-ribosylation [100, 101]. Similar to PARP, sirtuin (SIRT) proteins are NAD^+ dependent [100]. These critical deacetylases regulate metabolic homeostasis through activation of transcriptional regulators, including cAMP response element binding protein (CREB) and peroxisome proliferator-activated receptors (PPARs) [100]. As DNA damage increases and PARP-1 activity increases, NAD^+ availability for SIRTs declines [100]. This alters cellular energy metabolism from declining SIRT activity and results in increased levels of free PAR which can translocate to the cytoplasm and induce the nuclear transfer of apoptosis-inducing factor (AIF) from the mitochondria to initiate cell death (Figure 2.25) [100].

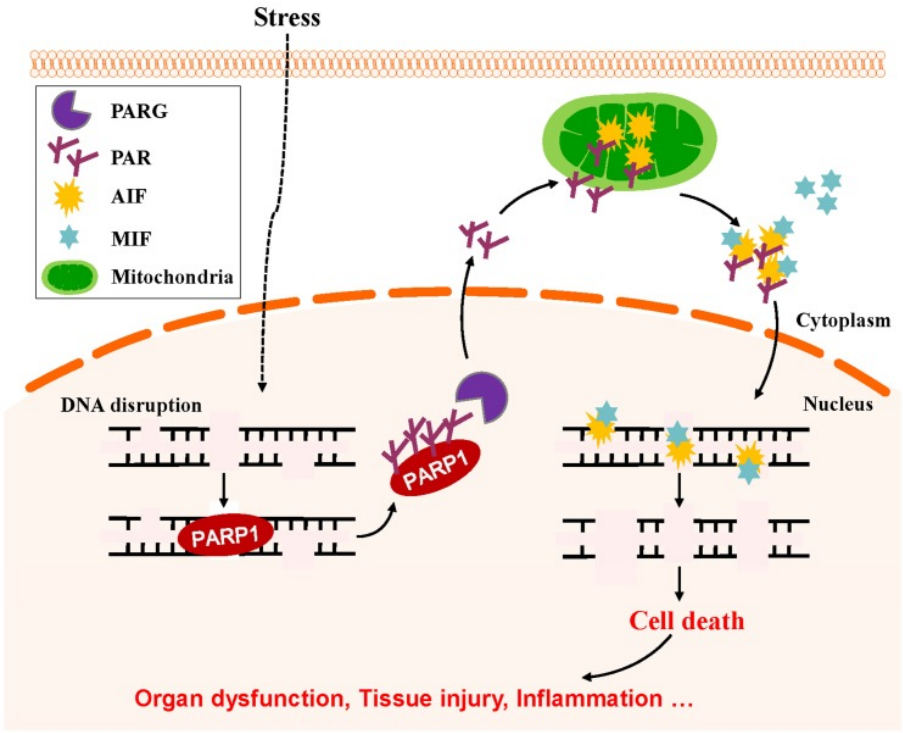

Figure 2.25. PARP-1-mediated cell death by triggering AIF release from mitochondria. Figure from Ke et al. (2019) [100].

Oxidative stress and disease: Oxidative stress is central to the development of many chronic diseases [5]. Accumulated damage to macromolecules leads to accelerated aging as well as the development of cancer and chronic diseases including cancer, ocular and respiratory diseases, diabetes mellitus (DM), and neurodegenerative, cardiovascular, hepatic, renal, and respiratory diseases [3].

Disruption of redox balance underlies cancer development, progression, and metastasis [102]. Oxidative damage to DNA plays a significant role in tumor development and elevated ROS have been detected in almost all cancers [103]. ROS affect malignant transformation and tumorigenesis largely through their role in induction of DNA sequence changes [2]. In addition, elevated ROS along with down-regulation of cellular antioxidant enzymes lead to malignant transformations in key cellular signals, including NF-κB and Nrf2 [102]. Furthermore, NOX and xanthine oxidase activity are augmented by ROS, leading to inflammatory oxidative conditions

and massive production of ROS, further accelerating ROS damage to cellular components [102], indicating that the elevated ROS allow not only for cancer cell survival but the inhibition of protective cellular mechanisms [12]. Cancerous cells have also been shown to upregulate antioxidant protein expression to prevent ROS-induced apoptotic signaling [103].

Ocular diseases, including dry eye disease, age-related macular degeneration, and cataracts, are thought to be a result of common exposure to environmental oxidants such as light exposure, ultraviolet rays, ionizing radiation, pathogenic microbes, irritants, and chemical pollutants [104, 105]. The overexpression of ROS on the ocular surface is attributed to prolonged exposure to atmospheric oxygen and inadequate antioxidant defense [106]. The high concentrations of ROS lead to oxidative damage to macromolecules within the eyes the which causes the degeneration of tissue leading to ocular disease [104]. Excessive light exposure reduces lipofuscin autofluorescence and generates ROS through photooxidation where electron orbitals are altered and direct bond breakage occurs [28].

ROS attack also contributes to intracellular stress signaling which initiates a pro-inflammatory response, reducing tear quality and secretion [105]. The proinflammatory phenotype results in functional and morphological changes to the retinal pigment epithelium, endothelial cells, and retinal ganglion cells, and promote the onset of non-cancerous ocular diseases, particularly through its negative effect on tear fluid [28]. Tear fluid is critical to eye health as it naturally contains several antioxidants to protect the eyes from ROS, but when tear film is rendered instable from inadequate tear fluid, the ocular surface experiences tear hyperosmolarity and a damaged tear lipid layer, leading to water evaporation from the eye [105]. Moreover, excessive ROS can damage the myelin sheath of the ocular surface nerves which can negatively affect vision through alteration in the blink reflex, injury repair, and tear production and secretion [105,

107].Tear fluid is critical to eye health as it naturally contains several antioxidants to protect the eyes from ROS, but when tear film is rendered instable from inadequate tear fluid, the ocular surface experiences tear hyperosmolarity and a damaged tear lipid layer, leading to water evaporation from the eye [105]. Moreover, excessive ROS can damage the myelin sheath of the ocular surface nerves which can negatively affect vision through alteration in the blink reflex, injury repair, and tear production and secretion [105, 107].

Onset and progression of pulmonary disorders, such as chronic obstructive pulmonary disease, asthma, and acute respiratory distress syndrome, are heavily influenced by oxidative stress given the nature of the lung's constant exposure to environmental oxidants, such as cigarette smoke and air pollutants, and molecular oxygen [108]. Airborne toxicants contain ROS, especially cigarette smoke which contains over 4000 oxygen-derived chemicals such as epoxides, peroxides, and semiquinones [109. In addition, the lungs naturally produce ROS/RNS through the actions of NOS, xanthine oxidase, NOX, and cytochrome c oxidase {Thimmulappa, 2019 #1984]. NO production is upregulated by environmental toxins and increases proangiogenic factors as well as induces mitochondrial alterations, further increasing ROS production and damage to cellular integrity [28]. Exogenous ROS exposure also triggers inflammatory responses in the lungs, increasing macrophage activity, ultimately resulting in a lowered antioxidant defense system and increased ROS production in lung epithelial cells [110]. Pulmonary disorders are largely characterized by chronic inflammation and airflow obstruction [109]. The lungs are particularly susceptible to oxidative stress and chronic inflammation given their large surface area and high blood supply [110]. This damage results in lung degeneration, chronic inflammation, and tumor development within the lungs [110].

The relationship between DM and oxidative stress has been extensively researched and it has been concluded that oxidative stress plays a role in the vascular complications seen in DM, particularly in type 2 DM (T2DM) [111]. T2DM is associated with high ROS production due to both hyperglycemia and the insulin resistance [111]. Excessive ROS production is a result of autooxidation of glucose, glycated proteins, and glycation of antioxidants – limiting the ability to neutralize other ROS and causing dysfunction of protein function. Glycated proteins include glycosylated hemoglobin, albumin, and lens crystalline [59]. Moreover, high levels of glucose – "glucotoxicity" – stimulates excessive mitochondrial respiration, producing excessive ROS and NADPH [58, 59], and the ketones produced in DM generate ROS, notably superoxide anions through reaction with transition metals [112]. To lower glucose concentrations in a hyperglycemic setting, aldose reductase converts intracellular glucose to sorbitol using NADPH in the cytoplasm [113]. Since NADPH is a key redox cofactor, this ultimately decreases cellular antioxidant capacity [113]. Furthermore, membrane-bound NOX is activated by AGEs produced by glucotoxicity, generating additional ROS [59]. The increased oxidative stress renders vascular tissue susceptible to oxidation because of the high ROS and RNS production with insufficient antioxidant capacity, leading to vascular dysfunction and tissue damage [111, 112].

Neurodegenerative diseases, such as Parkinson's and Alzheimer's disease, are associated with increased oxidative stress due to damage to neurons and increased inflammatory responses in the central nervous system (CNS) [114]. High levels of CNS inflammation and ROS production/damage has also been found to contribute to diseases such as Huntington's disease and multiple sclerosis [115, 116]. The brain has a high consumption of oxygen and is enriched in polyunsaturated fatty acids (PUFA) which are especially vulnerable to ROS attack and lipid peroxidation [117]. The brain also contains high concentrations of transition metals, namely iron

and copper, which actively participate in ROS reactions through the Fenton and Haber-Weiss reactions [117]. Neurodegenerative diseases are characterized by increased apoptosis and necrosis, as well as dysfunction of neuronal cells by excessive ROS activity [117]. Elevated levels of lipid peroxidation byproducts, as well as accumulation of protein aggregates, further contribute to mitochondrial dysfunction and cellular failure in neurodegenerative diseases [117].

Development of CVD is correlated with oxidative stress due to the vascular tissue damage from ROS and oxidized cholesterol, high inflammatory response, and increased cellular senescence [5]. The endothelium is a key modulator of vascular tone, vessel wall formation, and thromboresistance, largely through its production of vasodilator nitric oxide via NOS [118]. A reduced availability of nitric oxide leads to an altered balance between vasodilator and vasoconstrictor molecules, resulting in the accumulation of vasoconstrictor and prothrombotic products, increasing the risk of cardiovascular events [118]. As mentioned, nitric oxide serves as a critical vasodilator, modulating vascular tone and inhibiting thrombosis [32]. However, nitric oxide rapidly reacts with superoxide to yield peroxynitrite, which is highly reactive and can form peroxynitrous acid through protonation [33, 34]. This reaction initiates the decay if peroxynitrous acid into a hydroxyl radical and nitrogen dioxide radical, both of which are highly reactive and lead to the uncoupling of NOS by oxidizing its cysteine residues [33, 34]. This uncoupling leads to activation of the endothelium, resulting in the activation of NF-κB and production of pro-inflammatory cytokines, as well as the overproduction of ROS by NOX, rendering NO inactive through its reactions with superoxide [118]. In parallel, the increase in NOX-mediated ROS production results in oxidation of low-density lipoprotein (LDL) - the initial step of atherosclerosis [118-121]. Activated endothelial cells will express leukocyte adhesion molecules, including vascular cell adhesion molecule (VCAM-1) to mediate the adhesion of circulating leukocytes

(monocytes and T cells) [118, 120, 121]. When these monocytes from the blood travel to the damaged site, they differentiate into macrophages when stimulated by oxidized cholesterol [122]. These macrophages will digest the oxidized cholesterol molecules and initiate a pro-inflammatory response [122]. In addition, the macrophages change into foam cells which accumulate to form plaque, resulting in atherosclerosis [122]. Formation of atherosclerotic plaques then leads to the development of coronary artery disease (CAD). Furthermore, ROS activate matrix metalloproteinases in the endothelial cells which lead to plaque rupture and acute myocardial infarction [119]. Excessive ROS also mitigates cardiac hypertrophy through the activity of angiotensin-II (Ang-II). Ang-II generates ROS which activate ROS-signaling kinases and contribute to the expression of hypertrophic factor beta-myosin heavy chain [119]. Ang-II also stimulates NADPH to generate additional ROS which ultimately contributes to hypertrophy development [119].

Oxidative stress contributes to the initiation and progression of liver damage [123]. Exposure to alcohol, drugs, pollutants, and irradiation subjects the liver to increasing detoxification processes, which normally create ROS as a byproduct [123]. Hepatocyte mitochondria and ER are primary ROS producers and activity of these two organelles is upregulated under acute and chronic exposure to alcohol, a high-calorie diet, drug overdose, environmental pollutants, and heavy metals [124]. Under the conditions of oxidative stress, hepatocytes activate Nrf2 to upregulate cytoprotective genes [124], but when ROS concentrations remain uncontrolled, disturbances to redox balance and subsequent hepatic fat accumulation lead to the development liver disease [125]. The liver is responsible for synthesizing cholesterol, and ROS attack on lipid metabolism results in hepatic cholesterol accumulation and impairs hepatocyte regeneration [124]. Moreover, disturbances in lipid metabolism as a result of ROS attack results in hepatic lipid accumulation,

which itself increases ROS production through action on the mitochondria, ER, and NOX [125]. To adapt to the lipid accumulation, mitochondria will downregulate the ETC and preserve the mitochondrial fatty acid oxidation [125]. However, this stimulates ROS overproduction outside of the ETC through upregulation of NOX activity and ER stress, though the mechanisms responsible remain unclear [125]. Chronic lipid accumulation contributes to the development of non-alcoholic fatty liver disease (NAFLD) and its progression non-alcoholic steatohepatitis NASH (Figure 2.26) [126]. Non-alcoholic fatty liver disease (NAFLD) resembles the histopathological features of alcoholic liver disease (ALD), but patients do not have significant alcohol consumption which could be attributed to the disease etiology [127]. A subset of NAFLD patients suffer from NASH which includes not only steatosis, but hepatic inflammation [127]. NAFLD is associated with increased sensitivity to oxidative stress and liver fibrosis and is characterized by steatosis, mixed lobular inflammation, hepatocellular cell death, and hydropic degeneration [128]. In addition to the altered metabolism of lipids in NAFLD, cytokines, particularly TNF-α, are overexpressed and further contribute to NASH and hepatocellular apoptosis [128].

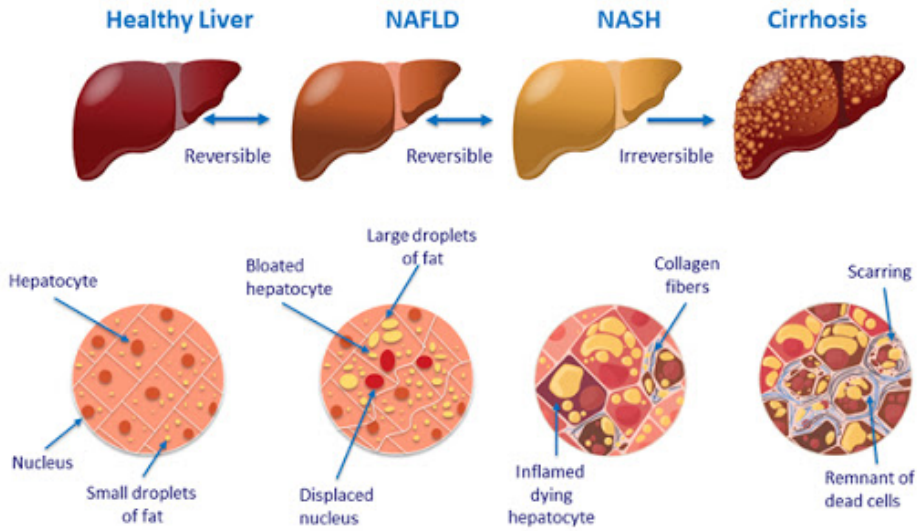

Figure 2.26. NAFLD: progression of disease. Figure from Diehl and Day (2017) [129].

Liver fibrosis arises from activation of hepatic stellate cells (HSCs) [130]. HSCs are found in the subendothelial space between hepatocytes and sinusoidal endothelial cells and are major storage sites of vitamin A for the liver and respond to liver injury to heal damage upon activation by inflammatory signals [131, 132]. HSCs amplify the inflammatory response through production of chemokines, particularly monocyte and neutrophil chemoattractants, and action as antigen presenting cells to stimulate lymphocyte proliferation and hepatocyte apoptosis [132]. Kupffer cells are the hepatic resident macrophages and release ROS and cytokines in response to these inflammatory signals [131]. Kupffer cells are also responsible for HSC activation by secretion of platelet-derived growth factor (PDGF) [131]. In response to PDGF, HSCs are activated and proliferate into myofibroblast-like cells to participate in fibrogenesis by migrating to the site of liver injury and producing extracellular matrix (ECM) components, including collagen and adhesive glycoproteins [131]. Following acute liver injury, hepatic parenchymal cells will regenerate to replace the apoptotic cells, and this is associated with an acute inflammatory response and limited ECM protein deposition by HSCs [131]. However, when the liver undergoes repeated injury such as through oxidative stress and chronic inflammation, liver regeneration fails and the hepatocytes are instead replaced with ECM, namely fibrillar collagen as HSCs lose their normal storage of vitamin A from persistent injury repair (Figure 2.27) [130, 131]. This process results in the onset of liver fibrosis and is associated with a chronic pro-inflammatory state [131]. The progression of liver fibrosis and buildup of scar tissue results in a the hardening of the liver and cirrhosis, characterized by the distortion of hepatic vasculature and architecture [133].

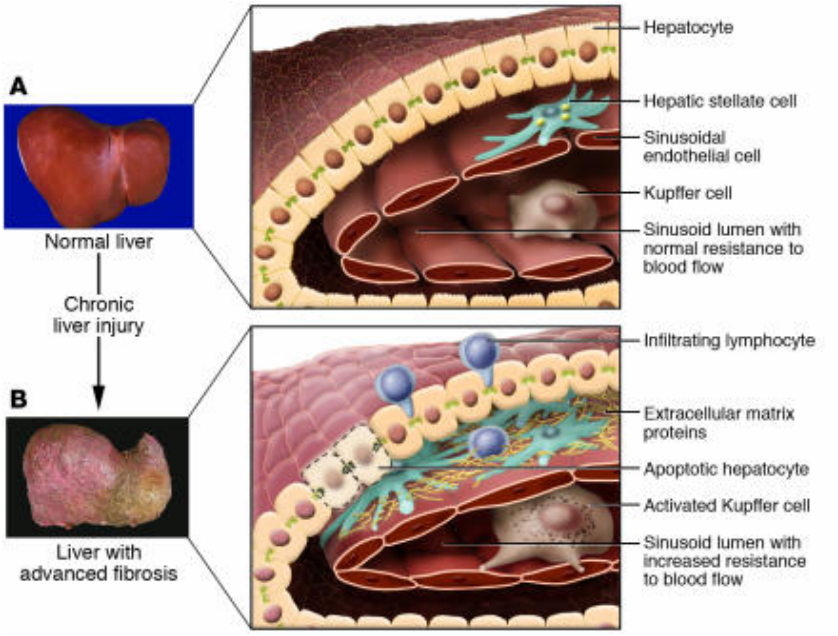

Figure 2.27. Changes in hepatic architecture associated with advanced hepatic fibrosis. Figure from Bataller and Brenner (2005) [131].

The kidneys are vulnerable to oxidative stress given their role in detoxification and regulation of extracellular fluid [134]. Kidney diseases include acute kidney injury (AKI) and chronic kidney disease (CKD) [135]. Within the kidneys, ROS are primarily produced by the mitochondria and NOX [135], particularly in the proximal tubules [134]. The proximal tubules are critical for reabsorption of water and solutes, and because of this, they have high oxygen demands [136]. If they are injured, such as through AKI, the epithelial cells will become activated and allow for inflammatory cell infiltration [136]. As a result, damage to renal cells from oxidative stress results in increased levels of uremic and nephrotoxins with prime polymorphonuclear cells that set up a vicious cycle by NF-κB activation, resulting in additional ROS and pro-inflammatory cytokine production [135, 136]. By exposing the kidneys to large amounts of oxidants and inflammation, it depletes antioxidant stores and leads to tissue malfunction [134]. CKD is characterized by a loss in kidney structure and function over time, with common causes including T2DM, hypertension, and polycystic kidney disease [136]. Plasma markers for oxidative stress –

indicative of systemic oxidative stress – are elevated in CKD patients [136]. Therefore, oxidative stress is considered a prognostic factor in CKD treatment [135]. Chronic inflammation, endothelial dysfunction, and oxidative stress are contributors to the vicious cycle that results in progression of CKD and its systemic complications [136]. Alteration to kidney function results in dysregulated metabolic waste disposal, leading to the accumulation of toxins and further contributing to oxidative stress [136]. Moreover, oxidative stress resulting in both liver and kidney dysfunction increases risk for progression of secondary chronic diseases, such as CVD and T2DM [134, 136].

To protect cellular machinery against the deleterious effects of oxidative stress, the body produces and stores antioxidants, both enzymatic and non-enzymatic, to neutralize ROS/RNS and regulate their concentrations [45].

Cellular antioxidant protection

Antioxidant defense systems are found within cellular membranes, cytoplasm, and organelles, and are responsible for sequestering the ROS and RNS, rendering them non-reactive (or less reactive) [5]. Much like ROS and RNS production, the sources of antioxidants are exogenous and endogenous [5], and the two sources act interactively to maintain redox balance [137].

Exogenous antioxidants: Primary exogenous sources of antioxidants include vitamins, phenolic compounds, carotenoids, and trace minerals. Vitamin C, also known as ascorbic acid, is a water-soluble vitamin that neutralizes ROS non-enzymatically [138]. Ascorbic acid is an important intracellular and extracellular antioxidant and participates in a variety of reduction reactions in aqueous environments [139]. In redox reactions, ascorbic acid is converted to semihydroascorbic acid radical (also known as monodehydroscorbate or ascorbate radical) and dehydroascorbic acid via its action as an electron donor. Dehydroascorbate reductase will then

regenerate ascorbic acid from semihydroascorbic acid radical or dehydroascorbic acid through the donation of electrons by GSH or other electron donors such as NADH [140]. Vitamin E, also known as α-tocopherol, is an important fat-soluble vitamin that also participates in ROS reactions, but in the lipid membrane [141]. Vitamin E is vital in neutralizing lipid peroxyl radicals to prevent the cycle of lipid peroxidation as a result of these radicals [141]. Vitamin E radicals are considered stable and therefore do not react with neighboring unsaturated fatty acids in the cellular membrane, protecting the integrity of the plasma membrane [141]. Similar to vitamin E, vitamin D has been shown to function as a lipid membrane antioxidant to inhibit lipid peroxidation [142, 143], however the potential role of vitamin D as an antioxidant remains controversial [144]. Trace elements zinc and selenium, as well as copper and manganese, act as cofactors of antioxidant enzymes [145]. Copper, zinc, and manganese are cofactors for SOD, whereas selenium is a pivotal part of the GPx active site [145]. Iron in its ferrous (Fe^{2+}) and ferric (Fe^{3+}) states serve as electron donors and acceptors and are active participants in the Fenton reaction in which hydroxyl and peroxyl radicals are produced in effort to neutralize hydrogen peroxide and oxygen radicals [145]. Several other exogenous antioxidants are obtained through the diet, including carotenoids: β-carotene, lycopene, lutein, zeaxanthin, phenolic acids: chlorogenic acids, gallic acid, caffeic acid, flavonols: quercetin, kaempferol, and myricetin, flavanols: proanthocyanidins and catechine, anthocyanidins: cyanidin and pelargonidin, isoflavones: genistein, daidzein, and glycitein, flavanones: naringenin, eriodictyol, and hesperetin, and flavones: luteolin and apigenin [137].

Dietary impact on antioxidants: Exogenous antioxidants are largely supplied from the diet [137]. Fruits and vegetables contain high amounts of antioxidants, such as flavonoids, vitamins C and E, carotenoids, and minerals, as well as precursors to other antioxidants such as GSH [146, 147]. Therefore, diets enriched with fruits and vegetables serve as viable avenues to combating

oxidative stress [146]. Following a vegetarian and/or vegan diet includes a high amount of antioxidants given the inclusion of large amounts of fruits and vegetables and these diets have been linked to lower levels of diabetes, cancer, and obesity [147]. Following a Western-type diet includes high amounts of saturated fat, meats, sugar, and refined grains, with limited consumption of fruits and vegetables [147]. Consumption of a Western-type diet has been linked to cancer, chronic disease, and high levels of oxidative damage, and is therefore not recommended to prevent oxidative stress [147]. The Dietary Approaches to Stop Hypertension (DASH) diet is recommended for those with chronic diseases such as T2DM, CVD, and obesity, and it emphasizes foods low in saturated fats while encouraging green leafy vegetables, whole grains, legumes, nuts and seeds, and fish [147]. The DASH diet has been associated with increased antioxidant status and lower oxidative stress in obese individuals [147, 148]. Much like the DASH diet, the Mediterranean diet, which emphasizes intake of fruits, vegetables, nuts, legumes, and extra virgin olive oil, with limits on eggs and sweets and red meat, is correlated with higher antioxidant levels and reduced risk for chronic disease [147, 149]. Lastly, consuming isolated antioxidant supplements, such as those containing polyphenols, vitamin C and E, and carotenoids, offer an additional avenue to increase antioxidant status [137]. However, it is important to not consume isolated antioxidant supplements in excess, as they can have a toxic and prooxidant effect if consumed in high doses [137]. If consumed safely, supplementing with antioxidants or their precursors help replenish and maintain antioxidant capacity in tissues [150].

Endogenous antioxidants: Primary endogenous enzymatic antioxidants include superoxide dismutase (SOD), catalase (CAT), and GSH-linked antioxidant enzyme glutathione peroxidase (GPx) (Figure 2.28) [5, 137]. SOD catalyzes the reduction reaction of superoxide to hydrogen peroxide which is then converted to water (H_2O) and molecular oxygen by CAT, GPx, and Prx [5,

137]. GPx1 is ubiquitously expressed intracellularly [151, 152], whereas GPx2 is specific to the gastrointestinal tract [153], GPx3 to the plasma and extracellular environment [154], and GPx4 as a phospholipid hydroperoxide [155]. GPx reduces reactive ROS and RNS to non-toxic forms through the reaction of GPx and GSH [5, 137]. Additional endogenous antioxidant enzymes include thioredoxin reductase (TR) and glucose-6-phosphate dehydrogenase (GAPDH) [137]. In effort to neutralize hydrogen peroxide, Prx oxidizes thioredoxin (Trx) [81]. TR then reduces oxidized Trx using the reducing NADPH cofactor [81]. GAPDH regenerates NADPH through enzymatic conversion of glucose-6-photosphate to 6-phosphogluconolactone, increasing the availability of the critical redox cofactor [81]. Non-enzymatic endogenous antioxidants include proteins and non-proteins such as bilirubin, β-carotene, albumin, lipoic acid, NADPH, coenzyme Q, and uric acid [5, 137]. Of all endogenous antioxidants, GSH is considered the most abundant and is critical to cellular protection against ROS and RNS [70].

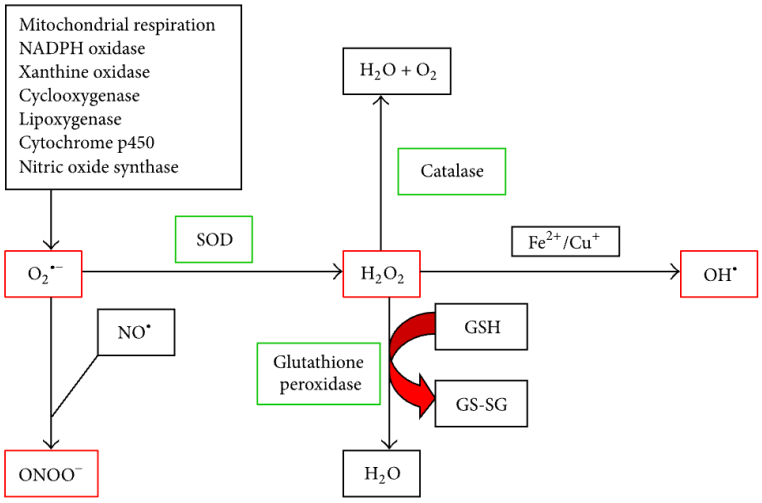

Figure 2.28. Major prooxidant-antioxidant reactions relevant in biological system. Figure from Biswas (2016) [156].

The glutathione redox system

History of glutathione: GSH was first discovered in 1888 and called "philothion", meaning love and sulfur in Greek [157]. Joseph de Rey-Pailhade isolated the molecule in yeast cells and found that the compound reacted spontaneously with sulfur to form hydrogen sulfide [158]. From there, Frederick Gowland Hopkins further characterized the GSH structure by isolating it in liver, skeletal muscle, and yeast, and in 1921 he suggested that the compound is a dipeptide containing glutamic acid and cysteine [157]. Hopkins called the compound "glutathione" and in 1927, Hunter and Eagles suggested that the compound could be a tripeptide [157]. In 1929, Hopkins concluded that GSH was a tripeptide with the addition of glycine (Figure 2.29) [158]. GSH is now documented as a tripeptide L-γ-glutamyl-L-cysteinyl-glycine synthesized from precursor amino acids glutamate, cysteine, and glycine [159].

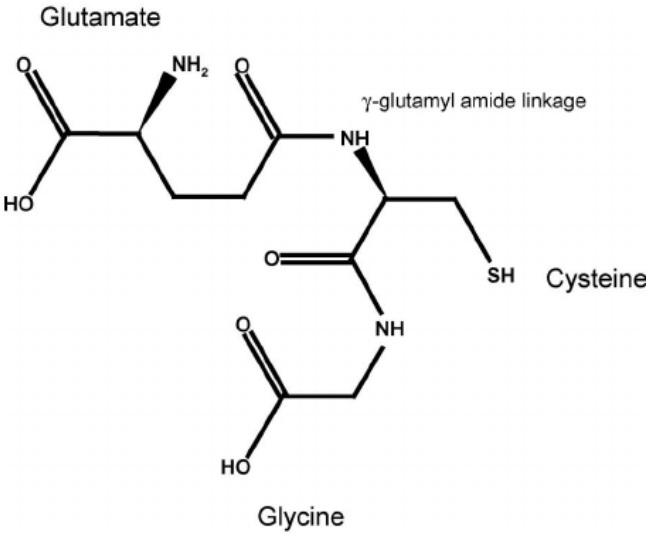

Figure 2.29. The structure of GSH. Franco et al. (2007) [160].

Glutathione cellular functions: GSH is a ubiquitous tripeptide used to combat oxidative stress in all mammalian cells [161]. It is the most abundant low molecular weight thiol antioxidant in mammals [162] and protects against both reactive oxygen species (ROS) and reactive nitrogen

species (RNS) and their deleterious actions on proteins, lipids, and DNA [163]. It is primarily found in its reduced form, GSH, while approximately 1% is found in the oxidized form, GSSG [163]. GSH is water-soluble and is produced exclusively in the cytosol where it is then transported to subcellular organelles [164]. The three major reservoirs of GSH are the cytosol (90% of cellular GSH), mitochondria (10%), and the ER (<1%) [147, 165]. GSH is the major reducing agent for disulfides and peroxides [166], and the antioxidant function of GSH is reliant on its cysteine residue because of its thiol group and redox properties [159]. Whereas cysteine is reactive and susceptible to oxidation, the addition of glutamate and glycine allows for the GSH molecule to stabilize and maintain intracellular redox balance [167]. GSH has many critical roles, most notably its action as a strong nucleophile through detoxification of electrophiles, including peroxide [168]. Glutathione transferases (GSTs) are phase II detoxification enzymes found in the cytosol that catalyze the conjugation of electrophiles, xenobiotics, and peroxidized lipids to GSH, rendering them water-soluble and eligible for breakdown [169-171]. Up to 10% of cystolic proteins are GSTs [169, 172] and GSTs can function as transport proteins as they bind toxins [173]. Similarly, GSH is a substrate for formaldehyde dehydrogenase which forms *S*-formyl-glutathione in effort to remove formaldehyde [174, 175]. Formaldehyde is produced from methionine, choline, methanol, sarcosine, and xenobiotic metabolism, but is a known carcinogen [174]. GSH is also involved in modulation of cell proliferation and apoptosis [161, 165], recycling of vitamins C and E [164, 176, 177], cysteine storage [160, 165, 178], and maintenance of thiol status of proteins [165]. Protein functionality is affected by their thiol groups due to their effect on tertiary and quaternary protein structure, as well as enzyme active sites [167]. The reactivity of sulfhydryl groups to proteins is regulated by S-glutathionylation and S-nitrosylation in protein post-translational modification [167]. Both reactions affect cellular signaling through their role in protein alteration [167]. In S-

glutathionylation, GSH binds to proteins through its cysteine residue, enhancing or suppressing the protein activity [167]. S-glutathionylation also renders the protein susceptible to degradation through proteolysis or sulfhydryl overoxidation [167]. In S-nitrosylation, NO covalently bonds to the sulfhydrl cysteine residue of a protein, altering the protein function. GSH S-nitrosylation can then occur, forming S-nitrosoglutathione, which serves as a NO reservoir and transfer NO groups in transnitrosylation reactions [167]. Lastly, GSH is required for prostanoid metabolism where it is utilized by endoperoxide isomerase for prostaglandin H_2 conversion to prostaglandins D2 and E2 [165]. Oxidative stress accelerates the rate of GSH conversion to GSSG, thereby decreasing the ratio GSH/GSSG; such a shift has major impacts on cellular signaling [179], thiol disulfide exchange reactions [180], and cell proliferation [165]. The GSH/GSSG ratio is a key redox sensor and determines the rate of S-glutathionylation and S-nitrosylation alterations [167]. Cellular GSH concentrations reflect the synthesis, metabolism, and transport of the molecule [160], and it is synthesized *de novo* (new) as well as through salvage (recovery of precursors from catabolism) [163].

GSH synthesis: The *de novo* synthesis of GSH involves a two-step enzymatic process (Figures 2.30 and 2.31) [157, 160]. First, γ-glutamylcysteine synthetase, commonly referred to now as glutamate cysteine ligase (GCL), catalyzes the synthesis of γ-glutamylcysteine by forming a γ-linkage peptide bond between glutamate and the amino group of cysteine (its γ-carboxyl group) [160]. This is done through the hydrolysis of ATP [163]. Glutamate is provided from the conversion of glutamine via normal metabolic pathways via glutaminase [147]. γ-glutamylcysteine has a very strong affinity for GSH synthetase which allows it to be more resistant to of γ-glutamylcyclotransferase, an intracellular peptidase that hydrolyzes it into the constituent amino acids [174, 181]. From there, glycine is added to γ-glutamylcysteine by GSH synthetase (GS)

[160]. This endothermic reaction consumes one ATP molecule [160]. The C-terminal glycine provides protection against the degenerative action of γ-glutamylcyclotransferase [160]. The presence of GSH acts as a feedback mechanism to inhibit GCL activity [160], and cysteine acts as the rate limiting amino acid in GSH *de novo* synthesis [147]. The γ-peptide bond with glutamate protects GSH from peptidases, while the cysteine sulfhydryl group renders GSH an excellent electron donor for electrophile neutralization [167]. The availability of precursors is essential to the formation of GSH, and several amino acids are involved in the GSH pathway, either directly or indirectly [147]. Furthermore, glutamate shares a saturable transporter with the oxidized form of cysteine (cystine) and the two compete for absorption [147]. The synthetic capacity of GSH from its precursors has been shown to diminish with age and dysfunction of the liver [182], but the nature of the mechanisms are not well understood [183].

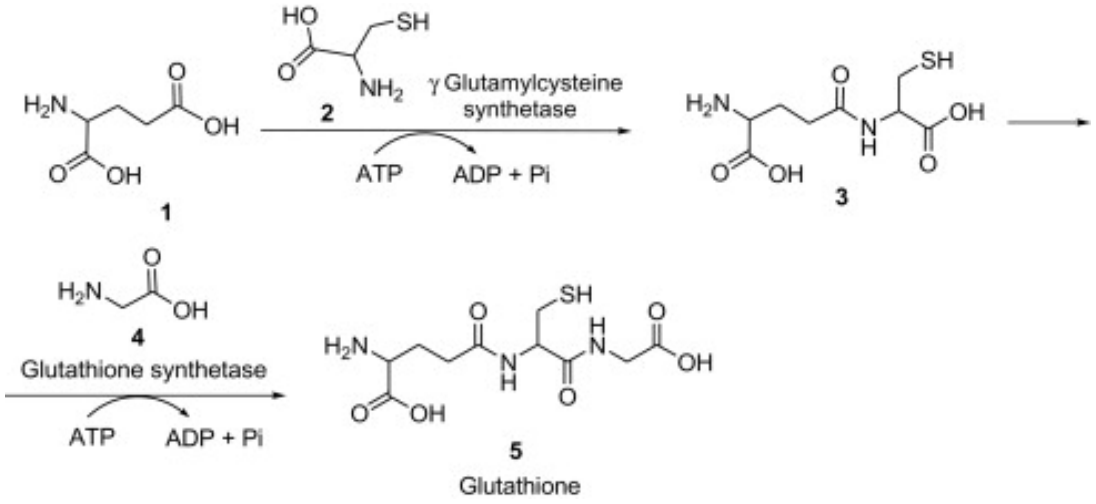

Figure 2.30. Biosynthesis of GSH. Figure from Alanazi, Mostafa, and Al-Badr (2015) [157].

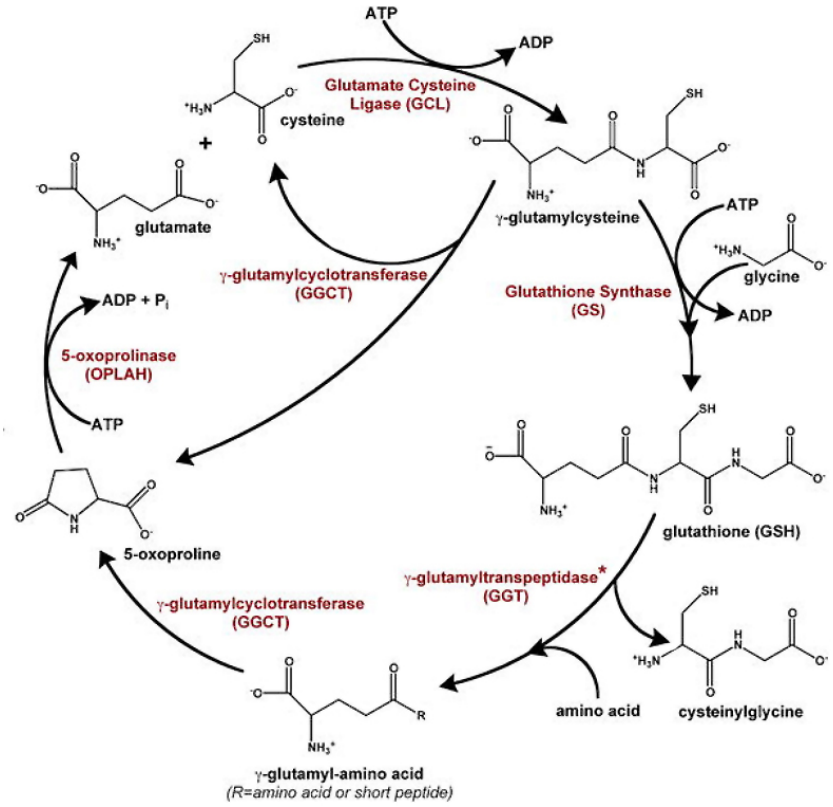

Figure 2.31. *De novo* synthesis of GSH. Figure from Hansen and Harris (2015) [184, 185].

GSH recycling: The salvage synthesis of GSH involves either the reduction of its disulfide form GSSG via the reducing agent NADPH, or through recycling of precursors [160]. GSH is oxidized to its dimer GSSG or other GSTs when GSH is consumed during redox reactions via GPx. Examples of this include reducing reactive oxygen species (ROS), such as H_2O_2 to H_2O [186], or as a direct result of GSH reactions with electrophilic compounds (Figure 2.32) [187, 188]. GSH is maintained in its reduced state through the action of specific enzymes, glutathione reductases (GR), that reduce the disulfide GSSG to regenerate the sulfhydryl GSH via NADPH [164]. GRs are found throughout the cell and have a high affinity for both NADPH and GSSG [158]. *In vitro*, dihydronicotinamide adenine dinucleotide (NADH) and NADPH can serve as the hydrogen donor for GSSG, but only NADPH can perform this action *in vivo* [189].

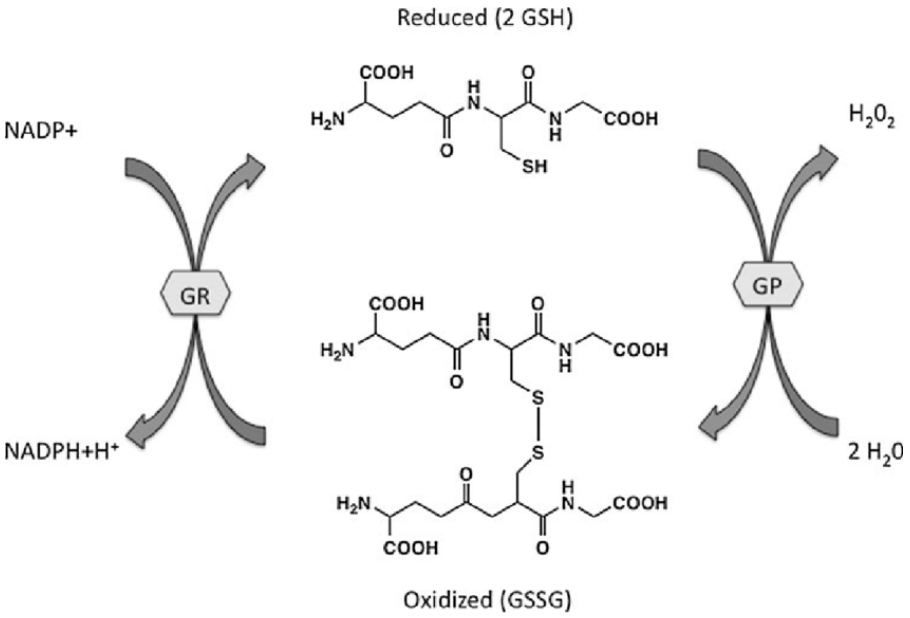

Figure 2.32. Glutathione recycling. Figure from Xiong et al. (2011) [190].

GSH can also be broken down and degraded for access to precursors glutamate, cysteine, and glycine through the gamma-glutamyl cycle. γ-L-glutamyltranspeptidase (GGT; also known as γ-glutamyltransferase) is found at the apical surface of the cellular membrane and catalyzes the degradation of GSH to cysteinyl-glycine and glutamic acid by removing the γ-glutamyl moiety from GSH (Figure 2.33) [160]. From there, cysteinyl-glycine can be hydrolyzed by dipeptidases and the amino acids can be used again for the synthesis of GSH [160]. This degradation process occurs exclusively in the extracellular space on the surface of cells that express GGT [191] as the N-terminal of glutamate is connected to the cysteine by its γ-carboxyl group which allows it to be resistant to hydrolysis by common intracellular peptidases outside of GGT [163]. GGT also decomposes GSSG and GSH conjugates which can then be excreted into bile or removed via mercapturic acid in the urine [192]. In total, the metabolism of GSH and its related enzymes are represented in Figure 2.34.

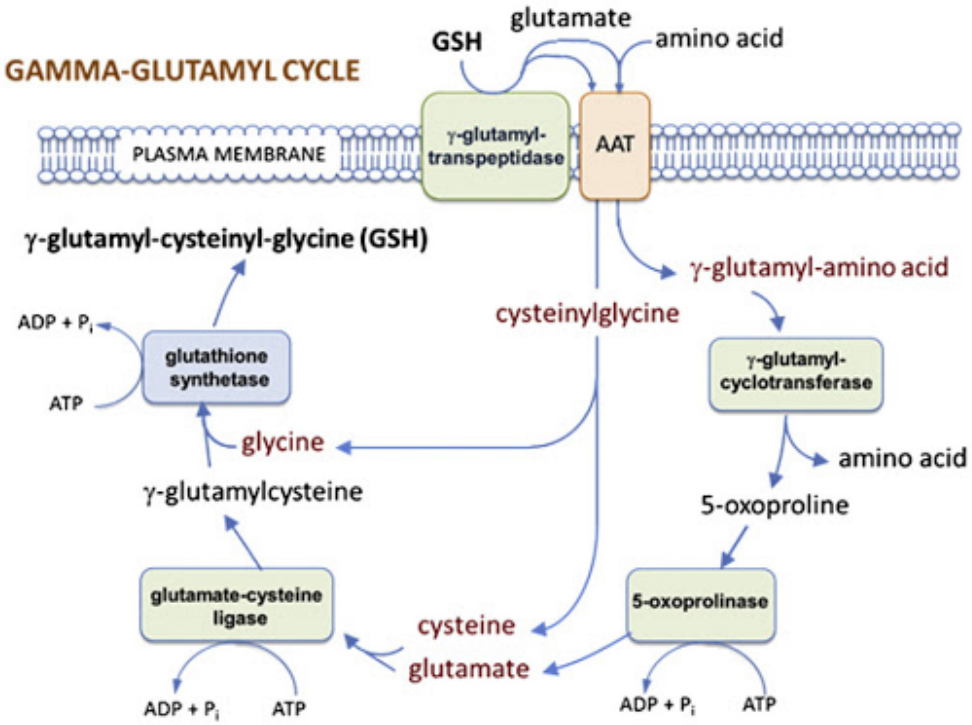

Figure 2.33. The gamma-glutamyl cycle and *de novo* synthesis of GSH. Figure from Nebraska Redox Biology Center Education Portal [185].

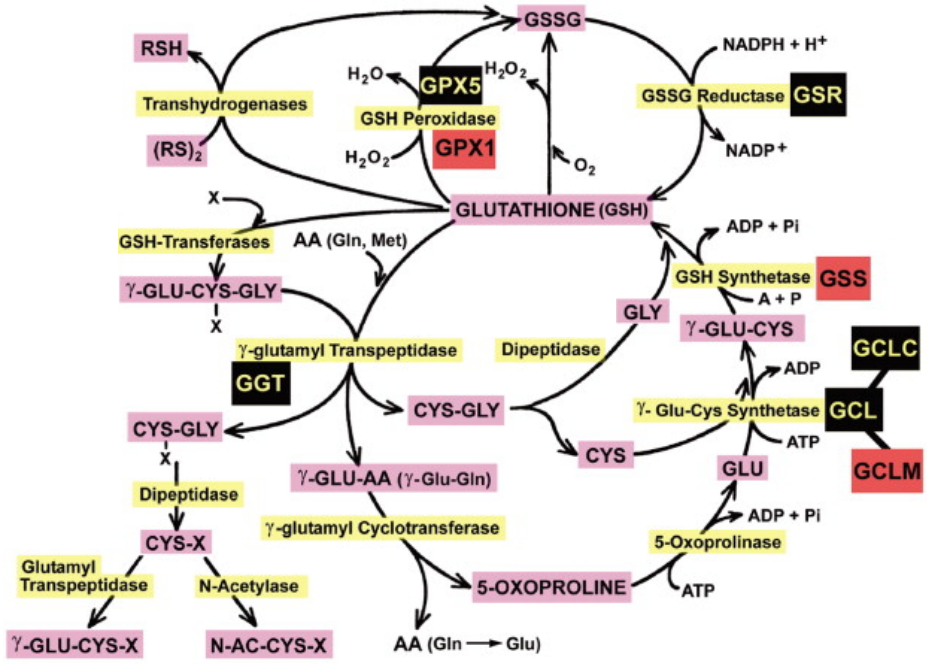

Figure 2.34. GSH metabolic pathway. Figure from Tosic et al. (2006) [193].

Digestion and cellular absorption of GSH and constituent amino acids: Dietary GSH is subject to normal proteolytic digestion and is primarily consumed in the upper jejunum where GGT breaks it down into its constituent amino acids by the enzymatic action of GGT (Figure 2.35) [147, 182, 194]. Extracellular GSH cannot be absorbed and instead cells require it to be degraded to its constituents before transport into the cell [185]. Through the action of GGT, glycine, glutamate, and cysteine are absorbed to be utilized for GSH synthesis or exported for transport [195]. GGT is located on the outer leaf of the enterocyte's membrane and acts as a glutathionase enzyme to release constituent amino acids for absorption through the respective amino acid transporters [185]. This effect remains true with injected GSH as a large proportion disappears after injection as a result of GGT action [196]. Under normal conditions, cellular GSH concentrations are regulated by both the rates of GSH synthesis and export, and GSH levels are influenced by the availability of precursors, nutrition, hormones, and stress levels, diurnal variations, and other physiological states such as protein energy malnutrition, cancer, heat shock, and pregnancy [174, 197]. Outside of transport of amino acid precursors, GSH can be released into circulation from cells where it is rapidly catabolized by plasma membrane-bound GGT, thus the half-life is only 2-6 hours [191, 198, 199]. How GSH is transported into circulation is poorly defined, with transporters appearing to be tissue-specific; For example, in the liver, Mrp2 mediates GSH transport from hepatocytes into bile whereas Mrp1 and Oatp1 mediates GSH efflux from hepatocytes into blood [191], whereas in the kidney basolateral membrane, Oat3 has been demonstrated to transport GSH, and Oat1 and NaC2 are likely carriers [200].

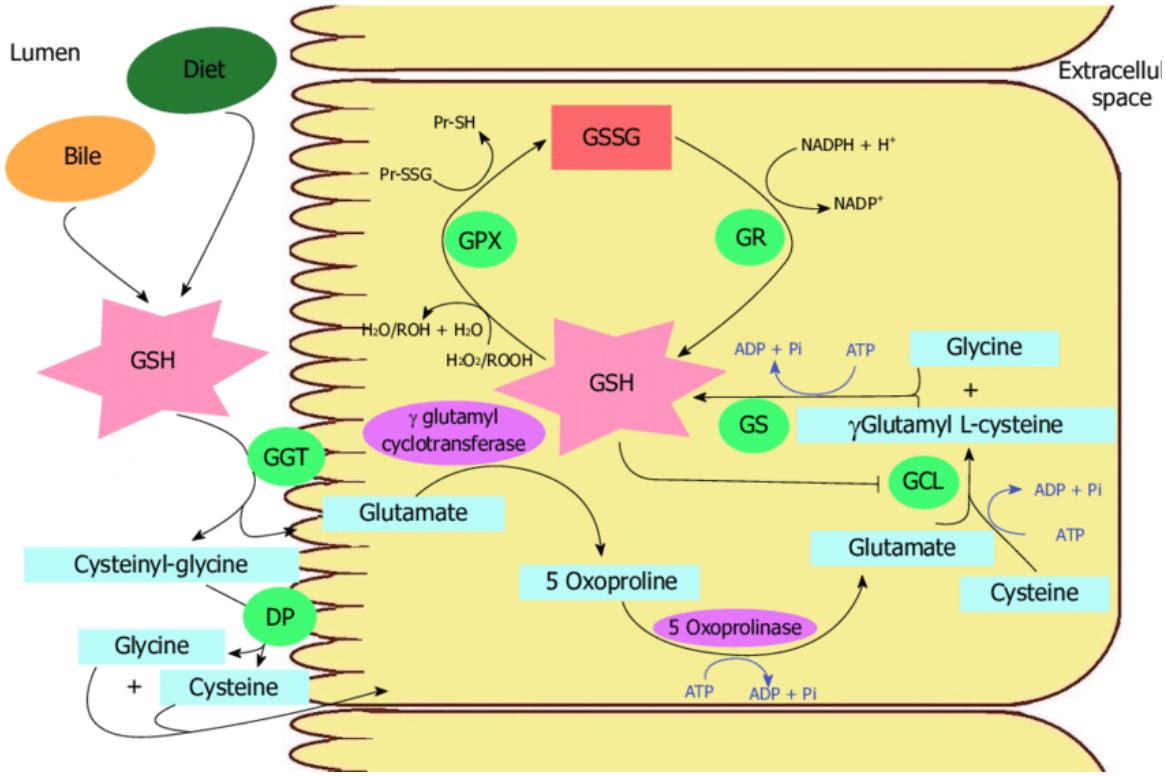

Figure 2.35. Intestinal glutathione metabolism. Figure from Moine et al. (2018) [201].

Glutathione concentrations are tissue-specific: GSH is ubiquitously expressed and intracellular concentrations are highest within the cytosol, mitochondria, and ER [202]. Intracellular GSH concentrations typically fall between 0.5 to 10 mM [163]. However, concentrations of glutathione depend on tissue of origin and variation in concentrations is related to cellular function [203]. The liver, kidney, pancreas, and heart are vital metabolic organs that have significant levels of GSH [204]. Liver and kidney tissue contain high levels of GSH attributed to their functions in detoxification and high exposure to oxidants and reactive electrophiles [205]. Similarly, GSH is the major antioxidant in the brain and is found in high concentrations in brain regions susceptible to oxidative stress, such as the prefrontal cortex [206]. The small-intestinal epithelium, the liver, and the renal proximal tubule are the main participants in the GSH interorgan metabolism (Figure 2.36) [200]. The liver is the major producer and exporter of GSH [174], and as such, is the main source of extracellular and plasma GSH [200, 207]. Hepatocytes export GSH

by transport into bile or plasma [200]. Biliary GSH is either degraded by GGT or is transported to the small-intestinal lumen to be degraded [200]. From there, the enterohepatic circulation transports the constituent amino acids for GSH resynthesis in the liver [200]. Plasma GSH and its respective amino acids are translocated to the brain via the blood brain barrier (Figure 2.37) [208]. The kidneys extract plasma GSH through glomerular filtration or through basolateral uptake [200]. The kidneys are considered the major consumer of plasma GSH, with glomerular filtration removing 30% of plasma GSH and basolateral uptake removing 50% [200, 209].

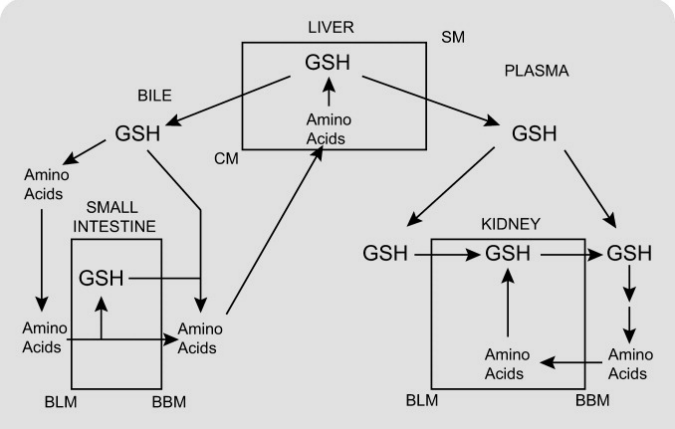

Figure 2.36. GSH interorgan metabolism. Figure from Lash (2009) [200].

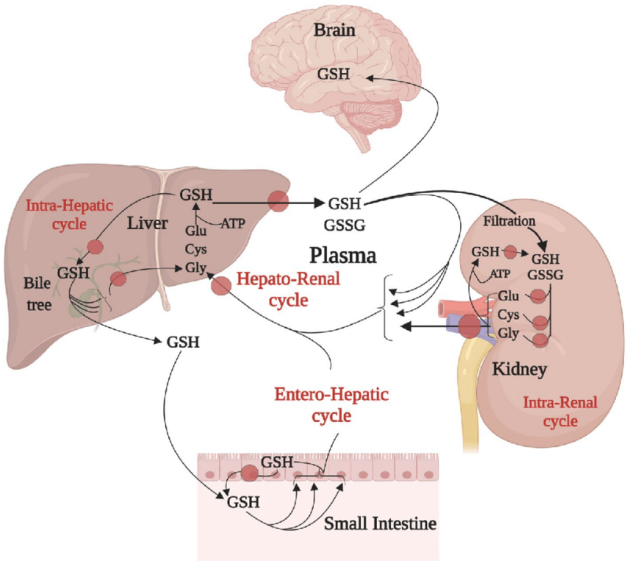

Figure 2.37. Interorgan GSH transport. Figure from Dwivedi et al. (2020) [208].

Interaction with other antioxidants: GSH is not only important for directly scavenging ROS and RNS, but it is also important in the regeneration of other critical antioxidants such as vitamin C and vitamin E (Figures 2.38 and 2.39) [210]. GSH regenerates vitamin C by acting as an electron donor in the enzymatic action of dehydroascorbate reductase [140]. Furthermore, since ROS and RNS found in aqueous environments are substrates for both vitamin C and GSH, vitamin C can spare GSH by reducing its substrates [211]. Vitamin C can then go on to regenerate lipophilic vitamin E nonenzymatically at the lipid/water interface by serving as a reducing agent for vitamin E [141, 177]. Vitamin E is correlated with GSH concentrations and supplementation of vitamin E significantly increases GSH stores [212]. The interaction is where GSH status is conserved by other antioxidants, and vice versa, is seen between GSH and vitamin A, SOD, and catalase, where proper function and concentrations of these antioxidants conserve GSH levels [137].

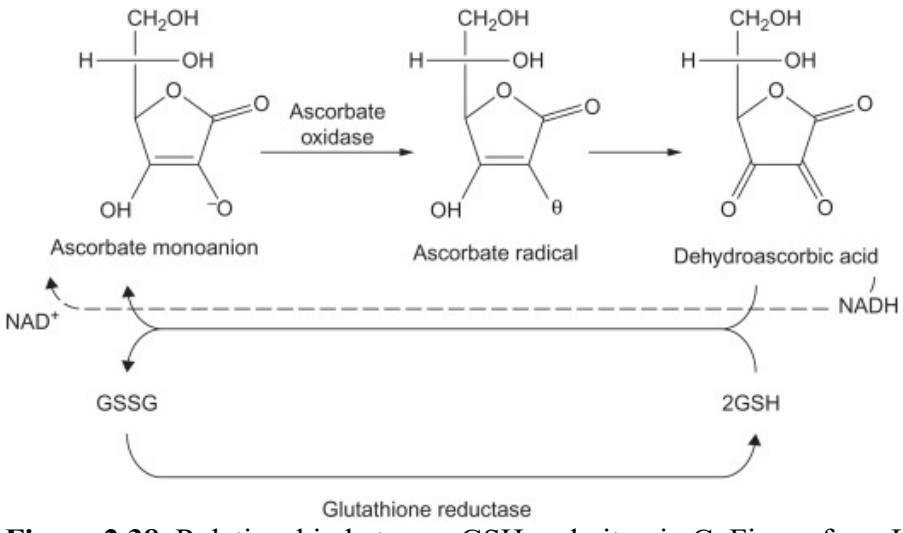

Figure 2.38. Relationship between GSH and vitamin C. Figure from Litwack (2018) [213].

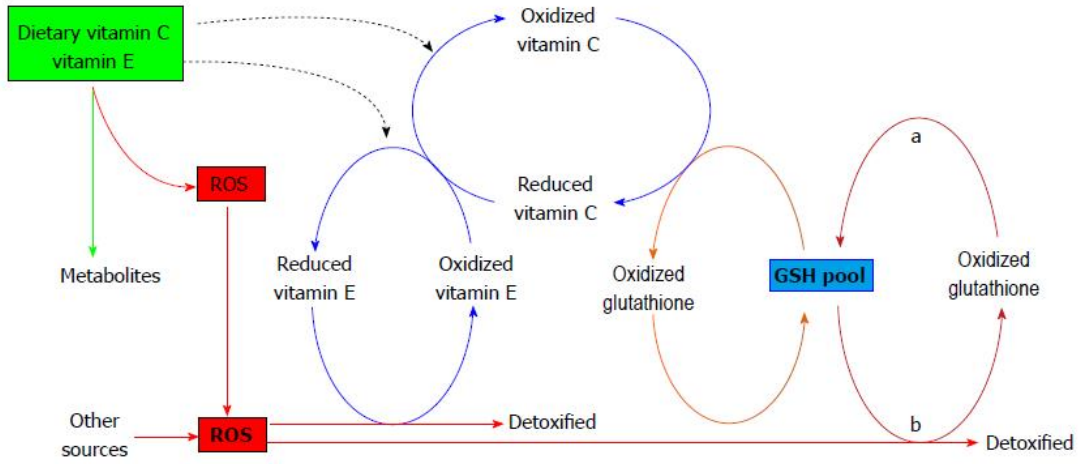

Figure 2.39. Relationship between GSH, vitamin C, and vitamin E, and detoxification of ROS. Figure from Zhou et al. (2015) [210].

Glutathione and its relationship with disease

Having high concentrations of GSH and GSH/GSSG, as well as total glutathione (GSH + 2GSSG) is associated with having heightened antioxidant activity and protection against cellular damage, tissue degeneration, and disease progression [175]. Alternatively, an increase in oxidative stress leads to an increase in GSH oxidation and consequently, higher levels of GSSG which negatively impacts cell activities and thiol disulfide exchange reactions [180]. Consequently, changes in GSH homeostasis has been linked to the aging process [175, 214], development of cancer [175, 215], cognitive decline [214-219], HIV [214] and AIDS [215], DM [215, 220], obesity [221], heart disease [215], liver disease [188, 202, 222-224], and kidney disease injury [225, 226].

Glutathione, aging, and cancer: A significant age-related reduction of GSH along with an increase in GSSG has been documented in the brain [227, 228], circulating whole blood, plasma and erythrocytes [229-234], lymphocytes [229, 234], gastric mucosa [233], as well as the lungs, kidneys, liver, and spleen [228, 229]. Furthermore, whole blood GSSG has been shown to increase with age [235]. This shift is owed to an alteration in redox balance toward oxidation and a decrease

in GSH synthesis [236, 237]. Though mechanisms of this change are not well understood, rescue of GSH status through supplementation of precursors has been shown to improve age-related oxidative stress and GSH synthesis [237]. The role of GSH in cancer development and progression is two-fold, with GSH deficiency increasing susceptibility to oxidative stress and mutagenesis through DNA damage and increased inflammation, while elevated GSH levels and synthesis enzymes in neoplastic cells provide chemoresistance and protect against anticancer agents through resistance to oxidative stress, inflammation, and apoptosis [238-242].

Glutathione and neurodegeneration: Dementia is a symptom of neurodegenerative disease and implies a cognitive decline which impairs a person's daily function [243]. Alternatively, mild cognitive impairment is one where the subject is cognitively impaired but not to the extent of demented with diminished daily function [243]. Alzheimer's disease is a neurodegenerative disorder in which neuropathological features appear, namely neuritic plaques and neurofibrillary tangles [243]. An additional common neurodegenerative disorder is Parkinson's disease (PD) where non-motor manifestations arise which can dramatically impair the subject's quality of life through degeneration of motility and muscle control [244]. A decrease in GSH concentrations in the brain has been associated with psychiatric disorders [245] and cognition problems, including Alzheimer's disease, Parkinson's disease, and mild cognitive impairment [217, 246]. Altered GSH metabolism leads to oxidative stress which furthers neuronal degeneration [247]. Furthermore, oxidative stress plays an important role in the pathogenesis of cognitive diseases and that depletion of GSH is directly correlated to functional outcomes [217]. Moreover, hippocampal and cortical GSH correlates with declines in cognitive function and differentiate between mild cognitive impairment and Alzheimer's disease [218]. Even in a healthy adult population, decreased GSH

levels were associated with cognitive function decline without a significant increase in inflammation [219].

Glutathione and HIV: HIV infection leads to CD4+T cell deficiency and loss of immunity through the destruction of CD4+T cells and thus, loss of production of cytokines IFN-γ, IL-2, and IL-12. IFN-γ is responsible for activating macrophages, neutrophils, and dendritic cells to produce ROS and destroy pathogens, as well as activating CD8+T and natural killer cells to induce apoptosis of target pathogenic cells [248]. HIV-infected individuals experience disturbed glutathione homeostasis, rendering them susceptible to oxidative stress and cellular dysfunction [249] through loss of CD4+T cells [248]. Moreover, HIV infection results in increased proinflammatory cytokine release which results in additional ROS production [248]. HIV^+ people have decreased GSH in plasma [250, 251], lungs [252], and peripheral blood mononuclear cells [253], and depleted GSH promotes HIV expression as well as impairs T cell function in HIV^+ patients [254]. Furthermore, *in vitro* studies demonstrate that decreased GSH decreases cell survival [255], alters T cell function [256], and increases HIV replication and activation of NF-κB [257, 258].

Glutathione, DM, and obesity: Hyperglycemia leads to an increase in ROS production through autoxidation of glucose, protein glycation, and polyol metabolism activation [259]. This increase in ROS is associated with oxidative stress which has been suggested to affect the progression of diabetic complications [259]. Deficient GSH synthesis has been documented in those with poorly controlled type 1 DM (T1DM) and T2DM – a result of both limited precursor availability and increased GSH utilization as a result of oxidative stress [237, 260]. Retention of GSH status has been shown to prevent diabetic complications, including microvascular complications [261] and diabetic nephropathy [259]. Similarly, The glutathione redox system is

associated with the development of obesity and its associated comorbidities [262]. Fat accumulation and insulin resistance are associated with increased oxidative stress in those with metabolic syndrome [263]. Furthermore, symptoms of metabolic syndrome and diabetes, such as hyperlipidemia and hyperglycemia lead to increased oxidative stress levels and alter, and in some cases deplete, circulating GSH stores [263]. Adipocyte fat stores affect metabolic homeostasis and are heavily redox-regulated as a result of fatty acid β oxidation [264]. Subcutaneous adipose tissues (SAT) and visceral adipose tissues (VAT) differ in their contribution to disease progression and contribution to metabolic risk, with an increased VAT to SAT stores classifying the subject as metabolically obese or "at risk" compared to a metabolically healthy subject who has higher SAT to VAT stores [264]. Obese women were found to have lower GSH in both VAT and SAT compared to the normal weight individuals, and NADPH was found to increase in the VAT of these obese women [264]. However, there is also evidence that slight decrements in GSH improves resistance to obesity and protect against insulin resistance while increasing energy expenditure due to the stimulation of the Nrf2 pathway as a result of GSH reduction (Figure 2.40) [262].

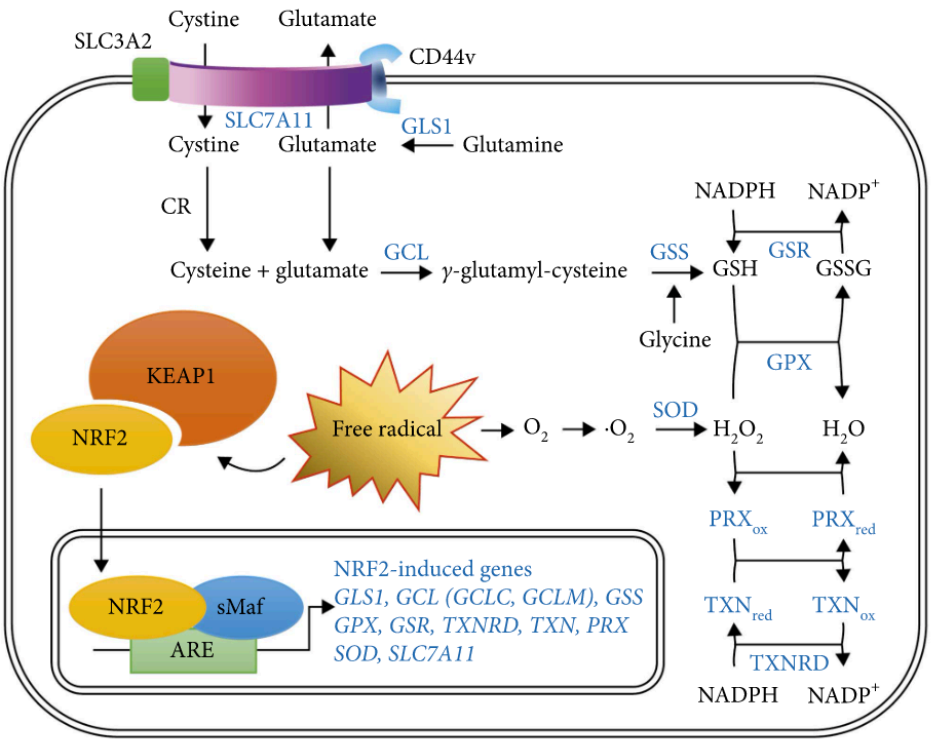

Figure 2.40. Nrf2-mediated pathway of glutathione synthesis. Figure from Woo et al. (2019) [81].

Glutathione and heart disease: Oxidative vascular injury as a result of increased oxidative stress and radical production in the vessel walls leads to the development of CVD [265]. Accumulation of oxidized LDL, cholesterol, fats, and cellular waste products in the damaged area of the arterial wall modulates the progression of atherosclerosis [118, 122]. Because of this, it has been hypothesized that having higher antioxidant levels, such as GSH, prevents CVD development and/or attenuate its effects. The effect of GSH redox status on cardiovascular disease outcomes has been studied using animal models and in the clinical realm. Research using animal models supports the notion that improving antioxidant status, specifically GSH status, improves cardiovascular outcomes [266, 267]. Furthermore, reduced GPx levels have been associated with increased LDL oxidation levels in both mice and humans [268]. In humans, it has been shown that fasting plasma total glutathione is lower in those will CVD compared to healthy controls of both

sexes, allowing the authors to conclude that a low total glutathione status is a risk factor for CVD [265]. Blood samples from patients with CAD revealed significantly less GSH and lower activity of erythrocyte GPx compared to healthy controls [269]. GSH status has also been measured in patients with CVD of different cardiovascular functional classes with different structural heart diseases [266, 267]. Damy et al. found that blood GSH is worse in those with congestive heart failure (CHF) compared to healthy controls, and blood GSH levels are correlated with worsening functional status, even in asymptomatic patients [270]. Moreover, GSH content localized to the atrial also decreases with worsening heart function and CAD advancement [265], showing that blood GSH levels correlates with the severity of CHF. Lastly, by raising GSH levels through supplementation of amino acids and micronutrients that consequently affect GSH status, beneficial effects were found in CVD patients along with improved cardiovascular outcomes [147].

Glutathione and liver disease: The liver contains the highest amount of GSH compared to any other tissue, and this is in part due to its role in releasing GSH into the sinusoidal blood and bile [271]. Sinusoidal GSH determines the systemic availability of GSH whereas biliary GSH serves as a source of precursors for intestinal GSH synthesis [202]. Locally, GSH is important for hepatocyte proliferation and liver regeneration through its role in cell signaling [202]. Liver diseases are associated with low hepatic GSH levels due to nutritional deficiency, oxidative stress, and decreased expression of GSH synthesis genes [202]. Alternatively, extremely high GSH levels confers a proliferative advantage for certain liver cancers, including hepatocellular carcinoma (HCC) [188, 222], as HCC cells demonstrate higher activation of the antioxidant response element (ARE), AP-1, and NF-κB elements which are responsible for increased GS expression and result in higher GSH concentrations [272]. In addition, patients with alcoholic liver disease (ALD) commonly have low hepatic and circulating GSH levels, as well as reduced cysteine availability,

a necessary precursor to GSH synthesis [273, 274]. Glutathione dysregulation is apparent in NAFLD cases with decreased liver GSH in both NAFLD and NASH [223]. As stated prior, oxidative stress may contribute to the clinical progression from NAFLD to NASH, and therefore GSH is a potential therapeutic to halting the progression [126]. Lastly, activated HSCs synthesize pro-fibrogenic factors which in-turn inhibit GCL expression [202]. Decreased GCL expression leads to decreased liver GSH concentrations, which then exacerbates liver fibrosis [126]. Interestingly, mice placed on a high fat diet showed an increase in intracellular GSSG which sensitized hepatocytes to TNF-α and lead to suppressed activation of NF-κB, separate from a reduction in GSH [275], indicating that rescue of GSH is not entirely necessary for decreased hepatic inflammation.

Glutathione and renal disease: The kidneys require a constant and adequate supply of GSH to maintain normal function due to exposure to oxidants and electrophiles, as well as for aerobic metabolism in the proximal tubules [276]. Elevated oxidative stress is associated with progression of CKD [277], and antioxidant status, including GSH and GPx levels, are often depleted in chronic kidney disease (CKD) due to chronic renal injury [225, 226]. CKD is associated with dysregulation of renal mitochondrial and decline in mitochondrial content, resulting in increased inflammation and ROS production [278]. As renal damage progresses, these mitochondrial insults continue resulting in an overproduction of ROS and subsequent damage to renal mitochondrial DNA, membrane permeability, and altered Ca^{2+} homeostasis [278]. This mitochondrial dysfunction then leads to production of uremic toxins [279], proteinuria [280, 281], transformation of tubular epithelial cells to mesenchymal cells [282, 283], and altered oxidative phosphorylation in tubular epithelial cells [279]. Additionally, activity of NADPH and xanthine oxidases are upregulated in CKD, further contributing to ROS production [278]. Oxidative stress in CKD is linked with risk

of complications, and the leading cause of mortality in CKD patients is CVD due to increased oxidative stress [226]. Restoration of GSH levels in the kidneys is considered a therapeutic against CKD and for prevention of CKD-related complications [284, 285]. GSH replenishment is associated with mitigating the consequences of uremia, the accumulation of renal waste products, and reducing the impact of ROS production [285].

Influence of diet and physical activity on glutathione metabolism

Impact of supplementary amino acids, micronutrients, and overall diet on glutathione homeostasis[1]*:* Due to the strong cytoprotective effects of GSH, it could be a therapeutic option to maintain cellular integrity and slow tissue degeneration in various diseases. Researchers have tested the impact of administering GSH through several routes, including intravenously [286], intranasally [287], orally [194, 288, 289], sublingually [182], via inhalation [290], and transdermally [291]. Given the invasiveness and financial burden of many of these routes, oral administration is considered most convenient [182]. Yet, the efficacy of oral GSH against oxidative stress is still controversial due to several unresolved issues [292]. Notably, oral GSH supplementation had no effect on oxidative stress biomarkers or GSH concentrations in red blood cells (RBC) isolated from healthy human subjects [194, 293], a finding that may be attributable to GSH digestion. The primary site of dietary GSH digestion is the upper jejunum [294], where the enzyme GGT breaks down GSH to its constituent amino acids [194]. GGT is also expressed in the liver [295], and these combined actions limit the amount of dietary GSH that enters the circulation. Furthermore, most cells simply cannot absorb intact GSH, instead requiring it to be first broken down by GGT into its constituent amino acids [195]. Because of these issues, researchers have instead turned to supplementation of individual GSH precursors to improve GSH status. Several

[1] Adapted from Gould RL, Pazdro R. Impact of Supplementary Amino Acids, Micronutrients, and Overall Diet on Glutathione Homeostasis. *Nutrients*. 2019;11(5):1056. Reprinted here with permission of publisher.

amino acids intersect with the GSH pathway, and altering the concentrations of those amino acids, either directly or indirectly, can modify cellular GSH homeostasis.

Effect of Individual Amino Acid Supplementation

L-Glutamine: L-Glutamine is the most abundant free amino acid in the body [296]. Through normal metabolic pathways, glutamine is converted to glutamate, which is used in the intracellular synthesis of GSH. It has been postulated that through direct oral supplementation of glutamine, GSH levels would consequently increase. It must be noted that long-term glutamine supplementation should not exceed >40 g/day due to its negative effects on biochemical pathways [297]. Glutamine not only competes for absorption against other amino acids such as cystine, but also impairs endogenous glutamate synthesis [297]. Furthermore, glutamine supplementation can increase ammonia production while also impairing ammonia transport and detoxification [297]. Overall, glutamine supplementation appears to be beneficial in HIV^+ individuals [298], but not in ICU patients or those with sickle-cell disease [299-301]. It is crucial that future research efforts expand beyond RBC, as RBC lack mitochondria, producing a unique biochemical milieu that may not fully represent other cell types [296].

L-Glycine: Glycine is one of three amino acids used to form GSH [302], so it has been postulated that its oral supplementation may stimulate GSH biosynthesis [303]. Glycine seems to improve GSH concentrations in animals with higher levels of oxidative stress [303-305]. When supplemented in the diet, glycine may exert a beneficial effect via promotion of GSH biosynthesis and attenuation of oxidation, which in turn protects against endothelial and vascular dysfunction [304]. There is evidence that glycine supplementation could be even more effective when orally supplemented with cysteine in older HIV-infected individuals [306]. The role of glycine

supplementation in improving GSH status warrants further research given its broad, beneficial influence on the GSH pathway.

Cysteine pro-drugs: *L*-cysteine is the rate limiting amino acid in *de novo* synthesis of GSH [164], so naturally, cysteine supplementation should be investigated as a possible approach to improve GSH status and counter disease-associated oxidative stress. Yet according to studies on this topic, direct administration of cysteine is limited by spontaneous oxidation to its corresponding disulfide cystine [307], significant toxicity [308-313], and mutagenicity risks [314, 315]. Because of these issues, focus has shifted from cysteine to its precursors, which may provide an alternate avenue to raising GSH concentrations by increasing the available cysteine pool. The efficacy of cysteine precursors *N*-acetylcysteine (NAC), *S*-Adenosyl-*L*-methionine (AdoMet), and *L*-2-oxothiazolidine-4-carboxylate (OTC) supplementation on GSH levels are evaluated in the next sections. Methionine is also a cysteine prodrug that increases RBC GSH levels when supplemented orally [316], but supplementing with methionine is not recommended due to the increased risk of raising homocysteine levels [317, 318], so it will not be discussed in this review.

NAC is a cysteine precursor that, when administered orally, increases GSH concentrations in individuals with GSH deficiency caused by infections, genetic defects, or metabolic disorders [319]. Orally administered NAC is readily absorbed in the stomach and gut [320] and then converted to cysteine in the liver [321], where it is used locally for GSH synthesis or transported throughout the body to individual tissues [322]. Pharmokinetics studies have revealed that NAC is almost entirely metabolized by the liver and kidneys [321], and as a result, NAC is nearly undetectable in plasma [323]. Therefore, measuring NAC in plasma is not representative of NAC status [323]. Overall, orally administered NAC is an effective way to replenish GSH in HIV-infected patients [298, 324-326], but more research is needed to better understand the effect of

NAC supplementation on GSH levels in healthy individuals. Despite its potential benefits, NAC is limited by potentially harmful side effects, such as nausea or gastric distress, but investigators hypothesize that the intestinal side effects found in the trial may have been due to the ingestion of the excipient, which contained lactose [319].

AdoMet is a precursor to the transsulfuration pathway, the metabolic pathway responsible for condensing homocysteine to form cystathionine, which is then converted to cysteine [327]. Patients with ALD or NAFLD were found to exhibit low hepatic GSH levels, which were replenished after oral AdoMet treatment (1.2 g/day for 6 months) [328]. Rodent studies have supported this finding, concluding that AdoMet supplementation is effective at attenuating liver injury by increasing GSH levels [329-333]. In baboons, supplementation of oral AdoMet resulted in significant hepatic uptake of the molecule, and eventually, restored GSH levels [334]. AdoMet supplementation does not appear to have a significant effect on homocysteine concentrations in healthy individuals [335], so supplementation of this amino acid may be a viable source of increasing GSH levels without deleterious consequences of increased homocysteine.

OTC is converted to cysteine through 5-oxoprolinase in cells [214] and has been used to elevate GSH concentrations in animal models [336-341] and humans [342, 343]. Much like the other cysteine prodrugs, OTC supplementation has been evaluated for its effect on GSH homeostasis in populations with low GSH statuses. In a study conducted on rats with liver injury due to alcohol or a high-fat diet (HFD), oral supplementation of OTC for 1 month resulted in increased circulating GSH levels [336]. Furthermore, OTC protected against liver injury [336]. In another study, PEM rats receiving daily OTC significantly increased GSH in the lungs, but OTC was not as effective as protein repletion in restoring blood GSH levels [344]. In healthy humans, oral OTC supplementation was found to increase the lymphatic GSH concentration 2 to 3 hours

after ingestion, but plasma GSH remained unaffected [342]. Studies suggest that OTC may be a safe and viable option for elevating GSH concentrations, but some limitations remain unaddressed. A study by Nishina, Ohta, and Obuka (1987) found that intraperitoneal delivery of OTC increased hepatic GSH concentrations in guinea pigs, but decreased renal GSH levels [345]. It was suggested that hepatic OTC was used to form cysteine for GSH synthesis, whereas in the kidney, OTC promoted GSH turnover instead [345].

L-Serine: The transsulfuration pathway is a major source of sulfur for GSH formation [346]. In the pathway, cystathionine β-synthase, along with vitamin B_6, condenses homocysteine and serine to ultimately form cysteine [346]. Presently, research on oral serine supplementation on GSH homeostasis is limited and mostly confined to rodent models with high levels of oxidative stress. In experimental models of oxidative stress, serine appears to conserve tissue GSH levels and attenuate oxidative damage [347-351].

Taurine: Cysteine is a necessary metabolic precursor for taurine synthesis, so it has been postulated that taurine supplementation would spare cysteine for eventual incorporation into GSH [352]. In research studies on this topic, animals were supplemented with taurine intraperitoneally [352], via drinking water [353-358], or intragastric intubation [359]. When investigators supplemented diabetic rats with taurine, lens GSSG and GSSG/GSH ratio levels decreased while GSH levels were not affected [360]. In rabbits on a high-cholesterol diet, taurine failed to affect hepatic GSH levels [361]. However, taurine supplementation normalized GSH and GSSG levels in iron-overloaded mice [358] and increased renal and hepatic GSH levels in rats with hypothyroidism [357]. Effects of taurine on the enzymes GPx and GR have been evaluated in both rodent and human studies. Taurine supplementation recovered hepatic GR activity in diabetic rats [362], whereas hepatic GPx levels remained unaltered by taurine supplementation in type I and

type II diabetic mice [363]. However, when young adults were orally supplemented with taurine (50 mg/kg for 2 weeks) after performing eccentric exercise, RBC GPx levels were elevated [364]. Overall, these results point to a limited impact of taurine on GSH, implying that other amino acid or micronutrient supplements may be a more effective option at targeting and raising GSH concentrations.

Effects of Micronutrient Supplementation

α-tocopherol (vitamin E): Fat-soluble vitamins (A, D, E, and K) have been evaluated for their potential effects on GSH homeostasis. These vitamins exhibit antioxidant properties, and there is evidence that status of vitamin A [365, 366], vitamin D [367-369] and vitamin K [370] may affect GSH levels; supplementation has also been associated with adverse effects [366]. Vitamin E is a lipid-soluble antioxidant that protects the cell membrane against oxidation and supports other antioxidant reactions, including those involving GSH [371]. Studies suggest that vitamin E supplementation may prevent GSH oxidation and ultimately increase its levels in tissues. Based on animal [371-375] and clinical studies [304, 376-378], it appears that vitamin E, when taken in safe doses, has the potential to increase RBC and brain GSH concentrations. However, when vitamin E-deficient thalassemic children were supplemented with vitamin E for (200 mg/day) for 4-8 weeks, RBC GPx activity decreased [379] and supplementation of 400 mg/day for 2 months failed to raise plasma GSH levels in elderly cardiovascular patients [380].

Pyridoxine (vitamin B6): Pyridoxal 5'-phosphate (PLP), the biologically active form of vitamin B_6, is a coenzyme in the conversion of homocysteine to cysteine, which supports GSH biosynthesis [381]. PLP is also a powerful antioxidant that has an indirect role in GSH homeostasis via sequestering free radical species to spare cellular GSH concentrations [382, 383]. Homocysteinemia and chromium toxicity are high stress environments wherein vitamin B_6 is

especially critical for maintaining GSH pools [383-385]. Oral vitamin B_6 supplementation increased renal and hepatic GSH levels in rats with chromium-induced toxicity [384, 385] and increased hepatic GSH levels in homocysteinemic rats, despite the fact that homocysteine levels remained high [383]. Conversely, vitamin B_6 supplementation had no effect on hepatic GSH levels in control rats, with or without supplementation [383], nor did it alter GPx levels in homocysteinemic rats [381]. Unexpectedly, vitamin B_6 supplementation increased blood GPx levels of control rats, indicating that the vitamin may directly stimulate the GSH redox system under normal conditions [386]. Vitamin B_6 also affects GSH status of human patients. HCC patients exhibit high levels of oxidative stress, and when 33 HCC patients – who had recently undergone a tumor resection – were supplemented with vitamin B_6 (50 mg/day) for 3 months, plasma GSH/GSSG ratios and GR activity unexpectedly decreased while GSSG and GPx levels did not change [387]. The authors hypothesized that the decline in GSH came from redistribution of GSH molecules from plasma to RBC [387]. The impact of vitamin B_6 supplementation with other vitamins has been also evaluated [388, 389]. Combined vitamin B_6 (200 mg/day) and folic acid (15 mg/day) supplementation for 1 month increased RBC and whole blood GSH levels in both hemodialysis patients and healthy patients [389]. Similarly, Parkinson's disease patients supplemented with folic acid and vitamins B_{12} and B_6 had improved GSH status [388]. At this time, recommendations on B_6 supplementation cannot be made due to the limited clinical research and conflicting results on the effect of vitamin B_6 supplementation on GSH concentrations. Future research on vitamin B_6 supplementation is warranted given the possibility of beneficial effects on GSH status.

Ascorbate (vitamin C): Ascorbate, a potent free radical scavenger, and GSH are biochemically intertwined [390, 391]. GSH actively recycles oxidized dehydroascorbate back to

ascorbate [392], and GSH deficiency is accompanied by low tissue levels of ascorbate [391]. It has also been predicted that increasing ascorbate levels ultimately spares GSH pools [211]. Rodent studies have shown that ascorbate supplementation improves GSH and its associated ratio concentrations [176, 383, 393]. But in weanling rats supplemented with ascorbate in high doses for 4 months, RBC GSH concentrations actually decreased [394]. Moreover, there was a significant increase in GPx activity in RBC and plasma [394]. Similarly, heart GPx and GSSG levels increased after 5 weeks of high ascorbate supplementation in guinea pigs [395]. Investigators attributed these negative results to peroxidative stress induced by the high ascorbate doses [394]. Healthy adults have been supplemented with ascorbate to better understand the vitamin's effects on GSH homeostasis and have found that 500 mg/day for 2-3 weeks significantly improves RBC GSH [396]. Furthermore, ascorbate supplementation (500 or 1000 mg/day) was found to increase lymphocyte GSH levels in healthy adults [397]. Ascorbate has also been combined with vitamin E since the two vitamins have an additive effect against oxidative stress [176]. When ascorbate was supplemented (500 mg/day) with vitamin E (400 IU/day) for 2 months in cardiovascular disease patients, GPx levels were significantly higher than those without supplementation [398]. Moreover, supplementation of the two vitamins increased GPx activity in women consuming oral contraceptives, a population that has been found to have decreased antioxidant status [399]. Based on this evidence, ascorbate, if used in safe and tolerable doses, appears to attenuate GSH depletion under stress conditions and promote an increased antioxidant status.

Selenium (Se): In the enzymatic reduction of hydrogen peroxide to water, GSH is utilized by GPx, a selenoprotein that requires Se for proper functioning [400, 401]. Researchers have predicted that increasing Se would increase cellular GPx expression and lower oxidative damage

in tissues. Indeed, oral Se supplementation has been shown to improve GSH status in rodents [373, 402-404]. Clinical interventions have been conducted to determine whether Se exerts a comparable effect in humans. Supplementing women with Se (200 mcg/day) for 4 weeks increased platelet, whole blood, plasma, and liver GPx expression levels [405]. In another study, 45 patients with chronic kidney disease (CKD) were supplemented with 200 mcg of Se for 3 months, and their RBC GPx activities increased [406]. The same dosage was used in 53 chronic renal failure patients, and Se increased plasma GPx among those in the early stages of the disease, but not in end stage renal disease patients [407]. Zachara et al. evaluated the effect of Se supplementation in patients undergoing hemodialysis (HD). When dialyzed uremic patients were supplemented with 300 mcg Se after each hemodialysis session (3 times/week) for 3 months, GSH levels did not change, but GPx activity increased after only 1 month of supplementation [408]. Overall, the relationship between Se status and GPx activity has been inconsistent, with some studies concluding that Se supplementation has no effect on GPx activity in healthy individuals [409-411] or in those with mucopolysaccharidosis [412], while others found beneficial effects [413-415]. Such conflicting outcomes could be a result of oral Se supplementation acting in a tissue-specific manner on GSH homeostasis [416]. Although Se could be a viable option to increase GPx activity in individuals with high oxidative stress, Se supplementation may be most effective in combination with another therapeutic known to directly increase GSH. After all, without GSH, an increase in GPx may not induce significant health effects.

Magnesium (Mg): Mg is an important mineral whose status has been linked to oxidative damage [417]. When diabetic rats were orally supplemented with Mg, blood concentrations of total glutathione and GSH increased [418]. However, since whole blood was analyzed, it is possible that the effect was driven by increased GSH secretion from cells [418]. In addition,

women of unexplained infertility or early miscarriage were found to have abnormal RBC-Mg levels, and when these women were supplemented orally with Mg (600 mg/day) for 4 months, those who still had abnormal RBC-Mg levels also had significantly lower RBC GPx levels [419]. After 2 additional months of Mg supplementation, RBC-Mg levels and GPx concentrations were normalized in all women [419]. Furthermore, when atopic asthmatic children (4 to 16-year-olds) were orally supplemented with Mg for 3 months, blood GSH levels increased while blood GSSG remained unaffected [420]. But when pregnant women (24-28 weeks) with gestational diabetes were supplemented with 250 mg Mg/day for 6 weeks, plasma GSH concentrations did not significantly change [421]. Based on these clinical trials, it is possible that Mg supplementation may provide antioxidant protection. Importantly, more research is needed to identify the optimal dose of Mg supplementation to boost GSH metabolism.

Overall Diet Effects

The Mediterranean Diet (MedDiet): The Mediterranean diet (MedDiet) emphasizes high intakes of extra virgin olive oil, vegetables, fruits, cereals, nuts, pulses and legumes, and moderate intakes of fish, dairy, and red wine, while limiting intakes of eggs and sweet foods [422]. There is typically no specific serving size recommended, but instead, emphasis is placed on frequency of food consumption [422]. The diet's effect on oxidative stress levels has been a subject of investigation, given its high content of Se, essential fatty acids, fiber, and antioxidants [423]. Using data from the Twins Heart Study, researchers explored a potential association between the MedDiet and GSH levels [424]. Adherence to the MedDiet, based on Mediterranean Diet Scores (MDS), showed an inverse association with plasma GSSG, resulting in higher GSH/GSSG ratios, independent of familial and genetic factors [424]. In addition, the MedDiet was found to enhance GPx activity in patients with atrial fibrillation [425] and increase mammary gland GSH levels in

monkeys that were on the diet for 31 months [426]. In a cross-sectional study of healthy working men and women, MDS were positively associated with plasma GSH levels while similar diets, such as the Alternative Healthy Eating Index and the DASH diet, were not [427]. These conclusions were independent of BMI, an important factor given the strong correlation between fat accumulation and increased systemic oxidative stress [428].

The DASH Diet: The DASH diet was developed in the 1990s and rose in popularity once the National Institutes of Health began supporting research efforts to identify dietary interventions that were efficacious against hypertension [429]. The DASH diet was found to decrease systolic blood pressure by 6-11 mm Hg in both hypertensive and normotensive individuals and is therefore considered a first-line therapy for hypertension today [429]. The DASH diet includes the following servings of foods per day: 5 fruits and vegetables, 7 carbohydrates, 2 low fat dairy products, no more than 2 lean meats, as well as 2-3 servings nuts and seeds per week [429]. The DASH diet emphasizes the consumption of "healthy" carbohydrates (e.g., green leafy vegetables, whole grains, legumes) and "good" fats (e.g., foods low in saturated fats, nuts, avocados, fish) [429]. The DASH diet also promotes low sodium intake (<1,500 mg/day) and reduction of processed food consumption [430]. Because of these recommendations, the DASH diet has been named an excellent dietary intervention for those with other chronic diseases such as DM, heart disease, and obesity [430]. Chronic disease patients often have impaired GSH statuses and heightened GSSG levels [431]. It has been postulated that the DASH diet may assist in controlling metabolic profiles of those suffering from a chronic disease, in part through its positive impact on GSH status. When the DASH diet was implemented in overweight men and women with NAFLD for 8 weeks without other lifestyle modifications [432], plasma GSH concentrations significantly increased [432]. In addition, plasma total glutathione levels increased in overweight and obese women with polycystic

ovarian syndrome who adhered to the DASH diet for 8 weeks [433]. Furthermore, pregnant women diagnosed with gestational diabetes at 24 to 28 weeks gestation were assigned to either a standard American diet or the DASH diet with 2400 mg sodium per day for 4 weeks [430], and those in the latter group had significantly higher plasma total glutathione levels [430]. In conclusion, the DASH diet appears to be a feasible dietary strategy for increasing total glutathione levels.

Other diets: Naturally, vegetarian diets exclude meat, a significant source of amino acids needed for GSH biosynthesis [434]. Yet vegetarian and vegan diets include substantial amounts of fruits and vegetables, which are naturally high in antioxidants [435, 436], and these diets are associated with lower rates of obesity, cancer, and diabetes [437]. A vegetarian diet appears to positively influence GSH levels in some populations, such as patients with type 2 diabetes [438] and cardiovascular disease [265]. However, other studies found no significant differences in GSH status between vegetarians and fish or meat eaters [435, 439, 440]. And yet another study found that a vegan diet with low protein intake results in significantly lower blood GSH levels compared to omnivores and lacto-ovo-vegetarians [434]. A Western-type diet is characterized by high amounts of meats, saturated fat, refined grains, and sugar, with low amounts of fruits and vegetables [441]. The Western diet has been associated with increased risks of cancer and other chronic diseases [426] and is commonly used to experimentally induce oxidative stress and antioxidant depletion [426, 442-444], including impaired GSH synthesis [443]. Furthermore, Western-type diets are correlated with low vitamin B_6 [445], methionine [444], and cysteine [444] status, as well as high homocysteine levels [446], suggesting that the diet may affect GSH homeostasis through its effects on precursor availability. Overall, the diet is associated with excessive body fat, insulin resistance, and poor health [447], so an alternative diet emphasizing plants and less processed foods is recommended.

Other Supplementation Sources

Whey protein: Whey protein is a rich source of cysteine, so research is being conducted on its relationship with GSH status. Evidence suggests that the consumption of whey protein can raise intracellular GSH levels in healthy individuals [448]. In addition, whey protein intake was found to increase lymphocyte GSH levels in CF patients [449]. More research is needed to evaluate the true effect of whole whey protein supplementation on GSH homeostasis.

Sublingual and liposomal GSH supplements: Oral GSH supplementation is not the most effective means of increasing GSH status, so researchers anticipate that alternate forms of oral GSH may be more promising. Notably, food-grade sublingual and liposomal GSH supplements have been designed. Sublingual forms of GSH have received significant attention because sublingual compounds are able to by-pass hepatic first-pass metabolism and degradation, maintaining supplement bioavailability [182]. A 3-week randomized crossover study was conducted on metabolic syndrome patients, where they were supplemented with oral GSH (450 mg/day), oral NAC (200 mg/day), or a sublingual form of GSH (450 mg/day) [182]. Compared to the oral GSH group, sublingual GSH resulted in a significant increase in both total plasma glutathione and plasma GSH [182]. Plasma vitamin E levels also increased in the sublingual GSH group, a result not found in either the oral GSH or NAC supplemented groups [182]. To supplement with lipoceutical GSH, GSH is first packaged into liposomes, small droplets that fuse with cellular membranes, directly releasing their contents into target cells. Recent studies have underscored the beneficial effects of liposomal GSH on intracellular GSH concentrations [450, 451]. For instance, liposomal GSH was given to children (3-13 years old) with autism spectrum disorder, and the treatment significantly increased plasma GSH, cysteine, and taurine levels [291]. To date, a limited number of animal and clinical interventions have evaluated the efficacy of

liposomal GSH [291, 451, 452]. Future research is warranted and needs to weigh potential benefits of these pharmaceuticals against their high costs.

Conclusion

GSH is an exciting and promising therapeutic target against oxidative stress. Given the low bioavailability of oral GSH, researchers have supplemented with compounds that directly or indirectly affect the GSH system. The list of supplements discussed in this review is not exhaustive, and other amino acids and micronutrients, or their combinations, may have significant effects on GSH homeostasis in specific populations. It is important to ensure that interventions are tested in various age groups, in particular because pediatric populations have been consistently understudied. And it is important to consider the health status of each population under investigation, as dysfunction of the liver and other essential organs can impede the body's ability to synthesize GSH and thus, nutraceutical supplementation may not be as effective as it would be in healthy individuals. Investigators must also consider the analytical method used to quantify GSH and GSSG in each study. GSH and GSSG are often quantified via colorimetric assays [453], high performance liquid chromatography (HPLC) [454], and mass spectrometry [455]. A particular benefit of mass spectrometry and HPLC with electrochemical detection is the direct measurement of GSH without derivatization [454]. Finally, in each study, the source of GSH should be carefully selected. For instance, GSH levels would ideally be measured in serum and RBC, in tandem, to address the fact that GSH may be redistributed from the serum to RBC during times of stress or tissue injury. Overall, supplementation of amino acids and micronutrients, as well as implementation of diet strategies offer safe and non-invasive strategies to improve GSH status and protect the body from oxidative stress in various diseases and conditions.

Regulation of glutathione by physical activity: The use of exercise and physical activity to modulate mammalian glutathione metabolism has been evaluated. Physical activity events can cause oxidation of GSH in blood, skeletal muscle, and the liver [456, 457]. However, lifelong and regular physical activity upregulates antioxidant systems [458] and ultimately increases GSH availability in skeletal muscle tissue [456]. Muscular exercise naturally promotes free radical production [459] and levels of GSSG in the blood increase after exhaustive physical exercise in both rodents and humans, values return back to normal after one hour of rest, and GSH values do not significantly change [460]. Alternatively, chronic inactivity results in a decrease of GSH levels [456]. These findings are attributed to the beneficial adaptive changes that arise in various tissues, particularly the heart and skeletal muscle, in response to regular physical activity [456]. Endurance training can strengthen antioxidant defenses [456], and aerobic exercise training and circuit weight training, as well as the combination of the two, in healthy sedentary individuals significantly improved GSH/GSSG due to significant decreases in GSSG levels [461]. Strength training has also been shown to have a positive effect on GSH homeostasis [456]. Overall, exercise-induced increases in free radical production, particularly in the skeletal muscle, appear to have a positive adaptation effect on antioxidant mechanisms which prevents increases in oxidative stress that could be detrimental to human health [459].

Genetics of glutathione and disease risk

Genes involved in glutathione homeostasis and the effects of disruption in their expression: Given the relevance of glutathione to human health, researchers have investigated the deletion and polymorphisms of critical enzymes involved in GSH synthesis and recycling, namely *GS, GPx GCLM, GCLC, and GR*, to understand the physiological effects of these genes.

Knockout (KO) animal studies allow researchers to study the phenotypic effect of an absent gene, elucidating gene function *in vivo* [462]. This approach has been applied to understand the function of genes involved in glutathione metabolism. $GS^{-/-}$ KO mice are deficient in GSH and the disruption is embryonic lethal by day 7.5, whereas $GS^{+/-}$ heterozygous mice survive and exhibit no phenotypic changes nor changes in GSH status [463]. $Gpx1^{-/-}$ KO mice exhibit no phenotypic changes, but when mice are deficient in both Gpx1 and Gpx2 (gastrointestinal-specific Gpx), they present with inflammatory bowel disease [464]. $Gpx5^{-/-}$ KO males exhibited no differences in fertility or development, whereas $Gpx5^{-/-}$ females experienced a higher incidence of miscarriages and developmental defects [465]. $Gclm^{-/-}$ KO mice are rendered viable and fertile yet exhibit chronic GSH depletion [466] and are more susceptible to oxidative stress [467]. Alternatively, $Gclc^{-/-}$ KO mice die before gestational day 13, and its heterozygous $Gclc^{+/-}$ counterpart is viable and fertile with a chronic GSH deficiency [468]. Disruption of *Gclc* synthesis in both young and aged mice exhibit mitochondrial damage and neurodegeneration in the hippocampus and cerebral cortex as a result of heightened oxidative stress [469]. Lastly, $GR^{-/-}$ KO mice [470] and $GR1^{a1Neu}$ mice (mice treated with a mutagen to exhibit GR depletion) [471] did not exhibit significant changes to GSH status, an effect attributed to the compensatory mechanism of Trx and TR in reducing GSSG to GSH in the absence of adequate GR [470, 471].

The candidate gene approach is a type of genetic association study where researchers test the effects of genetic variants of a potentially contributing gene on phenotypes of interest [472]. These studies are influential in identifying genes that may have small, but biologically relevant, effects [472]. A caveat to candidate gene studies is that they rely on the knowledge of potential candidate genes, typically identified through animal studies, as well as known biology of the disease being investigated [472]. The candidate gene approach has been applied to human genetic

association studies where investigators have assessed the effect of polymorphisms in glutathione metabolism genes on disease risk and/or progression. Several SNPs of *GPx1* have been identified in humans and are associated with increased risk of breast cancer [473] and its prognosis [474], CKD [475], prostate cancer [476], coronary artery disease [477], and acute myeloid leukemia [477]. A *GPx1* variant is associated with kidney complications in T1DM patients [478] and a variant in *GPx3* is associated with an increased risk for arterial ischemic stroke in young adults and children [479]. Interestingly, polymorphisms in *GPx (GPx4, 5,* and *6)* have been associated with prepubertal childhood obesity in Spanish children, despite retaining normal circulating GPx activity [480]. However, these associations are not consistent across all studies [481-486]. SNPs of *GCLC* have been associated with hemolytic anemia and neurological disorders as a result of low intracellular GSH [487]. Additionally, polymorphisms of the *GCLC* gene have been correlated with cystic fibrosis lung disease severity [488], chronic obstructive pulmonary disease (COPD) [489], and idiosyncratic drug reactions in HIV/AIDS patients [490]. In a Japanese population, those with polymorphisms in *GCLC* or *GCLM*, or both, were at risk for developing anti-tuberculosis drug-induced hepatic toxicity when treated for pulmonary tuberculosis [491]. However, conflicting evidence has been observed for *GCLM* SNPs on schizophrenia, as a *GCLM* polymorphism associated with schizophrenia in Europeans [193] was not found to be associated with schizophrenia in a Japanese population [492]. Similarly, a candidate gene study investigating the effect of variants in *GS, GCLC,* and *GCLM* observed no significant association between genotype and schizophrenia [493]. Studies have been conducted investigating the relationship between variants in glutathione metabolism genes and autism, but associations are not clear and oxidative stress risk on autism may involve a multi-SNP interaction between polymorphisms in glutathione genes and other antioxidant genes [494]. Associations with *GS* and susceptibility to

lung function growth deficits following exposure to air pollutants in children have been observed [495]. Though not directly related to the basic glutathione synthesis and recycling, polymorphisms in *GST* genes have been investigated to assess their role in disease risk. *GST* SNPs have been associated with CKD [496], Alzheimer's and Parkinson's disease [497], prostate [498] and colorectal cancer [499], autism spectrum disorder [500], schizophrenia [501], HCC [502], and COPD [503].

Complete deficiency of glutathione metabolism genes are rare and are classified as inherited metabolic disorders [471]. GPx1 deficiency is associated with hemolytic anemia [504-508]. GPx3 deficiency has been documented in patients with a history of arterial thrombosis [509, 510]. However, these case studies reported partial or complete deficiency of circulating GPx, and to date, there is no documented defect in the *GPx1* gene that unequivocally results in hemolytic syndromes or other physical manifestations, and the associations may be coincidental or related to maternal selenium intake during pregnancy [504, 507]. *In vivo*, GCLC and GCLM deficiency are collectively documented as GCL deficiency since both subunits are required for proper *GCL* function [511]. Limited (<10) cases of GCL deficiency have been documented [512-516]. Patients with GCL deficiency have reduced erythrocyte glutathione, hemolytic anemia, and neurological dysfunction, but the disorder is not lethal [511]. GS deficiency is a class of rare genetic disorders that are more common than GCL deficiencies, though there are only less than 100 cases documented worldwide [471]. Patients with GS deficiency exhibit 5-oxoprolineuria, hemolytic anemia, as well as neurological disorders, and typically die in childhood [471]. GR deficiency is also extremely rare with less than 10 reported cases and clinical findings include hemolytic anemia, thalassemia, and pancytopenia [517-519].

Glutathione concentrations are dependent on genetic background:[2] Much of our current knowledge of the glutathione system has been generated using classic biochemical techniques, but recent studies have revealed that valuable insight could be attained through genetic analyses. Early evidence for the effects of genetic variation on the glutathione system emerged from comparisons of common classical inbred mouse strains [520, 521]. Rebrin et al. found that the GSH/GSSG ratios of C57BL/6 (B6) mice were significantly higher than those of DBA/2 (D2) mice in several distinct brain regions: cerebral cortex/hippocampus, striatum, cerebellum, and brainstem [522]. Additional studies found that B6 mice display higher erythrocyte GSH/GSSG ratios than D2 mice [523], and higher GSH/GSSG ratios and GSH levels in heart [524] and skeletal muscle [524] as well. Following those discoveries, more comprehensive strain panels were assembled and utilized. Tsuchiya et al. used a panel of 14 diverse inbred mouse strains and discovered significant variation in hepatic GSH levels and GSH/GSSG ratios between strains [525]. Zhou et al. used an expanded strain panel consisting of 30 genetically-diverse inbred mouse strains and quantified GSH levels, GSSG levels, and GSH/GSSG ratios in their livers and kidneys [526]. Those phenotypes exhibited nearly threefold ranges and mostly moderate to high heritabilities [526]. Specifically, estimated heritabilities of hepatic GSH phenotypes ranged from R2=0.37 (GSSG levels) to 0.68 (GSH/GSSG), while the heritabilities of renal phenotypes ranged from R2=0.25 (GSH levels) to 0.66 (GSH/GSSG) (unpublished data). Importantly, the estimated heritabilities overlapped with those obtained from humans [527], suggesting that knowledge gained from mouse studies may indeed be relevant to the human condition [526].

[2] Adapted from Gould RL, Zhou Y, Yakaitis CL, Love K, Reeves J, Kong W, Coe E, Xiao Y, and Pazdro R. Heritability of the aged glutathione phenotype is dependent on tissue of origin. *Mamm Genome*. 2018;29(9-10):619-31. Reprinted here with permission of publisher.

Heritability of glutathione phenotypes remains significant at old age: Despite this compelling evidence, studies investigating the role in GSH metabolism have been confined to young-adult to adult subjects [525-529]. To evaluate the role of genetics on glutathione metabolism at old age, Gould et al. performed a strain survey using 19 mouse strains and investigated GSH, GSSG, total glutathione, and GSH/GSSG heritability [203]. Their results agreed with Zhou et al. and concluded that GSH levels were not only dependent on strain and significant at old age, but that heritabilities were tissue-specific (Figure 2.41) [203]. Moreover, those results agree with those published in humans where GSH levels in the brain remained stable, or even increased, across age [530].

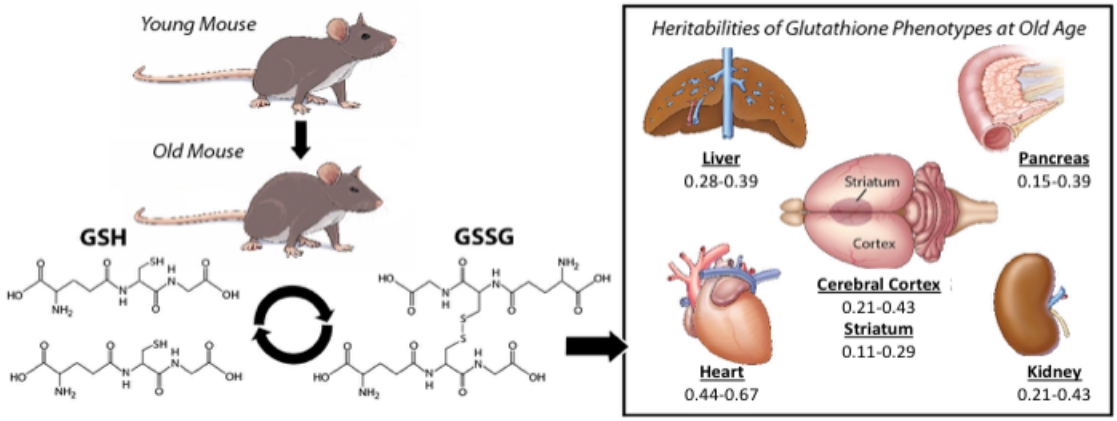

Figure 2.41. Heritabilities of glutathione phenotypes at old age. Figure from Gould et al. (2018) [203].

Purpose and Significance

Despite emerging evidence indicating that genetic background dictates a proportion of glutathione variation, no genetic mapping study has been conducted to map the loci and genes influencing glutathione concentrations in individual tissues. As a result, human candidate gene studies are isolated to canonical genes with established functions in glutathione formation and

recycling (i.e., GCL, GS, GR, and GPx). Initial genetic analyses from animal and clinical models concluded that genetic background impacts glutathione concentrations and suggest that novel genes and loci are responsible for glutathione variation on a tissue-specific level. Given the relevance of glutathione to human health and disease, it is critical that we understand the role of genotype on glutathione so that we can better inform candidate gene studies and improve treatments aimed at rescuing GSH status.

Purpose of dissertation research: Research into the genetic control of glutathione has largely been directed at investigating the effect of polymorphisms in canonical genes related to glutathione metabolism to identify their effect on disease. Recent research has shown that glutathione phenotypes are heritable and driven by genetics, and that novel genes outside of genes responsible for GSH synthesis and recycling may be responsible for tissue-specific variation. Despite glutathione's critical physiological role as a cytoprotectant, we still do not fully understand 1) the influence of genetics on natural variation in glutathione in a genetically diverse population's individual tissues, and 2) the impact of that variation on health outcomes. The purpose of this dissertation research is to improve our understanding of the complex redox system by defining genomic regions and candidate genes associated with the hepatic and renal glutathione redox system using a forward-genetics approach. To date, no other laboratory has investigated the impact of genetic background on tissue-specific glutathione phenotypes using genetic association mapping in an outbred animal model. Our genetic hypothesis predicts that concentrations of the glutathione redox system are, in part, predetermined by genetic background, and that novel genes outside of the known canonical glutathione genes are responsible for this variation. Moreover, we predict that tissue-specific glutathione variation will correlate with outcomes of liver and kidney function. Candidate gene studies involve the testing of pre-specified genes of interest, therefore

genes identified through these studies will better inform future human genetic studies and refine candidate gene approaches focused on redox biochemistry at an individual tissue level. By better understanding the genetic regulation of this critical antioxidant system, as well as its biological and physiological relevance, we can better understand the use and impact of clinical treatments attempting to modulate glutathione homeostasis, and ultimately improve patient outcomes.

CHAPTER 3

QUANTITATIVE TRAIT MAPPING IN DIVERSITY OUTBRED MICE IDENTIFIES NOVEL GENOMIC REGIONS ASSOCIATED WITH THE HEPATIC GLUTATHIONE REDOX SYSTEM[3]

[3] Gould RL, Craig SC, McClatchy S, Churchill G, Pazdro R. Quantitative trait mapping in Diversity Outbred mice identifies novel genomic regions associated with the hepatic glutathione redox system. To be submitted to *Redox Biology*.

Abstract

The tripeptide glutathione (GSH) is instrumental to antioxidant protection and xenobiotic metabolism, and the ratio of its reduced and oxidized forms (GSH/GSSG) indicates the cellular redox environment and maintains key aspects of cellular signaling. Disruptions in GSH levels and GSH/GSSG have long been tied to various chronic diseases, and many studies have examined whether variant alleles in genes responsible for GSH synthesis and metabolism are associated with increased disease risk. However, past studies have been limited to established, canonical GSH genes, though emerging evidence suggests that novel loci and genes influence the GSH redox system in specific tissues. The present study marks the most comprehensive effort to date to directly identify genetic loci associated with the GSH redox system. We employed the Diversity Outbred (DO) mouse population, a model of human genetics, and measured GSH and the essential redox cofactor NADPH in liver, the organ with the highest levels of GSH in the body. Under normal physiological conditions, we observed substantial variation in hepatic GSH and NADPH levels and their redox balances, and discovered a novel, significant quantitative trait locus (QTL) on murine chromosome 16 underlying GSH/GSSG; bioinformatics analyses revealed *Socs1* to be the most likely candidate gene. We also discovered novel QTL associated with hepatic NADP+ levels and NADP+/NADPH, as well as unique candidate genes behind each trait. Overall, these findings transform our understanding of the GSH redox system, revealing genetic loci that govern it and proposing new candidate genes to investigate in future mechanistic endeavors.

Introduction

Glutathione is a ubiquitous and versatile intracellular antioxidant [164]. A tripeptide comprised of glycine, glutamate, and cysteine, its biochemical functions are mediated by a sulfhydryl group on the cysteine residue [531]. In the cell, glutathione mostly exists in its reduced thiol form (GSH), and enzymes such as glutathione peroxidase (GPx) and glutaredoxins convert it to the dimer glutathione disulfide (GSSG), which is recycled back to two molecules of GSH via NADPH-dependent glutathione reductase (GR) [164, 532]. Though GSH and GSSG are in a constant state of flux, their levels – and the ratio GSH/GSSG, or 2GSH/GSSG – provide an informative glimpse into the redox environment of the cell and shifts in these values often indicate oxidative stress [164, 167]. Furthermore, decreases in tissue GSH levels and GSH/GSSG, and corresponding increases in GSSG levels, have been observed in a wide array of chronic diseases including liver disease [202, 233], chronic kidney disease [226, 285], heart disease [265, 270], diabetes mellitus [533-535], and obesity [262].

Because of the close relationship between GSH and chronic diseases, many studies have sought to determine whether variant alleles in genes encoding GSH-related enzymes, including GPx and GR, predict chronic disease risk in human populations. *GPX1* polymorphisms have been associated with increased risk of breast cancer [473, 474], chronic kidney disease [475], prostate cancer [476], coronary artery disease [477], acute myeloid leukemia [477], and kidney complications in T1DM patients [478]. Moreover, variants in *GPX* isoforms have been associated with risk for arterial ischemic stroke in young adults and children (*GPX3*) [479] and prepubertal childhood obesity (*GPX4, 5,* and *6*) [480]. Yet it should be noted that these trends have not been consistent across all populations [481-486]. Other studies have examined the disease relevance of polymorphisms in genes involved in glutathione biosynthesis, notably glutathione cysteine ligase

(GCL) and glutathione synthetase (GS), which directly affect cellular GSH concentrations [487]. Polymorphisms in the catalytic subunit of GCL (*GCLC*) have been associated with cystic fibrosis [488], chronic obstructive pulmonary disease [489], pulmonary tuberculosis [536], drug sensitivity in human tumor cell lines [537], methylmercury retention [538], vasomotor function, and myocardial infarction [539, 540]. Functional polymorphisms in GCL modifier subunit (*GCLM*) have been linked with ischemic heart disease and vasomotor function [540, 541], and in some cases, schizophrenia [193, 492, 493]. Lastly, polymorphisms in *GS* have been associated with susceptibility to lung dysfunction and lung cancer, as well as patient survival [495, 542]. Mutations in these genes have also been found in patients with inborn errors in glutathione metabolism, though the diseases are rare [515, 517, 519, 543, 544].

While most genetics studies have focused on core genes with established functions in GSH biosynthesis and metabolism, emerging evidence suggests that novel loci and genes impact tissue GSH dynamics as well. Multiple studies have shown that GSH and GSSG levels and GSH/GSSG are heritable in mice [203, 522-524, 526] and humans [527] alike, and Zhou et al. discovered new genetic loci associated with hepatic GSH levels and GSH/GSSG in mice [526]. However, those genes were found using a panel of inbred mouse strains, which do not fully reflect the human condition, and many *in silico* mapping tools have limited power and a predisposition toward false positives [545-547]. Thus, more powerful and comprehensive approaches are needed to identify genes that truly govern tissue GSH levels and redox balance, and ultimately, affect chronic disease risk.

In the present study, we performed genome-wide analysis of hepatic GSH and GSSG levels, as well as GSH/GSSG, in the Diversity Outbred (DO) mouse stock, which models the genetic diversity of humans and facilitates high-precision mapping of quantitative trait loci (QTL)

[548, 549]. To best understand the genetics of the entire GSH system [160], we expanded our analysis to include the redox cofactor NADPH, which is essential for GSH recycling [550], and its precursor NADH. To our knowledge, this is the most comprehensive genetic mapping study to focus on tissue GSH homeostasis, and overall, our results point to novel loci and candidate genes that will vastly expand our understanding of this essential redox system and its regulation.

Materials and Methods

Mice: Male and female Diversity Outbred (DO) mice (J:DO; JAX® #009376) from generations 30, 32, and 35 were purchased from The Jackson Laboratory (Bar Harbor, ME USA); the DO stock was originally generated from eight inbred founder strains: A/J (AJ), C57BL/6J (B6), 129S1/SvImJ (129), NOD/ShiLtJ (NOD), NZO/HlLtJ (NZO), CAST/EiJ (CAST), PWK/PhJ (PWK), and WSB/EiJ (WSB). All mice arrived at 4 weeks of age and were given *ad libitum* access to water and standard chow diet (LabDiet®, St. Louis, MO USA, product 5053) and kept on a 12-hour light-dark cycle. These conditions were maintained until the mice were sacrificed at 5-6 months of age. Prior to sacrifice, and during the light cycle, all mice were fasted for 3-4 hours. Then mice were humanely euthanized by cervical dislocation and tissues were collected for analysis. A total of 351 mice (174 males, 177 females) were sacrificed, and at the time of harvest, total body weight (g), liver weight (g), and liver weight/body weight (%) were documented (Supplementary Tables S3.1 – S3.3; Supplementary Figure S3.1). The University of Georgia Institutional Animal Care and Use Committee (IACUC) approved all methods and procedures involving animals in accordance with the ethical standards of the institution (AUP #A2016-07-016), and all methods and procedures were carried out in accordance with the National Institutes of Health guide for the care and use of Laboratory animals (NIH Publications No. 8023, revised 1978).

Assessment of hepatic total glutathione, GSH, GSSG, and redox ratios: Samples of liver tissue were promptly harvested from each mouse after humane euthanasia. Tissues were rinsed with ice-cold PBS, promptly blotted on a paper towel, and flash frozen in liquid nitrogen. Within 12 hours of each harvest, samples were homogenized in PBS containing 10 mM diethylenetriaminepentaacetic acid (DTPA) and promptly acidified with an equal volume of ice-cold 10% perchloric acid (PCA) containing 1 mM DTPA as previously described [203, 454]. Acidified samples underwent centrifugation (15,000 RPM at 4°C for 15 minutes) and the acidified supernatant was collected and filtered. Filtered supernatant samples were stored at -80°C until analysis, and all samples were analyzed within 6 months. GSH and GSSG concentrations were quantified in each sample by HPLC coupled with electrochemical detection (Dionex Ultimate 3000, Thermo Fisher Scientific, Waltham, MA USA) based on previously published methods [454]. A conditioning cell was set to +500 mV and placed immediately before the boron-doped diamond cell which was set at +1475 mV with a cleaning potential at +1900 mV between samples. The mobile phase consisted of 4.0% acetonitrile, 0.1% pentafluoropropionic acid, and 0.02% ammonium hydroxide. The flow rate was maintained at 0.22 mL/min and injection volumes were set at 5.0 μL. Peaks were quantified using external GSH and GSSG standards, external calibration, and the Chromeleon Chromatography Data System Software (Dionex Version 7.2, Thermo Fisher Scientific, Waltham, MA USA). Total glutathione concentrations were determined by calculating $[GSH] + [2GSSG]$ and all glutathione concentrations were standardized to total protein (Pierce BCA Protein Assay, Thermo Fisher Scientific, Waltham, MA USA) and expressed in nM/mg protein. The ratio of GSH/GSSG was then calculated. Another commonly reported measurement related to GSH dynamics and oxidative stress is the redox potential E_h of the redox couple [551-

556]. To calculate the redox potential (E_h) of the GSSG-GSH pair ($2GSH \rightarrow GSSG + 2e^- + 2H^+$) in each liver sample, we used the Nernst equation at 40°C:

$$E_h = E_0 + \frac{RT}{nF} \ln \left[\frac{(ox)}{(red)}\right]$$

E_h = measured cell potential, E_0 = standard electrode potential for GSSG/2GSH (-264 mV at pH 7.4 [552-554]), R = gas constant (8.3145 J x mol^{-1} x K^{-1}), T = temperature in Kelvin (313.15 K), n = number of electrons transferred (2), F = Faraday's constant (96485 C x mol^{-1}), ox = molar concentration of oxidant (GSSG), and red = molar concentration of reductant (GSH). The exponential of GSH reflects the stoichiometry where 2 GSH are oxidized per 1 GSSG formed [551]. Tissue concentrations of GSH and GSSG (nmol/mg protein) were expressed in molar concentrations [555, 556] using a conversion factor of 500 µL/mg of protein. The final equation used to calculate E_h (mV) for the GSSG-GSH couple was:

$$E_h(mV) = -264 + 31 \log \left[\frac{(GSSG)}{(GSH)^2}\right]$$

Assessment of hepatic NADPH, $NADP^+$, $NADP^+$/NADPH, and NADH: Liver samples collected at harvest were rinsed with ice-cold PBS, blotted on a paper towel, and flash frozen in liquid nitrogen. Within 12 hours of each harvest, samples were homogenized, processed, and analyzed by kit (NADP/NADPH Quantification Kit and NAD/NADH Quantification Kit, MilliporeSigma, Burlington, MA USA) according to the manufacturer's instructions. All nicotinamide adenine dinucleotide (NAD) phenotypes were standardized to total protein (Pierce BCA Protein Assay, Thermo Fisher Scientific, Waltham, MA USA) and expressed in pmol/µg protein.

Genotyping: Genotyping was performed on all 351 DO samples. DNA was extracted from tail tips collected at sacrifice and subsequently genotyped using the third-generation Mouse

Universal Genotyping Array (GigaMUGA) [557] performed by GeneSeek (Neogen Genomics, Lincoln, NE USA, 68504). This 143K-probe array is built on the Illumina Infinium II platform and has been optimized for genetic mapping in the DO populations.

Quantitative trait loci (QTL) mapping: Genome scans were performed using 347 (172 male, 175 female) of the original 351 DO samples; 2 mice were excluded from QTL analysis because they were XO females, and 2 were excluded due to low call rates. Prior to analysis, all phenotypic data underwent *z*-score transformation to ensure normality [558]. We then performed genomes scans using R/qtl2 software [549], and for each phenotype, scans included sex and experimental cohort as additive covariates. Each genome scan model also accounted for kinship among the DO mice using the "leave one chromosome out" (LOCO) method [549, 559]. Significance thresholds were determined for individual traits by performing 1000 permutations [549, 560, 561], and we applied a suggestive threshold (p-value ≤ 0.20) for reporting QTL loci based on the permutation analysis [561]. A 95% Bayesian credible interval was calculated around each peak using the R/qtl2 *find_peaks* and *bayes_int* functions [549, 560]. Genes within Bayesian credible intervals ± 1 Mbp were plotted using R/qtl2 via connection with the Mouse Genome Informatics (MGI) database. All genotype data and genotype probabilities are publicly available through figshare (https://doi.org/10.6084/m9.figshare.c.5360501.v1). All source code, phenotype data, and other files used in QTL analyses are available through a public GitHub repository (https://doi.org/10.5281/zenodo.4683881).

Candidate gene analysis: To interrogate the plausibility of candidate genes within significant and suggestive loci, we used an integrative bioinformatics approach that queried databases for expression, phenotypic, and functional annotations based on previously published methods [562, 563]. First, we identified all protein-coding and functional RNA genes within the

significant QTL intervals ± 1 Mbp reported by R/qtl2 using the Unified Mouse Genome Feature Catalog within the Mouse Genome Informatics (MGI) database [563]. Second, for each genome feature in the region, we compiled expression annotations from the bioinformatics resources listed in Supplementary Table S3.4. Gene expression annotations were collected from the EBI Expression Atlas (EEA) [564] and the Gene eXpression Database (GXD) [565] through MGI [566]. Functional annotations were collected using InterPro [567] and Gene Ontology (GO) annotations [568, 569] obtained through MGI [566]. All phenotypic data relevant to the liver were collected from PheWeb [570] and Ensembl BioMart [571].

Statistical Analysis: IBM SPSS Statistics version 26 (SPSS Inc., Chicago, IL USA) was used to detect the significance of relationships between variables of interest. Mann-Whitney tests were used to compare variables between sex to elucidate any sex-effects between variables, and the test includes a U statistic and a standard error. RStudio version 1.3.1093 (RStudio, PBC., Boston, MA USA) and R version 4.0.2 (R Foundation for Statistical Computing, Vienna, Austria) were used to evaluate correlations between values and rank-based Spearman's rho (ρ) was calculated for each relationship. A relationship between variables was considered statistically significant if the p-value was less than 0.05.

Results

Hepatic GSH and NADPH redox systems vary significantly among outbred mice: In a large cohort of genetically-diverse DO mice, we measured hepatic concentrations of GSH and GSSG, as well as GSH/GSSG, and found that under normal physiological conditions, these phenotypes vary widely (Table 3.1; Figure 3.1). Hepatic concentrations of total glutathione and GSH exhibited an over 11-fold difference, ranging from 10.183 to 117.232 nmol/mg and 9.843 to 113.359 nmol/mg, respectively. Hepatic GSSG concentrations ranged from 0.140 to 2.288 nmol/mg,

reflecting a 16-fold difference, and GSH/GSSG ranged from 31.894 to 177.181, over a 5-fold difference. We observed a significant degree of variation in hepatic E_h with a range of -215.556 to -166.948 mV, a 1.3-fold difference. There were no sex effects observed for any of these phenotypes (Supplementary Tables S3.5 and S3.6).

A similar degree of variation was observed in the redox cofactor NADPH and its precursor NADH (Table 3.1; Figure 3.2). $NADP^+$ concentrations ranged from 0.157 to 2.575 pmol/µg, over a 16-fold difference, while its reduced form NADPH ranged from 0.011 to 0.898 pmol/µg, over an 81-fold difference. $NADP^+$/NADPH ranged from 0.460 to 161.363, over a 350-fold difference. NADH ranged from 0.293 to 7.572 pmol/µg, over a 25-fold difference. Sex-specific values are found in Supplementary Tables S3.5 and S3.6.

Table 3.1. Descriptive statistics for hepatic redox system metabolites in DO mice.

Phenotype:	**N**	**x̄**	**Median**	**SD**	**Min**	**Max**
Total Glutathione (nmol/mg)	346	45.945	43.045	19.215	10.183	117.232
GSH (nmol/mg)	346	44.695	41.971	18.708	9.843	113.359
GSSG (nmol/mg)	347	0.627	0.558	0.346	0.140	2.288
GSH/GSSG	346	78.052	74.714	25.120	31.894	177.181
E_h (mV)	346	-195.278	-195.477	7.707	-215.556	-166.948
NADPH (pmol/µg)	335	0.262	0.238	0.170	0.011	0.898
$NADP^+$ (pmol/µg)	331	0.981	0.890	0.450	0.157	2.575
$NADP^+$/NADPH	319	9.888	3.694	19.499	0.460	161.363
NADH (pmol/µg)	332	2.788	2.788	1.233	0.293	7.572

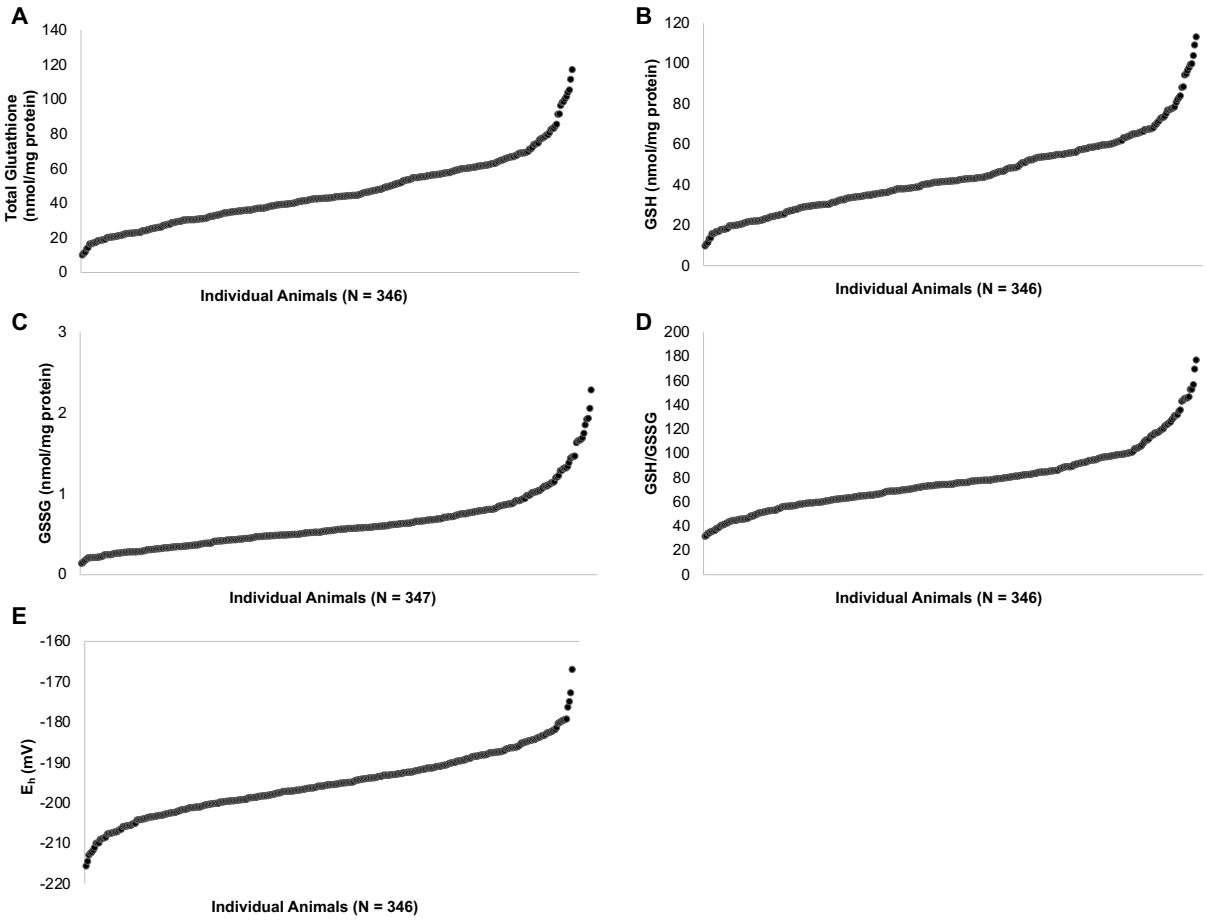

Figure 3.1. Variation in hepatic glutathione concentrations and redox balance in the DO population.

Hepatic concentrations of **A.** Total Glutathione (GSH + 2GSSG, expressed in nmol/mg); **B.** GSH (nmol/mg); **C.** GSSG (nmol/mg); **D.** GSH/GSSG; and **E.** Redox Potential of the GSSG-GSH couple, indicated as E_h (mV) were measured in a population of DO mice. Values are arranged from smallest to largest, and the N for each measurement is provided underneath each panel.

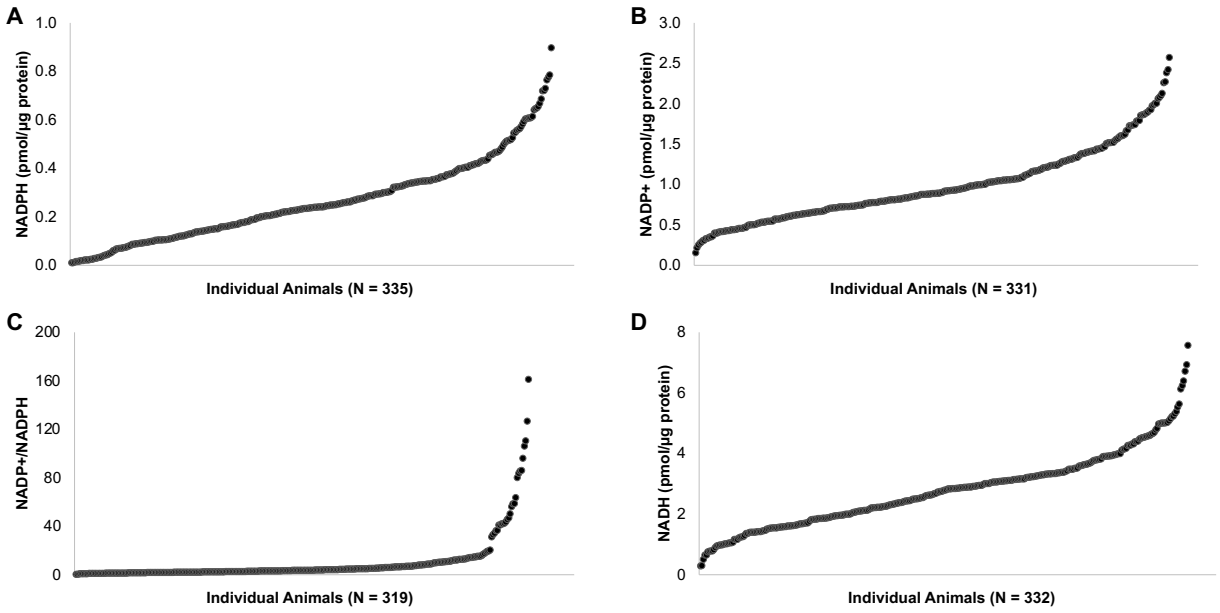

Figure 3.2. Variation in hepatic NAD(P)H concentrations and redox balances in the DO population.
Hepatic concentrations of **A.** NADPH (pmol/µg); **B.** $NADP^+$ (pmol/µg); **C.** $NADP^+$/NADPH; and **D.** NADH (pmol/µg) in a population of DO mice. Values are arranged from smallest to largest, and the N for each measurement is provided underneath each panel.

We screened for statistical associations among variables and discovered multiple significant correlations. Association results are listed in Table 3.2 and shown visually in Figure 3.3. Hepatic total glutathione concentrations were positively correlated with GSH concentrations ($\rho = 1.000$, $p = <0.001$), GSSG concentrations ($\rho = 0.801$, $p = <0.001$), and GSH/GSSG levels ($\rho = 0.120$, $p = 0.026$), and were strongly negatively correlated with E_h levels ($\rho = -0.799$, $p = <0.001$). Hepatic GSH concentrations were positively correlated with GSSG concentrations ($\rho = 0.791$, $p = <0.001$) and GSH/GSSG levels ($\rho = 0.137$, $p = 0.011$), and were negatively correlated with E_h levels ($\rho = -0.810$, $p = <0.001$). Hepatic GSSG concentrations were negatively correlated with GSH/GSSG levels ($\rho = -0.443$, $p = <0.001$) and E_h levels ($\rho = -0.326$, $p = <0.001$). Hepatic GSH/GSSG levels were negatively correlated with E_h levels ($\rho = -0.652$, $p = <0.001$).

Hepatic NADPH concentrations were positively correlated with total glutathione concentrations ($\rho = 0.265$, $p = <0.001$), GSH concentrations ($\rho = 0.267$, $p = <0.001$), and GSSG concentrations ($\rho = 0.203$, $p = <0.001$), and negatively correlated with $NADP^+$ concentrations ($\rho = -0.278$, $p = <0.001$), $NADP^+$/NADPH levels ($\rho = -0.846$, $p = <0.001$) and E_h levels ($\rho = -0.234$, $p = <0.001$). Hepatic $NADP^+$ concentrations were negatively correlated with total glutathione concentrations ($\rho = -0.306$, $p = <0.001$), GSH concentrations ($\rho = -0.306$, $p = <0.001$), GSSG concentrations ($\rho = -0.269$, $p = <0.001$), and $NADP^+$ concentrations ($\rho = -0.142$, $p = 0.010$), and positively correlated with $NADP^+$/NADPH levels ($\rho = 0.711$, $p = <0.001$) and E_h levels ($\rho = 0.226$, $p = <0.001$). Hepatic $NADP^+$/NADPH levels were positively correlated with E_h levels ($\rho = 0.240$, $p = <0.001$) and negatively correlated with total glutathione concentrations ($\rho = -0.296$, $p = <0.001$), GSH concentrations ($\rho = -0.297$, $p = <0.001$), and GSSG concentrations ($\rho = -0.233$, $p = <0.001$). Neither NADPH or $NADP^+$, nor the $NADP^+$/NADPH ratio were found to be correlated with GSH/GSSG ($p = 119$, $p = 0.850$, and $p = 0.208$, respectively). Hepatic NADH concentrations were positively correlated with NADPH ($\rho = 0.191$, $p = 0.001$), total glutathione concentrations ($\rho = 0.250$, $p = <0.001$), GSH concentrations ($\rho = 0.253$, $p = <0.001$), GSSG concentrations ($\rho = 0.123$, $p = 0.025$), GSH/GSSG levels ($\rho = 0.186$, $p = 0.001$), and were negatively correlated with $NADP^+$/NADPH levels ($\rho = -0.181$, $p = 0.001$), and E_h levels ($\rho = -0.307$, $p = <0.001$).

Relationships between redox phenotypes and liver weights were also observed, with positive associations between liver weights and total glutathione concentrations ($\rho = 0.137$, $p = 0.011$), GSH concentrations ($\rho = 0.136$, $p = 0.012$), and GSSG concentrations ($\rho = 0.176$, $p = 0.001$). Liver weights were also positively correlated with NADPH concentrations ($\rho = 0.203$, $p = <0.001$) and negatively correlated with $NADP^+$ concentrations ($\rho = -0.218$, $p = <0.001$) and

$NADP^+$/NADPH ($\rho = -0.262$, $p = <0.001$). NADH was not correlated with liver weight ($\rho = -0.063$, $p = 0.253$).

Table 3.2. Statistical relationships among markers of the hepatic GSH redox system as well as liver weights.
Spearman's rho (ρ) was calculated for each variable combination. Total glutathione, GSH, and GSSG concentrations were standardized as nmol/mg protein. Concentrations of NADPH, NADP, and NADH were standardized as pmol/µg protein. E_h was expressed as mV. Liver weight was reported in grams (g). *indicates a significant relationship ($p \leq 0.05$).

Variables	**ρ**	**p-value**
Total Glutathione, GSH	1.000*	<0.001
Total Glutathione, GSSG	0.801*	<0.001
Total Glutathione, GSH/GSSG	0.120*	0.026
Total Glutathione, E_h	-0.799*	<0.001
Total Glutathione, NADPH	0.265*	<0.001
Total Glutathione, $NADP^+$	-0.306*	<0.001
Total Glutathione, $NADP^+$/NADPH	-0.296*	<0.001
Total Glutathione, NADH	0.250*	<0.001
GSH, GSSG	0.791*	<0.001
GSH, GSH/GSSG	0.137*	0.011
GSH, E_h	-0.810*	<0.001
GSH, NADPH	0.267*	<0.001
GSH, $NADP^+$	-0.306*	<0.001
GSH, $NADP^+$/NADPH	-0.297*	<0.001
GSH, NADH	0.253*	<0.001
GSSG, GSH/GSSG	-0.443*	<0.001
GSSG, E_h	-0.326*	<0.001
GSSG, NADPH	0.203*	<0.001
GSSG, $NADP^+$	-0.269*	<0.001
GSSG, $NADP^+$/NADPH	-0.233*	<0.001
GSSG, NADH	0.123*	0.025
GSH/GSSG, E_h	-0.652*	<0.001
E_h, NADPH	-0.234*	<0.001
E_h, $NADP^+$	0.226*	<0.001
E_h, $NADP^+$/NADPH	0.240*	<0.001
E_h, NADH	-0.307*	<0.001
NADPH, $NADP^+$	-0.278*	<0.001
NADPH, $NADP^+$/NADPH	-0.846*	<0.001

NADPH, NADH	0.191*	0.001
$NADP^+$, $NADP^+$/NADPH	0.711*	<0.001
$NADP^+$, NADH	-0.142*	0.010
$NADP^+$/NADPH, NADH	-0.181*	0.001
Liver Weight, Total Glutathione	0.137*	0.011
Liver Weight, GSH	0.136*	0.012
Liver Weight, GSSG	0.176*	0.001
Liver Weight, GSH/GSSG	-0.089	0.099
Liver Weight, E_h	-0.050	0.349
Liver Weight, NADPH	0.203*	<0.001
Liver Weight, $NADP^+$	-0.218*	<0.001
Liver Weight, $NADP^+$/NADPH	-0.262*	<0.001
Liver Weight, NADH	-0.063	0.253

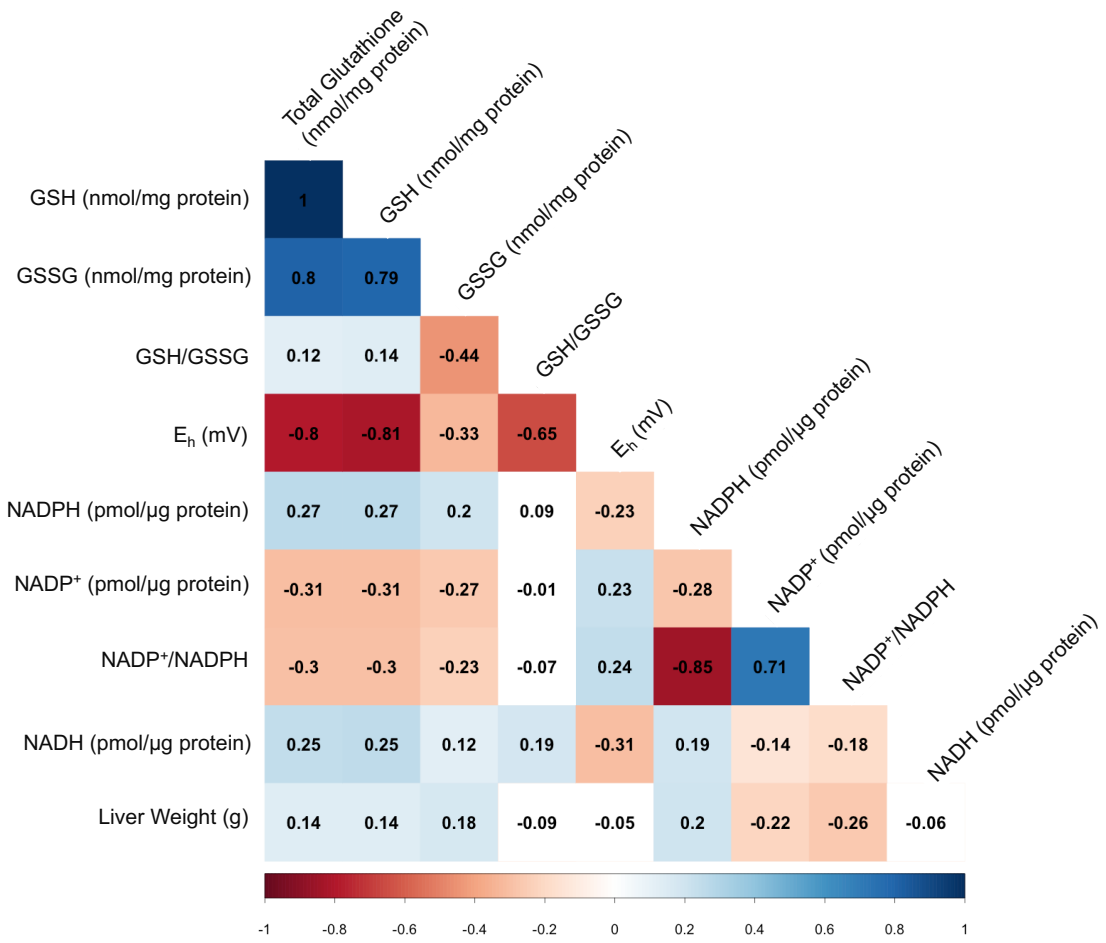

Figure 3.3. Correlation matrix of statistical relationships among markers of the hepatic GSH redox system and liver weights.
Spearman's rho (ρ) was calculated for each variable combination and is listed within each corresponding box. Total glutathione, GSH, and GSSG concentrations were standardized as nmol/mg protein. Concentrations of NADPH, NADP, and NADH were standardized as pmol/µg protein. E_h was expressed as mV. Liver weight was reported in grams (g). A colored box indicates a significant relationship ($p \leq 0.05$). An uncolored (white) box indicates an insignificant relationship ($p > 0.05$).

QTL mapping of the hepatic GSH redox system: We performed QTL analysis using R/qtl2 on all measured markers of the GSH redox system (Figure 3.4). Here we outline the results of statistically significant peaks, yet it should be noted that multiple other peaks surpassed LOD scores of 6 but failed to surpass significance thresholds calculated through 1000 permutation tests. Genome-wide scans for hepatic concentrations of total glutathione and GSH revealed a suggestive

peak (LOD scores 6.755 and 6.748, respectively) on mouse chromosome 14 (founder allele effects and candidate gene results are included in Supplementary Figures S3.2 and S3.3). Mapping GSH/GSSG and E_h revealed a significant (p-value ≤ 0.05) peak on mouse chromosome 16 at 8.998 Mbp (LOD scores 8.224 and 8.598, respectively). Given that the peak position was the same between the two scans, we focused on GSH/GSSG results, which are outlined in Figure 3.5, while E_h results are provided in Supplementary Figure S3.4.

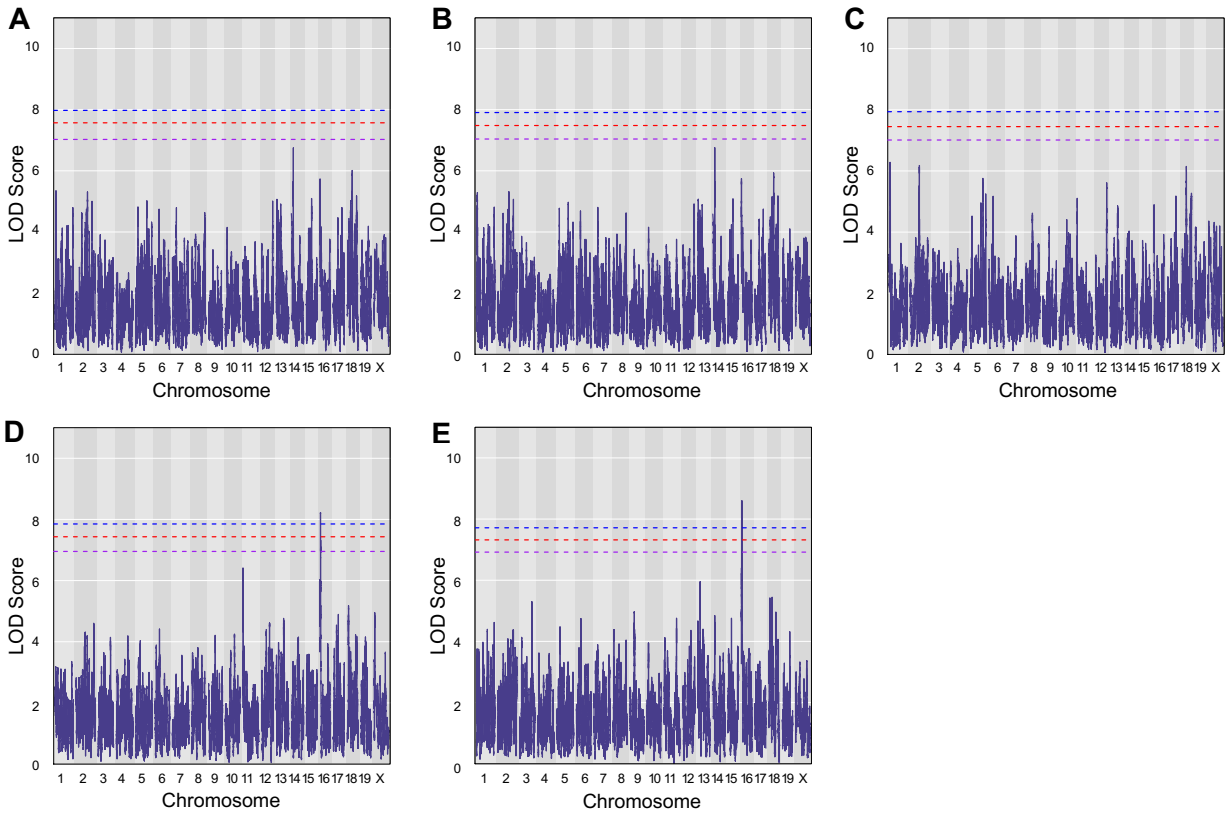

Figure 3.4. QTL results for markers of the GSH redox system.
Genome-wide scans of hepatic **A.** Total Glutathione (GSH + 2GSSG, expressed in nmol/mg); **B.** GSH (nmol/mg); **C.** GSSG (nmol/mg); **D.** GSH/GSSG; and **E.** Redox Potential of the GSSG-GSH couple (E_h, expressed as mV). Permutation-derived significance thresholds are indicated by colored lines at significance (α) levels 0.05 (blue), 0.1 (red), and 0.2 (purple).

The genome-wide scan for GSH/GSSG revealed a significant peak on mouse chromosome 16 with a QTL interval of 8.865 – 10.077 Mbp (Figure 3.5A). Within the interval, founder allele

effects were extrapolated, showing that the AJ allele contributes to a higher GSH/GSSG, whereas the PWK allele contributes to a lower GSH/GSSG (Figure 3.5B). Genes found within this interval ± 1 Mbp were plotted using R/qtl2 through connection with the MGI database (Figure 3.5C), and functional RNA and protein-coding genes were collected and screened for physiological relevance using existing expression, functional, and phenotypic annotations (Supplementary Table S3.7). The QTL interval contained 66 possible candidate genes: 29 protein-coding, 35 non-coding RNA, and 2 unclassified (GRCm38/mm10; gene query performed November 2020, Feature Type "gene" [563]). 30 of the 66 GSH/GSSG candidate genes had limited hepatic expression annotations and were therefore excluded. Of the remaining 36 candidate genes, 22 were limited to hepatic expression data only, and the remaining 14 candidate genes had annotations with functional relevance to the GSH redox system: transmembrane protein 114 (*Tmem114*), predicted gene 5767 (*Gm5767*), RIKEN cDNA 1810013L24 gene (*1810013L24Rik*), ribosomal protein L39-like (*Rpl39l*), activating transcription factor 7 interacting protein 2 (*Atf7ip2*), predicted gene 1600 (*Gm1600*), nucleotide binding protein 1 (*Nubp1*), trans-golgi network vesicle protein 23A (*Tvp23a*), class II transactivator (*Ciita*), *C*-type lectin domain family 16, member A (*Clec16a*), suppressor of cytokine signalling-1 (*Socs1*), protamine 3 (*Prm3*), protamine 2 (*Prm2*), and LPS-induced TN factor (*Litaf*). Based on functional and phenotypic annotations, *Socs1* (Chr16:10783808–10785536 bp; 5.81 cM; GRCm38) was determined to be the most likely candidate gene within the interval. SOCS1 functions as a negative regulator of cytokine signaling, including the JAK/STAT-signaling pathway, as well as insulin and toll-like receptor (TLR) signal transduction [572]. Importantly, SOCS1 has been involved in p53 activation and subsequent repression of the transcription of SLC7A11 [573] – a cystine/glutamate antiporter and regulator of intracellular cysteine concentrations, the rate-limiting precursor for GSH biosynthesis [165, 574].

As a result of its suppression of *SLC7A11*, SOCS1 expression has been found to negatively correlate with GSH levels [573]. Furthermore, SOCS1 negatively regulates the nuclear factor-κB (NF-κB) transcription complex, specifically the p65 subunit, by acting as a ubiquitin ligase and prompting proteasome-mediated degradation [575]. NF-κB is transcription factor and activation of NF-κB is critical in maintaining cellular GSH concentrations [576] and expression of enzymes involved in GSH synthesis [577].

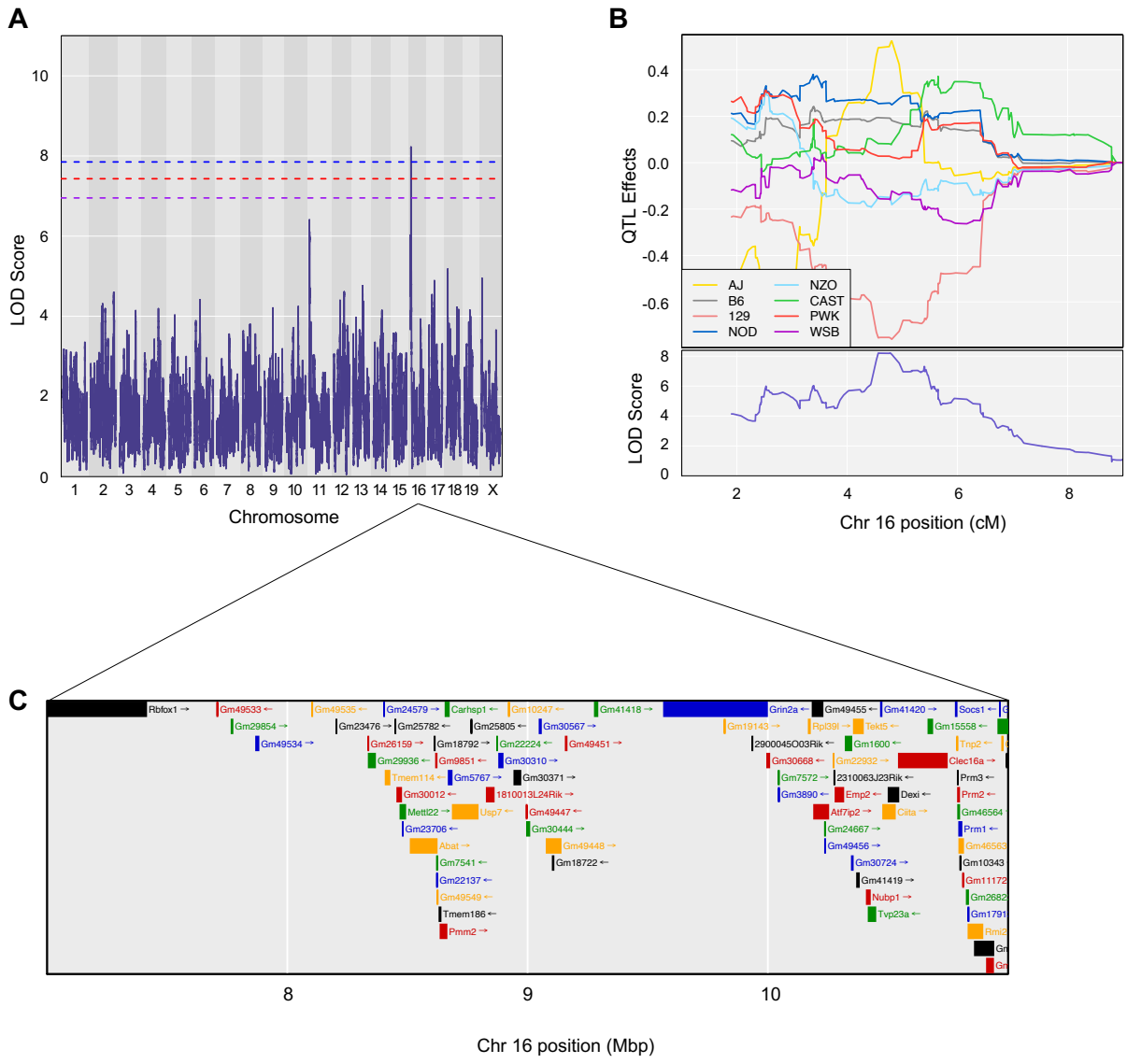

Figure 3.5. High-resolution association mapping for hepatic GSH/GSSG in outbred mice reveals a significant QTL on mouse chromosome 16.
A. Genome-wide scan of hepatic GSH/GSSG in outbred mice shows a QTL with peak LOD score 8.224 at 8.998 Mbp (4.779 cM) on mouse chromosome 16. Permutation-derived significance thresholds are indicated by colored lines at significance (α) levels 0.05 (blue), 0.1 (red), and 0.2 (purple). **B.** The founder allele QTL effects indicate that the PWK allele contributes to a lower hepatic GSH/GSSG concentration, whereas the AJ allele contributes to a higher hepatic GSH/GSSG concentration. Each colored line represents a DO founder allele as indicated in the legend. The differences between strains are considered significant when the LOD score (bottom) crosses significance thresholds (panel A). **C.** Candidate genes found within the QTL interval relative to the MGI database. E_h (mV) genome scan resulted in the same significant QTL interval on mouse chromosome 16 compared to GSH/GSSG (Supplementary Figure S3.4).

QTL mapping of the hepatic NAD(P)H phenotypes: Genome-wide scans were conducted for the following NADPH redox phenotypes: NADPH, $NADP^+$, $NADP^+$/NADPH, and NADH (Figure 3.6). Scans for NADPH and NADH included peaks that surpassed LOD score 6 or more yet failed to reach significance. The genome-wide scan for $NADP^+$ revealed a suggestive peak (p-value ≤ 0.20) on mouse chromosome 3 at 110.517 Mbp (LOD score 7.032) with a QTL interval of 109.677 – 115.729 Mbp (Figure 3.7A). Founder allele effects showed that the WSB and PWK alleles contribute to a higher $NADP^+$ concentration, whereas the NOD and CAST alleles contribute to a lower $NADP^+$ concentration (Figure 3.7B). Genes located within this interval ± 1 Mbp were plotted using R/qtl2 (Figure 3.7C) and existing biological annotations were collected. The QTL interval contained 85 possible candidate genes: 38 protein-coding, 37 non-coding RNA, and 10 unclassified (Supplementary Table S3.8; GRCm38/mm10; gene query performed November 2020, Feature Type "gene" [563]). 52 of the 85 $NADP^+$ candidate genes had no hepatic expression and were therefore excluded. Of the remaining 33 candidate genes, 8 had no additional functional or phenotypic annotations related to hepatic redox function. The remaining 25 candidate genes were: chloride channel CLIC-like 1 (*Clcc1*), G-protein signalling modulator 2 (*Gpsm2*), AKNA domain containing 1 (*Aknad1*), syntaxin binding protein 3 (*Stxbp3*), PRP38 pre-mRNA processing factor 38 (yeast) domain containing B (*Prpf38b*), HEN1 methyltransferase homolog 1 (*Henmt1*), family with sequence similarity 102, member B (*Fam102b*), solute carrier family 25, member 54 (*Slc25a54*), vav 3 oncogene (*Vav3*), netrin G1 (*Ntng1*), protein arginine N-methyltransferase 6 (*Prmt6*), RNA-binding region containing 3 (*Rnpc3*), olfactomedin 3 (*Olfm3*), RIKEN cDNA A930005H10 gene (*A930005H10Rik*), diphthamide biosynthesis 5 (*Dph5*), solute carrier family 30 (zinc transporter), member 7 (*Slc30a7*), exostoses-like 2 (*Extl2*), vascular cell adhesion molecule 1 (*Vcam1*), CDC14 cell division cycle 14A (*Cdc14a*), RNA 3'-terminal phosphate

cyclase (*Rtca*), dihydrolipoamide branched chain transacylase E2 (*Dbt*), leucine rich repeat containing 39 (*Lrrc39*), tRNA methyltransferase 13 (*Trmt13*), SAS-6 centriolar assembly protein (*Sass6*), and solute carrier family 35 (UDP-N-acetylglucosamine (UDP-GlcNAc) transporter), member 3 (*Slc35a3*). Evaluation of functional and phenotypic annotations did not point to a single candidate with a direct link to NADP+ regulation. Yet a subsequent literature search suggested that *Vav3, Vcam1,* and *Cdc14a* were the most likely genes influencing $NADP^+$ concentrations. Vav3 (Chr3:109340653–109685698 bp; 48.13 cM; GRCm38) is a Rho GTPase regulating guanine nucleotide exchange factor (GEF) [578]. The Vav protein family, including Vav3, are key activators of the Card9/NF-κB pathway in immunity [579]. VCAM-1 (Chr3: 116110020 – 116129688 bp; 50.17 cM; GRCm38) expression is upregulated by NF-κB and increases in oxidative stress [580, 581], and VCAM-1 activates NADPH oxidase in endothelial cells [582]. CDC14A (Chr3: 116272553–116428741bp; 50.24 cM; GRCm38) is a phosphoprotein-phosphatase involved in cell cycle progression [583]. CDC14A has been found to dephosphorylate tumor suppressor p53 and is thought to regulate the function of p53 [584, 585] whose actions are critical in regulating NADPH redox status and NADPH production through the pentose phosphate pathway [586, 587]. We were unable to find research supporting the involvement of Vav3, Vcam-1, or Cdc14a's involvement with hepatic NF-κB or p53, nor their influence on hepatic $NADP^+$.

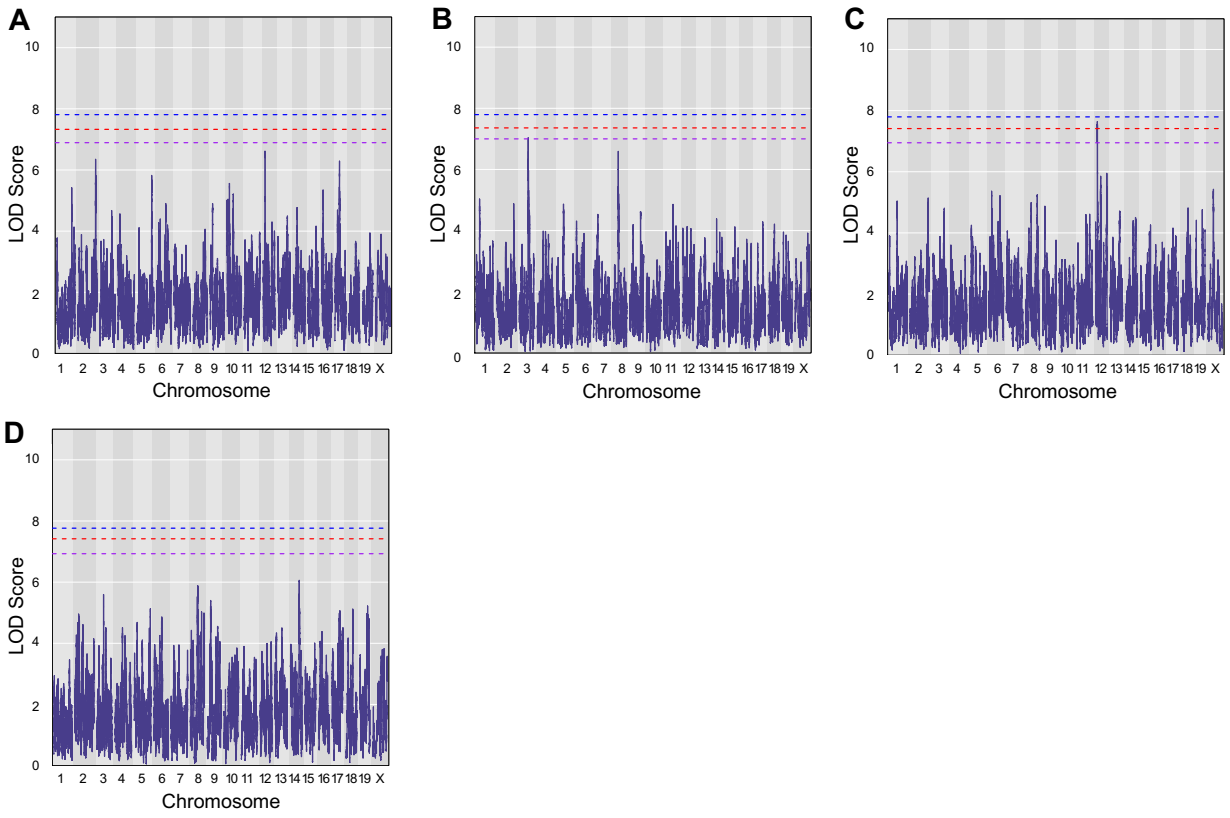

Figure 3.6. QTL results for hepatic NAD(P)H phenotypes.
Genome-wide scans of hepatic **A.** NADPH (pmol/µg); **B.** $NADP^+$ (pmol/µg); **C.** $NADP^+$/NADPH; and **D.** NADH (pmol/µg). Permutation-derived significance thresholds are indicated by colored lines at significance (α) levels 0.05 (blue), 0.1 (red), and 0.2 (purple).

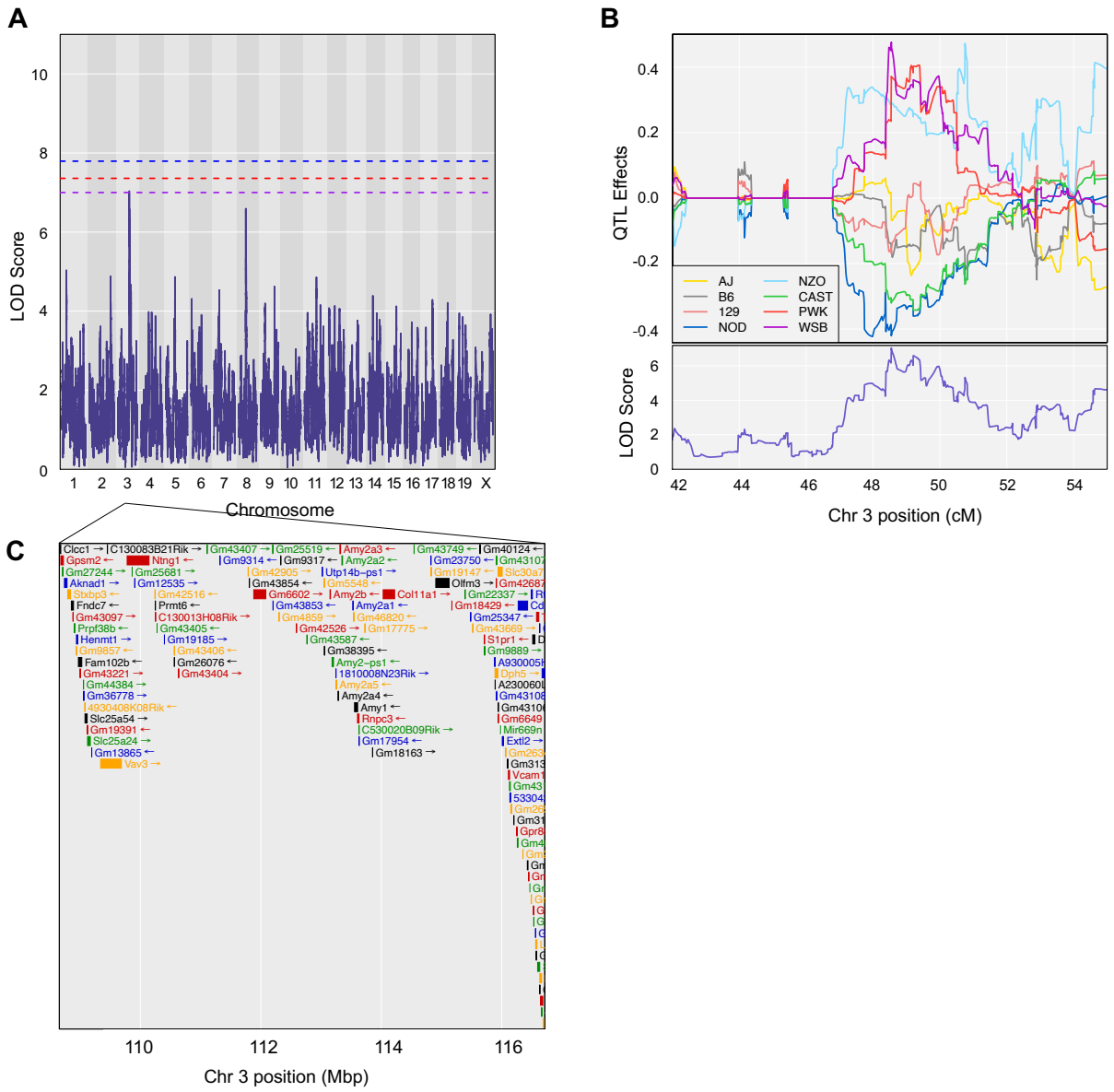

Figure 3.7. High-resolution association mapping for hepatic NADP$^+$ in outbred mice reveals a suggestive QTL on mouse chromosome 3.

A. Genome-wide scan of hepatic NADP$^+$ (pmol/µg) in outbred mice shows a QTL with peak LOD score 7.032 at 110.517 Mbp (48.547 cM) on mouse chromosome 3. Permutation-derived significance thresholds are indicated by colored lines at significance (α) levels 0.05 (blue), 0.1 (red), and 0.2 (purple). **B.** The founder allele QTL effects indicate that the NOD and CAST alleles contribute to a lower hepatic NADP$^+$ concentration, whereas the WSB and PWK alleles contribute to a higher hepatic NADP$^+$ concentration. Each colored line represents a DO founder allele as indicated in the legend. The differences between strains are considered significant when the LOD score (bottom) crosses significance thresholds (panel A). **C.** Candidate genes found within the QTL interval relative to the MGI database.

The genome-wide scan for $NADP^+$/NADPH revealed a suggestive peak (p-value ≤ 0.10) on mouse chromosome 12 at 28.626 Mbp (LOD score 7.637) with a QTL interval of 28.562 – 29.394 Mbp (Figure 3.8A). Founder allele effects were extrapolated within the interval and show that the WSB and B6 alleles contribute to a higher $NADP^+$/NADPH concentration, whereas the NOD and PWK alleles contribute to a lower $NADP^+$/NADPH concentration (Figure 3.8B). Genes found within this credible interval ± 1 Mbp were plotted using R/qtl2 through connection with the MGI database (Figure 3.8C) for collection of functional RNA and protein coding genes. The QTL interval contained 51 possible candidate genes: 15 protein-coding, 34 non-coding RNA, and 2 unclassified (GRCm38/mm10; gene query performed November 2020, Feature Type "gene" [563]). Biological annotations were collected (Supplementary Table S3.9), and 36 of the 51 $NADP^+$/NADPH candidate genes had no hepatic expression annotations and were therefore excluded. 6 of the remaining 15 candidate genes did not have additional functional or phenotypic annotations related to hepatic redox function, and the remaining 8 candidate genes were: SRY (sex determining region Y)-box 11 (*Sox11*), collectin sub-family member 11 (*Colec11*), ribosomal protein S7 (*Rps7*), ribonuclease H1 (*Rnaseh1*), acireductone dioxygenase 1 (*Adi1*), myelin transcription factor 1-like (*Myt1l*), peroxidasin (*Pxdn*), thyroid peroxidase (*Tpo*), and syntrophin, gamma 2 (*Sntg2*). A comprehensive literature search on each gene failed to suggest evidence of their influence on hepatic $NADP^+$/NADPH levels or redox homeostasis.

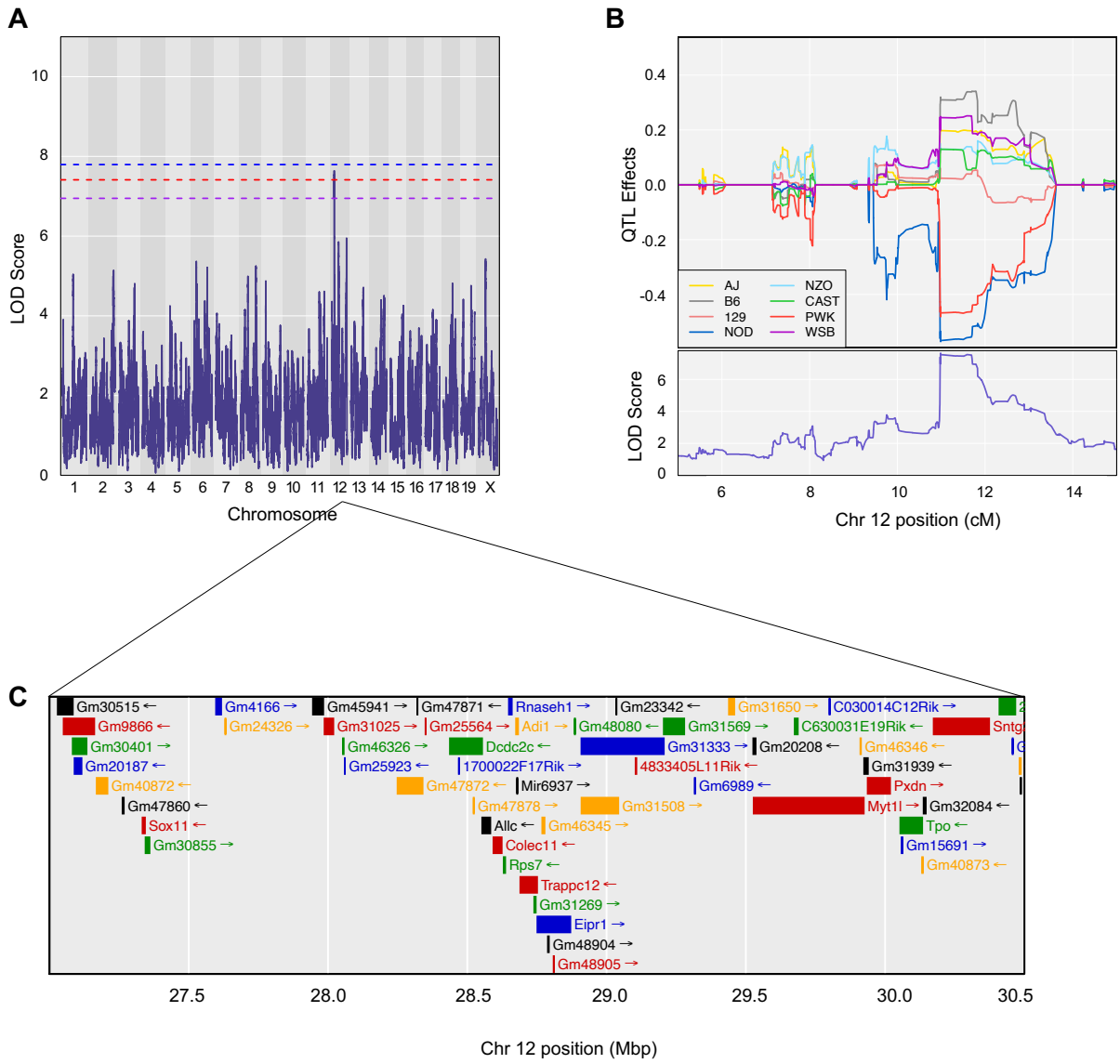

Figure 3.8. High-resolution association mapping for hepatic NADP$^+$/NADPH in outbred mice reveals a suggestive QTL on mouse chromosome 12.
A. Genome-wide scan of GSH in outbred mice shows a QTL with peak LOD score 7.637 at 28.626 Mbp (10.987 cM) on mouse chromosome 12. Permutation-derived significance thresholds are indicated by colored lines at significance (α) levels 0.05 (blue), 0.1 (red), and 0.2 (purple). **B.** The founder allele QTL effects indicate that the NOD and PWK alleles contribute to a lower hepatic NADP$^+$/NADPH concentration, whereas the WSB and B6 alleles contribute to a higher hepatic NADP$^+$/NADPH concentration. Each colored line represents a DO founder allele as indicated in the legend. The differences between strains are considered significant when the LOD score (bottom) crosses significance thresholds (panel A). **C.** Candidate genes found within the QTL interval relative to the MGI database.

Discussion

GSH maintains the cellular redox environment and declines in its concentrations and GSH/GSSG are closely associated with oxidative stress and chronic disease. Recent studies have suggested that genetics has a prominent role in regulating the GSH redox system [203, 522-524, 526, 527], and that novel, as yet unidentified, genes and loci may directly regulate GSH dynamics. The present study was conducted to define the loci and candidate genes underlying the GSH redox system, results that could shift existing paradigms surrounding redox regulation.

In this study, hepatic glutathione phenotypes varied widely, with an 11-fold difference in hepatic GSH and a 5-fold difference in GSH/GSSG. Variation in liver glutathione status has the potential to impact global glutathione status, as the liver is the major producer and exporter of GSH [174], regulating the systemic availability of GSH [200, 207]. Moreover, in humans, circulating GSH/GSSG is often measured as an indicator of oxidative stress and liver injury [588], and an altered GSH status is linked to the onset and progression of liver disease [202, 223]. Our results suggest that the status of the GSH redox system may be controlled at a tissue-specific level, potentially impacting the risk for liver disease. Future research will identify if this variation has an impact on liver tissue health.

Genome-wide association mapping revealed a novel locus for GSH/GSSG on murine chromosome 16 at 8.998 Mbp ($p \leq 0.05$) harboring 66 candidate genes (Figure 3.9). Via bioinformatic database query, we identified *Socs1* as the most plausible candidate gene for multiple reasons. First, Socs1 is involved in activation of p53[573], a critical tumor suppressor that has been closely tied to redox systems andoxidative stress [91]. In low oxidative stress conditions, p53 contributes to antioxidant protection by upregulating Gpx and other stress resistance genes to ensure cell survival [91]. Yet in high oxidative stress conditions, p53 acts as a prooxidant to

increase levels of stress which ultimately leads to cell death [91]. p53 also negatively regulates nuclear factor E2-related factor 2 (Nrf2), a critical antioxidant transcription factor [589], and by inhibiting Nrf2 action, p53 represses the expression of genes involved in glutathione metabolism (namely, *GCLM, GCLC, GR*, and cysteine transporter *SLC7A11*) [471, 590, 591], further increasing oxidative stress or inducing apoptosis [91]. SLC7A11, also referred to as xCT, is the regulator of intracellular cysteine levels – the rate limiting precursor to GSH biosynthesis – and low levels of cysteine result in decreased GSH biosynthesis [592] [165, 574, 593]. Moreover, SLC7A11 has been implicated as a SOCS1-dependent p53 target gene and expression of *SOCS1* is negatively correlated with expression of SLC7A11 and GSH levels [573]. In addition, to SOCS1's role in p53 signaling, SOCS1 functions as a negative regulator of cytokine signaling and suppresses NF-κB [572]. NF-κB is a transcription factor that responds to oxidative stress to influence cell survival, differentiation, and proliferation by increasing expression of inflammatory cytokines, as well as antioxidant and anti-apoptotic proteins [594]. NF-κB confers resistance to oxidative stress by maintaining cellular GSH concentrations [576], as well as basal GCLC and GCLM expression which regulates GSH synthesis [577]. SOCS1 negatively regulates the NF-κB transcription complex by acting as a ubiquitin ligase and prompting proteasome-mediated degradation [575, 595]. Increased degradation of NF-κB as a result of amplified SOCS1 could therefore result in decreased GSH synthesis due to a lack of available synthesis enzymes as well as an increased need for GSH in the inflammation process [576, 577]. Lastly, in mice, increased Socs1 is associated with enlarged liver (MP:0000599), hepatic necrosis (MP:0001654), hepatic steatosis (MP:0002628), liver degeneration (MP:0003103), and liver inflammation (MP:0001860) [566, 596]. Alternatively, $Socs1^{-/-}$ knockout mice are rendered perinatal lethal [597], and the gene deletion results in severe liver inflammation [597]. Furthermore, Socs1 methylation in mouse liver

is associated with advancement of liver fibrosis [597]. In humans, a *SOCS1* variant (rs243330) in obese humans is associated non-alcoholic fatty liver disease and insulin resistance [598]. Given this evidence, we propose that *Socs1* has an indirect effect on hepatic GSH/GSSG levels through its role in the p53 and NF-κB pathways. Further research validating the effect of variants in Socs1 on GSH/GSSG levels is warranted.

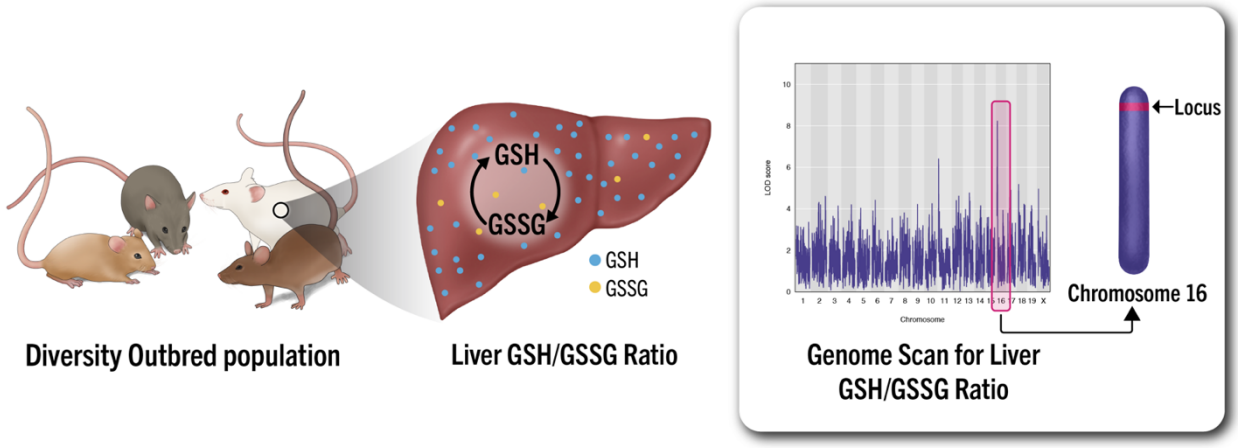

Figure 3.9. Graphical abstract.

Genetic mapping conducted for the NADPH redox system phenotypes revealed suggestive QTL for $NADP^+$ on mouse chromosome 3 at 110.517 Mbp ($p \leq 0.20$) and $NADP^+$/NADPH on mouse chromosome 12 at 28.626 Mbp ($p \leq 0.10$). Candidate gene analysis for $NADP^+$ and $NADP^+$/NADPH was inconclusive, with a possible 25 candidate genes for $NADP^+$ (*Clcc1, Gpsm2, Aknad1, Stxbp3, Prpf38b, Henmt1, Fam102b, Slc25a54, Vav3, Ntng1, Prmt6, Rnpc3, Olfm3, A930005H10Rik, Dph5, Slc30a7, Extl2, Vcam1, Cdc14a, Rtca, Dbt, Lrrc39, Trmt13, Sass6,* and *Slc35a3*) and 9 candidate genes for $NADP^+$/NADPH (*Sox11, Colec11, Rps7, Rnaseh1, Adi1, Myt1l, Pxdn, Tpo,* and *Sntg2*). A collection of functional and phenotypic annotations suggests that *Vav3, Vcam1,* and *Cdc14a* are the most likely genes influencing $NADP^+$ concentrations, though

there is a lack of literature specific to their role in hepatic redox metabolism. Future studies will be conducted to narrow and eventually select the causative gene.

Previous genetic analysis was conducted on liver and kidney glutathione phenotypes (GSH, GSSG, GSH/GSSG) *in silico* using haplotype association mapping (HAM) which revealed novel loci regulating glutathione status [526]. We compiled all QTL peaks with LOD scores > 6 (Supplementary Table S3.10) and compared them to the HAM peaks found *in silico.* We did not observe any direct overlap between our hepatic glutathione QTL and the hepatic HAM results. However, we did draw a comparison between a HAM peak reported from Zhou et al. (2014) and our $NADP^+$ genome scan results. We observed a QTL peak for $NADP^+$ on mouse chromosome 8 at 61.237 (60.722 – 65.378) Mbp which was in proximity to the HAM peaks reported by Zhou et al. (2014) for hepatic GSH on mouse chromosome 8 at 56.109 Mbp and for renal GSSG on mouse chromosome 8 at 54.793 – 55.416 Mbp. Moreover, we documented a QTL peak for hepatic GSSG on chromosome 1 at 21.043 (18.793 – 22.050) Mbp which was in proximity to the HAM peak observed for renal GSH on chromosome 1 at 20.259 Mbp. These results indicate that there could be shared regulatory mechanisms between the hepatic and renal glutathione redox systems.

Genes involved in GSH synthesis and metabolism failed to reach significance in our high-resolution genetic mapping. The genome scan reports genomic regions whose allelic variation significantly contributes to variation in the phenotype of interest, and our genome scans report that the regions housing GSH synthesis and recycling genes did not significantly alter glutathione phenotypes. We suspected this is due to lack of genotype variation in the DO animals for those specific genes. To investigate the effects of allelic variation on GSH, GSSG, total glutathione, GSH/GSSG, and E_h, founder allele effects were visualized in genetic regions of Gpx1 (Chromosome 9 59.24 cM), Gclc (Chromosome 9 43.36 cM), Gclm (Chromosome 3 52.94 cM),

Gs (Chromosome 2 77.26 cM), and Gr (Chromosome 8 20.69 cM) (Supplementary Table S3.11) [596]. The founder allele effects indicate that there are no founder haplotypes in proximity to the Gpx1, Gclc, Gclm, Gs, or Gr gene locations that contribute to a significantly lower or higher glutathione phenotype concentration (Supplementary Figure S3.5 – S3.9). These results support our conclusion that the differences in glutathione phenotype concentrations are generated independently of variation in genes supporting classical GSH synthesis and recycling, and rather are due to novel regulatory loci.

The present study was accompanied by some limitations. Though the study included representation of both male and female mice, a subset of males (N = 63) had to be individually housed due to aggressive behavior. Excessive fighting has been associated with additive stress in mice [599], which had the potential of negatively influencing glutathione homeostasis due to its sensitivity toward external stressors [203]. To address this factor, we performed Mann-Whitney tests comparing variables in mice to their housing group size and found that mice single-housed did not have significantly different levels of glutathione, NADH, NADP(H), or liver weights. Furthermore, there is always a possibility for variation in glutathione quantification due to HPLC from possible exposure to oxidants as a result of being on the sample plate. To address this potential problem, all samples were thawed on the sample plate at 4°C and analyzed in duplicates within 4 hours of being put on the plate.

Conclusion

It is thought that hepatic oxidative stress is controlled by GSH and NADPH status [600]. To our knowledge, this is the first study to employ a computational genome analysis of glutathione phenotypes within hepatic tissue using the DO. Our results indicate that there is 1) a large natural variation in the GSH and NADPH redox systems in a genetically diverse population, and 2)

GSH/GSSG, $NADP^+$, and $NADP^+$/NADPH may be regulated by genetic factors outside of canonical regulatory genes. We documented a novel locus influencing hepatic GSH/GSSG on murine chromosome 16 and identified *Socs1* as a the most likely gene influencing GSH/GSSG levels. In addition, we identified numerous candidate genes influencing $NADP^+$ and $NADP^+$/NADPH status. The evidence we provide linking novel loci with the glutathione redox system underscores the physiological relevance to humans, whose glutathione redox balance has previously been found to vary based on genetic background [527]. Moreover, these findings emphasize the importance of considering genetic background in glutathione redox studies. GSH metabolism and its related NADPH cofactor are critical to longevity and delay of chronic disease onset, and thus it is imperative that we better understand their genetic regulation to identify if certain genes and alleles confer resistance or susceptibility to oxidative stress and disease. This study utilized precise systems genetics to understand the genetic regulation of the GSH and NADPH redox systems and represents a new framework for investigating biochemical systems using a forward-genetics approach.

Supplementary Table S3.1. Descriptive statistics for weights of DO mice.

Phenotype:	N	x̄	Median	SD	Min	Max
Body Weight (g)	347	39.545	39.000	8.679	18.500	64.800
Liver Weight (g)	347	1.723	1.645	0.520	0.662	3.720
Liver Weight/Body Weight (%)	347	4.337	4.262	0.712	2.641	7.190

Supplementary Table S3.2. Descriptive statistics for weights of male DO mice.

Phenotype:	N	x̄	Median	SD	Min	Max
Body Weight (g)	172	42.832	42.300	7.809	25.700	64.800
Liver Weight (g)	172	1.986	1.874	0.510	1.091	3.720
Liver Weight/Body Weight (%)	172	4.629	4.604	0.700	3.262	7.190

Supplementary Table S3.3. Descriptive statistics for weights of female DO mice.

Phenotype:	N	x̄	Median	SD	Min	Max
Body Weight (g)	175	36.315	35.200	8.288	18.500	60.600
Liver Weight (g)	175	1.464	1.394	0.383	0.662	2.915
Liver Weight/Body Weight (%)	175	4.050	4.022	0.600	2.641	6.201

Supplementary Table S3.4. Databases queried for biological annotations for candidate gene prioritization.
*Resource accessed through the Mouse Genome Informatics website (MGI; http://www.informatics.jax.org/). **Datasets include GRCm38.p6 (mouse) and GRCh38.p13 (humans).

Database (Abbreviation)	Annotation Type	URL	Reference
EBI Expression Atlas (EEA) *	Expression	https://www.ebi.ac.uk/gxa/home/	[564]
Gene eXpression Database (GXD) *	Expression	http://www.informatics.jax.org/expression.shtml	[565]
InterPro	Functional	http://www.ebi.ac.uk/interpro/	[567]
Gene Ontology (GO) *	Functional	http://www.geneontology.org/	[568, 569]
Ensembl BioMart**	Phenotypic	https://m.ensembl.org/info/data/biomart/	[571]
PheWeb	Phenotypic	http://pheweb.sph.umich.edu/	[570]

Supplementary Table S3.5. Descriptive statistics for hepatic redox system metabolites in male DO mice.

Phenotype:	N	$\bar{x}$	Median	SD	Min	Max
Total Glutathione (nmol/mg)	171	49.311	44.404	20.872	10.183	117.232
GSH (nmol/mg)	171	47.975	43.243	20.307	9.843	113.359
GSSG (nmol/mg)	172	0.672	0.586	0.379	0.153	2.288
GSH/GSSG	171	78.643	76.275	25.182	34.344	169.761
E_h (mV)	171	-196.293	-196.157	7.829	-214.418	-166.948
NADPH (pmol/µg)	171	0.331	0.295	0.164	0.026	0.898
$NADP^+$ (pmol/µg)	156	0.765	0.727	0.329	0.157	2.006
$NADP^+$/NADPH	155	3.421	2.392	3.752	0.460	34.344
NADH (pmol/µg)	157	2.710	2.835	1.082	0.293	5.394

Supplementary Table S3.6. Descriptive statistics for hepatic redox system metabolites in female DO mice.

Phenotype:	**N**	**$\bar{x}$**	**Median**	**SD**	**Min**	**Max**
Total Glutathione (nmol/mg)	175	42.656	41.289	16.864	11.813	105.566
GSH (nmol/mg)	175	41.489	40.335	16.437	11.532	103.986
GSSG (nmol/mg)	175	0.583	0.523	0.305	0.140	1.925
GSH/GSSG	175	77.473	74.137	25.119	31.894	177.181
E_h (mV)	175	-194.287	-195.026	7.476	-215.556	-174.872
NADPH (pmol/µg)	164	0.191	0.154	0.145	0.011	0.730
$NADP^+$ (pmol/µg)	175	1.174	1.062	0.456	0.401	2.575
$NADP^+$/NADPH	164	16.000	6.260	25.518	1.036	161.363
NADH (pmol/µg)	175	2.858	2.753	1.354	0.304	7.572

Supplementary Table S3.7. GSH/GSSG candidate genes and their relevant annotations (Chr16:8.865–10.077 ± 1 Mbp; GRCm38/mm10).[a]

				Expression		Functional		Phenotypic (liver-related)		
MGI Gene symbol	**Genome coordinates (strand)**	**Type**	**Known glutathione gene**	**GXD (MGI)**	**EEA**	**Inter Pro**	**GO**	**PW**	**EBM**	**Relevance to hepatic GSH redox system[b]**
Rbfox1	Chr16:5885355-7411526 (+)	protein coding gene	No	--	--	--	--	--	--	None
Gm29854	Chr16:7767891-7771595 (+)	lncRNA gene	No	--	--	--	--	--	--	None – predicted gene
Gm49534	Chr16:7870102-7879859 (+)	lncRNA gene	No	--	--	--	--	--	--	None – predicted gene
Gm23476	Chr16:8203975-8204248 (+)	unclassified non-coding RNA gene	No	--	--	--	--	--	--	None – predicted gene
Gm26159	Chr16:8336993-8337096 (+)	snRNA gene	No	--	--	--	--	--	--	None – predicted gene
Gm29936	Chr16:8338906-8365012 (-)	lncRNA gene	No	--	--	--	--	--	--	None – predicted gene
Gm24579	Chr16:8402814-8402945 (+)	snoRNA gene	No	--	--	--	--	--	--	None – predicted gene
Tmem114	Chr16:8409276-8425136 (-)	protein coding gene	No	X	--	--	X	--	--	Expressed in mouse liver; GO:0016324; GO:0016327; GO:0008150; GO:0016021; GO:0016020; GO:0003674; GO:0005886
Gm25782	Chr16:8449498-8449786 (-)	unclassified non-coding RNA gene	No	--	X	--	--	--	--	Expressed in mouse liver
Gm30012	Chr16:8457687-8471155 (-)	lncRNA gene	No	--	--	--	--	--	--	None – predicted gene
Mettl22	Chr16:8470757-8490205 (+)	protein coding gene	No	X	X	--	--	--	--	Expressed in mouse liver

Gm23706	Chr16:8480660-8480741 (-)	snoRNA gene	No	--	X	--	--	--	--	Expressed in mouse liver
Abat	Chr16:8513429-8621568 (+)	protein coding gene	No	X	X	--	--	--	--	Expressed in mouse liver
Gm9851	Chr16:8618949-8621218 (-)	protein coding gene	No	--	--	--	--	--	--	None – predicted gene
Gm22137	Chr16:8623163-8623270 (-)	miRNA gene	No	--	X	--	--	--	--	Expressed in mouse liver
Tmem186	Chr16:8633731-8637711 (-)	protein coding gene	No	X	X	--	--	--	--	Expressed in mouse liver
Pmm2	Chr16:8637613-8657608 (+)	protein coding gene	No	X	X	--	--	--	--	Expressed in mouse liver
Carhsp1	Chr16:8658580-8672153 (-)	protein coding gene	No	X	X	--	--	--	--	Expressed in mouse liver
Gm5767	Chr16:8680770-8683911 (+)	protein coding gene	No	--	X	--	X	--	--	Expressed in mouse liver; GO:0008150; GO:0005575; GO:0003674
Usp7	Chr16:8688722-8757067 (-)	protein coding gene	No	--	--	--	--	--	--	None
Gm25805	Chr16:8766169-8766276 (-)	snRNA gene	No	--	X	--	--	--	--	Expressed in mouse liver
1810013L24Rik	Chr16:8830100-8858922 (+)	protein coding gene	No	--	X	--	X	--	--	Expressed in mouse liver; GO:0008150; GO:0005575; GO:0003674
Gm22224	Chr16:8873079-8873171 (-)	rRNA gene	No	--	X	--	--	--	--	Expressed in mouse liver
Gm30310	Chr16:8881614-8896050 (+)	lncRNA gene	No	--	--	--	--	--	--	None – predicted gene
Gm30371	Chr16:8961301-8969900 (+)	lncRNA gene	No	--	--	--	--	--	--	None – predicted gene
Gm30444	Chr16:8997527-9007799 (+)	lncRNA gene	No	--	--	--	--	--	--	None – predicted gene
Gm30567	Chr16:9054647-9055420 (+)	lncRNA gene	No	--	X	--	--	--	--	Expressed in mouse liver
Gm49448	Chr16:9079396-9137444 (+)	lncRNA gene	No	--	--	--	--	--	--	None – predicted gene

Gm49451	Chr16:9.15877-9.162334 (+)	lncRNA gene	No	--	--	--	--	--	--	None – predicted gene
Gm41418	Chr16:9.279972-9.290565 (+)	lncRNA gene	No	--	--	--	--	--	--	None – predicted gene
Grin2a	Chr16:9567898-9995560 (-)	protein coding gene	No	X	X	--	--	--	--	Expressed in mouse liver
2900045O03Rik	Chr16:9935230-9935830 (-)	unclassified non-coding RNA gene	No	--	--	--	--	--	--	None
Gm30668	Chr16:9997209-10005988 (-)	lncRNA gene	No	--	--	--	--	--	--	None – predicted gene
Rpl39l	Chr16:10.170197-10.174911 (+)	protein coding gene	No	--	X	--	X	--	--	Expressed in mouse liver; GO:0022625
Gm49455	Chr16:10.186293-10.227524 (-)	lncRNA gene	No	--	--	--	--	--	--	None – predicted gene
Atf7ip2	Chr16:10192649-10250731 (+)	protein coding gene	No	X	X	--	X	X	--	Expressed in mouse liver; Associated with cancer of liver and intrahepatic bile duct; GO:0008150; GO:0003674; GO:0005634
Gm24667	Chr16:10237918-10238020 (+)	snRNA gene	No	--	X	--	--	--	--	Expressed in mouse liver
Gm22932	Chr16:10273750-10273821 (+)	miRNA gene	No	--	X	--	--	--	--	Expressed in mouse liver
2310063J23Rik	Chr16:10276947-10277122 (-)	unclassified gene	No	--	--	--	--	--	--	None – predicted gene
Emp2	Chr16:10281749-10313968(-)	protein coding gene	No	X	X	--	--	--	--	Expressed in mouse liver
Gm1600	Chr16:10324105-10331285 (-)	lncRNA gene	No	--	X	--	--	--	--	Expressed in mouse liver; GO:0008150; GO:0005575; GO:0003674
Gm30724	Chr16:10349642-10353405 (+)	lncRNA gene	No	--	--	--	--	--	--	None – predicted gene
Tekt5	Chr16:10357952-10395455 (-)	protein coding gene	No	X	X	--	--	--	--	Expressed in mouse liver

Gm41419	Chr16:10371350-10378925 (+)	lncRNA gene	No	--	--	--	--	--	--	None – predicted gene
Nubp1	Chr16:10411948-10424428 (+)	protein coding gene	No	X	X	X	X	--	--	Expressed in mouse liver; GO:0051539; GO:0005524; GO:0042995; GO:0030030; GO:0006879; GO:0051642; GO:0005929; GO:0005737; GO:0005856; GO:0005829; GO:0016226; GO:0051536; GO:0046872; GO:0010826; GO:0000166; GO:0005634; GO:0005886; GO:0005515; GO:0072697; GO:0001558
Tvp23a	Chr16:10420557-10447362 (-)	protein coding gene	No	--	X	--	X	--	--	Expressed in mouse liver; GO:0030173; GO:0003674; GO:0009306; GO:0016192
Gm41420	Chr16:10470003-10473103 (+)	lncRNA gene	No	--	--	--	--	--	--	None – predicted gene
Ciita	Chr16:10480059-10528418 (+)	protein coding gene	No	X	X	X	X	--	--	Expressed in mouse liver; GO:0033613; GO:0005524; GO:0009986; GO:0005829; GO:0005525; GO:0006954; GO:0016301; GO:0000122; GO:0045892; GO:0046597; GO:0005654; GO:0000166; GO:0005634; GO:0016310; GO:0016605; GO:0045345; GO:0045348; GO:0045944; GO:0045893; GO:0044877; GO:0008022; GO:0006355; GO:0046677; GO:0034341; GO:0000976; GO:0016740; GO:0016746
Dexi	Chr16:10530207-10543054 (-)	protein coding gene	No	X	X	--	--	--	--	Expressed in mouse liver

Clec16a	Chr16:10545339-10744878 (+)	protein coding gene	No	X	X	X	X	--	--	Expressed in mouse liver; GO:0006914; GO:0009267; GO:0005829; GO:0036020; GO:0016197; GO:0005768; GO:0008333; GO:0005794; GO:0016021; GO:0005770; GO:0005764; GO:0016020; GO:1901097; GO:1904766; GO:1901525; GO:0032435; GO:1901098; GO:1904263; GO:0005515; GO:1901096; GO:0031982
Gm15558	Chr16:10669248-10683539 (-)	lncRNA gene	No	--	X	--	--	--	--	Expressed in mouse liver
Socs1	Chr16:10783808-10785536 (-)	protein coding gene	No	X	X	X	X	--	X	Expressed in mouse liver; GO:0046935; GO:0071230; GO:0071345; GO:0071407; GO:0019221; GO:0005737; GO:0036464; GO:0031410; GO:0045444; GO:0005159; GO:0035556; GO:0019210; GO:0043377; GO:0046627; GO:0046426; GO:0009968; GO:0042532; GO:0005654; GO:0005634; GO:0005942; GO:0046854; GO:0043372; GO:0045591; GO:0005515; GO:0019901; GO:0007259; GO:0010533; GO:0001817; GO:0040008; GO:0060334; GO:0043551; GO:0001932; GO:0046425; GO:0042509; Associated with enlarged liver, hepatic steatosis, hepatic necrosis, liver degeneration, and liver inflammation (EBM)

Tnp2	Chr16:10787935-10788655 (-)	protein coding gene	No	--	--	--	--	--	--	None
Prm3	Chr16:10790508-10790914 (-)	protein coding gene	No	--	X	--	X	--	--	Expressed in mouse liver; GO:0030154; GO:0005694; GO:0030261; GO:0005737; GO:0003677; GO:0030317; GO:0007275; GO:0000786; GO:0005634; GO:0007283
Prm2	Chr16:10791377-10792105 (-)	protein coding gene	No	--	X	--	X	--	--	Expressed in mouse liver; GO:0030154; GO:0005694; GO:0030261; GO:0003677; GO:0006323; GO:0007275; GO:0000786; GO:0005634; GO:0006997; GO:0007286; GO:0007283
Gm46564	Chr16:Syntenic	lncRNA gene	No	--	--	--	--	--	--	None – predicted gene
Prm1	Chr16:10796332-10796823 (-)	protein coding gene	No	X	X	--	--	--	--	Expressed in mouse liver
Gm46563	Chr16:10797943-10812726 (+)	lncRNA gene	No	--	X	--	--	--	--	Expressed in mouse liver
Gm11172	Chr16:10812915-10812994 (+)	protein coding gene	No	--	--	--	--	--	--	None – predicted gene
Gm26822	Chr16:10827927-10833507 (+)	lncRNA gene	No	--	--	--	--	--	--	None – predicted gene
Rmi2	Chr16:10835059-10843235 (+)	protein coding gene	No	X	X	--	--	--	--	Expressed in mouse liver
Gm21859	Chr16:10912012-10914797 (-)	lncRNA gene	No	--	--	--	--	--	--	None – predicted gene
Litaf	Chr16:10959273-1099312 (-)	protein coding gene	No	X	X	X	X	--	--	Expressed in mouse liver; GO: 0071222; GO:0005737; GO:0098559; GO:0098560; GO:0098574; GO:0009898; GO:0003677; GO:0001228; GO:0005768; GO:0005794; GO:0043231; GO:0005765;

										GO:0005764; GO:0016020; GO:0046872; GO:1901223; GO:0005654; GO:0005634; GO:0005886; GO:0045944; GO:0005515; GO:0001817; GO:0032496; GO:0000978; GO:0050699; GO:0008270
Gm26268	Chr16:10965724-10965849 (+)	miRNA gene	No	X	X	--	--	--	--	Expressed in mouse liver
Gm19955	Chr16:10975209-10977392 (-)	unclassified gene	No	--	--	--	--	--	--	None – predicted gene
Gm24961	Chr16:10994386-10994569 (+)	snRNA gene	No	--	--	--	--	--	--	None – predicted gene

[a] Resource abbreviations: **EBM,** Ensembl BioMart; **EEA,** EBI Expression Atlas; **GO,** Gene Ontology; **GXD,** Gene eXpression Database; **MGI,** Mouse Genome Informatics; **PW,** PheWeb

[b] ID terms: **GO:0016324:** apical plasma membrane; **GO:0016327:** apicolateral plasma membrane; **GO:0008150:** biological process; **GO:0016021:** integral component of membrane; **GO:0016020:** membrane; **GO:0003674:** molecular function; **GO:0022625:** cytosolic large ribosomal subunit; **GO:0005886:** plasma membrane; **GO:0005575:** cellular_component; **GO:0005829:** cytosol; **GO:0005634:** nucleus; **GO:0008022:** protein C-terminus binding; **GO:0051539:** 4 iron, 4 sulfur cluster binding; **GO:0042995:** cell projection; **GO:0030030:** cell projection organization; **GO:0006879:** cellular iron ion homeostasis; **GO:0051642:** centrosome localization; **GO:0005929:** cilium; **GO:0005856:** cytoskeleton; **GO:0016226:** iron-sulfur cluster assembly; **GO:0051536:** iron-sulfur cluster binding; **GO:0010826:** negative regulation of centrosome duplication; **GO:0072697:** protein localization to cell cortex; **GO:0001558:** regulation of cell growth; **GO:0030173:** integral component of Golgi membrane; **GO:0009306:** protein secretion; **GO:0016192:** vesicle-mediated transport; **GO:0033613:** activating transcription factor binding; **GO:0005524:** ATP binding; **GO:0009986:** cell surface; **GO:0005525:** GTP binding; **GO:0006954:** inflammatory response; **GO:0016301:** kinase activity; **GO:0000122:** negative regulation of transcription by RNA polymerase II; **GO:0045892:** negative regulation of transcription, DNA-templated; **GO:0046597:** negative regulation of viral entry into host cell; **GO:0000166:** nucleotide binding; **GO:0016310:** phosphorylation; **GO:0016605:** PML body; **GO:0045345:** positive regulation of MHC class I biosynthetic process; **GO:0045348:** positive regulation of MHC class II biosynthetic process; **GO:0045893:** positive regulation of transcription, DNA-templated; **GO:0044877:** protein-containing complex binding; **GO:0006355:** regulation of transcription, DNA-templated; **GO:0046677:** response to antibiotic; **GO:0034341:** response to interferon-gamma; **GO:0000976:** transcription regulatory region sequence-specific DNA binding; **GO:0016740:** transferase activity; **GO:0016746:** transferase activity, transferring acyl groups; **GO:0006914:** autophagy; **GO:0009267:** cellular response to starvation; **GO:0036020:** endolysosome membrane; **GO:0016197:** endosomal transport; **GO:0008333:** endosome to lysosome transport; **GO:0005770:** late endosome; **GO:1901097:** negative regulation of autophagosome maturation; **GO:1904766:** negative regulation of

macroautophagy by TORC1 signaling; **GO:1901525:** negative regulation of mitophagy; **GO:0032435:** negative regulation of proteasomal ubiquitin-dependent protein catabolic process; **GO:1901098:** positive regulation of autophagosome maturation; **GO:1904263:** positive regulation of TORC1 signaling; **GO:1901096:** regulation of autophagosome maturation; **GO:0031982:** vesicle; **GO:0046935:** 1-phosphatidylinositol-3-kinase regulator activity; **GO:0071230:** cellular response to amino acid stimulus; **GO:0071345:** cellular response to cytokine stimulus; **GO:0071407:** cellular response to organic cyclic compound; **GO:0019221:** cytokine-mediated signaling pathway; **GO:0005737:** cytoplasm; **GO:0036464:** cytoplasmic ribonucleoprotein granule; **GO:0031410:** cytoplasmic vesicle; **GO:0045444:** fat cell differentiation; **GO:0005159:** insulin-like growth factor receptor binding; **GO:0035556:** intracellular signal transduction; **GO:0019210:** kinase inhibitor activity; **GO:0043377:** negative regulation of CD8-positive, alpha-beta T cell differentiation; **GO:0046627:** negative regulation of insulin receptor signaling pathway; **GO:0046426:** negative regulation of receptor signaling pathway via JAK-STAT; **GO:0009968:** negative regulation of signal transduction; **GO:0042532:** negative regulation of tyrosine phosphorylation of STAT protein; **GO:0005654:** nucleoplasm; **GO:0005942:** phosphatidylinositol 3-kinase complex; **GO:0046854:** phosphatidylinositol phosphorylation; **GO:0043372:** positive regulation of CD4-positive, alpha-beta T cell differentiation; **GO:0045591:** positive regulation of regulatory T cell differentiation; **GO:0005515:** protein binding; **GO:0019901:** protein kinase binding; **GO:0007259:** receptor signaling pathway via JAK-STAT; **GO:0010533:** regulation of activation of Janus kinase activity; **GO:0001817:** regulation of cytokine production**; GO:0032496:** response to lipopolysaccharide; **GO:0000978:** RNA polymerase II cis-regulatory region sequence-specific DNA binding; **GO:0050699:** WW domain binding; **GO:0008270:** zinc ion binding; **GO:0040008:** regulation of growth; **GO:0060334:** regulation of interferon-gamma-mediated signaling pathway; **GO:0043551:** regulation of phosphatidylinositol 3-kinase activity; **GO:0001932:** regulation of protein phosphorylation; **GO:0046425:** regulation of receptor signaling pathway via JAK-STAT; **GO:0042509:** regulation of tyrosine phosphorylation of STAT protein; **GO:0030154:** cell differentiation; **GO:0005694:** chromosome; **GO:0030261:** chromosome condensation; **GO:0030317:** flagellated sperm motility; **GO:0007275:** multicellular organism development; **GO:0000786:** nucleosome; **GO:0007283:** spermatogenesis; **GO:0006323:** DNA packaging; **GO:0006997:** nucleus organization; **GO:0007286:** spermatid development; **GO:0071222:** cellular response to lipopolysaccharide; **GO:0098559:** cytoplasmic side of early endosome membrane; **GO:0098560:** cytoplasmic side of late endosome membrane; **GO:0098574:** cytoplasmic side of lysosomal membrane; **GO:0009898:** cytoplasmic side of plasma membrane; **GO:0003677:** DNA binding; **GO:0001228:** DNA-binding transcription activator activity, RNA polymerase II-specific; **GO:0005768:** endosome; **GO:0005794:** Golgi apparatus; **GO:0043231:** intracellular membrane-bounded organelle; **GO:0005765:** lysosomal membrane; **GO:0005764:** lysosome; **GO:0046872:** metal ion binding; **GO:1901223:** negative regulation of NIK/NF-kappaB signaling; **GO:0045944:** positive regulation of transcription by RNA polymerase II

Supplementary Table S3.8. $NADP^+$ candidate genes and their relevant annotations (Chr3: 109.677–115.729 ± 1 Mbp; GRCm38/mm10).[a]

				Expression		Functional		Phenotypic (liver-related)		
MGI Gene symbol	**Genome coordinates (strand)**	**Type**	**Known $NADP^+$ gene**	**GXD**	**EEA**	**Inter Pro**	**GO**	**PW**	**EBM**	**Relevance to hepatic NADPH redox system[b]**
Clcc1	Chr3:108653913-108678840 (+)	protein coding gene	No	X	--	--	X	--	--	Expressed in mouse liver; GO:0005254; GO:0034707; GO:1902476; GO:0006821; GO:0005737; GO:0005783; GO:0005794; GO:0016021; GO:0043231; GO:0006811; GO:0016020; GO:0044233; GO:0005634
Gpsm2	Chr3:108678638-108722309 (-)	protein coding gene	No	X	X	X	X	--	--	Expressed in mouse liver; GO:0045177; GO:0005938; GO:0099738; GO:0007049; GO:0051301; GO:0005813; GO:0005737; GO:0005856; GO:0005829; GO:0070840; GO:0000132; GO:0005092; GO:0001965; GO:0030695; GO:0042802; GO:0097575; GO:0060487; GO:0051661; GO:0016020; GO:0007052; GO:0097431; GO:0000166; GO:0005886; GO:1904778; GO:1905832; GO:0005515; GO:0032991; GO:0008022;

										GO:0019904; GO:0043621; GO:0031291; GO:0060236
Gm27244	Chr3:108708908-108712653 (+)	lncRNA gene	No	--	--	--	--	--	--	None – predicted gene
Aknad1	Chr3:108739658-108782309 (+)	protein coding gene	No	X	--	X	X	--	--	Expressed in mouse liver; GO:0008150; GO:0003674
Stxbp3	Chr3:108793180-108840502 (-)	protein coding gene	No	X	--	--	X	--	--	Expressed in mouse liver; GO:0016324; GO:0016323; GO:0007420; GO:0001678; GO:0071346; GO:0005737; GO:0005829; GO:0006887; GO:0030073; GO:0006886; GO:0016020; GO:0045955; GO:0046325; GO:0007269; GO:0045335; GO:0005886; GO:0070527; GO:0031091; GO:0098793; GO:0005515; GO:0044877; GO:0022615; GO:0015031; GO:0032868; GO:0030141; GO:0042581; GO:0017075; GO:0019905; GO:0070820; GO:0006904; GO:0016192
Fndc7	Chr3:108853678-108890008 (-)	protein coding gene	No	--	--	--	--	--	--	None
Prpf38b	Chr3:108902805-108911727 (-)	protein coding gene	No	X	--	--	X	--	--	Expressed in mouse liver; GO:0006397; GO:0005634; GO:0071011; GO:0008380; GO:0005681
Henmt1	Chr3:108940059-108960774 (+)	protein coding gene	No	X	--	--	X	--	--	Expressed in mouse liver; GO:0005737; GO:0031047;

										GO:0046872; GO:0032259; GO:0008168; GO:0005634; GO:0008171; GO:0034587; GO:0030422; GO:0003723; GO:0001510; GO:0008173; GO:0090486; GO:0016740
Gm9857	Chr3:108939873-108940446 (-)	protein coding gene	No	--	--	--	--	--	--	None – predicted gene
Fam102b	Chr3:108970997-109027607 (-)	protein coding gene	No	X	--	--	X	--	--	Expressed in mouse liver; GO:0008150; GO:0005575; GO:0003674
Gm43221	Chr3:109000024-109002094 (+)	lncRNA gene	No	--	--	--	--	--	--	None – predicted gene
Gm44384	Chr3:109055634-109055747 (+)	miRNA gene	No	--	--	--	--	--	--	None – predicted gene
Gm36778	Chr3:109055708-109065353 (+)	lncRNA gene	No	--	--	--	--	--	--	None – predicted gene
4930408K08Rik	Chr3:109078590-109080414 (-)	lncRNA gene	No	--	--	--	--	--	--	None
Slc25a54	Chr3:109080499-109116582 (+)	protein coding gene	No	X	X	--	X	--	--	Expressed in mouse liver; GO:0005347; GO:0015867; GO:0033391; GO:0005829; GO:0005815; GO:0005739; GO:1901679
Gm19391	Chr3:109120533-109122895 (-)	lncRNA gene	No	--	--	--	--	--	--	None – predicted gene
Slc25a24	Chr3:109123149-109168409 (+)	protein coding gene	No	--	--	--	--	--	--	None
Vav3	Chr3:109340653-109685698 (+)	protein coding gene	No	X	X	X	X	--	--	Expressed in mouse liver; GO:0001525; GO:0050853; GO:0016477; GO:0030031;

										GO:0006974; GO:0005737; GO:0005154; GO:0005085; GO:0001772; GO:0007229; GO:0035556; GO:0030032; GO:0046872; GO:0030593; GO:0005886; GO:0030890; GO:0045785; GO:0043552; GO:0005515; GO:0043087; GO:0035023; GO:0042493; GO:0007264; GO:0006906
C130083B21Rik	Chr3:109450901-109454701 (+)	unclassified gene	No	--	--	--	--	--	--	None
Ntng1	Chr3:109780040-110144011 (-)	protein coding gene	No	X	--	--	X	--	--	Expressed in mouse liver; GO:0031225; GO:0046658; GO:0099029; GO:0009887; GO:0007409; GO:0070831; GO:0050839; GO:0098632; GO:0030154; GO:0016477; GO:0098978; GO:0043256; GO:0016020; GO:0050804; GO:0007275; GO:0007399; GO:0005886; GO:0005515; GO:2001222; GO:0150011; GO:0010975; GO:0098685; GO:0034446; GO:0099560; GO:0009888
Gm25681	Chr3:109863780-109863885 (+)	snRNA gene	No	--	--	--	--	--	--	None – predicted gene
Gm42516	Chr3:110243862-110244628 (-)	unclassified gene	No	--	--	--	--	--	--	None – predicted gene

Prmt6	Chr3:110246109-110250998 (-)	protein coding gene	No	X	--	X	X	--	--	Expressed in mouse liver; GO:0006974; GO:0090398; GO:0003682; GO:0006325; GO:0006281; GO:0008469; GO:0042393; GO:0034970; GO:0016571; GO:0042054; GO:0070612; GO:0070611; GO:0044020; GO:0032259; GO:0008168; GO:0031064; GO:0051572; GO:0000122; GO:0045892; GO:0005730; GO:0005654; GO:0005634; GO:0019919; GO:0035246; GO:0016274; GO:0035242; GO:0035241; GO:0005515; GO:0006479; GO:0010821; GO:1901796; GO:0016740
C130013H08Rik	Chr3:110250015-110253706 (+)	lncRNA gene gene	No	X	--	--	--	--	--	Expressed in mouse liver
Gm26076	Chr3:110564437-110564541 (-)	snRNA	No	--	--	--	--	--	--	None – predicted gene
Gm43404	Chr3:110634323-110636856 (+)	unclassified gene	No	--	--	--	--	--	--	None – predicted gene
Gm42905	Chr3:111789492-111791102 (+)	unclassified gene	No	--	--	--	--	--	--	None – predicted gene
Gm6602	Chr3:111881903-112082001 (+)	lncRNA gene	No	--	--	--	--	--	--	None – predicted gene
Gm25519	Chr3:112198915-112199041 (-)	snoRNA gene	No	--	--	--	--	--	--	None – predicted gene

1810008N23Rik	Chr3:113247453-113248289 (-)	unclassified non-coding RNA gene	No	--	--	--	--	--	--	None
Amy2a5	Chr3:113249178-113258699 (-)	protein coding gene	No	--	--	--	--	--	--	None
Amy2a4	Chr3:113279843-113291449 (-)	protein coding gene	No	--	--	--	--	--	--	None
Amy2a3	Chr3:113312455-113324052 (-)	protein coding gene	No	--	--	--	--	--	--	None
Amy2a2	Chr3:113345055-113356658 (-)	protein coding gene	No	--	--	--	--	--	--	None
Amy2a1	Chr3:113529403-113532428 (-)	protein coding gene	No	--	--	--	--	--	--	None
Gm46820	Chr3:Syntenic	lncRNA gene	No	--	--	--	--	--	--	None – predicted gene
Amy1	Chr3:113555952-113577750 (-)	protein coding gene	No	X	X	--	--	--	--	Expressed in mouse liver
Rnpc3	Chr3:113605067-113630149 (-)	protein coding gene	No	X	--	X	X	--	--	Expressed in mouse liver; GO:0000398; GO:0003676; GO:0005654; GO:0005634; GO:0097157; GO:0003723; GO:0030626; GO:0005689
C530020B09Rik	Chr3:113629853-113631283 (+)	unclassified non-coding RNA gene	No	--	--	--	--	--	--	None
Col11a1	Chr3:114030540-114220718 (+)	protein coding gene	No	X	X	--	--	--	--	Expressed in mouse liver
Gm23750	Chr3:114824154-114824285 (-)	snoRNA gene	No	--	--	--	--	--	--	None – predicted gene
Olfm3	Chr3:114904078-115125722 (+)	protein coding gene	No	X	--	X	X	--	--	Expressed in mouse liver; GO:0032281; GO:0030054;

										GO:0005576; GO:0005615; GO:0042462; GO:0005794; GO:0005515; GO:0045202
Gm22337	Chr3:115391554-115391685 (+)	snoRNA gene	No	--	--	--	--	--	--	None – predicted gene
Gm25347	Chr3:115484016-115484136 (-)	miRNA gene	No	--	--	--	--	--	--	None – predicted gene
Gm40124	Chr3:115636693-115641726(-)	lncRNA gene	No	--	--	--	--	--	--	None – predicted gene
S1pr1	Chr3:115710433-115715055 (-)	protein coding gene	No	X	X	--	--	--	--	Expressed in mouse liver
Gm9889	Chr3:115715150-115716728 (+)	lncRNA gene	No	--	--	--	--	--	--	None – predicted gene
A930005H10Rik	Chr3:115881581-115888130 (-)	lncRNA gene	No	X	--	--	X	--	--	Expressed in mouse liver; GO:0008150; GO:0005575; GO:0003674
Dph5	Chr3:115888116-115934361 (+)	protein coding gene	No	X	--	X	X	--	--	Expressed in mouse liver; GO:0005575; GO:0004164; GO:0032259; GO:0008168; GO:0017183; GO:0016740
A230060L02Rik	Chr3:115889261-115892275 (+)	unclassified gene	No	--	--	--	--	--	--	None
Gm42687	Chr3:115910370-115910533 (+)	unclassified gene	No	--	--	--	--	--	--	None – predicted gene
Gm43107	Chr3:115913809-115914063 (-)	unclassified gene	No	--	--	--	--	--	--	None – predicted gene
Gm43108	Chr3:115913890-115914182 (+)	unclassified gene	No	--	--	--	--	--	--	None – predicted gene
Slc30a7	Chr3:115938973-116007406 (-)	protein coding gene	No	X	--	X	X	--	--	Expressed in mouse liver; GO:0008324; GO:0006812; GO:0005737; GO:0031410;

										GO:0005794; GO:0016021; GO:0006811; GO:0016020; GO:0048471; GO:0055085; GO:0031982; GO:0008270; GO:0006829
Mir669n	Chr3:115979902-115979955 (+)	miRNA gene	No	--	--	--	--	--	--	None
Extl2	Chr3:116007462-116029017 (+)	protein coding gene	No	X	X	X	X	--	--	Expressed in mouse liver; GO:0035248; GO:0005829; GO:0005783; GO:0001888; GO:0047237; GO:0005539; GO:0016021; GO:0030145; GO:0016020; GO:0046872; GO:0006044; GO:0005654; GO:0006486; GO:0016740; GO:0016757; GO:0019276
Gm26344	Chr3:116065788-116065919 (-)	snoRNA gene	No	--	--	--	--	--	--	None – predicted gene
Gm31384	Chr3:116093593-116102373 (+)	lncRNA gene	No	--	--	--	--	--	--	None – predicted gene
Vcam1	Chr3:116110020-116129688 (-)	protein coding gene	No	X	X	X	X	--	--	Expressed in mouse liver; GO:0071065; GO:0009308; GO:0031225; GO:0045177; GO:0035584; GO:0060945; GO:0007155; GO:0050839; GO:0098609; GO:0140039; GO:0060326; GO:0007160; GO:0071944; GO:0009986; GO:1904646; GO:0071333; GO:0060710; GO:0005769; GO:0060669; GO:0005783;

										GO:0005615; GO:0030175; GO:0005794; GO:0007507; GO:0007157; GO:0034113; GO:0060384; GO:0016021; GO:0005887; GO:0005178; GO:0007159; GO:0050901; GO:0016020; GO:0005902; GO:0005886; GO:0002102; GO:0042102; GO:0008131; GO:0042383; GO:0016032; GO:0061032
Gm43109	Chr3:116128451-116141016 (+)	lncRNA gene	No	--	--	--	--	--	--	None – predicted gene
5330425B07Rik	Chr3:116148110-116149136 (+)	lncRNA gene	No	--	--	--	--	--	--	None
Gm26544	Chr3:116150479-116165821 (+)	lncRNA gene	No	--	--	--	--	--	--	None – predicted gene
Gm31651	Chr3:116200408-116202713 (+)	lncRNA gene	No	--	--	--	--	--	--	None – predicted gene
Gpr88	Chr3:116249654-116253503 (-)	protein coding gene	No	X	X	--	--	--	--	Expressed in mouse liver
Gm46839	Chr3:116257944-116269982 (+)	lncRNA gene	No	--	--	--	--	--	--	None – predicted gene
Cdc14a	Chr3:116272553-116428741 (-)	protein coding gene	No	X	X	X	X	--	--	Expressed in mouse liver; GO:0007049; GO:0051301; GO:0042995; GO:0005813; GO:0060271; GO:0005737; GO:0005856; GO:0005829; GO:0016311; GO:0016787; GO:1902636; GO:0060091; GO:0000226; GO:0000278;

										GO:0071850; GO:0072686; GO:0016604; GO:0005730; GO:0005654; GO:0005634; GO:0016791; GO:0004721; GO:0032467; GO:0006470; GO:0004722; GO:0004725; GO:0008138; GO:0007096; GO:0007605; GO:0000922; GO:0032426
Gm29151	Chr3:116350103-116352888 (+)	lncRNA gene	No	--	--	--	--	--	--	None – predicted gene
Gm40125	Chr3:116424251-116435432 (+)	lncRNA gene	No	--	--	--	--	--	--	None – predicted gene
Gm22361	Chr3:116448391-116448564 (-)	snRNA gene	No	--	--	--	--	--	--	None – predicted gene
Gm26358	Chr3:116466619-116466715 (+)	snoRNA gene	No	--	--	--	--	--	--	None – predicted gene
Rtca	Chr3:116488963-116508203 (-)	protein coding gene	No	X	--	--	X	--	--	Expressed in mouse liver; GO:0005524; GO:0003824; GO:0016874; GO:0005654; GO:0000166; GO:0005634; GO:0003963; GO:0006396
Gm26530	Chr3:Syntenic	lncRNA gene	No	--	--	--	--	--	--	None – predicted gene
Dbt	Chr3:116513070-116549981 (+)	protein coding gene	No	X	X	X	X	--	--	Expressed in mouse liver; GO:0016407; GO:0005737; GO:0005829; GO:0043754; GO:0031405; GO:0015630; GO:0042645; GO:0005739; GO:0016740; GO:0016746; GO:0031625

Gm43651	Chr3:116532149-116532587(+)	unclassified gene	No	--	--	--	--	--	--	None – predicted gene
Lrrc39	Chr3:116562973-116583134 (+)	protein coding gene	No	X	--	--	X	--	--	Expressed in mouse liver; GO:0005737; GO:0043231; GO:0004722; GO:0007165
Gm42940	Chr3:116572063-116574424 (-)	unclassified gene	No	X	--	--	--	--	--	Expressed in mouse liver
Trmt13	Chr3:116581093-116614587 (-)	protein coding gene	No	X	--	--	X	--	--	Expressed in mouse liver; GO:0005575; GO:0046872; GO:0032259; GO:0008168; GO:0016740; GO:0106050; GO:0030488; GO:0008175; GO:0008033
Sass6	Chr3:116594982-116631004 (+)	protein coding gene	No	X	--	--	X	--	--	Expressed in mouse liver; GO:0007049; GO:0034451; GO:0005814; GO:0007099; GO:0005813; GO:0051298; GO:0005737; GO:0005856; GO:0005829; GO:0098536
Gm42893	Chr3:116629173-116630984 (-)	lncRNA gene	No	--	--	--	--	--	--	None – predicted gene
Mfsd14a	Chr3:116631164-116662677 (-)	protein coding gene	No	X	X	--	--	--	--	Expressed in mouse liver
Gm42457	Chr3:116631671-116632209 (+)	lncRNA gene	No	--	--	--	--	--	--	None – predicted gene
Gm43191	Chr3:116641902-116681260 (-)	protein coding gene	No	--	--	--	--	--	--	None – predicted gene
4930512P04Rik	Chr3:116663732-116664155 (+)	lncRNA gene	No	X	--	--	--	--	--	Expressed in mouse liver
Slc35a3	Chr3:116669469-116712708 (-)	protein coding gene	No	X	--	--	X	--	--	Expressed in mouse liver; GO:0008643; GO:0005794;

										GO:0000139; GO:0030173; GO:0016021; GO:0016020; GO:0090481; GO:0015165; GO:0005459; GO:1990569
Gm40126	Chr3:116690388-116693380 (-)	lncRNA gene	No	--	--	--	--	--	--	None – predicted gene

[a] Resource abbreviations: **EBM,** Ensembl BioMart; **EEA,** EBI Expression Atlas; **GO,** Gene Ontology; **GXD,** Gene eXpression Database; **MGI,** Mouse Genome Informatics; **PW,** PheWeb

[b] ID terms: **GO:0005254:** chloride channel activity; **GO:0034707:** chloride channel complex; **GO:1902476:** chloride transmembrane transport; **GO:0006821:** chloride transport; **GO:0005737:** cytoplasm; **GO:0005783:** endoplasmic reticulum; **GO:0005794:** Golgi apparatus; **GO:0016021:** integral component of membrane; **GO:0043231:** intracellular membrane-bounded organelle; **GO:0006811:** ion transport; **GO:0016020:** membrane; **GO:0044233:** mitochondria-associated endoplasmic reticulum membrane; **GO:0005634:** nucleus; **GO:0045177:** apical part of cell; **GO:0005938:** cell cortex; **GO:0099738:** cell cortex region; **GO:0007049:** cell cycle; **GO:0051301:** cell division; **GO:0005813:** centrosome; **GO:0005856:** cytoskeleton; **GO:0005829:** cytosol; **GO:0070840:** dynein complex binding; **GO:0000132:** establishment of mitotic spindle orientation; **GO:0005092:** GDP-dissociation inhibitor activity; **GO:0001965:** G-protein alpha-subunit binding; **GO:0030695:** GTPase regulator activity; **GO:0042802:** identical protein binding; **GO:0097575:** lateral cell cortex; **GO:0060487:** lung epithelial cell differentiation; **GO:0051661:** maintenance of centrosome location; **GO:0007052:** mitotic spindle organization; **GO:0097431:** mitotic spindle pole; **GO:0000166:** nucleotide binding; **GO:0005886:** plasma membrane; **GO:1904778:** positive regulation of protein localization to cell cortex; **GO:1905832:** positive regulation of spindle assembly; **GO:0005515:** protein binding; **GO:0032991:** protein-containing complex; **GO:0008022:** protein C-terminus binding; **GO:0019904:** protein domain specific binding; **GO:0043621:** protein self-association; **GO:0031291:** Ran protein signal transduction; **GO:0060236:** regulation of mitotic spindle organization; **GO:0008150:** biological_process; **GO:0003674:** molecular_function; **GO:0016324:** apical plasma membrane; **GO:0016323:** basolateral plasma membrane; **GO:0007420:** brain development; **GO:0001678:** cellular glucose homeostasis; **GO:0071346:** cellular response to interferon-gamma; **GO:0006887:** exocytosis; **GO:0030073:** insulin secretion; **GO:0006886:** intracellular protein transport; **GO:0045955:** negative regulation of calcium ion-dependent exocytosis; **GO:0046325:** negative regulation of glucose import; **GO:0007269:** neurotransmitter secretion; **GO:0045335:** phagocytic vesicle; **GO:0070527:** platelet aggregation; **GO:0031091:** platelet alpha granule; **GO:0098793:** presynapse; **GO:0044877:** protein-containing complex binding; **GO:0022615:** protein to membrane docking; **GO:0015031:** protein transport; **GO:0032868:** response to insulin; **GO:0030141:** secretory granule; **GO:0042581:** specific granule; **GO:0017075:** syntaxin-1 binding; **GO:0019905:** syntaxin binding; **GO:0070820:** tertiary granule; **GO:0006904:** vesicle docking involved in exocytosis; **GO:0016192:** vesicle-mediated transport; **GO:0006397:** mRNA processing; **GO:0071011:** precatalytic spliceosome; **GO:0008380:** RNA splicing; **GO:0005681:** spliceosomal complex; **GO:0031047:** gene silencing by RNA; **GO:0046872:** metal ion binding; **GO:0032259:** methylation; **GO:0008168:** methyltransferase activity; **GO:0008171:** O-methyltransferase activity; **GO:0034587:** piRNA metabolic process; **GO:0030422:**

production of siRNA involved in RNA interference; **GO:0003723:** RNA binding; **GO:0001510:** RNA methylation; **GO:0008173:** RNA methyltransferase activity; **GO:0090486:** small RNA 2'-O-methyltransferase; **GO:0016740:** transferase activity; **GO:0005575:** cellular_component; **GO:0005347:** ATP transmembrane transporter activity; **GO:0015867:** ATP transport; **GO:0033391:** chromatoid body; **GO:0005815:** microtubule organizing center; **GO:0005739:** mitochondrion; **GO:1901679:** nucleotide transmembrane transport; **GO:0001525:** angiogenesis; **GO:0050853:** B cell receptor signaling pathway; **GO:0016477:** cell migration; **GO:0030031:** cell projection assembly; **GO:0006974:** cellular response to DNA damage stimulus; **GO:0005154:** epidermal growth factor receptor binding; **GO:0005085:** guanyl-nucleotide exchange factor activity; **GO:0001772:** immunological synapse; **GO:0007229:** integrin-mediated signaling pathway; **GO:0035556:** intracellular signal transduction; **GO:0030032:** lamellipodium assembly; **GO:0030593:** neutrophil chemotaxis; **GO:0030890:** positive regulation of B cell proliferation; **GO:0045785:** positive regulation of cell adhesion; **GO:0043552:** positive regulation of phosphatidylinositol 3-kinase activity; **GO:0043087:** regulation of GTPase activity; **GO:0035023:** regulation of Rho protein signal transduction; **GO:0042493:** response to drug; **GO:0007264:** small GTPase mediated signal transduction; **GO:0006906:** vesicle fusion; **GO:0031225:** anchored component of membrane; **GO:0046658:** anchored component of plasma membrane; **GO:0099029:** anchored component of presynaptic active zone membrane; **GO:0009887:** animal organ morphogenesis; **GO:0007409:** axonogenesis; **GO:0070831:** basement membrane assembly; **GO:0050839:** cell adhesion molecule binding; **GO:0098632:** cell-cell adhesion mediator activity; **GO:0030154:** cell differentiation; **GO:0098978:** glutamatergic synapse; **GO:0043256:** laminin complex; **GO:0050804:** modulation of chemical synaptic transmission; **GO:0007275:** multicellular organism development; **GO:0007399:** nervous system development; **GO:2001222:** regulation of neuron migration; **GO:0150011:** regulation of neuron projection arborization; **GO:0010975:** regulation of neuron projection development; **GO:0098685:** Schaffer collateral - CA1 synapse; **GO:0034446:** substrate adhesion-dependent cell spreading; **GO:0099560:** synaptic membrane adhesion; **GO:0009888:** tissue development; **GO:0090398:** cellular senescence; **GO:0003682:** chromatin binding; **GO:0006325:** chromatin organization; **GO:0006281:** DNA repair; **GO:0008469:** histone-arginine N-methyltransferase activity; **GO:0042393:** histone binding; **GO:0034970:** histone H3-R2 methylation; **GO:0016571:** histone methylation; **GO:0042054:** histone methyltransferase activity; **GO:0070612:** histone methyltransferase activity (H2A-R3 specific); **GO:0070611:** histone methyltransferase activity (H3-R2 specific); **GO:0044020:** histone methyltransferase activity (H4-R3 specific); **GO:0031064:** negative regulation of histone deacetylation; **GO:0051572:** negative regulation of histone H3-K4 methylation; **GO:0000122:** negative regulation of transcription by RNA polymerase II; **GO:0045892:** negative regulation of transcription, DNA-templated; **GO:0005730:** nucleolus; **GO:0005654:** nucleoplasm; **GO:0019919:** peptidyl-arginine methylation, to asymmetrical-dimethyl arginine; **GO:0035246:** peptidyl-arginine N-methylation; **GO:0016274:** protein-arginine N-methyltransferase activity; **GO:0035242:** protein-arginine omega-N asymmetric methyltransferase activity; **GO:0035241:** protein-arginine omega-N monomethyltransferase activity; **GO:0006479:** protein methylation; **GO:0010821:** regulation of mitochondrion organization; **GO:1901796:** regulation of signal transduction by p53 class mediator; **GO:0000398:** mRNA splicing, via spliceosome; **GO:0003676:** nucleic acid binding; **GO:0097157:** pre-mRNA intronic binding; **GO:0030626:** U12 snRNA binding; **GO:0005689:** U12-type spliceosomal complex; **GO:0032281:** AMPA glutamate receptor complex; **GO:0030054:** cell junction; **GO:0005576:** extracellular region; **GO:0005615:** extracellular space; **GO:0042462:** eye photoreceptor cell development;

GO:0045202: synapse; **GO:0004164:** diphthine synthase activity; **GO:0017183:** peptidyl-diphthamide biosynthetic process from peptidyl-histidine; **GO:0008324:** cation transmembrane transporter activity; **GO:0006812:** cation transport; **GO:0031410:** cytoplasmic vesicle; **GO:0048471:** perinuclear region of cytoplasm; **GO:0055085:** transmembrane transport; **GO:0031982:** vesicle; **GO:0008270:** zinc ion binding; **GO:0006829:** zinc ion transport; **GO:0035248:** alpha-1,4-N-acetylgalactosaminyltransferase activity; **GO:0001888:** glucuronyl-galactosyl-proteoglycan 4-alpha-N-acetylglucosaminyltransferase activity; **GO:0047237:** glucuronylgalactosylproteoglycan 4-beta-N-acetylgalactosaminyltransferase activity; **GO:0005539:** glycosaminoglycan binding; **GO:0030145:** manganese ion binding; **GO:0006044:** N-acetylglucosamine metabolic process; **GO:0006486:** protein glycosylation; **GO:0016757:** transferase activity, transferring glycosyl groups; **GO:0019276:** UDP-N-acetylgalactosamine metabolic process; **GO:0071065:** alpha9-beta1 integrin-vascular cell adhesion molecule-1 complex; **GO:0009308:** amine metabolic process; **GO:0035584:** calcium-mediated signaling using intracellular calcium source; **GO:0060945:** cardiac neuron differentiation; **GO:0007155:** cell adhesion; **GO:0098609:** cell-cell adhesion; **GO:0140039:** cell-cell adhesion in response to extracellular stimulus; **GO:0060326:** cell chemotaxis; **GO:0007160:** cell-matrix adhesion; **GO:0071944:** cell periphery; **GO:0009986:** cell surface; **GO:1904646:** cellular response to amyloid-beta; **GO:0071333:** cellular response to glucose stimulus; **GO:0060710:** chorio-allantoic fusion; **GO:0005769:** early endosome; **GO:0060669:** embryonic placenta morphogenesis; **GO:0009897:** external side of plasma membrane; **GO:0030175:** filopodium; **GO:0007507:** heart development; **GO:0007157:** heterophilic cell-cell adhesion via plasma membrane cell adhesion molecules; **GO:0034113:** heterotypic cell-cell adhesion; **GO:0060384:** innervation; **GO:0005887:** integral component of plasma membrane; **GO:0005178:** integrin binding; **GO:0007159:** leukocyte cell-cell adhesion; **GO:0050901:** leukocyte tethering or rolling; **GO:0005902:** microvillus; **GO:0002102:** podosome; **GO:0042102:** positive regulation of T cell proliferation; **GO:0008131:** primary amine oxidase activity; **GO:0042383:** sarcolemma; **GO:0016032:** viral process; **GO:0061032:** visceral serous pericardium development; **GO:0042995:** cell projection; **GO:0060271:** cilium assembly; **GO:0016311:** dephosphorylation; **GO:0016787:** hydrolase activity; **GO:1902636:** kinociliary basal body; **GO:0060091:** kinocilium; **GO:0000226:** microtubule cytoskeleton organization; **GO:0000278:** mitotic cell cycle; **GO:0071850:** mitotic cell cycle arrest; **GO:0072686:** mitotic spindle; **GO:0016604:** nuclear body; **GO:0016791:** phosphatase activity; **GO:0004721:** phosphoprotein phosphatase activity; **GO:0032467:** positive regulation of cytokinesis; **GO:0006470:** protein dephosphorylation; **GO:0004722:** protein serine/threonine phosphatase activity; **GO:0004725:** protein tyrosine phosphatase activity; **GO:0008138:** protein tyrosine/serine/threonine phosphatase activity; **GO:0007096:** regulation of exit from mitosis; **GO:0007605:** sensory perception of sound; **GO:0000922:** spindle pole; **GO:0032426:** stereocilium tip; **GO:0005524:** ATP binding; **GO:0003824:** catalytic activity; **GO:0016874:** ligase activity; **GO:0003963:** RNA-3'-phosphate cyclase activity; **GO:0006396:** RNA processing; **GO:0016407:** acetyltransferase activity; **GO:0043754:** dihydrolipoyllysine-residue (2-methylpropanoyl)transferase activity; **GO:0031405:** lipoic acid binding; **GO:0015630:** microtubule cytoskeleton; **GO:0042645:** mitochondrial nucleoid; **GO:0016746:** transferase activity, transferring acyl groups; **GO:0031625:** ubiquitin protein ligase binding; **GO:0007165:** signal transduction; **GO:0005575:** cellular_component; **GO:0046872:** metal ion binding; **GO:0032259:** methylation; **GO:0008168:** methyltransferase activity; **GO:0016740:** transferase activity; **GO:0106050:** tRNA 2'-O-methyltransferase activity; **GO:0030488:** RNA methylation; **GO:0008175:** tRNA methyltransferase activity; **GO:0008033:** tRNA

processing; **GO:0034451:** centriolar satellite; **GO:0005814:** centriole; **GO:0007099:** centriole replication; **GO:0051298:** centrosome duplication; **GO:0098536:** deuterosome; **GO:0008643:** carbohydrate transport; **GO:0000139:** Golgi membrane; **GO:0030173:** integral component of Golgi membrane; **GO:0090481:** pyrimidine nucleotide-sugar transmembrane transport; **GO:0015165:** pyrimidine nucleotide-sugar transmembrane transporter activity; **GO:0005459:** UDP-galactose transmembrane transporter activity; **GO:1990569:** UDP-N-acetylglucosamine transmembrane transport

Supplementary Table S3.9. $NADP^+$/NADPH candidate genes and their relevant annotations (Chr12:28.562–29.394 ± 1 Mbp; GRCm38/mm10).[a]

				Expression		Functional		Phenotypic (liver-related)		
MGI Gene symbol	**Genome coordinates (strand)**	**Type**	**Known NADP(H) gene**	**GXD (MGI)**	**EEA**	**Inter Pro**	**GO**	**PW**	**EBM**	**Relevance to hepatic NADPH redox system[b]**
Gm30515	Chr12:27028993-27083546 (-)	lncRNA gene	No	--	--	--	--	--	--	None – predicted gene
Gm9866	Chr12:27140796-27160516 (-)	lncRNA gene	No	--	--	--	--	--	--	None – predicted gene
Gm30401	Chr12:27083550-27126264 (+)	lncRNA gene	No	--	--	--	--	--	--	None – predicted gene
Gm20187	Chr12:27090237-27114995 (-)	lncRNA gene	No	--	--	--	--	--	--	None – predicted gene
Gm40872	Chr12:27169772-27208051 (-)	lncRNA gene	No	--	--	--	--	--	--	None – predicted gene
Sox11	Chr12:27334264-27342574 (-)	protein coding gene	No	X	X	X	X	--	--	Expressed in mouse liver; GO:0009653; GO:0003211; GO:0030154; GO:0000987; GO:0061386; GO:0061303; GO:0003677; GO:0001228; GO:0003700; GO:0000981; GO:0048557; GO:0048704; GO:0061029; GO:0021782; GO:0014009; GO:0060022; GO:0002089; GO:0060174; GO:0060425; GO:0007275; GO:0060548; GO:0010629; GO:0060253; GO:0050672; GO:0000122; GO:2000678; GO:0007399; GO:0014032; GO:0001841; GO:0060563; GO:0030182; GO:0003357; GO:0005654; GO:0005634;

										GO:0003151; GO:0005886; GO:0030513; GO:0008284; GO:0010628; GO:0035332; GO:0046887; GO:2001111; GO:0050769; GO:0045666; GO:0045778; GO:0045669; GO:2000648; GO:0045944; GO:0045893; GO:0006355; GO:0000978; GO:0035914; GO:0001501; GO:0060023; GO:0061053; GO:0021510; GO:0048485; GO:0000976; GO:0060412
Gm30855	Chr12:27345154-27359081 (+)	lncRNA gene	No	--	--	--	--	--	--	None – predicted gene
Gm4166	Chr12:27598201-27615362 (+)	lncRNA gene	No	--	--	--	--	--	--	None – predicted gene
Gm24326	Chr12:27631803-27631927 (+)	snoRNA gene	No	--	--	--	--	--	--	None – predicted gene
Gm45941	Chr12:27946042-27982234 (+)	lncRNA gene	No	X	--	--	--	--	--	Expressed in mouse liver
Gm31025	Chr12:27995008-28010046 (+)	lncRNA gene	No	--	--	--	--	--	--	None – predicted gene
Gm46326	Chr12:28045318-28056040 (+)	lncRNA gene	No	--	--	--	--	--	--	None – predicted gene
Gm25923	Chr12:28060391-28060528 (-)	rRNA gene	No	X	--	--	--	--	--	Expressed in mouse liver
Gm47872	Chr12:28249759-28339409 (-)	lncRNA gene	No	--	--	--	--	--	--	None – predicted gene
Gm47871	Chr12:28320635-28321058 (-)	lncRNA gene	No	--	--	--	--	--	--	None – predicted gene
Gm25564	Chr12:28350263-28350394 (+)	snoRNA gene	No	--	--	--	--	--	--	None – predicted gene
Dcdc2c	Chr12:28437795-28552399 (-)	protein coding gene	No	--	--	--	--	--	--	None – predicted gene

1700022F17Rik	Chr12:28469868-28470623 (-)	protein coding gene	No	--	--	--	--	--	--	None
Allc	Chr12:28553755-28582523 (-)	protein coding gene	No	--	--	--	--	--	--	None
Colec11	Chr12:28594173-28623377 (-)	protein coding gene	No	X	--	--	--	X	--	Expressed in mouse liver; Associated with vitamin-B complex deficiency; GO:0019730; GO:0120153; GO:0005509; GO:0030246; GO:0005581; GO:0006956; GO:0001867; GO:0003677; GO:0005576; GO:0005615; GO:0042806; GO:0002376; GO:0045087; GO:0005537; GO:0046872; GO:0007275; GO:0070492
Rps7	Chr12:28630854-28635953 (-)	protein coding gene	No	X	--	--	--	X	--	Expressed in mouse liver; Associated with vitamin-B complex deficiency; GO:0030154; GO:0005813; GO:0005737; GO:0005856; GO:0022627; GO:0005622; GO:0003730; GO:0048027; GO:2000059; GO:1904667; GO:0001843; GO:0005730; GO:0005634; GO:0008266; GO:0010628; GO:1902255; GO:0032991; GO:0019901; GO:0050821; GO:1990904; GO:0042274; GO:0005840; GO:0006364; GO:0032040; GO:0003735; GO:0045202; GO:0006412; GO:1990948
Rnaseh1	Chr12:28649602-28659589 (+)	protein coding gene	No	X	X	X	X	X	--	Expressed in mouse liver; Associated with vitamin-B complex deficiency;

										GO:0005737; GO:0043137; GO:0004519; GO:0016787; GO:0042802; GO:0000287; GO:0046872; GO:0006264; GO:0005739; GO:0004518; GO:0003676; GO:0005634; GO:0004523; GO:0090502
Adi1	28675231-28682175 (+)	protein coding gene	No	X	X	--	X	X	--	Expressed in mouse liver; Associated with vitamin-B complex deficiency; GO:0010309; GO:0008652; GO:0005737; GO:0051213; GO:0019509; GO:0016020; GO:0046872; GO:0009086; GO:0006555; GO:0005634; GO:0016491; GO:0005886
Mir6937	Chr12:28679325-28679389 (+)	miRNA gene	No	--	--	--	--	--	--	None
Trappc12	Chr12:28690628-28750472 (-)	protein coding gene	No	X	--	--	--	--	--	Expressed in mouse liver
Gm31269	Chr12:28740601-28745568 (+)	lncRNA gene	No	--	--	--	--	--	--	None – predicted gene
Eipr1	Chr12:28751802-28867494 (+)	protein coding gene	No	X	X	--	--	--	--	Expressed in mouse liver
Gm46345	Chr12:28766912-28777111 (+)	protein coding gene	No	--	--	--	--	--	--	None – predicted gene
Gm48904	Chr12:28789669-28792612 (+)	unclassified gene	No	--	--	--	--	--	--	None – predicted gene
Gm48905	Chr12:28810138-28811191 (+)	lncRNA gene	No	--	--	--	--	--	--	None – predicted gene
Gm31333	Chr12:29141929-29199768 (+)	lncRNA gene	No	X	--	--	--	--	--	Expressed in mouse liver
Gm31508	Chr12:28910229-29041874 (+)	lncRNA gene	No	X	--	--	--	--	--	Expressed in mouse liver
Gm23342	Chr12:29035180-29035294 (-)	rRNA gene	No	--	--	--	--	--	--	None – predicted gene

4833405L11Rik	Chr12:29104487-29106850 (-)	lncRNA gene	No	--	--	--	--	--	--	None
Gm31569	Chr12:29205647-29278718 (+)	lncRNA gene	No	--	--	--	--	--	--	None – predicted gene
Gm31650	Chr12:29439514-29458362 (+)	lncRNA gene	No	--	--	--	--	--	--	None – predicted gene
Gm20208	Chr12:29526958-29531102 (-)	lncRNA gene	No	--	--	--	--	--	--	None – predicted gene
Myt1l	Chr12:29528384-29923213 (+)	protein coding gene	No	X	X	X	X	--	--	Expressed in mouse liver; GO:0030154; GO:0005694; GO:0050897; GO:0001228; GO:0003700; GO:0000981; GO:0001227; GO:0046872; GO:0007275; GO:0000122 ; GO:0007399; GO:0048666; GO:0030182; GO:0048663; GO:0048665; GO:0005634; GO:0045944; GO:0005515; GO:0006357; GO:0006355; GO:0044323; GO:0000978; GO:0000977; GO:0003713; GO:0140110; GO:0008270
C630031E19Rik	Chr12:29675630-29686445 (-)	lncRNA gene	No	--	--	--	--	--	--	None
C030014C12Rik	Chr12:29800369-29801178 (+)	unclassified gene	No	--	--	--	--	--	--	None
Gm46346	Chr12:29911433-29915292 (-)	lncRNA gene	No	--	--	--	--	--	--	None – predicted gene
Gm31939	Chr12:29925005-29937987 (-)	lncRNA gene	No	--	--	--	--	--	--	None – predicted gene
Pxdn	Chr12:29937608-30017658 (+)	protein coding gene	No	X	X	X	X	--	--	Expressed in mouse liver; GO:0019806; GO:0062023; GO:0030199; GO:0005783; GO:0030198; GO:0005201; GO:0005576; GO:0005615;

										GO:0020037; GO:0042744; GO:0046872; GO:0016491; GO:0004601; GO:0006979
Tpo	Chr12:30054659-30132624 (-)	protein coding gene	No	X	X	X	X	--	--	Expressed in mouse liver; GO:0005509; GO:0009986; GO:0035162; GO:0005615; GO:0020037; GO:0042446; GO:0042744; GO:0016021; GO:0004447; GO:0016020; GO:0046872; GO:0005739; GO:0016491; GO:0004601; GO:0005886; GO:0006979; GO:0006590
Gm15691	Chr12:30059657-30062113 (+)	lncRNA gene	No	--	--	--	--	--	--	None – predicted gene
Gm40873	Chr12:30133220-30135401 (-)	lncRNA gene	No	--	--	--	--	--	--	None – predicted gene
Gm32084	Chr12:30138447-30145820 (-)	lncRNA gene	No	--	--	--	--	--	--	None – predicted gene
Sntg2	Chr12:30174482-30373375 (-)	protein coding gene	No	X	--	--	--	--	--	Expressed in mouse liver; GO:0003779; GO:0005737; GO:0005856; GO:0016010; GO:0005622; GO:0016020; GO:0097109; GO:0005654; GO:0030165; GO:0005886; GO:0005515; GO:0005198
2310016D03Rik	Chr12:30410559-30467358 (-)	lncRNA gene	No	--	--	--	--	--	--	None
Gm25865	Chr12:30457968-30458071 (-)	miRNA gene	No	--	--	--	--	--	--	None – predicted gene
Gm28806	Chr12:30482822-30487052 (-)	lncRNA gene	No	--	--	--	--	--	--	None – predicted gene

[a] Resource abbreviations: **EBM,** Ensembl BioMart; **EEA,** EBI Expression Atlas; **GO,** Gene Ontology; **GXD,** Gene eXpression Database; **MGI,** Mouse Genome Informatics; **PW,** PheWeb

[b] ID terms: **GO:0009653:** anatomical structure morphogenesis; **GO:0003211:** cardiac ventricle formation; **GO:0030154:** cell differentiation; **GO:0000987:** cis-regulatory region sequence-specific DNA binding; **GO:0061386:** closure of optic fissure;

GO:0061303: cornea development in camera-type eye; **GO:0003677:** DNA binding; **GO:0001228:** DNA-binding transcription activator activity, RNA polymerase II-specific; **GO:0003700:** DNA-binding transcription factor activity; **GO:0000981:** DNA-binding transcription factor activity, RNA polymerase II-specific; **GO:0048557:** embryonic digestive tract morphogenesis; **GO:0048704:** embryonic skeletal system morphogenesis; **GO:0061029:** eyelid development in camera-type eye; **GO:0021782:** glial cell development; **GO:**0014009: glial cell proliferation; **GO:0060022:** hard palate development; **GO:0002089:** lens morphogenesis in camera-type eye; **GO:0060174:** limb bud formation; **GO:0060425:** lung morphogenesis; **GO:0007275:** multicellular organism development; **GO:0060548:** negative regulation of cell death; **GO:0010629:** negative regulation of gene expression; **GO:0060253:** negative regulation of glial cell proliferation; **GO:0050672:** negative regulation of lymphocyte proliferation; **GO:0000122:** negative regulation of transcription by RNA polymerase II; **GO:2000678:** negative regulation of transcription regulatory region DNA binding; **GO:0007399:** nervous system development; **GO:0014032:** neural crest cell development; **GO:0001841:** neural tube formation; **GO:0060563:** neuroepithelial cell differentiation; **GO:0030182:** neuron differentiation; **GO:0003357:** noradrenergic neuron differentiation; **GO:0005654:** nucleoplasm; **GO:0005634:** nucleus; **GO:0003151:** outflow tract morphogenesis; **GO:0005886:** plasma membrane; **GO:0030513:** positive regulation of BMP signaling pathway; **GO:0008284:** positive regulation of cell population proliferation; **GO:0010628:** positive regulation of gene expression; **GO:0035332:** positive regulation of hippo signaling; **GO:0046887:** positive regulation of hormone secretion; **GO:2001111:** positive regulation of lens epithelial cell proliferation; **GO:0050769:** positive regulation of neurogenesis; **GO:0045666:** positive regulation of neuron differentiation; **GO:0045778:** positive regulation of ossification; **GO:0045669:** positive regulation of osteoblast differentiation; **GO:2000648:** positive regulation of stem cell proliferation; **GO:0045944:** positive regulation of transcription by RNA polymerase II; **GO:0045893:** positive regulation of transcription, DNA-templated; **GO:0006355:** regulation of transcription, DNA-templated; **GO:0000978:** RNA polymerase II cis-regulatory region sequence-specific DNA binding; **GO:0035914:** skeletal muscle cell differentiation; **GO:0001501:** skeletal system development; **GO:0060023:** soft palate development; **GO:0061053:** somite development; **GO:0021510:** spinal cord development; **GO:0048485:** sympathetic nervous system development; **GO:0000976:** transcription regulatory region sequence-specific DNA binding; **GO:0060412:** ventricular septum morphogenesis; **GO:0019730:** antimicrobial humoral response; **GO:0120153:** calcium-dependent carbohydrate binding; **GO:0005509:** calcium ion binding; **GO:0030246:** carbohydrate binding; **GO:0005581:** collagen trimer; **GO:0006956:** complement activation; **GO:0001867:** complement activation, lectin pathway; **GO:0005576:** extracellular region; **GO:0005615:** extracellular space; **GO:0042806:** fucose binding; **GO:0002376:** immune system process; **GO:0045087:** innate immune response; **GO:0005537:** mannose binding; **GO:0046872:** metal ion binding; **GO:0070492:** oligosaccharide binding; **GO:0005813:** centrosome; **GO:0005737:** cytoplasm; **GO:0005856:** cytoskeleton; **GO:0022627:** cytosolic small ribosomal subunit; **GO:0005622:** intracellular anatomical structure; **GO:0003730:** mRNA 3'-UTR binding; **GO:0048027:** mRNA 5'-UTR binding; **GO:2000059:** negative regulation of ubiquitin-dependent protein catabolic process; **GO:1904667:** negative regulation of ubiquitin protein ligase activity; **GO:0001843:** neural tube closure; **GO:0005730:** nucleolus; **GO:0008266:** poly(U) RNA binding; **GO:1902255:** positive regulation of intrinsic apoptotic signaling pathway by p53 class mediator; **GO:0032991:** protein-containing complex; **GO:0019901:** protein kinase binding; **GO:0050821:** protein stabilization; **GO:1990904:** ribonucleoprotein complex; **GO:0042274:** ribosomal small

subunit biogenesis; **GO:0005840:** ribosome; **GO:0006364:** rRNA processing; **GO:0032040:** small-subunit processome; **GO:0003735:** structural constituent of ribosome; **GO:0045202:** synapse; **GO:0006412:** translation; **GO:1990948:** ubiquitin ligase inhibitor activity; **GO:0043137:** DNA replication, removal of RNA primer; **GO:0004519:** endonuclease activity; **GO:0016787:** hydrolase activity; **GO:0042802**: identical protein binding; **GO:0000287:** magnesium ion binding; **GO:0006264:** mitochondrial DNA replication; **GO:0005739:** mitochondrion; **GO:0004518:** nuclease activity; **GO:0003676:** nucleic acid binding; **GO:0004523:** RNA-DNA hybrid ribonuclease activity; **GO:0090502:** RNA phosphodiester bond hydrolysis, endonucleolytic; **GO:0010309:** acireductone dioxygenase [iron(II)-requiring] activity; **GO:0008652:** cellular amino acid biosynthetic process; **GO:0051213:** dioxygenase activity; **GO:0019509:** L-methionine salvage from methylthioadenosine; **GO:0016020:** membrane; **GO:0009086:** methionine biosynthetic process; **GO:0006555:** methionine metabolic process; **GO:0016491:** oxidoreductase activity; **GO:0005694:** chromosome; **GO:0050897:** cobalt ion binding; **GO:0001227:** DNA-binding transcription repressor activity, RNA polymerase II-specific; **GO:0048666:** neuron development; **GO:0048663:** neuron fate commitment; **GO:0048665:** neuron fate specification; **GO:0005515:** protein binding; **GO:0006357:** regulation of transcription by RNA polymerase II; **GO:0044323:** retinoic acid-responsive element binding; **GO:0000977:** RNA polymerase II transcription regulatory region sequence-specific DNA binding; **GO:0003713:** transcription coactivator activity; **GO:0140110**: transcription regulator activity; **GO:0008270:** zinc ion binding; **GO:0019806:** bromide peroxidase activity; **GO:0062023:** collagen-containing extracellular matrix; **GO:0030199:** collagen fibril organization; **GO:0005783:** endoplasmic reticulum; **GO:0030198:** extracellular matrix organization; **GO:0005201:** extracellular matrix structural constituent; **GO:0020037:** heme binding; **GO:0042744:** hydrogen peroxide catabolic process; **GO:0004601:** peroxidase activity; **GO:0006979:** response to oxidative stress; **GO:0009986:** cell surface; **GO:0035162:** embryonic hemopoiesis; **GO:0042446:** hormone biosynthetic process; **GO:0016021:** integral component of membrane; **GO:0004447:** iodide peroxidase activity; **GO:0006590:** thyroid hormone generation; **GO:0003779:** actin binding; **GO:0016010:** dystrophin-associated glycoprotein complex; **GO:0097109:** neuroligin family protein binding; **GO:0030165:** PDZ domain binding; **GO:0005198:** structural molecule activity

Supplementary Table S3.10. Results of high-resolution association mapping of hepatic GSH and NADPH redox systems. Significant QTL position and respective Bayesian credible interval included in parentheses in Mbp. Peaks with LOD scores > 6 included within the table. Total glutathione, GSH, and GSSG standardized to nmol/mg. E_h expressed in mV. NADH, $NADP^+$ and NADPH standardized to pmol/µg.

Phenotype	LOD	Chr	QTL Position (Mbp)	QTL Position (cM)	p-value	Marker ID
Total Glutathione	6.748	14	22.506 (22.058 – 22.528)	12.355 (12.035 – 12.377)	p < 0.30	UNC23688811
Total Glutathione	6.011	18	51.537 (35.120 – 76.532)	28.097 (18.887 – 51.726)	p < 0.70	UNCHS046265
GSH	6.755	14	22.506 (22.058 – 22.528)	12.355 (12.035 – 12.377)	p < 0.35	UNC23688811
GSSG	6.283	1	21.043 (18.793 – 22.050)	6.502 (5.847 – 8.186)	p < 0.50	JAX00243875
GSSG	6.178	2	91.523 (78.897 – 91.656)	50.598 (47.166 – 50.641)	p < 0.60	UNCHS005746
GSSG	6.149	18	53.075 (50.199 – 82.487)	28.328 (27.234 – 55.913)	p < 0.60	UNC29274589
GSH/GSSG	6.407	11	6.017 (5.568 – 7.583)	3.906 (3.664 – 4.782)	p < 0.40	JAX00023998
GSH/GSSG	8.224	16	8.998 (8.865 – 10.077)	4.779 (4.433 – 5.470)	p < 0.05	UNC26310160
E_h	6.480	16	6.997 (3.526 – 8.225)	3.373 (2.074 – 3.621)	P < 0.40	UNC26285513
E_h	8.598	16	8.998 (8.865 – 10.324)	4.779 (4.433 – 5.579)	p < 0.05	UNC26310160
NADPH	6.352	2	173.408 (173.133 – 174.508)	96.424 (95.769 – 97.976)	p < 0.45	JAX00512108
NADPH	6.612	12	28.626 (28.578 – 29.450)	10.987 (10.975 – 11.927)	p < 0.30	UNC20792752
NADPH	6.287	17	51.366 (50.164 – 52.542)	26.684 (25.861 – 27.425)	p < 0.50	UNC28000164
$NADP^+$	7.032	3	110.517 (109.677 – 115.729)	48.547 (48.380 – 50.024)	p < 0.20	UNCHS009832
$NADP^+$	6.590	8	61.237 (60.722 – 65.378)	30.937 (30.901 – 32.757)	p < 0.40	UNC14852712
$NADP^+$/NADPH	7.637	12	28.626 (28.562 – 29.394)	10.987 (10.972 – 11.864)	p < 0.10	UNC20792752
NADH	6.062	14	100.731 (99.320 – 102.809)	50.508 (49.350 – 52.844)	p < 0.65	UNC24615532

Supplementary Table S3.11. Genes involved in GSH synthesis and recycling.
Gene locations listed in bp, as well as in cM for location on the Genetic Map (GRCm38/mm10).

Gene	Sequence Map (bp) – mouse	Genetic Map (cM) – mouse
Glutathione peroxidase (Gpx1)	Chr9:108339080-108340342	Chromosome 9, 59.24 cM
Glutathione cysteine ligase – catalytic subunit (Gclc)	Chr9:77754535-77794485	Chromosome 9, 43.36 cM
Glutamate-cysteine ligase – modifier subunit (Gclm)	Chr3:122245487-122267215	Chromosome 3, 52.94 cM
Glutathione synthetase (Gs)	Chr2:155563181-155592810	Chromosome 2, 77.26 cM
Glutathione reductase (Gr)	Chr8:33653238-33698162	Chromosome 8, 20.69 cM

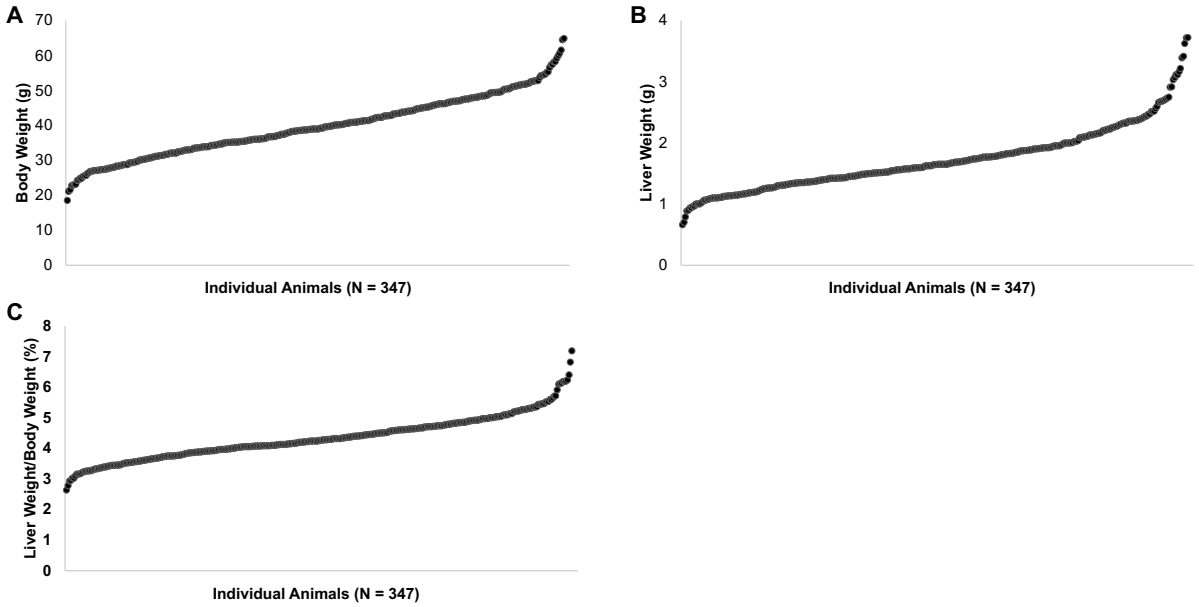

Supplementary Figure S3.1. Variation of weights in the DO population.
A. Body Weight (g); **B.** Liver Weight (g); and **C.** Liver Weight/Body Weight (%) were measured in a population of DO mice. Values are arranged from smallest to largest, and the N for each measurement is provided underneath each panel.

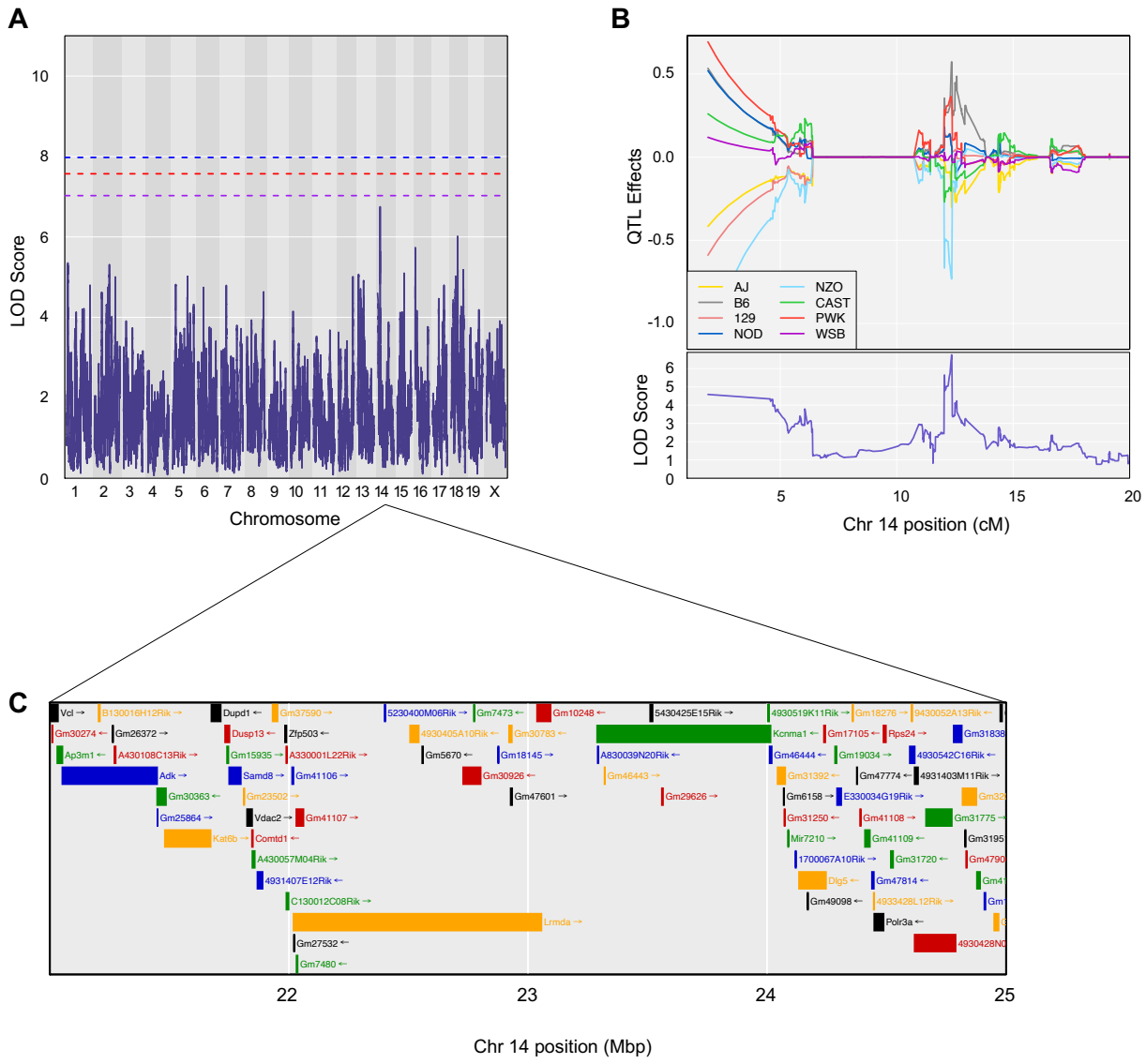

Supplementary Figure S3.2. High-resolution association mapping for hepatic total glutathione in outbred mice reveals a suggestive QTL on mouse chromosome 14.
A. Genome-wide scan of hepatic total glutathione in outbred mice shows a QTL with peak LOD score 6.478 at 22.506 Mbp (12.355 cM) on mouse chromosome 14. Permutation-derived significance thresholds are indicated by colored lines at significance (α) levels 0.05 (blue), 0.1 (red), and 0.2 (purple). **B.** The founder allele QTL effects indicate that the NZO allele contributes to a lower hepatic GSH concentration, whereas the B6 allele contributes to a higher hepatic total glutathione concentration. Each colored line represents a DO founder allele as indicated in the legend. The differences between strains are considered significant when the LOD score (bottom) crosses significance thresholds (panel A). **C.** Candidate genes found within the QTL interval relative to the MGI database (GRCm38/mm10; gene query performed November 2020, Feature Type "gene" [563]). Genes in the interval include *Vcl, Ap3m1, Adk, B130016H12Rik, Gm26372, A430108C13Rik, Gm30363, Gm25864, Kat6b, Dupd1, Dusp13, Gm15935, Samd8, Gm23502, Vdac2, Comtd1, A430057M04Rik, 4931407E12Rik, Gm37590, Zfp503, A330001L22Rik, C130012C08Rik, Gm41106, Lrmda, Gm27532, Gm41107, Gm7480, 5230400M06Rik,*

4930405A10Rik, Gm30926, Gm30783, Gm47601, Gm10248, Kcnma1, A830039N20Rik, 5430425E15Rik, Gm29626, 4930519K11Rik, Gm46444, Gm31392, Gm31250, Mir7210, 1700067A10Rik, Dlg5, Gm49098, Gm17105, E330034G19Rik, Gm47774, Gm41108 , Gm41109, Gm47814, 4933428L12Rik, Polr3a, Rps24, Gm31720, 4930542C16Rik, 9430052A13Rik, 4931403M11Rik, 4930428N03Rik, Gm31775, Gm31838, Gm32008, Gm31951, Gm47906, Gm41110, Gm10398, Gm32068, Gm41111. Hepatic GSH genome scan resulted in the same significant QTL interval on mouse chromosome 14 (Supplementary Figure S3.3).

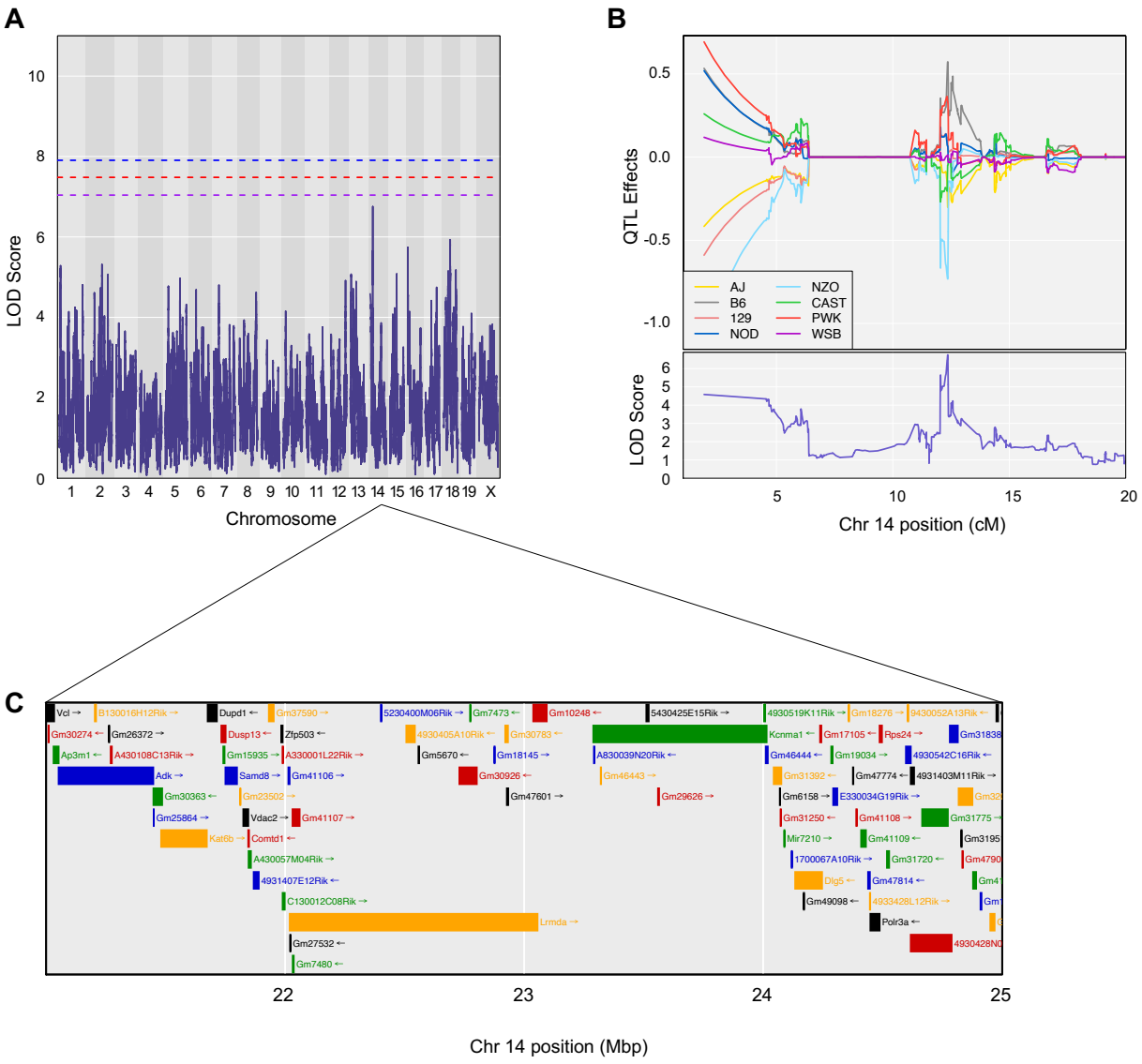

Supplementary Figure S3.3. High-resolution association mapping for hepatic GSH in outbred mice reveals a suggestive QTL on mouse chromosome 14.
A. Genome-wide scan of hepatic GSH in outbred mice shows a QTL with peak LOD score 6.755 at 22.506 Mbp (12.355 cM) on mouse chromosome 14. Permutation-derived significance thresholds are indicated by colored lines at significance (α) levels 0.05 (blue), 0.1 (red), and 0.2 (purple). **B.** The founder allele QTL effects indicate that the NZO allele contributes to a lower hepatic GSH concentration, whereas the B6 allele contributes to a higher hepatic GSH concentration. Each colored line represents a DO founder allele as indicated in the legend. The differences between strains are considered significant when the LOD score (bottom) crosses significance thresholds (panel A). **C.** Candidate genes found within the QTL interval relative to the MGI database (GRCm38/mm10; gene query performed November 2020, Feature Type "gene" [563]). Genes in the interval include *Vcl, Ap3m1, Adk, B130016H12Rik, Gm26372, A430108C13Rik, Gm30363, Gm25864, Kat6b, Dupd1, Dusp13, Gm15935, Samd8, Gm23502, Vdac2, Comtd1, A430057M04Rik, 4931407E12Rik, Gm37590, Zfp503, A330001L22Rik,*

C130012C08Rik, Gm41106, Lrmda, Gm27532, Gm41107, Gm7480, 5230400M06Rik, 4930405A10Rik, Gm30926, Gm30783, Gm47601, Gm10248, Kcnma1, A830039N20Rik, 5430425E15Rik, Gm29626, 4930519K11Rik, Gm46444, Gm31392, Gm31250, Mir7210, 1700067A10Rik, Dlg5, Gm49098, Gm17105, E330034G19Rik, Gm47774, Gm41108 , Gm41109, Gm47814, 4933428L12Rik, Polr3a, Rps24, Gm31720, 4930542C16Rik, 9430052A13Rik, 4931403M11Rik, 4930428N03Rik, Gm31775, Gm31838, Gm32008, Gm31951, Gm47906, Gm41110, Gm10398, Gm32068, Gm41111. Hepatic total glutathione genome scan resulted in the same significant QTL interval on mouse chromosome 14 (Supplementary Figure S3.2).

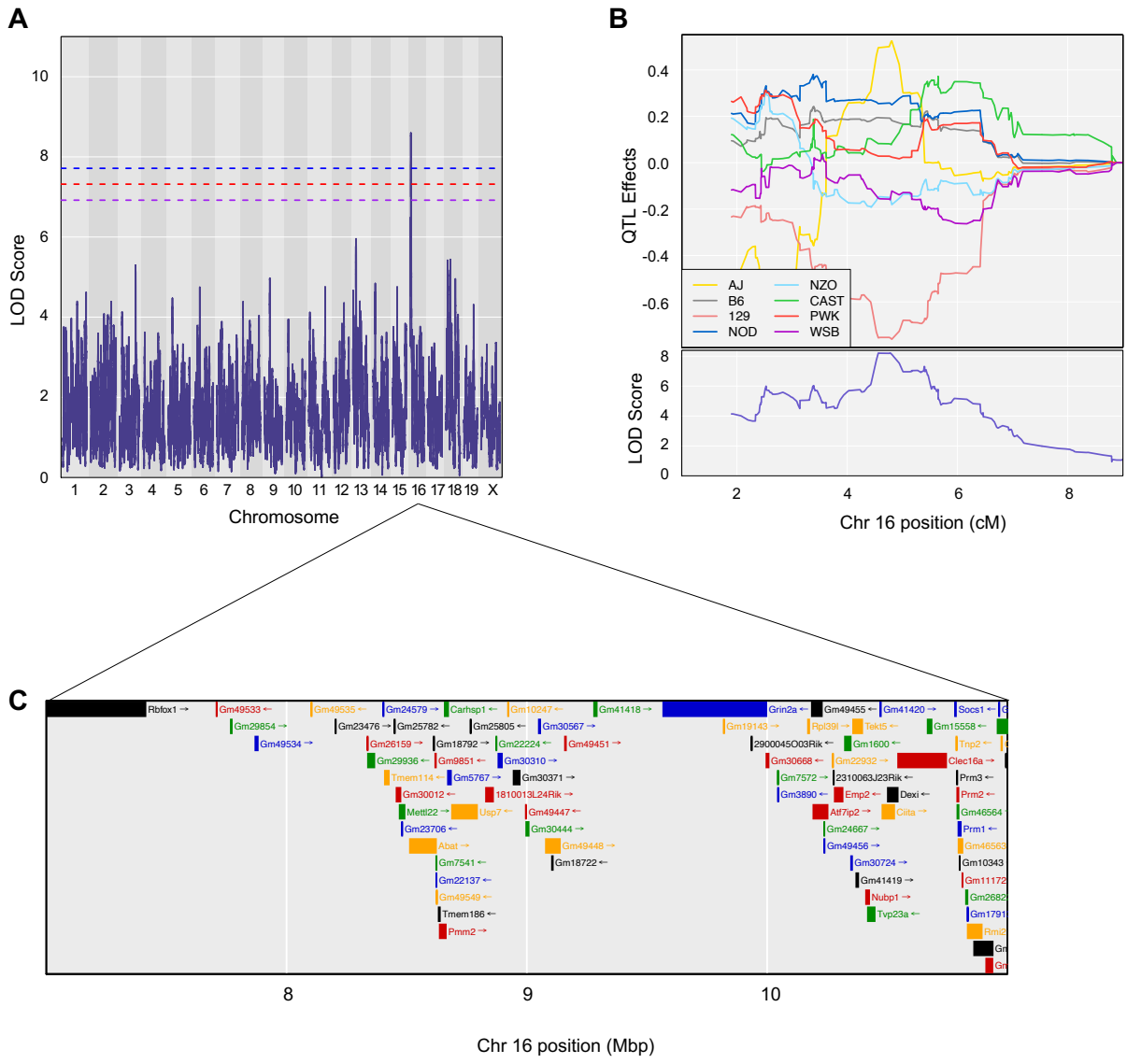

Supplementary Figure S3.4. High-resolution association mapping for hepatic E_h in outbred mice reveals a significant QTL on mouse chromosome 16.
A. Genome-wide scan of hepatic E_h in outbred mice shows a QTL with peak LOD score 8.598 at 8.998 Mbp (4.779 cM) on mouse chromosome 14. Permutation-derived significance thresholds are indicated by colored lines at significance (α) levels 0.05 (blue), 0.1 (red), and 0.2 (purple). **B.** The founder allele QTL effects indicate that the PWK allele contributes to a lower hepatic GSH concentration, whereas the AJ allele contributes to a higher hepatic GSH concentration. Each colored line represents a DO founder allele as indicated in the legend. The differences between strains are considered significant when the LOD score (bottom) crosses significance thresholds (panel A). **C.** Candidate genes found within the QTL interval relative to the MGI database.

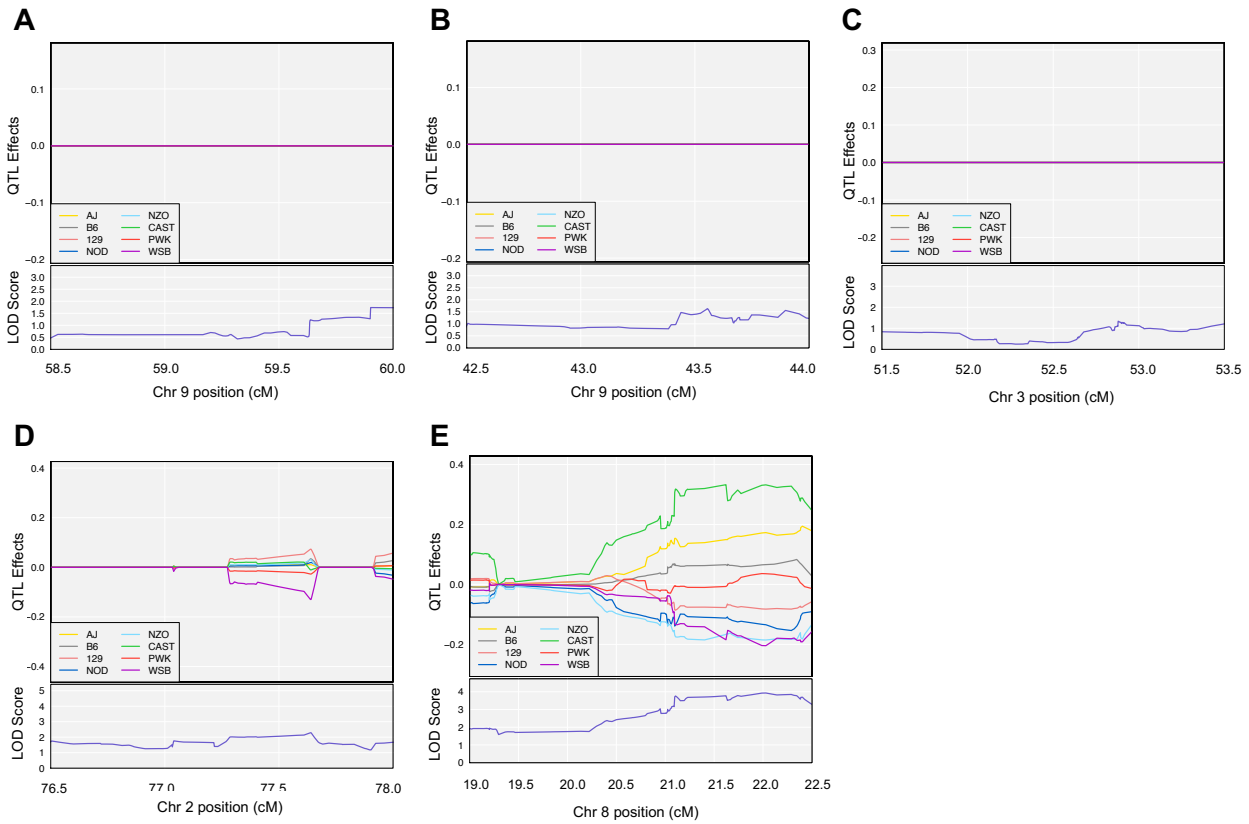

Supplementary Figure S3.5. Investigating founder allele effects on genes involved in glutathione metabolism using high-resolution mapping for hepatic total glutathione.
Each colored line represents a DO founder allele as indicated in the legend. The differences between strains are considered significant when the LOD score (bottom) is large enough surpass phenotype-specific permutation-derived significance thresholds. The founder allele QTL effects indicate that there are no alleles found in proximity to the **A.** Gpx1 gene location (Chromosome 9, 59.24 cM), **B.** Gclc gene location (Chromosome 9, 43.36 cM), **C.** Gclm gene location (Chromosome 3, 52.94 cM), **D.** Gs gene location (Chromosome 2, 77.26), and **E.** Gr gene location (Chromosome 8, 20.69) that contribute to a significantly lower or higher total glutathione concentration.

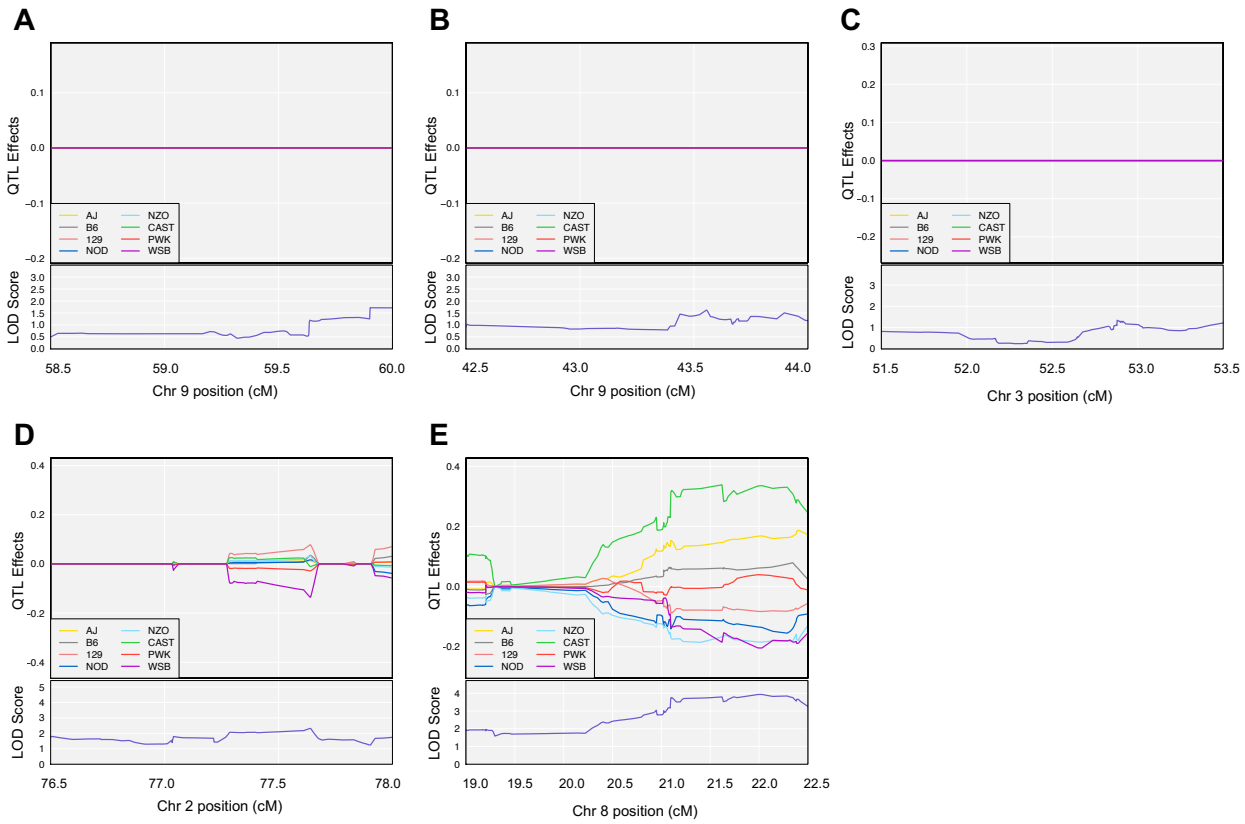

Supplementary Figure S3.6. Investigating founder allele effects on genes involved in glutathione metabolism using high-resolution mapping for hepatic GSH.
Each colored line represents a DO founder allele as indicated in the legend. The differences between strains are considered significant when the LOD score (bottom) is large enough surpass phenotype-specific permutation-derived significance thresholds. The founder allele QTL effects indicate that there are no alleles found in proximity to the **A.** Gpx1 gene location (Chromosome 9, 59.24 cM), **B.** Gclc gene location (Chromosome 9, 43.36 cM), **C.** Gclm gene location (Chromosome 3, 52.94 cM), **D.** Gs gene location (Chromosome 2, 77.26), and **E.** Gr gene location (Chromosome 8, 20.69) that contribute to a significantly lower or higher GSH concentration.

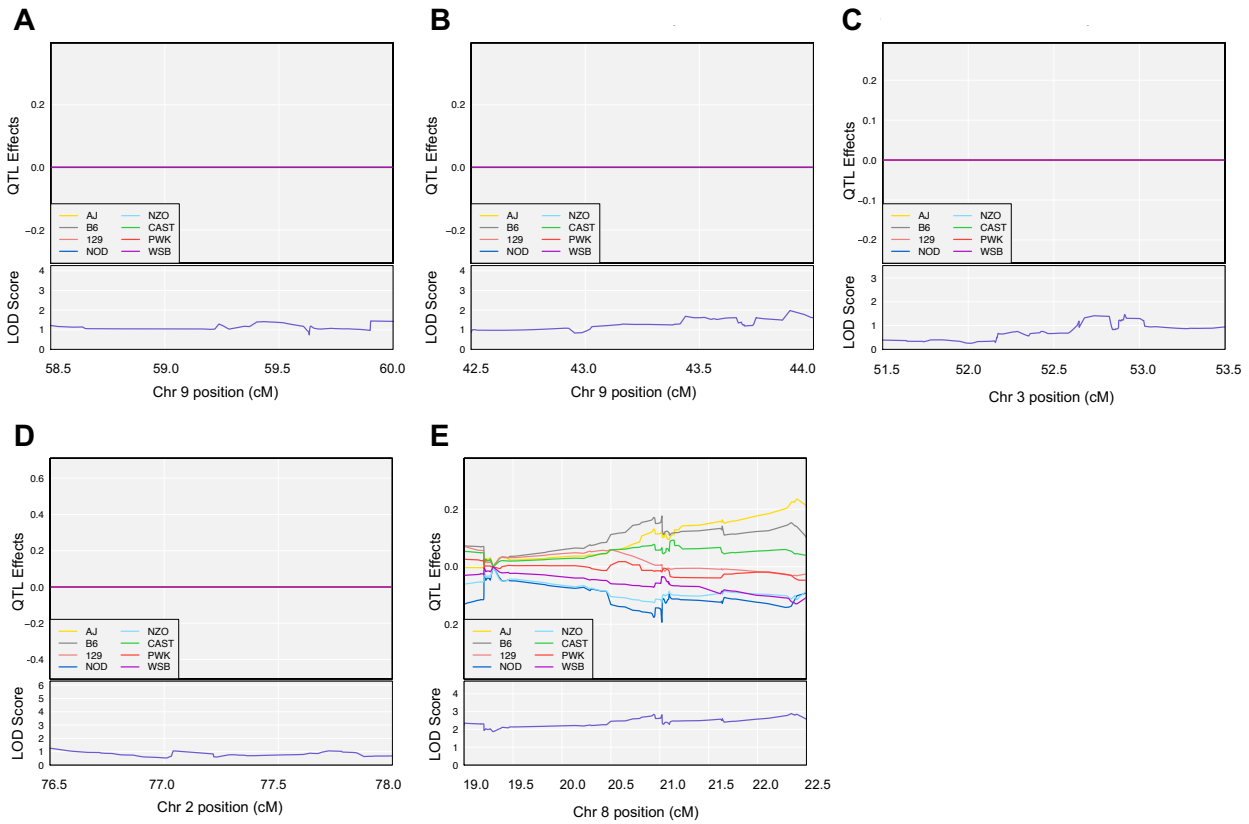

Supplementary Figure S3.7. Investigating founder allele effects on genes involved in glutathione metabolism using high-resolution mapping for hepatic GSSG.
Each colored line represents a DO founder allele as indicated in the legend. The differences between strains are considered significant when the LOD score (bottom) is large enough surpass phenotype-specific permutation-derived significance thresholds. The founder allele QTL effects indicate that there are no alleles found in proximity to the **A.** Gpx1 gene location (Chromosome 9, 59.24 cM), **B.** Gclc gene location (Chromosome 9, 43.36 cM), **C.** Gclm gene location (Chromosome 3, 52.94 cM), **D.** Gs gene location (Chromosome 2, 77.26), and **E.** Gr gene location (Chromosome 8, 20.69) that contribute to a significantly lower or higher GSSG concentration.

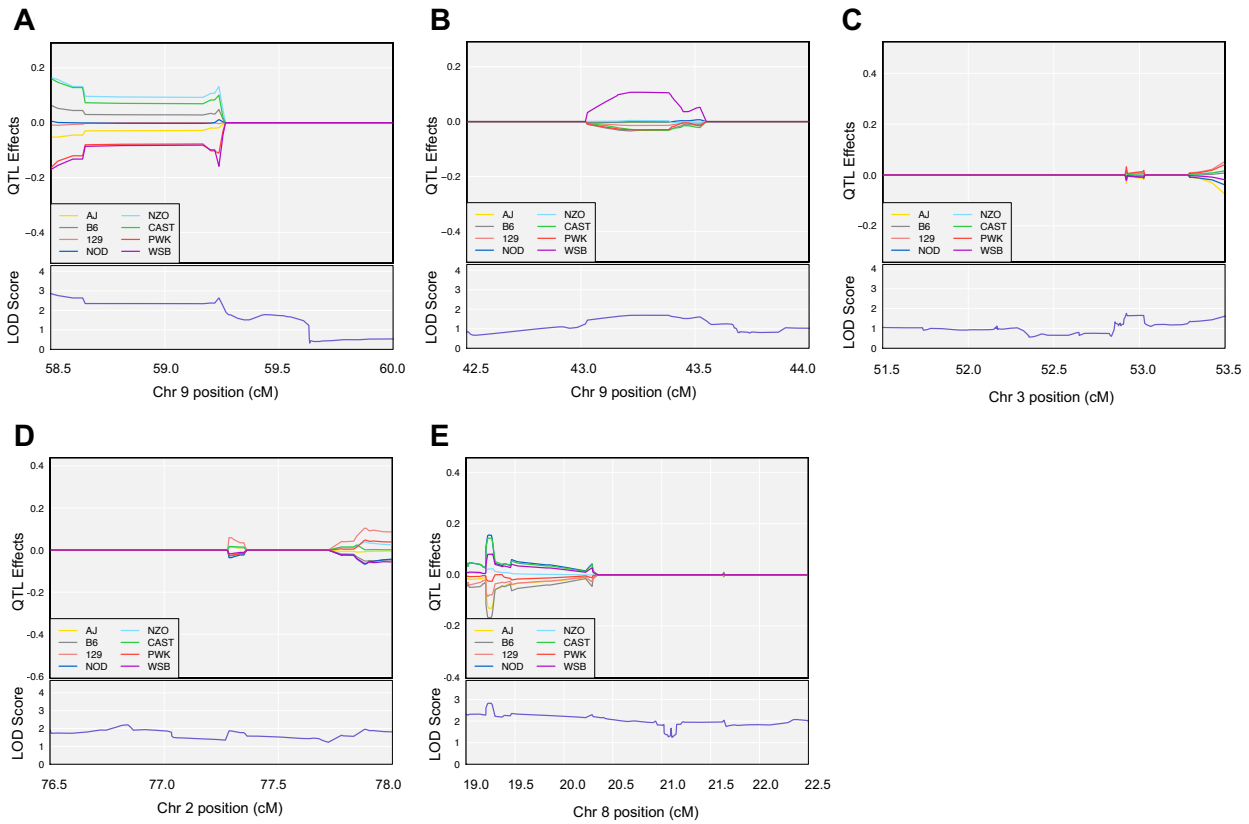

Supplementary Figure S3.8. Investigating founder allele effects on genes involved in glutathione metabolism using high-resolution mapping for hepatic GSH/GSSG.

Each colored line represents a DO founder allele as indicated in the legend. The differences between strains are considered significant when the LOD score (bottom) is large enough surpass phenotype-specific permutation-derived significance thresholds. The founder allele QTL effects indicate that there are no alleles found in proximity to the **A.** Gpx1 gene location (Chromosome 9, 59.24 cM), **B.** Gclc gene location (Chromosome 9, 43.36 cM), **C.** Gclm gene location (Chromosome 3, 52.94 cM), **D.** Gs gene location (Chromosome 2, 77.26), and **E.** Gr gene location (Chromosome 8, 20.69) that contribute to a significantly lower or higher GSH/GSSG concentration.

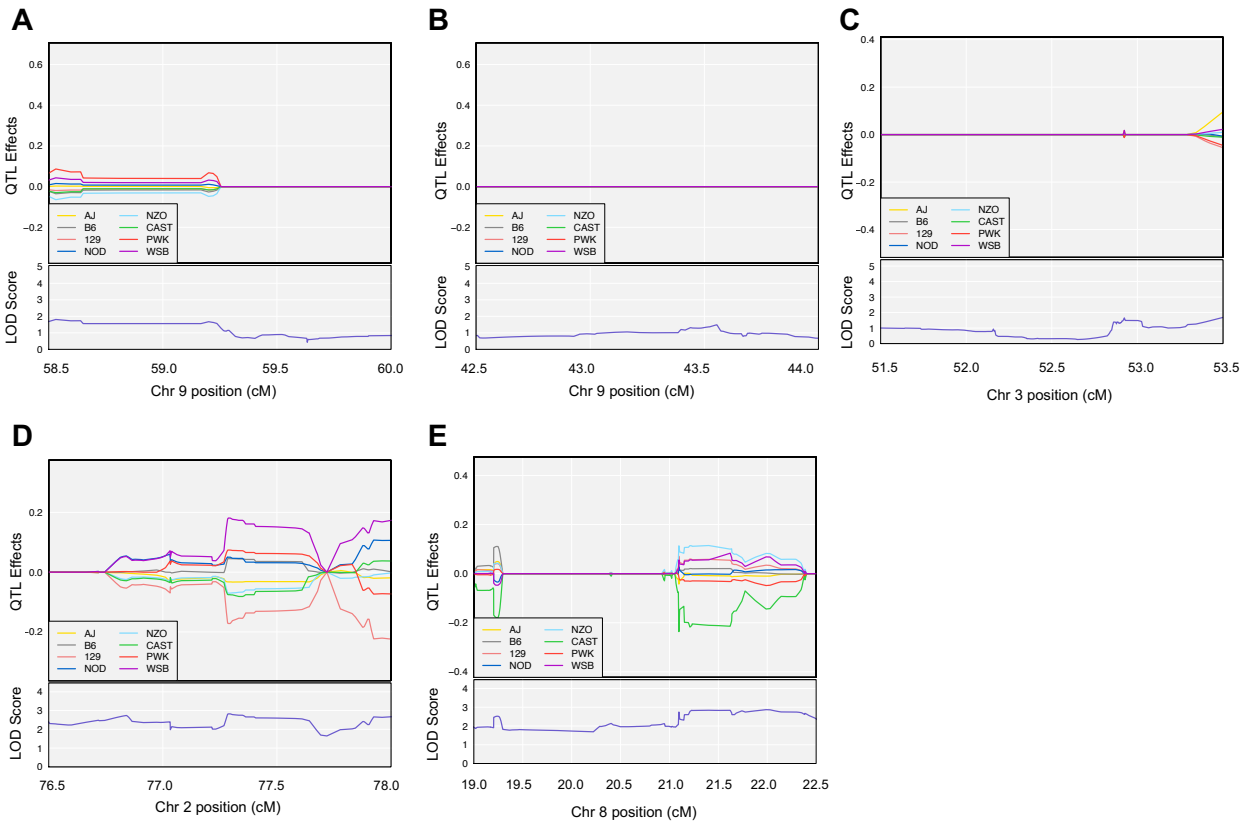

Supplementary Figure S3.9. Investigating founder allele effects on genes involved in glutathione metabolism using high-resolution mapping for hepatic E_h.
Each colored line represents a DO founder allele as indicated in the legend. The differences between strains are considered significant when the LOD score (bottom) is large enough surpass phenotype-specific permutation-derived significance thresholds. The founder allele QTL effects indicate that there are no alleles found in proximity to the **A.** Gpx1 gene location (Chromosome 9, 59.24 cM), **B.** Gclc gene location (Chromosome 9, 43.36 cM), **C.** Gclm gene location (Chromosome 3, 52.94 cM), **D.** Gs gene location (Chromosome 2, 77.26), and **E.** Gr gene location (Chromosome 8, 20.69) that contribute to a significantly lower or higher E_h concentration.

CHAPTER 4

SYSTEMS GENETICS APPROACH TO HISTOPATHOLOGICAL MARKERS OF NON-ALCOHOLIC FATTY LIVER DISEASE AND THEIR RELATIONSHIPS WITH HEPATIC REDOX SYSTEMS[4]

[4] Gould RL, Craig SC, Stanton J, McClatchy S, Churchill G, Williams D, Johns M, Chase K, Thiesfeldt D, Pazdro R. "Systems genetics approach to histopathological markers of non-alcoholic fatty liver disease and their relationships with hepatic redox systems" To be submitted to *Scientific Reports*.

Abstract

Oxidative stress plays a central role in non-alcoholic fatty liver disease (NAFLD) pathogenesis. Glutathione (GSH) is a critical antioxidant found within the liver whose neutralization of reactive oxygen species protects against the onset of oxidative stress and liver injury. Recent evidence conducted in outbred mice has documented over a 10-fold variation in hepatic GSH, as well as a 16-fold variation in its oxidized form, GSSG. Yet how this variation impacts onset and progression of NAFLD remains to be determined. In this follow-up study, we scored histopathological outcomes of NAFLD in liver sections from the same mice to identify the statistical relationships between the hepatic GSH and NADPH redox systems and NAFLD. In addition, we utilized high-resolution genetic mapping technologies to identify novel QTL peaks regulating hepatic steatosis and serum aminotransferase aspartate transaminase (AST) levels. Comparison of genetic mapping results revealed shared loci between hepatic GSSG and steatosis. These findings improve our understanding of the relationship between NAFLD and the hepatic GSH redox system in a genetically diverse model.

Introduction

Non-alcoholic fatty liver disease (NAFLD) is the most common chronic liver condition in the United States, with an estimated 25% of Americans living with NAFLD [601]. It is characterized by accumulation of 5-10% of triglyceride-based fat in hepatocytes in the absence of alcohol consumption [602], and represents a wide spectrum of liver injury that encompasses steatosis, steatohepatitis, fibrosis and cirrhosis [601, 603]. The disease is associated with obesity [604], type 2 diabetes mellitus [605], dyslipidemia [606], and metabolic syndrome [607], as well as an increased cardiovascular disease risk [608], as the liver is a key determinant of metabolic abnormalities through its role in production and metabolism of triglycerides and glucose [607]. Hepatic steatosis is the hallmark of NAFLD and is typically a result of abnormal lipid metabolism due to insulin resistance [603]. Fat deposition, inflammation and liver cell damage can then cause fibrosis, or scarring, of the liver [292]. NAFLD is thought to be a product of both environmental and genetic factors [608], but the complete mechanism in which hepatic steatosis progresses to nonalcoholic steatohepatitis (NASH) remains unknown [603].

Oxidative stress is a deleterious imbalance between the production and removal of reactive oxygen/nitrogen species (RONS) [12]. It plays a central role in NAFLD pathogenesis [125], but it remains unclear what initiates this process and how it progresses [292]. Glutathione is a crucial antioxidant composed of glutamate, cysteine, and glycine, that modulates oxidative stress [174]. It is recycled from its reduced form, GSH, to its oxidized form, GSSG, as it sequesters reactive oxygen species (ROS) [164]. Hepatic GSSG is then reduced back to GSH through the enzymatic action of NADPH-dependent glutathione reductase (GR) [164, 532]. Hepatic GSH is important for detoxification and protection against oxidative stress [609, 610], as accumulation of ROS leads to liver injury and ultimately liver disease [123]. It is clear that targeting hepatic oxidative stress is a

promising strategy to both prevent and treat NAFLD [125, 275], yet conflicting evidence has been documented regarding the relationship between glutathione and NAFLD. A diminished hepatic and blood GSH capacity was found in animals with steatosis, and human patients with NAFLD were found to have low levels of GSH precursor glycine [611] as well as glycine's precursor serine. Because of this, Gaggini et al. (2018) propose measurement of glutamate, serine, and glycine status as a holistic marker of liver disease severity [612]. However, discrepancies remain on whether these trends are consistent across studies, as some have documented heightened antioxidant status compared to healthy controls – a possible adaptive response to oxidative stress [125].

Despite compelling evidence that glutathione is related to NAFLD, it is still unclear what effect natural variation in glutathione has on liver function and pathology. The Diversity Outbred (DO) mice prove an excellent model for addressing this gap in knowledge, as they are genetically heterogenous, with over 45 million single nucleotide polymorphisms (SNPs) [558], and display broad ranges of phenotypes [548]. We previously showed that markers of the hepatic GSH redox system vary widely in DO mice [Chapter 3], and this subsequent study sought to investigate the functional impact of this variation on histological markers of NAFLD and clinical biomarkers indicative of liver function. Furthermore, a genetic mapping analysis software, R/qtl2, has been specifically developed for the DO strain [549], and we utilized those technologies to build upon current literature linking genetic background with NAFLD histopathology [613]. Brial et al. (2019) previously performed quantitative trait loci (QTL) analysis in intercrossed inbred mice (129S6xBALB/c) to elucidate the genetic influence on NAFLD histological scores, and the genome-wide linkage mapping demonstrated that QTL mapping is relevant to NAFLD histopathology outcomes [613]. Our study expands upon this through QTL analysis of the DO mouse model. To better understand the impact of hepatic glutathione variation on liver function,

we assessed liver sections from a large cohort of DO animals and scored them for presence of steatosis and hydropic degeneration, as well as quantified serum aminotransferases AST and ALT. We then assessed the genetic and statistical relationships between histopathological outcomes, serum AST and ALT, and markers of the hepatic GSH and NADPH redox systems.

Materials and Methods

Animals and genotyping: The DO mice (N = 346; 171 males, 175 females) used for the study and their genotyping were previously described [Chapter 3]. Liver weight (g) and body weight (g) were documented at sacrifice. The University of Georgia Institutional Animal Care and Use Committee (IACUC) approved all methods and procedures involving animals in accordance with the ethical standards of the institution (AUP #A2016 07-016).

Clinical measurements and analysis: Fasting blood was collected after a 3-4 hour fast during the light cycle at 3 months of age via the submandibular vein after being briefly anesthetized with 2.75% isoflurane via an isoflurane chamber. All blood samples clotted for 30 minutes to 1 hour and were then immediately centrifuged at 10,000 RPM (9,391 RCF) at 4°C for 5 minutes for serum extraction. Serum samples were stored at -80°C until analysis. Serum samples were submitted to and analyzed by the Clinical Pathology Department at the University of Georgia Veterinary Medical Center. Alanine transaminase (ALT) and aspartate transaminase (AST) were quantified using the cobas 6000 c501 Analyzer (Roche Diagnostics, Indianapolis, IN USA). The ratio of AST/ALT was calculated by comparing [AST] to [ALT].

Quantification of markers of the hepatic GSH and NADPH redox systems: Protocol for measurement of hepatic redox phenotypes were described previously [Chapter 3]. Hepatic glutathione phenotypes include the reduced form GSH, oxidized form GSSG, total glutathione (GSH+2GSSG), glutathione ratio GSH/GSSG, and glutathione redox potential (E_h). Hepatic

NAD(P)H phenotypes include reduced form NADH, as well as the reduced and oxidized form of nicotinamide adenine dinucleotide phosphate NADPH and $NADP^+$, respectively.

Preservation, staining, and imaging of liver tissue: A longitudinal section of the left, right, and median lobes were taken from each mouse liver. The sections were promptly fixed in formalin, paraffin embedded, serially sectioned to 5μm, mounted on adhesive slides, and stained with hematoxylin and eosin (H&E) and Picrosirius Red. Whole slide images were obtained using an Aperio AT2 automated digital whole slide scanner (Leica Biosystems, Buffalo Grove, IL) and slides were analyzed.

Development of histological scoring system in mice: To define the variation of steatosis, hydropic degeneration, and fibrosis in mouse liver, histological samples from all 346 mice were analyzed. Steatosis was determined by analyzing overall hepatocellular vesicular steatosis. Hydropic degeneration was defined as enlarged and rounded hepatocytes with clear cytoplasm. The fibrosis score was used to describe the amount of inflammation (the intensity of inflammation/breakdown of tissue) in the liver. To validate the scoring system, all slides of mouse were blindly analyzed by a board-certified pathologist (JS) and five scientists with basic histological experience (BG, DW, DT, MJ, KJ). The scientists estimated the percentage of steatosis (Table 4.1), hydropic degeneration (Table 4.2), and fibrosis (Table 4.3) based on scales adapted from previously published methods for liver steatosis [614, 615], hydropic degeneration [616], and fibrosis [617-619]. For H&E-stained slides, four TIFF images were taken at 20x using Aperio ImageScope 12.1 (Leica Biosystems, Buffalo Grove, IL) from each liver lobe (left, median, and right) for a total of twelve images per mouse. All scientists graded the individual images and scores between the researchers were then averaged and rounded to the nearest whole number for a final grade for both steatosis and hydropic degeneration in each mouse liver. For Picrosirius red-stained

slides, whole-slide images were assessed using Aperio ImageScope 12.1 (Leica Biosystems, Buffalo Grove, IL) and a grade of fibrosis was assigned for each lobe (left, median, and right), then averaged and rounded to the nearest whole number for a final fibrosis grade for each mouse.

Table 4.1. Grading system for hepatic steatosis.

Grade	% hepatocytes	Description
0	0% – 5%	Absent
1	>5% – 20%	Very mild
2	>20% – 50%	Mild
3	>50 – 75%	Moderate
4	>75 – 90%	Severe
5	>90%	Very severe

Table 4.2. Grading system for hepatic hydropic degeneration.

Grade	% hepatocytes	Description
0	0% – 5%	Absent
1	>5% – 20%	Very mild
2	>20% – 50%	Mild
3	>50 – 75%	Moderate
4	>75 – 90%	Severe
5	>90%	Very severe

Table 4.3. Grading system for hepatic fibrosis (METAVIR scoring system) [617-619].

Grade	Fibrosis
F0	No fibrosis
F1	Portal fibrosis without septa
F2	Portal fibrosis with few septa
F3	Septal fibrosis without cirrhosis
F4	Cirrhosis

Quantitative trait loci (QTL) mapping: Genome scans were performed in 346 DO samples using the R/qtl2 software [549] as previously described [Chapter 3]. Genome scans included sex and experimental cohort as additive covariates. Rank *z*-score transformation was used on each phenotype to ensure normality, and kinship among the DO mice was accounted for using the "leave one chromosome out" (LOCO) method [549, 559]. 1000 permutation tests were run for each

genome scan to determine autosomal significance thresholds [549, 560, 561]. For phenotypes with suggestive or significant QTL peaks on the X chromosome, separate permutation tests (18090 total) were run for the X chromosome using the *perm_Xsp = TRUE* function. A suggestive threshold ($p \leq 0.20$) was applied for reporting loci [561], and a 95% Bayesian credible interval was determined for each peak around the reported QTL position [549, 560]. Genes within the intervals were plotted through connection with the Mouse Genome Informatics (MGI) database. All genotype data and genotype probabilities are publicly available through figshare (https://doi.org/10.6084/m9.figshare.c.5360501.v1). All source code, phenotype data, and other files used in QTL analyses are available through a public GitHub repository (https://doi.org/10.5281/zenodo.4683951).

Candidate gene prioritization: Databases for expression, phenotypic, and functional annotations were queried using methods for candidate gene prioritization involving an integrative bioinformatics approach described previously [Chapter 3].

Statistical Analysis: We used RStudio version 1.3.1093 (RStudio, PBC., Boston, MA) and R version 4.0.2 (R Foundation for Statistical Computing, Vienna, Austria) to identify relationships between variables. Rank-based Spearman's rho (ρ) was calculated to identify correlations between values. Wilcoxon Rank Sum tests were conducted to identify relationships between variables by histological grades.

Results

Serum aminotransferases and hepatic histopathological outcomes vary significantly in outbred mice: To date, no reference values have been formally established for AST or ALT in mice given the variation in values between strains. This study sought to identify the variation in an outbred population housed under standard conditions (Table 4.4; Figure 4.1). We observed over

an 8.5-fold difference in AST values with a range of 27 to 233 U/L. This effect was not sex-specific, with both males and females exhibiting a 7.8-fold difference (27 to 212 U/L) and 8.3-fold difference (28 to 233 U/L), respectively (Supplementary Tables S4.1 and S4.2). Similarly, ALT varied with a 4-fold difference across values (14 to 60 U/L). Much like AST, this variation in ALT was not sex-specific, with ALT values from males ranging from 15 to 60 U/L and female ranging from 14 to 56 U/L. Lastly, we quantified the ratio of the two transaminases, AST/ALT, given its relationship with and use as an indicator of liver function [620-622]. We observed a 9-fold difference in AST/ALT values (0.867 to 7.833), a result of the variation in male animals. Though males exhibited the highest degree in variation, females exhibited a large variation as well with ratios ranging from 1.036 to 6.704, over a 6-fold difference.

Table 4.4. Descriptive statistics of serum aminotransferases in DO mice.

Phenotype:	**N**	**x̄**	**Median**	**SD**	**Min**	**Max**
AST (U/L)	343	59	49	32	27	233
ALT (U/L)	342	26	24	7	14	60
AST/ALT	341	2.293	2.000	1.038	0.867	7.833

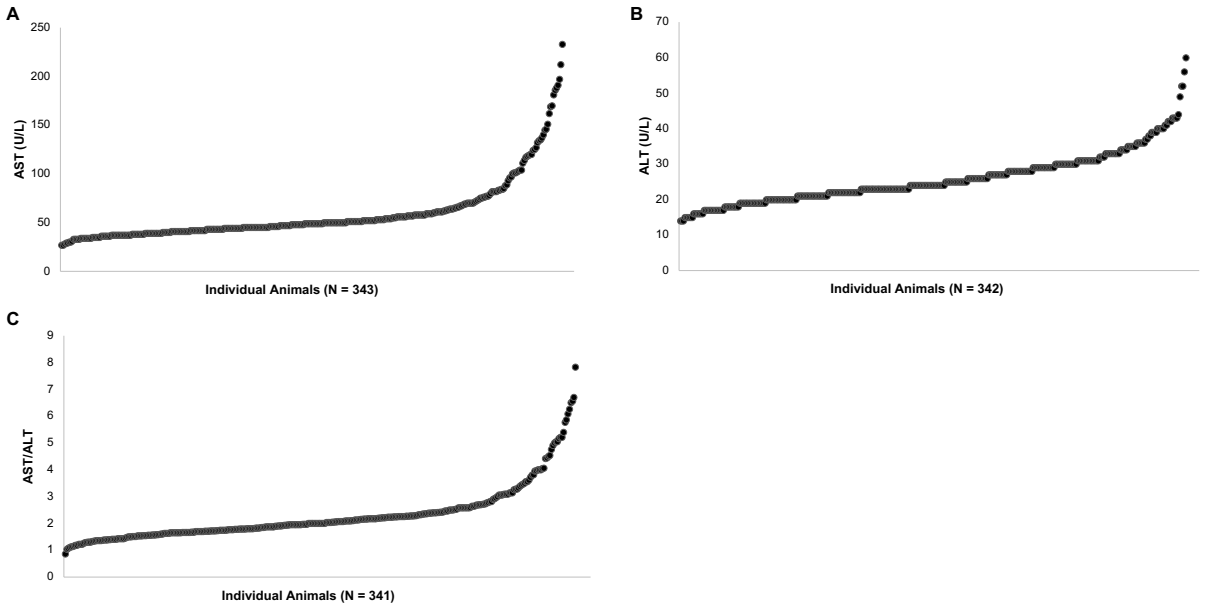

Figure 4.1. Variation in serum transaminases in the DO population.
Serum aminotransferases **A.** AST (U/L); **B.** ALT (U/L); and **C.** AST/ALT; were measured in a population of DO mice. Values are arranged from smallest to largest, and the N for each measurement is provided underneath each panel.

We graded liver sections from the 346 mice for steatosis, hydropic degeneration, and fibrosis. After surveying these sections, we observed a wide variance in the trait outcomes (Figures 4.2 – 4.4). 84.4% of mouse livers (N = 292) did not exhibit steatosis and were designated a grade 0; 10.4% of livers (N = 36) exhibited very mild steatosis (grade 1); 2.6% of livers (N= 9) exhibited mild steatosis (grade 2), and 2.3% (N = 8) exhibited moderate steatosis (grade 3) (Figure 4.2). No samples were designated a grade 4 (severe) for steatosis, and 1 liver received a grade 5 (severe steatosis). A wide variety of hydropic degeneration was observed, with 4.0% of livers (N = 14) receiving a grade 0 (no evidence of hydropic degeneration), 8.1% of livers (N = 28) receiving a grade 1 (very mild), and 16.1% (N = 56) receiving a grade 2 (mild) (Figure 4.3). The majority of livers exhibited moderate to severe hydropic degeneration (31.1%, N = 108; 34.6%, N = 120, respectively), and 6.1% (N = 21) received a grade 5 (very severe). We observed limited variation in fibrosis (Figure 4), with 95.1% of animals (N = 329) in Grade F0, 4.6% (N = 16) in Grade F1,

and 0.3% (N = 1) in Grade F2. There were 0 animals that scored an F3 or F4 grade for fibrosis. We observed no obvious sex differences in histological grades (Supplementary Tables S4.1 and S4.2).

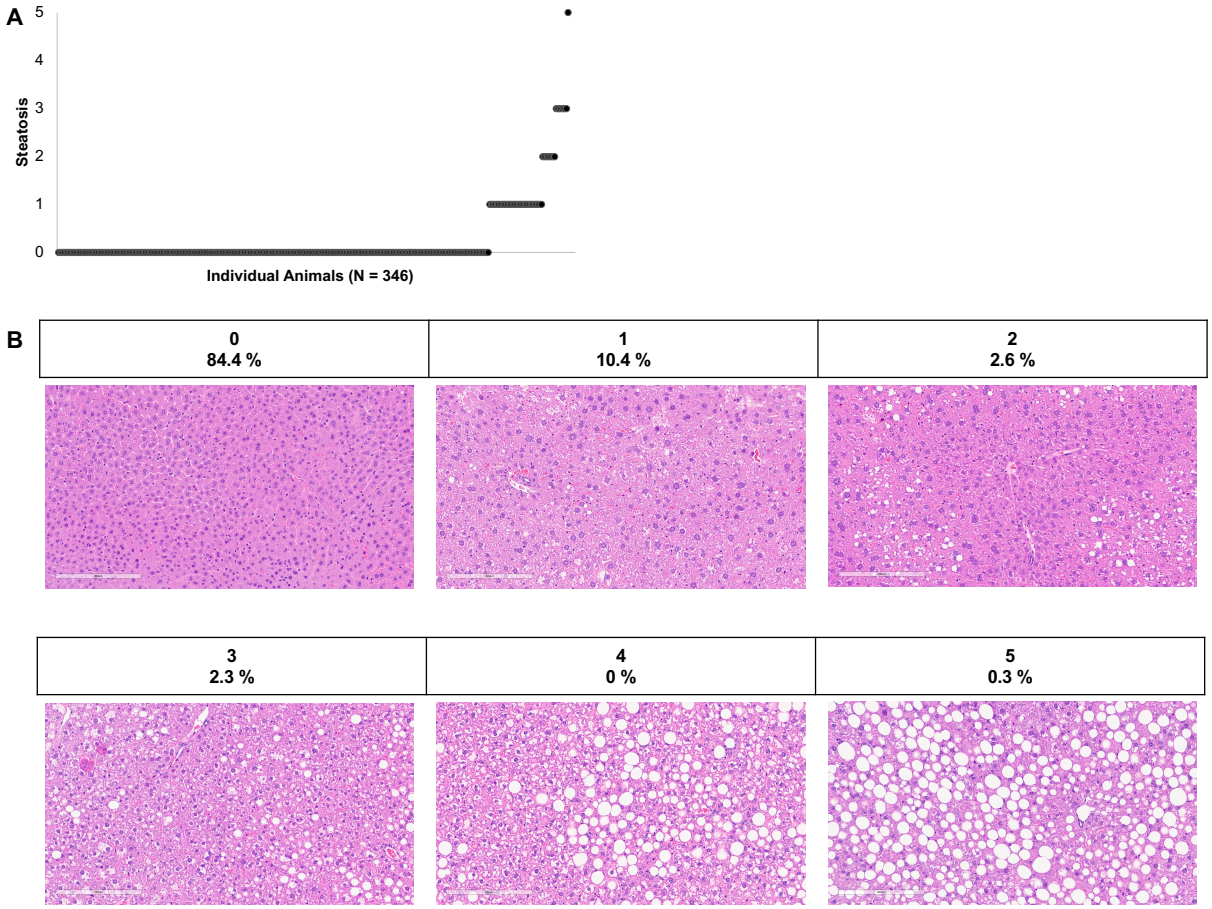

Figure 4.2. Variation in hepatic steatosis in the DO population.
A. Distribution of hepatic steatosis (grades 0 – 5); **B.** Variation in histological steatosis grade in 346 outbred mice. Percent of animals in each grading category listed below each histological grade. All images taken at 20x magnification.

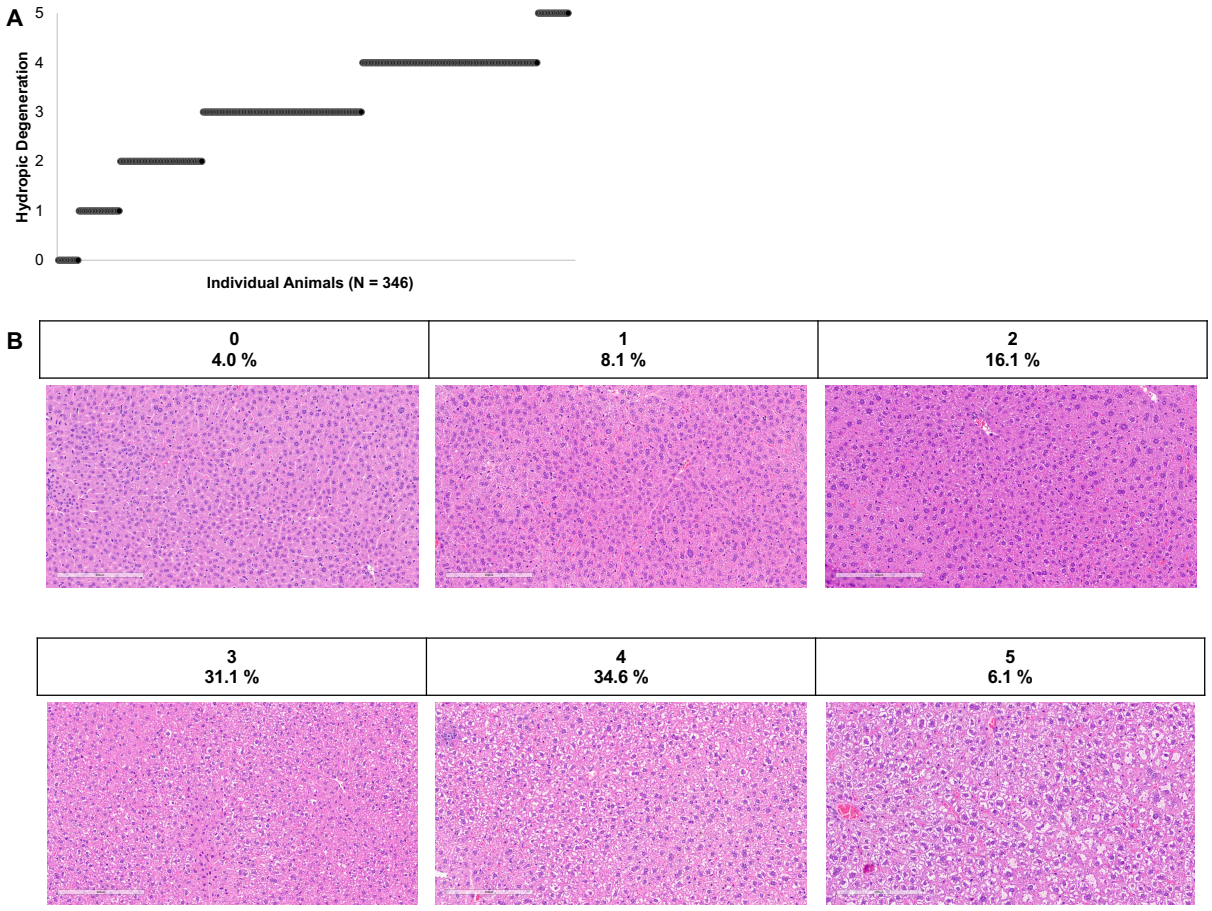

Figure 4.3. Variation in hepatic hydropic degeneration in the DO population.
A. Distribution of hepatic hydropic degeneration (grades 0 – 5). **B.** Variation in histological steatosis grade in 346 outbred mice. Percent of animals in each grading category listed below each histological grade. All images taken at 20x magnification.

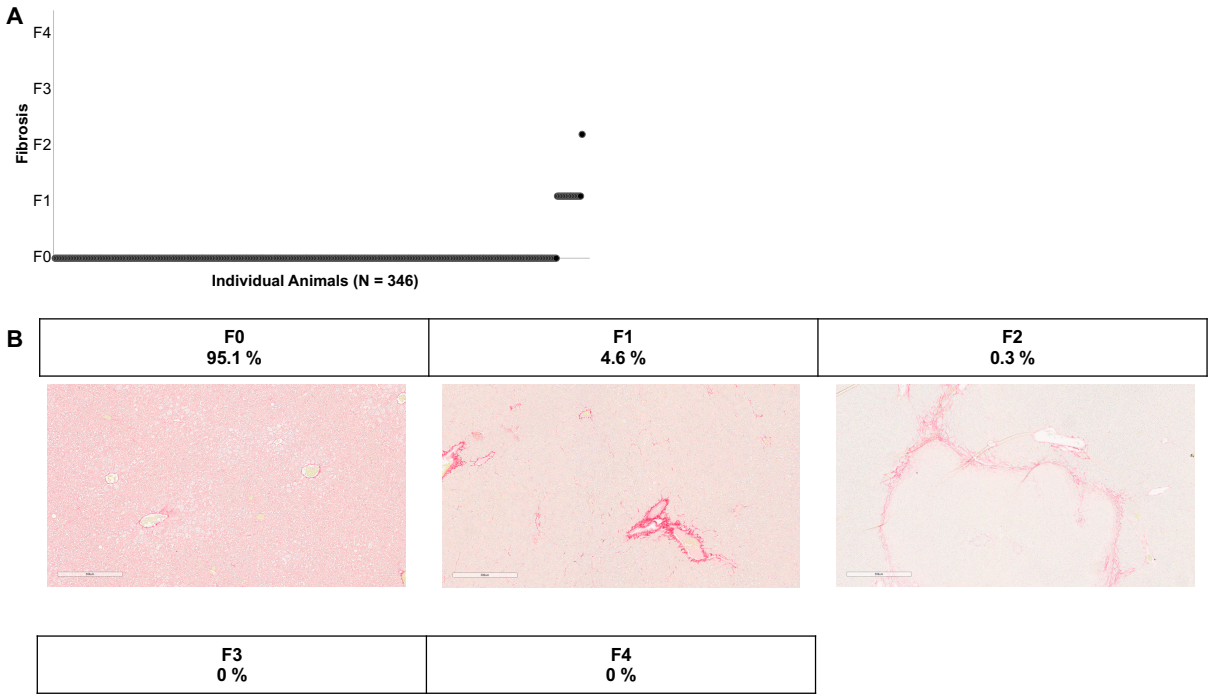

Figure 4.4. Variation in hepatic fibrosis in the DO population.
A. Distribution of hepatic fibrosis (grades F0 – F4). **B.** Variation in histological fibrosis grade in 346 outbred mice. Percent of animals in each grading category listed below each histological grade. All images taken at 20x magnification.

Variation in body weight, liver weight, and markers of the hepatic GSH and NADPH redox systems from these animals were previously described [Chapter 3]. To identify potential relationships between those traits and the serum aminotransferases, we calculated Spearman correlations for each relationship which generated many significant associations (Tables 4.5 – 4.7). Both liver weight and body weight were negatively correlated with AST concentrations (ρ = -0.160, p = 0.003 and ρ = -0.205, p = <0.001, respectively) and AST/ALT levels (ρ = -0.416, p = <0.001 and ρ = -0.381, p = <0.001, respectively), and positively correlated with ALT concentrations (ρ = 0.298, p = <0.001 and ρ = 0.197, p = <0.001, respectively). AST concentrations was positively correlated with ALT concentrations (ρ = 0.504, p = <0.001) and AST/ALT levels (ρ = 0.564, p = <0.001). ALT concentrations were negatively correlated with AST/ALT levels (ρ

= -0.355, p = <0.001). AST concentrations were positively correlated with hepatic total glutathione concentrations (ρ = 0.177, p = 0.001), hepatic GSH concentrations (ρ = 0.179, p = 0.001), hepatic GSSG concentrations (ρ = 0.109, p = 0.043), and hepatic E_h levels (ρ = -0.185, p = 0.001), but not hepatic GSH/GSSG levels (p = 0.098), nor hepatic NADPH concentrations (p = 0.572), hepatic $NADP^+$ concentrations (p = 0.304), hepatic $NADP^+$/NADPH levels (p = 0.582), or hepatic NADH concentrations (p = 0.051). ALT concentrations were positively correlated with hepatic $NADP^+$ concentrations (ρ = 0.152, p = 0.006), hepatic total glutathione concentrations (ρ = 0.131, p = 0.015), hepatic GSH concentrations (ρ = 0.132, p = 0.015), and hepatic GSSG concentrations (ρ = 0.127, p = 0.018), but was not correlated with hepatic NADPH (p = 0.203), hepatic $NADP^+$/NADPH (p = 0.082), or hepatic NADH (p = 0.976). However, ALT concentrations were not correlated with hepatic GSH/GSSG levels (p = 0.770) or hepatic E_h levels (p = 0.104). AST/ALT levels were correlated with hepatic NADH concentrations (ρ = 0.144, p = 0.009), but not hepatic NADPH concentrations (p = 0.600), hepatic $NADP^+$ concentrations (p = 0.496), or hepatic $NADP^+$/NADPH levels (p = 0.628). AST/ALT levels were correlated with hepatic total glutathione concentrations (ρ = 0.115, p = 0.034), hepatic GSH concentrations (ρ = 0.116, p = 0.033), and hepatic E_h levels (ρ = -0.146, p = 0.007).

Table 4.5. Statistical relationships between variables and AST (U/L).
Spearman's rho (ρ) was calculated for each variable combination and listed within each corresponding box. *indicates a significant relationship ($p \leq 0.05$).

Variables	**ρ**	**p-value**
Liver Weight (g)	-0.160*	0.003
Body Weight (g)	-0.205*	<0.001
ALT (U/L)	0.504*	<0.001
AST/ALT	0.564*	<0.001
Hepatic NADPH (pmol/μg)	0.031	0.572
Hepatic $NADP^+$ (pmol/μg)	-0.057	0.304
Hepatic $NADP^+$/NADPH	-0.031	0.582
Hepatic NADH (pmol/μg)	0.108	0.051
Hepatic Total Glutathione (nmol/mg)	0.177*	0.001
Hepatic GSH (nmol/mg)	0.179*	0.001
Hepatic GSSG (nmol/mg)	0.109*	0.043
Hepatic GSH/GSSG (nmol/mg)	0.090	0.098
Hepatic E_h (mV)	-0.185*	0.001
Steatosis	-0.080	0.142
Hydropic Degeneration	-0.115*	0.034
Fibrosis	-0.004	0.947

Table 4.6. Statistical relationships between variables and ALT (U/L).
Spearman's rho (ρ) was calculated for each variable combination and listed within each corresponding box. *indicates a significant relationship ($p \leq 0.05$).

Variables	**ρ**	**p-value**
Liver Weight (g)	0.298*	<0.001
Body Weight (g)	0.197*	<0.001
AST (U/L)	0.504*	<0.001
AST/ALT	-0.355*	0.000
Hepatic NADPH (pmol/μg)	0.070	0.203
Hepatic $NADP^+$ (pmol/μg)	-0.152*	0.006
Hepatic $NADP^+$/NADPH	-0.098	0.082
Hepatic NADH (pmol/μg)	-0.002	0.976
Hepatic Total Glutathione (nmol/mg)	0.131*	0.015
Hepatic GSH (nmol/mg)	0.132*	0.015
Hepatic GSSG (nmol/mg)	0.127*	0.018
Hepatic GSH/GSSG (nmol/mg)	-0.016	0.770
Hepatic E_h (mV)	-0.088	0.104
Steatosis	0.066	0.221
Hydropic Degeneration	0.013	0.818
Fibrosis	-0.022	0.689

Table 4.7. Statistical relationships between variables and AST/ALT.
Spearman's rho (ρ) was calculated for each variable combination and listed within each corresponding box. *indicates a significant relationship ($p \leq 0.05$).

Variables	**ρ**	**p-value**
Liver Weight (g)	-0.416*	<0.001
Body Weight (g)	-0.381*	<0.001
AST (U/L)	0.564*	<0.001
ALT (U/L)	-0.355*	0.000
Hepatic NADPH (pmol/μg)	-0.029	0.600
Hepatic $NADP^+$ (pmol/μg)	0.038	0.496
Hepatic $NADP^+$/NADPH	0.027	0.628
Hepatic NADH (pmol/μg)	0.144*	0.009
Hepatic Total Glutathione (nmol/mg)	0.115*	0.034
Hepatic GSH (nmol/mg)	0.116*	0.033
Hepatic GSSG (nmol/mg)	0.041	0.449
Hepatic GSH/GSSG (nmol/mg)	0.099	0.067
Hepatic E_h (mV)	-0.146*	0.007
Steatosis	-0.121*	0.026
Hydropic Degeneration	-0.130*	0.016
Fibrosis	0.023	0.678

To be consistent with fasting times needed for precise hepatic glutathione measurement, mice were fasted for 3-4 hours prior to sacrifice where blood glucose was collected at sacrifice via the tail vein using FreeStyle Lite test strips and glucometer (Abbott Laboratories, Chicago, IL USA) and expressed as mg/dL. Spearman correlations were calculated for relationships with glucose and included in Supplementary Table S4.3. Glucose concentrations were correlated with body weight ($\rho = 0.363$, $p = <0.001$), liver weight ($\rho = 0.394$, $p = <0.001$), AST concentrations ($\rho = -0.167$, $p = 0.002$) and AST/ALT levels ($\rho = -0.181$, $p = 0.001$). Glucose concentrations were not correlated with ALT concentrations, nor hepatic NADH concentrations, but were correlated with hepatic NADPH concentrations ($\rho = 0.233$, $p = <0.001$), hepatic $NADP^+$ concentrations ($\rho = -0.176$, $p = 0.001$), and hepatic $NADP^+$/NADPH levels ($\rho = -0.275$, $p = <0.001$). Glucose concentrations were not correlated with hepatic total glutathione concentrations ($p = 0.235$), hepatic GSH concentrations ($p = 0.227$), hepatic GSSG concentrations ($p = 0.460$), hepatic

GSH/GSSG levels ($p = 0.427$), hepatic E_h levels ($p = 0.241$), steatosis ($p = 0.127$), or fibrosis ($p = 0.792$), but were correlated with hydropic degeneration ($\rho = 0.316$, $p = <0.001$).

Lastly, we screened for statistical relationships with hepatic histological scores (Tables 4.8 – 4.10). Liver weight was correlated with both steatosis and hydropic degeneration grades ($\rho = 0.272$, $p = <0.001$ and $\rho = 0.387$, $p = <0.001$, respectively). Similarly, body weight was correlated with steatosis and hydropic degeneration grades ($\rho = 0.304$, $p = <0.001$ and $\rho = 0.352$, $p = <0.001$, respectively). AST/ALT levels, but not the two transaminases individually, were correlated with steatosis grades ($\rho = -0.121$, $p = 0.026$). Likewise, hepatic GSH/GSSG levels were correlated with steatosis grades ($\rho = -0.176$, $p = 0.001$). Lastly, steatosis and hydropic degeneration grades were correlated ($\rho = 0.116$, $p = 0.031$). Both AST concentrations and AST/ALT levels were negatively correlated with hydropic degeneration ($\rho = -0.115$, $p = 0.034$ and $\rho = -0.130$, $p = 0.016$, respectively). Given the lack of variation in fibrosis, we assessed correlations cautiously. Fibrosis was positively correlated with hepatic $NADP^+$ concentrations ($\rho = 0.111$, $p = 0.043$) and negatively correlated with hepatic total glutathione concentrations ($\rho = -0.112$, $p = 0.037$) and hepatic GSH concentrations ($\rho = -0.112$, $p = 0.037$).

Table 4.8. Statistical relationships between variables and steatosis.
Spearman's rho (ρ) was calculated for each variable combination and listed within each corresponding box. *indicates a significant relationship ($p \leq 0.05$).

Variables	**ρ**	**p-value**
Liver Weight (g)	0.272*	<0.001
Body Weight (g)	0.304*	<0.001
AST (U/L)	-0.080	0.142
ALT (U/L)	0.066	0.221
AST/ALT	-0.121*	0.026
Hepatic NADPH (pmol/μg)	-0.001	0.983
Hepatic $NADP^+$ (pmol/μg)	0.010	0.849
Hepatic $NADP^+$/NADPH	-0.021	0.708
Hepatic NADH (pmol/μg)	0.051	0.353
Hepatic Total Glutathione (nmol/mg)	0.013	0.808
Hepatic GSH (nmol/mg)	0.009	0.867
Hepatic GSSG (nmol/mg)	0.092	0.089
Hepatic GSH/GSSG (nmol/mg)	-0.176*	0.001
Hepatic E_h (mV)	0.078	0.146
Hydropic Degeneration	0.116*	0.031
Fibrosis	0.007	0.901

Table 4.9. Statistical relationships between variables and hydropic degeneration.
Spearman's rho (ρ) was calculated for each variable combination and listed within each corresponding box. *indicates a significant relationship ($p \leq 0.05$).

Variables	**ρ**	**p-value**
Liver Weight (g)	0.387*	<0.001
Body Weight (g)	0.352*	<0.001
AST (U/L)	-0.115*	0.034
ALT (U/L)	0.013	0.818
AST/ALT	-0.130*	0.016
Hepatic NADPH (pmol/μg)	0.075	0.169
Hepatic $NADP^+$ (pmol/μg)	0.075	0.176
Hepatic $NADP^+$/NADPH	-0.019	0.738
Hepatic NADH (pmol/μg)	0.100	0.070
Hepatic Total Glutathione (nmol/mg)	0.105	0.052
Hepatic GSH (nmol/mg)	0.105	0.052
Hepatic GSSG (nmol/mg)	0.084	0.120
Hepatic GSH/GSSG (nmol/mg)	0.008	0.876
Hepatic E_h (mV)	-0.091	0.091
Steatosis	0.116*	0.031
Fibrosis	-0.043	0.425

Table 4.10. Statistical relationships between variables and fibrosis.
Spearman's rho (ρ) was calculated for each variable combination and listed within each corresponding box. *indicates a significant relationship ($p \leq 0.05$).

Variables	**ρ**	**p-value**
Liver Weight (g)	-0.055	0.305
Body Weight (g)	-0.034	0.524
AST (U/L)	-0.004	0.947
ALT (U/L)	-0.022	0.689
AST/ALT	0.023	0.678
Hepatic NADPH (pmol/μg)	0.006	0.915
Hepatic $NADP^+$ (pmol/μg)	0.111*	0.043
Hepatic $NADP^+$/NADPH	0.087	0.123
Hepatic NADH (pmol/μg)	-0.037	0.503
Hepatic Total Glutathione (nmol/mg)	-0.112*	0.037
Hepatic GSH (nmol/mg)	-0.112*	0.037
Hepatic GSSG (nmol/mg)	-0.070	0.195
Hepatic GSH/GSSG (nmol/mg)	-0.036	0.510
Hepatic E_h (mV)	0.090	0.096
Steatosis	0.007	0.901
Hydropic Degeneration	-0.043	0.425

To better understand the relationship between the hepatic glutathione and NAD redox system phenotypes, serum transaminases, and histological grades, we plotted values by histological grade (Figures 4.5 and 4.6). We were unable to plot comparisons between values and fibrosis grades given insufficient histological observations in grades beyond F0 and F1. We observed significant variation in several values by steatosis grade (Figure 4.5). Liver weight was significantly different between grades 0 and 1 ($p = 0.005$), grades 0 and 2 ($p = <0.001$), and grades 0 and 3 ($p = 0.002$), as well as between grades 1 and 2 ($p = 0.011$) and grades 1 and 3 ($p = 0.032$). Body weight was similar in that it differed between steatosis grades 0 and 1 ($p = <0.001$), grades 0 and 2 ($p = 0.001$), and grades 0 and 3 ($p = 0.007$). Concentrations of glutathione phenotypes were not significantly different between steatosis grades. Hepatic We observed no differences between steatosis grades for hepatic NADPH concentrations or hepatic $NADP^+$/NADPH levels, but concentrations of hepatic $NADP^+$ did differ between steatosis grades 0 and 3 ($p = 0.010$), as

well as between steatosis grades 1 and 3 ($p = 0.005$). NADH concentrations were significantly different between steatosis grades 2 and 3 ($p = 0.012$). Neither AST or ALT concentrations, nor the ratio of the two (AST/ALT) differed between steatosis grades. Comparison of phenotypes by hydropic degeneration grade revealed many significant differences between grades (Figure 4.6). Hepatic total glutathione concentrations were significantly different between grades 2 and 5 ($p = 0.011$), 3 and 4 ($p = 0.014$), and 3 and 5 ($p = 0.005$). Hepatic GSH concentrations followed the same trend with differing concentrations between hydropic degeneration grades 2 and 5 ($p = 0.012$), 3 and 4 ($p = 0.012$), and 3 and 5 ($p = 0.005$). Hepatic GSSG concentrations differed between grades 2 and 5 ($p = 0.010$), 3 and 5 ($p = 0.006$), and 4 and 5 ($p = 0.023$). Hepatic GSH/GSSG concentrations did not differ by grades whereas hepatic E_h differed between grades 3 and 4 ($p = 0.010$) and grades 3 and 5 ($p = 0.022$). Hepatic $NADP^+$ concentrations differed between grades 0 and 4 ($p = 0.030$) and hepatic NADH differing between grades 3 and 4 ($p = 0.015$). AST/ALT, but not AST (U/L) or ALT (U/L) individually, were significantly different between grades 1 and 5 ($p = 0.037$). Lastly, we observed many significant differences between liver weight (g) and body weight (g) across hydropic degeneration grades. Liver weight was significantly different between grades 0 and 2 ($p = 0.020$), grades 0 and 3 ($p = 0.004$), grades 0 and 4 ($p = <0.001$), and grades 0 and 5 ($p = <0.001$), grades 1 and 3 ($p = 0.024$), grades 1 and 4 ($p = <0.001$), grades 1 and 5 ($p = <0.001$), grades 2 and 4 ($p = <0.001$), grades 2 and 5 ($p = <0.001$), grades 3 and 4 ($p = <0.001$), grades 3 and 5 ($p = <0.001$), and grades 4 and 5 ($p = <0.001$). Similarly, body weight was significantly different between grades 0 and 1 ($p = 0.039$), grades 0 and 2 ($p = <0.001$), grades 0 and 3 ($p = <0.001$), grades 0 and 4 ($p = <0.001$), grades 0 and 5 ($p = <0.001$), grades 1 and 4 ($p = < 0.001$), grades 1 and 5 ($p = <0.001$), grades 2 and 4 ($p = <0.001$), grades 2 and 5 ($p = <0.001$), grades 3 and 4 ($p = <0.001$), and grades 3 and 5 ($p = 0.001$).

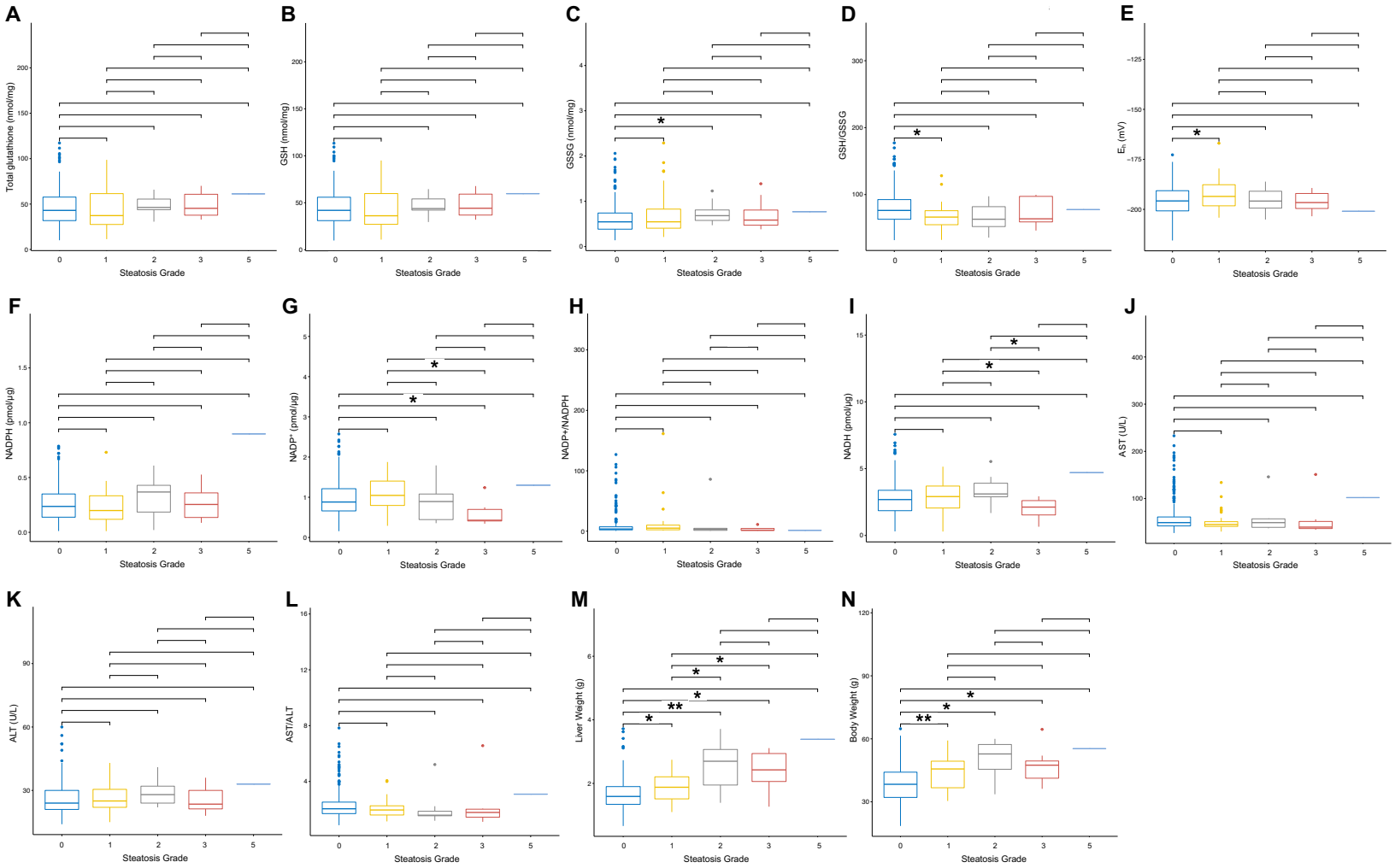

Figure 4.5. Distribution of variables by steatosis grade.
A. Hepatic Total Glutathione (nmol/mg) **B.** Hepatic GSH (nmol/mg) **C.** Hepatic GSSG (nmol/mg) **D.** Hepatic GSH/GSSG **E.** Hepatic E_h (mV) **F.** Hepatic NADH (pmol/µg) **G.** Hepatic $NADP^+$ (pmol/µg) **H.** Hepatic NADPH (pmol/µg) **I.** Hepatic NADP/NADPH **J.** AST (U/L) **K.** ALT (U/L) **L.** AST/ALT **M.** Liver Weight (g). **N.** Body Weight (g). *indicates a p-value ≤ 0.05, **indicates a p-value ≤ 0.001.

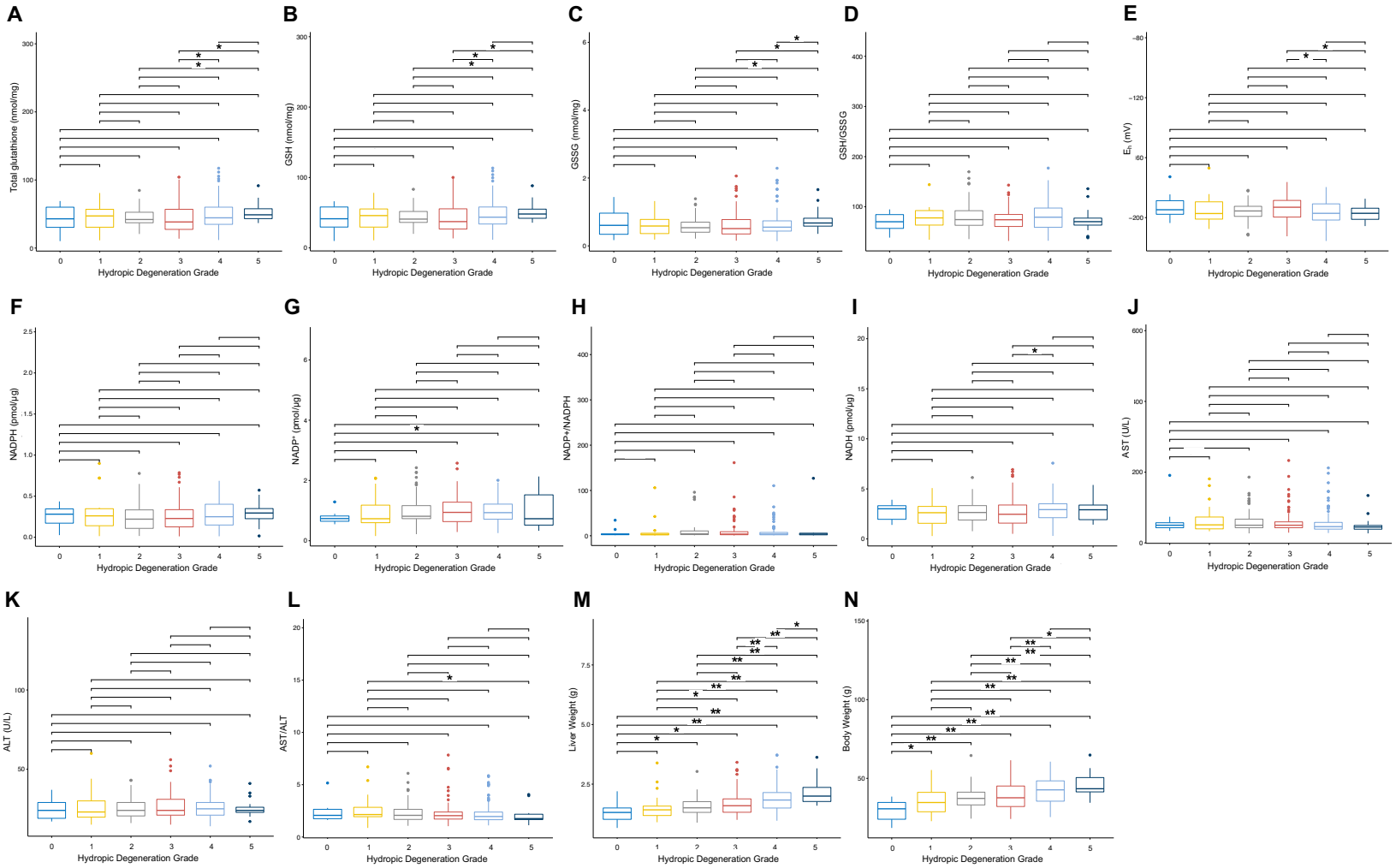

Figure 4.6. Distribution of variables by hydropic degeneration grade.
A. Hepatic GSH (nmol/mg) **B.** Hepatic GSSG (nmol/mg) **C.** Hepatic Total Glutathione (nmol/mg) **D.** Hepatic GSH/GSSG **E.** Hepatic E_h **F.** Hepatic NADH (pmol/µg) **G.** Hepatic $NADP^+$ (pmol/µg) **H.** Hepatic NADPH (pmol/µg) **I.** Hepatic NADP/NADPH **J.** AST (U/L) **K.** ALT (U/L) **L.** AST/ALT **M.** Liver Weight (g). **N.** Body Weight (g). *indicates a p-value ≤ 0.05, **indicates a p-value ≤ 0.001.

QTL mapping of serum aminotransferases and NAFLD histopathological scores: To identify the impact of genetic background on these clinical biomarkers and hepatic histopathological outcomes, we performed QTL analysis with the R/qtl2 package (Figure 4.7) [549]. Given the lack of variation of fibrosis, we did not perform QTL mapping using fibrosis as the phenotype of interest. The genome-wide scan for AST concentrations revealed 1 suggestive peak ($p \leq 0.10$) on mouse chromosome 2 at 12.200 Mbp (LOD score 7.444) and 1 significant peak ($p \leq 0.05$) on mouse chromosome 16 at 57.518 Mbp (LOD score 7.808) (Figure 4.7A). The genome-wide scan for steatosis revealed 1 significant peak on mouse chromosome 18 at 17.065 Mbp (LOD score 8.775). In addition, a peak on mouse chromosome X at 51.515 Mbp (LOD score 7.266) was observed for steatosis, though this peak failed to pass significance thresholds (Figure 4.7D). Given the suggestive nature of the peak on chromosome X, candidate gene results and founder allele QTL effects are included in Supplementary Table S4.4 and Figure S4.1. The genome scans for ALT, AST/ALT, and hydropic degeneration did not include QTL peaks that surpassed the significance thresholds (Figure 4.7B, Figure 4.7C, and Figure 4.7E, respectively).

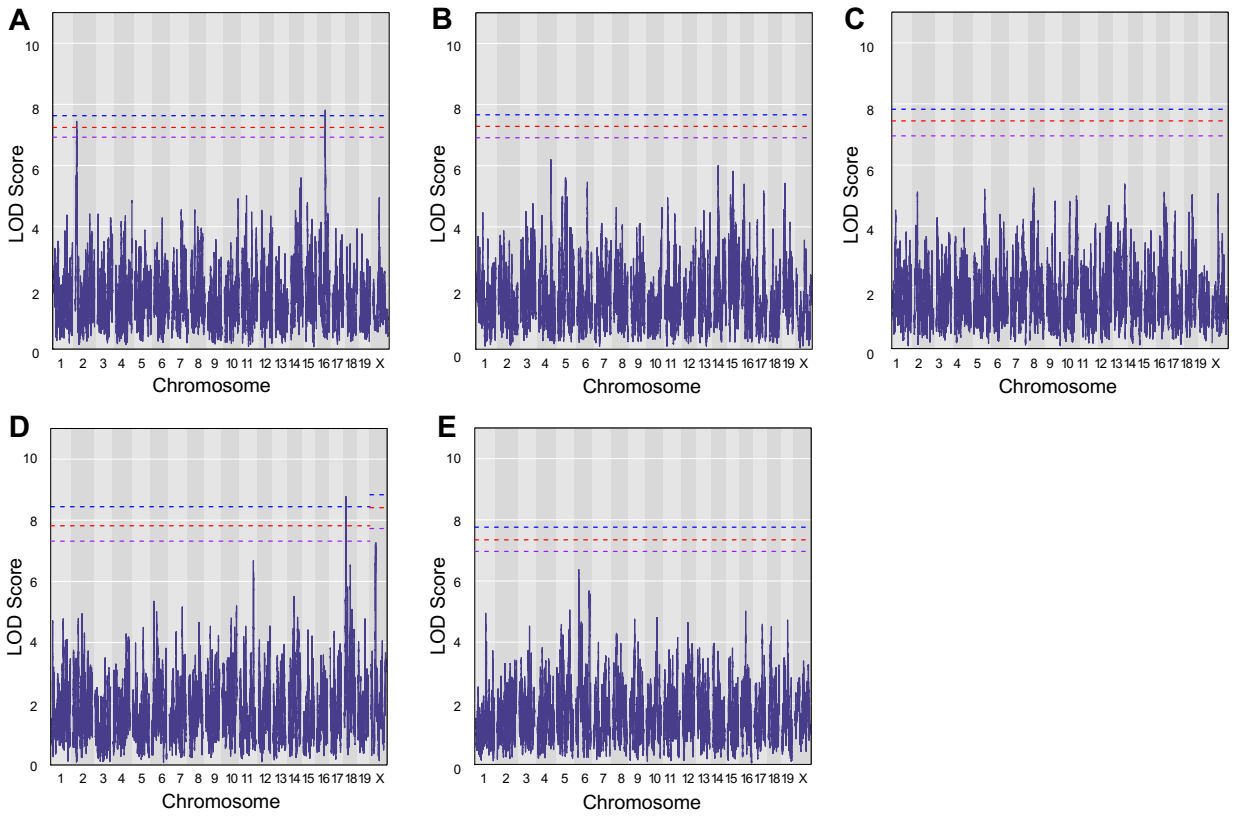

Figure 4.7. QTL results for serum aminotransferases and NAFLD histopathological scores. Genome-wide scans of **A.** AST (U/L); **B.** ALT (U/L); **C.** AST/ALT; **D.** Hepatic Steatosis; and **E.** Hepatic Hydropic Degeneration. Permutation-derived significance thresholds are indicated by colored lines at (α) levels 0.05 (blue), 0.10 (red), and 0.20 (purple).

The genome-wide scan for AST revealed a suggestive peak on mouse chromosome 2 at 12.200 Mbp with a QTL interval of 10.653 – 13.057 Mbp (Figure 4.8A). Founder allele effects were extrapolated within the interval and show that the CAST allele contributes to a lower AST concentration and the WSB allele contributes to a higher AST concentration (Figure 4.8B). We identified genes located within this interval ± 1 Mbp using R/qtl2 through connection with the MGI database (Figure 4.8C), and functional RNA and protein-coding genes were collected and screened for physiological relevance using existing expression, functional, and phenotypic annotations. Given that circulating AST is expressed from several tissues, most notably the heart, liver, skeletal muscle, and kidneys [623], we compiled biological annotations related to those

tissues of interest. The QTL interval contained 187 possible candidate genes: 23 protein-coding, 140 non-coding RNA, and 24 unclassified (Supplementary Table S4.5; GRCm38/mm10; gene query performed December 2020, Feature Type "gene" [563]). We compiled expression, functional, and phenotypic annotations for each gene within the QTL interval to identify candidates with relevance to AST function based on known experimental evidence. 74 of the 187 candidate genes had no heart, liver, skeletal muscle, or kidney expression annotations and were excluded. Out of the remaining 113 candidate genes, 75 did not have additional functional or phenotypic annotations, and the remaining 38 candidate genes were: TATA-box binding protein associated factor 3 (*Taf3*), ATP synthase, H+ transporting, mitochondrial F1 complex, gamma polypeptide 1 (*Atp5c1*), Kin17 DNA and RNA binding protein (*Kin*), inter-alpha trypsin inhibitor, heavy chain 2 (*Itih2*), inter-alpha (globulin) inhibitor H5 (*Itih5*), predicted gene 13261 (*Gm13261*), Scm-like with four mbt domains 2 (*Sfmbt2*), microRNA 466m (*Mir466m*), microRNA 466f-1 (*Mirr466f-1*), microRNA 669f (*Mir669f*), microRNA 669a-3 (*Mir669a-3*), microRNA 467a-1 (*Mir467a-1*), microRNA 467b (*Mir467b*), microRNA 669a-5 (*Mir669a-5*), microRNA 467e (*Mir467e*), microRNA 467d (*Mir467d*), microRNA 466 (*Mir466*), microRNA 297c (*Mir297c*), microRNA 669a-2 (*Mir669a-2*), microRNA 466d (*Mir466d*), microRNA 466d (*Mir669o*), microRNA 466g (*Mir466g*), microRNA 466l (*Mir466l*), protein kinase C, theta (*Prkcq*), 6-phosphofructo-2-kinase/fructose-2,6-biphosphatase 3 (*Pfkfb3*), RNA binding motif protein 17 (*Rbm17*), interleukin 2 receptor, alpha chain (*Il2ra*), interleukin 15 receptor, alpha chain (*Il15ra*), F-box DNA helicase 1 (*Fbh1*), ankyrin repeat domain 16 (*Ankrd16*), integrin alpha 8 (*Itga8*), RIKEN cDNA E030013I19 gene (*E030013I19Rik*), MINDY lysine 48 deubiquitinase 3 (*Mindy3*), phosphotriesterase related (*Pter*), C1q-like 3 (*C1ql3*), Ras suppressor protein 1 (*Rsu1*), predicted gene 13270 (*Gm13270*), and cubilin (intrinsic factor-cobalamin receptor) (*Cubn*).

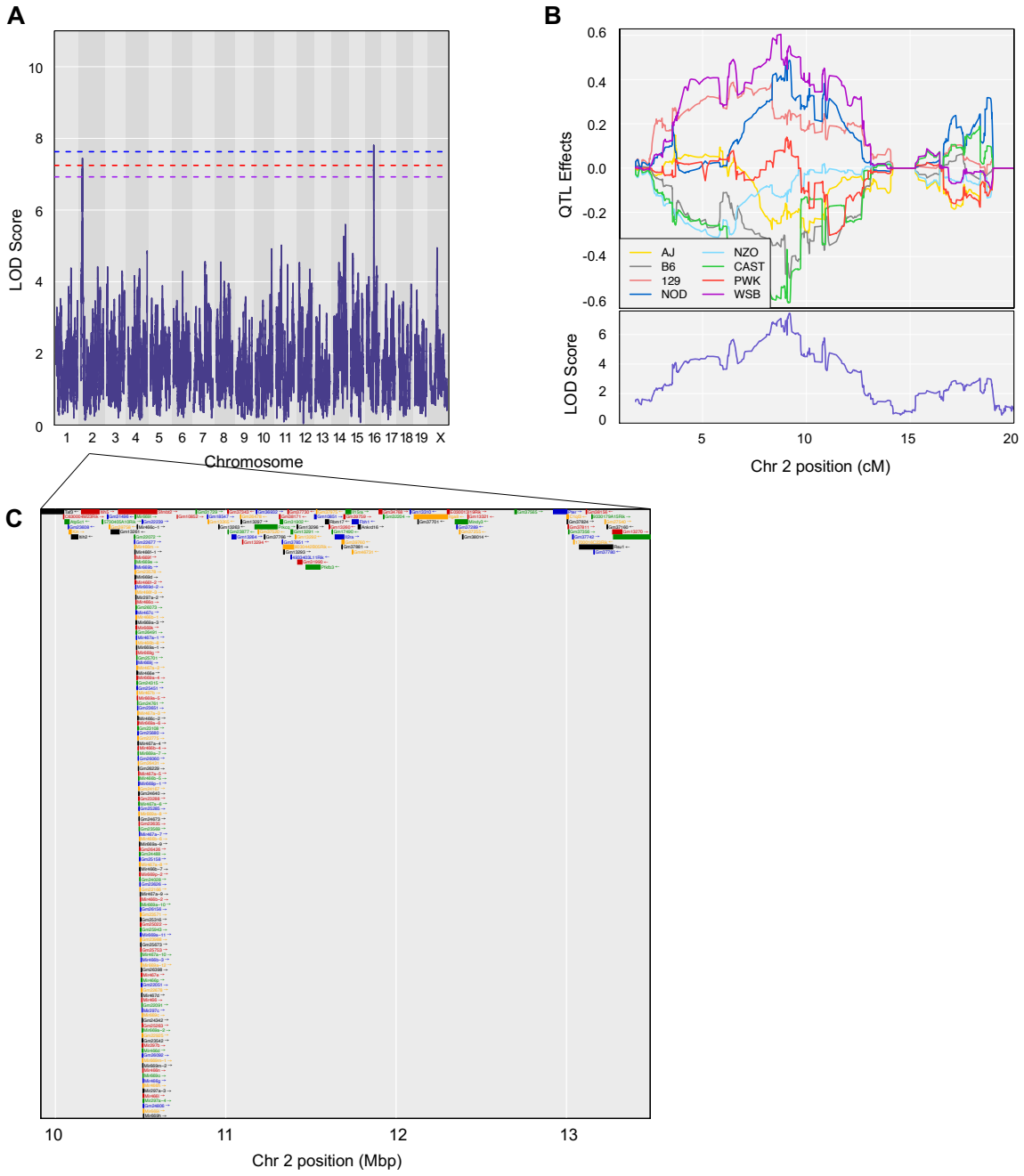

Figure 4.8. High-resolution association mapping for AST in outbred mice reveals a suggestive QTL on mouse chromosome 2.

A. Genome-wide scan of AST in outbred mice shows a QTL with peak LOD score 7.444 at 12.200 Mbp (9.177 cM) on mouse chromosome 2. Permutation-derived significance thresholds are indicated by colored lines at significance (α) levels 0.05 (blue), 0.10 (red), and 0.20 (purple). **B.** The founder allele QTL effects indicate that the CAST allele contributes to a lower AST concentration, whereas the WSB allele contributes to a higher AST concentration. Each colored line represents a DO founder allele as indicated in the legend. The differences between strains are considered significant when the LOD score (bottom) crosses significance thresholds (panel A). **C.** Candidate genes found within the QTL interval relative to the MGI database.

The genome-wide scan for AST revealed a significant peak on mouse chromosome 16 at 57.518 Mbp with a QTL interval of 57.069 – 59.755 Mbp (Figure 4.9A). Founder allele effects showed that the CAST allele contributes to a lower AST concentration, whereas the NZO allele contributes to a higher AST concentration (Figure 4.9B). Functional RNA and protein coding genes within the interval ± 1 Mbp (Figure 4.9C) were screened using biological annotations, and the QTL interval contained 82 possible candidate genes: 50 protein-coding, 26 non-coding RNA, and 6 unclassified (Supplementary Table S4.6; GRCm38/mm10; gene query performed December 2020, Feature Type "gene" [563]). 48 of the 82 candidate genes had no heart, liver, skeletal muscle, or kidney expression annotations and were excluded. Out of the remaining 34 genes, 11 had no additional functional or phenotypic annotations, and the remaining 23 candidate genes were: interphotoreceptor matrix proteoglycan 2 (*Impg2*), ABI gene family, member 3 (NESH) binding protein (*Abi3bp*), Trk-fused gene (*Tfg*), adhesion G protein-coupled receptor G7 (*Adgrg7*), transmembrane protein 45a (*Tmem45a*), transmembrane protein 45A2 (*Tmem45a2*), translocase of outer mitochondrial membrane 70A (*Tomm70a*), nitrilase family, member 2 (*Nit2*), TBC1 domain family, member 23 (*Tbc1d23*), cms small ribosomal subunit 1 (*Cmss1*), filamin A interacting protein 1-like (*Filip1l*), collagen, type VIII, alpha 1 (*Col8a1*), discoidin, CUB and LCCL domain containing 2 (*Dcbld2*), ST3 beta-galactoside alpha-2,3-sialyltransferase 6 (*St3gal6*), coproporphyrinogen oxidase (*Cpox*), G protein-coupled receptor 15 (*Gpr15*), claudin domain containing 1 (*Cldnd1*), olfactory receptor 173 (*Olfr173*), olfactory receptor 201 (*Olfr201*), ribosomal oxygenase 2 (*Riox2*), beta-gamma crystallin domain containing 3 (*Crybg3*), ADP-ribosylation factor-like 6 (*Arl6*), and Eph receptor A6 (*Epha6*). It is unlikely that olfactory receptor genes *Olfr173* and *Olfr201* are candidates for influence on AST concentration, given their primary function in smell perception (GO:0050911, GO:0007608, GO:0005549).

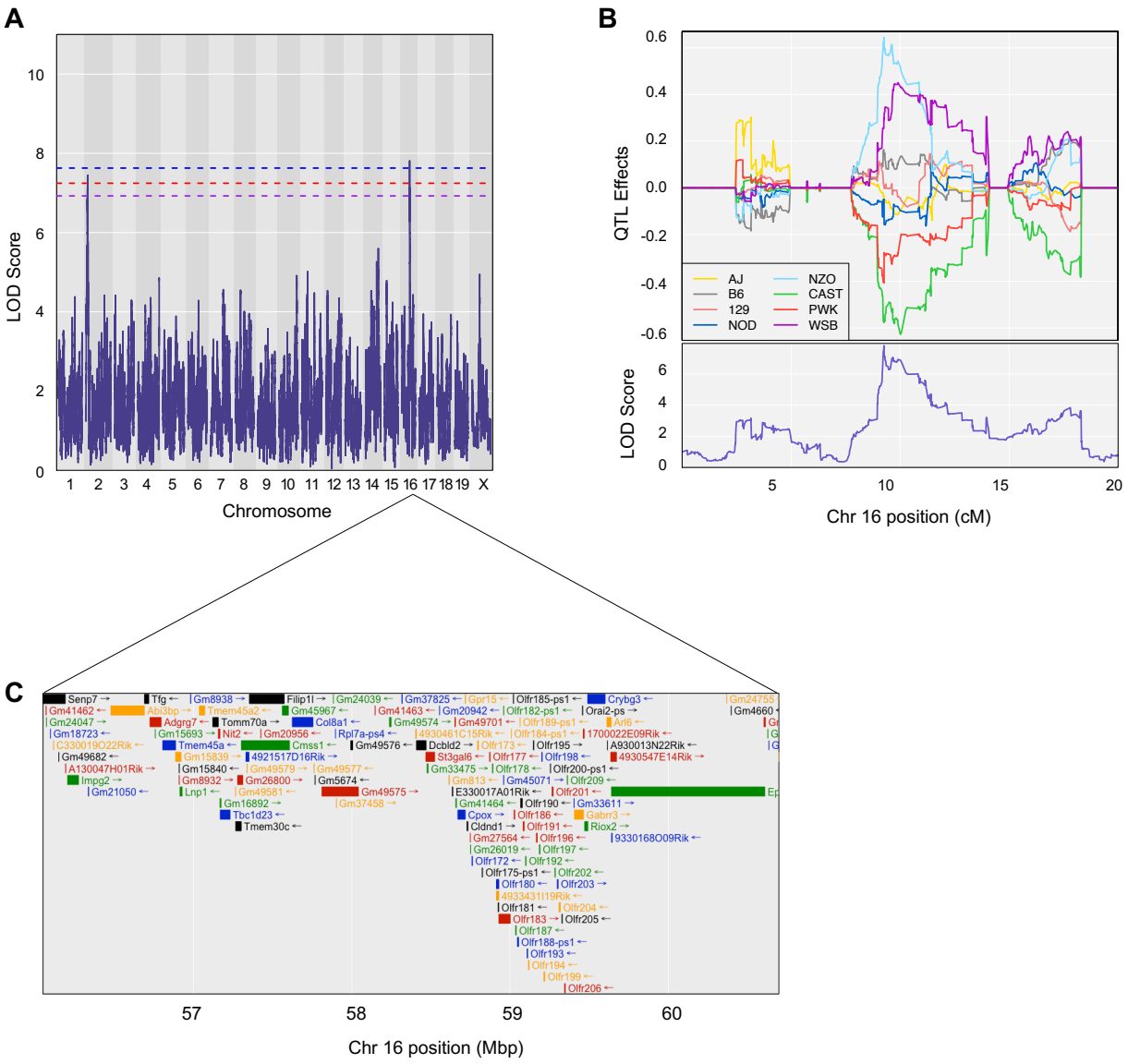

Figure 4.9. High-resolution association mapping for AST in outbred mice reveals a significant QTL on mouse chromosome 16.
A. Genome-wide scan of AST in outbred mice shows a QTL with peak LOD score 7.808 at 57.518 Mbp (34.263 cM) on mouse chromosome 16. Permutation-derived significance thresholds are indicated by colored lines at significance (α) levels 0.05 (blue), 0.10 (red), and 0.20 (purple). **B.** The founder allele QTL effects indicate that the CAST allele contributes to a lower AST concentration, whereas the NZO allele contributes to a higher AST concentration. Each colored line represents a DO founder allele as indicated in the legend. The differences between strains are considered significant when the LOD score (bottom) crosses significance thresholds (panel A). **C.** Candidate genes found within the QTL interval relative to the MGI database.

The genome-wide scan for steatosis revealed a significant peak on mouse chromosome 18 at 17.065 Mbp with a QTL interval of 16.842 – 17.710 Mbp (Figure 4.10A). Founder allele effects were extrapolated within the interval and show that the CAST allele contributes to a higher steatosis grade, whereas the NOD allele contributes to a lower steatosis grade (Figure 4.10B). Functional RNA and protein coding genes within the interval were collected (Figure 4.10C) and screened for using biological annotations and physiological relevance to hepatic steatosis. The QTL interval contained 19 possible candidate genes: 1 protein-coding, 17 non-coding RNA, and 1 unclassified (Supplementary Table S4.7; GRCm38/mm10; gene query performed December 2020, Feature Type "gene" [563]). 17 of the 19 steatosis candidate genes had limited to no hepatic expression annotations and were excluded. Out of the remaining 2 candidate genes, 1 did not have additional functional or phenotypic annotations. The remaining candidate gene was cadherin-2 (*Cdh2*) (Chr18:16588877–16809246 bp; GRCmm38). N-cadherin, also known as cadherin-2 (CDH2), functions as a transmembrane protein to mediate cell-cell adhesion [624]. Matrix metalloproteinase-24 (MMP-24) is responsible for cleaving CDH2 to facilitate cell-cell interactions, and MMP-24 has been shown to be upregulated during liver regeneration [625].

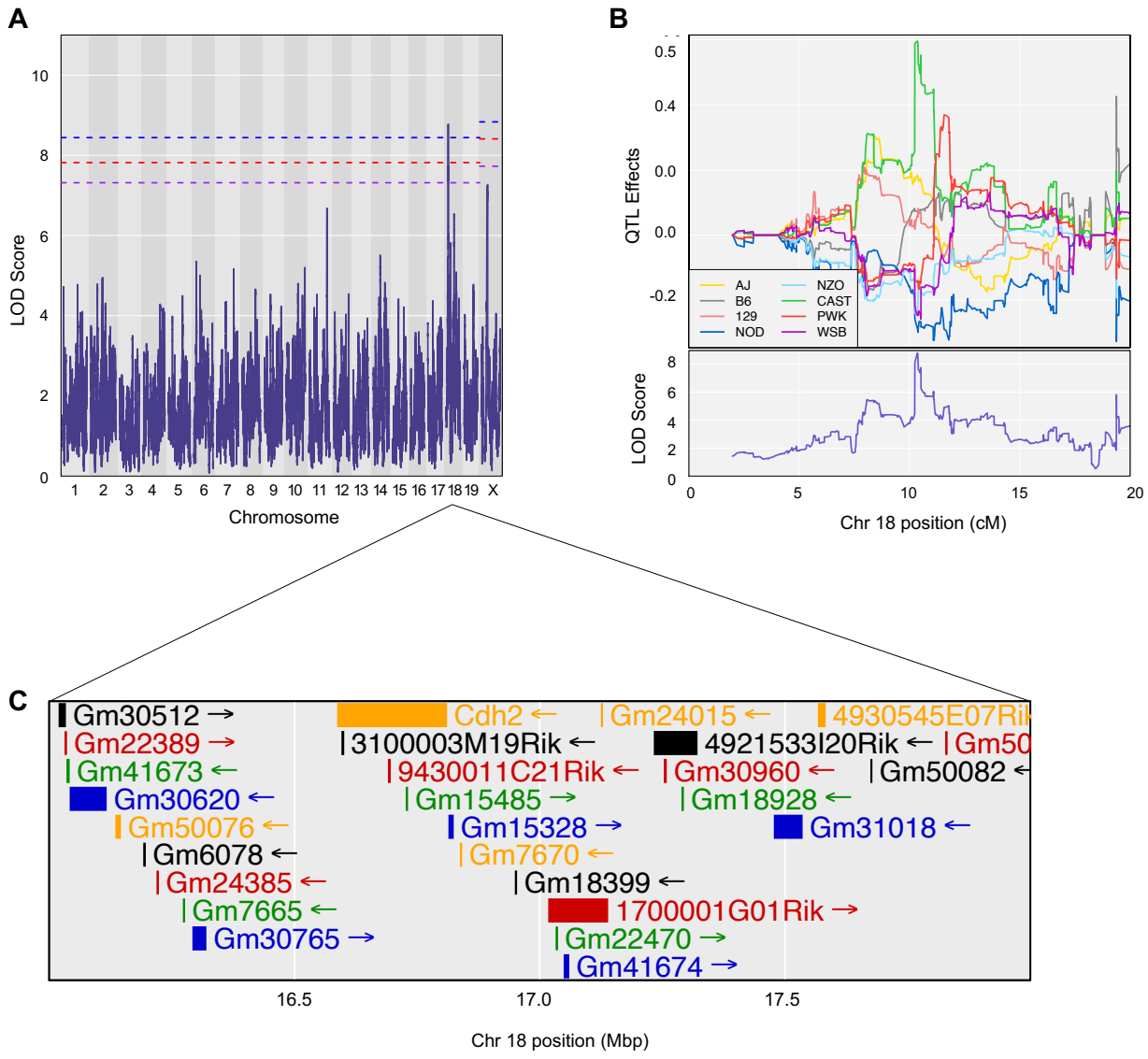

Figure 4.10. High-resolution association mapping for hepatic steatosis in outbred mice reveals a significant QTL on mouse chromosome 18.
A. Genome-wide scan of hepatic steatosis in outbred mice shows a QTL with peak LOD score 8.775 at 17.065 Mbp (10.357 cM) on mouse chromosome 18. Permutation-derived significance thresholds are indicated by colored lines at significance (α) levels 0.05 (blue), 0.10 (red), and 0.20 (purple). **B.** The founder allele QTL effects indicate that the NOD allele contributes to a lower hepatic steatosis grade, whereas the CAST allele contributes to a higher hepatic steatosis grade. Each colored line represents a DO founder allele as indicated in the legend. The differences between strains are considered significant when the LOD score (bottom) crosses significance thresholds (panel A). **C.** Candidate genes found within the QTL interval relative to the MGI database.

Discussion

Despite growing evidence that NAFLD progression is related to oxidative stress, the relationship between hepatic redox variation and NAFLD histopathology remains unclear. We used a large cohort of genetically-diverse mice – the DO model – to disentangle these complex relationships and better understand the genetic regulation of common NAFLD markers: steatosis and hydropic degeneration. This research study was designed to 1) quantify the variation in NAFLD histopathological outcomes and serum aminotransferases AST and ALT in an outbred population under standard conditions, 2) use precise genetic analysis techniques to isolate QTL related to those phenotypes, and 3) elucidate relationships between these markers of NAFLD and liver function with markers of the GSH and NADPH redox systems.

To our knowledge, this is the first study to identify the natural variation of the AST and ALT aminotransferases in a large cohort of outbred mice. Both of these aminotransferases are commonly measured in the clinical setting as serum enzyme biomarkers of liver injury [626]. ALT is considered to be a more sensitive biomarker of hepatic steatosis [627, 628], and has the greatest concentration in the liver, unlike its counterpart AST which is found in high concentrations within heart, liver, skeletal muscle, and kidneys. Regardless, the ratio AST/ALT is often used an indicator for etiology of the underlying liver disease, including as NAFLD [629] and cirrhosis [620]. We quantified serum AST (U/L), ALT (U/L), and AST/ALT in all DO mice and observed a wide variation in these biomarkers. Neither variation was sex-specific, and AST varied from 27 to 233 U/L while ALT varied from 15 to 60 U/L. We observed over a 9-fold difference in AST/ALT with ratios ranging from 0.867 to 7.833, with males having the largest variation and females exhibiting a slightly smaller range from 1.036 to 6.704. At this time, there are no established murine reference values for AST, ALT, or their ratio, as concentrations are dependent on strain background. These

findings represent the natural variation of these commonly measured aminotransferases from both male and female outbred mice under standard conditions and emphasize the importance for inclusion of genetic background when analyzing AST, ALT, or AST/ALT in mouse models.

To elucidate the role of genetic background on the aminotransferase concentrations, we used the R/qtl2 software package to perform QTL analysis on AST, ALT, and AST/ALT with sex and experimental cohort as additive covariates. The QTL peaks for ALT and AST/ALT failed to reach significance (Supplementary Table S4.8), whereas the genome scan for AST revealed a suggestive peak ($p \leq 0.10$) on mouse chromosome 2 at 12.200 Mbp with a LOD score of 7.444, and a significant peak ($p \leq 0.05$) on mouse chromosome 16 at 57.518 Mbp with a LOD score of 7.808. Genes located within the QTL intervals for each peak were investigated for candidate gene prioritization using documented biological annotations. We performed an extensive literature search into each gene and were unable to find evidence linking the candidate genes from mouse chromosome 2 and 16 with AST. Given that serum AST has multiple tissues of origin and is not specific to the liver, along with the multiple etiologies that could lead to a variation in circulating AST, we were unable to narrow down the candidate gene list to propose genes responsible causing the natural variation in AST. However, we used this information to identify if these QTL peaks overlapped between those found from genome scans of hepatic histological scores and markers of the hepatic GSH and NADPH redox systems [Chapter 3]. Genome scans of the markers of the GSH and NADPH redox systems did not have peaks with a LOD score greater than 6 on mouse chromosome 2 or 16 in intervals near those found in the AST genome scan. Hepatic GSH/GSSG had a significant peak found on mouse chromosome 16, but the QTL interval was between 8.865 – 10.077 Mbp and we therefore concluded that these peaks were not related to one another.

NAFLD histopathological outcomes in these outbred rodents are reflective of NAFLD etiology and progression in humans [615]. To identify the natural variation in histopathological outcomes related to NAFLD, we graded liver samples from 347 DO mice for steatosis, hydropic degeneration, and fibrosis. Variation of steatosis spanned from 0 (absent) to 5 (severe steatosis), with 84.4% (N = 292) of livers exhibiting no presence of steatosis. Progressed hydropic degeneration was apparent in mouse liver samples evidenced by grade variation spanning from 0 to 5, with 65.7% of livers earning a grade of 3 or 4. We observed much less variation in fibrosis than other histopathological outcomes, with N = 329 (95.1%) not exhibiting any signs of fibrosis (grade 0). We suspect this is due to the animals being young-adult old under standard conditions, and that fibrosis would have needed more time or the introduction of a stressor to develop. These findings establish a baseline for natural variation in histological findings of the liver, and future DO studies should account for this when investigating liver-based pathologies. Moreover, we sought to identify the statistical relationships between histological outcomes and other variables of interest. Confirming our assumption that steatosis would be linked to enlarged liver weight (g), we observed a moderate correlation between the two ($\rho = 0.240$, $p = <0.001$). Steatosis was mildly correlated with AST/ALT and GSH/GSSG ($\rho = -0.132$, $p = 0.026$ and $\rho = -0.171$, $p = 0.001$, respectively), but no other aminotransferases or hepatic redox phenotypes. We also observed a mild correlation between steatosis and hydropic degeneration ($\rho = 0.136$, $p = 0.031$), as well as between hydropic degeneration and AST/ALT ($\rho = -0.110$, $p = 0.016$) and AST at ($\rho = -0.139$, $p = 0.034$). Hydropic degeneration was not observed to be correlated with any hepatic redox phenotypes.

Despite lack of correlations between histological grades and redox phenotypes as a whole, we used Wilcoxon Rank Sum tests to identify the significant differences in these variables by

histological grade. Given the strong correlation of increased liver weight to steatosis progression [630, 631], we expected to find a difference between liver weight (g) and steatosis grade. Liver weight (g) significantly increased in a steatosis grade-dependent manner between grades 0, 1, 2, and 3 with the exception of no significant difference between grades 2 and 3. Hepatic $NADP^+$ concentrations differed between grades 0 and 3 and grades 1 and 3, and hepatic NADH concentrations differed between steatosis grades 2 and 3. We did not observe any significant differences between hepatic glutathione phenotypes or serum aminotransferases when separated and compared by steatosis grade. However, we did observe significant differences in hepatic total glutathione concentrations, hepatic GSH concentrations, hepatic GSSG concentrations, and hepatic E_h levels by hydropic degeneration grade. Both hepatic total glutathione concentrations and hepatic GSH concentrations increased between hydropic degeneration grades 2 and 5, 3 and 4, and 3 and 5. Similarly, hepatic GSSG concentrations increased between hydropic generation grades 2 and 5, 3 and 5, and 4 and 5, while hepatic E_h levels decreased between grades 3 and 4, and grades 3 and 5. Lastly, hepatic $NADP^+$ concentrations increased from grades 0 and 4 and hepatic NADH concentrations increased from hydropic degeneration grades 3 and 4. These results better inform us on the risk of NAFLD progression from change in redox status and suggests that our GSH and NADPH redox systems are altered as hepatic hydropic degeneration progresses.

Lastly, to identify the genetic determinants of steatosis and hydropic generation, we conducted QTL mapping on the two histological outcomes. No significant peaks for hydropic degeneration were found, but the genome scan for steatosis revealed a significant peak on mouse chromosome 18 at 17.065 Mbp with a LOD score of 8.775. This peak did not overlap with QTL results previously found for markers of the GSH and NADPH redox systems [Chapter 3]. Interestingly, the CAST allele was found to be associated with low AST (U/L) concentrations (in

both QTL peaks on mouse chromosome 2 and 16), a higher steatosis grade, and lower $NADP^+$ (pmol/μg) concentrations, whereas the WSB allele was associated with a higher AST (U/L) concentration (QTL peak on mouse chromosome 2), as well as higher hepatic $NADP^+$ (pmol/μg) and $NADP^+$/NADPH concentrations.

When comparing QTL results from genome scans of histological scores with those from serum aminotransferases (Supplementary Table S4.8) and with those previously discovered from genome scans of hepatic markers of the GSH and NADPH redox systems [Chapter 3], we found a QTL interval for steatosis on mouse chromosome 18 at 56.619 (58.499 – 69.153) Mbp (LOD score 6.540) overlapping with a QTL found for hepatic total glutathione on mouse chromosome 18 at 51.537 (35.120 – 76.532) Mbp (LOD score 6.011) and hepatic GSSG on mouse chromosome 18 at 53.075 (50.199 – 82.487) Mbp (LOD score 6.149). Additionally, we compared our findings to those of hepatic and renal glutathione genome scans discovered *in silico* using haplotype association mapping (HAM) [526]. We found a QTL peak for ALT on mouse chromosome 4 at 134.295 (132.970 – 135.609) Mbp (LOD score 6.206) to be in proximity to a HAM peak for hepatic GSSG on mouse chromosome 4 at 130.724 Mbp. Furthermore, we observed our QTL peak for steatosis on mouse chromosome 18 at 17.065 (16.482 – 17.710) Mbp (LOD score 8.775) to be in proximity to HAM peaks reported for renal GSH and GSH/GSSG at 14.646 – 16.605 Mbp and 12.293 Mbp, respectively. These findings further suggest that the hepatic and renal glutathione system are related to those responsible for variation in hepatic steatosis and ALT levels, and future studies will be conducted to narrow and eventually select causative genes.

Genome-wide association mapping in 346 DO mice revealed a novel QTL peak influencing hepatic steatosis on mouse chromosome 18 at 17.065 Mbp (LOD score 8.775) which included 19 candidate genes. Published biological annotations concluded that *Cdh2* was the most plausible

candidate gene in the QTL region. It is possible that other genes in this region are responsible for variation in steatosis grades, but we investigated *Cdh2* given its function and relevance to liver function and metabolism. Cdh2 is a transmembrane protein involved in cell-cell adhesion. Matrix metalloproteinase-24 (MMP-24) cleaves CDH2 to facilitate cell-cell interactions, and MMP-24 has been shown to be upregulated during liver regeneration [625]. In addition, microRNA-194 (miR-194) targets genes that are involved in hepatic epithelial-mesenchymal transition as well as motility, of which *Cdh2* is included [632], and expression of this microRNA is lost as hepatocellular carcinoma progresses in mice [633]. *Cdh2* has also been implicated in fibrosis progression as endothelial cells transition to mesenchymal cells and gain the ability to express mesenchymal proteins, including *Cdh2* [633, 634], and a clinical trial investigating NASH patients found that *CDH2* was linked to fibrosis improvement [635]. *Cdh2* expression is upregulated during epithelial-to-mesenchymal transitions (EMT) [636, 637] and endothelial-to-mesenchymal transitions (EndMT) [638], processes that are involved in NAFLD progression [639, 640]. Moreover, the hedgehog pathway mediates the EMT response in NAFLD liver injury repair [641], and *Cdh2* is a critical gene involved in hedgehog signaling in the liver [642]. Limited mouse genome-wide association studies (GWAS) are available on NAFLD and our literature search failed to find mouse GWAS linking *Cdh2* to NAFLD, though human GWAS have revealed CDH2 to be linked with hepatic steatosis [643]. Moreover, human GWAS found that a specific variant of *CDH2* (rs11083271-A) has been linked with the pathology of NAFLD [644]. Given this evidence, we propose that *Cdh2* expression could be influencing hepatic steatosis progression through its role in cell-cell adhesion. The next steps of this research involve investigating and validating the role of *Cdh2* on hepatic steatosis in a NAFLD model. Interestingly, QTL mapping conducted by Brial et al. (2019) observed a peak for macrovesicular and microvesicular steatosis at

approximately 20 cM (10–30 cM) on mouse chromosome 18, which is in close proximity to the QTL peak we observed here on mouse chromosome 18 at 10.357 cM (17.065 Mbp) [613]. Interestingly, in leptin-receptor deficient (*db/db* mice) that develop type 2 diabetes mellitus, *Cdh2* expression and protein concentrations are markedly increased [645]. Proteonomic and bioinformatic analysis of diabetic mouse liver linked hepatic lipid metabolism, inflammation, ER stress, and insulin resistance with *Cdh2* upregulation, potentially mediated by JNK [645].

This study was accompanied by some limitations. This study was designed to evaluate the natural variation in histopathological outcomes of NAFLD, and we therefore did not incorporate an intervention to induce NAFLD. Due to the age of the mice and lack of intervention, we were able to identify the variation in hepatic steatosis, hydropic degeneration, and fibrosis, but we were unable to utilize the QTL mapping technology to identify the influence of genetics on fibrosis outcomes due to lack of fibrosis progression. Furthermore, the mice were kept in a sterile environment and the room underwent standard screening for infections that could have resulted in hepatic infection and adenomas, however we cannot rule out all possible infections.

Conclusion

Hepatic glutathione status is closely tied with the onset and progression of NAFLD due to its role as a cytoprotectant against oxidative stress. Previous research from DO mice under standard conditions found that markers of the GSH and NADPH redox systems vary within hepatic tissue and that genetic background influences hepatic GSH/GSSG. Those results suggested that the status of the GSH redox system may be controlled at a tissue-specific level, potentially impacting the risk for liver disease, and this follow-up study investigated the impact of that variation on liver health and NAFLD histopathological outcomes. We documented the variation of hepatic steatosis, hydropic degeneration, and fibrosis, as well as serum AST and ALT, and then evaluated the

statistical and genetic relationships between hepatic redox phenotypes and these outcomes. Genetic mapping identified a novel QTL peak on mouse chromosome 18 at 56.619 Mbp associated with hepatic steatosis, and bioinformatic analysis identified *Cdh2* as a plausible candidate in steatosis progression. Future research investigating the role of *Cdh2* on hepatic steatosis in a NAFLD model is warranted. Overall, these findings improve our understanding of the complex relationship between glutathione and NAFLD histopathology, as well as better inform candidate gene studies investigating NAFLD progression.

Supplementary Table S4.1. Descriptive statistics of serum aminotransferases in male DO mice.

Phenotype:	**N**	**$\bar{x}$**	**Median**	**SD**	**Min**	**Max**
AST (U/L)	170	56	47	29	27	212
ALT (U/L)	169	27	26	8	15	60
AST/ALT	169	2.048	1.789	0.886	0.867	7.833

Supplementary Table S4.2. Descriptive statistics of serum aminotransferases in female DO mice.

Phenotype:	**N**	**$\bar{x}$**	**Median**	**SD**	**Min**	**Max**
AST (U/L)	173	62	50	35	28	233
ALT (U/L)	173	24	23	7	14	56
AST/ALT	172	2.534	2.200	1.120	1.036	6.704

Supplementary Table S4.3. Statistical relationships between variables and glucose (mg/dL). Spearman's rho (ρ) was calculated for each variable combination and listed within each corresponding box. *indicates a significant relationship ($p < 0.05$).

Variables	**ρ**	**p-value**
Liver Weight (g)	0.394*	<0.001
Body Weight (g)	0.363*	<0.001
AST (U/L)	-0.167*	0.002
ALT (U/L)	0.009	0.865
AST/ALT	-0.181*	0.001
Hepatic NADPH (pmol/μg)	0.233*	<0.001
Hepatic $NADP^+$ (pmol/μg)	-0.176*	0.001
Hepatic $NADP^+$/NADPH	-0.275*	<0.001
Hepatic NADH (pmol/μg)	-0.023	0.675
Hepatic Total Glutathione (nmol/mg)	0.064	0.235
Hepatic GSH (nmol/mg)	0.065	0.227
Hepatic GSSG (nmol/mg)	0.040	0.460
Hepatic GSH/GSSG (nmol/mg)	0.043	0.427
Hepatic E_h (mV)	-0.063	0.241
Steatosis	0.082	0.127
Hydropic Degeneration	0.316*	<0.001
Fibrosis	0.014	0.792

Supplementary Table S4.4. Steatosis candidate genes and their relevant annotations (ChrX: 47.372–51.838 ± 1 Mbp; GRCm38/mm10).[a]

				Expression (liver)		Functional		Phenotypic (liver-related)		
MGI Gene symbol	**Genome coordinates (strand)**	**Type**	**Known steatosis gene**	**GXD (MGI)**	**EEA**	**Inter Pro**	**GO**	**PW**	**EBM**	**Relevance to hepatic steatosis[b]**
4930515L19Rik	ChrX:46267559-46328911 (-)	lncRNA gene	No	--	--	--	--	--	--	None – predicted gene
Actrt1	ChrX:46329007-46330345 (-)	protein coding gene	No	--	--	--	--	--	--	None
Gm29242	ChrX:46473585-46774099 (-)	lncRNA gene	No	--	--	--	--	--	--	None – predicted gene
Gm5636	ChrX:47433043-47436541 (-)	unclassified gene	No	--	--	--	--	--	--	None – predicted gene
Gm39510	ChrX:47465791-47466863 (-)	lncRNA gene	No	--	--	--	--	--	--	None – predicted gene
Smarca1	ChrX:47809370-47892613 (-)	protein coding gene	No	X	X	X	X	--	--	Expressed in mouse liver; GO:0036310; GO:0008094; GO:0005524; GO:0043044; GO:0007420; GO:0090537; GO:0000785; GO:0003682; GO:0006325; GO:0006338; GO:0003677; GO:0004386; GO:0016787; GO:0016818; GO:0043231; GO:0030182; GO:0003676; GO:0005654; GO:0031491; GO:0070615; GO:0000166; GO:0005634; GO:0016589; GO:0045944; GO:0045893; GO:2000177; GO:0006355; GO:0008134
Ocrl	ChrX:47912387-47965868 (+)	protein coding gene	No	X	X	X	X	--	--	Expressed in mouse liver; GO:0042995; GO:0030030; GO:0005929; GO:0060271; GO:0005905; GO:0030136;

										GO:0005737; GO:0031410; GO:0016311; GO:0005769; GO:0005768; GO:0005794; GO:0005096; GO:0016787; GO:0052659; GO:0052658; GO:0046855; GO:0052745; GO:0004445; GO:0001701; GO:0016020; GO:0005634; GO:0004439; GO:0046856; GO:0001750; GO:0005886; GO:0043087; GO:0007165; GO:0031267; GO:0005802
Apln	ChrX:48025146-48034853	protein coding gene	No	X	X	X	X	--	--	Expressed in mouse liver; GO:0001525; GO:0031704; GO:0060183; GO:0060976; GO:0042756; GO:0005576; GO:0007631; GO:0007369; GO:0007186; GO:0005179; GO:0042802; GO:0007275; GO:0045776; GO:0040037; GO:0010629; GO:1904706; GO:0045906; GO:0048471; GO:0008284; GO:0051466; GO:0051461; GO:1904022; GO:0045823; GO:0031652; GO:0042327; GO:1902895; GO:1905564; GO:0050878; GO:0043576; GO:0002026; GO:0005102; GO:0007165
Xpnpep2	ChrX:48108725-48136981 (+)	protein coding gene	No	X	X	--	X	--	--	Expressed in mouse liver; GO:0004177; GO:0031225; GO:0070062; GO:0016787; GO:0016020; GO:0046872; GO:0070006; GO:0008233; GO:0005886; GO:0006508

Sash3	ChrX:48146436-48161565 (+)	protein coding gene	No	X	X	X	X	--	X	Expressed in mouse liver; GO:0005737; GO:0048873; GO:0005634; GO:0002821; GO:0030890; GO:0043372; GO:0002639; GO:0032729; GO:0032733; GO:0032743; GO:0032753; GO:0051251; GO:0046622; GO:0002726; GO:0042102; GO:0032760; Abnormal inflammatory response (EBM)
Zdhhc9	ChrX:48171967-48208702 (-)	protein coding gene	No	X	X	X	X	--	--	Expressed in mouse liver; GO:0005829; GO:0005783; GO:0005794; GO:0016021; GO:0031228; GO:0016020; GO:0016409; GO:0002178; GO:0018230; GO:0019706; GO:0018345; GO:0006612; GO:0043849; GO:0016740; GO:0016746
Gm24038	ChrX:48230286-48230444 (+)	snRNA gene	No	--	--	--	--	--	--	None – predicted gene
Gm39511	ChrX:48254336-48256792 (-)	lncRNA gene	No	--	--	--	--	--	--	None – predicted gene
Utp14a	ChrX:48256934-48282450 (+)	protein coding gene	No	X	X	--	X	--	--	Expressed in mouse liver; GO:0005829; GO:0005730; GO:0005634; GO:0042254; GO:0006364; GO:0032040; GO:0030154; GO:0051321; GO:0007275; GO:0007283
9530027J09Rik	ChrX:48276792-48285426 (-)	lncRNA gene	No	--	--	--	--	--	--	None
Gm22528	ChrX:48299579-48299682 (+)	snRNA gene	No	--	--	--	--	--	--	None – predicted gene
Gm22612	ChrX:48307043-48307143 (+)	snRNA gene	No	--	--	--	--	--	--	None – predicted gene

Bcorl1	ChrX:48341358-48408049 (+)	protein coding gene	No	X	X	X	X	--	--	Expressed in mouse liver; GO:0006325; GO:0003674; GO:0005654; GO:0005634; GO:0005886
Elf4	ChrX:48411049-48463132 (-)	protein coding gene	No	X	X	X	X	--	X	Expressed in mouse liver; GO:0030154; GO:0003677; GO:0001228; GO:0003700; GO:0000981; GO:0045087; GO:0001787; GO:0001866; GO:0016604; GO:0005654; GO:0005634; GO:0016605; GO:0045944; GO:0045893; GO:0006357; GO:0006355; GO:0000978; GO:0043565; GO:1990837; Abnormal inflammatory response (EBM)
5033418A18Rik	ChrX:48441605-48443111 (-)	unclassified gene	No	--	--	--	--	--	--	None
Aifm1	ChrX:48474944-48513563 (-)	protein coding gene	No	X	X	X	X	--	--	Expressed in mouse liver; GO:0006919; GO:0008637; GO:0006915; GO:0005737; GO:0005829; GO:0003677; GO:0004174; GO:0071949; GO:0050660; GO:0070059; GO:0016020; GO:0005743; GO:0005758; GO:0005741; GO:0033108; GO:0032981; GO:0005739; GO:0016174; GO:0051402; GO:0030182; GO:0005634; GO:0016491; GO:0016651; GO:0043065; GO:0010942; GO:0043525; GO:0005515; GO:0046983; GO:0045041; GO:1902510; GO:0006979; Abnormal cell

										physiology, oxidative stress (EBM)
Gm39512	ChrX:Syntenic	lncRNA gene	No	--	--	--	--	--	--	None – predicted gene
Rab33a	ChrX:48519285-48530232 (+)	protein coding gene	No	--	--	--	--	--	--	None
Zfp280c	ChrX:48541625-48594504 (-)	protein coding gene	No	X	--	--	--	--	--	Expressed in mouse liver
Slc25a14	ChrX:48623418-48662298 (+)	protein coding gene	No	X	X	X	X	--	X	Expressed in mouse liver; GO:0015297; GO:0016021; GO:0071423; GO:0015140; GO:0016020; GO:0005740; GO:0005743; GO:0031966; GO:0006839; GO:0005739; GO:0015131; GO:0015729; GO:0035435; GO:0071422; GO:0015141; GO:1902358; GO:0015116; GO:0008272; GO:0015117; GO:0015709; Abnormal circulating alanine transaminase level (EBM)
Gm27828	ChrX:48644340-48644458 (+)	miRNA gene	No	X	X	--	--	--	--	Expressed in mouse liver
Gpr119	ChrX:48667979-48674478 (-)	protein coding gene	No	--	--	--	--	--	--	None
Rbmx2	ChrX:48695004-48710719 (+)	protein coding gene	No	X	X	X	X	--	--	Expressed in mouse liver; GO:0019882; GO:0005768; GO:0005794; GO:0003924; GO:0005525; GO:0016020; GO:0000166; GO:0005886; GO:0032482; GO:0006397; GO:0000398; GO:0003676; GO:0005634; GO:0071011; GO:0003723; GO:0008380;

										GO:0005681; GO:0005686; GO:0071005
Gm595	ChrX:48841466-48877713 (-)	protein coding gene	No	--	--	--	--	--	--	None – predicted gene
Gm35107	ChrX:48884927-48906068 (+)	lncRNA gene	No	--	--	--	--	--	--	None – predicted gene
Enox2	ChrX:49009707-49288243 (-)	protein coding gene	No	X	X	X	X	--	--	Expressed in mouse liver; GO:0022900; GO:0009897; GO:0005576; GO:0016020; GO:0003676; GO:0016491; GO:0005886; GO:0015035; GO:0040008; GO:0048511; GO:0007624
Gm39513	ChrX:49286916-49315605 (+)	lncRNA gene	No	--	--	--	--	--	--	None – predicted gene
Gm14696	ChrX:49313321-49345237 (-)	lncRNA gene	No	--	--	--	--	--	--	None – predicted gene
Gm14697	ChrX:49332409-49447972 (-)	lncRNA gene	No	--	--	--	--	--	--	None – predicted gene
Arhgap36	ChrX:49463945-49500244 (+)	protein coding gene	No	X	X	X	X	--	--	Expressed in mouse liver; GO:0005096; GO:0007165
Olfr1320	ChrX:49683504-49684463 (+)	protein coding gene	No	--	--	--	--	--	--	None
Olfr1321	ChrX:49726973-49727932 (-)	protein coding gene	No	--	--	--	--	--	--	None
Igsf1	ChrX:49782536-49797749 (-)	protein coding gene	No	X	X	--	X	--	--	Expressed in mouse liver; GO:0038102; GO:0015026; GO:0005576; GO:0034711; GO:0016021; GO:0016020; GO:0032926; GO:2000272; GO:0006355
n-R5s6	ChrX:49879307-49879394 (+)	rRNA gene	No	--	--	--	--	--	--	None
Olfr1322	ChrX:49885469-49886401 (-)	protein coding gene	No	--	--	--	--	--	--	None

Olfr1323	ChrX:50009306-50010235 (-)	protein coding gene	No	--	--	--	--	--	--	None
Gm23385	ChrX:50022621-50022915 (+)	unclassified non-coding RNA gene	No	--	--	--	--	--	--	None – predicted gene
Gm22288	ChrX:50405813-50405919 (+)	snRNA gene	No	--	--	--	--	--	--	None – predicted gene
Olfr1324	ChrX:50425496-50426494 (-)	protein coding gene	No	--	--	--	--	--	--	None
Gm35612	ChrX:50537389-50562598 (+)	lncRNA gene	No	--	--	--	--	--	--	None – predicted gene
Firre	ChrX:50563120-50635321 (-)	lncRNA gene	No	X	X	--	X	--	--	Expressed in mouse liver; GO:0010467; GO:0003674; GO:0005654; GO:0005634
Stk26	ChrX:50841174-50893103 (+)	protein coding gene	No	X	--	--	X	--	--	Expressed in mouse liver; GO:0016324; GO:0006915; GO:0005524; GO:0071944; GO:0009267; GO:0005737; GO:0005829; GO:0005794; GO:0005798; GO:0000139; GO:0042802; GO:0016301; GO:0000287; GO:0016020; GO:0046872; GO:0030033; GO:0030336; GO:0000166; GO:0048471; GO:0016310; GO:0046777; GO:0042803; GO:0004672; GO:0006468; GO:0106310; GO:0004674; GO:0106311; GO:0042981; GO:1903205; GO:0042542; GO:0016740
Frmd7	ChrX:50895180-50942710 (-)	protein coding gene	No	X	--	X	X	--	--	Expressed in mouse liver; GO:0042995; GO:0005856; GO:0005829; GO:0030426; GO:0005085; GO:0032091; GO:0051497; GO:0007399;

										GO:0043025; GO:0043005; GO:0005654; GO:0005886; GO:0010592; GO:0051057; GO:0005515; GO:0050790; GO:0010975
Rap2c	ChrX:51003912-51018018 (-)	protein coding gene	No	X	X	X	X	--	--	Expressed in mouse liver; GO:0005923; GO:0044291; GO:0005737; GO:0005829; GO:0005768; GO:0090557; GO:0019003; GO:0003924; GO:0005525; GO:0016787; GO:0016020; GO:0030336; GO:0000166; GO:0005886; GO:0031954; GO:0032486; GO:0055037; GO:0055038; GO:0061097; GO:0007165; GO:0003713
Mbnl3	ChrX:51117269-51206532 (-)	protein coding gene	No	X	X	--	X	--	--	Expressed in mouse liver; GO:0005737; GO:0046872; GO:0006397; GO:0007275; GO:0045662; GO:0005654; GO:0005634; GO:0000381; GO:0043484; GO:0003723; GO:0008380
Gm23417	ChrX:51219110-51219192 (-)	miRNA gene	No	--	--	--	--	--	--	None – predicted gene
Hs6st2	ChrX:51387212-51681856 (-)	protein coding gene	No	X	X	--	X	--	--	Expressed in mouse liver; GO:0017095; GO:0015015; GO:0016021; GO:0016020; GO:0008146; GO:0016740
Gm35727	ChrX:51681757-51864066 (+)	lncRNA gene	No	--	--	--	--	--	--	None – predicted gene
2900011F02Rik	ChrX:51682089-51683755 (+)	unclassified gene	No	--	--	--	--	--	--	None
Usp26	ChrX:51753959-51801233 (-)	protein coding gene	No	--	--	--	--	--	--	None

Gm22539	ChrX:51844685-51844801 (+)	snoRNA gene	No	--	--	--	--	--	--	None – predicted gene
1700080O16Rik	ChrX:51968695-51972772 (-)	protein coding gene	No	--	--	--	--	--	--	None
Gm35790	ChrX:51972854-51974700 (+)	lncRNA gene	No	--	--	--	--	--	--	None – predicted gene
Gpc4	ChrX:52053021-52165252 (-)	protein coding gene	No	X	X	X	X	--	X	Expressed in mouse liver; GO:0031225; GO:0046658; GO:0099026; GO:0016477; GO:0009986; GO:0062023; GO:0009897; GO:0005576; GO:0005615; GO:0098978; GO:0016020; GO:0005886; GO:0098696; GO:1905606; GO:1905475; GO:0009966; GO:0045202; GO:0099560; GO:0016055; Abnormal fasting circulating glucose level (EBM)
Gpc3	ChrX:52272426-52613950 (-)	protein coding gene	No	X	X	X	X	--	--	Expressed in mouse liver; GO:0031225; GO:0046658; GO:0009887; GO:0009948; GO:0010171; GO:0030282; GO:0001658; GO:0016477; GO:0072111; GO:0072203; GO:0009986; GO:0062023; GO:0060976; GO:0035116; GO:0005887; GO:0001822; GO:0030324; GO:0005764; GO:0016020; GO:0072138; GO:0072180; GO:0090090; GO:0008285; GO:0050680; GO:0045926; GO:0010466; GO:0045879; GO:0030316; GO:0030414; GO:0060422; GO:0005886; GO:0030513;

										GO:0090263; GO:0045807; GO:0046326; GO:0045732; GO:0045880; GO:2000096; GO:0005515; GO:0060828; GO:0040008; GO:2000050; GO:1905475; GO:0009966; GO:0009617
Gm14582	ChrX:52296181-52333679 (+)	lncRNA gene	No	X	--	--	--	--	--	Expressed in mouse liver
D230050J18Rik	ChrX:52350175-52351810 (-)	unclassified gene	No	--	--	--	--	--	--	None
Mir6384	ChrX:52378121-52378181 (-)	miRNA gene	No	X	--	--	--	--	--	Expressed in mouse liver
Mir717	ChrX:52422407-52422515 (-)	miRNA gene	No	X	--	--	--	--	--	Expressed in mouse liver
A630012P03Rik	ChrX:52575843-52619047 (+)	lncRNA gene	No	X	--	--	--	--	--	Expressed in mouse liver
Mir363	ChrX:52741693-52741767 (-)	miRNA gene	No	--	--	--	--	--	--	None
Mir92-2	ChrX:52741838-52741928 (-)	miRNA gene	No	--	--	--	--	--	--	None
Mir19b-2	ChrX:52741983-52742066 (-)	miRNA gene	No	X	--	--	X	--	--	Expressed in mouse liver; GO:0007569; GO:1990830; GO:0060291; GO:0043066; GO:0002903; GO:0009617; GO:0016442
Mir20b	ChrX:52742113-52742192 (-)	miRNA gene	No	--	--	--	--	--	--	None
Mir18b	ChrX:52742331-52742413 (-)	miRNA gene	No	--	--	--	--	--	--	None
Mir106a	ChrX:52742503-52742567 (-)	miRNA gene	No	X	--	--	X	--	--	Expressed in mouse liver; GO:0036294; GO:1904322; GO:0071241; GO:1990830; GO:0070062; GO:0060291; GO:0043066; GO:0002903;

										GO:0009617; GO:0009611; GO:0016442
Kis2	ChrX:52742563-52744593 (-)	lncRNA gene	No	--	--	--	--	--	--	None
Gm42407	ChrX:52760995-52763973 (+)	lncRNA gene	No	--	--	--	--	--	--	None – predicted gene
Ccdc160	ChrX:52791200-52799468 (+)	protein coding gene	No	X	X	--	X	--	--	Expressed in mouse liver; GO:0005829; GO:0003677; GO:0001228; GO:0003700; GO:0000981; GO:0008544; GO:0042802; GO:0030216; GO:0043922; GO:0016604; GO:0005730; GO:0005654; GO:0005634; GO:0005886; GO:0045944; GO:0006357; GO:0006355; GO:0000978; GO:0043565; GO:1990837; GO:0005667; GO:0042060
Phf6	ChrX:52912266-52956943 (+)	protein coding gene	No	X	X	X	X	--	--	Expressed in mouse liver; GO:0001835; GO:0005694; GO:0000775; GO:0003677; GO:0019899; GO:0042393; GO:0042826; GO:0000776; GO:0046872; GO:0000122; GO:0005730; GO:0005654; GO:0005634; GO:0051219; GO:0006357; GO:0043021; GO:0097110; GO:0015631
Hprt	ChrX:52988137-53021659 (+)	protein coding gene	No	X	X	X	X	--	--	Expressed in mouse liver; GO:0046083; GO:0006168; GO:0021954; GO:0021895; GO:0005737; GO:0005829; GO:0048813; GO:0042417; GO:0046038; GO:0032263; GO:0007625; GO:0052657; GO:0006178; GO:0046100;

										GO:0004422; GO:0043103; GO:0042802; GO:0046040; GO:0032264; GO:0007626; GO:0046651; GO:0000287; GO:0046872; GO:0009116; GO:0000166; GO:0045964; GO:0051289; GO:0006164; GO:0006166; GO:0001975; GO:0021756; GO:0001913; GO:0016740; GO:0016757

[a] Resource abbreviations: **EBM,** Ensembl BioMart; **EEA,** EBI Expression Atlas; **GO,** Gene Ontology; **GXD,** Gene eXpression Database; **MGI,** Mouse Genome Informatics; **PW,** PheWeb

[b] ID terms: **GO:0036310:** annealing helicase activity; **GO:0008094:** ATPase, acting on DNA; **GO:0005524:** ATP binding; **GO:0043044:** ATP-dependent chromatin remodeling; **GO:0007420:** brain development; **GO:0090537:** CERF complex; **GO:0000785:** chromatin; **GO:0003682:** chromatin binding; **GO:0006325:** chromatin organization; **GO:0006338:** chromatin remodeling; **GO:0003677:** DNA binding; **GO:0004386:** helicase activity; **GO:0016787:** hydrolase activity; **GO:0016818:** hydrolase activity, acting on acid anhydrides, in phosphorus-containing anhydrides; **GO:0043231:** intracellular membrane-bounded organelle; **GO:0030182:** neuron differentiation; **GO:0003676:** nucleic acid binding; **GO:0005654:** nucleoplasm; **GO:0031491:** nucleosome binding; **GO:0070615:** nucleosome-dependent ATPase activity; **GO:0000166:** nucleotide binding; **GO:0005634:** nucleus; **GO:0016589:** NURF complex; **GO:0045944:** positive regulation of transcription by RNA polymerase II; **GO:0045893:** positive regulation of transcription, DNA-templated; **GO:2000177:** regulation of neural precursor cell proliferation; **GO:0006355:** regulation of transcription, DNA-templated; **GO:0008134:** transcription factor binding; **GO:0042995:** cell projection; **GO:0030030:** cell projection organization; **GO:0005929:** cilium; **GO:0060271:** cilium assembly; **GO:0005905:** clathrin-coated pit; **GO:0030136:** clathrin-coated vesicle; **GO:0005737:** cytoplasm; **GO:0031410:** cytoplasmic vesicle; **GO:0016311:** dephosphorylation; **GO:0005769:** early endosome; **GO:0005768:** endosome; **GO:0005794:** Golgi apparatus; **GO:0005096:** GTPase activator activity; **GO:0052659:** inositol-1,3,4,5-tetrakisphosphate 5-phosphatase activity; **GO:0052658:** inositol-1,4,5-trisphosphate 5-phosphatase activity; **GO:0046855:** inositol phosphate dephosphorylation; **GO:0052745:** inositol phosphate phosphatase activity; **GO:0004445:** inositol-polyphosphate 5-phosphatase activity; **GO:0001701:** in utero embryonic development; **GO:0016020:** membrane; **GO:0004439:** phosphatidylinositol-4,5-bisphosphate 5-phosphatase activity; **GO:0046856:** phosphatidylinositol dephosphorylation; **GO:0001750:** photoreceptor outer segment; **GO:0005886:** plasma membrane; **GO:0043087:** regulation of GTPase activity; **GO:0007165:** signal transduction; **GO:0031267:** small GTPase binding; **GO:0005802:** trans-Golgi network; **GO:0001525:** angiogenesis; **GO:0031704:** apelin receptor binding; **GO:0060183:** apelin receptor signaling pathway; **GO:0060976:** coronary vasculature development; **GO:0042756:** drinking behavior; **GO:0005576:** extracellular region; **GO:0007631:** feeding behavior; **GO:0007369:** gastrulation; **GO:0007186:** G protein-coupled receptor signaling pathway; **GO:0005179:** hormone activity; **GO:0042802:** identical protein binding; **GO:0007275:**

multicellular organism development; **GO:0045776:** negative regulation of blood pressure; **GO:0040037:** negative regulation of fibroblast growth factor receptor signaling pathway; **GO:0010629:** negative regulation of gene expression; **GO:1904706:** negative regulation of vascular associated smooth muscle cell proliferation; **GO:0045906:** negative regulation of vasoconstriction; **GO:0048471:** perinuclear region of cytoplasm; **GO:0008284:** positive regulation of cell population proliferation; **GO:0051466:** positive regulation of corticotropin-releasing hormone secretion; **GO:0051461:** positive regulation of corticotropin secretion; **GO:1904022:** positive regulation of G protein-coupled receptor internalization; **GO:0045823:** positive regulation of heart contraction; **GO:0031652:** positive regulation of heat generation; **GO:0042327:** positive regulation of phosphorylation; **GO:1902895:** positive regulation of pri-miRNA transcription by RNA polymerase II; **GO:1905564:** positive regulation of vascular endothelial cell proliferation; **GO:0050878:** regulation of body fluid levels; **GO:0043576:** regulation of respiratory gaseous exchange; **GO:0002026:** regulation of the force of heart contraction; **GO:0005102:** signaling receptor binding; **GO:0004177:** aminopeptidase activity; **GO:0031225:** anchored component of membrane; **GO:0070062:** extracellular exosome; **GO:0046872:** metal ion binding; **GO:0070006:** metalloaminopeptidase activity; **GO:0008233:** peptidase activity; **GO:0006508:** proteolysis; **GO:0048873:** homeostasis of number of cells within a tissue; **GO:0002821:** positive regulation of adaptive immune response; **GO:0030890:** positive regulation of B cell proliferation; **GO:0043372:** positive regulation of CD4-positive, alpha-beta T cell differentiation; **GO:0002639:** positive regulation of immunoglobulin production; **GO:0032729:** positive regulation of interferon-gamma production; **GO:0032733:** positive regulation of interleukin-10 production; **GO:0032743:** positive regulation of interleukin-2 production; **GO:0032753:** positive regulation of interleukin-4 production; **GO:0051251:** positive regulation of lymphocyte activation; **GO:0046622:** positive regulation of organ growth; **GO:0002726:** positive regulation of T cell cytokine production; **GO:0042102:** positive regulation of T cell proliferation; **GO:0032760:** positive regulation of tumor necrosis factor production; **GO:0005829:** cytosol; **GO:0005783:** endoplasmic reticulum; **GO:0016021:** integral component of membrane; **GO:0031228:** intrinsic component of Golgi membrane; **GO:0016409:** palmitoyltransferase activity; **GO:0002178:** palmitoyltransferase complex; **GO:0018230:** peptidyl-L-cysteine S-palmitoylation; **GO:0019706:** protein-cysteine S-palmitoyltransferase activity; **GO:0018345:** protein palmitoylation; **GO:0006612:** protein targeting to membrane; **GO:0043849:** Ras palmitoyltransferase activity; **GO:0016740:** transferase activity; **GO:0016746:** transferase activity, transferring acyl groups; **GO:0005730:** nucleolus; **GO:0042254:** ribosome biogenesis; **GO:0006364:** rRNA processing; **GO:0032040:** small-subunit processome; **GO:0030154:** cell differentiation; **GO:0051321:** meiotic cell cycle; **GO:0007283:** spermatogenesis; **GO:0003674:** molecular_function; **GO:0001228:** DNA-binding transcription activator activity, RNA polymerase II-specific; **GO:0003700:** DNA-binding transcription factor activity; **GO:0000981:** DNA-binding transcription factor activity, RNA polymerase II-specific; **GO:0045087:** innate immune response; **GO:0001787:** natural killer cell proliferation; **GO:0001866:** NK T cell proliferation; **GO:0016604:** nuclear body; **GO:0016605:** PML body; **GO:0006357:** regulation of transcription by RNA polymerase II; **GO:0000978:** RNA polymerase II cis-regulatory region sequence-specific DNA binding; **GO:0043565:** sequence-specific DNA binding; **GO:1990837:** sequence-specific double-stranded DNA binding; **GO:0006919:** activation of cysteine-type endopeptidase activity involved in apoptotic process; **GO:0008637:** apoptotic mitochondrial changes; **GO:0006915:** apoptotic process; **GO:0004174:** electron-transferring-flavoprotein dehydrogenase activity; **GO:0071949:** FAD binding; **GO:0050660:** flavin adenine dinucleotide

binding; **GO:0070059:** intrinsic apoptotic signaling pathway in response to endoplasmic reticulum stress; **GO:0005743:** mitochondrial inner membrane; **GO:0005758:** mitochondrial intermembrane space; **GO:0005741:** mitochondrial outer membrane; **GO:0033108:** mitochondrial respiratory chain complex assembly; **GO:0032981:** mitochondrial respiratory chain complex I assembly; **GO:0005739:** mitochondrion; **GO:0016174:** NAD(P)H oxidase H2O2-forming activity; **GO:0051402:** neuron apoptotic process; **GO:0016491:** oxidoreductase activity; **GO:0016651:** oxidoreductase activity, acting on NAD(P)H; **GO:0043065:** positive regulation of apoptotic process; **GO:0010942:** positive regulation of cell death; **GO:0043525:** positive regulation of neuron apoptotic process; **GO:0005515:** protein binding; **GO:0046983:** protein dimerization activity; **GO:0045041:** protein import into mitochondrial intermembrane space; **GO:1902510:** regulation of apoptotic DNA fragmentation; **GO:0006979:** response to oxidative stress; **GO:0015297:** antiporter activity; **GO:0071423:** malate transmembrane transport; **GO:0015140:** malate transmembrane transporter activity; **GO:0005740:** mitochondrial envelope; **GO:0031966:** mitochondrial membrane; **GO:0006839:** mitochondrial transport; **GO:0015131:** oxaloacetate transmembrane transporter activity; **GO:0015729:** oxaloacetate transport; **GO:0035435:** phosphate ion transmembrane transport; **GO:0071422:** succinate transmembrane transport; **GO:0015141:** succinate transmembrane transporter activity; **GO:1902358:** sulfate transmembrane transport; **GO:0015116:** sulfate transmembrane transporter activity; **GO:0008272:** sulfate transport; **GO:0015117:** thiosulfate transmembrane transporter activity; **GO:0015709:** thiosulfate transport; **GO:0019882:** antigen processing and presentation; **GO:0003924:** GTPase activity; **GO:0005525:** GTP binding; **GO:0032482:** Rab protein signal transduction; **GO:0006397:** mRNA processing; **GO:0000398:** mRNA splicing, via spliceosome; **GO:0071011:** precatalytic spliceosome; **GO:0003723:** RNA binding; **GO:0008380:** RNA splicing; **GO:0005681:** spliceosomal complex; **GO:0005686:** U2 snRNP; **GO:0071005:** U2-type precatalytic spliceosome; **GO:0022900:** electron transport chain; **GO:0009897:** external side of plasma membrane; **GO:0015035:** protein disulfide oxidoreductase activity; **GO:0040008:** regulation of growth; **GO:0048511:** rhythmic process; **GO:0007624:** ultradian rhythm; **GO:0038102:** activin receptor antagonist activity; **GO:0015026:** coreceptor activity; **GO:0034711:** inhibin binding; **GO:0032926:** negative regulation of activin receptor signaling pathway; **GO:2000272:** negative regulation of signaling receptor activity; **GO:0010467:** gene expression; **GO:0016324:** apical plasma membrane; **GO:0071944:** cell periphery; **GO:0009267:** cellular response to starvation; **GO:0005798:** Golgi-associated vesicle; **GO:0000139:** Golgi membrane; **GO:0016301:** kinase activity; **GO:0000287:** magnesium ion binding; **GO:0030033:** microvillus assembly; **GO:0030336:** negative regulation of cell migration; **GO:0016310:** phosphorylation; **GO:0046777:** protein autophosphorylation; **GO:0042803:** protein homodimerization activity; **GO:0004672:** protein kinase activity; **GO:0006468:** protein phosphorylation; **GO:0106310:** protein serine kinase activity; **GO:0004674:** protein serine/threonine kinase activity; **GO:0106311:** protein threonine kinase activity; **GO:0042981:** regulation of apoptotic process; **GO:1903205:** regulation of hydrogen peroxide-induced cell death; **GO:0042542:** response to hydrogen peroxide; **GO:0005856:** cytoskeleton; **GO:0030426:** growth cone; **GO:0005085:** guanyl-nucleotide exchange factor activity; **GO:0032091:** negative regulation of protein binding; **GO:0051497:** negative regulation of stress fiber assembly; **GO:0007399:** nervous system development; **GO:0043025:** neuronal cell body; **GO:0043005:** neuron projection; **GO:0010592:** positive regulation of lamellipodium assembly; **GO:0051057:** positive regulation of small GTPase mediated signal transduction; **GO:0050790:** regulation of catalytic activity; **GO:0010975:** regulation of neuron projection development; **GO:0005923:** bicellular tight junction; **GO:0044291:** cell-cell contact

zone; **GO:0090557:** establishment of endothelial intestinal barrier; **GO:0019003:** GDP binding; **GO:0031954:** positive regulation of protein autophosphorylation; **GO:0032486:** Rap protein signal transduction; **GO:0055037:** recycling endosome; **GO:0055038:** recycling endosome membrane; **GO:0061097:** regulation of protein tyrosine kinase activity; **GO:0003713:** transcription coactivator activity; **GO:0045662:** negative regulation of myoblast differentiation; **GO:0000381:** regulation of alternative mRNA splicing, via spliceosome; **GO:0043484:** regulation of RNA splicing; **GO:0017095:** heparan sulfate 6-O-sulfotransferase activity; **GO:0015015:** heparan sulfate proteoglycan biosynthetic process, enzymatic modification; **GO:0008146:** sulfotransferase activity; **GO:0046658:** anchored component of plasma membrane; **GO:0099026:** anchored component of presynaptic membrane; **GO:0016477:** cell migration; **GO:0009986:** cell surface; **GO:0062023:** collagen-containing extracellular matrix; **GO:0005615:** extracellular space; **GO:0098978:** glutamatergic synapse; **GO:0098696:** regulation of neurotransmitter receptor localization to postsynaptic specialization membrane; **GO:1905606:** regulation of presynapse assembly; **GO:1905475:** regulation of protein localization to membrane; **GO:0009966:** regulation of signal transduction; **GO:0045202:** synapse; **GO:0099560:** synaptic membrane adhesion; **GO:0016055:** Wnt signaling pathway; **GO:0009887:** animal organ morphogenesis; **GO:0009948:** anterior/posterior axis specification; **GO:0010171:** body morphogenesis; **GO:0030282:** bone mineralization; **GO:0001658:** branching involved in ureteric bud morphogenesis; **GO:0072111:** cell proliferation involved in kidney development; **GO:0072203:** cell proliferation involved in metanephros development; **GO:0035116:** embryonic hindlimb morphogenesis; **GO:0005887:** integral component of plasma membrane; **GO:0001822:** kidney development; **GO:0030324:** lung development; **GO:0005764:** lysosome; **GO:0072138:** mesenchymal cell proliferation involved in ureteric bud development; **GO:0072180:** mesonephric duct morphogenesis; **GO:0090090:** negative regulation of canonical Wnt signaling pathway; **GO:0008285:** negative regulation of cell population proliferation; **GO:0050680:** negative regulation of epithelial cell proliferation; **GO:0045926:** negative regulation of growth; **GO:0010466:** negative regulation of peptidase activity; **GO:0045879:** negative regulation of smoothened signaling pathway; **GO:0030316:** osteoclast differentiation; **GO:0030414:** peptidase inhibitor activity; **GO:0060422:** peptidyl-dipeptidase inhibitor activity; **GO:0030513:** positive regulation of BMP signaling pathway; **GO:0090263:** positive regulation of canonical Wnt signaling pathway; **GO:0045807:** positive regulation of endocytosis; **GO:0046326:** positive regulation of glucose import; **GO:0045732:** positive regulation of protein catabolic process; **GO:0045880:** positive regulation of smoothened signaling pathway; **GO:2000096:** positive regulation of Wnt signaling pathway, planar cell polarity pathway; **GO:0060828:** regulation of canonical Wnt signaling pathway; **GO:2000050:** regulation of non-canonical Wnt signaling pathway; **GO:0009617:** response to bacterium; **GO:0007569:** cell aging; **GO:1990830:** cellular response to leukemia inhibitory factor; **GO:0060291:** long-term synaptic potentiation; **GO:0043066:** negative regulation of apoptotic process; **GO:0002903:** negative regulation of B cell apoptotic process; **GO:0016442:** RISC complex; **GO:0036294:** cellular response to decreased oxygen levels; **GO:1904322:** cellular response to forskolin; **GO:0071241:** cellular response to inorganic substance; **GO:0009611:** response to wounding; **GO:0008544:** epidermis development; **GO:0030216:** keratinocyte differentiation; **GO:0043922:** negative regulation by host of viral transcription; **GO:0005667:** transcription regulator complex; **GO:0042060:** wound healing; **GO:0001835:** blastocyst hatching; **GO:0005694:** chromosome; **GO:0000775:** chromosome, centromeric region; **GO:0019899:** enzyme binding; **GO:0042393:** histone binding; **GO:0042826:** histone deacetylase binding; **GO:0000776:** kinetochore; **GO:0000122:** negative regulation of transcription by

RNA polymerase II; **GO:0051219:** phosphoprotein binding; **GO:0043021:** ribonucleoprotein complex binding; **GO:0097110:** scaffold protein binding; **GO:0015631:** tubulin binding; **GO:0046083:** adenine metabolic process; **GO:0006168:** adenine salvage; **GO:0021954:** central nervous system neuron development; **GO:0021895:** cerebral cortex neuron differentiation; **GO:0048813:** dendrite morphogenesis; **GO:0042417:** dopamine metabolic process; **GO:0046038:** GMP catabolic process; **GO:0032263:** GMP salvage; **GO:0007625:** grooming behavior; **GO:0052657:** guanine phosphoribosyltransferase activity; **GO:0006178:** guanine salvage; **GO:0046100:** hypoxanthine metabolic process; **GO:0004422:** hypoxanthine phosphoribosyltransferase activity; **GO:0043103:** hypoxanthine salvage; **GO:0046040:** IMP metabolic process; **GO:0032264:** IMP salvage; **GO:0007626:** locomotory behavior; **GO:0046651:** lymphocyte proliferation; **GO:0009116:** nucleoside metabolic process; **GO:0045964:** positive regulation of dopamine metabolic process; **GO:0051289:** protein homotetramerization; **GO:0006164:** purine nucleotide biosynthetic process; **GO:0006166:** purine ribonucleoside salvage; **GO:0001975:** response to amphetamine; **GO:0021756:** striatum development; **GO:0001913:** T cell mediated cytotoxicity; **GO:0016757:** transferase activity, transferring glycosyl groups

Supplementary Table S4.5. AST candidate genes and their relevant annotations (Chr2: 10.653–13.057 ± 1 Mbp; GRCm38/mm10).[a]

				Expression		Functional		Phenotypic		
MGI Gene symbol	**Genome coordinates (strand)**	**Type**	**Known AST gene**	**GXD (MGI)**	**EEA**	**Inter Pro**	**GO**	**PW**	**EBM**	**Relevance to AST[b]**
Taf3	Chr2:9914552-10048596 (-)	protein coding gene	No	X	X	X	X	X	--	Expressed in all mouse tissues of interest; GO:0051457; GO:0046872; GO:0043433; GO:0000122; GO:0031965; GO:0005654; GO:0005634; GO:0002039; GO:0005515; GO:0046982; GO:0006357; GO:0006366; GO:0005669; GO:0140416
C630004 M23Rik	Chr2:10047838-10049519 (+)	unclassified gene	No	X	X	--	--	--	--	Expressed in mouse heart, brain, and liver
Atp5c1	Chr2:10056030-10080510 (-)	protein coding gene	No	X	X	--	X	X	--	Expressed in mouse heart, brain, and liver; GO:0016887; GO:0006754; GO:0046034; GO:0015986; GO:0006811; GO:0016020; GO:0042776; GO:0005743; GO:0005753; GO:0000275; GO:0005739; GO:0043209; GO:0046933; GO:0045261
Gm23608	Chr2:10075653-10075780 (-)	snoRNA gene	No	X	X	--	--	--	--	Expressed in all mouse tissues of interest
Kin	Chr2:156558786-156649568 (+)	protein coding gene	No	X	X	--	X	X	--	Expressed in all mouse tissues of interest; GO:0006974; GO:0005737; GO:0003677; GO:0006310; GO:0006281; GO:0006260; GO:0003690; GO:0043231; GO:0046872; GO:0006397; GO:0016363; GO:0005654; GO:0005634; GO:0032991; GO:0003723

Itih2	Chr2:10094591-10130683 (-)	protein coding gene	No	X	X	--	X	X	--	Expressed in all mouse tissues of interest; GO:0062023; GO:0005576; GO:0030212; GO:0010466; GO:0030414; GO:0004867
Itih5	Chr2:10153571-10256529 (+)	protein coding gene	No	X	X	--	X	X	--	Expressed in all mouse tissues of interest; GO:0062023; GO:0005576; GO:0030212; GO:0010466; GO:0030414; GO:0004867
5730405A10Rik	Chr2:10276439-10277418 (+)	unclassified gene	No	--	--	--	--	--	--	None
Gm31496	Chr2:10305663-10307590 (-)	lncRNA gene	No	--	--	--	--	--	--	None – predicted gene
Gm39758	Chr2:10317088-10320201 (-)	lncRNA gene	No	--	--	--	--	--	--	None – predicted gene
Gm13261	Chr2:10339283-10374041 (-)	lncRNA gene	No	X	X	--	X	--	--	Expressed in mouse liver; GO:0008150; GO:0005575; GO:0003674
Sfmbt2	Chr2:10370510-10595253 (+)	protein coding gene	No	X	X	--	X	X	X	Expressed in all mouse tissues of interest; GO:0016235; GO:0003682; GO:0005829; GO:0042393; GO:0043231; GO:0010629; GO:0045892; GO:0016604; GO:0016607; GO:0005654; GO:0005634; GO:0006355; GO:0003714
Gm22072	Chr2:10465287-10465407 (+)	miRNA gene	No	X	--	--	--	--	--	Expressed in mouse heart and liver
Gm22677	Chr2:10465760-10465867 (+)	miRNA gene	No	X	--	--	--	--	--	Expressed in mouse heart and liver
Mir466m	Chr2:10466663-10466746 (+)	miRNA gene	No	X	--	--	X	--	--	Expressed in mouse heart and liver; GO:0016442
Mir466f-1	Chr2:10466944-10467037 (+)	miRNA gene	No	X	--	--	X	--	--	Expressed in mouse liver; GO:0071230

Mir669f	Chr2:10467229-10467349 (+)	miRNA gene	No	X	--	--	X	--	--	Expressed in mouse heart and liver; GO:0071230; GO:0016442
Mir669e	Chr2:10467495-10467613 (+)	miRNA gene	No	X	--	--	--	--	--	Expressed in mouse heart and liver
Mir669b	Chr2:10467790-10467886 (+)	miRNA gene	No	X	--	--	--	--	--	Expressed in mouse liver
Gm23578	Chr2:10468069-10468172 (+)	miRNA gene	No	X	--	--	--	--	--	Expressed in mouse liver
Mir669d	Chr2:10468343-10468463 (+)	miRNA gene	No	X	--	--	--	--	--	Expressed in mouse liver
Mir466f-2	Chr2:10468675-10468768 (+)	miRNA gene	No	--	--	--	--	--	--	None
Mir669l	Chr2:10468971-10469068 (+)	miRNA gene	No	--	--	--	--	--	--	Expressed in mouse heart
Mir669d-2	Chr2:10471644-10471729 (+)	miRNA gene	No	X	--	--	--	--	--	Expressed in mouse heart and liver
Mir466f-3	Chr2:10471953-10472046 (+)	miRNA gene	No	X	--	--	--	--	--	Expressed in mouse liver
Mir297a-2	Chr2:10472254-10472343 (+)	miRNA gene	No	X	--	--	--	--	--	Expressed in mouse liver
Mir466o	Chr2:10472540-10472623 (+)	miRNA gene	No	X	--	--	--	--	--	Expressed in mouse liver
Gm26073	Chr2:10473351-10473477 (+)	miRNA gene	No	X	--	--	--	--	--	Expressed in mouse liver
Mir467c	Chr2:10473931-10474027 (+)	miRNA gene	No	X	--	--	--	--	--	Expressed in mouse liver
Mir466b-1	Chr2:10474219-10474300 (+)	miRNA gene	No	X	--	--	--	--	--	Expressed in mouse liver
Mir669a-3	Chr2:10474433-10474541 (+)	miRNA gene	No	X	--	--	X	--	--	Expressed in mouse liver; GO:2001015; GO:0010468
Mir669k	Chr2:10475300-1047542 (+)	miRNA gene	No	X	--	--	--	--	--	Expressed in mouse liver
Gm26491	Chr2:10475500-10475620 (+)	miRNA gene	No	X	--	--	--	--	--	Expressed in mouse heart and liver

Mir467a-1	Chr2:10476346-10476418 (+)	miRNA gene	No	X	--	--	X	--	--	Expressed in mouse liver; GO:1990830; GO:0060291; GO:0030307; GO:0016442; GO:0007605
Mir466b-8	Chr2:10476628-10476713 (+)	miRNA gene	No	--	--	--	--	--	--	None
Mir669a-1	Chr2:10476853-10476949 (+)	miRNA gene	No	--	--	--	--	--	--	None
Mir669g	Chr2:10477150-10477272 (+)	miRNA gene	No	X	--	--	--	--	--	Expressed in mouse liver
Gm25701	Chr2:10477710-10477836 (+)	miRNA gene	No	X	--	--	--	--	--	Expressed in mouse liver
Mir669j	Chr2:10477910-10478030 (+)	miRNA gene	No	X	--	--	--	--	--	Expressed in mouse liver
Mir467a-2	Chr2:10478798-10478880 (+)	miRNA gene	No	--	--	--	--	--	--	None
Mir466e	Chr2:10479088-10479171 (+)	miRNA gene	No	--	--	--	--	--	--	None
Mir669a-4	Chr2:10479315-10479401 (+)	miRNA gene	No	--	--	--	--	--	--	None
Gm24315	Chr2:10480165-10480291 (+)	miRNA gene	No	--	--	--	--	--	--	None – predicted gene
Gm25451	Chr2:10480365-10480485 (+)	miRNA gene	No	X	--	--	--	--	--	Expressed in mouse liver
Mir467b	Chr2:10481248-10481320 (+)	miRNA gene	No	X	--	--	X	--	--	Expressed in mouse skeletal muscle; GO:1990830; GO:0071356; GO:0060291
Mir466c-1	Chr2:10481534-10481617 (+)	miRNA gene	No	X	--	--	--	--	--	Expressed in mouse heart
Mir669a-5	Chr2:10481761-10481847 (+)	miRNA gene	No	X	--	--	X	--	--	Expressed in mouse liver; GO:2001015; GO:0010468
Gm24761	Chr2:10482612-10482738 (+)	miRNA gene	No	--	--	--	--	--	--	None – predicted gene
Gm23651	Chr2:10482812-10482931 (+)	miRNA gene	No	--	--	--	--	--	--	None – predicted gene

Mir467a-3	Chr2:10483678-10483760 (+)	miRNA gene	No	--	--	--	--	--	--	None
Mir466c-2	Chr2:10483966-10484055 (+)	miRNA gene	No	--	--	--	--	--	--	None
Mir669a-6	Chr2:10484196-10484282 (+)	miRNA gene	No	--	--	--	--	--	--	None
Gm23108	Chr2:10484490-10484613 (+)	miRNA gene	No	--	--	--	--	--	--	None – predicted gene
Gm25680	Chr2:10485051-10485176 (+)	miRNA gene	No	--	--	--	--	--	--	None – predicted gene
Gm22775	Chr2:10485250-10485369 (+)	miRNA gene	No	--	--	--	--	--	--	None – predicted gene
Mir467a-4	Chr2:10486135-10486217 (+)	miRNA gene	No	--	--	--	--	--	--	None
Mir466b-4	Chr2:10486423-10486512 (+)	miRNA gene	No	--	--	--	--	--	--	None
Mir669a-7	Chr2:10486653-10486739 (+)	miRNA gene	No	--	--	--	--	--	--	None
Gm26060	Chr2:10486946-10487068 (+)	miRNA gene	No	--	--	--	--	--	--	None – predicted gene
Gm26431	Chr2:10487507-10487633 (+)	miRNA gene	No	--	--	--	--	--	--	None – predicted gene
Gm26229	Chr2:10487704-10487824 (+)	miRNA gene	No	--	--	--	--	--	--	None – predicted gene
Mir467a-5	Chr2:10488599-10488681 (+)	miRNA gene	No	--	--	--	--	--	--	None
Mir466b-5	Chr2:10488887-10488974 (+)	miRNA gene	No	--	--	--	--	--	--	None
Mir669p-1	Chr2:10489116-10489202 (+)	miRNA gene	No	--	--	--	--	--	--	None
Gm24167	Chr2:10489410-10489533 (+)	miRNA gene	No	--	--	--	--	--	--	None – predicted gene
Gm24640	Chr2:10489971-10490096 (+)	miRNA gene	No	--	--	--	--	--	--	None – predicted gene
Gm23288	Chr2:10490167-10490287 (+)	miRNA gene	No	--	--	--	--	--	--	None – predicted gene

Mir467a-6	Chr2:10491048-10491130 (+)	miRNA gene	No	--	--	--	--	--	--	None
Gm25285	Chr2:10491336-10491425 (+)	miRNA gene	No	--	--	--	--	--	--	None – predicted gene
Mir669a-8	Chr2:10491566-10491652 (+)	miRNA gene	No	--	--	--	--	--	--	None
Gm24673	Chr2:10491860-10491983 (+)	miRNA gene	No	--	--	--	--	--	--	None – predicted gene
Gm22635	Chr2:10492421-10492546 (+)	miRNA gene	No	--	--	--	--	--	--	None – predicted gene
Gm23569	Chr2:10492620-10492739 (+)	miRNA gene	No	--	--	--	--	--	--	None – predicted gene
Mir467a-7	Chr2:10493510-10493592 (+)	miRNA gene	No	--	--	--	--	--	--	None
Mir466b-6	Chr2:10493798-10493887 (+)	miRNA gene	No	--	--	--	--	--	--	None
Mir669a-9	Chr2:10494028-10494114 (+)	miRNA gene	No	--	--	--	--	--	--	None
Gm26426	Chr2:10494321-10494443 (+)	miRNA gene	No	--	--	--	--	--	--	None
Gm24488	Chr2:10494882-10495008 (+)	miRNA gene	No	--	--	--	--	--	--	None – predicted gene
Gm25158	Chr2:10495079-10495199 (+)	miRNA gene	No	--	--	--	--	--	--	None – predicted gene
Mir467a-8	Chr2:10495980-10496062 (+)	miRNA gene	No	--	--	--	--	--	--	None
Mir466b-7	Chr2:10496268-10496355 (+)	miRNA gene	No	X	--	--	--	--	--	Expressed in mouse liver
Mir669p-2	Chr2:10496497-10496583 (+)	miRNA gene	No	--	--	--	--	--	--	None
Gm24028	Chr2:10496791-10496914 (+)	miRNA gene	No	--	--	--	--	--	--	None – predicted gene
Gm22626	Chr2:10497352-10497477 (+)	miRNA gene	No	--	--	--	--	--	--	None – predicted gene
Gm22166	Chr2:10497548-10497668 (+)	miRNA gene	No	--	--	--	--	--	--	None – predicted gene

Mir467a-9	Chr2:10498393-10498475 (+)	miRNA gene	No	--	--	--	--	--	--	None
Mir466b-2	Chr2:10498685-10498766 (+)	miRNA gene	No	--	--	--	--	--	--	None
Mir669a-10	Chr2:10498911-10498997 (+)	miRNA gene	No	--	--	--	--	--	--	None
Gm26156	Chr2:10499204-10499326 (+)	miRNA gene	No	X	--	--	--	--	--	Expressed in mouse heart and liver
Gm23571	Chr2:10499763-10499889 (+)	miRNA gene	No	X	--	--	--	--	--	Expressed in mouse liver
Gm25316	Chr2:10499966-10500083 (+)	miRNA gene	No	X	--	--	--	--	--	Expressed in mouse liver
Gm25022	Chr2:10500822-10500904 (+)	miRNA gene	No	--	--	--	--	--	--	None – predicted gene
Gm25943	Chr2:10501109-10501198 (+)	miRNA gene	No	--	--	--	--	--	--	None – predicted gene
Mir669a-11	Chr2:10501339-10501425 (+)	miRNA gene	No	X	--	--	--	--	--	Expressed in mouse liver
Gm23988	Chr2:10501633-10501754 (+)	miRNA gene	No	X	--	--	--	--	--	Expressed in mouse liver
Gm25673	Chr2:10502191-10502317 (+)	miRNA gene	No	X	--	--	--	--	--	Expressed in mouse liver
Gm25753	Chr2:10502391-10502511 (+)	miRNA gene	No	X	--	--	--	--	--	Expressed in mouse liver
Mir467a-10	Chr2:10503273-10503355 (+)	miRNA gene	No	--	--	--	--	--	--	None
Mir466b-3	Chr2:10503565-10503645 (+)	miRNA gene	No	X	--	--	--	--	--	Expressed in mouse liver
Mir669a-12	Chr2:10503791-10503877 (+)	miRNA gene	No	--	--	--	--	--	--	None
Gm26398	Chr2:10504647-10504773 (+)	miRNA gene	No	X	--	--	--	--	--	Expressed in mouse liver
Mir467e	Chr2:10505721-10505807 (+)	miRNA gene	No	X	--	--	X	--	--	Expressed in mouse liver; GO:0016442
Mir466p	Chr2:10506006-10506094 (+)	miRNA gene	No	--	--	--	--	--	--	None

Gm22051	Chr2:10506555-10506681 (+)	miRNA gene	No	X	--	--	--	--	--	Expressed in mouse liver
Gm22678	Chr2:10506755-10506855 (+)	miRNA gene	No	--	--	--	--	--	--	None – predicted gene
Mir467d	Chr2:10507630-10507714 (+)	miRNA gene	No	X	--	--	X	--	--	Expressed in mouse heart; GO:0071222
Mir466	Chr2:10507918-10507990 (+)	miRNA gene	No	X	--	--	X	--	--	Expressed in mouse liver; GO:0071391; GO:1904322; GO:0071241; GO:0010468
Gm22091	Chr2:10508453-10508579 (+)	miRNA gene	No	X	--	--	--	--	--	Expressed in mouse heart and liver
Mir297c	Chr2:10509016-10509113 (+)	miRNA gene	No	X	--	--	X	--	--	Expressed in mouse liver; GO:1990830
Mir669c	Chr2:10509296-10509404 (+)	miRNA gene	No	--	--	--	--	--	--	None
Gm24342	Chr2:10509584-10509687 (+)	miRNA gene	No	X	--	--	--	--	--	Expressed in mouse liver
Gm25263	Chr2:10509885-10509984 (+)	miRNA gene	No	X	--	--	--	--	--	Expressed in mouse liver
Mir669a-2	Chr2:10510164-10510260 (+)	miRNA gene	No	X	--	--	X	--	--	Expressed in mouse heart and liver; GO:2001015;GO:0010468
Gm22239	Chr2:10510461-10510563 (+)	miRNA gene	No	X	--	--	--	--	--	Expressed in mouse liver
Gm22925	Chr2:10510791-10510892 (+)	miRNA gene	No	X	--	--	--	--	--	Expressed in mouse heart and liver
Gm23542	Chr2:10511370-10511465 (+)	miRNA gene	No	--	--	--	--	--	--	None – predicted gene
Mir297b	Chr2:10511667-10511775 (+)	miRNA gene	No	X	--	--	--	--	--	Expressed in mouse heart
Mir466d	Chr2:10511967-10512062 (+)	miRNA gene	No	X	--	--	X	--	--	Expressed in mouse liver; GO:0045944; GO:0016442
Gm26092	Chr2:10512203-10512299 (+)	miRNA gene	No	--	X	--	--	--	--	Expressed in mouse brain
Mir669m-1	Chr2:10512790-10512887 (+)	miRNA gene	No	X	--	--	--	--	--	Expressed in mouse liver

Mir669m-2	Chr2:10513434-10513531 (+)	miRNA gene	No	X	--	--	--	--	--	Expressed in mouse heart and liver
Mir466n	Chr2:10513741-10513834 (+)	miRNA gene	No	X	--	--	--	--	--	Expressed in mouse liver
Mir669o	Chr2:10514300-10514395 (+)	miRNA gene	No	X	--	--	X	--	--	Expressed in mouse heart; GO:0016442
Mir466g	Chr2:10514595-10514674 (+)	miRNA gene	No	X	--	--	X	--	--	Expressed in mouse heart and liver; GO:0071230; GO:0016442
Mir466h	Chr2:10514891-10514971 (+)	miRNA gene	No	--	--	--	--	--	--	None
Mir297a-3	Chr2:10515820-10515921 (+)	miRNA gene	No	X	--	--	--	--	--	Expressed in mouse heart
Mir466l	Chr2:10516097-10516217 (+)	miRNA gene	No	X	--	--	X	--	--	Expressed in mouse liver; GO:0070935; GO:0035925; GO:0045944; GO:0045727; GO:0061013; GO:0006357
Mir297a-4	Chr2:10517067-10517164 (+)	miRNA gene	No	X	--	--	--	--	--	Expressed in mouse heart and liver
Gm24806	Chr2:10517337-10517426 (+)	miRNA gene	No	X	--	--	--	--	--	Expressed in mouse heart and liver
Mir669i	Chr2:10517604-10517730 (+)	miRNA gene	No	X	--	--	--	--	--	Expressed in mouse heart and liver
Mir669h	Chr2:10518155-10518279 (+)	miRNA gene	No	X	--	--	--	--	--	Expressed in mouse heart and liver
Gm10852	Chr2:10715338-10715369 (+)	protein coding gene	No	--	--	--	--	--	--	None – predicted gene
Gm31729	Chr2:10825745-10828322 (+)	lncRNA gene	No	--	--	--	--	--	--	None – predicted gene
Gm37343	Chr2:11013808-11013918 (-)	unclassified gene	No	--	X	--	--	--	--	Expressed in mouse brain and kidney
Gm23877	Chr2:11014762-11014890 (-)	snoRNA gene	No	--	--	--	--	--	--	None – predicted gene
Gm13264	Chr2:11036874-11060129 (+)	lncRNA gene	No	--	--	--	--	--	--	None – predicted gene

Gm26478	Chr2:11087781-11087913 (-)	snRNA gene	No	--	--	--	--	--	--	None – predicted gene
Prkcq	Chr2:11172108-11301222 (+)	protein coding gene	No	X	X	--	X	X	X	Expressed in all mouse tissues of interest; GO:0016235; GO:0005524; GO:0060326; GO:0034451; GO:0005737; GO:0002376; GO:0001772; GO:0006954; GO:0035556; GO:0016301; GO:0016020; GO:0006509; GO:0046872; GO:0046627; GO:0070233; GO:0031594; GO:0000166; GO:0005634; GO:0018105; GO:0016310; GO:0005886; GO:0051491; GO:0032740; GO:0032743; GO:0032753; GO:0051092; GO:0042307; GO:0050714; GO:0051496; GO:0050870; GO:0042102; GO:0051973; GO:1904355; GO:0032212; GO:2000318; GO:2000570; GO:0005515; GO:0004672; GO:0004697; GO:0018215; GO:0006468; GO:0004674; GO:0010389; GO:0090330; GO:0006355; GO:0042383; GO:0016740; abnormal muscle cell glucose uptake (EBM)
Gm36932	Chr2:11181012-11181940 (+)	unclassified gene	No	X	--	--	--	--	--	Expressed in mouse heart, skeletal muscle, and liver
Gm37520	Chr2:11190641-11193312 (-)	unclassified gene	No	X	--	--	--	--	--	Expressed in mouse skeletal muscle and liver
Gm37766	Chr2:11227297-11229863 (+)	unclassified gene	No	X	--	--	--	--	--	Expressed in mouse liver

Gm38171	Chr2:11315372-11319874 (-)	lncRNA gene	No	X	--	--	--	--	--	Expressed in mouse heart, skeletal muscle, and liver
Gm31902	Chr2:Syntenic	lncRNA gene	No	--	--	--	--	--	--	None – predicted gene
Gm37851	Chr2:11332825-11333713 (+)	unclassified gene	No	X	--	--	--	--	--	Expressed in mouse liver
8030442B05Rik	Chr2:11338366-11398500 (-)	lncRNA gene	No	X	--	--	--	--	--	Expressed in mouse heart
Gm13293	Chr2:11339489-11344106 (+)	lncRNA gene	No	X	--	--	--	--	--	Expressed in mouse skeletal muscle
Gm37730	Chr2:11365241-11367451 (-)	unclassified gene	No	--	--	--	--	--	--	None
Gm13291	Chr2:11385003-11387064 (+)	lncRNA gene	No	X	--	--	--	--	--	Expressed in mouse heart
4933403L11Rik	Chr2:11383787-11384907 (-)	unclassified gene	No	--	--	--	--	--	--	None
Gm31990	Chr2:11422527-11447447 (-)	lncRNA gene	No	--	--	--	--	--	--	None – predicted gene
Pfkfb3	Chr2:11471430-11554071 (-)	protein coding gene	No	X	X	--	X	X	X	Expressed in all mouse tissues of interest; GO:0003873; GO:0005829; GO:0004331; GO:0006003; GO:0005654; increased circulating HDL cholesterol level (EBM)
Gm10851	Chr2:11521642-11529973 (+)	lncRNA gene	No	X	X	--	--	--	--	Expressed in mouse heart, kidney, skeletal muscle, and liver
Gm37975	Chr2:11532596-11534694 (-)	unclassified gene	No	X	X	--	--	--	--	Expressed in mouse skeletal muscle and liver
Rbm17	Chr2:11585439-11603199 (-)	protein coding gene	No	X	X	X	X	X	--	Expressed in all mouse tissues of interest; GO:0000380; GO:0006397; GO:0000398; GO:0003676; GO:0005654; GO:0005634; GO:0005515; GO:0032991; GO:0003723;

										GO:0008380; GO:0000375; GO:0005681
Gm17490	Chr2:11625606-11626264 (-)	protein coding gene	No	X	--	--	--	--	--	Expressed in mouse heart and liver
Il2ra	Chr2:11642807-11693193 (+)	protein coding gene	No	X	X	--	X	X	X	Expressed in mouse heart, brain, skeletal muscle, and liver; GO:0006924; GO:0009986; GO:0009897; GO:0002376; GO:0006954; GO:0002437; GO:0016021; GO:0019976; GO:0004911; GO:0016020; GO:0050728; GO:0050672; GO:0042130; GO:0007219; GO:0042104; GO:0045582; GO:0042102; GO:0005515; GO:0046013; GO:0002664; GO:0043029; decreased circulating cholesterol, glucose, and serum albumin levels, decreased heart weight and increased heart rate, enlarged lymph nodes, increased circulating phosphate level (EBM)
Gm39760	Chr2:11682688-11694615 (-)	lncRNA gene	No	--	--	--	--	--	--	None – predicted gene
Gm37881	Chr2:11683126-11683546 (+)	unclassified gene	No	X	X	--	--	--	--	Expressed in mouse heart, skeletal muscle, and liver
Gm39759	Chr2:11693611-11699526 (+)	lncRNA gene	No	--	--	--	--	--	--	None – predicted gene
Il15ra	Chr2:11705172-11733985 (+)	protein coding gene	No	X	X	X	X	X	X	Expressed in mouse heart, skeletal muscle, and liver; GO:0009986; GO:0031410; GO:0005576; GO:0016021; GO:0035723; GO:0042010;

										GO:0016020; GO:0010977; GO:0005634; GO:0005886; GO:0032825; GO:0050766; GO:0019901; GO:0007259; abnormal NK and T cell physiology, increased interleukin-2 secretion (EBM)
Fbh1	Chr2:11742573-11777582 (-)	protein coding gene	No	X	X	--	X	X	--	Expressed in all mouse tissues of interest; GO:0043138; GO:0005524; GO:0008219; GO:0006974; GO:0000785; GO:0005694; GO:0003677; GO:0000737; GO:0003678; GO:0006281; GO:0015616; GO:0000724; GO:0003690; GO:0004386; GO:0016787; GO:0035562; GO:2000042; GO:0000166; GO:0005634; GO:1902231; GO:0001934; GO:0005515; GO:0016567; GO:0000725; GO:0031297; GO:0072429; GO:0019005; GO:0003697
Gm46731	Chr2:11743778-11745198 (-)	protein coding gene	No	--	--	--	--	--	--	None – predicted gene
Ankrd16	Chr2:11777876-11790329 (+)	protein coding gene	No	X	X	--	X	X	--	Expressed in all mouse tissues of interest; GO:0005737; GO:0003674; GO:0005634; GO:0006400
Gm32204	Chr2:11925843-11927868 (+)	protein coding gene	No	--	--	--	--	--	--	None – predicted gene
Itga8	Chr2:12106632-12301922 (-)	protein coding gene	No	X	X	--	X	X	X	Expressed in all mouse tissues of interest; GO:0045177; GO:0007155; GO:0030154; GO:0007160; GO:0030030; GO:0009986; GO:0032591;

										GO:0005783; GO:0045184; GO:0030198; GO:0042472; GO:0016021; GO:0008305; GO:0007229; GO:0001822; GO:0016020; GO:0007613; GO:0046872; GO:0001656; GO:0007275; GO:0007399; GO:0043204; GO:0005886; GO:2000721; GO:0030511; GO:0014069; GO:0048745; GO:0034446; increased circulating calcium, sodium, and triglyceride levels (EBM)
Gm37701	Chr2:12128643-12129742 (-)	unclassified gene	No	--	X	--	--	--	--	Expressed in mouse kidney and brain
E030013I19Rik	Chr2:12301246-12312315 (+)	lncRNA gene	No	X	X	--	X	--	--	Expressed in mouse heart, kidney, and liver; GO:0008150; GO:0005575; GO:0003674
Mindy3	Chr2:12347263-12419470 (-)	protein coding gene	No	X	X	--	X	X	--	Expressed in all mouse tissues of interest; GO:0006915; GO:0008234; GO:0016787; GO:1990380; GO:0031965; GO:0005654; GO:0005634; GO:0008233; GO:0071108; GO:0018215; GO:0006508; GO:0004843
Gm37289	Chr2:12357095-12358496 (-)	unclassified gene	No	X	X	--	--	--	--	Expressed in mouse heart and liver
Gm37255	Chr2:12372212-12375271 (-)	unclassified gene	No	X	X	--	--	--	--	Expressed in mouse heart, kidney, skeletal muscle, and liver
Gm38014	Chr2:12389872-12392483 (-)	unclassified gene	No	X	X	--	--	--	--	Expressed in mouse heart, brain, skeletal muscle, and liver

Gm37565	Chr2:12697417-12706853 (+)	lncRNA gene	No	X	X	--	--	--	--	Expressed in mouse heart and liver
Pter	Chr2:12924041-13003455 (+)	protein coding gene	No	X	X	X	X	X	--	Expressed in all mouse tissues of interest; GO:0009056; GO:0016787; GO:0016788; GO:0046872; GO:0008270; abnormal heart sounds (PW)
C1ql3	Chr2:13003457-13011806 (-)	protein coding gene	No	X	--	--	X	X	X	Expressed in mouse heart, brain, skeletal muscle, and liver; GO:0005581; GO:0005576; GO:0042802; GO:0005515; GO:0050807; abnormal heart sounds (PW)
Gm37824	Chr2:13004365-13007600 (+)	unclassified gene	No	X	X	--	--	--	--	Expressed in mouse heart, skeletal muscle, and liver
Gm37811	Chr2:13009886-13012486 (+)	unclassified gene	No	X	--	--	--	--	--	Expressed in mouse liver
Gm37356	Chr2:13012624-13014236 (+)	unclassified gene	No	X	X	--	--	--	--	Expressed in mouse kidney, brain, skeletal muscle and liver
Gm37742	Chr2:13036126-13040104 (+)	unclassified gene	No	X	--	--	--	--	--	Expressed in mouse kidney
1700016C23Rik	Chr2:13042601-13045493 (-)	unclassified gene	No	--	--	--	--	--	--	None
Rsu1	Chr2:13076967-13271438 (-)	protein coding gene	No	X	X	--	X	X	--	Expressed in all mouse tissues of interest; GO:0005925; GO:0003674; GO:0010811; GO:0043547; GO:2000179; GO:0007265; GO:0007165; abnormal heart sounds (PW)
Gm38156	Chr2:13116176-13118435 (-)	unclassified gene	No	X	--	--	--	--	--	Expressed in mouse heart, skeletal muscle, and liver
9330179A15Rik	Chr2:13149539-13149962 (+)	unclassified gene	No	--	--	--	--	--	--	None
Gm37780	Chr2:13161751-13163623 (-)	unclassified gene	No	X	X	--	--	--	--	Expressed in all mouse tissues of interest

Gm27540	Chr2:13226828-13227014 (+)	unclassified non-coding RNA gene	No	X	X	--	--	--	--	Expressed in mouse heart, brain, skeletal muscle, and liver
Gm37160	Chr2:13238939-13240627 (-)	unclassified gene	No	X	X	--	--	--	--	Expressed in mouse heart, brain, skeletal muscle, and liver
Gm13270	Chr2:13271577-13309275 (+)	lncRNA gene	No	X	X	--	X	--	--	Expressed in mouse heart, skeletal muscle, and liver; GO:0008150; GO:0005575; GO:0003674
Cubn	Chr2:13276338-13491813 (-)	protein coding gene	No	X	X	--	X	X	X	Expressed in all mouse tissues of interest; GO:0045177; GO:0016324; GO:0005903; GO:0031526; GO:0005509; GO:0038024; GO:0008203; GO:0005905; GO:0030135; GO:0031419; GO:0042366; GO:0015889; GO:0005737; GO:0020028; GO:0030139; GO:0030666; GO:0005783; GO:0005768; GO:0070062; GO:0005794; GO:0005798; GO:0030492; GO:0042802; GO:0001701; GO:0006629; GO:0042953; GO:0043202; GO:0005764; GO:0016020; GO:0046872; GO:0005886; GO:0005515; GO:0032991; GO:0042803; GO:0015031; GO:0043235; GO:0006898; GO:0009617; GO:0007584; GO:0038023; GO:0008202; abnormal heart morphology (EBM)

[a] Resource abbreviations: **EBM,** Ensembl BioMart; **EEA,** EBI Expression Atlas; **GO,** Gene Ontology; **GXD,** Gene eXpression Database; **MGI,** Mouse Genome Informatics; **PW,** PheWeb

[b] ID terms: **GO:0051457:** maintenance of protein location in nucleus; **GO:0046872:** metal ion binding; **GO:0043433:** negative regulation of DNA-binding transcription factor activity; **GO:0000122:** negative regulation of transcription by RNA polymerase II; **GO:0031965:** nuclear membrane; **GO:0005654:** nucleoplasm; **GO:0005634:** nucleus; **GO:0002039:** p53 binding; **GO:0005515:** protein binding; **GO:0046982:** protein heterodimerization activity; **GO:0006357:** regulation of transcription by RNA polymerase II; **GO:0006366:** transcription by RNA polymerase II; **GO:0005669:** transcription factor TFIID complex; **GO:0140416:** transcription regulator inhibitor activity; **GO:0016887:** ATPase activity; **GO:0006754:** ATP biosynthetic process; **GO:0046034:** ATP metabolic process; **GO:0015986:** ATP synthesis coupled proton transport; **GO:0006811:** ion transport; **GO:0016020:** membrane; **GO:0042776:** mitochondrial ATP synthesis coupled proton transport; **GO:0005743:** mitochondrial inner membrane; **GO:0005753:** mitochondrial proton-transporting ATP synthase complex; **GO:0000275:** mitochondrial proton-transporting ATP synthase complex, catalytic sector F(1); **GO:0005739:** mitochondrion; **GO:0043209:** myelin sheath; **GO:0046933:** proton-transporting ATP synthase activity, rotational mechanism; **GO:0045261:** proton-transporting ATP synthase complex, catalytic core F(1); **GO:0006974:** cellular response to DNA damage stimulus; **GO:0005737:** cytoplasm; **GO:0003677:** DNA binding; **GO:0006310:** DNA recombination; **GO:0006281:** DNA repair; **GO:0006260:** DNA replication; **GO:0003690:** double-stranded DNA binding; **GO:0043231:** intracellular membrane-bounded organelle; **GO:0006397:** mRNA processing; **GO:0016363:** nuclear matrix; **GO:0032991:** protein-containing complex; **GO:0003723:** RNA binding; **GO:0062023:** collagen-containing extracellular matrix; **GO:0005576:** extracellular region; **GO:0030212:** hyaluronan metabolic process; **GO:0010466:** negative regulation of peptidase activity; **GO:0030414:** peptidase inhibitor activity; **GO:0004867:** serine-type endopeptidase inhibitor activity; **GO:0008150:** biological_process; **GO:0005575:** cellular_component; **GO:0003674:** molecular_function; **GO:0016235:** aggresome; **GO:0003682:** chromatin binding; **GO:0005829:** cytosol; **GO:0042393:** histone binding; **GO:0010629:** negative regulation of gene expression; **GO:0045892:** negative regulation of transcription, DNA-templated; **GO:0016604:** nuclear body; **GO:0016607:** nuclear speck; **GO:0006355:** regulation of transcription, DNA-templated; **GO:0003714:** transcription corepressor activity; **GO:0016442:** RISC complex; **GO:0071230:** cellular response to amino acid stimulus; **GO:2001015:** negative regulation of skeletal muscle cell differentiation; **GO:0010468:** regulation of gene expression; **GO:1990830:** cellular response to leukemia inhibitory factor; **GO:0060291:** long-term synaptic potentiation; **GO:0030307:** positive regulation of cell growth; **GO:0007605:** sensory perception of sound; **GO:0071356:** cellular response to tumor necrosis factor; **GO:0071222:** cellular response to lipopolysaccharide; **GO:0071391:** cellular response to estrogen stimulus; **GO:1904322:** cellular response to forskolin; **GO:0071241:** cellular response to inorganic substance; **GO:0045944:** positive regulation of transcription by RNA polymerase II; **GO:0070935:** 3'-UTR-mediated mRNA stabilization; **GO:0035925:** mRNA 3'-UTR AU-rich region binding; **GO:0045727:** positive regulation of translation; **GO:0061013:** regulation of mRNA catabolic process;**GO:0005524:** ATP binding; **GO:0060326:** cell chemotaxis; **GO:0034451:** centriolar satellite; **GO:0002376:** immune system process; **GO:0001772:** immunological synapse; **GO:0006954:** inflammatory response; **GO:0035556:** intracellular signal transduction; **GO:0016301:** kinase activity; **GO:0006509:** membrane protein ectodomain proteolysis; **GO:0046627:** negative regulation of insulin receptor signaling pathway; **GO:0070233:** negative regulation of T cell apoptotic process; **GO:0031594:** neuromuscular junction; **GO:0000166:** nucleotide binding; **GO:0018105:** peptidyl-serine phosphorylation; **GO:0016310:** phosphorylation; **GO:0005886:** plasma membrane; **GO:0051491:** positive regulation of filopodium

assembly; **GO:0032740:** positive regulation of interleukin-17 production; **GO:0032743:** positive regulation of interleukin-2 production; **GO:0032753:** positive regulation of interleukin-4 production; **GO:0051092:** positive regulation of NF-kappaB transcription factor activity; **GO:0042307:** positive regulation of protein import into nucleus; **GO:0050714:** positive regulation of protein secretion; **GO:0051496:** positive regulation of stress fiber assembly; **GO:0050870:** positive regulation of T cell activation; **GO:0042102:** positive regulation of T cell proliferation; **GO:0051973:** positive regulation of telomerase activity; **GO:1904355:** positive regulation of telomere capping; **GO:0032212:** positive regulation of telomere maintenance via telomerase; **GO:2000318:** positive regulation of T-helper 17 type immune response; **GO:2000570:** positive regulation of T-helper 2 cell activation; **GO:0004672:** protein kinase activity; **GO:0004697:** protein kinase C activity; **GO:0018215:** protein phosphopantetheinylation; **GO:0006468:** protein phosphorylation; **GO:0004674:** protein serine/threonine kinase activity; **GO:0010389:** regulation of G2/M transition of mitotic cell cycle; **GO:0090330:** regulation of platelet aggregation; **GO:0042383:** sarcolemma; **GO:0016740:** transferase activity; **GO:0003873:** 6-phosphofructo-2-kinase activity; **GO:0004331:** fructose-2,6-bisphosphate 2-phosphatase activity; **GO:0006003:** fructose 2,6-bisphosphate metabolic process; **GO:0000380:** alternative mRNA splicing, via spliceosome; **GO:0000398:** mRNA splicing, via spliceosome; **GO:0003676:** nucleic acid binding; **GO:0008380:** RNA splicing; **GO:0000375:** RNA splicing, via transesterification reactions; **GO:0005681:** spliceosomal complex; **GO:0006924:** activation-induced cell death of T cells; **GO:0009986:** cell surface; **GO:0009897:** external side of plasma membrane; **GO:0002437:** inflammatory response to antigenic stimulus; **GO:0016021:** integral component of membrane; **GO:0019976:** interleukin-2 binding; **GO:0004911:** interleukin-2 receptor activity; **GO:0050728:** negative regulation of inflammatory response; **GO:0050672:** negative regulation of lymphocyte proliferation; **GO:0042130:** negative regulation of T cell proliferation; **GO:0007219:** Notch signaling pathway; **GO:0042104:** positive regulation of activated T cell proliferation; **GO:0045582:** positive regulation of T cell differentiation; **GO:0046013:** regulation of T cell homeostatic proliferation; **GO:0002664:** regulation of T cell tolerance induction; **GO:0043029:** T cell homeostasis; **GO:0031410:** cytoplasmic vesicle; **GO:0035723:** interleukin-15-mediated signaling pathway; **GO:0042010:** interleukin-15 receptor activity; **GO:0010977:** negative regulation of neuron projection development; **GO:0032825:** positive regulation of natural killer cell differentiation; **GO:0050766:** positive regulation of phagocytosis; **GO:0019901:** protein kinase binding; **GO:0007259:** receptor signaling pathway via JAK-STAT; **GO:0043138:** 3'-5' DNA helicase activity; **GO:0005524:** ATP binding; **GO:0008219:** cell death; **GO:0006974:** cellular response to DNA damage stimulus; **GO:0000785:** chromatin; **GO:0005694:** chromosome; **GO:0003677:** DNA binding; **GO:0000737:** DNA catabolic process, endonucleolytic; **GO:0003678:** DNA helicase activity; **GO:0006281:** DNA repair; **GO:0015616:** DNA translocase activity; **GO:0000724:** double-strand break repair via homologous recombination; **GO:0003690:** double-stranded DNA binding; **GO:0004386:** helicase activity; **GO:0016787:** hydrolase activity; **GO:0035562:** negative regulation of chromatin binding; **GO:2000042:** negative regulation of double-strand break repair via homologous recombination; **GO:0000166:** nucleotide binding; **GO:1902231:** positive regulation of intrinsic apoptotic signaling pathway in response to DNA damage; **GO:0001934:** positive regulation of protein phosphorylation; **GO:0016567:** protein ubiquitination; **GO:0000725:** recombinational repair; **GO:0031297:** replication fork processing; **GO:0072429:** response to intra-S DNA damage checkpoint signaling; **GO:0019005:** SCF ubiquitin ligase complex; **GO:0003697:** single-stranded DNA binding; **GO:0006400:** tRNA modification; **GO:0045177:** apical part of cell; **GO:0007155:** cell adhesion; **GO:0030154:** cell differentiation;

GO:0007160: cell-matrix adhesion; **GO:0030030:** cell projection organization; **GO:0032591:** dendritic spine membrane; **GO:0005783:** endoplasmic reticulum; **GO:0045184:** establishment of protein localization; **GO:0030198:** extracellular matrix organization; **GO:0042472:** inner ear morphogenesis; **GO:0008305:** integrin complex; **GO:0007229:** integrin-mediated signaling pathway; **GO:0001822:** kidney development; **GO:0007613:** memory; **GO:0001656:** metanephros development; **GO:0007275:** multicellular organism development; **GO:0007399:** nervous system development; **GO:0043204:** perikaryon; **GO:2000721:** positive regulation of transcription from RNA polymerase II promoter involved in smooth muscle cell differentiation; **GO:0030511:** positive regulation of transforming growth factor beta receptor signaling pathway; **GO:0014069:** postsynaptic density; **GO:0048745:** smooth muscle tissue development; **GO:0034446:** substrate adhesion-dependent cell spreading; **GO:0006915:** apoptotic process; **GO:0008234:** cysteine-type peptidase activity; **GO:1990380:** Lys48-specific deubiquitinase activity; **GO:0008233:** peptidase activity; **GO:0071108:** protein K48-linked deubiquitination; **GO:0006508:** proteolysis; **GO:0004843:** thiol-dependent ubiquitin-specific protease activity; **GO:0009056:** catabolic process; **GO:0016788:** hydrolase activity, acting on ester bonds; **GO:0008270:** zinc ion binding; **GO:0005581:** collagen trimer; **GO:0042802:** identical protein binding; **GO:0050807:** regulation of synapse organization; **GO:0005925:** focal adhesion; **GO:0010811:** positive regulation of cell-substrate adhesion; **GO:0043547:** positive regulation of GTPase activity; **GO:2000179:** positive regulation of neural precursor cell proliferation; **GO:0007265:** Ras protein signal transduction; **GO:0007165:** signal transduction; **GO:0016324:** apical plasma membrane; **GO:0005903:** brush border; **GO:0031526:** brush border membrane; **GO:0005509:** calcium ion binding; **GO:0038024:** cargo receptor activity; **GO:0008203:** cholesterol metabolic process; **GO:0005905:** clathrin-coated pit; **GO:0030135:** coated vesicle; **GO:0031419:** cobalamin binding; **GO:0042366:** cobalamin catabolic process; **GO:0015889:** cobalamin transport; **GO:0020028:** endocytic hemoglobin import into cell; **GO:0030139:** endocytic vesicle; **GO:0030666:** endocytic vesicle membrane; **GO:0005768:** endosome; **GO:0070062:** extracellular exosome; **GO:0005794:** Golgi apparatus; **GO:0005798:** Golgi-associated vesicle; **GO:0030492:** hemoglobin binding; **GO:0001701:** in utero embryonic development; **GO:0006629:** lipid metabolic process; **GO:0042953:** lipoprotein transport; **GO:0043202:** lysosomal lumen; **GO:0005764:** lysosome; **GO:0042803:** protein homodimerization activity; **GO:0015031:** protein transport; **GO:0043235:** receptor complex; **GO:0006898:** receptor-mediated endocytosis; **GO:0009617:** response to bacterium; **GO:0007584:** response to nutrient; **GO:0038023:** signaling receptor activity; **GO:0008202:** steroid metabolic process

Supplementary Table S4.6. AST candidate genes and their relevant annotations (Chr16: 57.069–59.755 ± 1 Mbp; GRCm38/mm10).[a]

				Expression		Functional		Phenotypic		
MGI Gene symbol	**Genome coordinates (strand)**	**Type**	**Known AST gene**	**GXD (MGI)**	**EEA**	**Inter Pro**	**GO**	**PW**	**EBM**	**Relevance to AST[b]**
Senp7	Chr16:56057526-56190031 (+)	protein coding gene	No	--	--	--	--	--	--	None
Gm41462	Chr16:56067819-56069664 (-)	lncRNA gene	No	--	--	--	--	--	--	None – predicted gene
Gm24047	Chr16:56070563-56070666 (+)	miRNA gene	No	X	X	--	--	--	--	Expressed in mouse skeletal muscle and liver
C330019O22Rik	Chr16:56115269-56116255 (-)	unclassified gene	No	--	--	--	--	--	--	None
A130047H01Rik	Chr16:56191090-56193351 (+)	unclassified gene	No	--	--	--	--	--	--	None
Impg2	Chr16:56204313-56273756 (+)	protein coding gene	No	--	X	X	X	X	--	Expressed in mouse liver; GO:0042995; GO:0031012; GO:0005201; GO:0005576; GO:0008201; GO:0008201; GO:0005540; GO:0005540; GO:0016021; GO:0033165; GO:0016020; GO:0043235; GO:0007601
Abi3bp	Chr16:56477878-56690135 (+)	protein coding gene	No	X	--	--	X	--	--	Expressed in mouse skeletal muscle; GO:0005518; GO:0062023; GO:0031012; GO:0030198; GO:0005201; GO:0005539; GO:0008201; GO:0005614; GO:0010811
Tfg	Chr16:56690332-56717450 (-)	protein coding gene	No	X	--	X	X	X	--	Expressed in mouse skeletal muscle and liver; GO:0005737; GO:0005829; GO:0070971; GO:0006888; GO:0042802; GO:0043231; GO:0005515

Adgrg7	Chr16:56724609-56795855 (-)	protein coding gene	No	X	--	--	X	--	X	Expressed in mouse skeletal muscle and liver; GO:0007189; GO:0007166; GO:0004930; GO:0007186; GO:0016021; GO:0005887; GO:0016020; GO:0007165; GO:0004888
Tmem45a	Chr16:56805161-56886166 (-)	protein coding gene	No	X	X	--	X	X	--	Expressed in mouse heart, kidney, skeletal muscle, and liver; GO:0008150; GO:0016021; GO:0005887; GO:0016020; GO:0003674
Gm15839	Chr16:56886367-56921506 (+)	lncRNA gene	No	--	--	--	--	--	--	None – predicted gene
Lnp1	Chr16:56914344-56928061 (-)	protein coding gene	No	X	--	X	--	X	--	Expressed in mouse heart
Tmem45a2	Chr16:57036967-57071346 (-)	protein coding gene	No	X	--	--	X	--	--	Expressed in mouse skeletal muscle and liver; GO:0008150; GO:0005575; GO:0003674
Tomm70a	Chr16:57121714-57154530 (+)	protein coding gene	No	X	X	--	X	--	--	Expressed in all mouse tissues of interest; GO:0002218; GO:0098586; GO:0016021; GO:0031307; GO:0016020; GO:0005741; GO:0005742; GO:0005739; GO:0061052; GO:0002230; GO:0032728; GO:1904591; GO:0005515; GO:0006626; GO:0042981
Nit2	Chr16:57156665-57167332 (-)	protein coding gene	No	X	X	X	X	X	--	Expressed in all mouse tissues of interest; GO:0006528; GO:0005813; GO:0005737; GO:0005829; GO:0006541; GO:0016787; GO:0005739; GO:0006807; GO:0050152; GO:0006107

Gm16892	Chr16:57167401-57174413 (+)	lncRNA gene	No	X	X	--	--	--	--	Expressed in all mouse tissues of interest
Tbc1d23	Chr16:57168862-57231504 (-)	protein coding gene	No	X	X	X	X	X	X	Expressed in all mouse tissues of interest; GO:0007420; GO:0031410; GO:1990403; GO:0005794; GO:0007275; GO:0031175; GO:0032755; GO:0005515; GO:0050727; GO:0032680; GO:0042147; GO:0005802; GO:0016192; GO:0099041; GO:0071203; Increased inflammatory response, increased circulating interleukin-6 and tumor necrosis factor levels (EBM)
Tmem30c	Chr16:57266139-57292865 (-)	protein coding gene	No	--	--	--	--	--	--	None
Gm26800	Chr16:57280890-57281496 (+)	lncRNA gene	No	X	X	--	--	--	--	Expressed in mouse heart and skeletal muscle
Cmss1	Chr16:57302000-57606864 (-)	protein coding gene	No	X	X	--	X	X	--	Expressed in all mouse tissues of interest; GO:0008150; Other disorders of biliary tract (PW)
4921517D16Rik	Chr16:57331951-57335432 (+)	lncRNA gene	No	X	--	--	--	--	--	Expressed in mouse heart, skeletal muscle, and liver
Gm49579	Chr16:57338310-57340403 (+)	lncRNA gene	No	X	--	--	--	X	--	Expressed in all mouse tissues of interest
Filip1l	Chr16:57353277-57572804 (+)	protein coding gene	No	X	--	--	X	--	--	Expressed in all mouse tissues of interest; GO:0008150; GO:0005737; GO:0016020; GO:0003674; GO:0005634
Gm45967	Chr16:Syntenic	lncRNA gene	No	--	--	--	--	--	--	None – predicted gene
Col8a1	Chr16:57624258-57754737 (-)	protein coding gene	No	X	--	--	X	X	X	Expressed in all mouse tissues of interest; GO:0001525; GO:0005604; GO:0048593;

										GO:0007155; GO:0062023; GO:0005581; GO:0050673; GO:0031012; GO:0030198; GO:0005201; GO:0030020; GO:0005576; GO:0005615; GO:0010811; Obstruction of bile duct (PW)
Gm49575	Chr16:57811487-58042341 (+)	lncRNA gene	No	--	--	--	--	--	--	None – predicted gene
Gm24039	Chr16:57884008-57884139 (-)	snoRNA gene	No	--	--	--	--	--	--	None – predicted gene
Gm37458	Chr16:57902933-57903342 (+)	unclassified gene	No	--	--	--	--	--	--	None – predicted gene
Gm49576	Chr16:57993538-58006023 (-)	lncRNA gene	No	--	--	--	--	--	--	None – predicted gene
Gm41463	Chr16:58147017-58148684 (-)	lncRNA gene	No	--	--	--	--	--	--	None – predicted gene
Gm49574	Chr16:58238104-58249239 (+)	lncRNA gene	No	--	--	--	--	--	--	None – predicted gene
Gm37825	Chr16:58316785-58319071 (-)	unclassified gene	No	--	--	--	--	--	--	None – predicted gene
4930461C15Rik	Chr16:58404878-58408276 (-)	lncRNA gene	No	--	--	--	--	--	--	None
Dcbld2	Chr16:58408535-58469745 (+)	protein coding gene	No	X	X	--	X	X	X	Expressed in all mouse tissues of interest; GO:0009986; GO:0016021; GO:0005887; GO:0016020; GO:0030308; GO:0042060; Secondary hyperparathyroidism (of renal origin), type 2 diabetes with renal manifestations (PW)
St3gal6	Chr16:58469742-58524260 (-)	protein coding gene	No	X	--	--	X	X	--	Expressed in all mouse tissues of interest; GO:0052798; GO:0006464; GO:0006664; GO:0005794; GO:0016021; GO:0016020; GO:0009311;

										GO:0006486; GO:0097503; GO:0008373; GO:0016740; GO:0016757
Gm33475	Chr16:58475943-58483165 (+)	lncRNA gene	No	--	--	--	--	--	--	None – predicted gene
Gm49701	Chr16:58651490-58655244 (-)	lncRNA gene	No	X	--	--	--	--	--	Expressed in mouse liver
Gm41464	Chr16:58657485-58663452 (-)	lncRNA gene	No	--	--	--	--	--	--	None – predicted gene
Cpox	Chr16:58670208-58680391 (+)	protein coding gene	No	X	X	--	X	X	X	Expressed in all mouse tissues of interest; GO:0004109; GO:0005737; GO:0005829; GO:0006783; GO:0042802; GO:0016020; GO:0005743; GO:0005758; GO:0005739; GO:0016491; GO:0006779; GO:0006813; GO:0042803; GO:0006782; GO:0005391; GO:0006814; GO:0005212
Gpr15	Chr16:58717433-58719070 (-)	protein coding gene	No	X	--	--	X	X	X	Expressed in mouse kidney and skeletal muscle; GO:0015026; GO:0005737; GO:0005768; GO:0004930; GO:0007186; GO:0016021; GO:0016020; GO:0005886; GO:0007165; GO:0072678; GO:0046718; GO:0001618; Increased interleukin-17 and interferon-gamma secretion (EBM)
Cldnd1	Chr16:58727910-58734247 (+)	protein coding gene	No	X	X	X	X	X	--	Expressed in all mouse tissues of interest; GO:0016324; GO:0008150; GO:0016021; GO:0016020; GO:0003674
Gm27564	Chr16:58749589-58749684 (-)	miRNA gene	No	X	--	--	--	--	--	Expressed in mouse heart and liver

Gm26019	Chr16:58751478-58751596 (-)	snoRNA gene	No	X	X	--	--	--	--	Expressed in mouse heart, kidney, and liver
Olfr172	Chr16:58760152-58761240 (-)	protein coding gene	No	X	--	--	--	--	--	Expressed in mouse liver
Olfr173	Chr16:58796779-58797942 (-)	protein coding gene	No	X	--	--	X	--	--	Expressed in mouse skeletal muscle; GO:0007186; GO:0016021; GO:0004984; GO:0007608; GO:0005549
Olfr175-ps1	Chr16:58823781-58826761 (-)	protein coding gene	No	--	--	--	--	--	--	None
Olfr177	Chr16:58869403-58873148 (-)	protein coding gene	No	--	--	--	--	--	--	None
Olfr178	Chr16:58889259-58890218 (-)	protein coding gene	No	--	--	--	--	--	--	None
Olfr180	Chr16:58915686-58918486 (-)	protein coding gene	No	--	--	--	--	--	--	None
4933431I19Rik	Chr16:58914303-58929392 (-)	unclassified non-coding RNA gene	No	--	--	--	--	--	--	None
Olfr181	Chr16:58925557-58928644 (-)	protein coding gene	No	--	--	--	--	--	--	None
Olfr183	Chr16:58995357-59001441 (+)	protein coding gene	No	--	--	--	--	--	--	None
Olfr186	Chr16:59026923-59027927 (-)	protein coding gene	No	--	--	--	--	--	--	None
Olfr187	Chr16:59035780-59039749 (-)	protein coding gene	No	--	--	--	--	--	--	None
Olfr190	Chr16:59074155-59075078 (-)	protein coding gene	No	--	--	--	--	--	--	None
Olfr191	Chr16:59085552-59086481 (-)	protein coding gene	No	--	--	--	--	--	--	None
Olfr193	Chr16:59109625-59110633 (-)	protein coding gene	No	--	--	--	--	--	--	None
Olfr194	Chr16:59119148-59120068 (-)	protein coding gene	No	--	--	--	--	--	--	None

Olfr195	Chr16:59148852-59149778 (+)	protein coding gene	No	--	--	--	--	--	--	None
Olfr196	Chr16:59166647-59170454 (-)	protein coding gene	No	--	--	--	--	--	--	None
Olfr198	Chr16:59201504-59202424 (-)	protein coding gene	No	--	--	--	--	--	--	None
Olfr199	Chr16:59215685-59216611 (-)	protein coding gene	No	--	--	--	--	--	--	None
Olfr201	Chr16:59268739-59269665 (-)	protein coding gene	No	X	--	--	X	--	--	Expressed in mouse liver; GO:0007186; GO:0016021; GO:0005549; GO:0004984; GO:0007608
Olfr202	Chr16:59283572-59284495 (-)	protein coding gene	No	--	--	--	--	--	--	None
Olfr203	Chr16:59303155-59304075 (+)	protein coding gene	No	--	--	--	--	--	--	None
Olfr204	Chr16:59314488-59315405 (-)	protein coding gene	No	--	--	--	--	--	--	None
Olfr205	Chr16:59328590-59329507 (-)	protein coding gene	No	--	--	--	--	--	--	None
Olfr206	Chr16:59344722-59345726 (-)	protein coding gene	No	--	--	--	--	--	--	None
Olfr209	Chr16:59361224-59362240 (-)	protein coding gene	No	--	--	--	--	--	--	None
Gm33611	Chr16:59405026-59406161 (+)	lncRNA gene	No	--	--	--	--	--	--	None – predicted gene
Gabrr3	Chr16:59407382-59461739 (+)	protein coding gene	No	--	--	--	--	--	--	None
1700022E09Rik	Chr16:59466872-59469238 (-)	lncRNA gene	No	--	--	--	--	--	--	None
Riox2	Chr16:59471775-59492461 (+)	protein coding gene	No	X	X	--	X	X	X	Expressed in all mouse tissues of interest; GO:0016706; GO:0008283; GO:0005829; GO:0051213; GO:0051864; GO:0032453; GO:0070544; GO:0034720; GO:0042802;

										GO:0046872; GO:0005730; GO:0005654; GO:0005634; GO:0016491; GO:0018215; GO:0042127; GO:0042254; GO:0003714; GO:0005667; Abnormal immunoglobulin and circulating interferon-gamma and interleukin-4 levels, decreased inflammatory response and eosinophil, macrophage, and neutrophil cell numbers (EBM); Ill-defined descriptions and complications of heart disease, vitamin D deficiency (PW)
Crybg3	Chr16:59492088-59601047 (-)	protein coding gene	No	X	X	--	X	--	--	Expressed in all mouse tissues of interest; GO:0030246; GO:0002088; GO:0032991; GO:0051018; GO:0005212; GO:0007601
Arl6	Chr16:59612949-59639391 (-)	protein coding gene	No	X	X	X	X	X	X	Expressed in all mouse tissues of interest; GO:0005930; GO:0007420; GO:0042995; GO:0030030; GO:0005929; GO:0060271; GO:0005737; GO:0005856; GO:0005829; GO:0005525; GO:0006886; GO:0016020; GO:0046872; GO:0000166; GO:0005886; GO:0006471; GO:0005515; GO:1903441; GO:0061512; GO:0097499; GO:0015031; GO:1903445; GO:0007265; GO:0008589; GO:0010842; GO:0016192; GO:0016055

A930013N22Rik	Chr16:59615993-59616903 (-)	unclassified gene	No	--	--	--	--	--	--	None
4930547E14Rik	Chr16:59636945-59672993 (+)	lncRNA gene	No	--	--	--	--	--	--	None
Epha6	Chr16:59653483-60605531 (-)	protein coding gene	No	X	X	X	X	X	X	Expressed in mouse heart, brain, and skeletal muscle; GO:0005524; GO:0007411; GO:0005003; GO:0016021; GO:0005887; GO:0016301; GO:0016020; GO:0007275; GO:0043005; GO:0005654; GO:0000166; GO:0016310; GO:0033674; GO:0004672; GO:0006468; GO:0004713; GO:0043235; GO:0016740; GO:0005005; GO:0004714; GO:0007169; Abnormal kidney morphology (EBM)
9330168O09Rik	Chr16:59642029-59646310 (-)	unclassified gene	No	--	--	--	--	--	--	None
Gm24755	Chr16:60369054-60369163 (-)	miRNA gene	No	--	--	--	--	--	--	None – predicted gene
Gm9017	Chr16:60604766-60611236 (+)	lncRNA gene	No	--	--	--	--	--	--	None – predicted gene
Gm27784	Chr16:60699179-60699291 (-)	miRNA gene	No	X	--	--	--	--	--	Expressed in mouse heart

[a] Resource abbreviations: **EBM,** Ensembl BioMart; **EEA,** EBI Expression Atlas; **GO,** Gene Ontology; **GXD,** Gene eXpression Database; **MGI,** Mouse Genome Informatics; **PW,** PheWeb

[b] ID terms: **GO:0042995:** cell projection; **GO:0031012:** extracellular matrix; **GO:0005201:** extracellular matrix structural constituent; **GO:0005576:** extracellular region; **GO:0008201:** heparin binding; **GO:0008201:** heparin binding; **GO:0005540:** hyaluronic acid binding; **GO:0005540:** hyaluronic acid binding; **GO:0016021:** integral component of membrane; **GO:0033165:** interphotoreceptor matrix; **GO:0016020:** membrane; **GO:0043235:** receptor complex; **GO:0007601:** visual perception; **GO:0005518:** collagen binding; **GO:0062023:** collagen-containing extracellular matrix; **GO:0030198:** extracellular matrix organization; **GO:0005539:** glycosaminoglycan binding; **GO:0005614:** interstitial matrix; **GO:0010811:** positive regulation of cell-substrate adhesion; **GO:0005737:** cytoplasm; **GO:0005829:** cytosol; **GO:0070971:** endoplasmic reticulum exit site; **GO:0006888:** endoplasmic reticulum

to Golgi vesicle-mediated transport; **GO:0042802:** identical protein binding; **GO:0043231:** intracellular membrane-bounded organelle; **GO:0005515:** protein binding; **GO:0007189:** adenylate cyclase-activating G protein-coupled receptor signaling pathway; **GO:0007166:** cell surface receptor signaling pathway; **GO:0004930:** G protein-coupled receptor activity; **GO:0007186:** G protein-coupled receptor signaling pathway; **GO:0005887:** integral component of plasma membrane; **GO:0007165:** signal transduction; **GO:0004888:** transmembrane signaling receptor activity; **GO:0008150:** biological_process; **GO:0003674:** molecular_function; **GO:0005575:** cellular_component; **GO:0002218:** activation of innate immune response; **GO:0098586**: cellular response to virus; **GO:0031307:** integral component of mitochondrial outer membrane; **GO:0005741:** mitochondrial outer membrane; **GO:0005742:** mitochondrial outer membrane translocase complex; **GO:0005739:** mitochondrion; **GO:0061052:** negative regulation of cell growth involved in cardiac muscle cell development; **GO:0002230:** positive regulation of defense response to virus by host; **GO:0032728:** positive regulation of interferon-beta production; **GO:1904591:** positive regulation of protein import; **GO:0006626:** protein targeting to mitochondrion; **GO:0042981:** regulation of apoptotic process; **GO:0006528:** asparagine metabolic process; **GO:0005813:** centrosome; **GO:0006541:** glutamine metabolic process; **GO:0016787:** hydrolase activity; **GO:0006807:** nitrogen compound metabolic process; **GO:0050152:** omega-amidase activity; **GO:0006107:** oxaloacetate metabolic process; **GO:0007420:** brain development; **GO:0031410:** cytoplasmic vesicle; **GO:1990403:** embryonic brain development; **GO:0005794:** Golgi apparatus; **GO:0007275:** multicellular organism development; **GO:0031175:** neuron projection development; **GO:0032755:** positive regulation of interleukin-6 production; **GO:0050727:** regulation of inflammatory response; **GO:0032680:** regulation of tumor necrosis factor production; **GO:0042147:** retrograde transport, endosome to Golgi; **GO:0005802:** trans-Golgi network; **GO:0016192:** vesicle-mediated transport; **GO:0099041:** vesicle tethering to Golgi; **GO:0071203:** WASH complex; **GO:0005634:** nucleus; **GO:0001525:** angiogenesis; **GO:0005604:** basement membrane; **GO:0048593:** camera-type eye morphogenesis; **GO:0007155:** cell adhesion; **GO:0005581:** collagen trimer; **GO:0050673:** epithelial cell proliferation; **GO:0030020:** extracellular matrix structural constituent conferring tensile strength; **GO:0005615:** extracellular space; **GO:0009986:** cell surface; **GO:0030308:** negative regulation of cell growth; **GO:0042060:** wound healing; **GO:0052798:** beta-galactoside alpha-2,3-sialyltransferase activity; **GO:0006464:** cellular protein modification process; **GO:0006664:** glycolipid metabolic process; **GO:0009311:** oligosaccharide metabolic process; **GO:0006486:** protein glycosylation; **GO:0097503:** sialylation; **GO:0008373:** sialyltransferase activity; **GO:0016740:** transferase activity; **GO:0016757:** transferase activity, transferring glycosyl groups; **GO:0004109:** coproporphyrinogen oxidase activity; **GO:0006783:** heme biosynthetic process; **GO:0005743:** mitochondrial inner membrane; **GO:0005758:** mitochondrial intermembrane space; **GO:0016491:** oxidoreductase activity; **GO:0006779:** porphyrin-containing compound biosynthetic process; **GO:0006813:** potassium ion transport; **GO:0042803:** protein homodimerization activity; **GO:0006782:** protoporphyrinogen IX biosynthetic process; **GO:0005391:** P-type sodium:potassium-exchanging ATPase activity; **GO:0006814:** sodium ion transport; **GO:0005212:** structural constituent of eye lens; **GO:0015026:** coreceptor activity; **GO:0005768:** endosome; **GO:0005886:** plasma membrane; **GO:0072678:** T cell migration; **GO:0046718:** viral entry into host cell; **GO:0001618:** virus receptor activity; **GO:0016324:** apical plasma membrane; **GO:0004984:** olfactory receptor activity; **GO:0007608:** sensory perception of smell; **GO:0005549:** odorant binding; **GO:0016706:** 2-oxoglutarate-dependent dioxygenase activity; **GO:0008283:** cell population proliferation; **GO:0051213:** dioxygenase activity; **GO:0051864:** histone

demethylase activity (H3-K36 specific); **GO:0032453:** histone demethylase activity (H3-K4 specific); **GO:0070544:** histone H3-K36 demethylation; **GO:0034720:** histone H3-K4 demethylation; **GO:0046872:** metal ion binding; **GO:0005730:** nucleolus; **GO:0005654:** nucleoplasm; **GO:0018215:** protein phosphopantetheinylation; **GO:0042127:** regulation of cell population proliferation; **GO:0042254:** ribosome biogenesis; **GO:0003714:** transcription corepressor activity; **GO:0005667:** transcription regulator complex; **GO:0030246:** carbohydrate binding; **GO:0002088:** lens development in camera-type eye; **GO:0032991:** protein-containing complex; **GO:0051018:** protein kinase A binding; **GO:0005930:** axoneme; **GO:0030030:** cell projection organization; **GO:0005929:** cilium; **GO:0060271:** cilium assembly; **GO:0005856:** cytoskeleton; **GO:0005525:** GTP binding; **GO:0006886:** intracellular protein transport; **GO:0000166:** nucleotide binding; **GO:0006471:** protein ADP-ribosylation; **GO:1903441:** protein localization to ciliary membrane; **GO:0061512:** protein localization to cilium; **GO:0097499:** protein localization to non-motile cilium; **GO:0015031:** protein transport; **GO:1903445:** protein transport from ciliary membrane to plasma membrane; **GO:0007265:** Ras protein signal transduction; **GO:0008589:** regulation of smoothened signaling pathway; **GO:0010842:** retina layer formation; **GO:0016055:** Wnt signaling pathway; **GO:0005524:** ATP binding; **GO:0007411:** axon guidance; **GO:0005003:** ephrin receptor activity; **GO:0016301:** kinase activity; **GO:0043005:** neuron projection; **GO:0016310:** phosphorylation; **GO:0033674:** positive regulation of kinase activity; **GO:0004672:** protein kinase activity; **GO:0006468:** protein phosphorylation; **GO:0004713:** protein tyrosine kinase activity; **GO:0005005:** transmembrane-ephrin receptor activity; **GO:0004714:** transmembrane receptor protein tyrosine kinase activity; **GO:0007169:** transmembrane receptor protein tyrosine kinase signaling pathway

Supplementary Table S4.7. Steatosis candidate genes and their relevant annotations (Chr18: 16.842–17.710 ± 1 Mbp; GRCm38/mm10).[a]

				Expression (in liver)		Functional		Phenotypic (liver-related)		
MGI Gene symbol	**Genome coordinates (strand)**	**Type**	**Known steatosis gene**	**GXD (MGI)**	**EEA**	**Inter Pro**	**GO**	**PW**	**EBM**	**Relevance to hepatic steatosis[b]**
Gm30512	Chr18:16021506-16036283 (+)	lncRNA gene	No	--	--	--	--	--	--	None – predicted gene
Gm22389	Chr18:16033746-16034046 (+)	unclassified non-coding RNA gene	No	--	--	--	--	--	--	None – predicted gene
Gm41673	Chr18:16037135-16039879 (-)	lncRNA gene	No	--	--	--	--	--	--	None – predicted gene
Gm30620	Chr18:16043618-16115424 (-)	lncRNA gene	No	--	--	--	--	--	--	None – predicted gene
Gm50076	Chr18:16136887-16144450 (-)	lncRNA gene	No	--	--	--	--	--	--	None – predicted gene
Gm24385	Chr18:16221019-16221368 (-)	unclassified non-coding RNA gene	No	--	--	--	--	--	--	None – predicted gene
Gm30765	Chr18:16293824-16318593 (+)	lncRNA gene	No	--	--	--	--	--	--	None – predicted gene
Cdh2	Chr18:16588877-16809246 (-)	protein coding gene	Yes	X	X	X	X	--	--	Expressed in mouse liver; GO:0005912; GO:0045294; GO:0045177; GO:0016324; GO:0016327; GO:0016323; GO:0008013; GO:0048514; GO:0007420; GO:0048854; GO:0045296; GO:0016339; GO:0005509; GO:0016342; GO:0007155; GO:0098609; GO:0044331; GO:0098742; GO:0005911; GO:0007043; GO:0030054; GO:0016477; GO:0009986; GO:0021987;

										GO:0030864; GO:0005737; GO:0019899; GO:0005916; GO:0045295; GO:0010001; GO:0098978; GO:0007157; GO:0048872; GO:0007156; GO:0042802; GO:0016021; GO:0005887; GO:0099060; GO:0099059; GO:0014704; GO:0030027; GO:0016020; GO:0090497; GO:0046872; GO:0050804; GO:0090090; GO:0014032; GO:0060563; GO:0097118; GO:0097150; GO:0043005; GO:0050998; GO:0005886; GO:0044853; GO:0043410; GO:2000809; GO:0014069; GO:0005515; GO:0032991; GO:0044877; GO:0019901; GO:0072659; GO:0019903; GO:0060019; GO:0050770; GO:0031641; GO:0070445; GO:1902897; GO:0032880; GO:0035023; GO:0009966; GO:0051966; GO:0042383; GO:0051146; GO:0045202; GO:0007416; GO:0021537; GO:0030315; GO:0003323
3100003 M19Rik	Chr18:16597564-16599554 (-)	unclassified non-coding RNA gene	No	--	--	--	--	--	--	None
9430011C 21Rik	Chr18:16692356-16694549 (-)	unclassified gene	No	--	--	--	--	--	--	None
Gm15485	Chr18:16728733-16729678 (+)	lncRNA gene	No	X	X	--	--	--	--	Expressed in mouse liver

Gm15328	Chr18:16816407-16822783 (+)	lncRNA gene	No	--	--	--	--	--	--	None – predicted gene
1700001G01Rik	Chr18:17035508-17137559 (+)	lncRNA gene	No	--	--	--	--	--	--	None
Gm22470	Chr18:17034662-17034791 (+)	snoRNA gene	No	--	--	--	--	--	--	None – predicted gene
Gm41674	Chr18:17050571-17058297 (+)	lncRNA gene	No	--	--	--	--	--	--	None – predicted gene
Gm24015	Chr18:17126571-17126802 (-)	unclassified non-coding RNA gene	No	--	--	--	--	--	--	None – predicted gene
Gm30960	Chr18:17254639-17257022 (-)	lncRNA gene	No	--	--	--	--	--	--	None – predicted gene
Gm31018	Chr18:17478967-17533929 (-)	lncRNA gene	No	--	--	--	--	--	--	None – predicted gene
4930545E07Rik	Chr18:17568746-17580990 (-)	lncRNA gene	No	--	--	--	--	--	--	None

[a] Resource abbreviations: **EBM,** Ensembl BioMart; **EEA,** EBI Expression Atlas; **GO,** Gene Ontology; **GXD,** Gene eXpression Database; **MGI,** Mouse Genome Informatics; **PW,** PheWeb

[b] ID terms: **GO:0005912:** adherens junction; **GO:0045294:** alpha-catenin binding; **GO:0045177:** apical part of cell; **GO:0016324:** apical plasma membrane; **GO:0016327:** apicolateral plasma membrane; **GO:0016323:** basolateral plasma membrane; **GO:0008013:** beta-catenin binding; **GO:0048514:** blood vessel morphogenesis; **GO:0007420:** brain development; **GO:0048854:** brain morphogenesis; **GO:0045296:** cadherin binding; **GO:0016339:** calcium-dependent cell-cell adhesion via plasma membrane cell adhesion molecules; **GO:0005509:** calcium ion binding; **GO:0016342:** catenin complex; **GO:0007155:** cell adhesion; **GO:0098609:** cell-cell adhesion; **GO:0044331:** cell-cell adhesion mediated by cadherin; **GO:0098742:** cell-cell adhesion via plasma-membrane adhesion molecules; **GO:0005911:** cell-cell junction; **GO:0007043:** cell-cell junction assembly; **GO:0030054:** cell junction; **GO:0016477:** cell migration; **GO:0009986:** cell surface; **GO:0021987:** cerebral cortex development; **GO:0030864:** cortical actin cytoskeleton; **GO:0005737:** cytoplasm; **GO:0019899:** enzyme binding; **GO:0005916:** fascia adherens; **GO:0045295:** gamma-catenin binding; **GO:0010001:** glial cell differentiation; **GO:0098978:** glutamatergic synapse; **GO:0007157:** heterophilic cell-cell adhesion via plasma membrane cell adhesion molecules; **GO:0048872:** homeostasis of number of cells; **GO:0007156:** homophilic cell adhesion via plasma membrane adhesion molecules; **GO:0042802:** identical protein binding; **GO:0016021:** integral component of membrane; **GO:0005887:** integral component of plasma membrane; **GO:0099060:** integral component of postsynaptic specialization membrane; **GO:0099059:** integral component of presynaptic active zone membrane; **GO:0014704:** intercalated disc; **GO:0030027:** lamellipodium; **GO:0016020:** membrane; **GO:0090497:** mesenchymal cell migration; **GO:0046872:** metal ion binding; **GO:0050804:** modulation of chemical synaptic transmission; **GO:0090090:** negative regulation of canonical Wnt signaling pathway; **GO:0014032:** neural crest cell

development; **GO:0060563:** neuroepithelial cell differentiation; **GO:0097118:** neuroligin clustering involved in postsynaptic membrane assembly; **GO:0097150:** neuronal stem cell population maintenance; **GO:0043005:** neuron projection; **GO:0050998:** nitric-oxide synthase binding; **GO:0005886:** plasma membrane; **GO:0044853:** plasma membrane raft; **GO:0043410:** positive regulation of MAPK cascade; **GO:2000809:** positive regulation of synaptic vesicle clustering; **GO:0014069:** postsynaptic density; **GO:0005515:** protein binding; **GO:0032991:** protein-containing complex; **GO:0044877:** protein-containing complex binding; **GO:0019901:** protein kinase binding; **GO:0072659:** protein localization to plasma membrane; **GO:0019903:** protein phosphatase binding; **GO:0060019:** radial glial cell differentiation; **GO:0050770:** regulation of axonogenesis; **GO:0031641:** regulation of myelination; **GO:0070445:** regulation of oligodendrocyte progenitor proliferation; **GO:1902897:** regulation of postsynaptic density protein 95 clustering; **GO:0032880:** regulation of protein localization; **GO:0035023:** regulation of Rho protein signal transduction; **GO:0009966:** regulation of signal transduction; **GO:0051966:** regulation of synaptic transmission, glutamatergic; **GO:0042383:** sarcolemma; **GO:0051146:** striated muscle cell differentiation; **GO:0045202:** synapse; **GO:0007416:** synapse assembly; **GO:0021537:** telencephalon development; **GO:0030315:** T-tubule; **GO:0003323:** type B pancreatic cell development

Supplementary Table S4.8. Results of high-resolution association mapping in outbred mice of serum aminotransferases and hepatic histological scores.
Significant QTL position and respective Bayesian credible interval included in parentheses in Mbp on mouse chromosomes. Peaks with LOD scores > 6 included within the table. ALT and AST expressed as U/L.

Phenotype	LOD	Chr	QTL Position (Mbp)	QTL Position (cM)	p value	Marker ID
AST	7.444	2	12.200 (10.653 – 13.057)	9.177 (8.072 – 9.718)	$p < 0.10$	UNC2587898
AST	7.808	16	57.518 (57.069 – 59.755)	34.263 (34.190 – 35.267)	$p < 0.05$	UNCHS042906
ALT	6.206	4	134.295 (132.970 – 135.609)	66.663 (66.128 – 67.844)	$p < 0.55$	UNC8266620
ALT	6.001	14	50.061 (48.897 – 55.655)	25.923 (25.401 – 28.103)	$p < 0.65$	UNC23989426
Hydropic Degeneration	6.371	6	36.106 (35.897 – 142.658)	15.428 (15.373 – 74.478)	$p < 0.50$	UNCHS016962
Steatosis	6.680	11	111.241 (111.010 – 111.280)	75.185 (74.681 – 75.230)	$p < 0.45$	UNC20387893
Steatosis	6.297	11	112.469 (112.417 – 112. 568)	76.030 (75.921 – 76.354)	$p < 0.45$	UNC20409887
Steatosis	8.775	18	17.065 (16.842 – 17.710)	10.357 (10.240 – 10.522)	$p < 0.05$	UNC28802837
Steatosis	6.540	18	59.619 (58.499 – 69.153)	34.167 (33.267 – 42.903)	$p < 0.50$	UNCHS045468
Steatosis	7.266	X	51.515 (47.372 – 51.838)	28.171 (24.945 – 28.295)	$p < 0.25$	UNCHS048616

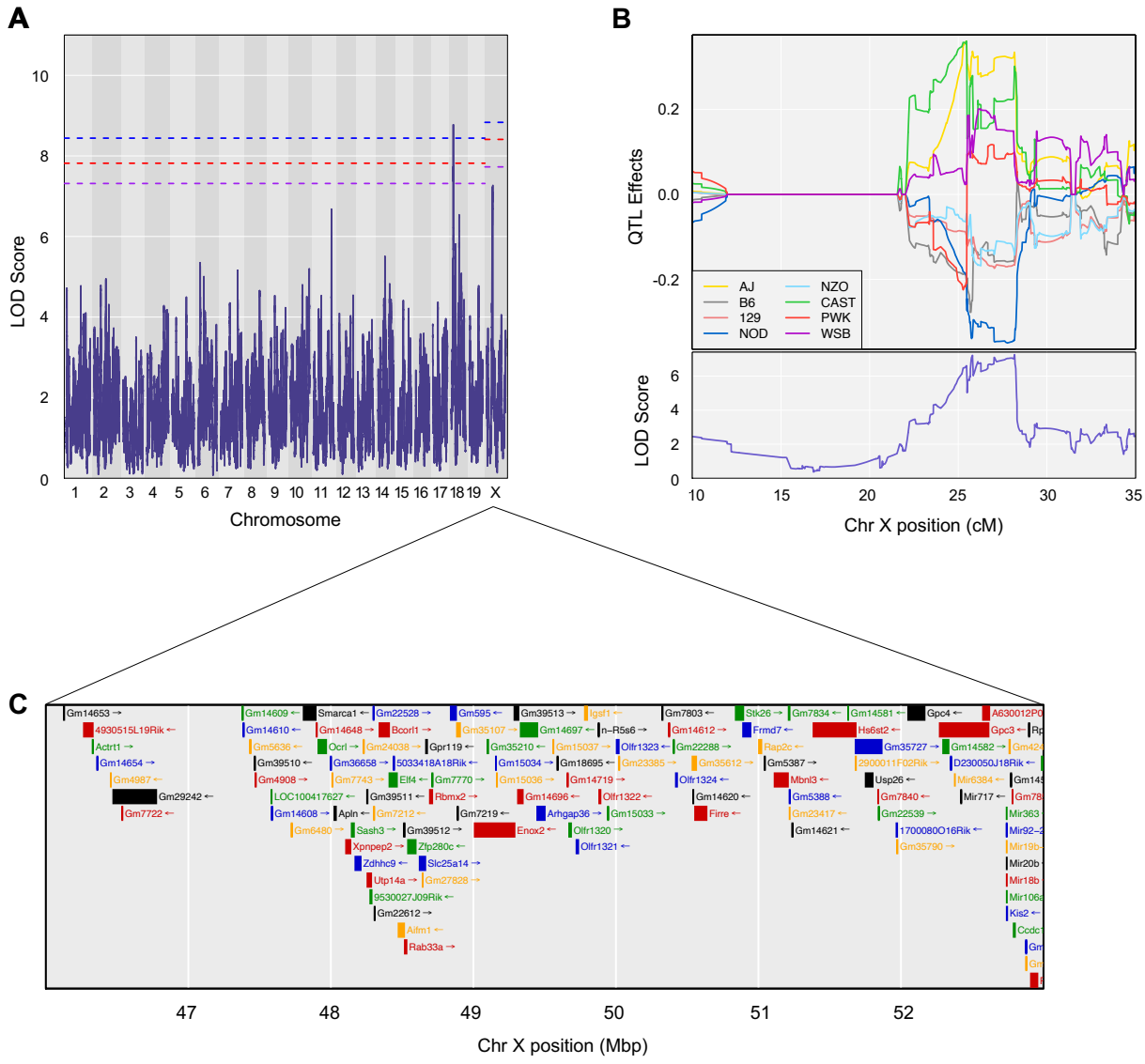

Supplementary Figure S4.1. High-resolution association mapping for hepatic steatosis in outbred mice reveals a suggestive QTL on mouse chromosome X.
A. Genome-wide scan of hepatic steatosis in outbred mice shows a QTL with peak LOD score 7.266 at 51.515 Mbp (28.171 cM) on mouse chromosome X. Permutation-derived significance thresholds are indicated by colored lines at significance (α) levels 0.05 (blue), 0.1 (red), and 0.2 (purple). Autosome LOD score thresholds were 7.32, 7.82, and 8.44 for p-values of 0.20, 0.10, and 0.05, respectively. X chromosome LOD score thresholds were 7.73, 8.41, and 8.43 for p-values of 0.20, 0.10, and 0.05, respectively. **B.** The founder allele QTL effects indicate that the NOD allele contributes to a lower hepatic steatosis grade, whereas the CAST and AJ alleles contribute to a higher hepatic steatosis grade. Each colored line represents a DO founder allele as indicated in the legend. The differences between strains are considered significant when the LOD score (bottom) crosses significance thresholds (panel A). **C.** Candidate genes found within the QTL interval relative to the MGI database.

CHAPTER 5

SYSTEMS GENETICS OF THE RENAL GLUTATHIONE REDOX SYSTEM[5]

[5] Gould RL, Craig SC, McClatchy S, Churchill G, Pazdro R. Systems genetics of the renal glutathione redox system. To be submitted to *Free Radical Biology & Medicine*.

Abstract

Glutathione is a critical cytoprotectant whose functions include actions as an antioxidant to support aerobic metabolism and neutralize reactive electrophiles. Proper maintenance of its reduced form, GSH, versus its oxidized form, GSSG, is thought to be essential in preventing oxidative stress and the onset of renal disease. Recent evidence has indicated that both GSH and GSSG are moderately determined by genetic background, and we recently used QTL mapping technologies to investigate the hepatic glutathione redox system which revealed novel loci responsible for hepatic glutathione variation. This follow-up study employed a similar framework to investigate the renal glutathione status of the same animals to identify if the two systems are under shared genetic control. Through high-resolution genetic mapping, we identified a suggestive QTL peak for renal GSH on mouse chromosome X at 51.602 Mbp. Using an integrative bioinformatics approach, we compiled expression, functional, and phenotypic data on the genetic region and identified *Aifm1* as the most plausible candidate gene influencing renal GSH levels. We observed that renal and hepatic glutathione vary to a similar degree with over a 10-fold variation in their GSH concentrations. Comparison of QTL results revealed that the two systems are under both individual and shared genetic control outside of canonical genes involved in GSH synthesis and recycling. These findings suggest that genes peripherally involved in regulating glutathione concentrations influence redox status and risk for oxidative stress at a tissue-specific level.

Introduction

Glutathione (GSH) is a key regulator of the cellular redox environment and serves as a critical antioxidant [646]. This crucial cytoprotectant is a tripeptide composed of glutamate, cysteine, and glycine, and is recycled to its oxidized form glutathione disulfide (GSSG) after neutralizing electrophiles and reactive oxygen species (ROS). Beyond its essential antioxidant activities, it functions in cell proliferation, detoxification of xenobiotics, and cysteine storage and transport [284]. To maintain a proper redox state, cells either increase cellular GSH concentrations *de novo* or through enzymatic reduction of GSSG via the enzymatic action of glutathione reductase (GR) with NADPH as the electron donor [174, 647, 648]. However, during times of oxidative stress, there is an imbalance of reactive oxygen species to available antioxidants [12] and consequently, the ratio of GSH to GSSG shifts, decreasing GSH/GSSG, negatively impacting cellular signaling [179], thiol disulfide exchange reactions [180], and cell proliferation [165]. The kidneys are dependent on adequate GSH concentrations to maintain function, support proper aerobic metabolism, and protect against exposure to reactive electrophiles [276]. Renal GSH status is supported by intracellular synthesis as well as external transport [276], including from hepatocytes which produce and export GSH [161, 649]. The kidneys are the primary consumer of circulating GSH, hydrolyzing it to its constituent amino acids and reabsorbing them for protein synthesis or resynthesis of GSH [650]. Kidneys have the highest turnover rate of glutathione [649, 651].

Proper renal glutathione homeostasis is essential to prevention of oxidative stress and progression of chronic disease, including chronic kidney disease (CKD) [225, 226, 652, 653]. Biomarkers of oxidative stress are elevated in the plasma at an early stage of CKD and increase with CKD stage progression [654]. Overproduction of ROS in renal tissue is a hallmark of CKD

[655]. As a result, oxidative stress machinery is a pharmacological target to prevent the onset of systemic comorbidities [655]. Unfortunately, oxidative stress increases with the use of traditional CKD therapies including dialysis. Recent evidence has emerged encouraging antioxidant therapy prior to renal replacement therapy to restore GSH concentrations [284]. Given the critical importance of renal glutathione to prevention of CKD and oxidative stress, researchers have investigated the role of polymorphisms in enzymes involved in glutathione homeostasis and have identified associations between genetic variants in glutathione peroxidases and glutathione S-transferases and CKD onset and progression [475, 496]. However, there is conflicting evidence on the clinical effects of these polymorphisms on renal health [656, 657]. Moreover, these polymorphisms address the impact of variants on global glutathione status, but do not address the causal agent for the disparities in renal glutathione documented across strains of inbred rodents [203, 526].

Recent evidence indicates that there is a large variation in glutathione phenotypes based on genetic background [203, 526]. A comprehensive strain panel composed of 30 inbred strains documented over a 3-fold difference in renal GSH/GSSG and identified novel candidate genes for renal glutathione homeostasis *in silico* [526]. Follow-up studies determined that this variation and heritability is maintained at old age, indicating that this genetic regulation is conserved across the lifespan [203]. These initial genetic analyses were the first to utilize genome mapping technologies to document the heritability and genetic regulation of renal glutathione, but the use of inbred strains in comprehensive genetic analyses is limited as they do not fully reflect the genetic diversity found in humans. To fully understand the genetic mechanisms responsible for renal glutathione variation, we employed an outbred model.

The Diversity Outbred (DO) mouse stock is a genetically diverse model that is phenotypically diverse and exhibit genetic diversity comparable to the average human genetic diversity [548]. This model allows for invasive tissue sampling and data from these samples can be used in high resolution genetic mapping. R/qtl2 is a powerful genome scan software that was specifically designed for quantitative trait loci (QTL) mapping of DO mice [548, 549]. In a previous genetic mapping study using the DO, we observed a large variation in hepatic glutathione levels and identified a novel locus on mouse chromosome 16 linked with hepatic redox status, indicating that R/qtl2 mapping can improve our understanding of the genetic influence on glutathione at a tissue-specific level [Chapter 3]. Given that renal glutathione is impacted by hepatic glutathione status [658, 659], we hypothesized that renal glutathione would also vary to the same degree as hepatic glutathione, and that two tissue systems would be regulated under shared genetic control. Despite published reports documenting novel genes and loci external to the traditional glutathione synthesis and recycling systems controlling renal glutathione homeostasis, no genetic mapping study has been conducted. A recent study has suggested that knowledge on biochemical redox systems can be gained through a forward-genetics approach [Chapter 3], and the present study employs those genetic mapping techniques to identify loci associated with the renal GSH redox system.

Materials and Methods

Animals and genotyping: The DO mice (N = 346, 171 males, 175 females) used for the study and their genotyping were previously described [Chapter 3]. Liver weight and body weight were obtained at sacrifice. The University of Georgia Institutional Animal Care and Use Committee (IACUC) approved all methods and procedures involving animals in accordance with the ethical standards of the institution (AUP #A2016 07-016).

Assessment of renal total glutathione, GSH, GSSG, and redox ratios: Samples of tissue were promptly harvested from each mouse after humane euthanasia and were rinsed with ice-cold PBS, blotted on a paper towel, and flash frozen in liquid nitrogen. Processing and quantification of renal total glutathione (GSH + 2GSSG), GSH, and GSSG, GSH/GSSG, and redox potential (E_h) were conducted as previously described [Chapter 3].

Clinical measurements and analysis: Fasting blood collection and serum isolation from all animals was described previously [Chapter 4]. Blood urea nitrogen (BUN) was quantified using the cobas 6000 c501 Analyzer (Roche Diagnostics, Indianapolis, IN USA) by the Clinical Pathology Department at the University of Georgia Veterinary Medical Center.

Quantitative trait loci (QTL) mapping: Genome scans were performed in the 346 DO samples using the R/qtl2 software [549] as previously described [Chapter 3]. Sex and experimental cohort were included in the genome scans as additive covariates. To ensure normality, each phenotype underwent rank *z*-score transformation, and kinship among the DO mice was accounted for using the "leave one chromosome out" (LOCO) method [549, 559]. 1000 permutation tests were run for each genome scan to determine autosomal significance thresholds [549, 560, 561]. For phenotypes with QTL peaks on the X chromosome, separate permutation tests (18090 total) were run for the X chromosome using the *perm_Xsp = TRUE* function. A suggestive threshold ($p \leq 0.20$) was applied for reporting loci [561], and a 95% Bayesian credible interval was determined for each peak around the reported QTL position [549, 560]. Genes within intervals were plotted in connection with the Mouse Genome Informatics (MGI) database. All genotype data and genotype probabilities are publicly available through figshare (https://doi.org/10.6084/m9.figshare.c.5360501.v1). All source code, phenotype data, and other

files used in QTL analyses are available through a public GitHub repository (https://doi.org/10.5281/zenodo.4683884).

Candidate gene analysis: Databases for expression, phenotypic, and functional annotations were queried using methods for candidate gene prioritization previously described [Chapter 3].

Statistical Analysis: RStudio version 1.3.1093 (RStudio, PBC., Boston, MA) and R version 4.0.2 (R Foundation for Statistical Computing, Vienna, Austria) were used to identify relationships between variables. We calculated Rank-based Spearman's rho (ρ) to report correlations between values. A relationship between variables with *p*-values less than 0.05 was considered statistically significant.

Results

Renal GSH redox system varies significantly among outbred mice: We quantified concentrations of the renal GSH redox system and serum BUN in a large cohort of outbred mice and observed wide variation in all phenotypes (Table 5.1; Figure 5.1). Renal total glutathione concentrations varied nearly 10-fold variation (5.069 to 49.074 nmol/mg), and similarly, renal GSH concentrations varied 10-fold (4.744 to 47.712 nmol/mg). Renal GSSG concentrations varied 18-fold, ranging from 0.088 to 1.612 nmol/mg, and renal GSH/GSSG levels, a 26-fold (6.855 to 177.900). Renal E_h levels ranged from -202.380 to -145.203 mV, a 1.4-fold difference. Serum BUN ranged from 14 to 48 mg/dL, over a 3-fold difference. There were no sex specific effects observed for any phenotype with the exception of renal GSSG (Supplementary Tables S5.1 and S5.2).

Table 5.1. Descriptive statistics for the renal GSH system phenotypes and serum BUN in DO mice.

Phenotype:	N	x̄	Median	SD	Min	Max
Total Glutathione (nmol/mg)	345	18.380	17.591	7.604	5.069	49.074
GSH (nmol/mg)	345	17.641	17.061	7.364	4.744	47.712
GSSG (nmol/mg)	345	0.370	0.300	0.256	0.088	1.612
GSH/GSSG	345	59.077	52.007	31.424	6.855	177.900
E_h (mV)	345	-177.845	-179.733	10.944	-202.380	-145.203
BUN (mg/dL)	338	24	23	5	14	48

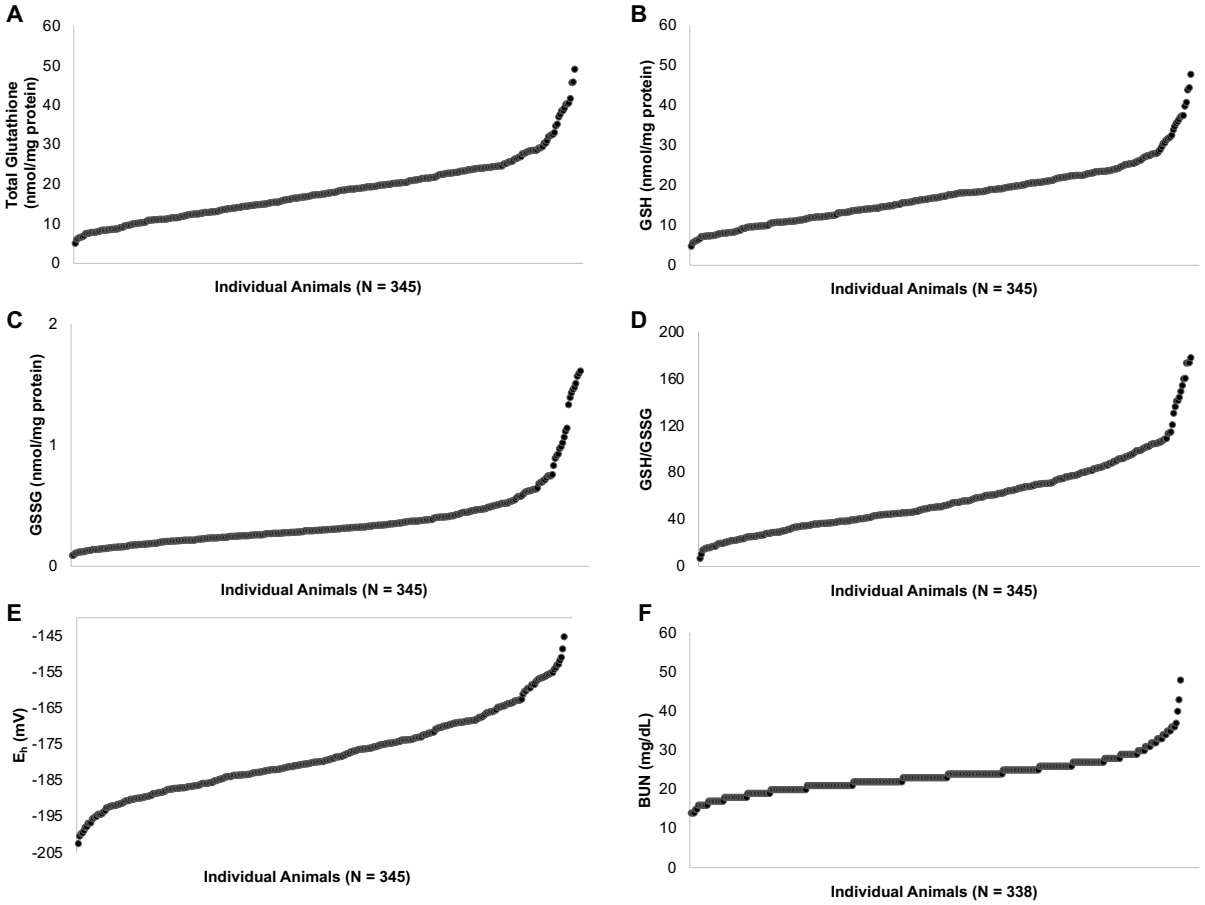

Figure 5.1. Variation in renal glutathione concentrations and serum BUN in the DO population. Renal concentrations of **A.** Total Glutathione (GSH + 2GSSG, expressed in nmol/mg); **B.** GSH (nmol/mg); **C.** GSSG (nmol/mg); **D.** GSH/GSSG; **E.** Redox Potential of the GSSG-GSH couple, indicated as E_h (mV); and **F.** BUN (mg/dL) were measured in a population of DO mice. Values are arranged from smallest to largest, and the N for each measurement is provided underneath each panel.

We evaluated the associations between renal GSH redox system phenotypes and observed that all renal glutathione phenotypes were moderately to strongly correlated with one another (Table 5.2). In addition, a large variation of phenotypes in the hepatic GSH and NADPH redox systems has previously been documented [Chapter 3] and we observed multiple significant correlations between the renal and hepatic GSH redox systems (Table 5.3). Renal total glutathione concentrations were correlated with hepatic total glutathione ($\rho = 0.193$, $p = <0.001$), hepatic GSH concentrations ($\rho = 0.193$, $p = <0.001$), hepatic GSSG concentrations ($\rho = 0.154$, $p = 0.004$), and hepatic E_h levels ($\rho = -0.145$, $p = 0.007$), but not hepatic GSH/GSSG ($p = 0.786$). Renal GSH concentrations were correlated with hepatic total glutathione concentrations ($\rho = 0.199$, $p = <0.001$), hepatic GSH concentrations ($\rho = 0.199$, $p = <0.001$), hepatic GSSG concentrations ($\rho = 0.157$, $p = 0.003$), and hepatic E_h levels ($\rho = -0.154$, $p = 0.004$), but not hepatic GSH/GSSG levels ($p = 0.681$). Renal GSSG concentrations were correlated with hepatic GSH/GSSG ($\rho = -0.126$, $p = 0.020$), but not hepatic total glutathione concentrations ($p = 0.300$), hepatic GSH concentrations ($p = 0.277$), hepatic GSSG concentrations ($p = 0.791$), and hepatic E_h levels ($p = 0.053$). Renal GSH/GSSG levels were correlated with hepatic total glutathione concentrations ($\rho = 0.216$, $p = <0.001$), hepatic GSH concentrations ($\rho = 0.219$, $p = <0.001$), hepatic GSSG concentrations ($\rho = 0.112$, $p = 0.037$), hepatic GSH/GSSG levels ($\rho = 0.150$, $p = 0.005$), and hepatic E_h levels ($\rho = -0.226$, $p = <0.001$). Renal E_h levels were correlated with hepatic total glutathione concentrations ($\rho = -0.244$, $p = <0.001$), hepatic GSH concentrations ($\rho = -0.246$, $p = <0.001$), hepatic GSSG concentrations ($\rho = -0.147$, $p = 0.006$), hepatic GSH/GSSG levels ($\rho = -0.124$, $p = 0.021$), and hepatic E_h levels ($\rho = 0.238$, $p = <0.001$). We also screened for associations between the renal GSH redox system and the hepatic NADPH redox system (Table 5.3). Renal total glutathione concentrations were correlated with hepatic NADPH concentrations ($\rho = 0.176$, $p = 0.001$), hepatic

$NADP^+$ concentrations (ρ = -0.260, p = <0.001), hepatic $NADP^+$/NADPH levels (ρ = -0.205, p = <0.001), but not hepatic NADH concentrations (p = 0.447). Renal GSH concentrations were correlated with hepatic NADPH concentrations (ρ = 0.187, p = 0.001), hepatic $NADP^+$ concentrations (ρ = -0.267, p = <0.001), hepatic $NADP^+$/NADPH levels (ρ = -0.217, p = <0.001), but not hepatic NADH concentrations (p = 0.385). Renal GSSG concentrations were correlated with hepatic NADPH concentrations (ρ = -0.113, p = 0.039), hepatic $NADP^+$/NADPH levels (ρ = 0.115, p = 0.041), hepatic NADH concentrations (ρ = -0.114, p = 0.038), but not $NADP^+$ concentrations (p = 0.432). Renal GSH/GSSG levels were correlated with hepatic NADPH concentrations (ρ = 0.256, p = <0.001), hepatic $NADP^+$ concentrations (ρ = -0.258, p = <0.001), hepatic $NADP^+$/NADPH levels (ρ = -0.293 p = <0.001), and hepatic NADH concentrations (ρ = -0.151, p = 0.006). Renal E_h levels were correlated with hepatic NADPH concentrations (ρ = -0.272, p = <0.001), hepatic $NADP^+$ (ρ = 0.311, p = <0.001), hepatic $NADP^+$/NADPH (ρ = 0.313, p = <0.001), and hepatic NADH (ρ = -0.136, p = 0.013).

Table 5.2. Statistical relationships among markers of the renal GSH redox system.
Spearman's rho (ρ) was calculated for each variable combination. Total glutathione, GSH, and GSSG concentrations were standardized as nmol/mg protein. E_h was expressed as mV. *indicates a significant relationship ($p \leq 0.05$).

Variables	**ρ**	**p-value**
Renal Total Glutathione, Renal GSH	0.998*	<0.001
Renal Total Glutathione, Renal GSSG	0.394*	<0.001
Renal Total Glutathione, Renal GSH/GSSG	0.360*	<0.001
Renal Total Glutathione, Renal E_h	-0.743*	<0.001
Renal GSH, Renal GSSG	0.352*	<0.001
Renal GSH, Renal GSH/GSSG	0.401*	<0.001
Renal GSH, Renal E_h	-0.773*	<0.001
Renal GSSG, Renal GSH/GSSG	-0.661*	<0.001
Renal GSSG, Renal E_h	0.263*	<0.001
Renal GSH/GSSG, Renal E_h	-0.879*	<0.001

Table 5.3. Statistical relationships among markers of the hepatic GSH, NADPH, and renal GSH redox systems.

Spearman's rho (ρ) was calculated for each variable combination. Hepatic and renal total glutathione, GSH, and GSSG concentrations were standardized as nmol/mg protein, and E_h was expressed as mV. NADPH, NADH, and $NADP^+$ were standardized as pmol/μg protein. *indicates a significant relationship ($p \leq 0.05$).

Variables	**ρ**	**p-value**
Renal Total Glutathione, Hepatic Total Glutathione	0.193*	<0.001
Renal Total Glutathione, Hepatic GSH	0.193*	<0.001
Renal Total Glutathione, Hepatic GSSG	0.154*	0.004
Renal Total Glutathione, Hepatic GSH/GSSG	0.015	0.786
Renal Total Glutathione, Hepatic E_h	-0.145*	0.007
Renal Total Glutathione, Hepatic NADPH	0.176*	0.001
Renal Total Glutathione, Hepatic $NADP^+$	-0.260*	<0.001
Renal Total Glutathione, Hepatic $NADP^+$/NADPH	-0.205*	<0.001
Renal Total Glutathione, Hepatic NADH	0.039	0.477
Renal GSH, Hepatic Total Glutathione	0.199*	<0.001
Renal GSH, Hepatic GSH	0.199*	<0.001
Renal GSH, Hepatic GSSG	0.157*	0.003
Renal GSH, Hepatic GSH/GSSG	0.022	0.681
Renal GSH, Hepatic E_h	-0.154*	0.004
Renal GSH, Hepatic NADPH	0.187*	0.001
Renal GSH, Hepatic $NADP^+$	-0.267*	<0.001
Renal GSH, Hepatic $NADP^+$/NADPH	-0.217*	<0.001
Renal GSH, Hepatic NADH	0.048	0.385
Renal GSSG, Hepatic Total Glutathione	-0.056	0.300
Renal GSSG, Hepatic GSH	-0.059	0.277
Renal GSSG, Hepatic GSSG	0.014	0.791
Renal GSSG, Hepatic GSH/GSSG	-0.126*	0.020
Renal GSSG, Hepatic E_h	0.105	0.053
Renal GSSG, Hepatic NADPH	-0.113*	0.039
Renal GSSG, Hepatic $NADP^+$	0.043	0.432
Renal GSSG, Hepatic $NADP^+$/NADPH	0.115*	0.041
Renal GSSG, Hepatic NADH	-0.114*	0.038
Renal GSH/GSSG, Hepatic Total Glutathione	0.216*	<0.001
Renal GSH/GSSG, Hepatic GSH	0.219*	<0.001
Renal GSH/GSSG, Hepatic GSSG	0.112*	0.037
Renal GSH/GSSG, Hepatic GSH/GSSG	0.150*	0.005
Renal GSH/GSSG, Hepatic E_h	-0.226*	<0.001
Renal GSH/GSSG, Hepatic NADPH	0.256*	<0.001
Renal GSH/GSSG, Hepatic $NADP^+$	-0.258*	<0.001
Renal GSH/GSSG, Hepatic $NADP^+$/NADPH	-0.293*	<0.001
Renal GSH/GSSG, Hepatic NADH	0.151*	0.006
Renal E_h, Hepatic Total Glutathione	-0.244*	<0.001
Renal E_h, Hepatic GSH	-0.246*	<0.001

Renal E_h, Hepatic GSSG	-0.147*	0.006
Renal E_h, Hepatic GSH/GSSG	-0.124*	0.021
Renal E_h, Hepatic E_h	0.238*	<0.001
Renal E_h, Hepatic NADPH	-0.272*	<0.001
Renal E_h, Hepatic $NADP^+$	0.311*	<0.001
Renal E_h, Hepatic $NADP^+$/NADPH	0.313*	<0.001
Renal E_h, Hepatic NADH	-0.136*	0.013

Similarly, we assessed associations with serum BUN (mg/dL) (Table 5.4). BUN concentrations were correlated with hepatic total glutathione concentrations ($\rho = 0.131$, $p = 0.016$), hepatic GSH concentrations ($\rho = 0.134$, $p = 0.014$), and hepatic E_h levels ($\rho = -0.123$, $p = 0.024$), but not hepatic GSSG concentrations ($p = 0.073$) or hepatic GSH/GSSG levels ($p = 0.501$). Additionally, BUN concentrations were correlated with NADH concentrations ($\rho = 0.152$, $p = 0.006$). We did not observe any significant correlations between BUN concentrations and renal total glutathione concentrations ($p = 0.220$), renal GSH concentrations ($p = 0.193$), renal GSSG concentrations ($p = 0.951$), renal GSH/GSSG levels ($p = 0.278$), renal E_h levels ($p = 0.148$), nor with hepatic NADPH concentrations ($p = 0.602$), $NADP^+$ concentrations ($p = 0.335$), or $NADP^+$/NADPH levels ($p = 0.489$). Lastly, we calculated Spearman's ρ for body weight (g) and liver weight (g) and the renal GSH redox system phenotypes (Supplementary Table S5.3). Body weight levels was negatively correlated with renal total glutathione, GSH, and GSSG concentrations ($\rho = -0.170$, $p = 0.002$, $\rho = -0.159$, $p = 0.003$; $\rho = -0.199$, $p = <0.001$, respectively). Liver weight levels were negatively correlated with renal total glutathione, renal GSH, GSSG concentrations ($\rho = -0.145$, $p = 0.007$; $\rho = -0.135$, $p = 0.012$; $\rho = -0.234$, $p = <0.001$, respectively), and positively correlated with renal GSH/GSSG levels ($\rho = 0.146$, $p = 0.006$).

Table 5.4. Statistical relationships with serum BUN (mg/dL).
Spearman's rho (ρ) was calculated for each variable combination. Hepatic and renal total glutathione, GSH, and GSSG concentrations were standardized as nmol/mg protein, and E_h was expressed as mV. NADPH, NADH, and $NADP^+$ were standardized as pmol/μg protein. *indicates a significant relationship ($p \leq 0.05$).

Variables	**ρ**	**p-value**
BUN, Renal Total Glutathione	0.067	0.220
BUN, Renal GSH	0.071	0.193
BUN, Renal GSSG	0.003	0.951
BUN, Renal GSH/GSSG	0.059	0.278
BUN, Renal E_h	-0.079	0.148
BUN, Hepatic Total Glutathione	0.131*	0.016
BUN, Hepatic GSH	0.134*	0.014
BUN, Hepatic GSSG	0.098	0.073
BUN, Hepatic GSH/GSSG	0.037	0.501
BUN, Hepatic E_h	-0.123*	0.024
BUN, Hepatic NADPH	0.029	0.602
BUN, Hepatic $NADP^+$	-0.054	0.335
BUN, Hepatic $NADP^+$/NADPH	-0.039	0.489
BUN, Hepatic NADH	0.152*	0.006

QTL mapping of the renal GSH redox system and serum BUN: We performed genome-wide analysis using R/qtl2 on all renal GSH redox system phenotypes (Figure 5.2). We initially ran 1000 permutation tests in each QTL scan to identify LOD score thresholds to assess significance for autosomes. For those with QTL peaks on mouse chromosome X, we ran separate permutation tests (18090 total) using the *perm_Xsp* function to identify X chromosome-specific significance thresholds. Peaks that surpassed significance thresholds were investigated using bioinformatic resources. Genome-wide scans for renal concentrations of total glutathione and GSH revealed a peak that surpassed LOD score of 6 but failed to surpass significance thresholds on mouse chromosome 11 (LOD scores 6.428 and 6.664, respectively). Candidate gene results for these peaks are included in Supplementary Table S5.4 and Supplementary Figures S5.1 and S5.2. Additionally, both renal total glutathione and GSH had suggestive QTL peaks ($p \leq 0.10$) on mouse chromosome X (LOD scores 7.105 and 6.962, respectively). Given that the peak position and QTL

intervals were the same between the two scans, genome scan results for renal GSH are included in Figure 5.3, and total glutathione results are found in Supplementary Figure S5.3.

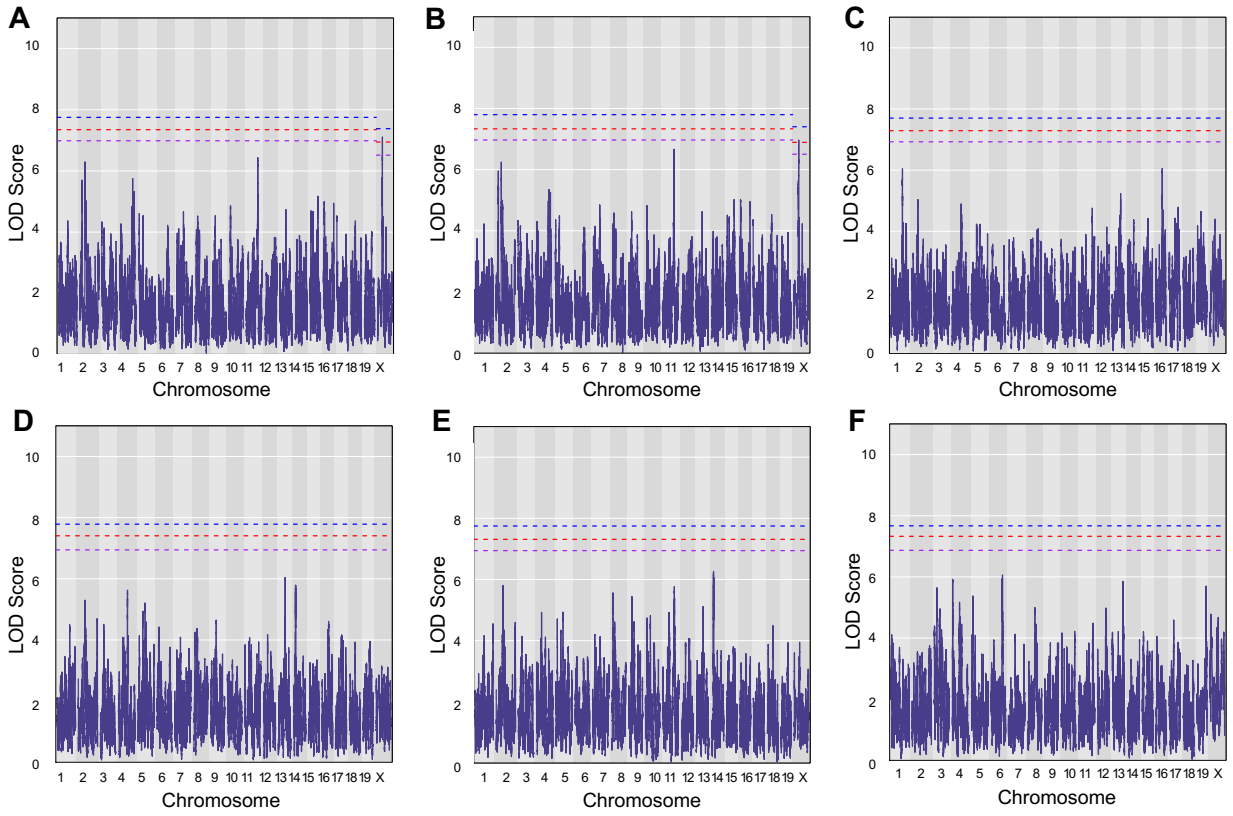

Figure 5.2. QTL results for markers of the renal GSH redox system and serum BUN. Genome-wide scans of renal **A.** Total Glutathione (GSH + 2GSSG, expressed in nmol/mg); **B.** GSH (nmol/mg); **C.** GSSG (nmol/mg); **D.** GSH/GSSG; **E.** Redox Potential of the GSSG-GSH couple (E_h, expressed as mV); and **F.** BUN (mg/dL). Permutation-derived significance thresholds are indicated by colored lines at significance (α) levels 0.05 (blue), 0.1 (red), and 0.2 (purple).

The genome-wide scan for renal GSH revealed a suggestive peak ($p \leq 0.10$) on mouse chromosome X at 51.602 Mbp with a QTL interval of 49.234 – 51.892 Mbp (Figure 5.3A). Founder allele effects revealed that the NOD, NZO, and 129 alleles contribute to a lower renal total glutathione and GSH, whereas the AJ and PWK alleles contribute to a higher renal total glutathione and GSH concentration (Figure 5.3B). Genes found within this interval ± 1 Mbp were plotted using R/qtl2 through connection with the MGI database (Figure 5.3C), and functional RNA

and protein coding genes were collected and screened for physiological relevance using existing expression, functional, and phenotypic annotations as previously described [Chapter 3]. The QTL interval contained 63 possible candidate genes: 29 protein-coding, 32 non-coding RNA, and 2 unclassified (Supplementary Table S5.5; GRCm38/mm10; gene query performed February 2021, Feature Type "gene" [563]). 36 of the 63 candidate genes had limited renal expression annotations and were excluded. Out of the remaining 27 candidate genes, 2 did not have additional functional annotations and were excluded. Out of the remaining 25 candidate genes, 4 genes had additional phenotypic annotations related to renal and/or redox function: apoptosis-inducing factor, mitochondrion-associated 1 (*Aifm1*), immunoglobulin superfamily, member 1 (*Igsf1*), glypican 3 (*Gpc3*), and coiled-coil domain containing protein 160 (*Ccdc160*).

Aifm1 (ChrX: 48474944–48513563 bp; 25.68 cM; GRCmm38) functions as a NADH oxidoreductase and regulator of apoptosis [660]. A query in Ensembl BioMart revealed that *Aifm1* is associated with increased catalase activity (MP:0011593), increased cellular sensitivity to hydrogen peroxide (MP:0008406), increased superoxide dismutase level (MP:0012660), and oxidative stress (MP:0003674) in mice. In humans, *AIFM1* was linked with combined oxidative phosphorylation deficiency 6 (300816) [571]. Igsf1 is a transmembrane glycoprotein whose function is largely unknown. It is expressed by thyrotropin (TSH)-producing cells in the pituitary gland and can cause central hypothyroidism [661]. We noted phenotypic annotations of *Igsf1* related to chronic kidney disease, Stage I or II ($p = 8.6e-7$) and pyelonephritis ($p = 4.1e-6$) in humans [570]. However, the large majority of Igsf1 expression and action is in the pituitary gland, and it is unlikely that *Igsf1* is responsible for glutathione metabolism variation in the s. *Gpc3* is part of the glypican family which are heparan sulfate proteoglycans linked to the cell surface through a glycosyl–phosphatidylinositol anchor [662]. *GPC3* was linked with Wilms Tumor

(194070), nephroblastoma (654), and Simpson–Golabi–Behmel (SGB) syndrome (373, 312870) in humans [571]. SGB overgrowth syndrome causes as wide variety of congenital defects, including renal dysplasia and nephromegaly [663]. *Gpc3*-deficient mice serve as a model of human renal dysplasia and GPC3 has been linked with modulating the actions of stimulatory and inhibitory growth factors during branching morphogenesis in renal tissue [664]. There is limited research on the action of GPC3 in the kidneys, though it has been shown to reduce cell proliferation in renal carcinoma cells [665]. We were unable to find literature documenting associations between *Gpc3* or *Igsf1* expression and oxidative stress. Lastly, *Ccdc160* was linked with nephritis and nephropathy without mention of glomerulonephritis ($p = 3.8e\text{-}5$) [570]. Limited biological annotations were available on *Ccdc160* as complete function remains unknown.

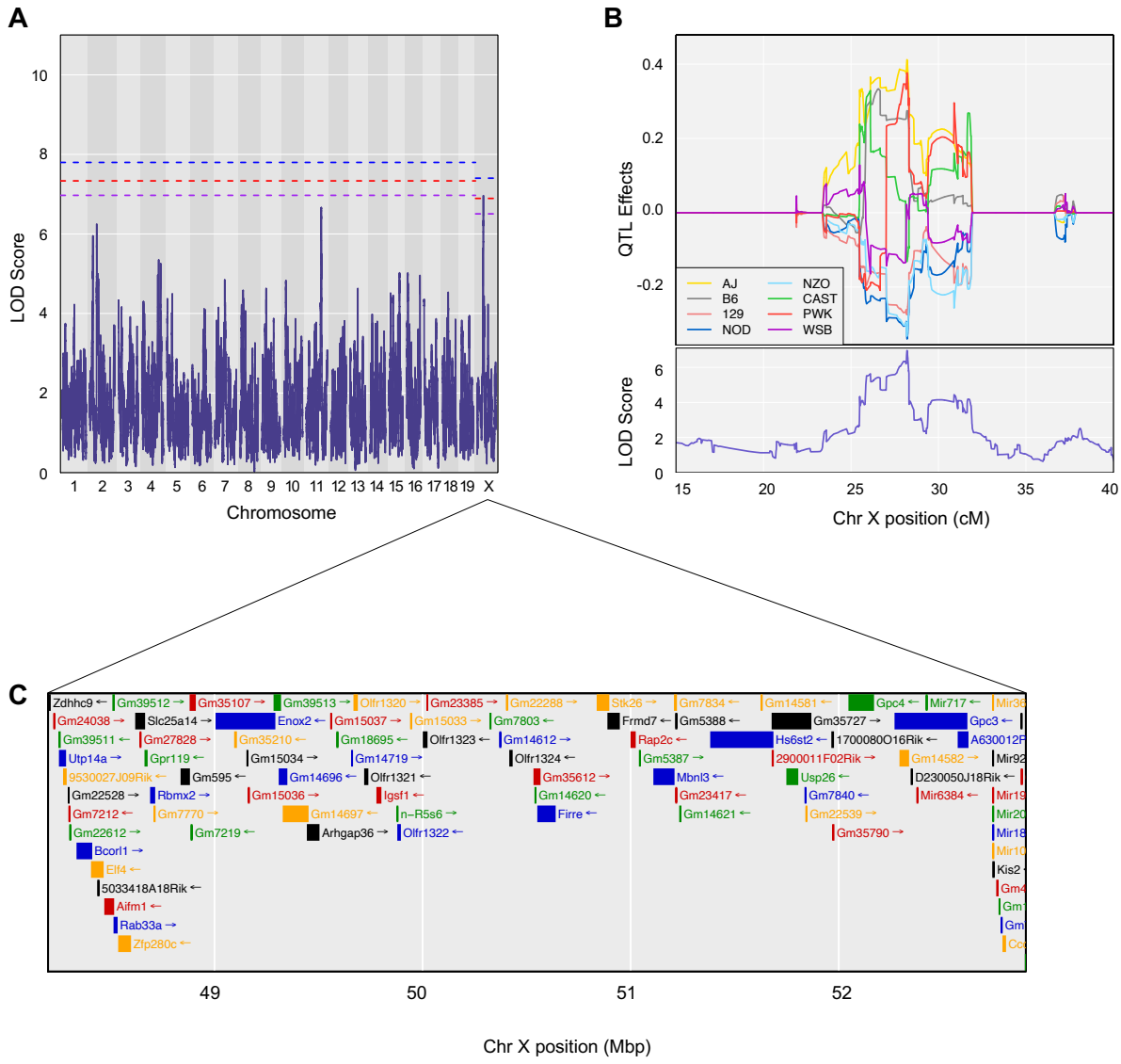

Figure 5.3. High-resolution association mapping for renal GSH in outbred mice reveals a suggestive QTL on mouse chromosome X.
A. Genome-wide scan of renal GSH (nmol/mg) in outbred mice shows a QTL with peak LOD score 6.962 at 51.602 Mbp (28.205 cM) on mouse chromosome X. Permutation-derived significance thresholds are indicated by colored lines at significance (α) levels 0.05 (blue), 0.1 (red), and 0.2 (purple). Autosome LOD score thresholds were 6.97, 7.33, and 7.80 for p-values of 0.20, 0.10, and 0.05, respectively. X chromosome LOD score thresholds were 6.50, 6.89, and 7.40 for p-values of 0.20, 0.10, and 0.05, respectively. **B.** The founder allele QTL effects indicate that the NOD, NZO, and 129 alleles contribute to a lower renal GSH (nmol/mg) concentration, whereas the AJ and PWK alleles contribute to a higher renal GSH (nmol/mg) concentration. Each colored line represents a DO founder allele as indicated in the legend. The differences between strains are considered significant when the LOD score (bottom) crosses significance thresholds (panel A). **C.** Candidate genes found within the QTL interval relative to the MGI database. The renal total glutathione genome scan resulted in the same suggestive QTL interval on mouse chromosome X compared to renal GSH (Supplementary Figure S5.3).

Discussion

Glutathione is a critical cytoprotectant in the kidneys. Adequate GSH is vital to maintain renal function and prevent the onset of oxidative stress and disease. Variation in renal glutathione has previously been documented in rodent strain panels, but inbred strains lack the degree of genetic diversity found in humans. To better understand the degree to which renal glutathione varies in genetically diverse individuals, we quantified markers of the renal GSH redox system in a large cohort of genetically diverse mice and performed QTL mapping to identify their genetic regulation.

We observed a 10-fold and 18-fold variation in renal GSH and GSSG, respectively, and nearly a 26-fold difference in renal GSH/GSSG. We previously documented a similar range of variation in hepatic glutathione phenotypes – over an 11-fold variation in hepatic total glutathione (nmol/mg) and GSH (nmol/mg) and a 16-fold variation in hepatic GSSG (nmol/mg) [Chapter 3]. To better understand the relationship between hepatic and renal GSH redox statuses, we compared the two systems (Figure 5.4) and observed similar trends compared to those previously published [526]. To better understand the statistical relationships between the two systems, we calculated Spearman ρ between variables. All renal glutathione phenotypes were moderately to strongly correlated with one another, and we observed multiple significant correlations between hepatic and renal glutathione. Notably, hepatic total glutathione, GSH, GSSG, and E_h were mildly correlated with renal total glutathione, GSH, GSH/GSSG, and E_h. Furthermore, hepatic GSH/GSSG was mildly correlated with renal GSSG, GSH/GSSG, and renal E_h. To identify whether these relationships extended to the related hepatic NAD redox system, we calculated Spearman ρ between renal glutathione phenotypes and hepatic NADPH (pmol/µg), $NADP^+$ (pmol/µg), $NADP^+$/NADPH, and NADH (pmol/µg). We observed several significant

relationships, including that hepatic NADPH and $NADP^+$/NADPH were correlated with all renal GSH redox system phenotypes. Hepatic $NADP^+$ concentrations were correlated with renal GSH, total glutathione, GSH/GSSG, and E_h concentrations, and hepatic NADH to renal GSSG, GSH/GSSG, and E_h. In total, these results point to the relatedness between the hepatic and renal redox systems and reflect the natural variation of the GSH redox systems in a genetically diverse population comparable to the human condition.

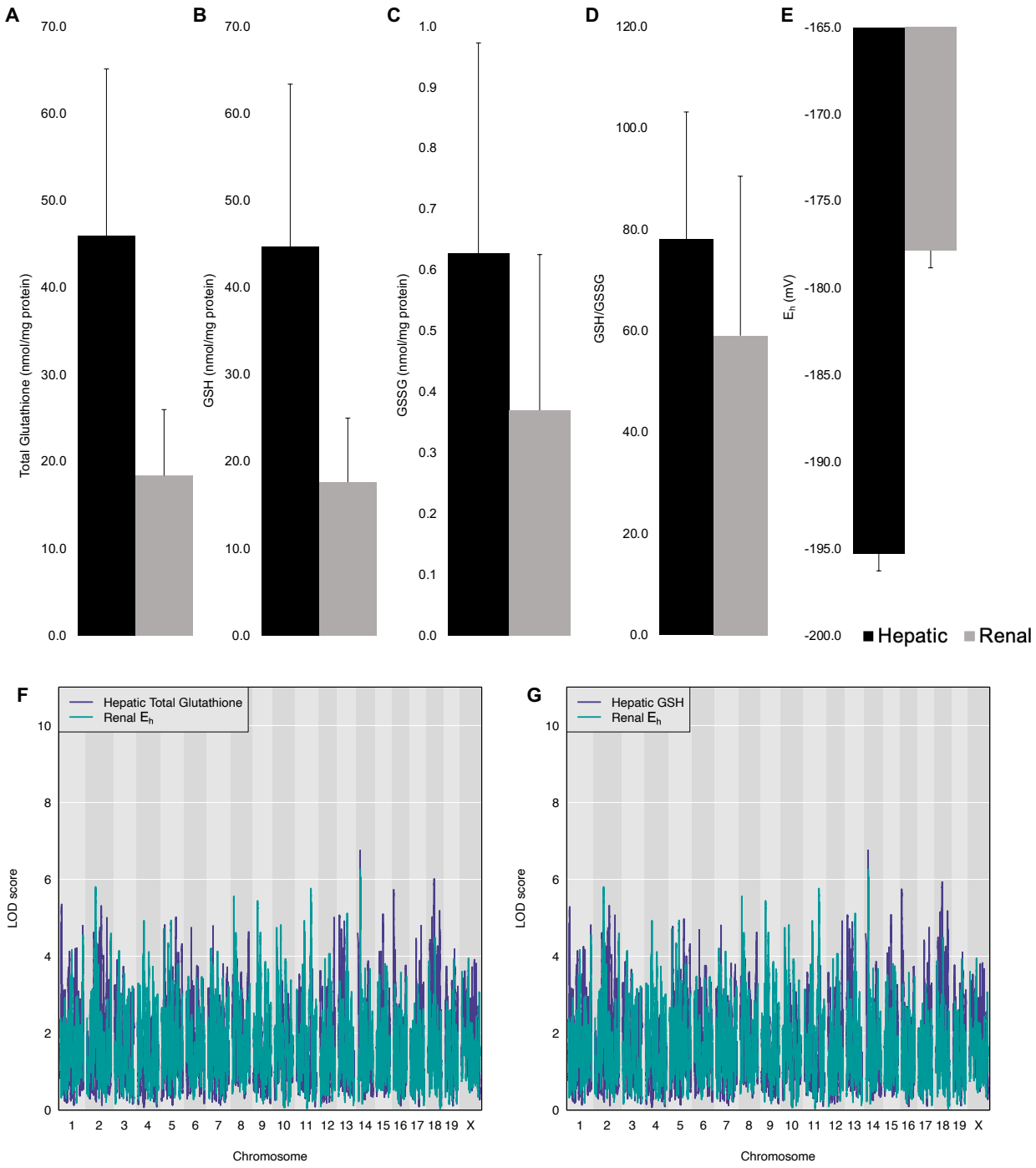

Figure 5.4. Comparison of renal and hepatic GSH redox systems.
A. Total Glutathione (GSH + 2 GSSG; expressed nmol/mg); **B.** GSH (nmol/mg); **C.** GSSG (nmol/mg); **D.** GSH/GSSG; and **E.** E_h (mV). Average ($\bar{x}$) ± SD for all outbred animals by tissue type. Overlapped QTL plots of **F.** Hepatic total glutathione and renal E_h; and **G.** Hepatic GSH and renal E_h.

To identify the genetic mechanisms responsible for this variation in renal GSH redox status, we utilized QTL mapping technology through R/qtl2. We identified a suggestive QTL peak for renal GSH and total glutathione on mouse chromosome X at 51.602 (49.234 – 51.892) Mbp. Renal total glutathione (GSH + 2GSSG) is largely derived from GSH concentrations, so it is not surprising that the two phenotypes had overlapping QTL peaks. A database query involving expression, functional, and phenotypic annotations was conducted and identified 4 protein coding candidate genes – *Aifm1, Igsf1, Gpc3,* and *Ccdc160*. Kidney-specific phenotypic annotations were documented for *Igsf1, Gpc3,* and *Ccdc160*, but functional annotations were unrelated to cellular redox function and are unlikely to be the candidate genes causing variation in renal glutathione status. We propose that *Aifm1* is the likely candidate gene responsible for variation in renal GSH and total glutathione concentrations given its function in regulating oxidative stress. Aifm1 is a flavoprotein that functions as a NADH oxidoreductase and regulator of apoptosis independent of the caspase pathway [660, 666] while also playing roles in electron transport, ROS generation, ferredoxin metabolism, and immune system regulation [667]. AIFM1 is normally confined to the mitochondrial intermembrane space where it acts as an electron acceptor/donor with oxidoreductase activity [668]. After an apoptotic insult, the mitochondrial outer membrane is permeabilized, and AIFM1 translocates to the cytosol and then nucleus to induce peripheral chromatin condensation and DNA fragmentation [669, 670]. Additionally, cytochrome *c* is released from the mitochondrial membrane as the membrane is permeabilized to initiate caspase-dependent apoptosis [671]. Loss of AIFM1 and cytochrome *c* increases oxidative stress and ROS generation by disrupting the mitochondrial respiratory chain and membrane potential [668]. In addition, increased levels of ROS can alter the conformation of NRF2–KEAP1–PGAM5 complex and cause its dissociation [672]. The separated PGAM5 binds to AIFM1 to catalyze its

dephosphorylation, and dephosphorylated AIFM1 then activates caspase-independent cell death and blocks inflammation [672]. Separated NRF2 can then upregulate expression of cytoprotective genes, including those involved in glutathione metabolism, to sequester ROS [672, 673]. *In vivo,* Aifm1 deficiency is associated with increased catalase activity (MP:0011593), increased cellular sensitivity to hydrogen peroxide (MP:0008406), increased superoxide dismutase level (MP:0012660), and increased sensitivity to oxidative stress (MP:0003674) in mice. Furthermore, it has been linked with combined oxidative phosphorylation deficiency 6 (300816) in humans [571] via complex I activity and assembly loss [674, 675]. Recent evidence has emerged indicating that Aifm1 is relevant to rodent and human renal pathologies. A partial knockdown of *Aifm1* in mice resulted in chronic disease (CKD) features with excess mitochondrial ROS production and *Nox4* upregulation, yet these mice retained their complex 1 activity [676]. In addition, patients with diabetic nephropathy had decreased *AIFM1* expression and protein concentrations in proportion to diminishing renal function [676], and a decrease in *AIFM1* expression may impair mitochondrial respiration, resulting in ROS generation and CKD progression [677]. Given this evidence, we propose that *Aifm1* expression could be influencing renal GSH and total glutathione through its regulation of the cellular redox environment and impact on ROS generation. The next step of this research is validating the effect of this candidate gene on glutathione status and oxidative stress in renal tissue.

The present study was designed to use precise genetic analysis techniques to identify overlapping loci, if any, between hepatic and renal glutathione phenotypes. We previously conducted genome association mapping for hepatic glutathione phenotypes from these animals and identified a novel locus responsible for variation in hepatic GSH/GSSG redox balance, indicating that there is knowledge to be gained through the use of QTL mapping technologies with

glutathione phenotypes [Chapter 3]. Renal glutathione is largely impacted by hepatic glutathione through interorgan metabolism of GSH [658, 659], and thus, we hypothesized that the two would be under shared genetic control. We compared all QTL results of renal glutathione phenotypes with LOD scores greater than 6 (Supplementary Table S5.6) with the results of those hepatic outcomes, as well as with those observed *in silico* for liver and glutathione phenotypes using HAM [526]. When comparing QTL peaks from renal glutathione with those from hepatic glutathione, we observed a QTL for renal E_h (mV) on mouse chromosome 14 at 22.959 (22.359 – 23.926) Mbp (LOD score 6.258) overlapping with a QTL peak observed for hepatic GSH and total glutathione on mouse chromosome 14 at 22.506 (22.058 – 22.528) Mbp (LOD score 6.755 and 6.748 for GSH and total glutathione, respectively) (Figure 4). Candidate gene results and founder allele effects for renal E_h are included in Supplementary Figures S5.4 (hepatic total glutathione and GSH results found in Supplementary Figures 3.2 and 3.3). These results indicate that the renal and hepatic GSH redox systems are under both shared and tissue-specific genetic control. In addition, we observed multiple comparisons between renal glutathione QTL and renal glutathione HAM peaks. A QTL peak for renal GSH and total glutathione on mouse chromosome 11 at 100.810 (100.059 – 101.369) Mbp (LOD score 6.664) and 100.804 (100.059 – 101.369) Mbp (LOD score 6.428), respectively, was in proximity to a HAM peak discovered for renal GSH at 93.177 Mbp on mouse chromosome 11. Similarly, a QTL peak for renal GSSG on mouse chromosome 1 at 144.970 (143.603 – 148.590) Mbp (LOD score 6.044) was in proximity to a HAM peak for renal GSH at 138.112 Mbp on mouse chromosome 1. Furthermore, the suggestive peak for renal GSH and total glutathione on mouse chromosome X at 51.602 (49.234 – 51.892) Mbp (LOD scores 6.962 and 7.105, respectively) overlapped with a peak discovered for hepatic steatosis on mouse chromosome X at 51.515 (47.372 – 51.838) Mbp (LOD score 7.266). Interestingly, a candidate gene from mouse

chromosome X for renal GSH variation, *GPC3*, has been evaluated as a marker for hepatocellular carcinoma (HCC) as its expression is increased in HCC hepatocytes and detectable in HCC serum, whereas it is undetectable in serum and hepatocytes of non-healthy patients [678]. When comparing QTL peaks observed for BUN, we found a QTL peak on mouse chromosome 6 at 127.602 (125.386 – 128.618) Mbp (LOD score 6.060) to be in proximity to a HAM peak discovered *in silico* for renal GSSG on mouse chromosome 6 at 134.119 Mbp. Lastly, we observed a QTL peak for renal GSSG on mouse chromosome 16 at 62.938 (61.291 – 72.202) Mbp (LOD score 6.048) in proximity to a significant QTL peak observed for AST on mouse chromosome 16 at 57.518 (57.069 – 59.755) Mbp (LOD score 7.808).

To identify the effect, if any, the variation in genomic regions encoding canonical GSH metabolism genes had on glutathione phenotype concentrations, we investigated the QTL reports for their specific genome locations to elucidate if there was allelic variation resulting in significant differences in glutathione concentrations. *De novo* synthesis and recycling of GSH intracellularly involves glutathione peroxidase 1 (GPx1), glutathione cysteine ligase – catalytic subunit (Gclc), glutathione cysteine ligase – modifier subunit (Gclm), glutathione synthetase (Gs), and Gr. Founder allele QTL effects were visualized for renal GSH, GSSG, total glutathione, GSH/GSSG, and E_h (mV) in genetic regions of Gpx1 (Chromosome 9 59.24 cM), Gclc (Chromosome 9 43.36 cM), Gclm (Chromosome 3 52.94 cM), Gs (Chromosome 2 77.26 cM), and Gr (Chromosome 8 20.69 cM) (Supplementary Figures S5.5 – S5.9). These plots indicate that there are no alleles found in proximity to synthesis or recycling enzyme gene locations that contribute to a significantly lower or higher glutathione phenotype concentration. These results support our hypothesis that the variation in renal GSH redox status markers is regulated by loci external to those housing canonical GSH synthesis and recycling genes.

This study was accompanied by a few limitations. Given that the glutathione system is sensitive to external stressors, we limited exposure to stressors throughout the duration of the study. However, N = 62 males had to be individually housed as a result of aggressive behavior. To ensure that housing conditions did not affect glutathione status, we performed Mann-Whitney tests and confirmed that all glutathione variables were not significantly different between animals individually housed versus housed in groups.

Conclusion

Glutathione is a critical cytoprotectant and regulator of cellular redox balance, with renal tissue dependent on GSH to maintain function and neutralize ROS to prevent oxidative stress and the onset of CKD. Recent evidence has documented natural variation in renal glutathione, as well as suggested novel genes associated with the renal GSH redox system. However, those studies were limited to inbred rodent strains and do not reflect the degree of genetic diversity in humans. We previously identified a large degree of hepatic glutathione variation in these outbred mice, and documented a novel locus influencing hepatic redox balance. Given the interorgan metabolism between hepatic and renal glutathione homeostasis [650], we hypothesized that renal glutathione would vary to the same degree as hepatic glutathione, and that the two systems would be under shared genetic control. We found that the two varied to similar degrees, with trends agreeing with those previously reported from strain surveys. Moreover, we classified both shared and tissue-specific loci controlling the hepatic and renal glutathione systems. Through QTL mapping, we identified a novel QTL peak for renal GSH and total glutathione on chromosome X and identified *Aifm1* as the most plausible candidate gene within that region. In summary, we employed a forward genetics approach to study renal glutathione – an approach that has not been previously used to study this tissue's redox system – and identified a novel locus controlling renal GSH. The next

stage of this research involves validation of the candidate genes using mechanistic approaches to elucidate their influence on renal GSH redox status, oxidative stress, and disease.

Supplementary Table S5.1. Descriptive statistics for renal glutathione and BUN for male DO mice.

Phenotype:	**N**	**$\bar{x}$**	**Median**	**SD**	**Min**	**Max**
Total Glutathione (nmol/mg)	170	17.965	17.307	7.010	6.699	49.074
GSH (nmol/mg)	170	17.345	16.813	6.821	6.234	47.712
GSSG (nmol/mg)	170	0.310	0.272	0.192	0.088	1.478
GSH/GSSG	170	67.313	61.430	33.502	19.668	177.900
E_h (mV)	170	-179.759	-181.617	10.143	-199.627	-154.232
BUN (mg/dL)	164	24	24	5	14	43

Supplementary Table S5.2. Descriptive statistics for renal glutathione and BUN for female DO mice.

Phenotype:	**N**	**$\bar{x}$**	**Median**	**SD**	**Min**	**Max**
Total Glutathione (nmol/mg)	175	18.783	18.852	8.139	5.069	45.835
GSH (nmol/mg)	175	17.928	17.722	7.864	4.744	44.401
GSSG (nmol/mg)	175	0.428	0.337	0.294	0.129	1.612
GSH/GSSG	175	51.077	45.453	27.045	6.855	173.517
E_h (mV)	175	-175.986	-176.454	11.394	-202.380	-145.203
BUN (mg/dL)	174	23	22	4	14	48

Supplementary Table S5.3. Spearman's Rank correlations between weights.
Liver weight and body weight expressed in grams (g). GSH, GSSG, and total glutathione were standardized as nmol/mg protein. E_h was expressed as mV and BUN was standardized as mg/dL. *indicates a significant relationship ($p < 0.05$).

Variables	**ρ**	**p-value**
Final Weight, Kidney Total Glutathione	-0.170*	0.002
Final Weight, Kidney GSH	-0.159*	0.003
Final Weight, Kidney GSSG	-0.199*	<0.001
Final Weight, Kidney GSH/GSSG	0.094	0.082
Final Weight, Kidney E_h	0.006	0.915
Final Weight, BUN	0.098	0.071
Liver Weight, Kidney Total Glutathione	-0.145*	0.007
Liver Weight, Kidney GSH	-0.135*	0.012
Liver Weight, Kidney GSSG	-0.234*	<0.001
Liver Weight, Kidney GSH/GSSG	0.146*	0.006
Liver Weight, Kidney E_h	-0.037	0.496
Liver Weight, BUN	0.106	0.052

Supplementary Table S5.4. Renal total glutathione and GSH and candidate genes and their relevant annotations (Chr11: 100.059–101.369 ± 1 Mbp; GRCm38/mm10).[a]

				Expression (kidney)		Functional		Phenotypic (kidney-related)		
MGI Gene symbol	**Genome coordinates (strand)**	**Type**	**Known redox gene**	**GXD (MGI)**	**EEA**	**Inter Pro**	**GO**	**PW**	**EBM**	**Relevance to renal glutathione[b]**
Top2a	Chr11:98992943-99024189 (-)	protein coding gene	No	X	X	--	X	--	--	Expressed in mouse kidney; GO:0030263; GO:0008094; GO:0005524; GO:0006974; GO:0005814; GO:0003682; GO:0000775; GO:0030261; GO:0007059; GO:0000793; GO:0005737; GO:0003677; GO:0008301; GO:0006266; GO:0006259; GO:0003916; GO:0003918; GO:0009330; GO:0006265; GO:0040016; GO:0019899; GO:0051309; GO:0007143; GO:0002244; GO:0042826; GO:0016853; GO:0000287; GO:0046872; GO:1905463; GO:0000228; GO:0005730; GO:0005654; GO:0000166; GO:0005634; GO:0043065; GO:0045870; GO:0045944; GO:0005515; GO:0032991; GO:0008022; GO:0046982; GO:0042803; GO:0005080; GO:0042752; GO:0000712; GO:0048511; GO:1990904; GO:0043565; GO:0000819; GO:0043130
Gm23451	Chr11:99017031-99017152 (-)	snoRNA gene	No	--	--	--	--	--	--	None – predicted gene

Igfbp4	Chr11:99040005-99052655 (+)	protein coding gene	No	X	--	X	X	--	--	Expressed in mouse kidney; GO:0005576; GO:0005615; GO:0019838; GO:0005520; GO:0031994; GO:0031995; GO:0043568; GO:0043410; GO:0005515; GO:0001558; GO:0010906; GO:0040008; GO:0043567; GO:0044342
Tns4	Chr11:99065678-99089306 (-)	protein coding gene	No	X	X	--	X	--	--	Expressed in mouse kidney; GO:0003779; GO:0006915; GO:0030054; GO:0005737; GO:0005856; GO:0005925; GO:0008104
Ccr7	Chr11:99144199-99155077 (-)	protein coding gene	No	X	X	X	X	--	--	Expressed in mouse kidney; GO:0007257; GO:0019722; GO:0019957; GO:0016493; GO:0038117; GO:0038121; GO:0060326; GO:0009986; GO:0071345; GO:0035757; GO:0035758; GO:0004950; GO:0006935; GO:0001768; GO:0009897; GO:0004930; GO:0007186; GO:0048872; GO:0006955; GO:0006954; GO:0016021; GO:0048535; GO:0002518; GO:0097022; GO:0097029; GO:0016020; GO:0005739; GO:0002408; GO:0032695; GO:2000107; GO:0045060; GO:0005886; GO:2000147; GO:0007204; GO:0002606; GO:2000510; GO:0051491; GO:2000526; GO:0043547; GO:0002922; GO:0002885; GO:2000522; GO:0032735; GO:0032731;

										GO:0010759; GO:0090023; GO:0050766; GO:0048260; GO:0010820; GO:2000525; GO:0042102; GO:0050862; GO:0045627; GO:2000412; GO:0032760; GO:0005515; GO:2000547; GO:0032649; GO:0032651; GO:0002649; GO:0032496; GO:0071731; GO:0034695; GO:0007165
Gm32249	Chr11:99168312-99175730 (+)	lncRNA gene	No	--	--	--	--	--	--	None – predicted gene
Smarce1	Chr11:99209047-99231017 (-)	protein coding gene	No	X	--	X	X	--	--	Expressed in mouse kidney; GO:0043044; GO:0006325; GO:0006338; GO:0003677; GO:0008080; GO:0071565; GO:0045892; GO:0007399; GO:0022008; GO:0071564; GO:0016922; GO:0005654; GO:0006337; GO:0005634; GO:0005515; GO:0047485; GO:0003723; GO:0016514; GO:0070603
Krt222	Chr11:99232761-99244085 (-)	protein coding gene	No	X	X	--	X	--	--	Expressed in mouse kidney; GO:0008150; GO:0005882; GO:0005198
Gm32385	Chr11:99243653-99305492 (+)	lncRNA gene	No	--	--	--	--	--	--	None – predicted gene
Krt24	Chr11:99279959-99285262 (-)	protein coding gene	No	X	--	--	X	--	--	Expressed in mouse kidney; GO:0016327; GO:0060706; GO:0071944; GO:0043034; GO:0016010; GO:0005882; GO:0007219; GO:0005886; GO:0005515; GO:0044877; GO:0042383; GO:0045214; GO:0008307; GO:0005198;

										GO:1990357; GO:0030018; GO:0008150
Krt25	Chr11:99315516-99322951 (-)	protein coding gene	No	X	X	--	X	--	--	Expressed in mouse kidney; GO:0007568; GO:0005737; GO:0007010; GO:0042633; GO:0031069; GO:0005882; GO:0045109; GO:0005515; GO:0046982; GO:0005198
Gm32502	Chr11:99322537-99333259 (+)	lncRNA gene	No	--	--	--	--	--	--	None – predicted gene
Krt26	Chr11:99328550-99337966 (-)	protein coding gene	No	--	X	--	X	--	--	Expressed in mouse kidney; GO:0008150; GO:0005882; GO:0005198
Krt27	Chr11:99345565-99351104 (-)	protein coding gene	No	X	--	--	X	--	--	Expressed in mouse kidney; GO:0005737; GO:0031069; GO:0005882; GO:0005198
Krt28	Chr11:99365007-99374903 (-)	protein coding gene	No	--	--	--	--	--	--	None
Krt10	Chr11:99385254-99389364 (-)	protein coding gene	No	X	X	--	X	--	--	Expressed in mouse kidney; GO:0071277; GO:0008092; GO:0008544; GO:0030855; GO:0005882; GO:0045109; GO:0045095; GO:0003334; GO:0045684; GO:0005515; GO:0005198
Gm11940	Chr11:99387340-99387897 (+)	lncRNA gene	No	X	X	--	--	--	--	Expressed in mouse kidney
Krt12	Chr11:99415666-99422259 (-)	protein coding gene	No	--	X	--	X	--	--	Expressed in mouse kidney; GO:0061303; GO:0060429; GO:0005882; GO:0002009; GO:0005198
A830036E02Rik	Chr11:99417243-99423098 (+)	lncRNA gene	No	--	--	--	--	--	--	None
Krt20	Chr11:99428403-99438150 (-)	protein coding gene	No	X	X	--	X	--	--	Expressed in mouse kidney; GO:0006915; GO:0009267; GO:0005737; GO:0005829;

										GO:0005882; GO:0045109; GO:0005515; GO:0050708; GO:0005198
Krt23	Chr11:99477973-99493120 (-)	protein coding gene	No	X	X	--	X	--	--	Expressed in mouse kidney; GO:0008150; GO:0005882; GO:0005198
Krt39	Chr11:99514114-99521338 (-)	protein coding gene	No	--	X	--	X	--	--	Expressed in mouse kidney; GO:0008150; GO:0005882; GO:0005198
Krt40	Chr11:99537485-99543158 (-)	protein coding gene	No	--	--	--	--	--	--	None
Krtap3-3	Chr11:99550132-99550863 (-)	protein coding gene	No	X	--	--	X	X	--	Expressed in mouse kidney; GO:0008150; GO:0005882; GO:0005198; Glomerulonephritis (PW)
Krtap3-2	Chr11:99555823-99556853 (-)	protein coding gene	No	--	--	--	--	--	--	None
Gm11939	Chr11:99559167-99559466 (-)	protein coding gene	No	--	--	--	--	--	--	None – predicted gene
Krtap3-1	Chr11:99566027-99566630 (-)	protein coding gene	No	X	--	--	X	X	--	Expressed in mouse kidney; GO:0008150; GO:0005882; GO:0045095; GO:0005198; Glomerulonephritis (PW)
Krtap1-5	Chr11:99579977-99581016 (-)	protein coding gene	No	X	--	--	--	X	--	Expressed in mouse kidney; GO:0008150; GO:0005575; GO:0003674; Glomerulonephritis (PW)
Gm32730	Chr11:99581773-9963125 (+)	lncRNA gene	No	--	--	--	--	--	--	None – predicted gene
Krtap1-4	Chr11:99583062-99583654 (-)	protein coding gene	No	--	--	--	--	--	--	None
Krtap1-3	Chr11:99590461-99591339 (-)	protein coding gene	No	--	--	--	--	--	--	None
Krtap9-3	Chr11:99597348-99598106 (-)	protein coding gene	No	X	--	--	X	--	--	Expressed in mouse kidney; GO:0008150; GO:0005882; GO:0045095; GO:0003674

Gm11938	Chr11:99602646-99603308 (-)	protein coding gene	No	X	--	--	X	--	--	Expressed in mouse kidney; GO:0008150; GO:0005575; GO:0003674
Gm11937	Chr11:99609794-99610189 (-)	protein coding gene	No	--	--	--	--	--	--	None – predicted gene
Krtap2-4	Chr11:99614019-99614846 (-)	protein coding gene	No	--	--	--	--	--	--	None
Gm11562	Chr11:99619598-99620404 (-)	protein coding gene	No	X	--	--	X	--	--	Expressed in mouse kidney; GO:0008150; GO:0005575; GO:0003674
Krtap4-1	Chr11:99627229-99628239 (-)	protein coding gene	No	--	--	--	--	--	--	None
Krtap4-2	Chr11:99634114-99635084 (-)	protein coding gene	No	--	--	--	--	--	--	None
Krtap4-7	Chr11:99643112-99644089 (-)	protein coding gene	No	--	--	--	--	--	--	None
Gm11555	Chr11:99649654-99650181 (-)	protein coding gene	No	--	--	--	--	--	--	None – predicted gene
Gm11563	Chr11:99657949-99658960 (-)	protein coding gene	No	--	--	--	--	--	--	None – predicted gene
Krtap4-6	Chr11:99665043-99665960 (-)	protein coding gene	No	--	--	--	--	--	--	None
Gm14190	Chr11:99690588-99690740 (-)	protein coding gene	No	--	--	--	--	--	--	None – predicted gene
Gm14180	Chr11:99734213-99734290 (-)	protein coding gene	No	--	--	--	--	--	--	None – predicted gene
Gm11595	Chr11:99771714-99772913 (-)	protein coding gene	No	--	--	--	--	--	--	None – predicted gene
Krtap4-8	Chr11:99780014-99780643 (-)	protein coding gene	No	--	--	--	--	--	--	None
Krtap4-9	Chr11:99785200-99786257 (+)	protein coding gene	No	--	--	--	--	--	--	None
Gm11596	Chr11:99792675-99793353 (-)	protein coding gene	No	--	--	--	--	--	--	None – predicted gene
Gm11569	Chr11:99798064-99798932 (-)	protein coding gene	No	--	--	--	--	--	--	None – predicted gene

Gm11554	Chr11:99803670-99804446 (-)	protein coding gene	No	--	--	--	--	--	--	None – predicted gene
Krtap4-13	Chr11:99809078-99809892 (-)	protein coding gene	No	--	--	--	--	--	--	None
Gm11564	Chr11:99814976-99815666 (-)	protein coding gene	No	--	--	--	--	--	--	None – predicted gene
2300003K06Rik	Chr11:99837148-99838066 (-)	protein coding gene	No	--	--	--	--	--	--	None
Krtap4-16	Chr11:99850655-99851605 (-)	protein coding gene	No	--	--	--	--	--	--	None
Gm26324	Chr11:99856308-99856414 (+)	snRNA gene	No	--	--	--	--	--	--	None – predicted gene
Gm11568	Chr11:99857917-99859060 (+)	protein coding gene	No	--	--	--	--	--	--	None – predicted gene
Gm11559	Chr11:99864476-99865571 (+)	protein coding gene	No	--	--	--	--	--	--	None – predicted gene
Krtap9-1	Chr11:99873389-99874000 (+)	protein coding gene	No	--	--	--	--	--	--	None
Gm11567	Chr11:99879187-99880229 (+)	protein coding gene	No	--	--	--	--	--	--	None – predicted gene
Krtap31-1	Chr11:99907920-99908890 (+)	protein coding gene	No	--	--	--	--	--	--	None
Gm11565	Chr11:99914751-99915671 (+)	protein coding gene	No	--	--	--	--	--	--	None – predicted gene
Krtap31-2	Chr11:99936291-99937225 (+)	protein coding gene	No	--	--	--	--	--	--	None
Krtap9-5	Chr11:99948475-99949551 (+)	protein coding gene	No	--	--	--	--	--	--	None
Krtap29-1	Chr11:99978025-99979053 (-)	protein coding gene	No	--	--	--	--	--	--	None
Krtap16-1	Chr11:99984710-99986597 (-)	protein coding gene	No	--	--	--	--	--	--	None
Krtap17-1	Chr11:99993234-99993994 (-)	protein coding gene	No	--	--	--	--	--	--	None
Krt33a	Chr11:100011199-100016212 (-)	protein coding gene	No	--	--	--	--	--	--	None

Krt33b	Chr11:100023634-100029868 (-)	protein coding gene	No	X	--	--	X	--	--	Expressed in mouse kidney; GO:0005882; GO:0005198
Krt34	Chr11:100037347-100041554 (-)	protein coding gene	No	X	--	--	X	--	--	Expressed in mouse kidney; GO:0005882; GO:0005198
Krt31	Chr11:100046646-100050551 (-)	protein coding gene	No	X	--	--	X	--	--	Expressed in mouse kidney; GO:0005882; GO:0005198; GO:0008150
Gm11571	Chr11:100052286-100085983 (+)	lncRNA gene	No	--	--	--	--	--	--	None – predicted gene
Krt32	Chr11:100080848-100088226 (-)	protein coding gene	No	--	X	--	X	--	--	Expressed in mouse kidney; GO:0005882; GO:0005198
Krt35	Chr11:100092192-100096224 (-)	protein coding gene	No	--	--	--	--	--	--	None
Krt36	Chr11:100102007-100105626 (-)	protein coding gene	No	X	--	--	X	--	--	Expressed in mouse kidney; GO:0005882; GO:0045111; GO:0045616; GO:0030280; GO:0005198
Gm12347	Chr11:100105771-100112106 (-)	lncRNA gene	No	--	--	--	--	--	--	None – predicted gene
Krt13	Chr11:100117327-100121566 (-)	protein coding gene	No	--	--	--	--	--	--	None
Krt15	Chr11:100131758-100135928 (-)	protein coding gene	No	X	X	--	X	--	--	Expressed in mouse kidney; GO:0005882; GO:0097110; GO:0005198; GO:0071944; GO:0005737; GO:0031069; GO:0045111; GO:0045109; GO:0031424; GO:0002009; GO:0030307; GO:0051798; GO:0045727; GO:0005515
Krt19	Chr11:100140810-100145926 (-)	protein coding gene	No	X	X	--	X	--	--	Expressed in mouse kidney; GO:0016327; GO:0060706; GO:0071944; GO:0043034; GO:0016010; GO:0005882; GO:0007219; GO:0005886; GO:0005515; GO:0044877; GO:0042383; GO:0045214;

										GO:0008307; GO:0005198; GO:1990357; GO:0030018
Gm39022	Chr11:100166884-100181390 (+)	lncRNA gene	No	--	--	--	--	--	--	None – predicted gene
Krt9	Chr11:100186781-100193246 (-)	protein coding gene	No	X	--	--	X	--	--	Expressed in mouse kidney; GO:0005882; GO:0045095; GO:0048471; GO:0007283; GO:0005198
Krt14	Chr11:100203162-100207510 (-)	protein coding gene	No	X	X	--	X	--	--	Expressed in mouse kidney; GO:0007568; GO:0045178; GO:0071944; GO:0005737; GO:0030855; GO:0042633; GO:0005882; GO:0045110; GO:0005622; GO:0045095; GO:1990254; GO:0005634; GO:0005515; GO:0005198; GO:0005856; GO:0061436; GO:0002376; GO:0006954; GO:0045087; GO:0045104; GO:0031424; GO:0030216; GO:0051546; GO:0002009; GO:0030336; GO:0005200; GO:0008150
Krt16	Chr11:100246091-100248902 (-)	protein coding gene	No	--	--	--	--	--	--	None
Krt17	Chr11:100256217-100261029 (-)	protein coding gene	No	X	X	--	X	--	--	Expressed in mouse kidney; GO:0071944; GO:0005737; GO:0031069; GO:0005882; GO:0045111; GO:0045109; GO:0031424; GO:0002009; GO:0030307; GO:0051798; GO:0045727; GO:0005515; GO:0005198; GO:0008150; GO:0005737

Krt42	Chr11:100262882-100269871 (-)	protein coding gene	No	X	--	--	X	--	--	Expressed in mouse kidney; GO:0008150; GO:0005737; GO:0005882; GO:0005198
Gm14206	Chr11:100278706-100291286 (-)	lncRNA gene	No	--	--	--	--	--	--	None – predicted gene
Gm12349	Chr11:100291671-100293711 (+)	lncRNA gene	No	X	X	--	--	--	--	
Eif1	Chr11:100319949-100322099 (+)	protein coding gene	No	X	--	X	X	--	--	Expressed in mouse kidney; GO:0009048; GO:0016282; GO:0043024; GO:0003723; GO:0006412; GO:0006413; GO:0003743
Gast	Chr11:100334407-100336996 (+)	protein coding gene	No	--	--	--	--	--	--	None
Hap1	Chr11:100347327-100356128 (-)	protein coding gene	No	X	X	X	X	--	--	Expressed in mouse kidney; GO:0008408; GO:0007568; GO:0006284; GO:0045454; GO:0006974; GO:0070301; GO:0005813; GO:0031490; GO:0005737; GO:0003684; GO:0003906; GO:0003677; GO:0080111; GO:0006310; GO:0006281; GO:0008311; GO:0008309; GO:0003691; GO:0004519; GO:0005783; GO:0004521; GO:0004527; GO:0016787; GO:0046872; GO:0005739; GO:0014912; GO:0051059; GO:0016607; GO:0004518; GO:0005730; GO:0005654; GO:0016491; GO:0048471; GO:0004528; GO:0008081; GO:1900087; GO:0045944; GO:0044877; GO:0042981; GO:0043488; GO:0003723; GO:0016890;

										GO:0000723; GO:0097698; GO:0003713; GO:0005667; GO:0008089; GO:0098957; GO:0005776; GO:0006914; GO:0043679; GO:0048403; GO:0030054; GO:0042995; GO:0030030; GO:0005814; GO:0021549; GO:0031410; GO:0005856; GO:0005829; GO:0030425; GO:0005768; GO:0006887; GO:0098982; GO:0030426; GO:0021979; GO:0042802; GO:0016234; GO:0044325; GO:0005764; GO:0048311; GO:0017022; GO:1902430; GO:0022008; GO:0043005; GO:0031175; GO:0048011; GO:0045742; GO:0090261; GO:0031587; GO:0050769; GO:0010976; GO:0032901; GO:1902857; GO:0032230; GO:0099524; GO:0099523; GO:0005515; GO:0019904; GO:0008104; GO:0006605; GO:0015031; GO:0017157; GO:1902513; GO:0099149; GO:0008090; GO:0005102; GO:0045202; GO:0047496
Gm20394	Chr11:100349696-100350889 (-)	lncRNA gene	No	X	X	--	--	--	--	Expressed in mouse kidney
Jup	Chr11:100368958-100397763 (-)	protein coding gene	No	X	--	--	X	--	--	Expressed in mouse kidney; GO:0015629; GO:0005912; GO:0045294; GO:0016327; GO:0086073; GO:0045296; GO:0016342; GO:0007155;

										GO:0050839; GO:0098609; GO:0005911; GO:0030054; GO:0016477; GO:0071681; GO:0005737; GO:0009898; GO:0106006; GO:0005856; GO:0005829; GO:0030057; GO:0002159; GO:0050982; GO:0005916; GO:0071665; GO:0014704; GO:0005882; GO:0016328; GO:0016020; GO:0043537; GO:0035257; GO:0005634; GO:0005886; GO:0045766; GO:0001954; GO:0051091; GO:0042307; GO:0045944; GO:0005515; GO:0044877; GO:0032993; GO:0019901; GO:0072659; GO:0019903; GO:0042127; GO:0086091; GO:0098911; GO:0043588; GO:0005198; GO:0003713; GO:0030018
Gm12348	Chr11:100401508-100402252 (+)	lncRNA gene	No	X	X	--	X	--	--	Expressed in mouse kidney; GO:0008150; GO:0005575; GO:0003674
P3h4	Chr11:100408467-100414716 (-)	protein coding gene	No	X	X	--	X	--	--	Expressed in mouse kidney; GO:0046849; GO:1902494; GO:0005518; GO:0032964; GO:0030199; GO:0005783; GO:0043231; GO:0017185; GO:0005515; GO:0000795
Fkbp10	Chr11:100415697-100424824 (+)	protein coding gene	No	X	X	--	X	--	--	Expressed in mouse kidney; GO:0035909; GO:0005509; GO:0030199; GO:0005783; GO:0085029; GO:0005528; GO:0001701; GO:0016853; GO:0016020; GO:0046872;

										GO:0005758; GO:0017185; GO:0018208; GO:0003755; GO:0005515; GO:0042060
Nt5c3b	Chr11:100422321-100441808 (-)	protein coding gene	No	X	X	X	X	--	--	Expressed in mouse kidney; GO:0005737; GO:0016787; GO:0000287; GO:0046872; GO:0000166; GO:0009117
Klhl10	Chr11:100441917-100457022 (+)	protein coding gene	No	X	X	X	X	--	--	Expressed in mouse kidney; GO:0005737; GO:0016787; GO:0000287; GO:0046872; GO:0000166; GO:0009117
Gm27374	Chr11:100442395-100442475 (-)	miRNA gene	No	--	X	--	--	--	--	Expressed in mouse kidney
2610002J23Rik	Chr11:100457125-100461693 (-)	unclassified gene	No	--	--	--	--	--	--	None
Klhl11	Chr11:100462614-100472741 (-)	protein coding gene	No	X	X	X	--	--	--	Expressed in mouse kidney
Acly	Chr11:100476353-100528000 (-)	protein coding gene	Yes	X	--	X	X	--	--	Expressed in mouse kidney; GO:0006085; GO:0006084; GO:0005524; GO:0003878; GO:0003824; GO:0006101; GO:0005737; GO:0005829; GO:0006633; GO:0008610; GO:0006629; GO:0046872; GO:0005739; GO:0005654; GO:0000166; GO:0006107; GO:0005886; GO:0005515; GO:0016740; GO:0046912
Mir7116	Chr11:100478411-100478480 (-)	miRNA gene	No	X	X	--	X	--	--	Expressed in mouse kidney; GO:0035690; GO:0002269; GO:0001774; GO:0003729; GO:0017148; GO:0070997; GO:0150103
n-TSgga1	Chr11:100538158-100538230 (+)	tRNA gene	No	--	--	--	--	--	--	None

Ttc25	Chr11:100545608-100572566 (+)	protein coding gene	No	X	X	X	X	--	--	Expressed in mouse kidney; GO:0097729; GO:0005930; GO:0007420; GO:0042995; GO:0090660; GO:0003341; GO:0005737; GO:0005856; GO:0060287; GO:0007507; GO:0030324; GO:0003674; GO:0120197; GO:0036158; GO:0120228; GO:0120229
Cnp	Chr11:100574904-100591729 (+)	protein coding gene	No	X	X	X	X	--	--	Expressed in mouse kidney; GO:0004113; GO:0008344; GO:0007409; GO:0042995; GO:0030551; GO:0009214; GO:0005737; GO:0005615; GO:0016787; GO:0016020; GO:0005874; GO:0000226; GO:0005902; GO:0005743; GO:0005741; GO:0043209; GO:0035748; GO:0048709; GO:0048471; GO:0005886; GO:0031143; GO:0046902; GO:0009636; GO:0003723; GO:0048513; GO:0006182; GO:0019934; GO:0005576; GO:0005615; GO:0003418; GO:0003419; GO:0005179; GO:0051427; GO:0008285; GO:0032966; GO:2000279; GO:0051447; GO:1900194; GO:0005184; GO:0001503; GO:0010753; GO:0043306; GO:0045669; GO:1900721; GO:0009791; GO:0032991; GO:0006457; GO:0007168; GO:0040014; GO:0022414; GO:0030141; GO:0005102

Dnajc7	Chr11:100582818-100620188 (-)	protein coding gene	No	X	--	X	X	--	--	Expressed in mouse kidney; GO:0051085; GO:0005737; GO:0005856; GO:0005829; GO:0031072; GO:0005654; GO:0005634
Nkiras2	Chr11:100619244-100627607 (+)	protein coding gene	No	X	X	--	X	--	--	Expressed in mouse kidney; GO:0005737; GO:0003924; GO:0005525; GO:0007249; GO:0000166
Zfp385c	Chr11:100627543-100692455 (-)	protein coding gene	No	--	--	--	--	--	--	None
Dhx58os	Chr11:100687417-100697520 (+)	antisense lncRNA gene	No	X	X	--	--	--	--	Expressed in mouse kidney
Gm38483	Chr11:100673387-100697529 (+)	lncRNA gene	No	--	--	--	--	--	--	None – predicted gene
Dhx58	Chr11:100694884-100704271 (-)	protein coding gene	No	X	X	X	X	--	--	Expressed in mouse kidney; GO:0005524; GO:0005737; GO:0051607; GO:0003677; GO:0003725; GO:0004386; GO:0016787; GO:0002376; GO:0045087; GO:0046872; GO:0045824; GO:0039534; GO:0039536; GO:0032480; GO:0000166; GO:0032728; GO:1900245; GO:1900246; GO:0032481; GO:0045088; GO:0009617; GO:0009615; GO:0003723; GO:0003724; GO:0003727; GO:0008270
Kat2a	Chr11:100704746-100712465 (-)	protein coding gene	No	X	X	X	X	--	--	Expressed in mouse kidney; GO:0016407; GO:0005671; GO:0071929; GO:0008283; GO:0005813; GO:0000785; GO:0003682; GO:0005694; GO:0005737; GO:0005856;

										GO:0010484; GO:0016573; GO:0004402; GO:0043997; GO:0000123; GO:0042826; GO:0016578; GO:0106229; GO:0043966; GO:0044154; GO:0043983; GO:0106077; GO:0106078; GO:0018393; GO:0048312; GO:0001701; GO:0007616; GO:0022037; GO:0030901; GO:0072686; GO:0035264; GO:0008080; GO:0046600; GO:0007399; GO:0001843; GO:0005634; GO:0045252; GO:0061733; GO:0106227; GO:2000727; GO:0031346; GO:0001819; GO:0045722; GO:0035066; GO:0045944; GO:0045893; GO:0005515; GO:0019903; GO:1903010; GO:0061035; GO:0031647; GO:0045589; GO:2000036; GO:0048167; GO:0050863; GO:0006355; GO:0001756; GO:0030914; GO:0021537; GO:0003713; GO:0008134; GO:0033276; GO:0016740; GO:0016746
Hspb9	Chr11:100713929-100714575 (+)	protein coding gene	No	X	X	X	X	--	--	Expressed in mouse kidney; GO:0008150; GO:0005737; GO:0003674; GO:0005634
Rab5c	Chr11:100715009-100738215 (-)	protein coding gene	No	X	--	--	X	--	--	Expressed in mouse kidney; GO:0098993; GO:0031410; GO:0005769; GO:0030139; GO:0006897; GO:0012505; GO:0005768; GO:0007032; GO:0019003; GO:0003924;

										GO:0005525; GO:0006886; GO:0005811; GO:0016020; GO:0000166; GO:0005886; GO:0048227; GO:0005515; GO:0015031; GO:0030100
Kcnh4	Chr11:100740376-100759942 (-)	protein coding gene	No	--	X	--	X	--	--	Expressed in mouse kidney; GO:0005887; GO:0071805; GO:0042391; GO:0005249
Hcrt	Chr11:100761693-100762931 (-)	protein coding gene	No	--	X	--	X	--	--	Expressed in mouse kidney; GO:0030054; GO:0005737; GO:0031410; GO:0042755; GO:0005783; GO:0060079; GO:0007631; GO:0008156; GO:0043267; GO:0051970; GO:0005184; GO:0007218; GO:0048471; GO:0007200; GO:0051928; GO:0120162; GO:0007204; GO:0051971; GO:0007205; GO:0046928; GO:0042594; GO:0030141; GO:0030431; GO:0045202; GO:0001659; GO:0031771; GO:0031772
Ghdc	Chr11:100766032-100770957 (-)	protein coding gene	No	X	X	--	X	--	--	Expressed in mouse kidney; GO:0016881; GO:0005737; GO:0005783; GO:0005634
Gm24358	Chr11:100774513-100774800 (-)	unclassified non-coding RNA gene	No	X	X	--	--	--	--	Expressed in mouse kidney
Stat5b	Chr11:100780731-100850724 (-)	protein coding gene	No	X	X	X	X	--	--	Expressed in mouse kidney; GO:0006953; GO:0071364; GO:0071363; GO:0032870; GO:0003682; GO:0019221; GO:0005737; GO:0005829; GO:0006952; GO:0046543; GO:0046544; GO:0003677;

										GO:0001228; GO:0003700; GO:0000981; GO:0003690; GO:0007565; GO:0035259; GO:0060397; GO:0042802; GO:0007595; GO:0019915; GO:0001889; GO:0001553; GO:0097531; GO:0001779; GO:0043066; GO:0045647; GO:0005634; GO:0048541; GO:0042104; GO:0045579; GO:0008284; GO:0051272; GO:0045648; GO:0045588; GO:0050729; GO:0032743; GO:0045621; GO:0045931; GO:0040018; GO:0032825; GO:0045954; GO:0032819; GO:0048661; GO:0045944; GO:0042448; GO:0005515; GO:0046983; GO:0007259; GO:0030155; GO:0042127; GO:0030856; GO:0040014; GO:0019218; GO:0006357; GO:0006355; GO:0032355; GO:0070672; GO:0070669; GO:0070670; GO:0032496; GO:0043434; GO:0000978; GO:0043565; GO:0007548; GO:0007165; GO:0019530; GO:0033077; GO:0043029; GO:0006366
Stat5a	Chr11:100859351-100885169 (+)	protein coding gene	No	X	--	X	X	--	--	Expressed in mouse kidney; GO:0071345; GO:0097011; GO:0071407; GO:0019221; GO:0005737; GO:0005829; GO:0006952; GO:0046543; GO:0046544; GO:0003677;

										GO:0001228; GO:0003700; GO:0000981; GO:0003690; GO:0060742; GO:0007565; GO:0060397; GO:0007595; GO:0019915; GO:0001553; GO:0030879; GO:0061180; GO:0060056; GO:0001779; GO:0043066; GO:0045647; GO:0033026; GO:0005654; GO:0005634; GO:0018108 ; GO:0048541; GO:0042301; GO:0042104; GO:0045579; GO:0043536; GO:0008284; GO:0001938; GO:0045588; GO:0050729; GO:0032743 GO:0045621; GO:0060376; GO:0070668; GO:0045931; GO:0040018; GO:0032825; GO:0045954; GO:0045944; GO:0060740; GO:0005515; GO:0007259; GO:0038026; GO:0030155; GO:0042127; GO:0030856; GO:0040014; GO:0019218; GO:0006357; GO:0006355; GO:0043434; GO:0000978; GO:0043565; GO:0007165; GO:0019530; GO:0033077; GO:0043029; GO:0006366; GO:0006953; GO:0071364; GO:0071363 ; GO:0032870; GO:0003682; GO:0051272; GO:0045648; GO:0032819; GO:0048661; GO:0042448; GO:0046983; GO:0032355; GO:0070672;

										GO:0070669; GO:0070670; GO:0032496; GO:0007548
Stat3	Chr11:100886806-100939594 (-)	protein coding gene	No	X	X	X	X	--	--	Expressed in mouse kidney; GO:0006953; GO:0048708; GO:0031730; GO:0008283; GO:0071345; GO:0032870; GO:0044320; GO:0071407; GO:0000785; GO:0031490; GO:0019221; GO:0005737; GO:0005829; GO:0006952; GO:0003677; GO:0001228; GO:0003700; GO:0000981; GO:0042755; GO:0097009; GO:0001754; GO:0035259; GO:0042593; GO:0098978; GO:0060396; GO:0060397; GO:0042802; GO:0006954; GO:0070102; GO:0030522; GO:0033210; GO:0005743; GO:0005739; GO:0050804; GO:0042789; GO:0010507; GO:0060548; GO:0008285; GO:0045820; GO:0010730; GO:1901215; GO:2001223; GO:2000635; GO:2000737; GO:0004879; GO:0005654; GO:0005634; GO:0016310; GO:0005886; GO:0045766; GO:2001171; GO:0030335; GO:0008284; GO:1900017; GO:0045648; GO:0010628; GO:2000637; GO:1902728; GO:0032733; GO:0032731; GO:0032755; GO:0032757; GO:1904685; GO:1905618; GO:0051092; GO:0045747;

										GO:1902895; GO:0045944; GO:0045893; GO:0032760; GO:1905564; GO:0099527; GO:0014069; GO:0070878; GO:0005515; GO:0046983; GO:0042803; GO:0006606; GO:0019901; GO:0019903; GO:0060019; GO:0007259; GO:0051726; GO:0042127; GO:0060259; GO:0046902; GO:0040014; GO:0006357; GO:0006355; GO:0034097; GO:0032355; GO:0044321; GO:0043434; GO:0000978; GO:0001103; GO:0090575; GO:0098685; GO:0043565; GO:0019953; GO:0007165; GO:0019827; GO:0001659; GO:0072540; GO:0072538; GO:0006366; GO:0008134; GO:0005667; GO:0000976
Gm46295	Chr11:100938338-100940242 (+)	lncRNA gene	No	--	--	--	--	--	--	None – predicted gene
Cavin1	Chr11:100956736-100970617 (-)	protein coding gene	No	X	--	--	X	--	--	Expressed in mouse kidney; GO:0005901; GO:0005737; GO:0006353; GO:0005783; GO:0042802; GO:0043231; GO:0016020; GO:0045121; GO:0005739; GO:0005634; GO:0005886; GO:2000147; GO:0005515; GO:0032991; GO:0009306; GO:0003723; GO:0019843; GO:0042134; GO:0009303; GO:0006363; GO:0006361

Atp6v0a1	Chr11:101009452-101063719 (+)	protein coding gene	Yes	X	X	X	X	--	--	Expressed in mouse kidney; GO:0051117; GO:0005737; GO:0031410; GO:0005829; GO:0005794; GO:0016021; GO:0030285; GO:0043231; GO:0043229; GO:0006811; GO:0016020; GO:0016607; GO:0048471; GO:0005886; GO:0005515; GO:1902600; GO:0015078; GO:0046961; GO:0033179; GO:0016241; GO:0008021; GO:1901998; GO:0007035; GO:0016471; GO:0000220
C030015 D21Rik	Chr11:101019349-101020026 (+)	unclassified gene	No	--	--	--	--	--	--	None
Mir6928	Chr11:101030340-101030409 (+)	miRNA gene	No	X	X	--	--	--	--	Expressed in mouse kidney
A930017 D03Rik	Chr11:101052325-101053852	unclassified gene	No	--	--	--	--	--	--	None
Naglu	Chr11:101070090-101077672 (+)	protein coding gene	No	X	X	X	X	--	--	Expressed in mouse kidney; GO:0004561; GO:0021680; GO:0070062; GO:0060119; GO:0045475; GO:0007040; GO:0042474; GO:0046548
Hsd17b1	Chr11:101078411-101080527 (+)	protein coding gene	No	X	X	X	X	--	--	Expressed in mouse kidney; GO:0072582; GO:0005737; GO:0005829; GO:0035410; GO:0004303; GO:1903924; GO:0006703; GO:0006629; GO:0050661; GO:0070401; GO:0016491; GO:0042803; GO:0005496; GO:0006694; GO:0061370; GO:0047035; GO:0030283

Coasy	Chr11:101082565-101086619 (+)	protein coding gene	No	X	--	--	X	--	--	Expressed in mouse kidney; GO:0005524; GO:0009058; GO:0003824; GO:0015937; GO:0005737; GO:0004140; GO:0016301; GO:0008152; GO:0005759; GO:0005739; GO:0000166; GO:0016779; GO:0004595; GO:0016310; GO:0016740
Mlx	Chr11:101087277-101092207 (+)	protein coding gene	No	X	X	X	X	--	--	Expressed in mouse kidney; GO:0005737; GO:0005829; GO:0003677; GO:0000981; GO:0001227; GO:0000122; GO:0045892; GO:0031965; GO:0006913; GO:0005654; GO:0005634; GO:0045944; GO:0005515; GO:0046983; GO:0046982; GO:0042803; GO:0006357; GO:0006355; GO:0000978; GO:0000977; GO:1990837; GO:0008134; GO:0035538; GO:0071333; GO:0008284; GO:0045723; GO:0045821; GO:0046889; GO:0019901; GO:0051726; GO:0006110; GO:0009749; GO:0005667
Psmc3ip	Chr11:101092141-101095435(-)	protein coding gene	No	X	X	--	X	--	--	Expressed in mouse kidney; GO:0050681; GO:0003677; GO:0050692; GO:0006310; GO:0030331; GO:0035259; GO:0051321; GO:0030374; GO:0005654; GO:0005634; GO:0045944; GO:0044877; GO:0007131; GO:0046966

Retreg3	Chr11:101096322-101119841 (-)	protein coding gene	No	X	X	X	X	--	--	Expressed in mouse kidney; GO:0016021; GO:0016020; GO:0003674; GO:0010976; GO:0032991; GO:0061709
Tubg1	Chr11:101119938-101126419 (+)	protein coding gene	No	X	X	X	X	--	--	Expressed in mouse kidney; GO:0045177; GO:0031252; GO:0005814; GO:0005813; GO:0036064; GO:0005929; GO:0000794; GO:0005737; GO:0005881; GO:0031122; GO:0005856; GO:0000930; GO:0003924; GO:0005525; GO:0042802; GO:0000212; GO:0005874; GO:0007017; GO:0000226; GO:0007020; GO:0005815; GO:0000278; GO:0000070; GO:1990498; GO:0007052; GO:0097730; GO:0000166; GO:0005634; GO:0000242; GO:0005827; GO:0005515; GO:0055037; GO:0007088; GO:0005819; GO:0005876; GO:0000922; GO:0005200
Gm27626	Chr11:101140454-101140509 (-)	miRNA gene	No	--	--	--	--	--	--	None – predicted gene
Tubg2	Chr11:101155907-101161787 (+)	protein coding gene	No	X	X	--	X	--	--	Expressed in mouse kidney; GO:0005813; GO:0005737; GO:0005881; GO:0031122; GO:0005856; GO:0000930; GO:0003924; GO:0005525; GO:0000212; GO:0005874; GO:0007017; GO:0000226; GO:0007020; GO:0000278; GO:0000070; GO:0007052; GO:0000166; GO:0005634;

										GO:0000242; GO:0005819; GO:0005876; GO:0005200
Plekhh3	Chr11:101162679-101171351 (-)	protein coding gene	No	X	X	X	X	--	--	Expressed in mouse kidney; GO:0005856; GO:0003674; GO:0007165
Cntnap1	Chr11:101174617-101190724 (+)	protein coding gene	No	X	X	X	X	--	--	Expressed in mouse kidney; GO:0030424; GO:0007155; GO:0030054; GO:0022010; GO:0007010; GO:0016021; GO:0016020; GO:0022011; GO:0043209; GO:0050885; GO:0050884; GO:0019227; GO:0031175; GO:0048812; GO:0030913; GO:0033270; GO:0048787; GO:0071205; GO:0002175; GO:0005918; GO:0017124
Ccr10	Chr11:101172998-101175443 (-)	protein coding gene	No	X	X	X	X	--	--	Expressed in mouse kidney; GO:0005884; GO:0019722; GO:0019957; GO:0016493; GO:0060326; GO:0070098; GO:0004950; GO:0006935; GO:0005829; GO:0005768; GO:0009897; GO:0004930; GO:0007186; GO:0006955; GO:0006954; GO:0016021; GO:0005887; GO:0043231; GO:0016020; GO:0031965; GO:0005654; GO:0005886; GO:0007204; GO:0005515; GO:0005044; GO:0007165; GO:0019956; GO:0009986; GO:0005783
Ezh1	Chr11:101191115-101226463 (-)	protein coding gene	No	X	X	X	X	--	--	Expressed in mouse kidney; GO:0003682; GO:0006325; GO:0006338; GO:0006348;

										GO:0000781; GO:0035098; GO:0036333; GO:0031507; GO:0070734; GO:0098532; GO:0018024; GO:0046976; GO:0097421; GO:0032259; GO:0008168; GO:0000122; GO:0005654; GO:0031493; GO:0005634; GO:0045944; GO:0005515; GO:1904772; GO:0003714; GO:0016740
D830013 H23Rik	Chr11:101245106-101246746 (-)	unclassified gene	No	--	--	--	--	--	--	None
Ramp2	Chr11:101246334-101248250 (+)	protein coding gene	No	X	--	X	X	--	--	Expressed in mouse kidney; GO:0007189; GO:0034333; GO:1990409; GO:0001605; GO:1903143; GO:1990410; GO:0097643; GO:0150057; GO:0097647; GO:0001525; GO:0070831; GO:0070830; GO:0006816; GO:0009986; GO:0032870; GO:0035924; GO:0015026; GO:0005737; GO:0007186; GO:0007507; GO:0016021; GO:0006886; GO:0016020; GO:2000352; GO:0043116; GO:0005886; GO:0045766; GO:0010628; GO:0032092; GO:2001214; GO:0072659; GO:0015031; GO:0043235; GO:0031623; GO:0008217; GO:0008277; GO:0002040; GO:0097084; GO:0001570
Vps25	Chr11:101253707-101259549 (+)	protein coding gene	No	X	--	X	X	--	--	Expressed in mouse kidney; GO:0005737; GO:0005829; GO:0005768; GO:0010008;

										GO:0000814; GO:0016020; GO:0005739; GO:0071985; GO:0007175; GO:0005634; GO:0042803; GO:0047485; GO:0015031; GO:0043328; GO:0005198
Wnk4	Chr11:101260567-101277409 (+)	protein coding gene	No	X	X	X	X	--	--	Expressed in mouse kidney; GO:0005524; GO:0005923; GO:0030054; GO:0030644; GO:0019869; GO:0006821; GO:0005737; GO:0005829; GO:0072156; GO:0035556; GO:0050801; GO:0006811; GO:0016301; GO:0016020; GO:0090188; GO:0010766; GO:0000166; GO:0016310; GO:1903288; GO:2000651; GO:0019870; GO:0005515; GO:0004672; GO:0008104; GO:0006468; GO:0106310; GO:0004674; GO:0106311; GO:0050794; GO:0070294; GO:0016740
Gm11615	Chr11:101264762-101266303 (-)	lncRNA gene	No	X	X	--	--	--	--	Expressed in mouse kidney
Coa3	Chr11:101277970-101278948 (-)	protein coding gene	No	X	--	--	X	--	X	Expressed in mouse kidney; GO:0016021; GO:0031305; GO:0016020; GO:0033617; GO:0005743; GO:0005739; GO:0003674; GO:0070131; Isolated cycochrome C oxidase deficiency, mitochondrial complex IV deficiency (EBM)

Cntd1	Chr11:101279203-101288701 (+)	protein coding gene	No	X	X	X	X	--	--	Expressed in mouse kidney; GO:0003674; GO:0007131; GO:0035861; GO:0007283
Becn1	Chr11:101288258-101302286 (-)	protein coding gene	No	X	X	X	X	--	--	Expressed in mouse kidney; GO:0050435; GO:0001525; GO:0006915; GO:0005776; GO:0000045; GO:0006914; GO:0000422; GO:0007049; GO:0051301; GO:0042149; GO:0006995; GO:0005737; GO:0031410; GO:0005856; GO:0051607; GO:0030425; GO:0045022; GO:0006897; GO:0005783; GO:0005768; GO:0043652; GO:0019898; GO:0005794; GO:0051020; GO:0042802; GO:0045324; GO:0007040; GO:0016236; GO:0016020; GO:0005739; GO:0000423; GO:0007080; GO:0043066; GO:1902902; GO:0010507; GO:0060548; GO:0008285; GO:1905672; GO:2000378; GO:0048666; GO:0005634; GO:0045335; GO:0000407; GO:0043548; GO:0035032; GO:0034271; GO:0034272; GO:1902425; GO:2000786; GO:0010508; GO:0010613; GO:2001244; GO:0005515; GO:0032991; GO:0019901; GO:0032801; GO:0050790; GO:0032465; GO:0098780; GO:0051707; GO:0005802; GO:0031625

Psme3	Chr11:101316213-101323537 (+)	protein coding gene	No	X	X	X	X	--	--	Expressed in mouse kidney; GO:0006915; GO:0007049; GO:0005737; GO:0005829; GO:0061133; GO:0042802; GO:0097371; GO:2001237; GO:0005654; GO:0005634; GO:0002039; GO:0010950; GO:0008537; GO:0000502; GO:2000045; GO:0061136
Aoc2	Chr11:101325063-101329702 (+)	protein coding gene	Yes	X	X	X	X	--	--	Expressed in mouse kidney; GO:0052595; GO:0009308; GO:0052594; GO:0006584; GO:0005507; GO:0046872; GO:0016491; GO:0052596; GO:0005886; GO:0008131; GO:0048038; GO:0052593; GO:0007601; GO:0005509; GO:0007155; GO:0009986; GO:0005737; GO:0005769; GO:0042755; GO:0005783; GO:0005615; GO:0005794; GO:0042802; GO:0016021; GO:0043231; GO:0002523; GO:0016020; GO:0005902; GO:1902283; GO:0002675; GO:0010828; GO:0002687; GO:0046982; GO:0008217; GO:0046677; GO:0035902
Aoc3	Chr11:101330606-101339430 (+)	protein coding gene	Yes	X	--	--	X	--	--	Expressed in mouse kidney; GO:0052595; GO:0009308; GO:0052594; GO:0005509; GO:0007155; GO:0009986; GO:0005507; GO:0005737; GO:0005769; GO:0042755; GO:0005783; GO:0005615; GO:0005794; GO:0042802;

										GO:0016021; GO:0043231; GO:0002523; GO:0016020; GO:0046872; GO:0005902; GO:1902283; GO:0016491; GO:0052596; GO:0005886; GO:0002675; GO:0010828; GO:0002687; GO:0008131; GO:0046982; GO:0048038; GO:0008217; GO:0046677; GO:0035902; GO:0052593
Gm28156	Chr11:101339660-101347939 (-)	lncRNA gene	No	--	--	--	--	--	--	None – predicted gene
4931418L13Rik	Chr11:101347973-101348573 (+)	unclassified gene	No	--	--	--	--	--	--	None
Gm25593	Chr11:101353342-101353437 (-)	miRNA gene	No	--	--	--	--	--	--	None – predicted gene
G6pc	Chr11:101367716-101377903 (+)	protein coding gene	No	X	--	--	X	--	--	Expressed in mouse kidney; GO:0042632; GO:0005783; GO:0006094; GO:0004346; GO:0051156; GO:0015760; GO:0042593; GO:0005980; GO:0005977; GO:0016787; GO:0016021; GO:0043231; GO:0055088; GO:0016020; GO:0035264; GO:0006796; GO:0042301; GO:0046838; GO:0016773; GO:0010468; GO:0008202; GO:0006641; GO:0046415
Gm25475	Chr11:101397590-101397768 (-)	snRNA gene	No	--	--	--	--	--	--	None – predicted gene
Gm27029	Chr11:101406664-101424796 (-)	protein coding gene	No	--	X	--	X	--	--	Expressed in mouse kidney; GO:0106074; GO:0006450; GO:0002196
Aarsd1	Chr11:101406839-101417615 (-)	protein coding gene	No	X	--	--	X	--	--	Expressed in mouse kidney; GO:0004813; GO:0006419;

										GO:0002161; GO:0004812; GO:0005524; GO:0005737; GO:0046872; GO:0003676; GO:0000166; GO:0005515; GO:0006450; GO:0002196; GO:0006412; GO:0043039
Ptges3l	Chr11:101418812-101425333 (-)	protein coding gene	No	X	--	--	X	--	--	Expressed in mouse kidney; GO:0051087; GO:0051131; GO:0005829; GO:0051879; GO:0005634; GO:0006457
Mir6929	Chr11:101419187-101419253 (-)	miRNA gene	No	X	--	--	--	--	--	Expressed in mouse kidney
Rundc1	Chr11:101425085-101435666 (+)	protein coding gene	No	X	X	--	X	--	--	Expressed in mouse kidney; GO:0090630; GO:0005096; GO:0006886; GO:0001701; GO:0050790
Rpl27	Chr11:101442298-101445529 (+)	protein coding gene	No	X	--	--	X	--	--	Expressed in mouse kidney; GO:0022625; GO:0022626; GO:0005730; GO:0005654; GO:1990904; GO:0005840; GO:0006364; GO:0003735
Ifi35	Chr11:101448412-101458701 (+)	protein coding gene	No	X	--	--	X	--	--	Expressed in mouse kidney; GO:0005737; GO:0005829; GO:0005615; GO:0042802; GO:0002281; GO:0016020; GO:0008285; GO:1901223; GO:0005634; GO:0050729; GO:0045089; GO:1901224; GO:0034145
Gm11626	Chr11:101456576-101457390 (-)	lncRNA gene	No	X	X	--	--	--	--	Expressed in mouse kidney
Vat1	Chr11:101458748-101466199 (-)	protein coding gene	No	X	--	X	X	--	--	Expressed in mouse kidney; GO:0015842; GO:0098656; GO:0030054; GO:0005737; GO:0031410; GO:0019899; GO:0015698; GO:0016021;

										GO:0016020; GO:0030001; GO:0051612; GO:0006836; GO:0033603; GO:0005335; GO:0051610; GO:0035725; GO:0045202; GO:0030672; GO:0043195; GO:0055085; GO:0022857; GO:0042910; GO:0042908; GO:0005741; GO:0005739; GO:0010637; GO:0016491; GO:0008270
Rnd2	Chr11:101468175-101471853 (+)	protein coding gene	No	X	X	X	X	--	--	Expressed in mouse kidney; GO:0007015; GO:0005938; GO:0016477; GO:0042995; GO:0030865; GO:0031410; GO:0005856; GO:0005769; GO:0007163; GO:0003924; GO:0005525; GO:0043231; GO:0016020; GO:0000166; GO:0005886; GO:0048672; GO:0005515; GO:0019901; GO:0047485; GO:0032956; GO:0008360; GO:0007264
Brca1	Chr11:101488764-101551955 (-)	protein coding gene	No	X	X	X	X	--	--	Expressed in mouse kidney; GO:0070531; GO:0031436; GO:0007049; GO:0006974; GO:0071681; GO:0071356; GO:0005813; GO:0007098; GO:0051298; GO:0043009; GO:0003682; GO:0005694; GO:0007059; GO:0000793; GO:0000794; GO:0005737; GO:0003684; GO:0003677; GO:0006310; GO:0006281; GO:0009048; GO:0006302; GO:0000724; GO:0019899; GO:0006633; GO:0006631;

										GO:0008630; GO:0000800; GO:0006629; GO:0046872; GO:0005759; GO:0007095; GO:0044818; GO:1902042; GO:0045717; GO:0035067; GO:0051572; GO:0051573; GO:0033147; GO:2000378; GO:0045892; GO:0016604; GO:0005654; GO:0005634; GO:0005886; GO:0045766; GO:0045739; GO:0010628; GO:0035066; GO:0051571; GO:2000617; GO:0051574; GO:2000620; GO:0070512; GO:0042307; GO:0031398; GO:0045944; GO:0045893; GO:0010575; GO:0006301; GO:0051865; GO:0032991; GO:0085020; GO:0016567; GO:0051726; GO:0044030; GO:0006349; GO:0006357; GO:0043627; GO:0010212; GO:1990904; GO:0003723; GO:0070063; GO:0003713; GO:0000976; GO:0016740; GO:0031625; GO:0004842; GO:0008270
Nbr1	Chr11:101552149-101581951 (+)	protein coding gene	No	X	X	X	X	--	--	Expressed in mouse kidney; GO:0005776; GO:0005737; GO:0031410; GO:0005829; GO:0043231; GO:0005770; GO:0005764; GO:0016236; GO:0046872; GO:0005758; GO:0005739; GO:0051019; GO:0045668; GO:0016604; GO:0005654; GO:0000407;

										GO:0005515; GO:0043235; GO:0030500; GO:0032872; GO:0043130; GO:0008270
Tmem106a	Chr11:101582242-101591788 (+)	protein coding gene	No	X	X	--	X	--	--	Expressed in mouse kidney; GO:0035780; GO:0035781; GO:0002376; GO:0045087; GO:0016021; GO:0042116; GO:0016020; GO:0003674; GO:0005886; GO:0043123; GO:0032731; GO:0032755; GO:0043410; GO:0045348; GO:1904407; GO:0032760
Gm11634	Chr11:101593743-101599256 (-)	protein coding gene	No	X	X	--	--	--	--	Expressed in mouse kidney
Gm26316	Chr11:101604850-101605040 (+)	snRNA gene	No	X	--	--	--	--	--	
Gm11635	Chr11:101610614-101615956 (+)	lncRNA gene	No	--	--	--	--	--	--	None – predicted gene
Rdm1	Chr11:101627242-101636089 (+)	protein coding gene	No	X	X	X	X	--	--	Expressed in mouse kidney; GO:0008150; GO:0005737; GO:0005829; GO:0003677; GO:0003676; GO:0005730; GO:0005634; GO:0003723
Gm23849	Chr11:101627366-101627556 (+)	snRNA gene	No	X	X	--	--	--	--	Expressed in mouse kidney
Gm24950	Chr11:101641748-101641938 (+)	snRNA gene	No	X	--	--	--	--	--	None – limited expression data
Gm23971	Chr11:101645740-101645930 (-)	snRNA gene	No	X	--	--	--	--	--	None – limited expression data
Rnu2-10	Chr11:101658238-101658424 (+)	snRNA gene	No	X	--	--	--	--	--	None – limited expression data
Arl4d	Chr11:101665541-101667832 (+)	protein coding gene	No	X	X	--	X	--	--	
Gm39391	Chr11:101696251-101697580 (+)	lncRNA gene	No	--	--	--	--	--	--	None – predicted gene

Dhx8	Chr11:101732956-101767358 (+)	protein coding gene	No	X	--	X	X	--	--	Expressed in mouse kidney; GO:0005524; GO:0071013; GO:0005829; GO:0004386; GO:0016787; GO:0042802; GO:0005622; GO:0006397; GO:0000398; GO:0016604; GO:0003676; GO:0005654; GO:0000166; GO:0005634; GO:0003723; GO:0003724; GO:0008380; GO:0005681; GO:0000390; GO:0071007
Etv4	Chr11:101769747-101785310 (-)	protein coding gene	No	X	X	--	X	--	--	Expressed in mouse kidney; GO:0060444; GO:0030154; GO:0005694; GO:0003677; GO:0001228; GO:0003700; GO:0000981; GO:0005622; GO:0008045; GO:0033600; GO:0005730; GO:0005634; GO:0010628; GO:0045618; GO:0045944; GO:0045893; GO:0006357; GO:0006355; GO:0000978; GO:0043565; GO:1990837; GO:0048863
Gm39392	Chr11:101785321-101789152 (+)	lncRNA gene	No	--	--	--	--	--	--	None – predicted gene
Meox1	Chr11:101877510-101894354 (-)	protein coding gene	No	X	X	X	X	--	--	Expressed in mouse kidney; GO:0003682; GO:0005737; GO:0003677; GO:0001228; GO:0003700; GO:0000981; GO:0071837; GO:0007275; GO:0005634; GO:0045944; GO:0006357; GO:0006355; GO:0000978; GO:0061056; GO:0043565; GO:1990837; GO:0061053; GO:0001757

Gm11551	Chr11:101886237-101891206 (+)	lncRNA gene	No	--	X	--	--	--	--	Expressed in mouse kidney
Gm33662	Chr11:101929194-101938003 (-)	lncRNA gene	No	--	--	--	--	--	--	None – predicted gene
4930417O22Rik	Chr11:101952421-101960573 (+)	lncRNA gene	No	--	--	--	--	--	--	None – predicted gene
Sost	Chr11:101962458-101967015 (-)	protein coding gene	No	--	X	X	X	--	--	Expressed in mouse kidney; GO:0036122; GO:0071374; GO:0005576; GO:0005794; GO:0008201; GO:0030514; GO:0090090; GO:0030279; GO:0031333; GO:0030178; GO:0001503; GO:0045893; GO:0005515; GO:0032991; GO:0008134; GO:0016055
Dusp3	Chr11:101971143-101987013 (-)	protein coding gene	No	X	--	X	X	--	--	Expressed in mouse kidney; GO:0071364; GO:0008092; GO:0005829; GO:0016311; GO:0016787; GO:0001772; GO:0000188; GO:0001701; GO:0033549; GO:0030336; GO:0050922; GO:0042059; GO:0070373; GO:0046329; GO:0043409; GO:0050868; GO:0050860; GO:0005654; GO:0005634; GO:0035335; GO:1990264; GO:0016791; GO:0004721; GO:0120183; GO:0045931; GO:0006470; GO:0019901; GO:0106306; GO:0004722; GO:0106307; GO:1990782; GO:0004725; GO:0008138; GO:0030971; GO:0051893; GO:0030165
Gm20659	Chr11:101971143-101971859 (+)	lncRNA gene	No	--	--	--	--	--	--	None – predicted gene

Cfap97d1	Chr11:101987056-101992264 (+)	protein coding gene	No	X	X	X	X	--	--	Expressed in mouse kidney; GO:0005575; GO:0003674; GO:0007288
Mpp3	Chr11:101999652-102027045 (-)	protein coding gene	No	X	X	X	X	--	--	Expressed in mouse kidney; GO:0030165

[a] Resource abbreviations: **EBM,** Ensembl BioMart; **EEA,** EBI Expression Atlas; **GO,** Gene Ontology; **GXD,** Gene eXpression Database; **MGI,** Mouse Genome Informatics; **PW,** PheWeb

[b] ID terms: **GO:0030263:** apoptotic chromosome condensation; **GO:0008094:** ATPase, acting on DNA; **GO:0005524:** ATP binding; **GO:0006974:** cellular response to DNA damage stimulus; **GO:0005814:** centriole; **GO:0003682:** chromatin binding; **GO:0000775:** chromosome, centromeric region; **GO:0030261:** chromosome condensation; **GO:0007059:** chromosome segregation; **GO:0000793:** condensed chromosome; **GO:0005737:** cytoplasm; **GO:0003677:** DNA binding; **GO:0008301:** DNA binding, bending; **GO:0006266:** DNA ligation; **GO:0006259:** DNA metabolic process; **GO:0003916:** DNA topoisomerase activity; **GO:0003918:** DNA topoisomerase type II (double strand cut, ATP-hydrolyzing) activity; **GO:0009330:** DNA topoisomerase type II (double strand cut, ATP-hydrolyzing) complex; **GO:0006265:** DNA topological change; **GO:0040016:** embryonic cleavage; **GO:0019899:** enzyme binding; **GO:0051309:** female meiosis chromosome separation; **GO:0007143:** female meiotic nuclear division; **GO:0002244:** hematopoietic progenitor cell differentiation; **GO:0042826:** histone deacetylase binding; **GO:0016853:** isomerase activity; **GO:0000287:** magnesium ion binding; **GO:0046872:** metal ion binding; **GO:1905463:** negative regulation of DNA duplex unwinding; **GO:0000228:** nuclear chromosome; **GO:0005730:** nucleolus; **GO:0005654:** nucleoplasm; **GO:0000166:** nucleotide binding; **GO:0005634:** nucleus; **GO:0043065:** positive regulation of apoptotic process; **GO:0045870:** positive regulation of single stranded viral RNA replication via double stranded DNA intermediate; **GO:0045944:** positive regulation of transcription by RNA polymerase II; **GO:0005515:** protein binding; **GO:0032991:** protein-containing complex; **GO:0008022:** protein C-terminus binding; **GO:0046982:** protein heterodimerization activity; **GO:0042803:** protein homodimerization activity; **GO:0005080:** protein kinase C binding; **GO:0042752:** regulation of circadian rhythm; **GO:0000712:** resolution of meiotic recombination intermediates; **GO:0048511:** rhythmic process; **GO:1990904:** ribonucleoprotein complex; **GO:0043565:** sequence-specific DNA binding; **GO:0000819:** sister chromatid segregation; **GO:0043130:** ubiquitin binding; **GO:0005576:** extracellular region; **GO:0005615:** extracellular space; **GO:0019838:** growth factor binding; **GO:0005520:** insulin-like growth factor binding; **GO:0031994:** insulin-like growth factor I binding; **GO:0031995:** insulin-like growth factor II binding; **GO:0043568:** positive regulation of insulin-like growth factor receptor signaling pathway; **GO:0043410:** positive regulation of MAPK cascade; **GO:0001558:** regulation of cell growth; **GO:0010906:** regulation of glucose metabolic process; **GO:0040008:** regulation of growth; **GO:0043567:** regulation of insulin-like growth factor receptor signaling pathway; **GO:0044342:** type B pancreatic cell proliferation; **GO:0003779:** actin binding; **GO:0006915:** apoptotic process; **GO:0030054:** cell junction; **GO:0005856:** cytoskeleton; **GO:0005925:** focal adhesion; **GO:0008104:** protein localization; **GO:0007257:** activation of JUN kinase activity; **GO:0019722:** calcium-mediated signaling; **GO:0019957:** C-C chemokine binding; **GO:0016493:** C-C chemokine receptor activity; **GO:0038117:** C-C motif chemokine 19 receptor activity; **GO:0038121:** C-C motif chemokine 21 receptor activity; **GO:0060326:** cell chemotaxis; **GO:0009986:** cell surface; **GO:0071345:** cellular response to cytokine stimulus; **GO:0035757:**

chemokine (C-C motif) ligand 19 binding; **GO:0035758:** chemokine (C-C motif) ligand 21 binding; **GO:0004950:** chemokine receptor activity; **GO:0006935:** chemotaxis; **GO:0001768:** establishment of T cell polarity; **GO:0009897:** external side of plasma membrane; **GO:0004930:** G protein-coupled receptor activity; **GO:0007186:** G protein-coupled receptor signaling pathway; **GO:0048872:** homeostasis of number of cells; **GO:0006955:** immune response; **GO:0006954:** inflammatory response; **GO:0016021:** integral component of membrane; **GO:0048535:** lymph node development; **GO:0002518:** lymphocyte chemotaxis across high endothelial venule; **GO:0097022:** lymphocyte migration into lymph node; **GO:0097029:** mature conventional dendritic cell differentiation; **GO:0016020:** membrane; **GO:0005739:** mitochondrion; **GO:0002408:** myeloid dendritic cell chemotaxis; **GO:0032695:** negative regulation of interleukin-12 production; **GO:2000107:** negative regulation of leukocyte apoptotic process; **GO:0045060:** negative thymic T cell selection; **GO:0005886:** plasma membrane; **GO:2000147:** positive regulation of cell motility; **GO:0007204:** positive regulation of cytosolic calcium ion concentration; **GO:0002606:** positive regulation of dendritic cell antigen processing and presentation; **GO:2000510:** positive regulation of dendritic cell chemotaxis; **GO:0051491:** positive regulation of filopodium assembly; **GO:2000526:** positive regulation of glycoprotein biosynthetic process involved in immunological synapse formation; **GO:0043547:** positive regulation of GTPase activity; **GO:0002922:** positive regulation of humoral immune response; **GO:0002885:** positive regulation of hypersensitivity; **GO:2000522:** positive regulation of immunological synapse formation; **GO:0032735:** positive regulation of interleukin-12 production; **GO:0032731:** positive regulation of interleukin-1 beta production; **GO:0010759:** positive regulation of macrophage chemotaxis; **GO:0090023:** positive regulation of neutrophil chemotaxis; **GO:0050766:** positive regulation of phagocytosis; **GO:0048260:** positive regulation of receptor-mediated endocytosis; **GO:0010820:** positive regulation of T cell chemotaxis; **GO:2000525:** positive regulation of T cell costimulation; **GO:0042102:** positive regulation of T cell proliferation; **GO:0050862:** positive regulation of T cell receptor signaling pathway; **GO:0045627:** positive regulation of T-helper 1 cell differentiation; **GO:2000412:** positive regulation of thymocyte migration; **GO:0032760:** positive regulation of tumor necrosis factor production; **GO:2000547:** regulation of dendritic cell dendrite assembly; **GO:0032649:** regulation of interferon-gamma production; **GO:0032651:** regulation of interleukin-1 beta production; **GO:0002649:** regulation of tolerance induction to self antigen; **GO:0032496:** response to lipopolysaccharide; **GO:0071731:** response to nitric oxide; **GO:0034695:** response to prostaglandin E; **GO:0007165:** signal transduction; **GO:0043044:** ATP-dependent chromatin remodeling; **GO:0006325:** chromatin organization; **GO:0006338:** chromatin remodeling; **GO:0008080:** N-acetyltransferase activity; **GO:0071565:** nBAF complex; **GO:0045892:** negative regulation of transcription, DNA-templated; **GO:0007399:** nervous system development; **GO:0022008:** neurogenesis; **GO:0071564:** npBAF complex; **GO:0016922:** nuclear receptor binding; **GO:0006337:** nucleosome disassembly; **GO:0047485:** protein N-terminus binding; **GO:0003723:** RNA binding; **GO:0016514:** SWI/SNF complex; **GO:0070603:** SWI/SNF superfamily-type complex; **GO:0008150:** biological_process; **GO:0005882:** intermediate filament; **GO:0005198:** structural molecule activity; **GO:0016327:** apicolateral plasma membrane; **GO:0060706:** cell differentiation involved in embryonic placenta development; **GO:0071944:** cell periphery; **GO:0043034:** costamere; **GO:0016010:** dystrophin-associated glycoprotein complex; **GO:0007219:** Notch signaling pathway; **GO:0044877:** protein-containing complex binding; **GO:0042383:** sarcolemma; **GO:0045214:** sarcomere organization; **GO:0008307:** structural constituent of muscle; **GO:1990357:** terminal web; **GO:0030018:** Z disc; **GO:0007568:** aging; **GO:0007010:** cytoskeleton organization;

GO:0042633: hair cycle; **GO:0031069:** hair follicle morphogenesis; **GO:0045109:** intermediate filament organization; **GO:0071277:** cellular response to calcium ion; **GO:0008092:** cytoskeletal protein binding; **GO:0008544:** epidermis development; **GO:0030855:** epithelial cell differentiation; **GO:0045095:** keratin filament; **GO:0003334:** keratinocyte development; **GO:0045684:** positive regulation of epidermis development; **GO:0061303:** cornea development in camera-type eye; **GO:0060429:** epithelium development; **GO:0002009:** morphogenesis of an epithelium; **GO:0009267:** cellular response to starvation; **GO:0005829:** cytosol; **GO:0050708:** regulation of protein secretion; **GO:0045111:** intermediate filament cytoskeleton; **GO:0045616:** regulation of keratinocyte differentiation; **GO:0030280:** structural constituent of skin epidermis; **GO:0097110:** scaffold protein binding; **GO:0031424:** keratinization; **GO:0030307:** positive regulation of cell growth; **GO:0051798:** positive regulation of hair follicle development; **GO:0045727:** positive regulation of translation; **GO:0048471:** perinuclear region of cytoplasm; **GO:0007283:** spermatogenesis; **GO:0045178:** basal part of cell; **GO:0045110:** intermediate filament bundle assembly; **GO:0005622:** intracellular anatomical structure; **GO:1990254:** keratin filament binding; **GO:0061436:** establishment of skin barrier; **GO:0002376:** immune system process; **GO:0045087:** innate immune response; **GO:0045104:** intermediate filament cytoskeleton organization; **GO:0030216:** keratinocyte differentiation; **GO:0051546:** keratinocyte migration; **GO:0030336:** negative regulation of cell migration; **GO:0005200:** structural constituent of cytoskeleton; **GO:0009048:** dosage compensation by inactivation of X chromosome; **GO:0016282:** eukaryotic 43S preinitiation complex; **GO:0043024:** ribosomal small subunit binding; **GO:0006412:** translation; **GO:0006413:** translational initiation; **GO:0003743:** translation initiation factor activity; **GO:0008408:** 3'-5' exonuclease activity; **GO:0006284:** base-excision repair; **GO:0045454:** cell redox homeostasis; **GO:0070301:** cellular response to hydrogen peroxide; **GO:0005813:** centrosome; **GO:0031490:** chromatin DNA binding; **GO:0003684:** damaged DNA binding; **GO:0003906:** DNA-(apurinic or apyrimidinic site) endonuclease activity; **GO:0080111:** DNA demethylation; **GO:0006310:** DNA recombination; **GO:0006281:** DNA repair; **GO:0008311:** double-stranded DNA 3'-5' exodeoxyribonuclease activity; **GO:0008309:** double-stranded DNA exodeoxyribonuclease activity; **GO:0003691:** double-stranded telomeric DNA binding; **GO:0004519:** endonuclease activity; **GO:0005783:** endoplasmic reticulum; **GO:0004521:** endoribonuclease activity; **GO:0004527:** exonuclease activity; **GO:0016787:** hydrolase activity; **GO:0014912:** negative regulation of smooth muscle cell migration; **GO:0051059:** NF-kappaB binding; **GO:0016607:** nuclear speck; **GO:0004518:** nuclease activity; **GO:0016491:** oxidoreductase activity; **GO:0004528:** phosphodiesterase I activity; **GO:0008081:** phosphoric diester hydrolase activity; **GO:1900087:** positive regulation of G1/S transition of mitotic cell cycle; **GO:0042981:** regulation of apoptotic process; **GO:0043488:** regulation of mRNA stability; **GO:0016890:** site-specific endodeoxyribonuclease activity, specific for altered base; **GO:0000723:** telomere maintenance; **GO:0097698:** telomere maintenance via base-excision repair; **GO:0003713:** transcription coactivator activity; **GO:0005667:** transcription regulator complex; **GO:0008089:** anterograde axonal transport; **GO:0098957:** anterograde axonal transport of mitochondrion; **GO:0005776:** autophagosome; **GO:0006914:** autophagy; **GO:0043679:** axon terminus; **GO:0048403:** brain-derived neurotrophic factor binding; **GO:0042995:** cell projection; **GO:0030030:** cell projection organization; **GO:0021549:** cerebellum development; **GO:0031410:** cytoplasmic vesicle; **GO:0030425:** dendrite; **GO:0005768:** endosome; **GO:0006887:** exocytosis; **GO:0098982:** GABA-ergic synapse; **GO:0030426:** growth cone; **GO:0021979:** hypothalamus cell differentiation; **GO:0042802:** identical protein binding; **GO:0016234:** inclusion body; **GO:0044325:** ion channel binding; **GO:0005764:** lysosome; **GO:0048311**:

mitochondrion distribution; **GO:0017022:** myosin binding; **GO:1902430:** negative regulation of amyloid-beta formation; **GO:0043005:** neuron projection; **GO:0031175:** neuron projection development; **GO:0048011:** neurotrophin TRK receptor signaling pathway; **GO:0045742:** positive regulation of epidermal growth factor receptor signaling pathway; **GO:0090261:** positive regulation of inclusion body assembly; **GO:0031587:** positive regulation of inositol 1,4,5-trisphosphate-sensitive calcium-release channel activity; **GO:0050769:** positive regulation of neurogenesis; **GO:0010976:** positive regulation of neuron projection development; **GO:0032901:** positive regulation of neurotrophin production; **GO:1902857:** positive regulation of non-motile cilium assembly; **GO:0032230:** positive regulation of synaptic transmission, GABAergic; **GO:0099524:** postsynaptic cytosol; **GO:0099523:** presynaptic cytosol; **GO:0019904:** protein domain specific binding; **GO:0006605:** protein targeting; **GO:0015031:** protein transport; **GO:0017157:** regulation of exocytosis; **GO:1902513:** regulation of organelle transport along microtubule; **GO:0099149:** regulation of postsynaptic neurotransmitter receptor internalization; **GO:0008090:** retrograde axonal transport; **GO:0005102:** signaling receptor binding; **GO:0045202:** synapse; **GO:0047496:** vesicle transport along microtubule; **GO:0015629:** actin cytoskeleton; **GO:0005912:** adherens junction; **GO:0045294:** alpha-catenin binding; **GO:0086073:** bundle of His cell-Purkinje myocyte adhesion involved in cell communication; **GO:0045296:** cadherin binding; **GO:0016342:** catenin complex; **GO:0007155:** cell adhesion; **GO:0050839:** cell adhesion molecule binding; **GO:0098609:** cell-cell adhesion; **GO:0005911:** cell-cell junction; **GO:0016477:** cell migration; **GO:0071681:** cellular response to indole-3-methanol; **GO:0009898:** cytoplasmic side of plasma membrane; **GO:0106006:** cytoskeletal protein-membrane anchor activity; **GO:0030057:** desmosome; **GO:0002159:** desmosome assembly; **GO:0050982:** detection of mechanical stimulus; **GO:0005916:** fascia adherens; **GO:0071665:** gamma-catenin-TCF7L2 complex; **GO:0014704:** intercalated disc; **GO:0016328:** lateral plasma membrane; GO:0043537**:** negative regulation of blood vessel endothelial cell migration; **GO:0035257:** nuclear hormone receptor binding; **GO:0045766:** positive regulation of angiogenesis; **GO:0001954:** positive regulation of cell-matrix adhesion; **GO:0051091:** positive regulation of DNA-binding transcription factor activity; **GO:0042307:** positive regulation of protein import into nucleus; **GO:0032993:** protein-DNA complex; **GO:0019901:** protein kinase binding; **GO:0072659:** protein localization to plasma membrane; **GO:0019903:** protein phosphatase binding; **GO:0042127:** regulation of cell population proliferation; **GO:0086091:** regulation of heart rate by cardiac conduction; **GO:0098911:** regulation of ventricular cardiac muscle cell action potential; **GO:0043588:** skin development; **GO:0046849:** bone remodeling; **GO:1902494:** catalytic complex; **GO:0005518:** collagen binding; **GO:0032964:** collagen biosynthetic process; **GO:0030199:** collagen fibril organization; **GO:0043231:** intracellular membrane-bounded organelle; **GO:0017185:** peptidyl-lysine hydroxylation; **GO:0000795:** synaptonemal complex; **GO:0035909:** aorta morphogenesis; **GO:0005509:** calcium ion binding; **GO:0030199:** collagen fibril organization; **GO:0085029:** extracellular matrix assembly; **GO:0005528:** FK506 binding; **GO:0001701:** in utero embryonic development;; **GO:0016853:** isomerase activity; **GO:0005758:** mitochondrial intermembrane space; **GO:0017185:** peptidyl-lysine hydroxylation; **GO:0018208:** peptidyl-proline modification; **GO:0003755:** peptidyl-prolyl cis-trans isomerase activity; **GO:0042060:** wound healing; **GO:0009117:** nucleotide metabolic process; **GO:0006085:** acetyl-CoA biosynthetic process; **GO:0006084:** acetyl-CoA metabolic process; **GO:0003878:** ATP citrate synthase activity; **GO:0003824:** catalytic activity; **GO:0006101:** citrate metabolic process; **GO:0006633:** fatty acid biosynthetic process; **GO:0008610:** lipid biosynthetic process; **GO:0006629:** lipid metabolic process; **GO:0006107:** oxaloacetate metabolic process;

GO:0016740: transferase activity; **GO:0046912:** transferase activity, transferring acyl groups, acyl groups converted into alkyl on transfer; **GO:0035690:** cellular response to drug; **GO:0002269:** leukocyte activation involved in inflammatory response; **GO:0001774:** microglial cell activation; **GO:0003729:** mRNA binding; **GO:0017148:** negative regulation of translation; **GO:0070997:** neuron death; **GO:0150103:** reactive gliosis; **GO:0097729:** 9+2 motile cilium; **GO:0005930:** axoneme; **GO:0007420:** brain development; **GO:0090660:** cerebrospinal fluid circulation; **GO:0003341:** cilium movement; **GO:0060287:** epithelial cilium movement involved in determination of left/right asymmetry; **GO:0007507:** heart development; **GO:0030324:** lung development; **GO:0003674:** molecular_function; **GO:0120197:** mucociliary clearance; **GO:0036158:** outer dynein arm assembly; **GO:0120228:** outer dynein arm docking complex; **GO:0120229:** protein localization to motile cilium; **GO:0004113:** 2',3'-cyclic-nucleotide 3'-phosphodiesterase activity; **GO:0008344:** adult locomotory behavior; **GO:0007409:** axonogenesis; **GO:0030551:** cyclic nucleotide binding; **GO:0009214:** cyclic nucleotide catabolic process; **GO:0005874:** microtubule; **GO:0000226:** microtubule cytoskeleton organization; **GO:0005902:** microvillus; **GO:0005743:** mitochondrial inner membrane; **GO:0005741:** mitochondrial outer membrane; **GO:0043209:** myelin sheath; **GO:0035748:** myelin sheath abaxonal region; **GO:0048709:** oligodendrocyte differentiation; **GO:0031143:** pseudopodium; **GO:0046902:** regulation of mitochondrial membrane permeability; **GO:0009636:** response to toxic substance; **GO:0048513:** animal organ development; **GO:0006182:** cGMP biosynthetic process; **GO:0019934:** cGMP-mediated signaling; **GO:0003418:** growth plate cartilage chondrocyte differentiation; **GO:0003419:** growth plate cartilage chondrocyte proliferation; **GO:0005179:** hormone activity; **GO:0051427:** hormone receptor binding; **GO:0008285:** negative regulation of cell population proliferation; **GO:0032966:** negative regulation of collagen biosynthetic process; **GO:2000279:** negative regulation of DNA biosynthetic process; **GO:0051447:** negative regulation of meiotic cell cycle; **GO:1900194:** negative regulation of oocyte maturation; **GO:0005184:** neuropeptide hormone activity; **GO:0001503:** ossification; **GO:0010753:** positive regulation of cGMP-mediated signaling; **GO:0043306:** positive regulation of mast cell degranulation; **GO:0045669:** positive regulation of osteoblast differentiation; **GO:1900721:** positive regulation of uterine smooth muscle relaxation; **GO:0009791:** post-embryonic development; **GO:0006457:** protein folding; **GO:0007168:** receptor guanylyl cyclase signaling pathway; **GO:0040014:** regulation of multicellular organism growth; **GO:0022414:** reproductive process; **GO:0030141:** secretory granule; **GO:0051085:** chaperone cofactor-dependent protein refolding; **GO:0031072:** heat shock protein binding; **GO:0003924:** GTPase activity; **GO:0005525:** GTP binding; **GO:0007249:** I-kappaB kinase/NF-kappaB signaling; **GO:0051607:** defense response to virus; **GO:0003725:** double-stranded RNA binding; **GO:0004386:** helicase activity; **GO:0045824:** negative regulation of innate immune response; **GO:0039534:** negative regulation of MDA-5 signaling pathway; **GO:0039536:** negative regulation of RIG-I signaling pathway; **GO:0032480:** negative regulation of type I interferon production; **GO:0032728:** positive regulation of interferon-beta production; **GO:1900245:** positive regulation of MDA-5 signaling pathway; **GO:1900246:** positive regulation of RIG-I signaling pathway; **GO:0032481:** positive regulation of type I interferon production; **GO:0045088:** regulation of innate immune response; **GO:0009617:** response to bacterium; **GO:0009615:** response to virus; **GO:0003724:** RNA helicase activity; **GO:0003727:** single-stranded RNA binding; **GO:0008270:** zinc ion binding; **GO:0016407:** acetyltransferase activity; **GO:0005671:** Ada2/Gcn5/Ada3 transcription activator complex; **GO:0071929:** alpha-tubulin acetylation; **GO:0008283:** cell population proliferation; **GO:0000785:** chromatin; **GO:0005694:** chromosome; **GO:0010484:** H3 histone

acetyltransferase activity; **GO:0016573:** histone acetylation; **GO:0004402:** histone acetyltransferase activity; **GO:0043997:** histone acetyltransferase activity (H4-K12 specific); **GO:0000123:** histone acetyltransferase complex; **GO:0016578:** histone deubiquitination; **GO:0106229:** histone glutaryltransferase activity; **GO:0043966:** histone H3 acetylation; **GO:0044154:** histone H3-K14 acetylation; **GO:0043983:** histone H4-K12 acetylation; **GO:0106077:** histone succinylation; **GO:0106078:** histone succinyltransferase activity; **GO:0018393:** internal peptidyl-lysine acetylation; **GO:0048312:** intracellular distribution of mitochondria; **GO:0007616:** long-term memory; **GO:0022037:** metencephalon development; **GO:0030901:** midbrain development; **GO:0072686:** mitotic spindle; **GO:0035264:** multicellular organism growth; **GO:0046600:** negative regulation of centriole replication; **GO:0001843:** neural tube closure; **GO:0045252:** oxoglutarate dehydrogenase complex; **GO:0061733:** peptide-lysine-N-acetyltransferase activity; **GO:0106227:** peptidyl-lysine glutarylation; **GO:2000727:** positive regulation of cardiac muscle cell differentiation; **GO:0031346:** positive regulation of cell projection organization; **GO:0001819:** positive regulation of cytokine production; **GO:0045722:** positive regulation of gluconeogenesis; **GO:0035066:** positive regulation of histone acetylation; **GO:0045893:** positive regulation of transcription, DNA-templated; **GO:1903010**: regulation of bone development; **GO:0061035:** regulation of cartilage development; **GO:0031647:** regulation of protein stability; **GO:0045589:** regulation of regulatory T cell differentiation; **GO:2000036:** regulation of stem cell population maintenance; **GO:0048167:** regulation of synaptic plasticity; **GO:0050863:** regulation of T cell activation; **GO:0006355:** regulation of transcription, DNA-templated; **GO:0001756:** somitogenesis; **GO:0030914:** STAGA complex; **GO:0021537:** telencephalon development; **GO:0008134:** transcription factor binding; **GO:0033276:** transcription factor TFTC complex; **GO:0016746:** transferase activity, transferring acyl groups; **GO:0098993:** anchored component of synaptic vesicle membrane; **GO:0005769:** early endosome; **GO:0030139:** endocytic vesicle; **GO:0006897:** endocytosis; **GO:0012505:** endomembrane system; **GO:0007032:** endosome organization; **GO:0019003:** GDP binding; **GO:0006886:** intracellular protein transport; **GO:0005811:** lipid droplet; **GO:0048227:** plasma membrane to endosome transport; **GO:0030100:** regulation of endocytosis; **GO:0005887:** integral component of plasma membrane; **GO:0071805:** potassium ion transmembrane transport; **GO:0042391:** regulation of membrane potential; **GO:0005249:** voltage-gated potassium channel activity; **GO:0042755:** eating behavior; **GO:0060079:** excitatory postsynaptic potential; **GO:0007631:** feeding behavior; **GO:0008156:** negative regulation of DNA replication; **GO:0043267:** negative regulation of potassium ion transport; **GO:0051970:** negative regulation of transmission of nerve impulse; **GO:0007218:** neuropeptide signaling pathway; **GO:0007200:** phospholipase C-activating G protein-coupled receptor signaling pathway; **GO:0051928:** positive regulation of calcium ion transport; **GO:0120162:** positive regulation of cold-induced thermogenesis; **GO:0051971:** positive regulation of transmission of nerve impulse; **GO:0007205:** protein kinase C-activating G protein-coupled receptor signaling pathway; **GO:0046928:** regulation of neurotransmitter secretion; **GO:0042594:** response to starvation; **GO:0030431:** sleep; **GO:0001659:** temperature homeostasis; **GO:0031771:** type 1 hypocretin receptor binding; **GO:0031772:** type 2 hypocretin receptor binding; **GO:0016881:** acid-amino acid ligase activity; **GO:0006953:** acute-phase response; **GO:0071364:** cellular response to epidermal growth factor stimulus; **GO:0071363:** cellular response to growth factor stimulus; **GO:0032870:** cellular response to hormone stimulus; **GO:0019221:** cytokine-mediated signaling pathway; **GO:0006952:** defense response; **GO:0046543:** development of secondary female sexual characteristics; **GO:0046544:** development of secondary male sexual characteristics; **GO:0001228:** DNA-binding transcription activator activity, RNA

polymerase II-specific; **GO:0003700:** DNA-binding transcription factor activity; **GO:0000981:** DNA-binding transcription factor activity, RNA polymerase II-specific; **GO:0003690:** double-stranded DNA binding; **GO:0007565:** female pregnancy; **GO:0035259:** glucocorticoid receptor binding; **GO:0060397:** growth hormone receptor signaling pathway via JAK-STAT; **GO:0007595:** lactation; **GO:0019915:** lipid storage; **GO:0001889:** liver development; **GO:0001553:** luteinization; **GO:0097531:** mast cell migration; **GO:0001779:** natural killer cell differentiation; GO:0043066**:** negative regulation of apoptotic process; **GO:0045647:** negative regulation of erythrocyte differentiation; **GO:0048541:** Peyer's patch development; **GO:0042104:** positive regulation of activated T cell proliferation; **GO:0045579:** positive regulation of B cell differentiation; **GO:0008284:** positive regulation of cell population proliferation; **GO:0051272:** positive regulation of cellular component movement; **GO:0045648:** positive regulation of erythrocyte differentiation; **GO:0045588:** positive regulation of gamma-delta T cell differentiation; **GO:0050729:** positive regulation of inflammatory response; **GO:0032743:** positive regulation of interleukin-2 production; **GO:0045621:** positive regulation of lymphocyte differentiation; **GO:0045931:** positive regulation of mitotic cell cycle; **GO:0040018:** positive regulation of multicellular organism growth; **GO:0032825:** positive regulation of natural killer cell differentiation; **GO:0045954:** positive regulation of natural killer cell mediated cytotoxicity; **GO:0032819:** positive regulation of natural killer cell proliferation; **GO:0048661:** positive regulation of smooth muscle cell proliferation; **GO:0042448:** progesterone metabolic process; **GO:0046983:** protein dimerization activity; **GO:0030155:** regulation of cell adhesion; **GO:0030856:** regulation of epithelial cell differentiation; **GO:0019218:** regulation of steroid metabolic process; **GO:0006357:** regulation of transcription by RNA polymerase II; **GO:0032355:** response to estradiol; **GO:0070672:** response to interleukin-15; **GO:0070669:** response to interleukin-2; **GO:0070670:** response to interleukin-4; **GO:0043434:** response to peptide hormone; **GO:0000978:** RNA polymerase II cis-regulatory region sequence-specific DNA binding; **GO:0007548:** sex differentiation; **GO:0033077:** T cell differentiation in thymus; **GO:0043029:** T cell homeostasis; **GO:0006366:** transcription by RNA polymerase II; **GO:0097011:** cellular response to granulocyte macrophage colony-stimulating factor stimulus; **GO:0071407:** cellular response to organic cyclic compound; **GO:0060742:** epithelial cell differentiation involved in prostate gland development; **GO:0030879:** mammary gland development; **GO:0061180:** mammary gland epithelium development; **GO:0060056:** mammary gland involution; **GO:0033026:** negative regulation of mast cell apoptotic process; **GO:0018108:** peptidyl-tyrosine phosphorylation; **GO:0042301:** phosphate ion binding; **GO:0043536:** positive regulation of blood vessel endothelial cell migration; **GO:0001938:** positive regulation of endothelial cell proliferation; **GO:0060376:** positive regulation of mast cell differentiation; **GO:0070668:** positive regulation of mast cell proliferation; **GO:0060740:** prostate gland epithelium morphogenesis; **GO:0007259:** receptor signaling pathway via JAK-STAT; **GO:0038026:** reelin-mediated signaling pathway; **GO:0019218:** regulation of steroid metabolic process; **GO:0043434:** response to peptide hormone; **GO:0048708:** astrocyte differentiation; **GO:0031730:** CCR5 chemokine receptor binding; **GO:0044320:** cellular response to leptin stimulus; **GO:0097009:** energy homeostasis; **GO:0001754:** eye photoreceptor cell differentiation; **GO:0042593:** glucose homeostasis; **GO:0098978:** glutamatergic synapse; **GO:0060396:** growth hormone receptor signaling pathway; **GO:0070102:** interleukin-6-mediated signaling pathway; **GO:0030522:** intracellular receptor signaling pathway; **GO:0033210:** leptin-mediated signaling pathway; **GO:0050804:** modulation of chemical synaptic transmission; **GO:0042789:** mRNA transcription by RNA polymerase II; **GO:0010507:** negative regulation of autophagy; **GO:0060548:** negative regulation of cell death; **GO:0045820:** negative

regulation of glycolytic process; **GO:0010730:** negative regulation of hydrogen peroxide biosynthetic process; **GO:1901215:** negative regulation of neuron death; **GO:2001223:** negative regulation of neuron migration; **GO:2000635:** negative regulation of primary miRNA processing; **GO:2000737:** negative regulation of stem cell differentiation; **GO:0004879:** nuclear receptor activity; **GO:0016310:** phosphorylation; **GO:2001171:** positive regulation of ATP biosynthetic process; **GO:0030335:** positive regulation of cell migration; **GO:1900017:** positive regulation of cytokine production involved in inflammatory response; **GO:0010628:** positive regulation of gene expression; **GO:2000637:** positive regulation of gene silencing by miRNA; **GO:1902728:** positive regulation of growth factor dependent skeletal muscle satellite cell proliferation; **GO:0032733:** positive regulation of interleukin-10 production; **GO:0032755:** positive regulation of interleukin-6 production; **GO:0032757:** positive regulation of interleukin-8 production; **GO:1904685:** positive regulation of metalloendopeptidase activity; **GO:1905618:** positive regulation of miRNA mediated inhibition of translation; **GO:0051092:** positive regulation of NF-kappaB transcription factor activity; **GO:0045747:** positive regulation of Notch signaling pathway; **GO:1902895:** positive regulation of pri-miRNA transcription by RNA polymerase II; **GO:1905564:** positive regulation of vascular endothelial cell proliferation; **GO:0099527:** postsynapse to nucleus signaling pathway; **GO:0014069:** postsynaptic density; **GO:0070878:** primary miRNA binding; **GO:0006606:** protein import into nucleus; **GO:0060019:** radial glial cell differentiation; **GO:0051726:** regulation of cell cycle; **GO:0034097:** response to cytokine; **GO:0001103:** RNA polymerase II repressing transcription factor binding; **GO:0090575:** RNA polymerase II transcription regulator complex; **GO:0098685:** Schaffer collateral - CA1 synapse; **GO:0019953:** sexual reproduction; **GO:0019827:** stem cell population maintenance; **GO:0072540:** T-helper 17 cell lineage commitment; **GO:0072538:** T-helper 17 type immune response; **GO:0005901:** caveola; **GO:0006353:** DNA-templated transcription, termination; **GO:0045121:** membrane raft; **GO:0009306:** protein secretion; **GO:0019843:** rRNA binding; **GO:0042134:** rRNA primary transcript binding; **GO:0009303:** rRNA transcription; **GO:0006363:** termination of RNA polymerase I transcription; **GO:0006361:** transcription initiation from RNA polymerase I promoter; **GO:0051117:** ATPase binding; **GO:0005794:** Golgi apparatus; **GO:0030285:** integral component of synaptic vesicle membrane; **GO:0043229:** intracellular organelle; **GO:0006811:** ion transport; **GO:1902600:** proton transmembrane transport; **GO:0015078:** proton transmembrane transporter activity; **GO:0046961:** proton-transporting ATPase activity, rotational mechanism; **GO:0033179:** proton-transporting V-type ATPase, V0 domain; **GO:0016241:** regulation of macroautophagy; **GO:0008021:** synaptic vesicle; **GO:1901998:** toxin transport; **GO:0007035:** vacuolar acidification; **GO:0016471:** vacuolar proton-transporting V-type ATPase complex; **GO:0000220:** vacuolar proton-transporting V-type ATPase, V0 domain; **GO:0004561:** alpha-N-acetylglucosaminidase activity; **GO:0021680:** cerebellar Purkinje cell layer development; **GO:0070062:** extracellular exosome; **GO:0060119:** inner ear receptor cell development; **GO:0045475:** locomotor rhythm; **GO:0007040:** lysosome organization; **GO:0042474:** middle ear morphogenesis; **GO:0046548:** retinal rod cell development; **GO:0072582:** 17-beta-hydroxysteroid dehydrogenase (NADP+) activity; **GO:0035410:** dihydrotestosterone 17-beta-dehydrogenase activity; **GO:0004303:** estradiol 17-beta-dehydrogenase activity; **GO:1903924:** estradiol binding; **GO:0006703:** estrogen biosynthetic process; **GO:0050661:** NADP binding; **GO:0070401:** NADP+ binding; **GO:0005496:** steroid binding; **GO:0006694:** steroid biosynthetic process; **GO:0061370:** testosterone biosynthetic process; **GO:0047035:** testosterone dehydrogenase (NAD+) activity; **GO:0030283:** testosterone dehydrogenase [NAD(P)] activity; **GO:0009058:** biosynthetic process; **GO:0015937:** coenzyme A

biosynthetic process; **GO:0004140:** dephospho-CoA kinase activity; **GO:0016301:** kinase activity; **GO:0008152:** metabolic process; **GO:0005759:** mitochondrial matrix; **GO:0016779:** nucleotidyltransferase activity; **GO:0004595:** pantetheine-phosphate adenylyltransferase activity; **GO:0001227:** DNA-binding transcription repressor activity, RNA polymerase II-specific; **GO:0000122:** negative regulation of transcription by RNA polymerase II; **GO:0031965:** nuclear membrane; **GO:0006913:** nucleocytoplasmic transport; **GO:0000977:** RNA polymerase II transcription regulatory region sequence-specific DNA binding; **GO:1990837:** sequence-specific double-stranded DNA binding; **GO:0035538:** carbohydrate response element binding; **GO:0071333:** cellular response to glucose stimulus; **GO:0045723:** positive regulation of fatty acid biosynthetic process; **GO:0045821:** positive regulation of glycolytic process; **GO:0046889:** positive regulation of lipid biosynthetic process; **GO:0006110:** regulation of glycolytic process; **GO:0009749:** response to glucose; **GO:0050681:** androgen receptor binding; **GO:0050692:** DNA binding domain binding; **GO:0030331:** estrogen receptor binding; **GO:0051321:** meiotic cell cycle; **GO:0030374:** nuclear receptor coactivator activity; **GO:0007131:** reciprocal meiotic recombination; **GO:0046966:** thyroid hormone receptor binding; **GO:0061709:** reticulophagy; **GO:0045177:** apical part of cell; **GO:0031252:** cell leading edge; **GO:0036064:** ciliary basal body; **GO:0005929:** cilium; **GO:0000794:** condensed nuclear chromosome; **GO:0005881:** cytoplasmic microtubule; **GO:0031122:** cytoplasmic microtubule organization; **GO:0000930:** gamma-tubulin complex; **GO:0000212:** meiotic spindle organization; **GO:0007017:** microtubule-based process; **GO:0007020:** microtubule nucleation; **GO:0005815:** microtubule organizing center; **GO:0000278:** mitotic cell cycle; **GO:0000070:** mitotic sister chromatid segregation; **GO:1990498:** mitotic spindle microtubule; **GO:0007052:** mitotic spindle organization; **GO:0097730:** non-motile cilium; **GO:0000242:** pericentriolar material; **GO:0005827:** polar microtubule; **GO:0055037:** recycling endosome; **GO:0007088:** regulation of mitotic nuclear division; **GO:0005819:** spindle; **GO:0005876:** spindle microtubule; **GO:0000922:** spindle pole; **GO:0030424:** axon; **GO:0022010:** central nervous system myelination; **GO:0022011:** myelination in peripheral nervous system; **GO:0050885:** neuromuscular process controlling balance; **GO:0050884:** neuromuscular process controlling posture; **GO:0019227:** neuronal action potential propagation; **GO:0048812:** neuron projection morphogenesis; **GO:0030913:** paranodal junction assembly; **GO:0033270:** paranode region of axon; **GO:0048787:** presynaptic active zone membrane; **GO:0071205:** protein localization to juxtaparanode region of axon; **GO:0002175:** protein localization to paranode region of axon; **GO:0005918:** septate junction; **GO:0017124:** SH3 domain binding; **GO:0005884:** actin filament; **GO:0070098:** chemokine-mediated signaling pathway; **GO:0005044:** scavenger receptor activity; **GO:0019956:** chemokine binding; **GO:0006348:** chromatin silencing at telomere; **GO:0000781:** chromosome, telomeric region; **GO:0035098:** ESC/E(Z) complex; **GO:0036333:** hepatocyte homeostasis; **GO:0031507:** heterochromatin assembly; **GO:0070734:** histone H3-K27 methylation; **GO:0098532:** histone H3-K27 trimethylation; **GO:0018024:** histone-lysine N-methyltransferase activity; **GO:0046976:** histone methyltransferase activity (H3-K27 specific); **GO:0097421:** liver regeneration; **GO:0032259:** methylation; **GO:0008168:** methyltransferase activity; **GO:0031493:** nucleosomal histone binding; **GO:1904772:** response to tetrachloromethane; **GO:0003714:** transcription corepressor activity; **GO:0007189:** adenylate cyclase-activating G protein-coupled receptor signaling pathway; **GO:0034333:** adherens junction assembly; **GO:1990409:** adrenomedullin binding; **GO:0001605:** adrenomedullin receptor activity; **GO:1903143:** adrenomedullin receptor complex; **GO:1990410:** adrenomedullin receptor signaling pathway; **GO:0097643:** amylin receptor activity; **GO:0150057:** amylin receptor complex 2; **GO:0097647:** amylin receptor signaling

pathway; **GO:0001525:** angiogenesis; **GO:0070831:** basement membrane assembly; **GO:0070830:** bicellular tight junction assembly; **GO:0006816:** calcium ion transport; **GO:0009986:** cell surface; **GO:0032870:** cellular response to hormone stimulus; **GO:0035924:** cellular response to vascular endothelial growth factor stimulus; **GO:0015026:** coreceptor activity; **GO:0007186:** G protein-coupled receptor signaling pathway; **GO:0007507:** heart development; **GO:2000352:** negative regulation of endothelial cell apoptotic process; **GO:0043116:** negative regulation of vascular permeability; **GO:0032092:** positive regulation of protein binding; **GO:2001214:** positive regulation of vasculogenesis; **GO:0072659:** protein localization to plasma membrane; **GO:0043235:** receptor complex; **GO:0031623:** receptor internalization; **GO:0008217:** regulation of blood pressure; **GO:0008277:** regulation of G protein-coupled receptor signaling pathway; **GO:0002040:** sprouting angiogenesis; **GO:0097084:** vascular associated smooth muscle cell development; **GO:0001570:** vasculogenesis; **GO:0010008:** endosome membrane; **GO:0000814:** ESCRT II complex; **GO:0071985:** multivesicular body sorting pathway; **GO:0007175:** negative regulation of epidermal growth factor-activated receptor activity; **GO:0043328:** protein transport to vacuole involved in ubiquitin-dependent protein catabolic process via the multivesicular body sorting pathway; **GO:0005923:** bicellular tight junction; **GO:0030644:** cellular chloride ion homeostasis; **GO:0019869:** chloride channel inhibitor activity; **GO:0006821:** chloride transport; **GO:0072156:** distal tubule morphogenesis; **GO:0035556:** intracellular signal transduction; **GO:0050801:** ion homeostasis; **GO:0090188:** negative regulation of pancreatic juice secretion; **GO:0010766:** negative regulation of sodium ion transport; **GO:1903288:** positive regulation of potassium ion import across plasma membrane; **GO:2000651:** positive regulation of sodium ion transmembrane transporter activity; **GO:0019870:** potassium channel inhibitor activity; **GO:0004672:** protein kinase activity; **GO:0006468:** protein phosphorylation; **GO:0106310:** protein serine kinase activity; **GO:0004674:** protein serine/threonine kinase activity; **GO:0106311:** protein threonine kinase activity; **GO:0050794:** regulation of cellular process; **GO:0070294:** renal sodium ion absorption; **GO:0031305:** integral component of mitochondrial inner membrane; **GO:0033617:** mitochondrial cytochrome c oxidase assembly; **GO:0070131:** positive regulation of mitochondrial translation; **GO:0035861:** site of double-strand break; **GO:0050435:** amyloid-beta metabolic process; **GO:0000045:** autophagosome assembly; **GO:0000422:** autophagy of mitochondrion; **GO:0007049:** cell cycle; **GO:0051301:** cell division; **GO:0042149:** cellular response to glucose starvation; **GO:0006995:** cellular response to nitrogen starvation; **GO:0051607:** defense response to virus; **GO:0030425:** dendrite; **GO:0045022:** early endosome to late endosome transport; **GO:0043652:** engulfment of apoptotic cell; **GO:0019898:** extrinsic component of membrane; **GO:0051020:** GTPase binding; **GO:0045324:** late endosome to vacuole transport; **GO:0007040:** lysosome organization; **GO:0016236:** macroautophagy; **GO:0000423:** mitophagy; **GO:0007080:** mitotic metaphase plate congression; **GO:1902902:** negative regulation of autophagosome assembly; **GO:1905672:** negative regulation of lysosome organization; **GO:2000378:** negative regulation of reactive oxygen species metabolic process; **GO:0048666:** neuron development; **GO:0045335:** phagocytic vesicle; **GO:0000407:** phagophore assembly site; **GO:0043548:** phosphatidylinositol 3-kinase binding; **GO:0035032:** phosphatidylinositol 3-kinase complex, class III; **GO:0034271:** phosphatidylinositol 3-kinase complex, class III, type I; **GO:0034272:** phosphatidylinositol 3-kinase complex, class III, type II; **GO:1902425:** positive regulation of attachment of mitotic spindle microtubules to kinetochore; **GO:2000786:** positive regulation of autophagosome assembly; **GO:0010508:** positive regulation of autophagy; **GO:0010613:** positive regulation of cardiac muscle hypertrophy; **GO:2001244:** positive regulation of intrinsic apoptotic signaling pathway; **GO:0032801:** receptor catabolic process;

GO:0050790: regulation of catalytic activity; **GO:0032465:** regulation of cytokinesis; **GO:0098780:** response to mitochondrial depolarization; **GO:0051707:** response to other organism; **GO:0005802:** trans-Golgi network; **GO:0031625:** ubiquitin protein ligase binding; **GO:0061133:** endopeptidase activator activity; **GO:0097371:** MDM2/MDM4 family protein binding; **GO:2001237:** negative regulation of extrinsic apoptotic signaling pathway; **GO:0002039:** p53 binding; **GO:0010950:** positive regulation of endopeptidase activity; **GO:0008537:** proteasome activator complex; **GO:0000502:** proteasome complex; **GO:2000045:** regulation of G1/S transition of mitotic cell cycle; **GO:0061136:** regulation of proteasomal protein catabolic process; **GO:0052595:** aliphatic-amine oxidase activity; **GO:0009308:** amine metabolic process; **GO:0052594:** aminoacetone:oxygen oxidoreductase(deaminating) activity; **GO:0006584:** catecholamine metabolic process; **GO:0005507:** copper ion binding; **GO:0052596:** phenethylamine:oxygen oxidoreductase (deaminating) activity; **GO:0008131:** primary amine oxidase activity; **GO:0048038:** quinone binding; **GO:0052593:** tryptamine:oxygen oxidoreductase (deaminating) activity; **GO:0007601:** visual perception; **GO:0002523:** leukocyte migration involved in inflammatory response; **GO:1902283:** negative regulation of primary amine oxidase activity; **GO:0002675:** positive regulation of acute inflammatory response; **GO:0010828:** positive regulation of glucose transmembrane transport; **GO:0002687:** positive regulation of leukocyte migration; **GO:0046677:** response to antibiotic; **GO:0035902:** response to immobilization stress; **GO:0042632:** cholesterol homeostasis; **GO:0006094:** gluconeogenesis; **GO:0004346:** glucose-6-phosphatase activity; **GO:0051156:** glucose 6-phosphate metabolic process; **GO:0015760:** glucose-6-phosphate transport; **GO:0005980:** glycogen catabolic process; **GO:0005977:** glycogen metabolic process; **GO:0055088:** lipid homeostasis; **GO:0006796:** phosphate-containing compound metabolic process; **GO:0046838:** phosphorylated carbohydrate dephosphorylation; **GO:0016773:** phosphotransferase activity, alcohol group as acceptor; **GO:0010468:** regulation of gene expression; **GO:0008202:** steroid metabolic process; **GO:0006641:** triglyceride metabolic process; **GO:0046415:** urate metabolic process; **GO:0106074:** aminoacyl-tRNA metabolism involved in translational fidelity; **GO:0006450:** regulation of translational fidelity; **GO:0002196:** Ser-tRNA(Ala) hydrolase activity; **GO:0004813:** alanine-tRNA ligase activity; **GO:0006419:** alanyl-tRNA aminoacylation; **GO:0002161:** aminoacyl-tRNA editing activity; **GO:0004812:** aminoacyl-tRNA ligase activity; **GO:0003676:** nucleic acid binding; **GO:0043039:** tRNA aminoacylation; **GO:0051087:** chaperone binding; **GO:0051131:** chaperone-mediated protein complex assembly; **GO:0051879:** Hsp90 protein binding; **GO:0090630:** activation of GTPase activity; **GO:0005096:** GTPase activator activity; **GO:0022625:** cytosolic large ribosomal subunit; **GO:0022626:** cytosolic ribosome; **GO:0005840:** ribosome; **GO:0006364:** rRNA processing; **GO:0003735:** structural constituent of ribosome; **GO:0002281:** macrophage activation involved in immune response; **GO:1901223:** negative regulation of NIK/NF-kappaB signaling; **GO:0045089:** positive regulation of innate immune response; **GO:1901224:** positive regulation of NIK/NF-kappaB signaling; **GO:0034145:** positive regulation of toll-like receptor 4 signaling pathway; **GO:0015842:** aminergic neurotransmitter loading into synaptic vesicle; **GO:0098656:** anion transmembrane transport; **GO:0015698:** inorganic anion transport; **GO:0030001:** metal ion transport; **GO:0051612:** negative regulation of serotonin uptake; **GO:0006836:** neurotransmitter transport; **GO:0033603:** positive regulation of dopamine secretion; **GO:0005335:** serotonin:sodium symporter activity; **GO:0051610:** serotonin uptake; **GO:0035725:** sodium ion transmembrane transport; **GO:0030672:** synaptic vesicle membrane; **GO:0043195:** terminal bouton; **GO:0055085:** transmembrane transport; **GO:0022857:** transmembrane transporter activity; **GO:0042910:** xenobiotic transmembrane transporter activity;

GO:0042908: xenobiotic transport; **GO:0010637:** negative regulation of mitochondrial fusion; **GO:0007015:** actin filament organization; **GO:0005938:** cell cortex; **GO:0030865:** cortical cytoskeleton organization; **GO:0007163:** establishment or maintenance of cell polarity; **GO:0048672:** positive regulation of collateral sprouting; **GO:0032956:** regulation of actin cytoskeleton organization; **GO:0008360:** regulation of cell shape; **GO:0007264:** small GTPase mediated signal transduction; **GO:0070531:** BRCA1-A complex; **GO:0031436:** BRCA1-BARD1 complex; **GO:0071356:** cellular response to tumor necrosis factor; **GO:0007098:** centrosome cycle; **GO:0051298:** centrosome duplication; **GO:0043009:** chordate embryonic development; **GO:0006302**: double-strand break repair; **GO:0000724:** double-strand break repair via homologous recombination; **GO:0006631:** fatty acid metabolic process; **GO:0008630:** intrinsic apoptotic signaling pathway in response to DNA damage; **GO:0000800:** lateral element; **GO:0007095:** mitotic G2 DNA damage checkpoint signaling; **GO:0044818:** mitotic G2/M transition checkpoint; **GO:1902042:** negative regulation of extrinsic apoptotic signaling pathway via death domain receptors; **GO:0045717:** negative regulation of fatty acid biosynthetic process; **GO:0035067:** negative regulation of histone acetylation; **GO:0051572:** negative regulation of histone H3-K4 methylation; **GO:0051573:** negative regulation of histone H3-K9 methylation; **GO:0033147:** negative regulation of intracellular estrogen receptor signaling pathway; **GO:0016604:** nuclear body; **GO:0045739:** positive regulation of DNA repair; **GO:0051571:** positive regulation of histone H3-K4 methylation; **GO:2000617:** positive regulation of histone H3-K9 acetylation; **GO:0051574:** positive regulation of histone H3-K9 methylation; **GO:2000620:** positive regulation of histone H4-K16 acetylation; **GO:0070512:** positive regulation of histone H4-K20 methylation; **GO:0031398:** positive regulation of protein ubiquitination; **GO:0010575:** positive regulation of vascular endothelial growth factor production; **GO:**0006301: postreplication repair; **GO:0051865:** protein autoubiquitination; **GO:0085020:** protein K6-linked ubiquitination; **GO:0016567:** protein ubiquitination; **GO:0044030:** regulation of DNA methylation; **GO:0006349:** regulation of gene expression by genetic imprinting; **GO:0043627:** response to estrogen; **GO:0010212:** response to ionizing radiation; **GO:0070063:** RNA polymerase binding; **GO:0000976:** transcription regulatory region sequence-specific DNA binding; **GO:0004842:** ubiquitin-protein transferase activity; **GO:0051019:** mitogen-activated protein kinase binding; **GO:0045668:** negative regulation of osteoblast differentiation; **GO:0005654:** nucleoplasm; **GO:0030500:** regulation of bone mineralization; **GO:0032872:** regulation of stress-activated MAPK cascade; **GO:0035780:** CD80 biosynthetic process; **GO:0035781:** CD86 biosynthetic process; **GO:0042116:** macrophage activation; **GO:0043123:** positive regulation of I-kappaB kinase/NF-kappaB signaling; **GO:0045348:** positive regulation of MHC class II biosynthetic process; **GO:1904407:** positive regulation of nitric oxide metabolic process; **GO:0071013:** catalytic step 2 spliceosome; **GO:0006397:** mRNA processing; **GO:0000398:** mRNA splicing, via spliceosome; **GO:0008380:** RNA splicing; **GO:0005681:** spliceosomal complex; **GO:0000390:** spliceosomal complex disassembly; **GO:0071007:** U2-type catalytic step 2 spliceosome; **GO:0060444:** branching involved in mammary gland duct morphogenesis; **GO:0030154:** cell differentiation; **GO:0008045:** motor neuron axon guidance; **GO:0033600:** negative regulation of mammary gland epithelial cell proliferation; **GO:0045618:** positive regulation of keratinocyte differentiation; **GO:0048863:** stem cell differentiation; **GO:0071837:** HMG box domain binding; **GO:0007275:** multicellular organism development; **GO:0061056:** sclerotome development; **GO:0061053:** somite development; **GO:0001757:** somite specification; **GO:0036122:** BMP binding; **GO:0071374:** cellular response to parathyroid hormone stimulus; **GO:0008201:** heparin binding; **GO:0030514:** negative regulation of BMP signaling pathway; **GO:0090090:** negative

regulation of canonical Wnt signaling pathway; **GO:0030279:** negative regulation of ossification; **GO:0031333:** negative regulation of protein-containing complex assembly; **GO:0030178:** negative regulation of Wnt signaling pathway; **GO:0016055:** Wnt signaling pathway; **GO:0016311:** dephosphorylation; **GO:0001772:** immunological synapse; **GO:0000188:** inactivation of MAPK activity; **GO:0033549:** MAP kinase phosphatase activity; **GO:0050922:** negative regulation of chemotaxis; **GO:0042059:** negative regulation of epidermal growth factor receptor signaling pathway; **GO:0070373:** negative regulation of ERK1 and ERK2 cascade; **GO:0046329:** negative regulation of JNK cascade; **GO:0043409:** negative regulation of MAPK cascade; **GO:0050868:** negative regulation of T cell activation; **GO:0050860:** negative regulation of T cell receptor signaling pathway; **GO:0035335:** peptidyl-tyrosine dephosphorylation; **GO:1990264:** peptidyl-tyrosine dephosphorylation involved in inactivation of protein kinase activity; **GO:0016791:** phosphatase activity; **GO:0004721:** phosphoprotein phosphatase activity; **GO:0120183:** positive regulation of focal adhesion disassembly; **GO:0006470:** protein dephosphorylation; **GO:0106306:** protein serine phosphatase activity; **GO:0004722:** protein serine/threonine phosphatase activity; **GO:0106307:** protein threonine phosphatase activity; **GO:1990782:** protein tyrosine kinase binding; **GO:0004725:** protein tyrosine phosphatase activity; **GO:0008138:** protein tyrosine/serine/threonine phosphatase activity; **GO:0030971:** receptor tyrosine kinase binding; **GO:0051893:** regulation of focal adhesion assembly; **GO:0030165:** PDZ domain binding; **GO:0005575:** cellular_component; **GO:0007288:** sperm axoneme assembly

Supplementary Table S5.5. Renal total glutathione and GSH candidate genes and their relevant annotations (ChrX:49.234–51.892 ± 1 Mbp; GRCm38/mm10).[a]

				Expression (kidney)		Functional		Phenotypic (kidney-related)		
MGI Gene symbol	**Genome coordinates (strand)**	**Type**	**Known redox gene**	**GXD (MGI)**	**EEA**	**Inter Pro**	**GO**	**PW**	**EBM**	**Relevance to renal glutathione[b]**
Zdhhc9	ChrX:48171967-48208702 (-)	protein coding gene	No	X	X	X	X	--	--	Expressed in mouse kidney; GO:0005829; GO:0005783; GO:0005794; GO:0016021; GO:0031228; GO:0016020; GO:0016409; GO:0002178; GO:0018230; GO:0019706; GO:0018345; GO:0006612; GO:0043849; GO:0016740; GO:0016746
Gm24038	ChrX:48230286-48230444 (+)	snRNA gene	No	--	--	--	--	--	--	None – predicted gene
Gm39511	ChrX:48254336-48256792 (-)	lncRNA gene	No	--	--	--	--	--	--	None – predicted gene
Utp14a	ChrX:48256934-48282450 (+)	protein coding gene	No	X	X	--	X	--	--	Expressed in mouse kidney; GO:0005829; GO:0005730; GO:0005634; GO:0042254; GO:0006364; GO:0032040
9530027J09Rik	ChrX:48276792-48285426 (-)	lncRNA gene	No	--	--	--	--	--	--	None
Gm22528	ChrX:48299579-48299682 (+)	snRNA gene	No	--	--	--	--	--	--	None – predicted gene
Gm22612	ChrX:48307043-48307143 (+)	snRNA gene	No	--	--	--	--	--	--	None – predicted gene
Bcorl1	ChrX:48341358-48408049 (+)	protein coding gene	No	X	X	X	X	--	--	Expressed in mouse kidney; GO:0006325; GO:0003674; GO:0005654; GO:0005634; GO:0005886
Elf4	ChrX:48411049-48463132 (-)	protein coding gene	No	X	X	X	X	--	--	Expressed in mouse kidney; GO:0030154; GO:0003677;

										GO:0001228; GO:0003700; GO:0000981; GO:0045087; GO:0001787; GO:0001866; GO:0016604; GO:0005654; GO:0005634; GO:0016605; GO:0045944; GO:0045893; GO:0006357; GO:0006355; GO:0000978; GO:0043565; GO:1990837
5033418A18Rik	ChrX:48441605-48443111 (-)	unclassified gene	No	--	--	--	--	--	--	None
Aifm1	ChrX:48474944-48513563 (-)	protein coding gene	Yes	X	X	X	X	--	X	Expressed in mouse kidney; GO:0006919; GO:0008637; GO:0006915; GO:0005737; GO:0005829; GO:0003677; GO:0004174; GO:0071949; GO:0050660; GO:0070059; GO:0016020; GO:0005743; GO:0005758; GO:0005741; GO:0033108; GO:0032981; GO:0005739; GO:0016174; GO:0051402; GO:0030182; GO:0005634; GO:0016491; GO:0016651; GO:0043065; GO:0010942; GO:0043525; GO:0005515; GO:0046983; GO:0045041; GO:1902510; GO:0006979; Increased catalase activity, increased cellular sensitivity to hydrogen peroxide, increased superoxide dismutase level, oxidative stress (EBM – mice); Combined Oxidative

										Phosphorylation Deficiency 6 (EBM – humans)
Gm39512	ChrX:Syntenic	lncRNA gene	No	--	--	--	--	--	--	None – predicted gene
Rab33a	ChrX:48519285-48530232 (+)	protein coding gene	No	X	X	X	X	--	--	Expressed in mouse kidney; GO:0019882; GO:0005768; GO:0005794; GO:0003924; GO:0005525; GO:0016020; GO:0000166; GO:0005886
Zfp280c	ChrX:48541625-48594504 (-)	protein coding gene	No	X	--	--	X	--	--	Expressed in mouse kidney; GO:0003677; GO:0000981; GO:0046872; GO:0003676; GO:0005634; GO:0006357; GO:0006355; GO:0000978
Slc25a14	ChrX:48623418-48662298 (+)	protein coding gene	No	X	X	X	X	--	--	Expressed in mouse kidney; GO:0015297; GO:0016021; GO:0071423; GO:0015140; GO:0016020; GO:0005740; GO:0005743; GO:0031966; GO:0006839; GO:0005739; GO:0015131; GO:0015729; GO:0035435; GO:0071422; GO:0015141; GO:0015116; GO:0008272; GO:0015117; GO:0015709
Gm27828	ChrX:48644340-48644458 (+)	miRNA gene	No	X	X	--	--	--	--	Expressed in mouse kidney
Gpr119	ChrX:48667979-48674478 (-)	protein coding gene	No	--	--	--	--	--	--	None
Rbmx2	ChrX:48695004-48710719 (+)	protein coding gene	No	X	X	X	X	--	--	Expressed in mouse kidney; GO:0006397; GO:0000398; GO:0003676; GO:0005634; GO:0071011; GO:0003723; GO:0008380; GO:0005681; GO:0005686; GO:0071005

Gm595	ChrX:48841466-48877713 (-)	protein coding gene	No	--	--	--	--	--	--	None – predicted gene
Gm35107	ChrX:48884927-48906068 (+)	lncRNA gene	No	--	--	--	--	--	--	None – predicted gene
Enox2	ChrX:49009707-49288243 (-)	protein coding gene	No	X	X	X	X	--	--	Expressed in mouse kidney; GO:0009897; GO:0005576; GO:0016020; GO:0003676; GO:0016491; GO:0005886; GO:0015035; GO:0040008; GO:0048511; GO:0007624
Gm39513	ChrX:49286916-49315605 (+)	lncRNA gene	No	--	--	--	--	--	--	None – predicted gene
Gm14696	ChrX:49313321-49345237 (-)	lncRNA gene	No	--	--	--	--	--	--	None – predicted gene
Gm14697	ChrX:49332409-49447972 (-)	lncRNA gene	No	--	--	--	--	--	--	None – predicted gene
Arhgap36	ChrX:49463945-49500244 (+)	protein coding gene	No	X	--	X	X	X	--	Expressed in mouse kidney; GO:0005096; GO:0007165; Disorders of phosphorus metabolism (PW)
Olfr1320	ChrX:49683504-49684463 (+)	protein coding gene	No	--	--	--	--	--	--	None
Olfr1321	ChrX:49726973-49727932 (-)	protein coding gene	No	--	--	--	--	--	--	None
Igsf1	ChrX:49782536-49797749 (-)	protein coding gene	No	--	X	--	X	X	--	Expressed in mouse kidney; GO:0038102; GO:0015026; GO:0005576; GO:0034711; GO:0016021; GO:0016020; GO:0032926; GO:0006355; CKD stage 1 and II + pyelonephritis (PW)
n-R5s6	ChrX:49879307-49879394 (+)	rRNA gene	No	--	--	--	--	--	--	None
Olfr1322	ChrX:49885469-49886401 (-)	protein coding gene	No	--	--	--	--	--	--	None

Olfr1323	ChrX:50009306-50010235 (-)	protein coding gene	No	--	--	--	--	--	--	None
Gm23385	ChrX:50022621-50022915 (+)	unclassified non-coding RNA gene	No	--	--	--	--	--	--	None – predicted gene
Gm22288	ChrX:50405813-50405919 (+)	snRNA gene	No	--	--	--	--	--	--	None – predicted gene
Olfr1324	ChrX:50425496-50426494 (-)	protein coding gene	No	--	--	--	--	--	--	None
Gm35612	ChrX:50537389-50562598 (+)	lncRNA gene	No	--	--	--	--	--	--	None
Firre	ChrX:50563120-50635321 (-)	lncRNA gene	No	X	X	--	X	--	--	Expressed in mouse kidney; GO:0010467; GO:0003674; GO:0005654; GO:0005634
Stk26	ChrX:50841174-50893103 (+)	protein coding gene	No	X	X	--	X	--	--	Expressed in mouse kidney; GO:0016324; GO:0006915; GO:0005524; GO:0071944; GO:0009267; GO:0005737; GO:0005829; GO:0005794; GO:0005798; GO:0000139; GO:0042802; GO:0016301; GO:0000287; GO:0016020; GO:0046872; GO:0030033; GO:0030336; GO:0000166; GO:0048471; GO:0016310; GO:0046777; GO:0042803; GO:0004672; GO:0006468; GO:0004674; GO:0042981l; GO:1903205; GO:0042542; GO:0016740
Frmd7	ChrX:50895180-50942710 (-)	protein coding gene	No	X	X	X	X	--	--	Expressed in mouse kidney; GO:0042995; GO:0005856; GO:0005829; GO:0030426; GO:0005085; GO:0032091; GO:0051497; GO:0007399;

										GO:0043025; GO:0043005; GO:0005654; GO:0005886; GO:0010592; GO:0051057; GO:0005515; GO:0050790; GO:0010975
Rap2c	ChrX:51003912-51018018 (-)	protein coding gene	No	X	X	X	X	--	--	Expressed in mouse kidney; GO:0005923; GO:0044291; GO:0005737; GO:0005829; GO:0005768; GO:0090557; GO:0019003; GO:0003924; GO:0005525; GO:0016787; GO:0016020; GO:0030336; GO:0000166; GO:0005886; GO:0031954; GO:0032486; GO:0055037; GO:0055038; GO:0061097; GO:0007165; GO:0003713
Mbnl3	ChrX:51117269-51206532 (-)	protein coding gene	No	--	X	--	X	--	--	Expressed in mouse kidney; GO:0005737; GO:0046872; GO:0006397; GO:0007275; GO:0045662; GO:0005654; GO:0005634; GO:0000381; GO:0043484; GO:0003723
Gm23417	ChrX:51219110-51219192 (-)	miRNA gene	No	--	--	--	--	--	--	None – predicted gene
Hs6st2	ChrX:51387212-51681856 (-)	protein coding gene	No	X	X	--	X	--	--	Expressed in mouse kidney; GO:0017095; GO:0015015; GO:0016021; GO:0016020; GO:0008146; GO:0016740
Gm35727	ChrX:51681757-51864066 (+)	lncRNA gene	No	--	--	--	--	--	--	None – predicted gene
2900011F02Rik	ChrX:51682089-51683755 (+)	unclassified gene	No	--	--	--	--	--	--	None
Usp26	ChrX:51753959-51801233 (-)	protein coding gene	No	--	--	--	--	--	--	None

Gm22539	ChrX:51844685-51844801 (+)	snoRNA gene	No	--	X	--	--	--	--	Expressed in mouse kidney
1700080O16Rik	ChrX:51968695-51972772 (-)	protein coding gene	No	--	--	--	--	--	--	None
Gm35790	ChrX:51972854-51974700 (+)	lncRNA gene	No	--	--	--	--	--	--	None – predicted gene
Gpc4	ChrX:52053021-52165252 (-)	protein coding gene	No	X	X	X	X	--	--	Expressed in mouse kidney; GO:0031225; GO:0046658; GO:0099026; GO:0016477; GO:0009986; GO:0062023; GO:0009897; GO:0005576; GO:0005615; GO:0098978; GO:0016020; GO:0005886; GO:0098696; GO:1905606; GO:1905475; GO:0009966; GO:0045202; GO:0099560; GO:0016055
Gpc3	ChrX:52272426-52613950 (-)	protein coding gene	No	X	X	X	X	--	X	Expressed in mouse kidney; GO:0031225; GO:0046658; GO:0009887; GO:0009948; GO:0010171; GO:0030282; GO:0001658; GO:0016477; GO:0072111; GO:0072203; GO:0009986; GO:0062023; GO:0060976; GO:0035116; GO:0005576; GO:0005887; GO:0001822; GO:0030324; GO:0005764; GO:0016020; GO:0072138; GO:0072180; GO:0090090; GO:0008285; GO:0050680; GO:0045926; GO:0010466; GO:0045879; GO:0030316; GO:0030414; GO:0060422; GO:0005886; GO:0030513; GO:0090263; GO:0045807; GO:0046326;

										GO:0045732; GO:0045880; GO:2000096; GO:0005515; GO:0060828; GO:0040008; GO:2000050; GO:1905475; GO:0009966; GO:0009617; Abnormal kidney morphology, development, and weight, enlarged kidney, hydronephrosis, abnormal kidney cortex physiology (EBM – mice); Wilms Tumor 1, Nephroblastoma, Simpson–Golabi–Behmel Syndrome (EBM – humans)
Gm14582	ChrX:52296181-52333679 (+)	lncRNA gene	No	--	--	--	--	--	--	None – predicted gene
D230050J18Rik	ChrX:52350175-52351810 (-)	unclassified gene	No	--	--	--	--	--	--	None
Mir6384	ChrX:52378121-52378181 (-)	miRNA gene	No	--	--	--	--	--	--	None
Mir717	ChrX:52422407-52422515 (-)	miRNA gene	No	--	--	--	--	--	--	None
A630012P03Rik	ChrX:52575843-52619047 (+)	lncRNA gene	No	--	--	--	--	--	--	None
Mir363	ChrX:52741693-52741767 (-)	miRNA gene	No	--	X	--	X	--	--	Expressed in mouse kidney; GO:1990830; GO:0043066; GO:0002903
Mir92-2	ChrX:52741838-52741928 (-)	miRNA gene	No	X	--	--	X	--	--	Expressed in mouse kidney; GO:0071230; GO:1990830; GO:0071260; GO:0060291; GO:0043066; GO:0002903; GO:0010468; GO:0007605
Mir19b-2	ChrX:52741983-52742066 (-)	miRNA gene	No	X	--	--	X	--	--	Expressed in mouse kidney; GO:0007569; GO:1990830; GO:0060291; GO:0043066;

										GO:0002903; GO:0009617; GO:0016442
Mir20b	ChrX:52742113-52742192 (-)	miRNA gene	No	--	X	--	X	--	--	Expressed in mouse kidney; GO:0036294; GO:1904322; GO:0071241; GO:1990830; GO:0070062; GO:0043066; GO:0002903; GO:0009611; GO:0016442; GO:0007605
Mir18b	ChrX:52742331-52742413 (-)	miRNA gene	No	--	X	--	X	--	--	Expressed in mouse kidney; GO:1990830; GO:0043066; GO:0002903
Mir106a	ChrX:52742503-52742567 (-)	miRNA gene	No	--	--	--	--	--	--	None
Kis2	ChrX:52742563-52744593 (-)	lncRNA gene	No	--	--	--	--	--	--	None
Gm42407	ChrX:52760995-52763973 (+)	lncRNA gene	No	--	--	--	--	--	--	None – predicted gene
Ccdc160	ChrX:52791200-52799468 (+)	protein coding gene	No	X	X	--	--	X	--	Expressed in mouse kidney; GO:0008150; GO:0005575; GO:0003674; Nephritis and nephropathy without mention of glomerulonephritis (PW)

[a] Resource abbreviations: **EBM,** Ensembl BioMart; **EEA,** EBI Expression Atlas; **GO,** Gene Ontology; **GXD,** Gene eXpression Database; **MGI,** Mouse Genome Informatics; **PW,** PheWeb

[b] ID terms: **GO:0005829:** cytosol; **GO:0005783:** endoplasmic reticulum; **GO:0005794:** Golgi apparatus; **GO:0016021:** integral component of membrane; **GO:0031228:** intrinsic component of Golgi membrane; **GO:0016020:** membrane; **GO:0016409:** palmitoyltransferase activity; **GO:0002178:** almitoyltransferase complex; **GO:0018230:** peptidyl-L-cysteine S-palmitoylation; **GO:0019706:** protein-cysteine S-palmitoyltransferase activity; **GO:0018345:** protein palmitoylation; **GO:0006612:** protein targeting to membrane; **GO:0043849:** Ras palmitoyltransferase activity; **GO:0016740:** transferase activity; **GO:0016746:** transferase activity, transferring acyl groups; **GO:0005730:** nucleolus; **GO:0005634:** nucleus; **GO:0042254:** ribosome biogenesis; **GO:0006364:** rRNA processing; **GO:0032040:** small-subunit processome; **GO:0006325:** chromatin organization; **GO:0003674:** molecular_function; **GO:0005654:** nucleoplasm; **GO:0005886:** plasma membrane; **GO:0030154:** cell differentiation; **GO:0003677:** DNA binding; **GO:0001228:** DNA-binding transcription activator activity, RNA polymerase II-specific; **GO:0003700:** DNA-binding transcription factor activity; **GO:0000981:** DNA-binding transcription factor activity, RNA polymerase II-specific; **GO:0045087:** innate immune

response; **GO:0001787:** natural killer cell proliferation; **GO:0001866:** NK T cell proliferation; **GO:0016604:** nuclear body; **GO:0016605:** PML body; **GO:0045944:** positive regulation of transcription by RNA polymerase II; **GO:0045893:** positive regulation of transcription, DNA-templated; **GO:0006357:** regulation of transcription by RNA polymerase II; **GO:0006355:** regulation of transcription, DNA-templated; **GO:0000978:** RNA polymerase II cis-regulatory region sequence-specific DNA binding; **GO:0043565:** sequence-specific DNA binding; **GO:1990837:** sequence-specific double-stranded DNA binding; **GO:0006919:** activation of cysteine-type endopeptidase activity involved in apoptotic process; **GO:0008637:** apoptotic mitochondrial changes; **GO:0006915:** apoptotic process; **GO:0005737:** cytoplasm; **GO:0004174:** electron-transferring-flavoprotein dehydrogenase activity; **GO:0071949:** FAD binding; **GO:0050660:** flavin adenine dinucleotide binding; **GO:0070059:** intrinsic apoptotic signaling pathway in response to endoplasmic reticulum stress; **GO:0005743:** mitochondrial inner membrane; **GO:0005758:** mitochondrial intermembrane space; **GO:0005741:** mitochondrial outer membrane; **GO:0033108:** mitochondrial respiratory chain complex assembly; **GO:0032981:** mitochondrial respiratory chain complex I assembly; **GO:0005739:** mitochondrion; **GO:0016174:** NAD(P)H oxidase H2O2-forming activity; **GO:0051402:** neuron apoptotic process; **GO:0030182:** neuron differentiation; **GO:0016491:** oxidoreductase activity; **GO:0016651:** oxidoreductase activity, acting on NAD(P)H; **GO:0043065:** positive regulation of apoptotic process; **GO:0010942:** positive regulation of cell death; **GO:0043525:** positive regulation of neuron apoptotic process; **GO:0005515:** protein binding; **GO:0046983:** protein dimerization activity; **GO:0045041:** protein import into mitochondrial intermembrane space; **GO:1902510:** regulation of apoptotic DNA fragmentation; **GO:0006979:** response to oxidative stress; **GO:0019882:** antigen processing and presentation; **GO:0005768:** endosome; **GO:0003924:** GTPase activity; **GO:0005525:** GTP binding; **GO:0000166:** nucleotide binding; **GO:0046872:** metal ion binding; **GO:0003676:** nucleic acid binding; **GO:0015297:** antiporter activity; **GO:0071423:** malate transmembrane transport; **GO:0015140:** malate transmembrane transporter activity; **GO:0005740:** mitochondrial envelope; **GO:0031966:** mitochondrial membrane; **GO:0006839:** mitochondrial transport; **GO:0015131:** oxaloacetate transmembrane transporter activity; **GO:0015729:** oxaloacetate transport; **GO:0035435:** phosphate ion transmembrane transport; **GO:0071422:** succinate transmembrane transport; **GO:0015141:** succinate transmembrane transporter activity; **GO:0015116:** sulfate transmembrane transporter activity; **GO:0008272:** sulfate transport; **GO:0015117:** thiosulfate transmembrane transporter activity; **GO:0015709:** thiosulfate transport; **GO:0006397:** mRNA processing; **GO:0000398:** mRNA splicing, via spliceosome; **GO:0071011:** precatalytic spliceosome; **GO:0003723:** RNA binding; **GO:0008380:** RNA splicing; **GO:0005681:** spliceosomal complex; **GO:0005686:** U2 snRNP; **GO:0071005:** U2-type precatalytic spliceosome; **GO:0009897:** external side of plasma membrane; **GO:0005576:** extracellular region; **GO:0015035:** protein disulfide oxidoreductase activity; **GO:0040008:** regulation of growth; **GO:0048511:** rhythmic process; **GO:0007624:** ultradian rhythm; **GO:0005096:** GTPase activator activity; **GO:0007165:** signal transduction; **GO:0038102:** activin receptor antagonist activity; **GO:0015026:** coreceptor activity; **GO:0034711:** inhibin binding; **GO:0032926:** negative regulation of activin receptor signaling pathway; **GO:0010467:** gene expression; **GO:0016324:** apical plasma membrane; **GO:0005524:** ATP binding; **GO:0071944:** cell periphery; **GO:0009267:** cellular response to starvation; **GO:0005798:** Golgi-associated vesicle; **GO:0000139:** Golgi membrane; **GO:0042802:** identical protein binding; **GO:0016301:** kinase activity; **GO:0000287:** magnesium ion binding; **GO:0030033:** microvillus assembly; **GO:0030336:** negative regulation of cell migration; **GO:0048471:** perinuclear region of

cytoplasm; **GO:0016310:** phosphorylation; **GO:0046777:** protein autophosphorylation; **GO:0042803:** protein homodimerization activity; **GO:0004672:** protein kinase activity; **GO:0006468:** protein phosphorylation; **GO:0004674:** protein serine/threonine kinase activity; **GO:0042981:** regulation of apoptotic process; **GO:1903205:** regulation of hydrogen peroxide-induced cell death; **GO:0042542:** response to hydrogen peroxide; **GO:0042995:** cell projection; **GO:0005856:** cytoskeleton; **GO:0030426:** growth cone; **GO:0005085:** guanyl-nucleotide exchange factor activity; **GO:0032091:** negative regulation of protein binding; **GO:0051497:** negative regulation of stress fiber assembly; **GO:0007399:** nervous system development; **GO:0043025:** neuronal cell body; **GO:0043005:** neuron projection; **GO:0010592:** positive regulation of lamellipodium assembly; **GO:0051057:** positive regulation of small GTPase mediated signal transduction; **GO:0050790:** regulation of catalytic activity; **GO:0010975:** regulation of neuron projection development; **GO:0005923:** bicellular tight junction; **GO:0044291:** cell-cell contact zone; **GO:0090557:** establishment of endothelial intestinal barrier; **GO:0019003:** GDP binding; **GO:0016787:** hydrolase activity; **GO:0031954:** positive regulation of protein autophosphorylation; **GO:0032486:** Rap protein signal transduction; **GO:0055037:** recycling endosome; **GO:0055038:** recycling endosome membrane; **GO:0061097:** regulation of protein tyrosine kinase activity; **GO:0003713:** transcription coactivator activity; **GO:0007275:** multicellular organism development; **GO:0045662:** negative regulation of myoblast differentiation; **GO:0000381:** regulation of alternative mRNA splicing, via spliceosome; **GO:0043484:** regulation of RNA splicing; **GO:0017095:** heparan sulfate 6-O-sulfotransferase activity; **GO:0015015:** heparan sulfate proteoglycan biosynthetic process, enzymatic modification; **GO:0008146:** sulfotransferase activity; **GO:0004197:** cysteine-type endopeptidase activity; **GO:0008234:** cysteine-type peptidase activity; **GO:0000082:** G1/S transition of mitotic cell cycle; **GO:0008233:** peptidase activity; **GO:0016579:** protein deubiquitination; **GO:0018215:** protein phosphopantetheinylation; **GO:0006508:** proteolysis; **GO:0004843:** thiol-dependent ubiquitin-specific protease activity; **GO:0006511:** ubiquitin-dependent protein catabolic process; **GO:0031225:** anchored component of membrane; **GO:0046658:** anchored component of plasma membrane; **GO:0099026:** anchored component of presynaptic membrane; **GO:0016477:** cell migration; **GO:0009986:** cell surface; **GO:0062023:** collagen-containing extracellular matrix; **GO:0009897:** external side of plasma membrane; **GO:0005615:** extracellular space; **GO:0098978:** glutamatergic synapse; **GO:0098696:** regulation of neurotransmitter receptor localization to postsynaptic specialization membrane; **GO:1905606:** regulation of presynapse assembly; **GO:1905475:** regulation of protein localization to membrane; **GO:0009966:** regulation of signal transduction; **GO:0045202:** synapse; **GO:0099560:** synaptic membrane adhesion; **GO:0016055:** Wnt signaling pathway; **GO:0009887:** animal organ morphogenesis; **GO:0009948:** anterior/posterior axis specification; **GO:0010171:** body morphogenesis; **GO:0030282:** bone mineralization; **GO:0001658:** branching involved in ureteric bud morphogenesis; **GO:0072111:** cell proliferation involved in kidney development; **GO:0072203:** cell proliferation involved in metanephros development; **GO:0060976:** coronary vasculature development; **GO:0035116:** embryonic hindlimb morphogenesis; **GO:0005887:** integral component of plasma membrane; **GO:0001822:** kidney development; **GO:0030324:** lung development; **GO:0005764:** lysosome; **GO:0072138:** mesenchymal cell proliferation involved in ureteric bud development; **GO:0072180:** mesonephric duct morphogenesis; **GO:0090090:** negative regulation of canonical Wnt signaling pathway; **GO:0008285:** negative regulation of cell population proliferation; **GO:0050680:** negative regulation of epithelial cell proliferation; **GO:0045926:** negative regulation of growth; **GO:0010466:** negative regulation of peptidase activity; **GO:0045879:** negative regulation of smoothened

signaling pathway; **GO:0030316:** osteoclast differentiation; **GO:0030414:** peptidase inhibitor activity; **GO:0060422:** peptidyl-dipeptidase inhibitor activity; **GO:0030513:** positive regulation of BMP signaling pathway; **GO:0090263:** positive regulation of canonical Wnt signaling pathway; **GO:0045807:** positive regulation of endocytosis; **GO:0046326:** positive regulation of glucose import; **GO:0045732:** positive regulation of protein catabolic process; **GO:0045880:** positive regulation of smoothened signaling pathway; **GO:2000096:** positive regulation of Wnt signaling pathway, planar cell polarity pathway; **GO:0060828:** regulation of canonical Wnt signaling pathway; **GO:2000050:** regulation of non-canonical Wnt signaling pathway; **GO:0009617:** response to bacterium; **GO:1990830:** cellular response to leukemia inhibitory factor; **GO:0043066:** negative regulation of apoptotic process; **GO:0002903:** negative regulation of B cell apoptotic process; **GO:0071230:** cellular response to amino acid stimulus; **GO:0071260:** cellular response to mechanical stimulus; **GO:0060291:** long-term synaptic potentiation; **GO:0010468:** regulation of gene expression; **GO:0007605:** sensory perception of sound; **GO:0007569:** cell aging; **GO:0060291:** long-term synaptic potentiation; **GO:0016442:** RISC complex; **GO:0036294:** cellular response to decreased oxygen levels; **GO:1904322:** cellular response to forskolin; **GO:0071241:** cellular response to inorganic substance; **GO:0070062:** extracellular exosome; **GO:0009611:** response to wounding; **GO:0008150:** biological_process; **GO:0005575:** cellular_component

Supplementary Table S5.6. Results of high-resolution association mapping in outbred mice of renal glutathione phenotypes grades and serum BUN.

Sex and experimental cohort are included as additive covariates. Significant QTL position and respective Bayesian credible interval included in parentheses in Mbp on mouse chromosomes. Peaks with LOD scores > 6 included within the table.

Phenotype	**LOD**	**Chr**	**QTL Position (Mbp)**	**QTL Position (cM)**	**p value**	**Marker ID**
Total Glutathione	6.298	2	52.657 (19.817 – 61.128)	30.193 (14.085 – 35.317)	$p < 0.50$	UNCHS004964
Total Glutathione	6.428	11	100.804 (100.059 – 101.369)	63.671 (63.395 – 64.832)	$p < 0.45$	UNCHS032045
Total Glutathione	7.105	X	51.602 (49.234 – 51.892)	28.205 (25.870 – 28.316)	$p < 0.10$	UNCHS048618
GSH	6.249	2	52.657 (19.817 – 64.003)	30.193 (14.085 – 37.364)	$p < 0.55$	UNCHS004964
GSH	6.664	11	100.810 (100.059 – 101.369)	63.682 (63.395 – 64.832)	$p < 0.40$	UNC20247833
GSH	6.962	X	51.602 (49.234 – 51.892)	28.205 (25.870 – 28.316)	$p < 0.10$	UNCHS048618
GSSG	6.044	1	144.970 (143.603 – 148.590)	63.069 (62.513 – 63.371)	$p < 0.65$	UNCHS002665
GSSG	6.048	16	62.938 (61.291 – 72.202)	36.457 (36.121 – 40.793)	$p < 0.65$	JAX00209445
GSH/GSSG	6.032	13	71.522 (71.458 – 72.209)	38.009 (37.975 – 38.731)	$p < 0.65$	UNC22827479
E_h	6.258	14	22.959 (22.359 – 23.926)	12.791 (12.204 – 14.152)	$p < 0.55$	UNCHS037607
BUN	6.060	6	127.602 (125.386 – 128.618)	62.438 (59.395 – 63.065)	$p < 0.65$	UNC12048942

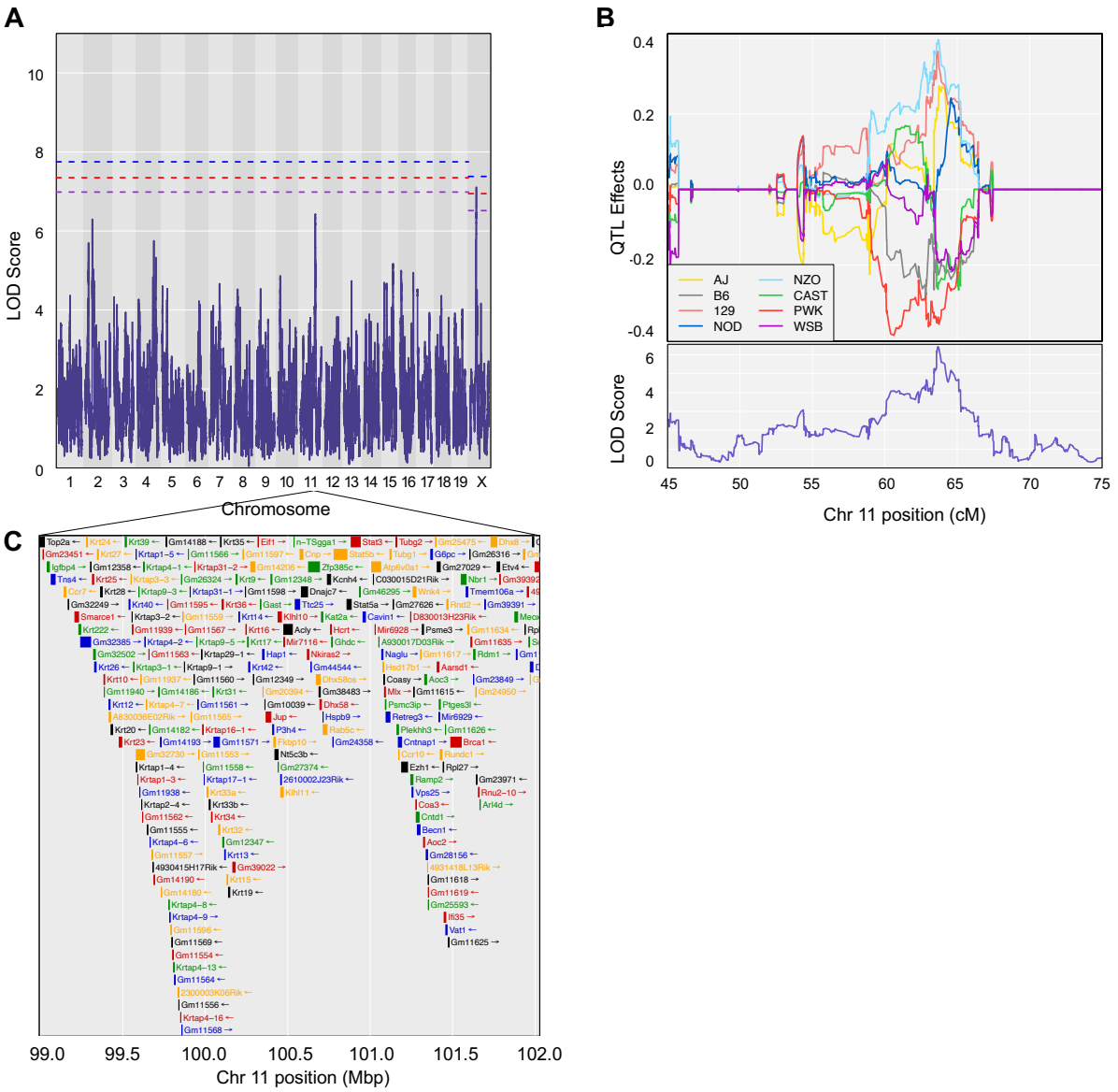

Supplementary Figure S5.1. High-resolution association mapping for renal total glutathione in outbred mice reveals a suggestive QTL on mouse chromosome 11.

A. Genome-wide scan of renal total glutathione in outbred mice shows a QTL with peak LOD score 6.428 at 100.804 Mbp (63.671 cM) on mouse chromosome 11. Permutation-derived significance thresholds are indicated by colored lines at significance (α) levels 0.05 (blue), 0.1 (red), and 0.2 (purple). Autosome LOD score thresholds were 6.99, 7.35, and 7.75 for p-values of 0.20, 0.10, and 0.05, respectively. X chromosome LOD score thresholds were 6.52, 6.95, and 7.38 for p-values of 0.20, 0.10, and 0.05, respectively. **B.** The founder allele QTL effects indicate that the PWK allele contributes to a lower renal total glutathione concentration, whereas the NZO and 129 alleles contributes to a higher renal total glutathione concentration. Each colored line represents a DO founder allele as indicated in the legend. The differences between strains are considered significant when the LOD score (bottom) crosses significance thresholds (panel A). **C.** Candidate genes found within the QTL interval relative to the MGI database. Renal total glutathione genome scan resulted in the same suggestive QTL interval on mouse chromosome 11 compared to renal GSH (Supplementary Figure S5.2).

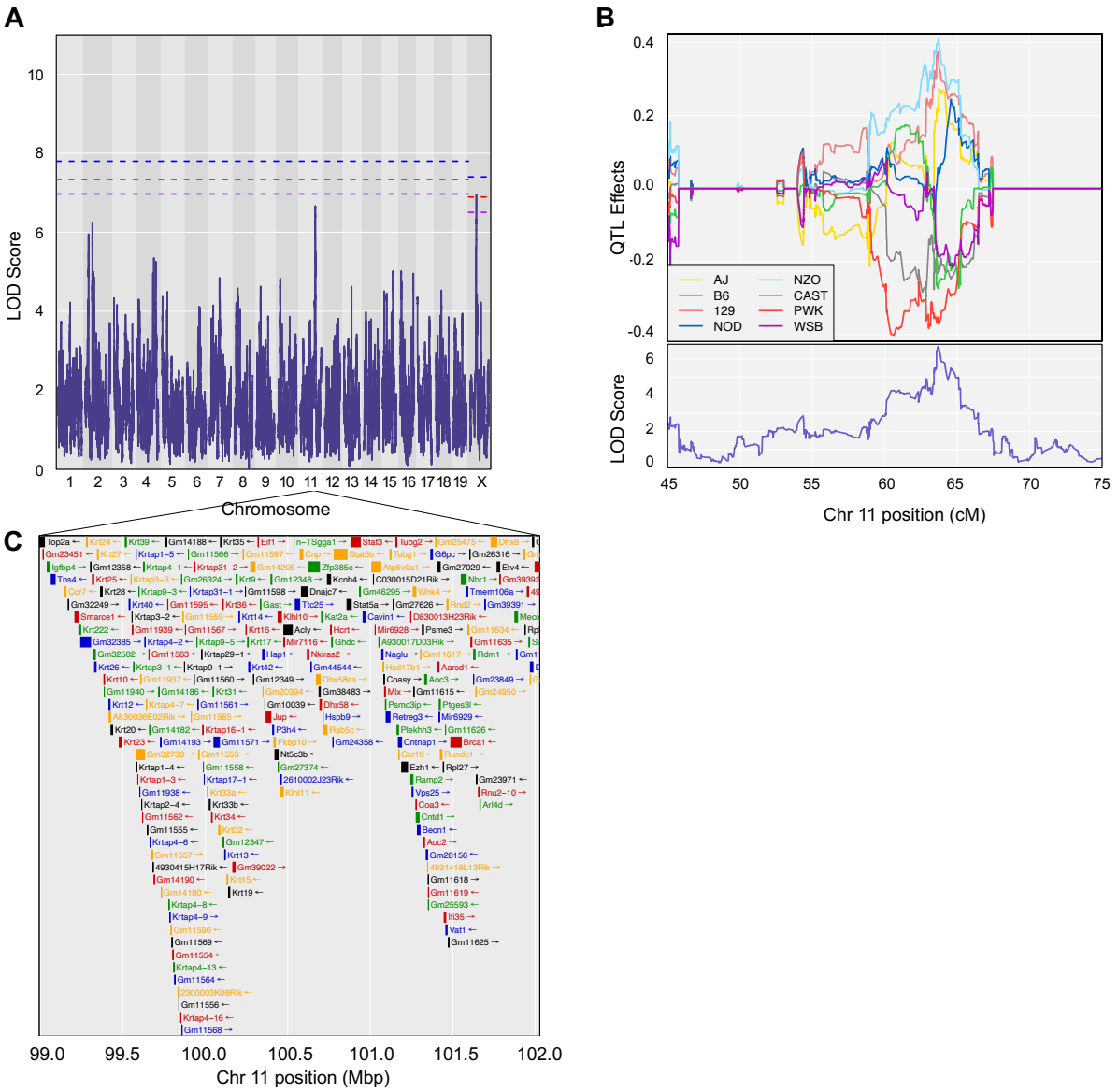

Supplementary Figure S5.2. High-resolution association mapping for renal GSH in outbred mice reveals a suggestive QTL on mouse chromosome 11.

A. Genome-wide scan of renal GSH in outbred mice shows a QTL with peak LOD score 6.664 at 100.810 Mbp (63.682 cM) on mouse chromosome 11. Permutation-derived significance thresholds are indicated by colored lines at significance (α) levels 0.05 (blue), 0.1 (red), and 0.2 (purple). Autosome LOD score thresholds were 6.97, 7.33, and 7.80 for p-values of 0.20, 0.10, and 0.05, respectively. X chromosome LOD score thresholds were 6.50, 6.89, and 7.40 for p-values of 0.20, 0.10, and 0.05, respectively. **B.** The founder allele QTL effects indicate that the PWK allele contributes to a lower renal GSH concentration, whereas the NZO and 129 alleles contributes to a higher renal GSH concentration. Each colored line represents a DO founder allele as indicated in the legend. The differences between strains are considered significant when the LOD score (bottom) crosses significance thresholds (panel A). **C.** Candidate genes found within the QTL interval relative to the MGI database. Renal GSH genome scan resulted in the same suggestive QTL interval on mouse chromosome 11 compared to renal total glutathione (Supplementary Figure S5.1).

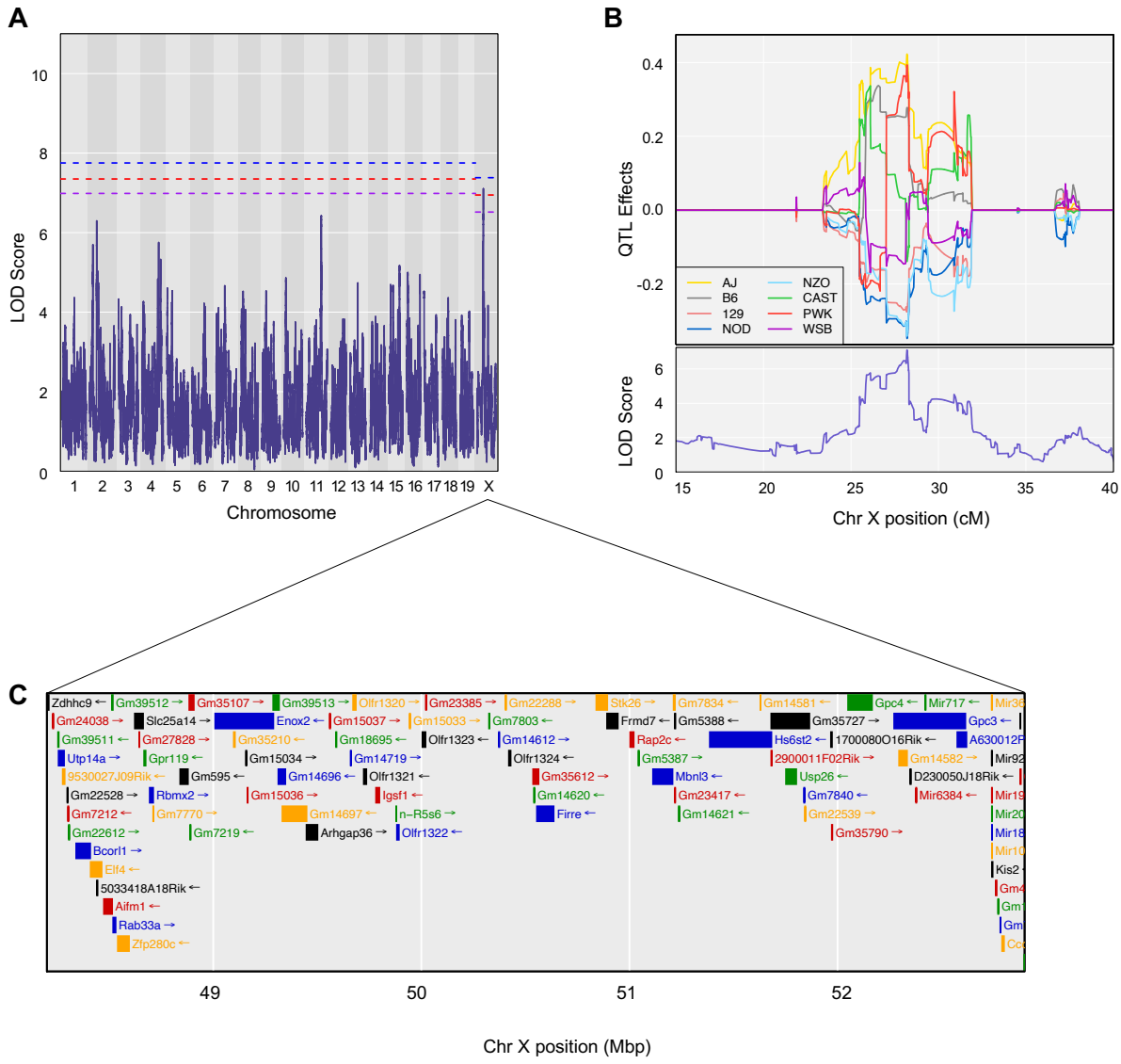

Supplementary Figure S5.3. High-resolution association mapping for renal total glutathione in outbred mice reveals a suggestive QTL on mouse chromosome X.
A. Genome-wide scan of renal total glutathione (nmol/mg) in outbred mice shows a QTL with peak LOD score 7.105 at 51.602 Mbp (28.205 cM) on mouse chromosome X. Permutation-derived significance thresholds are indicated by colored lines at significance (α) levels 0.05 (blue), 0.1 (red), and 0.2 (purple). Autosome LOD score thresholds were 6.99, 7.35, and 7.75 for p-values of 0.20, 0.10, and 0.05, respectively. X chromosome LOD score thresholds were 6.52, 6.95, and 7.38 for p-values of 0.20, 0.10, and 0.05, respectively. **B.** The founder allele QTL effects indicate that the NOD, NZO, and 129 alleles contribute to a lower renal total glutathione (nmol/mg) concentration, whereas the AJ and PWK alleles contribute to a higher renal total glutathione (nmol/mg) concentration. Each colored line represents a DO founder allele as indicated in the legend. The differences between strains are considered significant when the LOD score (bottom) crosses significance thresholds (panel A). **C.** Candidate genes found within the QTL interval relative to the MGI database. The renal GSH genome scan resulted in the same suggestive QTL interval on mouse chromosome X compared to renal total glutathione (Figure 5.3).

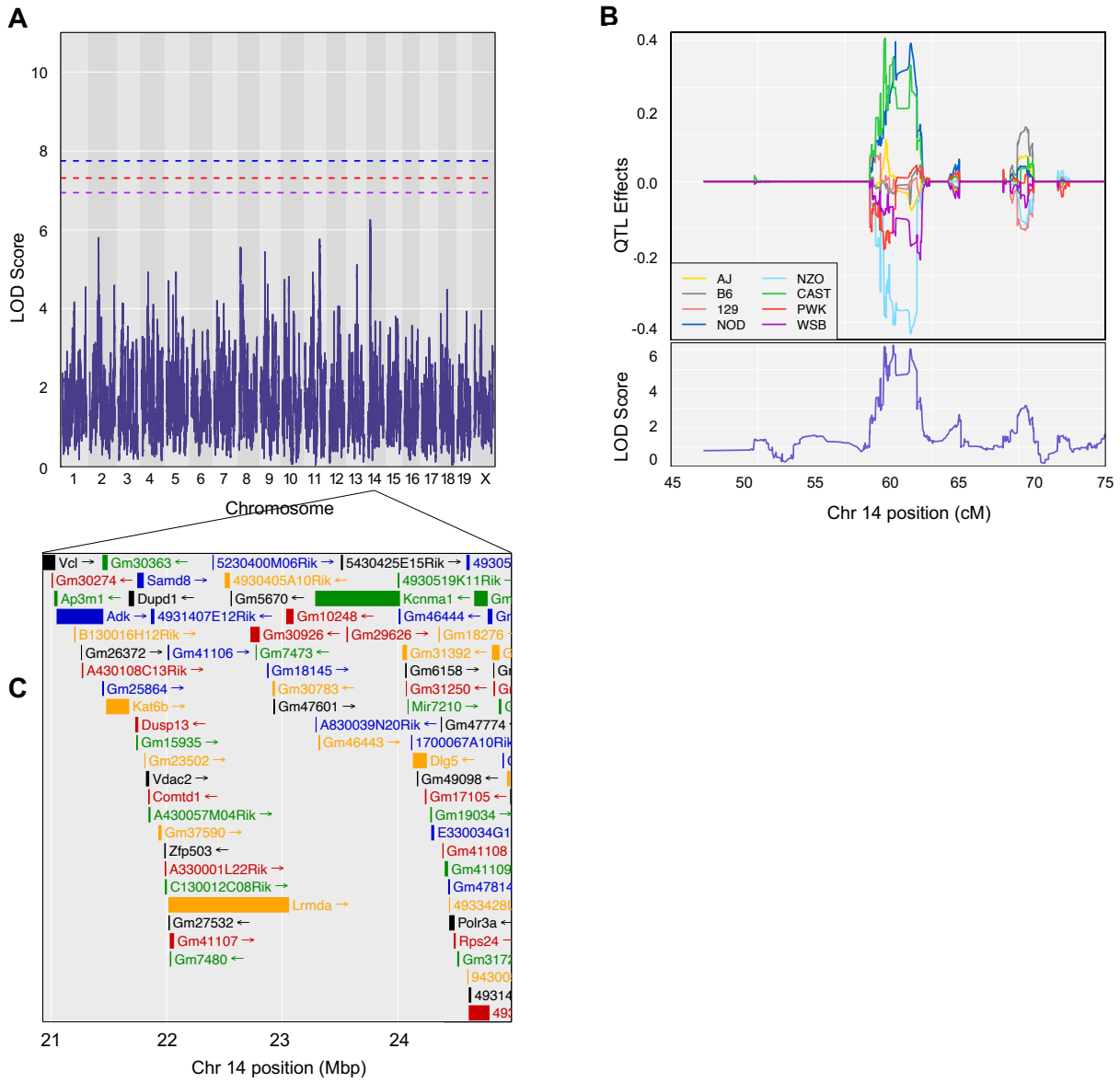

Supplementary Figure S5.4. High-resolution association mapping for renal E_h in outbred mice reveals a suggestive QTL on mouse chromosome 14.
A. Genome-wide scan of renal E_h in outbred mice shows a QTL with peak LOD score 6.258 at 22.959 Mbp (12.791 cM) on mouse chromosome 14. Permutation-derived significance thresholds are indicated by colored lines at significance (α) levels 0.05 (blue), 0.1 (red), and 0.2 (purple). **B.** The founder allele QTL effects indicate that the NZO allele contributes to a lower renal E_h concentration, whereas the NOD and CAST alleles contribute to a higher renal E_h concentration. Each colored line represents a DO founder allele as indicated in the legend. The differences between strains are considered significant when the LOD score (bottom) crosses significance thresholds (panel A). **C.** Candidate genes found within the QTL interval relative to the MGI database.

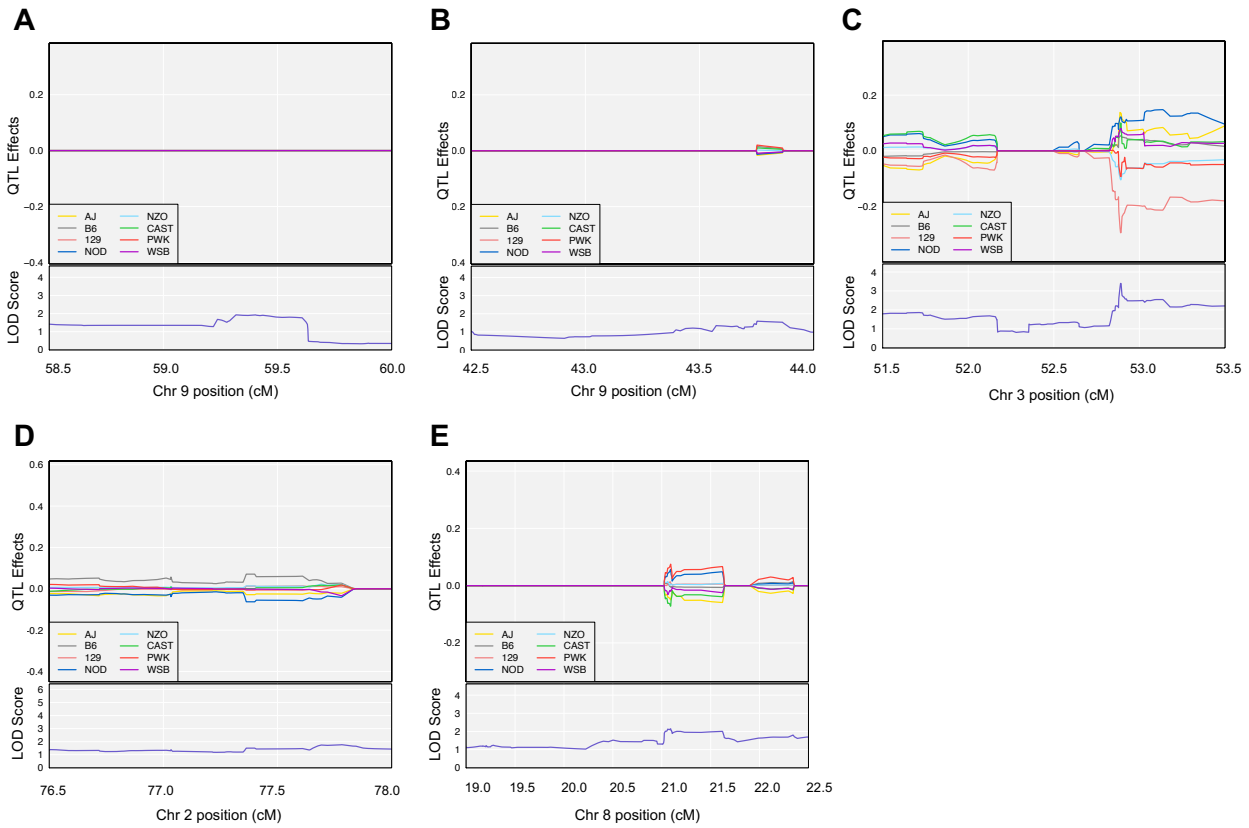

Supplementary Figure S5.5. Investigating founder allele effects on genes involved in glutathione metabolism using high-resolution mapping for renal total glutathione.
Each colored line represents a DO founder allele as indicated in the legend. The differences between strains are considered significant when the LOD score (bottom) is large enough surpass phenotype-specific permutation-derived significance thresholds. The founder allele QTL effects indicate that there are no alleles found in proximity to the **A.** Gpx1 gene location (Chromosome 9, 59.24 cM), **B.** Gclc gene location (Chromosome 9, 43.36 cM), **C.** Gclm gene location (Chromosome 3, 52.94 cM), **D.** Gs gene location (Chromosome 2, 77.26), and **E.** Gr gene location (Chromosome 8, 20.69) that contribute to a significantly lower or higher total glutathione concentration.

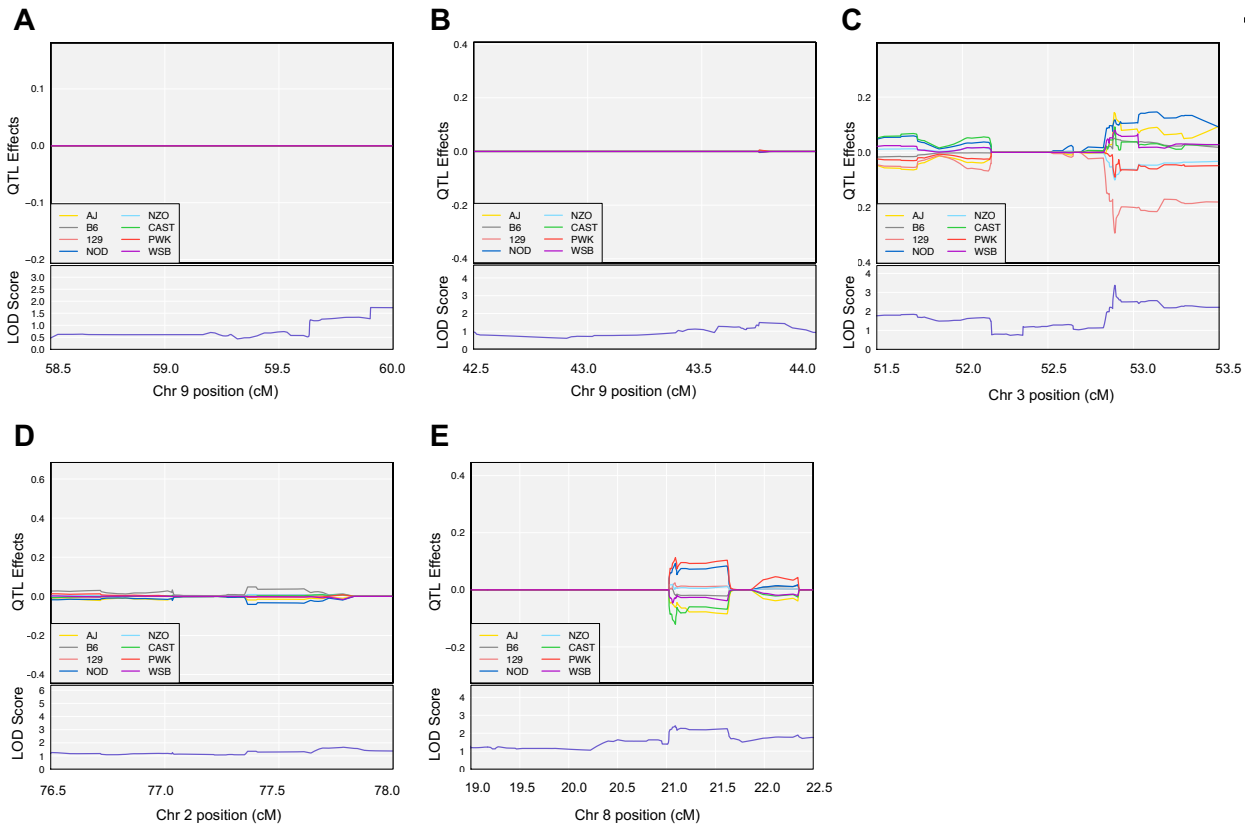

Supplementary Figure S5.6. Investigating founder allele effects on genes involved in glutathione metabolism using high-resolution mapping for renal GSH.
Each colored line represents a DO founder allele as indicated in the legend. The differences between strains are considered significant when the LOD score (bottom) is large enough surpass phenotype-specific permutation-derived significance thresholds. The founder allele QTL effects indicate that there are no alleles found in proximity to the **A.** Gpx1 gene location (Chromosome 9, 59.24 cM), **B.** Gclc gene location (Chromosome 9, 43.36 cM), **C.** Gclm gene location (Chromosome 3, 52.94 cM), **D.** Gs gene location (Chromosome 2, 77.26), and **E.** Gr gene location (Chromosome 8, 20.69) that contribute to a significantly lower or higher GSH concentration.

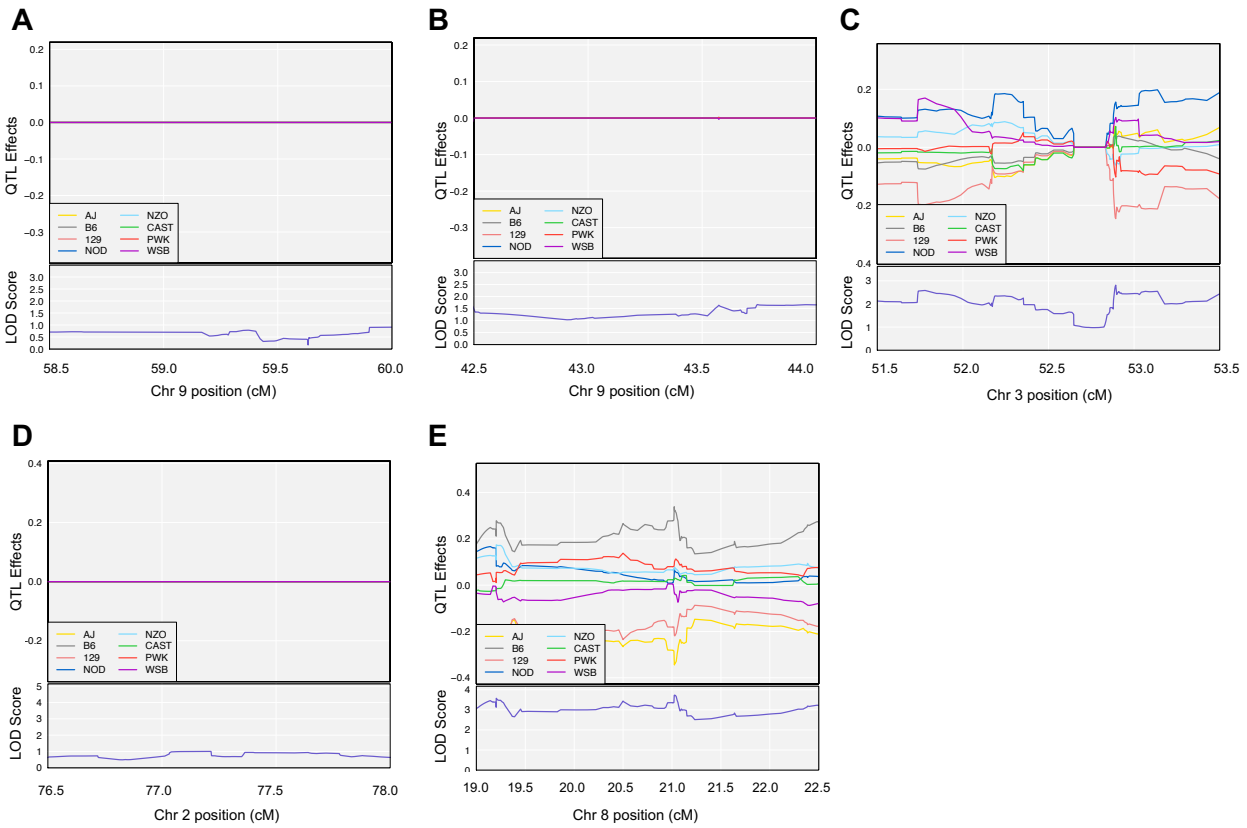

Supplementary Figure S5.7. Investigating founder allele effects on genes involved in glutathione metabolism using high-resolution mapping for renal GSSG.
Each colored line represents a DO founder allele as indicated in the legend. The differences between strains are considered significant when the LOD score (bottom) is large enough surpass phenotype-specific permutation-derived significance thresholds. The founder allele QTL effects indicate that there are no alleles found in proximity to the **A.** Gpx1 gene location (Chromosome 9, 59.24 cM), **B.** Gclc gene location (Chromosome 9, 43.36 cM), **C.** Gclm gene location (Chromosome 3, 52.94 cM), **D.** Gs gene location (Chromosome 2, 77.26), and **E.** Gr gene location (Chromosome 8, 20.69) that contribute to a significantly lower or higher GSSG concentration.

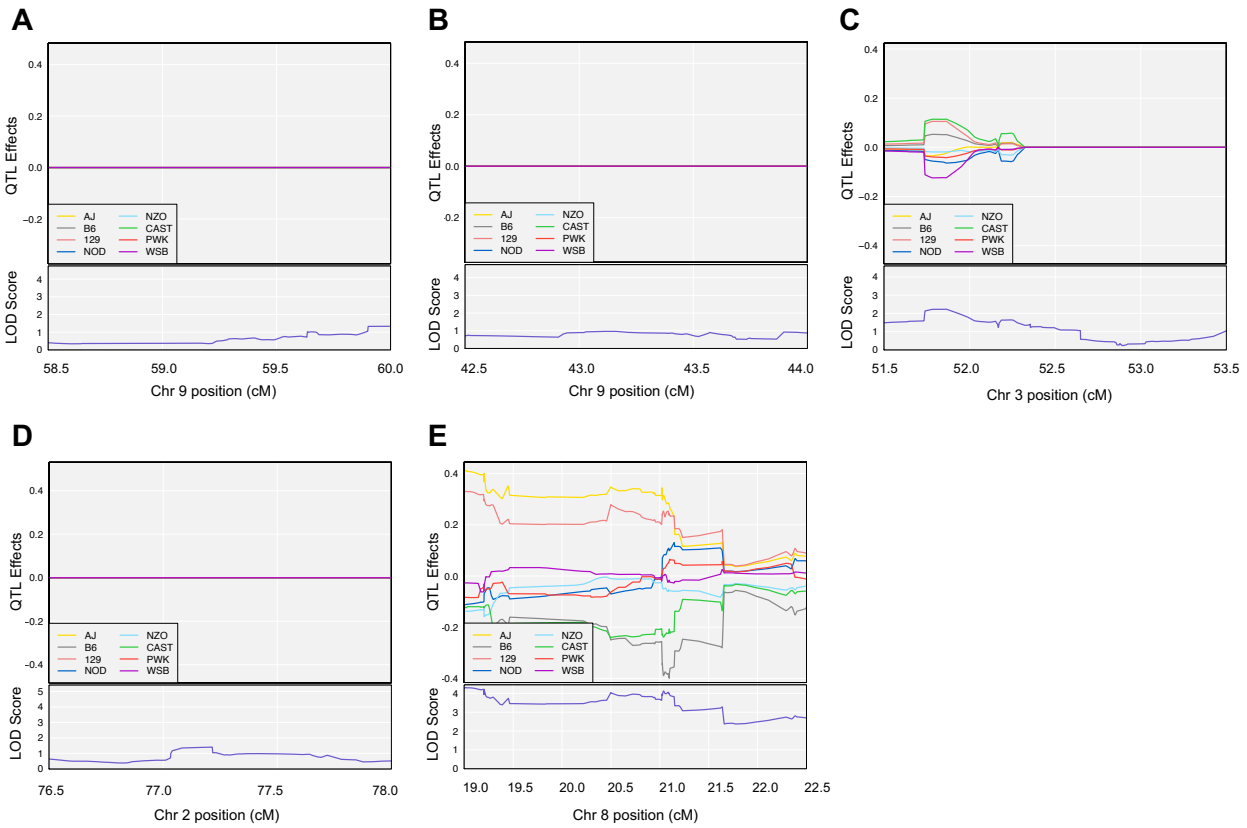

Supplementary Figure S5.8. Investigating founder allele effects on genes involved in GSH metabolism using high-resolution mapping for renal GSH/GSSG.
Each colored line represents a DO founder allele as indicated in the legend. The differences between strains are considered significant when the LOD score (bottom) is large enough surpass phenotype-specific permutation-derived significance thresholds. The founder allele QTL effects indicate that there are no alleles found in proximity to the **A.** Gpx1 gene location (Chromosome 9, 59.24 cM), **B.** Gclc gene location (Chromosome 9, 43.36 cM), **C.** Gclm gene location (Chromosome 3, 52.94 cM), **D.** Gs gene location (Chromosome 2, 77.26), and **E.** Gr gene location (Chromosome 8, 20.69) that contribute to a significantly lower or higher GSH/GSSG concentration.

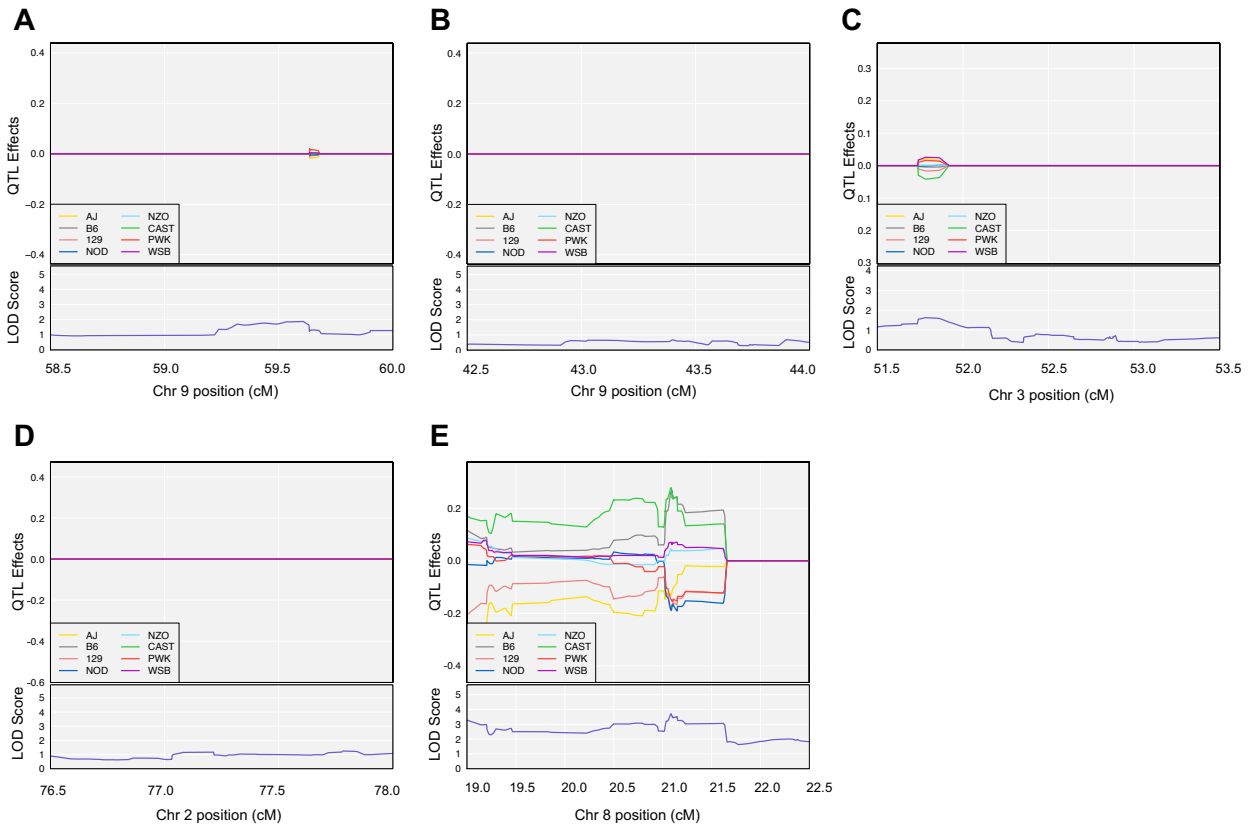

Supplementary Figure S5.9. Investigating founder allele effects on genes involved in glutathione metabolism using high-resolution mapping for renal E_h.

Each colored line represents a DO founder allele as indicated in the legend. The differences between strains are considered significant when the LOD score (bottom) is large enough surpass phenotype-specific permutation-derived significance thresholds. The founder allele QTL effects indicate that there are no alleles found in proximity to the **A.** Gpx1 gene location (Chromosome 9, 59.24 cM), **B.** Gclc gene location (Chromosome 9, 43.36 cM), **C.** Gclm gene location (Chromosome 3, 52.94 cM), **D.** Gs gene location (Chromosome 2, 77.26), and **E.** Gr gene location (Chromosome 8, 20.69) that contribute to a significantly lower or higher E_h concentration.

CHAPTER 6

CONCLUSIONS

Glutathione is a critical antioxidant that provides cells with essential protection against oxidative stress, xenobiotics, and other stressors. Cellular concentrations of glutathione reflect both its reduced, active form, GSH, and its oxidized form, GSSG. GSH is consumed through reduction-oxidation (redox) reactions and is recycled from GSSG back to GSH through the enzymatic action of glutathione reductase and reducing cofactor NADPH. In general, higher GSH levels and higher GSH/GSSG ratios protect against disease and oxidative stress. Recent evidence has revealed that glutathione phenotypes are heritable throughout aging, and that novel loci and genes may be responsible for variation in hepatic and renal glutathione. Yet to date, no genetic mapping study has been conducted on tissue-specific glutathione phenotypes. The objective of this dissertation was to investigate the genetic regulation of the GSH redox system in the liver and kidney and identify the impact of glutathione phenotype variation on health outcomes.

The study presented in Chapter 3 utilized a forward-genetics approach to quantify the natural variation in hepatic glutathione phenotypes and classify quantitative trait loci (QTL) associated with the variation. Over a 11-fold and 16-fold difference in hepatic GSH and GSSG, respectively, was observed. Through high-resolution genetic mapping, we documented a significant QTL peak for hepatic GSH/GSSG on mouse chromosome 16 at 8.998 Mbp, and suggestive peaks for hepatic $NADP^+$ and $NADP^+$/NADPH on mouse chromosome 3 at 110.517 Mbp and mouse chromosome 12 at 28.626 Mbp, respectively. Using an integrative bioinformatics approach, we identified *Socs1* as the most plausible candidate gene influencing hepatic

GSH/GSSG, and several candidate genes for the NADP(H) phenotypes. Importantly, this chapter demonstrated that knowledge is to be gained through the use of genetic mapping techniques on redox phenotypes and concluded that genes external to the basic GSH synthesis and recycling systems are responsible for glutathione variation.

The follow-up study presented in Chapter 4 evaluated the impact of hepatic glutathione variation on functional outcomes of liver health. Liver samples were collected from all outbred mice and scored for histopathological markers of non-alcoholic fatty liver disease: hepatic steatosis and hydropic degeneration. QTL mapping identified a significant QTL on mouse chromosome 18 at 17.065 Mbp associated with steatosis, as well as a significant peak on mouse chromosome 16 at 57.518 and suggestive peak on mouse chromosome 2 at 12.200 Mbp for aspartate aminotransferase. This was the first study to assess variation in NAFLD histopathological outcomes in a large, outbred cohort and advances our knowledge on the relationship between hepatic redox status and NAFLD progression.

Lastly, the study in Chapter 5, we applied a similar approach used in Chapter 3 to investigate the natural variation and genetic control of renal glutathione in DO mice. We quantified renal glutathione phenotypes and found that they varied to a similar degree compared to hepatic glutathione. In addition, genetic mapping identified a QTL peak on mouse chromosome X at 51.602 Mbp. This study classified both shared and tissue-specific loci associated with the hepatic and renal glutathione systems.

In total, this body of work presents evidence that glutathione is regulated by novel loci external to the basic glutathione metabolism systems at a tissue-specific level. We identified genomic regions responsible for hepatic and renal glutathione status, separately, and evaluated the impact of natural variation in glutathione on outcomes of health and non-alcoholic fatty liver

disease histopathology. These results support additional work into the impact of these novel genes on modulation of tissue-specific glutathione metabolism, oxidative stress, and disease. Overall, this dissertation research redefines our knowledge of redox biochemistry, its regulation, and better informs future candidate gene studies investigating glutathione and therapeutic approaches attempting to rescue and restore GSH levels.

REFERENCES

1. Rozantsev, E.G. and D.V. Loshadkin, *The history and modern problems of free radical chemistry. 100 years of free radical chemistry.* Design Monomer Polymer, 2001. 4(4): p. 281-300.

2. Knight, J.A., *Free radicals: their history and current status in aging and disease.* Ann Clin Lab Sci, 1998. 28(6): p. 331-46.

3. Phaniendra, A., D.B. Jestadi, and L. Periyasamy, *Free radicals: properties, sources, targets, and their implication in various diseases.* IJCB, 2015. 30(1): p. 11-26.

4. Petersen, R.C., M.S. Reddy, and P.R. Liu, *Advancements in Free-Radical Pathologies and an Important Treatment Solution with a Free-Radical Inhibitor.* SF J Biotechnol Biomed Eng, 2018. 1(1): p. 1003.

5. Liguori, I., et al., *Oxidative stress, aging, and diseases.* Clin Interv Aging, 2018. 13: p. 757-772.

6. Fenton, H.J.H., *LXXIII.—Oxidation of tartaric acid in presence of iron.* J Chem Soc Transact, 1894. 65(0): p. 899-910.

7. Gomberg, M., *AN INSTANCE OF TRIVALENT CARBON: TRIPHENYLMETHYL.* J Am Chem Soc, 1900. 22(11): p. 757-771.

8. Gerschman, R., et al., *Oxygen poisoning and x-irradiation: a mechanism in common.* Science, 1954. 119(3097): p. 623-6.

9. Harman, D., *Aging: A Theory Based on Free Radical and Radiation Chemistry.* J Gerontol, 1956. 11(3): p. 298-300.

10. Gutowski, M. and S. Kowalczyk, *A study of free radical chemistry: their role and pathophysiological significance.* Acta Biochim Pol, 2013. 60(1): p. 1-16.

11. Aprioku, J.S., *Pharmacology of free radicals and the impact of reactive oxygen species on the testis.* J Reprod Infertil, 2013. 14(4): p. 158-172.

12. Pizzino, G., et al., *Oxidative Stress: Harms and Benefits for Human Health.* Oxid Med Cell Longev, 2017. 2017: p. 8416763-8416763.

13. Pryor, W.A., et al., *Free radical biology and medicine: it's a gas, man!* Am J Physiol Regul Integr Comp Physiol, 2006. 291(3): p. R491-511.

14. Slater, T.F., *Free-radical mechanisms in tissue injury.* Biochem J, 1984. 222(1): p. 1-15.

15. Valko, M., H. Morris, and M.T. Cronin, *Metals, toxicity and oxidative stress.* Curr Med Chem, 2005. 12(10): p. 1161-208.

16. Aruoma, O.I., et al., *Copper-ion-dependent damage to the bases in DNA in the presence of hydrogen peroxide.* Biochem J, 1991. 273(Pt 3): p. 601-4.

17. Bahorun, T., et al., *Free Radicals and Antioxidants in Cardiovascular Health and Disease.* IJMU, 2006. 1.

18. Victor, V.M., M. Rocha, and M. De la Fuente, *Immune cells: free radicals and antioxidants in sepsis.* Int Immunopharmacol, 2004. 4(3): p. 327-47.

19. Henkel, R., *ROS and sperm DNA integrity – Implications of male accessory gland infections*, in *Clin Androl*. 2010. p. 481-488.

20. Finkel, T. and N.J. Holbrook, *Oxidants, oxidative stress and the biology of ageing.* Nature, 2000. 408(6809): p. 239-47.

21. Murphy, M.P., *How mitochondria produce reactive oxygen species.* Biochem J, 2009. 417(1): p. 1-13.

22. Nolfi-Donegan, D., A. Braganza, and S. Shiva, *Mitochondrial electron transport chain: Oxidative phosphorylation, oxidant production, and methods of measurement.* Redox Biol, 2020. 37: p. 101674.

23. Indo, H.P., et al., *A mitochondrial superoxide theory for oxidative stress diseases and aging.* J Clin Biochem Nutr, 2015. 56(1): p. 1-7.

24. Bleier, L. and S. Dröse, *Superoxide generation by complex III: From mechanistic rationales to functional consequences.* Biochim Biophys Acta Bioenerg, 2013. 1827(11): p. 1320-1331.

25. Ott, M., et al., *Mitochondria, oxidative stress and cell death.* Apoptosis, 2007. 12(5): p. 913-22.

26. Li, X., et al., *Targeting mitochondrial reactive oxygen species as novel therapy for inflammatory diseases and cancers.* J Hematol Onc, 2013. 6(1): p. 19.

27. Cao, S.S. and R.J. Kaufman, *Endoplasmic reticulum stress and oxidative stress in cell fate decision and human disease.* Antioxid Redox Signal, 2014. 21(3): p. 396-413.

28. Masuda, T., M. Shimazawa, and H. Hara, *Retinal Diseases Associated with Oxidative Stress and the Effects of a Free Radical Scavenger (Edaravone).* Oxid Med Cell Longev, 2017: p. 9208489-9208489.

29. Panday, A., et al., *NADPH oxidases: an overview from structure to innate immunity-associated pathologies.* Cell Mol Immunol, 2015. 12(1): p. 5-23.

30. Matesanz, N., et al., *Xanthine oxidase-derived extracellular superoxide anions stimulate activator protein 1 activity and hypertrophy in human vascular smooth muscle via c-Jun N-terminal kinase and p38 mitogen-activated protein kinases.* J Hypertens, 2007. 25(3): p. 609-18.

31. Assari, T., *Chronic Granulomatous Disease; fundamental stages in our understanding of CGD.* Medical Immunology (London, England), 2006. 5: p. 4.

32. Ghimire, K., et al., *Nitric oxide: what's new to NO?* Am J Physiol Cell Physiol, 2017. 312(3): p. C254-c262.

33. Radi, R., *Oxygen radicals, nitric oxide, and peroxynitrite: Redox pathways in molecular medicine.* Proc Natl Acad Sci, 2018. 115(23): p. 5839.

34. Lubos, E., D.E. Handy, and J. Loscalzo, *Role of oxidative stress and nitric oxide in atherothrombosis.* Front Biosci, 2008. 13: p. 5323-5344.

35. Johnson, R.T., et al., *Analysis of DNA repair in XP-HeLa hybrids; lack of correlation between excision repair of u.v. damage and adenovirus reactivation in an XP(D)-like cell line.* Carcinogenesis, 1986. 7(10): p. 1733-8.

36. Zangar, R.C., D.R. Davydov, and S. Verma, *Mechanisms that regulate production of reactive oxygen species by cytochrome P450.* Toxicol Appl Pharmacol, 2004. 199(3): p. 316-31.

37. Veith, A. and B. Moorthy, *Role of cytochrome P450s in the generation and metabolism of reactive oxygen species.* Curr Opin Toxicol, 2018. 7: p. 44-51.

38. Bae, Y.S., et al., *Regulation of reactive oxygen species generation in cell signaling.* Mol Cells, 2011. 32(6): p. 491-509.

39. Lobo, V., et al., *Free radicals, antioxidants and functional foods: Impact on human health.* Pharmacogn Rev, 2010. 4(8): p. 118-126.

40. Curtin, N.J., *DNA repair dysregulation from cancer driver to therapeutic target.* Nat Rev Cancer, 2012. 12(12): p. 801-817.

41. Srinivas, U.S., et al., *ROS and the DNA damage response in cancer.* Redox Biol, 2019. 25: p. 101084.

42. Cadet, J. and J.R. Wagner, *DNA base damage by reactive oxygen species, oxidizing agents, and UV radiation.* Perspect Biol, 2013. 5(2): p. a012559.

43. Clancy, S., *DNA damage & repair: mechanisms for maintaining DNA integrity.* Nat Sci Ed, 2008. 1(1): p. 103.

44. Singh, A., et al., *Oxidative Stress: Role and Response of Short Guanine Tracts at Genomic Locations.* Int J Mol Sci, 2019. 20(17): p. 4258.

45. Birben, E., et al., *Oxidative stress and antioxidant defense.* World Allergy Organ J, 2012. 5(1): p. 9-19.

46. Hofer, T., et al., *Hydrogen peroxide causes greater oxidation in cellular RNA than in DNA.* Biol Chem, 2005. 386(4): p. 333-7.

47. Alzaid, F., V.B. Patel, and V.R. Preedy, *Biomarkers of Oxidative Stress in Blood*, in *General Methods in Biomarker Research and their Applications*, V.R. Preedy and V.B. Patel, Editors. 2015, Springer Netherlands: Dordrecht. p. 567-594.

48. Butterfield, J.D. and C.P. McGraw, *Free radical pathology.* Stroke, 1978. 9(5): p. 443-445.

49. Su, L.-J., et al., *Reactive Oxygen Species-Induced Lipid Peroxidation in Apoptosis, Autophagy, and Ferroptosis.* Oxid Med Cell Longev, 2019. 2019: p. 5080843.

50. Ayala, A., M.F. Muñoz, and S. Argüelles, *Lipid peroxidation: production, metabolism, and signaling mechanisms of malondialdehyde and 4-hydroxy-2-nonenal.* Oxid Med Cell Longev, 2014. 2014: p. 360438-360438.

51. Gęgotek, A. and E. Skrzydlewska, *Biological effect of protein modifications by lipid peroxidation products.* Chem Phys Lipids, 2019. 221: p. 46-52.

52. Kikugawa, K. and M. Beppu, *Involvement of lipid oxidation products in the formation of fluorescent and cross-linked proteins.* Chem Phys Lipids, 1987. 44(2-4): p. 277-96.

53. Marnett, L.J., *Lipid peroxidation-DNA damage by malondialdehyde.* Mutat Res, 1999. 424(1-2): p. 83-95.

54. Gentile, F., et al., *DNA damage by lipid peroxidation products: implications in cancer, inflammation and autoimmunity.* AIMS Genet, 2017. 4(2): p. 103-137.

55. Saxena, A., H. Sonowal, and K.V. Ramana, *Chapter 32 - Transcriptional Factor Modulation by Lipid Peroxidation-Derived Aldehydes*, in *The Molecular Nutrition of Fats*, V.B. Patel, Editor. 2019, Academic Press. p. 419-431.

56. Kalish, J. and F.B. Pomposelli, *Chapter 55 - Diabetic Foot and Vascular Complications*, in *Endocrinology: Adult and Pediatric (Seventh Edition)*, J.L. Jameson, et al., Editors. 2016, W.B. Saunders: Philadelphia. p. 958-966.e2.

57. Mrowicka, M., *[Free-radical reactions in diabetes mellitus].* Pol Merkur Lekarski, 2005. 19(112): p. 571-6.

58. Matough, F.A., et al., *The role of oxidative stress and antioxidants in diabetic complications.* SQUMJ, 2012. 12(1): p. 5-18.

59. Kaneto, H., et al., *Role of Reactive Oxygen Species in the Progression of Type 2 Diabetes and Atherosclerosis.* Mediators of Inflammation, 2010. 2010: p. 453892.

60. Tan, A.L.Y., J.M. Forbes, and M.E. Cooper, *AGE, RAGE, and ROS in Diabetic Nephropathy.* Semin Nephrol, 2007. 27(2): p. 130-143.

61. Butterfield, D.A., et al., *Structural and functional changes in proteins induced by free radical-mediated oxidative stress and protective action of the antioxidants N-tert-butyl-alpha-phenylnitrone and vitamin E.* Ann N Y Acad Sci, 1998. 854: p. 448-62.

62. Davies, M.J., *Protein oxidation and peroxidation.* Biochem J, 2016. 473(7): p. 805-825.

63. Sibrian-Vazquez, M., et al., *Homocystamides promote free-radical and oxidative damage to proteins.* Proc Natl Acad Sci, 2010. 107(2): p. 551.

64. Pryor, W.A., X. Jin, and G.L. Squadrito, *One- and two-electron oxidations of methionine by peroxynitrite.* Proc Natl Acad Sci, 1994. 91(23): p. 11173-7.

65. Brodie, A.E. and D.J. Reed, *Cellular recovery of glyceraldehyde-3-phosphate dehydrogenase activity and thiol status after exposure to hydroperoxides.* Arch Biochem Biophys, 1990. 276(1): p. 212-8.

66. Chevion, M., E. Berenshtein, and E.R. Stadtman, *Human studies related to protein oxidation: protein carbonyl content as a marker of damage.* Free Radic Res, 2000. 33 Suppl: p. S99-108.

67. Thannickal, V.J. and B.L. Fanburg, *Reactive oxygen species in cell signaling.* Am J Physiol Lung Cell Mol Physiol, 2000. 279(6): p. L1005-L1028.

68. Turpaev, K.T., *Reactive oxygen species and regulation of gene expression.* Biochemistry, 2002. 67(3): p. 281-92.

69. Ryter, S.W., et al., *Mechanisms of Cell Death in Oxidative Stress.* Antioxid Redox Signal, 2006. 9(1): p. 49-89.

70. Espinosa-Diez, C., et al., *Antioxidant responses and cellular adjustments to oxidative stress.* Redox Biol, 2015. 6: p. 183-197.

71. Klotz, L.-O., et al., *Redox regulation of FoxO transcription factors.* Redox biology, 2015. 6: p. 51-72.

72. Ponugoti, B., G. Dong, and D. Graves, *Role of Forkhead Transcription Factors in Diabetes-Induced Oxidative Stress.* Exp Diab Res, 2012. 2012: p. 939751.

73. Vomund, S., et al., *Nrf2, the Master Regulator of Anti-Oxidative Responses.* Int J Mol Sci, 2017. 18(12): p. 2772.

74. Petri, S., S. Körner, and M. Kiaei, *Nrf2/ARE Signaling Pathway: Key Mediator in Oxidative Stress and Potential Therapeutic Target in ALS.* Neuro Res Int, 2012. 2012: p. 878030.

75. Bhakkiyalakshmi, E., D. Sireesh, and K.M. Ramkumar, *Chapter 12 - Redox Sensitive Transcription via Nrf2-Keap1 in Suppression of Inflammation*, in *Immunity and Inflammation in Health and Disease*, S. Chatterjee, W. Jungraithmayr, and D. Bagchi, Editors. 2018, Academic Press. p. 149-161.

76. Ma, Q., *Role of nrf2 in oxidative stress and toxicity.* Ann Rev Pharm Toxic, 2013. 53: p. 401-426.

77. Yalcin, S., et al., *Oxidative Stress-Mediated Activation of AKT/mTOR Signaling Pathway Leads to Myeloproliferative Syndrome in FoxO3 Null Mice: A Role for Lnk Adaptor Protein.* Blood, 2008. 112(11): p. 509-509.

78. Bendavit, G., et al., *Nrf2 Transcription Factor Can Directly Regulate mTOR: LINKING CYTOPROTECTIVE GENE EXPRESSION TO A MAJOR METABOLIC REGULATOR THAT GENERATES REDOX ACTIVITY.* J Biol Chem, 2016. 291(49): p. 25476-25488.

79. Wang, J., X. Yang, and J. Zhang, *Bridges between mitochondrial oxidative stress, ER stress and mTOR signaling in pancreatic β cells.* Cell Signal, 2016. 28(8): p. 1099-1104.

80. Su, K.-H. and C. Dai, *mTORC1 senses stresses: Coupling stress to proteostasis.* BioEssays, 2017. 39(5): p. 10.1002/bies.201600268.

81. Woo, Y., et al., *mTOR-Mediated Antioxidant Activation in Solid Tumor Radioresistance.* J Oncol, 2019. 2019: p. 5956867.

82. Lingappan, K., *NF-κB in Oxidative Stress.* Curr Opin Toxic, 2018. 7: p. 81-86.

83. Salzano, S., et al., *Linkage of inflammation and oxidative stress via release of glutathionylated peroxiredoxin-2, which acts as a danger signal.* Proc Natl Acad Sci, 2014. 111(33): p. 12157.

84. Liu, T., et al., *NF-κB signaling in inflammation.* Signal Transduct Target Ther, 2017. 2: p. 17023.

85. Naik, E. and V.M. Dixit, *Mitochondrial reactive oxygen species drive proinflammatory cytokine production.* J Exp Med, 2011. 208(3): p. 417-420.

86. Martinon, F., *Signaling by ROS drives inflammasome activation.* Eur J Immunol, 2010. 40(3): p. 616-9.

87. Yang, Y., et al., *Programmed cell death and its role in inflammation.* Mil Med Res, 2015. 2: p. 12-12.

88. Kerr, J.F.R., A.H. Wyllie, and A.R. Currie, *Apoptosis: A Basic Biological Phenomenon with Wideranging Implications in Tissue Kinetics.* British Journal of Cancer, 1972. 26(4): p. 239-257.

89. Redza-Dutordoir, M. and D.A. Averill-Bates, *Activation of apoptosis signalling pathways by reactive oxygen species.* Biochim Biophys Acta Mol Cell Res, 2016. 1863(12): p. 2977-2992.

90. Li, J. and J. Yuan, *Caspases in apoptosis and beyond.* Oncogene, 2008. 27(48): p. 6194-6206.

91. Liu, D. and Y. Xu, *p53, oxidative stress, and aging.* Antioxid Redox Signal, 2011. 15(6): p. 1669-1678.

92. Lane, D.P., *p53, guardian of the genome.* Nature, 1992. 358(6381): p. 15-16.

93. Zilfou, J.T. and S.W. Lowe, *Tumor suppressive functions of p53.* Cold Spring Harb Perspect Biol, 2009. 1(5): p. a001883-a001883.

94. Chandrasekaran, A., M.D.P.S. Idelchik, and J.A. Melendez, *Redox control of senescence and age-related disease.* Redox Biol, 2017. 11: p. 91-102.

95. Lawless, C., et al., *A stochastic step model of replicative senescence explains ROS production rate in ageing cell populations.* PloS one, 2012. 7(2): p. e32117-e32117.

96. Pole, A., M. Dimri, and G. Dimri, *Oxidative stress, cellular senescence and ageing.* AIMS Mol Sci, 2016. 3(3): p. 300-324.

97. Choi, K., et al., *Oxidative stress-induced necrotic cell death via mitochondira-dependent burst of reactive oxygen species.* Curr Neurovasc Res, 2009. 6(4): p. 213-22.

98. Koh, S.W.M. and J. Cheng, *The Choice of Apoptosis vs Necrosis in Oxidative Stress–Induced Death in Corneal Endothelial Cells in situ in Organ Cultures: The Effect of VIP.* Invest Ophthalmol Vis Sci, 2005. 46(13): p. 4712-4712.

99. Festjens, N., T. Vanden Berghe, and P. Vandenabeele, *Necrosis, a well-orchestrated form of cell demise: Signalling cascades, important mediators and concomitant immune response.* Biochim Biophys Acta Bioenerg, 2006. 1757(9): p. 1371-1387.

100. Ke, Y., et al., *The Role of PARPs in Inflammation-and Metabolic-Related Diseases: Molecular Mechanisms and Beyond.* Cells, 2019. 8(9): p. 1047.

101. Martínez-Zamudio, R.I. and H.C. Ha, *PARP1 enhances inflammatory cytokine expression by alteration of promoter chromatin structure in microglia.* Brain Behav, 2014. 4(4): p. 552-565.

102. Aggarwal, V., et al., *Role of Reactive Oxygen Species in Cancer Progression: Molecular Mechanisms and Recent Advancements.* Biomolecules, 2019. 9(11): p. 735.

103. Liou, G.-Y. and P. Storz, *Reactive oxygen species in cancer.* Free Rad Res, 2010. 44(5): p. 479-496.

104. Kruk, J., K. Kubasik-Kladna, and H.Y. Aboul-Enein, *The Role Oxidative Stress in the Pathogenesis of Eye Diseases: Current Status and a Dual Role of Physical Activity.* Mini Rev Med Chem, 2015. 16(3): p. 241-57.

105. Seen, S. and L. Tong, *Dry eye disease and oxidative stress.* Acta Ophthalmologica, 2018. 96(4): p. e412-e420.

106. Dogru, M., et al., *Potential Role of Oxidative Stress in Ocular Surface Inflammation and Dry Eye Disease.* Invest Ophthalmol Vis Sci, 2018. 59(14): p. DES163-DES168.

107. Shaheen, B.S., M. Bakir, and S. Jain, *Corneal nerves in health and disease.* Surv Ophthalmol, 2014. 59(3): p. 263-285.

108. Santus, P., et al., *Oxidative stress and respiratory system: pharmacological and clinical reappraisal of N-acetylcysteine.* COPD, 2014. 11(6): p. 705-717.

109. Thimmulappa, R.K., I. Chattopadhyay, and S. Rajasekaran, *Oxidative Stress Mechanisms in the Pathogenesis of Environmental Lung Diseases.* Oxid Stress Lung Dis, 2019: p. 103-137.

110. Liu, X. and Z. Chen, *The pathophysiological role of mitochondrial oxidative stress in lung diseases.* J Trans Med, 2017. 15(1): p. 207.

111. Asmat, U., K. Abad, and K. Ismail, *Diabetes mellitus and oxidative stress-A concise review.* SPJ, 2016. 24(5): p. 547-553.

112. Jain, S.K., K. Kannan, and G. Lim, *Ketosis (acetoacetate) can generate oxygen radicals and cause increased lipid peroxidation and growth inhibition in human endothelial cells.* Free Radic Biol Med, 1998. 25(9): p. 1083-8.

113. Forbes, J.M., M.T. Coughlan, and M.E. Cooper, *Oxidative Stress as a Major Culprit in Kidney Disease in Diabetes.* Diabetes, 2008. 57(6): p. 1446.

114. Barnham, K.J., C.L. Masters, and A.I. Bush, *Neurodegenerative diseases and oxidative stress.* Nat Rev Drug Discov, 2004. 3(3): p. 205-14.

115. Liu, Z., et al., *Oxidative Stress in Neurodegenerative Diseases: From Molecular Mechanisms to Clinical Applications.* Oxid Med Cell Longev, 2017. 2017: p. 2525967-2525967.

116. Ohl, K., K. Tenbrock, and M. Kipp, *Oxidative stress in multiple sclerosis: Central and peripheral mode of action.* Exp Neurol, 2016. 277: p. 58-67.

117. Singh, A., et al., *Oxidative Stress: A Key Modulator in Neurodegenerative Diseases.* Molecules, 2019. 24(8): p. 1583.

118. Senoner, T. and W. Dichtl, *Oxidative Stress in Cardiovascular Diseases: Still a Therapeutic Target?* Nutrients, 2019. 11(9): p. 2090.

119. Moris, D., et al., *The role of reactive oxygen species in the pathophysiology of cardiovascular diseases and the clinical significance of myocardial redox.* Annals of translational medicine, 2017. 5(16): p. 326-326.

120. Sirker, A., M. Zhang, and A.M. Shah, *NADPH oxidases in cardiovascular disease: insights from in vivo models and clinical studies.* Basic Res Cardiol, 2011. 106(5): p. 735-747.

121. Violi, F., et al., *NADPH Oxidase-2 and Atherothrombosis.* Atheroscl Thromb Vasc Biol, 2017. 37(2): p. 218-225.

122. Scott, J., *Pathophysiology and biochemistry of cardiovascular disease.* Curr Opin Gen Dev, 2004. 14(3): p. 271-279.

123. Li, S., et al., *The Role of Oxidative Stress and Antioxidants in Liver Diseases.* Int J Mol Sci, 2015. 16(11): p. 26087-26124.

124. Jadeja, R.N., R.V. Devkar, and S. Nammi, *Oxidative Stress in Liver Diseases: Pathogenesis, Prevention, and Therapeutics.* Oxid Med Cell Longev, 2017. 2017: p. 8341286.

125. Chen, Z., et al., *Role of oxidative stress in the pathogenesis of nonalcoholic fatty liver disease.* Free Radic Biol Med, 2020. 152: p. 116-141.

126. Irie, M., et al., *Reduced Glutathione suppresses Oxidative Stress in Nonalcoholic Fatty Liver Disease.* Euroasian journal of hepato-gastroenterology, 2016. 6(1): p. 13-18.

127. Al-Busafi, S.A., et al., *Antioxidant Therapy in Nonalcoholic Steatohepatitis.* Hepatitis Res Treat, 2012. 2012: p. 947575.

128. Marí, M., et al., *Mitochondrial glutathione, a key survival antioxidant.* Antioxid Redox Signal, 2009. 11(11): p. 2685-2700.

129. Diehl, A.M. and C. Day, *Cause, Pathogenesis, and Treatment of Nonalcoholic Steatohepatitis.* New England J Med, 2017. 377(21): p. 2063-2072.

130. Tsuchida, T. and S.L. Friedman, *Mechanisms of hepatic stellate cell activation.* Nat Rev Gastroenterol Hepatol, 2017. 14(7): p. 397-411.

131. Bataller, R. and D.A. Brenner, *Liver fibrosis.* JCI, 2005. 115(2): p. 209-218.

132. Friedman, S.L., *Hepatic stellate cells: protean, multifunctional, and enigmatic cells of the liver.* Physiol Rev, 2008. 88(1): p. 125-172.

133. Suk, K.T. and D.J. Kim, *Staging of liver fibrosis or cirrhosis: The role of hepatic venous pressure gradient measurement.* World J Hepatol, 2015. 7(3): p. 607-615.

134. Daenen, K., et al., *Oxidative stress in chronic kidney disease.* Pediatr Nephrol, 2019. 34(6): p. 975-991.

135. Rapa, S.F., et al., *Inflammation and Oxidative Stress in Chronic Kidney Disease-Potential Therapeutic Role of Minerals, Vitamins and Plant-Derived Metabolites.* Int J Mol Sci, 2019. 21(1): p. 263.

136. Gyurászová, M., et al., *Oxidative Stress in the Pathophysiology of Kidney Disease: Implications for Noninvasive Monitoring and Identification of Biomarkers.* Oxid Med Cell Longev, 2020. 2020: p. 5478708.

137. Bouayed, J. and T. Bohn, *Exogenous antioxidants--Double-edged swords in cellular redox state: Health beneficial effects at physiologic doses versus deleterious effects at high doses.* Oxid Med Cell Longev, 2010. 3(4): p. 228-237.

138. Padayatty, S.J., et al., *Vitamin C as an antioxidant: evaluation of its role in disease prevention.* J Am Coll Nutr, 2003. 22(1): p. 18-35.

139. Figueroa-Méndez, R. and S. Rivas-Arancibia, *Vitamin C in Health and Disease: Its Role in the Metabolism of Cells and Redox State in the Brain.* Front Physiol, 2015. 6: p. 397-397.

140. Sapper, H., et al., *The reversibility of the vitamin C redox system: electrochemical reasons and biological aspects.* Z Naturforsch C, 1982. 37(10): p. 942-6.

141. Niki, E., *Interaction of ascorbate and alpha-tocopherol.* Ann N Y Acad Sci, 1987. 498: p. 186-99.

142. Wiseman, H., *Vitamin D is a membrane antioxidant. Ability to inhibit iron-dependent lipid peroxidation in liposomes compared to cholesterol, ergosterol and tamoxifen and relevance to anticancer action.* FEBS Lett, 1993. 326(1-3): p. 285-8.

143. Saedisomeolia, A., et al., *Vitamin D status and its association with antioxidant profiles in diabetic patients: A cross-sectional study in Iran.* Indian J Med Sci, 2013. 67(1-2): p. 29-37.

144. Tagliaferri, S., et al., *The controversial role of vitamin D as an antioxidant: results from randomised controlled trials.* Nutr Res Rev, 2019. 32(1): p. 99-105.

145. Leung, F.Y., *Trace elements that act as antioxidants in parenteral micronutrition 11This paper was delivered at the January 18, 1998, workshop "Frontiers in Antioxidant Research: 14th Annual A.S.P.E.N. Workshop," which was held the day before the official start of the 22nd A.S.P.E.N. Clinical Congress in Orlando, FL.* J Nutr Biochem, 1998. 9(6): p. 304-307.

146. Harasym, J. and R. Oledzki, *Effect of fruit and vegetable antioxidants on total antioxidant capacity of blood plasma.* Nutrition, 2014. 30(5): p. 511-7.

147. Gould, R.L. and R. Pazdro, *Impact of Supplementary Amino Acids, Micronutrients, and Overall Diet on Glutathione Homeostasis.* Nutrients, 2019. 11(5).

148. Lopes, H.F., et al., *DASH diet lowers blood pressure and lipid-induced oxidative stress in obesity.* Hypertension, 2003. 41(3): p. 422-30.

149. Dai, J., et al., *Association between adherence to the Mediterranean diet and oxidative stress.* Am J Clin Nutr, 2008. 88(5): p. 1364-70.

150. Urso, M.L. and P.M. Clarkson, *Oxidative stress, exercise, and antioxidant supplementation.* Toxicology, 2003. 189(1-2): p. 41-54.

151. Cheng, W.-H., et al., *Cellular Glutathione Peroxidase Knockout Mice Express Normal Levels of Selenium-Dependent Plasma and Phospholipid Hydroperoxide Glutathione Peroxidases in Various Tissues.* J Nutr, 1997. 127(8): p. 1445-1450.

152. Lubos, E., J. Loscalzo, and D.E. Handy, *Glutathione peroxidase-1 in health and disease: from molecular mechanisms to therapeutic opportunities.* Antioxidants & redox signaling, 2011. 15(7): p. 1957-1997.

153. Chu, F.F., J.H. Doroshow, and R.S. Esworthy, *Expression, characterization, and tissue distribution of a new cellular selenium-dependent glutathione peroxidase, GSHPx-GI.* J Biol Chem, 1993. 268(4): p. 2571-6.

154. Takahashi, K. and H.J. Cohen, *Selenium-dependent glutathione peroxidase protein and activity: immunological investigations on cellular and plasma enzymes.* Blood, 1986. 68(3): p. 640-5.

155. Ursini, F., M. Maiorino, and C. Gregolin, *The selenoenzyme phospholipid hydroperoxide glutathione peroxidase.* Biochim Biophys Acta, 1985. 839(1): p. 62-70.

156. Biswas, S.K., *Does the Interdependence between Oxidative Stress and Inflammation Explain the Antioxidant Paradox?* Oxid Med Cell Longev, 2016. 2016: p. 5698931.

157. Alanazi, A.M., G.A.E. Mostafa, and A.A. Al-Badr, *Chapter Two - Glutathione*, in *Profiles of Drug Substances, Excipients and Related Methodology*, H.G. Brittain, Editor. 2015, Academic Press. p. 43-158.

158. Noctor, G., et al., *Glutathione.* Arabidopsis Book, 2011. 9: p. e0142-e0142.

159. Chakravarthi, S., C.E. Jessop, and N.J. Bulleid, *The role of glutathione in disulphide bond formation and endoplasmic-reticulum-generated oxidative stress.* EMBO reports, 2006. 7(3): p. 271-275.

160. Franco, R., et al., *The central role of glutathione in the pathophysiology of human diseases.* Arch Physiol Biochem, 2007. 113(4-5): p. 234-58.

161. Forman H, Z.H., Rinna A, *Glutathione: Overview of its protective roles, measurement, and biosynthesis.* Mol Aspects Med, 2009. 30(1-2): p. 1-12.

162. Lu, J. and A. Holmgren, *The thioredoxin antioxidant system.* Free Radic Biol Med, 2014. 66: p. 75-87.

163. Lushchak, V.I., *Glutathione Homeostasis and Functions: Potential Targets for Medical Interventions.* Journal of Amino Acids, 2012. 2012: p. 736837.

164. Pizzorno, J., *Glutathione!* Integr Med, 2014. 13(1): p. 8-12.

165. Lu, S.C., *Regulation of glutathione synthesis.* Mol Aspects Med, 2009. 30(1-2): p. 42-59.

166. Deponte, M., *Glutathione catalysis and the reaction mechanisms of glutathione-dependent enzymes.* Biochim Biophys Acta Gen Subj, 2013. 1830(5): p. 3217-3266.

167. Kalinina, E. and M. Novichkova, *Glutathione in Protein Redox Modulation through S-Glutathionylation and S-Nitrosylation.* Molecules, 2021. 26(2).

168. Mukwevho, E., Z. Ferreira, and A. Ayeleso, *Potential Role of Sulfur-Containing Antioxidant Systems in Highly Oxidative Environments.* Molecules, 2014. 19(12).

169. Mukanganyama, S., et al., *The evaluation of novel natural products as inhibitors of human glutathione transferase P1-1.* J Enzyme Inhib Med Chem, 2011. 26(4): p. 460-7.

170. Oakley, A., *Glutathione transferases: a structural perspective.* Drug Metab Rev, 2011. 43(2): p. 138-51.

171. Sheehan, D., et al., *Structure, function and evolution of glutathione transferases: implications for classification of non-mammalian members of an ancient enzyme superfamily.* Biochem J, 2001. 360(Pt 1): p. 1-16.

172. Boyer, T.D., *The glutathione S-transferases: an update.* Hepatology, 1989. 9(3): p. 486-96.

173. Litwack, G., B. Ketterer, and I.M. Arias, *Ligandin: a hepatic protein which binds steroids, bilirubin, carcinogens and a number of exogenous organic anions.* Nature, 1971. 234(5330): p. 466-7.

174. Wu, G., et al., *Glutathione metabolism and its implications for health.* J Nutr, 2004. 134(3): p. 489-92.

175. Townsend, D.M., K.D. Tew, and H. Tapiero, *The importance of glutathione in human disease.* Biomed Pharmacother, 2003. 57(3-4): p. 145-55.

176. Ryan, M.J., et al., *Vitamin E and C supplementation reduces oxidative stress, improves antioxidant enzymes and positive muscle work in chronically loaded muscles of aged rats.* Exp Gerontol, 2010. 45(11): p. 882-895.

177. Chan, A.C., *Partners in defense, vitamin E and vitamin C.* Can J Physiol Pharmacol, 1993. 71(9): p. 725-31.

178. Meister, A., M.E. Anderson, and O. Hwang, *Intracellular cysteine and glutathione delivery systems.* J Am Coll Nutr, 1986. 5(2): p. 137-51.

179. Zhang, H. and H.J. Forman, *Glutathione synthesis and its role in redox signaling.* Semin Cell Dev Biol, 2012. 23(7): p. 722-728.

180. Chakravarthi, S., C.E. Jessop, and N.J. Bulleid, *The role of glutathione in disulphide bond formation and endoplasmic-reticulum-generated oxidative stress.* EMBO Rep, 2006. 7(3): p. 271-275.

181. Wu, G., et al., *Glutathione Metabolism and Its Implications for Health.* The Journal of Nutrition, 2004. 134(3): p. 489-492.

182. Schmitt, B., et al., *Effects of N-acetylcysteine, oral glutathione (GSH) and a novel sublingual form of GSH on oxidative stress markers: A comparative crossover study.* Redox Biol, 2015. 6: p. 198-205.

183. Toroser, D. and R.S. Sohal, *Age-associated perturbations in glutathione synthesis in mouse liver.* Biochem J, 2007. 405(3): p. 583-589.

184. Hansen, J.M. and C. Harris, *Glutathione during embryonic development.* Biochim Biophys Acta, 2015. 1850(8): p. 1527-42.

185. Nebraska Redox Biology Center Education Portal. *Glutathione*. 2021.

186. Prabhakar R, V.T., Morokuma K, Musaev DG, *Elucidation of the mechanism of selenoprotein glutathione peroxidase (GPx)-catalyzed hydrogen peroxide reduction by two glutathione molecules: a density functional study.* Biochemistry, 2005. 44(35): p. 11864-11871.

187. Aquilano, K., S. Baldelli, and M.R. Ciriolo, *Glutathione: new roles in redox signaling for an old antioxidant.* Front Pharmacol, 2014. 5: p. 196-196.

188. Ballatori, N., et al., *Glutathione dysregulation and the etiology and progression of human diseases.* Biological chemistry, 2009. 390(3): p. 191-214.

189. Beutler, E., *Disorders Due to Enzyme Defects in the Red Blood Cell*, in *Adv Metab Dis*, R. Levine and R. Luft, Editors. 1972, Elsevier. p. 131-160.

190. Xiong, Y., et al., *S-glutathionylation: from molecular mechanisms to health outcomes.* Antioxid Redox Signal, 2011. 15(1): p. 233-270.

191. Ballatori, N., et al., *Plasma membrane glutathione transporters and their roles in cell physiology and pathophysiology.* Mol Aspects Med, 2009. 30(1-2): p. 13-28.

192. Zmorzyski, et al., *Significance of Polymorphisms and Expression of Enzyme-Encoding Genes Related to Glutathione in Hematopoietic Cancers and Solid Tumors.* BioMed Res Int, 2015. 2015: p. 6.

193. Tosic, M., et al., *Schizophrenia and oxidative stress: glutamate cysteine ligase modifier as a susceptibility gene.* Am J Hum Genet, 2006. 79(3): p. 586-92.

194. Allen, J. and R.D. Bradley, *Effects of oral glutathione supplementation on systemic oxidative stress biomarkers in human volunteers.* J Altern Complement Med, 2011. 17(9): p. 827-833.

195. Oz, H.S., T.S. Chen, and H. Nagasawa, *Comparative efficacies of 2 cysteine prodrugs and a glutathione delivery agent in a colitis model.* Transl Res, 2007. 150(2): p. 122-129.

196. Binkley, F., G.M. Christensen, and F.C. Wu, *Metabolism of glutathione. V. An effect of insulin.* J Biol Chem, 1951. 192(1): p. 29-34.

197. Ballatori, N., et al., *Glutathione dysregulation and the etiology and progression of human diseases.* Biol Chem, 2009. 390(3): p. 191-214.

198. Meister, A. and M.E. Anderson, *Glutathione.* Annu Rev Biochem, 1983. 52: p. 711-60.

199. Meister, A. and S.S. Tate, *Glutathione and related gamma-glutamyl compounds: biosynthesis and utilization.* Annu Rev Biochem, 1976. 45: p. 559-604.

200. Lash, L.H., *Renal glutathione transport: Identification of carriers, physiological functions, and controversies.* BioFactors, 2009. 35(6): p. 500-508.

201. Moine, L., et al., *Glutathione depleting drugs, antioxidants and intestinal calcium absorption.* World J Gastroenterol, 2018. 24: p. 4979-4988.

202. Lu, S.C., *Dysregulation of glutathione synthesis in liver disease.* Liver Res, 2020. 4(2): p. 64-73.

203. Gould, R.L., et al., *Heritability of the aged glutathione phenotype is dependent on tissue of origin.* Mamm Genome, 2018. 29(9): p. 619-631.

204. Githens, S., *Glutathione metabolism in the pancreas compared with that in the liver, kidney, and small intestine.* Int J Pancreatol, 1991. 8(2): p. 97-109.

205. Lash, L.H., *Role of glutathione transport processes in kidney function.* Toxicology and Applied Pharmacology, 2005. 204(3): p. 329-342.

206. Gawryluk, J.W., et al., *Decreased levels of glutathione, the major brain antioxidant, in post-mortem prefrontal cortex from patients with psychiatric disorders.* Int J Neuropsychopharmacol, 2011. 14(1): p. 123-30.

207. Ookhtens, M. and N. Kaplowitz, *Role of the Liver in Interorgan Homeostasis of Glutathione and Cyst(e)ine.* Semin Liver Dis, 1998. 18(04): p. 313-329.

208. Dwivedi, D., et al., *Glutathione in Brain: Overview of Its Conformations, Functions, Biochemical Characteristics, Quantitation and Potential Therapeutic Role in Brain Disorders.* Neurochem Res, 2020. 45: p. 1461–1480.

209. Anderson, M.E. and A. Meister, *Dynamic state of glutathione in blood plasma.* J Biol Chem, 1980. 255(20): p. 9530-3.

210. Zhou, S.-S., et al., *Vitamin paradox in obesity: Deficiency or excess?* World J Diabetes, 2015. 6(10): p. 1158-1167.

211. Waly, M.I., Z. Al-Attabi, and N. Guizani, *Low Nourishment of Vitamin C Induces Glutathione Depletion and Oxidative Stress in Healthy Young Adults.* Prev Nutr Food Sci, 2015. 20(3): p. 198-203.

212. Jain, S.K., R. McVie, and T. Smith, *Vitamin E supplementation restores glutathione and malondialdehyde to normal concentrations in erythrocytes of type 1 diabetic children.* Diabetes Care, 2000. 23(9): p. 1389-94.

213. Litwack, G., *Chapter 20 - Vitamins and Nutrition*, in *Human Biochemistry*, G. Litwack, Editor. 2018, Academic Press: Boston. p. 645-680.

214. Cacciatore, I., et al., *Prodrug Approach for Increasing Cellular Glutathione Levels.* Molecules, 2010. 15(3).

215. Wu G, F.Y., Yang S, Lupton JR, Turner ND, *Glutathione metabolism and its implications for health.* J Nutr, 2004. 134(3): p. 489-492.

216. Reid, M. and F. Jahoor, *Glutathione in disease.* Curr Opin Clin Nutr Metab Care, 2001. 4(1): p. 65-71.

217. Mandal, P.K., et al., *Cognitive Improvement with Glutathione Supplement in Alzheimer's Disease: A Way Forward.* Journal of Alzheimer's Disease, 2019. 68: p. 531-535.

218. Mandal, P.K., et al., *Brain Glutathione Levels – A Novel Biomarker for Mild Cognitive Impairment and Alzheimer & Disease.* Biol Psych, 2015. 78(10): p. 702-710.

219. Hajjar, I., et al., *Oxidative stress predicts cognitive decline with aging in healthy adults: an observational study.* J Neuroinflam, 2018. 15(1): p. 17.

220. Pastore, A., et al., *All glutathione forms are depleted in blood of obese and type 1 diabetic children.* Pediatr Diabetes, 2012. 13(3): p. 272-7.

221. Albuali, W.H., *Evaluation of oxidant-antioxidant status in overweight and morbidly obese Saudi children.* World J Clin Pediatr, 2014. 3(1): p. 6-13.

222. Huang, Z.-Z., et al., *Mechanism and significance of increased glutathione level in human hepatocellular carcinoma and liver regeneration.* The FASEB Journal, 2001. 15(1): p. 19-21.

223. Irie, M., et al., *Reduced Glutathione suppresses Oxidative Stress in Nonalcoholic Fatty Liver Disease.* Euroasian J Hepatogastroenterol, 2016. 6(1): p. 13-18.

224. Ramani, K., et al., *Mechanism and significance of changes in glutamate-cysteine ligase expression during hepatic fibrogenesis.* J Biol Chem, 2012. 287(43): p. 36341-55.

225. Zuo, M.-h., et al., *Clinical observation of the reduced glutathione in the treatment of diabetic chronic kidney disease.* J Cell Biochem, 2019. 120(5): p. 8483-8491.

226. Ling, X.C. and K.-L. Kuo, *Oxidative stress in chronic kidney disease.* Ren Replace Ther, 2018. 4(1): p. 53.

227. Zhu, Y., P.M. Carvey, and Z. Ling, *Age-related changes in glutathione and glutathione-related enzymes in rat brain.* Brain Res, 2006. 1090(1): p. 35-44.

228. Farooqui, M.Y., W.W. Day, and D.M. Zamorano, *Glutathione and lipid peroxidation in the aging rat.* Comp Biochem Physiol B, 1987. 88(1): p. 177-80.

229. Stohs, S.J., T. Lawson, and W.A. Al-Turk, *Changes in glutathione and glutathione metabolizing enzymes in erythrocytes and lymphocytes of mice as a function of age.* Gen Pharmacol, 1984. 15(3): p. 267-70.

230. Erden-Inal, M., E. Sunal, and G. Kanbak, *Age-related changes in the glutathione redox system.* Cell Biochem Funct, 2002. 20(1): p. 61-6.

231. Lang, C.A., et al., *Low blood glutathione levels in healthy aging adults.* J Lab Clin Med, 1992. 120(5): p. 720-5.

232. Matsubara, L.S. and P.E. Machado, *Age-related changes of glutathione content, glutathione reductase and glutathione peroxidase activity of human erythrocytes.* Braz J Med Biol Res, 1991. 24(5): p. 449-54.

233. Loguercio, C., et al., *Effect of liver cirrhosis and age on the glutathione concentration in the plasma, erythrocytes, and gastric mucosa of man.* Free Radic Biol Med, 1996. 20(3): p. 483-8.

234. Al-Turk, W.A., et al., *Changes in glutathione and its metabolizing enzymes in human erythrocytes and lymphocytes with age.* J Pharm Pharmacol, 1987. 39(1): p. 13-6.

235. Samiec, P.S., et al., *Glutathione in human plasma: decline in association with aging, age-related macular degeneration, and diabetes.* Free Radic Biol Med, 1998. 24(5): p. 699-704.

236. Liu, R. and J. Choi, *Age-associated decline in gamma-glutamylcysteine synthetase gene expression in rats.* Free Radic Biol Med, 2000. 28(4): p. 566-74.

237. Sekhar, R.V., et al., *Deficient synthesis of glutathione underlies oxidative stress in aging and can be corrected by dietary cysteine and glycine supplementation1–4.* Am J Clin Nutr, 2011. 94(3): p. 847-853.

238. Traverso, N., et al., *Role of Glutathione in Cancer Progression and Chemoresistance.* Oxid Med Cell Longev, 2013. 2013: p. 972913.

239. Calvert, P., et al., *Clinical studies of reversal of drug resistance based on glutathione.* Chem Biol Interact, 1998. 111-112: p. 213-224.

240. Godwin, A.K., et al., *High resistance to cisplatin in human ovarian cancer cell lines is associated with marked increase of glutathione synthesis.* Proc Natl Acad Sci, 1992. 89(7): p. 3070-4.

241. Mulcahy, R.T., S. Untawale, and J.J. Gipp, *Transcriptional up-regulation of gamma-glutamylcysteine synthetase gene expression in melphalan-resistant human prostate carcinoma cells.* Mol Pharmacol, 1994. 46(5): p. 909-14.

242. Estrela, J.M., A. Ortega, and E. Obrador, *Glutathione in cancer biology and therapy.* Crit Rev Clin Lab Sci, 2006. 43(2): p. 143-81.

243. Kelley, B.J. and R.C. Petersen, *Alzheimer's disease and mild cognitive impairment.* Neurologic clinics, 2007. 25(3): p. 577-v.

244. DeMaagd, G. and A. Philip, *Parkinson's Disease and Its Management: Part 1: Disease Entity, Risk Factors, Pathophysiology, Clinical Presentation, and Diagnosis.* P & T, 2015. 40(8): p. 504-532.

245. Andreazza, A.C., et al., *Decreased levels of glutathione, the major brain antioxidant, in post-mortem prefrontal cortex from patients with psychiatric disorders.* Int J Neuropsychopharmacol, 2011. 14(1): p. 123-130.

246. Feksa, L.R., et al., *Promotion of oxidative stress by L-tryptophan in cerebral cortex of rats.* Neurochem Int, 2006. 49(1): p. 87-93.

247. Aoyama, K. and T. Nakaki, *Impaired glutathione synthesis in neurodegeneration.* Int J Mol Sci, 2013. 14(10): p. 21021-21044.

248. Robinson, B., et al., *Liposomal-Glutathione as a Potential Therapeutic Agent to Control HIV-1 Infection and Tuberculosis.* Eur Med J, 2018. 3.

249. van der Ven, A.J., et al., *Glutathione homeostasis is disturbed in CD4-positive lymphocytes of HIV-seropositive individuals.* Eur J Clin Invest, 1998. 28(3): p. 187-93.

250. Eck, H.P., et al., *Low concentrations of acid-soluble thiol (cysteine) in the blood plasma of HIV-1-infected patients.* Biol Chem Hoppe Seyler, 1989. 370(2): p. 101-8.

251. Helbling, B., J. von Overbeck, and B.H. Lauterburg, *Decreased release of glutathione into the systemic circulation of patients with HIV infection.* Eur J Clin Invest, 1996. 26(1): p. 38-44.

252. Buhl, R., et al., *Systemic glutathione deficiency in symptom-free HIV-seropositive individuals.* Lancet, 1989. 2(8675): p. 1294-8.

253. de Quay, B., R. Malinverni, and B.H. Lauterburg, *Glutathione depletion in HIV-infected patients: role of cysteine deficiency and effect of oral N-acetylcysteine.* Aids, 1992. 6(8): p. 815-9.

254. Herzenberg, L.A., et al., *Glutathione deficiency is associated with impaired survival in HIV disease.* Proceedings of the National Academy of Sciences of the United States of America, 1997. 94(5): p. 1967-1972.

255. Adamson, G.M. and R.E. Billings, *Tumor necrosis factor induced oxidative stress in isolated mouse hepatocytes.* Arch Biochem Biophys, 1992. 294(1): p. 223-9.

256. Staal, F.J., et al., *Redox regulation of signal transduction: tyrosine phosphorylation and calcium influx.* Proc Natl Acad Sci, 1994. 91(9): p. 3619-22.

257. Staal, F.J., et al., *Intracellular thiols regulate activation of nuclear factor kappa B and transcription of human immunodeficiency virus.* Proc Natl Acad Sci, 1990. 87(24): p. 9943-7.

258. Mihm, S., et al., *Inhibition of HIV-1 replication and NF-kappa B activity by cysteine and cysteine derivatives.* Aids, 1991. 5(5): p. 497-503.

259. Ueno, Y., et al., *Dietary Glutathione Protects Rats from Diabetic Nephropathy and Neuropathy.* J Nutr, 2002. 132(5): p. 897-900.

260. Darmaun, D., et al., *Evidence for Accelerated Rates of Glutathione Utilization and Glutathione Depletion in Adolescents With Poorly Controlled Type 1 Diabetes.* Diabetes, 2005. 54(1): p. 190.

261. Lutchmansingh, F.K., et al., *Glutathione metabolism in type 2 diabetes and its relationship with microvascular complications and glycemia.* PloS one, 2018. 13(6): p. e0198626-e0198626.

262. Picklo, M.J., E.K. Long, and E.E. Vomhof-DeKrey, *Glutathionyl systems and metabolic dysfunction in obesity.* Nutr Rev, 2015. 73(12): p. 858-868.

263. Goutzourelas, N., et al., *GSH levels affect weight loss in individuals with metabolic syndrome and obesity following dietary therapy.* Exp Ther Med, 2018. 16(2): p. 635-642.

264. Jankovic, A., et al., *Differences in the redox status of human visceral and subcutaneous adipose tissues--relationships to obesity and metabolic risk.* Metabolism, 2014. 63(5): p. 661-71.

265. Shimizu, H., et al., *Relationship between plasma glutathione levels and cardiovascular disease in a defined population: the Hisayama study.* Stroke, 2004. 35(9): p. 2072-7.

266. Biswas, S.K., et al., *Depressed glutathione synthesis precedes oxidative stress and atherogenesis in Apo-E−/− mice.* Biochem Biophys Res Commun, 2005. 338(3): p. 1368-1373.

267. Rosenblat, M., et al., *Anti-oxidant and anti-atherogenic properties of liposomal glutathione: Studies in vitro, and in the atherosclerotic apolipoprotein E-deficient mice.* Atherosclerosis, 2007. 195(2): p. e61-e68.

268. Bajic, V.P., et al., *Glutathione; Redox Homeostasis; and Its Relation to Cardiovascular Disease.* Oxid Med Cell Longev, 2019. 2019: p. 14.

269. Bastani, A., et al., *Oxidant and antioxidant status in coronary artery disease.* Biomed Rep, 2018. 9(4): p. 327-332.

270. Damy, T., et al., *Glutathione deficiency in cardiac patients is related to the functional status and structural cardiac abnormalities.* PloS One, 2009. 4(3): p. e4871-e4871.

271. Stohs, S.J., et al., *Glutathione levels in hepatic and extrahepatic tissues of mice as a function of age.* AGE, 1980. 3(1): p. 11-14.

272. Huang, Z.Z., et al., *Mechanism and significance of increased glutathione level in human hepatocellular carcinoma and liver regeneration.* Faseb J, 2001. 15(1): p. 19-21.

273. Tsukamoto, H. and S.C. Lu, *Current concepts in the pathogenesis of alcoholic liver injury.* FASEB J, 2001. 15(8): p. 1335-1349.

274. Vendemiale, G., et al., *Effects of Oral S-Adenosyl-l-Methionine on Hepatic Glutathione in Patients with Liver Disease.* Scandinavian Journal of Gastroenterology, 1989. 24(4): p. 407-415.

275. Dou, X., et al., *Glutathione disulfide sensitizes hepatocytes to TNFα-mediated cytotoxicity via IKK-β S-glutathionylation: a potential mechanism underlying non-alcoholic fatty liver disease.* Exp Mol Med, 2018. 50(4): p. 7.

276. Lash, L.H., *Role of glutathione transport processes in kidney function.* Toxicol Appl Pharmacol, 2005. 204(3): p. 329-42.

277. Tbahriti, H.F., et al., *Effect of Different Stages of Chronic Kidney Disease and Renal Replacement Therapies on Oxidant-Antioxidant Balance in Uremic Patients.* Biochem Res Int, 2013. 2013: p. 358985.

278. Signorini, L., et al., *Naturally Occurring Compounds: New Potential Weapons against Oxidative Stress in Chronic Kidney Disease.* International journal of molecular sciences, 2017. 18(7): p. 1481.

279. Mutsaers, H.A., et al., *Uremic toxins inhibit renal metabolic capacity through interference with glucuronidation and mitochondrial respiration.* Biochim Biophys Acta, 2013. 1832(1): p. 142-50.

280. Su, M., et al., *Mitochondrial dysfunction is an early event in aldosterone-induced podocyte injury.* Am J Physiol Renal Physiol, 2013. 305(4): p. F520-31.

281. Zhao, M., et al., *PGC-1α overexpression protects against aldosterone-induced podocyte depletion: role of mitochondria.* Oncotarget, 2016. 7(11): p. 12150-62.

282. Yuan, Y., et al., *Mitochondrial dysfunction accounts for aldosterone-induced epithelial-to-mesenchymal transition of renal proximal tubular epithelial cells.* Free Radic Biol Med, 2012. 53(1): p. 30-43.

283. Zhang, A., et al., *Aldosterone induces epithelial-mesenchymal transition via ROS of mitochondrial origin.* Am J Physiol Renal Physiol, 2007. 293(3): p. F723-31.

284. Santangelo, F., et al., *Restoring glutathione as a therapeutic strategy in chronic kidney disease.* Nephrology Dialysis Transplantation, 2004. 19(8): p. 1951-1955.

285. Santangelo, F., et al., *Restoring glutathione as a therapeutic strategy in chronic kidney disease.* Nephrol Dial Transplant, 2004. 19(8): p. 1951-1955.

286. Hauser, R.A., et al., *Randomized, double-blind, pilot evaluation of intravenous glutathione in Parkinson's disease.* Mov Disord, 2009. 24(7): p. 979-83.

287. Mischley, L.K., et al., *Central nervous system uptake of intranasal glutathione in Parkinson's disease.* NPJ Parkinsons Dis, 2016. 2: p. 16002-16002.

288. Favilli, F., et al., *Effect of orally administered glutathione on glutathione levels in some organs of rats: role of specific transporters.* Br J Nutr, 1997. 78(2): p. 293-300.

289. Richie, J.P., Jr., et al., *Randomized controlled trial of oral glutathione supplementation on body stores of glutathione.* Eur J Nutr, 2015. 54(2): p. 251-63.

290. Prousky, J., *The treatment of pulmonary diseases and respiratory-related conditions with inhaled (nebulized or aerosolized) glutathione.* Evid Based Complement Alternat Med, 2008. 5(1): p. 27-35.

291. Kern, J.K., et al., *A clinical trial of glutathione supplementation in autism spectrum disorders.* Med Sci Monit, 2011. 17(12): p. CR677-CR682.

292. Honda, Y., et al., *Efficacy of glutathione for the treatment of nonalcoholic fatty liver disease: an open-label, single-arm, multicenter, pilot study.* BMC Gastroenterol, 2017. 17(1): p. 96-96.

293. Witschi, A., et al., *The systemic availability of oral glutathione.* Eur J Clin Pharmacol, 1992. 43(6): p. 667-9.

294. Hagen, T.M., et al., *Fate of dietary glutathione: disposition in the gastrointestinal tract.* Am J Physiol, 1990. 259(4 Pt 1): p. G530-5.

295. Hanigan, M.H., *Gamma-glutamyl transpeptidase: redox regulation and drug resistance.* Adv Cancer Res, 2014. 122: p. 103-141.

296. Valencia, E., A. Marin, and G. Hardy, *Impact of oral l-glutamine on glutathione, glutamine, and glutamate blood levels in volunteers.* Nutrition, 2002. 18(5): p. 367-370.

297. Holecek, M., *Side effects of long-term glutamine supplementation.* JPEN J Parenter Enteral Nutr, 2013. 37(5): p. 607-16.

298. Borges-Santos, M.D., et al., *Plasma glutathione of HIV+ patients responded positively and differently to dietary supplementation with cysteine or glutamine.* Nutrition, 2012. 28(7): p. 753-756.

299. Oldani, M., et al., *Glutamine Supplementation in Intensive Care Patients: A Meta-Analysis of Randomized Clinical Trials.* Medicine, 2015. 94(31): p. e1319.

300. Kumar, S., et al., *Effect of oral glutamine administration on oxidative stress, morbidity and mortality in critically ill surgical patients.* Indian J Gastroenterol, 2007. 26(2): p. 70-3.

301. Morris, C.R., et al., *Metabolic Fate of Oral Glutamine Supplementation within Plasma and Erythrocytes of Patients with Sickle Cell Disease: Preliminary Pharmacokinetics Results.* Blood, 2010. 116(21): p. 1636.

302. McCarty, M.F., J.H. O'Keefe, and J.J. DiNicolantonio, *Dietary Glycine Is Rate-Limiting for Glutathione Synthesis and May Have Broad Potential for Health Protection.* Ochsner J, 2018. 18(1): p. 81-87.

303. Wang, W., et al., *Glycine is a nutritionally essential amino acid for maximal growth of milk-fed young pigs.* Amino Acids, 2014. 46(8): p. 2037-2045.

304. Ruiz-Ramírez, A., et al., *Glycine restores glutathione and protects against oxidative stress in vascular tissue from sucrose-fed rats.* Clin Sci, 2014. 126(1): p. 19.

305. El-Hafidi, M., et al., *Glycine Increases Insulin Sensitivity and Glutathione Biosynthesis and Protects against Oxidative Stress in a Model of Sucrose-Induced Insulin Resistance.* Oxid Med Cell Longev, 2018. 2018: p. 12.

306. Nguyen, D., et al., *Effect of increasing glutathione with cysteine and glycine supplementation on mitochondrial fuel oxidation, insulin sensitivity, and body composition in older HIV-infected patients.* J Clin Endocrinol Metab, 2014. 99(1): p. 169-177.

307. McBean, G.J., *Cysteine, Glutathione, and Thiol Redox Balance in Astrocytes.* Antioxidants, 2017. 6(3): p. 62.

308. Olney, J.W., O.L. Ho, and V. Rhee, *Cytotoxic effects of acidic and sulphur containing amino acids on the infant mouse central nervous system.* Exp Brain Res, 1971. 14(1): p. 61-76.

309. Birnbaum, S.M., J.P. Greenstein, and M. Winitz, *Quantitative nutritional studies with water-soluble, chemically defined diets. II. Nitrogen balance and metabolism.* Arch Biochem Biophys, 1957. 72(2): p. 417-27.

310. Olney, J.W. and O.L. Ho, *Brain damage in infant mice following oral intake of glutamate, aspartate or cysteine.* Nature, 1970. 227(5258): p. 609-11.

311. Shapre, L.G., et al., *Brain damage and associated behavioral deficits following the administration of L-cysteine to infant rats.* Pharmacol Biochem Behav, 1975. 3(2): p. 291-298.

312. Anderson, M.E. and A. Meister, *Intracellular delivery of cysteine.* Methods Enzymol, 1987. 143: p. 313-25.

313. White, R.D., et al., *Toxicity evaluations of l-cysteine and Procysteine™, a cysteine prodrug, given once intravenously to neonatal rats.* Toxicol Lett, 1993. 69(1): p. 15-24.

314. Glatt, H., C.M. Protic-Sablji, and F. Oesch, *Mutagenicity of glutathione and cysteine in the Ames test.* Science, 1983. 220(4600): p. 961-3.

315. Glatt, H. and F. Oesch, *Mutagenicity of cysteine and penicillamine and its enantiomeric selectivity.* Biochem Pharmacol, 1985. 34(20): p. 3725-8.

316. Calkins, K.L., et al., *Effect of High-Dose Cysteine Supplementation on Erythrocyte Glutathione: A Double-Blinded, Randomized Placebo-Controlled Pilot Study in Critically Ill Neonates.* JPEN J Parenter Enteral Nutr, 2016. 40(2): p. 226-234.

317. Troen, A.M., et al., *The atherogenic effect of excess methionine intake.* Proc Natl Acad Sci, 2003. 100(25): p. 15089-15094.

318. Kim, S.-Y., H. Kim, and H. Min, *Effects of excessive dietary methionine on oxidative stress and dyslipidemia in chronic ethanol-treated rats.* Nutr Res Pract, 2015. 9(2): p. 144-149.

319. Atkuri, K.R., et al., *N-Acetylcysteine--a safe antidote for cysteine/glutathione deficiency.* Curr Opin Pharmacol, 2007. 7(4): p. 355-9.

320. Noszal, B., D. Visky, and M. Kraszni, *Population, acid-base, and redox properties of N-acetylcysteine conformers.* J Med Chem, 2000. 43(11): p. 2176-82.

321. Cotgreave, I.A., *N-acetylcysteine: pharmacological considerations and experimental and clinical applications.* Adv Pharmacol, 1997. 38: p. 205-27.

322. Griffith, O.W. and A. Meister, *Glutathione: interorgan translocation, turnover, and metabolism.* Proc Natl Acad Sci, 1979. 76(11): p. 5606-10.

323. Bridgeman, M.M., et al., *Cysteine and glutathione concentrations in plasma and bronchoalveolar lavage fluid after treatment with N-acetylcysteine.* Thorax, 1991. 46(1): p. 39-42.

324. De Rosa, S.C., et al., *N-acetylcysteine replenishes glutathione in HIV infection.* Eur J Clin Invest, 2000. 30(10): p. 915-929.

325. Paschalis, V., et al., *N-acetylcysteine supplementation increases exercise performance and reduces oxidative stress only in individuals with low levels of glutathione.* Free Radic Biol Med, 2018. 115: p. 288-297.

326. Cieslik, K.A., et al., *Improved Cardiovascular Function in Old Mice After N-Acetyl Cysteine and Glycine Supplemented Diet: Inflammation and Mitochondrial Factors.* J Gerontol A Biol Sci Med Sci, 2018. 73(9): p. 1167-1177.

327. Angelo, A. and J. Selhub, *Homocysteine and Thrombotic Disease.* Blood, 1997. 90(1): p. 1.

328. Vendemiale, G., et al., *Effects of oral S-adenosyl-L-methionine on hepatic glutathione in patients with liver disease.* Scand J Gastroenterol, 1989. 24(4): p. 407-15.

329. Song, Z., et al., *S-adenosylmethionine (SAMe) protects against acute alcohol induced hepatotoxicity in mice.* J Nutr Biochem, 2003. 14(10): p. 591-7.

330. Kaneshiro, Y., et al., *Augmentation of Mitochondrial Reduced Glutathione by S-Adenosyl-L-Methionine Administration in Ischemia-Reperfusion Injury of the Rat Steatotic Liver Induced by Choline-Methionine-Deficient Diet.* Eur Surg Res, 1998. 30(1): p. 34-42.

331. Colell, A., et al., *Selective glutathione depletion of mitochondria by ethanol sensitizes hepatocytes to tumor necrosis factor.* Gastroenterology, 1998. 115(6): p. 1541-51.

332. Seo Yeon, L. and K. and Kwang Suk, *Effects of S-Adenosylmethionine and Its Combinations With Taurine and/or Betaine on Glutathione Homeostasis in Ethanol-induced Acute Hepatotoxicity.* J Cancer Prev, 2016. 21(3): p. 164-172.

333. Fernandez-Checa, J.C., A. Colell, and C. Garcia-Ruiz, *S-Adenosyl-L-methionine and mitochondrial reduced glutathione depletion in alcoholic liver disease.* Alcohol, 2002. 27(3): p. 179-83.

334. Lieber, C.S., et al., *S-Adenosyl-L-methionine attenuates alcohol-induced liver injury in the baboon.* Hepatology, 1990. 11(2): p. 165-172.

335. Thompson, M.A., et al., *Dietary Supplement S-Adenosyl-l-Methionine (AdoMet) Effects on Plasma Homocysteine Levels in Healthy Human Subjects: A Double-Blind, Placebo-Controlled, Randomized Clinical Trial.* J Altern Complement Med, 2009. 15(5): p. 523-529.

336. Iimuro, Y., et al., *The glutathione precursor L-2-oxothiazolidine-4-carboxylic acid protects against liver injury due to chronic enteral ethanol exposure in the rat.* Hepatology, 2000. 31(2): p. 391-8.

337. Taylor, C.G., et al., *Elevation of lung glutathione by oral supplementation of L-2-oxothiazolidine-4-carboxylate protects against oxygen toxicity in protein-energy malnourished rats.* FASEB J, 1992. 6(12): p. 3101-3107.

338. Jain, A., et al., *L-2-oxothiazolidine-4-carboxylate, a cysteine precursor, stimulates growth and normalizes tissue glutathione concentrations in rats fed a sulfur amino acid-deficient diet.* J Nutr, 1995. 125(4): p. 851-6.

339. Held, P. and C.O. Harding, *L-2-oxothiazolidine-4-carboxylate supplementation in murine gamma-GT deficiency.* Free Radic Biol Med, 2003. 34(11): p. 1482-7.

340. Promsote, W., et al., *L-2-oxothiazolidine-4-carboxylic acid attenuates oxidative stress and inflammation in retinal pigment epithelium.* Mol Vis, 2014. 20: p. 73-88.

341. Zhang, Z., et al., *Effects of dietary protein and L-2-oxothiazolidine-4-carboxylate on rat brain glutathione concentration.* Nutr Res, 2002. 22(12): p. 1475-1486.

342. Porta, P., et al., *L-2-oxothiazolidine-4-carboxylic acid, a cysteine prodrug: pharmacokinetics and effects on thiols in plasma and lymphocytes in human.* J Pharmacol Exp Ther, 1991. 257(1): p. 331.

343. Korybalska, K., et al., *L-2-oxothiazolidine-4-carboxylate: an agent that modulates lipopolysaccharide-induced peritonitis in rats.* Perit Dial Int, 2002. 22(3): p. 293-300.

344. Levy, M.A., B. Sikorski, and T.M. Bray, *Selective elevation of glutathione levels in target tissues with L-2-oxothiazolidine-4-carboxylate (OTC) protects against hyperoxia-induced lung damage in protein-energy malnourished rats: implications for a new treatment strategy.* J Nutr, 1998. 128(4): p. 671-6.

345. Nishina, H., J. Ohta, and T. Ubuka, *Effect of L-2-oxothiazolidine-4-carboxylate administration on glutathione and cysteine concentrations in guinea pig liver and kidney.* Physiol Chem Phys Med NMR, 1987. 19(1): p. 9-13.

346. Lu, S.C., *Glutathione synthesis.* Biochim Biophys Acta, 2013. 1830(5): p. 3143-3153.

347. Zhou, X., et al., *Serine prevented high-fat diet-induced oxidative stress by activating AMPK and epigenetically modulating the expression of glutathione synthesis-related genes.* Biochim Biophys Acta Mol Basis Dis, 2018. 1864(2): p. 488-498.

348. Zhou, X., et al., *Serine alleviates oxidative stress via supporting glutathione synthesis and methionine cycle in mice.* Mol Nutr Food Res, 2017. 61(11).

349. Zhou, X., et al., *Effects of Dietary Serine Supplementation on Intestinal Integrity, Inflammation and Oxidative Status in Early-Weaned Piglets.* Cell Physiol Biochem, 2018. 48(3): p. 993-1002.

350. Sim, W.-C., et al., *L-Serine Supplementation Attenuates Alcoholic Fatty Liver by Enhancing Homocysteine Metabolism in Mice and Rats.* J Nutr, 2014. 145(2): p. 260-267.

351. Zhou, X., et al., *Long-Term l-Serine Administration Reduces Food Intake and Improves Oxidative Stress and Sirt1/NFκB Signaling in the Hypothalamus of Aging Mice.* Front Endocrinol, 2018. 9: p. 476-476.

352. Patriarca, S., et al., *Supplementation with N-acetylcysteine and taurine failed to restore glutathione content in liver of streptozotocin-induced diabetics rats but protected from oxidative stress.* Biochim Biophys Acta Mol Basis Dis, 2005. 1741(1): p. 48-54.

353. Lim, E., S. Park, and H. Kim, *Effect of taurine supplementation on the lipid peroxide formation and the activities of glutathione-related enzymes in the liver and islet of type I and II diabetic model mice.* Adv Exp Med Biol, 1998. 442: p. 99-103.

354. Yao, H.T., et al., *Effect of taurine supplementation on cytochrome P450 2E1 and oxidative stress in the liver and kidneys of rats with streptozotocin-induced diabetes.* Food Chem Toxicol, 2009. 47(7): p. 1703-9.

355. Saad, S.Y. and A.C. Al-Rikabi, *Protection effects of Taurine supplementation against cisplatin-induced nephrotoxicity in rats.* Chemotherapy, 2002. 48(1): p. 42-8.

356. Maclean, K.N., et al., *Taurine treatment prevents derangement of the hepatic gamma-glutamyl cycle and methylglyoxal metabolism in a mouse model of classical homocystinuria: regulatory crosstalk between thiol and sulfinic acid metabolism.* FASEB J, 2018. 32(3): p. 1265-1280.

357. Taş, S., et al., *The effect of taurine supplementation on oxidative stress in experimental hypothyroidism.* Cell Biochem Funct, 2006. 24(2): p. 153-158.

358. Oudit, G., et al., *Taurine Supplementation Reduces Oxidative Stress and Improves Cardiovascular Function in an Iron-Overload Murine Model.* Circulation, 2004. 109(15): p. 1877-1885.

359. Anand, P., et al., *Effects of Taurine on Glutathione Peroxidase, Glutathione Reductase and Reduced Glutathione Levels in Rats.* Pak J Biol Sci, 2011. 14(3): p. 219-225.

360. Obrosova, I.G. and M.J. Stevens, *Effect of dietary taurine supplementation on GSH and NAD(P)-redox status, lipid peroxidation, and energy metabolism in diabetic precataractous lens.* Invest Ophthalmol Vis Sci, 1999. 40(3): p. 680-8.

361. Balkan, J., et al., *Improving effect of dietary taurine supplementation on the oxidative stress and lipid levels in the plasma, liver and aorta of rabbits fed on a high-cholesterol diet.* Biosci Biotechnol Biochem, 2002. 66(8): p. 1755-8.

362. Foda, D., et al., *Protective and therapeutic impact of taurine on some biochemical, immunological and histological parameters in diabetic rats.* J App Pharm Sci., 2016. 6(10): p. 045-054.

363. Lim, E., S. Park, and H. Kim, *Effect of Taurine Supplementation on the Lipid Peroxide Formation and the Activities of Glutathione-Related Enzymes in the Liver and Islet of Type I and II Diabetic Model Mice*, in *Taurine 3: Cellular and Regulatory Mechanisms*, S. Schaffer, J.B. Lombardini, and R.J. Huxtable, Editors. 1998, Springer US: Boston, MA. p. 99-103.

364. da Silva, L.A., et al., *Effects of taurine supplementation following eccentric exercise in young adults.* Appl Physiol Nutr Metab, 2013. 39(1): p. 101-104.

365. Cha, J.-H., Q.-M. Yu, and J.-S. Seo, *Vitamin A supplementation modifies the antioxidant system in rats.* Nutr Res Pract, 2016. 10(1): p. 26-32.

366. Petiz, L.L., et al., *Vitamin A Oral Supplementation Induces Oxidative Stress and Suppresses IL-10 and HSP70 in Skeletal Muscle of Trained Rats.* Nutrients, 2017. 9(4): p. 353.

367. Jain, S.K., et al., *Vitamin D and L-cysteine levels correlate positively with GSH and negatively with insulin resistance levels in the blood of type 2 diabetic patients.* Eur J Clin Nutr, 2014. 68(10): p. 1148-53.

368. Alvarez, J.A., et al., *Vitamin D status is independently associated with plasma glutathione and cysteine thiol/disulphide redox status in adults.* Clin Endocrinol (Oxf), 2014. 81(3): p. 458-466.

369. Jain, S.K., R. Parsanathan, and A.E. Achari, *Positive association between reduced GSH and inadequacy/deficiency of 25-hydroxy-vitamin D in obese children.* FASEB J, 2017. 31(1_supplement): p. 799.12-799.12.

370. Sakamoto, W., et al., *The effect of vitamin K2 on bone metabolism in aged female rats.* Osteoporos Int, 2005. 16(12): p. 1604-10.

371. Marcus, S.R., M.V. Chandrakala, and H.A. Nadiger, *Interaction between vitamin E and glutathione in rat brain—effect of acute alcohol administration.* J Nutr Biochem, 1993. 4(6): p. 336-340.

372. Bucioli, S.A., et al., *Effects of vitamin E supplementation on renal non-enzymatic antioxidants in young rats submitted to exhaustive exercise stress.* BMC Complement Altern Med, 2011. 11(1): p. 133.

373. Scott, D.L., J. Kelleher, and M.S. Losowsky, *The influence of dietary selenium and vitamin E on glutathione peroxidase and glutathione in the rat.* Biochim Biophys Acta Gen Subj, 1977. 497(1): p. 218-224.

374. Yang, N.Y., et al., *Vitamin E supplementation and glutathione peroxidase activity.* Proc Soc Exp Biol Med, 1976. 151(4): p. 770-4.

375. Garg, M.C., D.P. Chaudhary, and D.D. Bansal, *Effect of vitamin E supplementation on diabetes induced oxidative stress in experimental diabetes in rats.* Indian J Exp Biol, 2005. 43(2): p. 177-80.

376. Costagliola, C. and M. Menzione, *Effect of vitamin E on the oxidative state of glutathione in plasma.* Clin Physiol Biochem, 1990. 8(3): p. 140-3.

377. Costagliola, C., et al., *Vitamin E and red blood cell glutathione.* Metabolism, 1985. 34(8): p. 712-714.

378. Sharma, A., et al., *Effect of glycemic control and vitamin E supplementation on total glutathione content in non-insulin-dependent diabetes mellitus.* Ann Nutr Metab, 2000. 44(1): p. 11-3.

379. Suthutvoravut, U., et al., *Vitamin E status, glutathione peroxidase activity and the effect of vitamin E supplementation in children with thalassemia.* J Med Assoc Thai, 1993. 76 Suppl 2: p. 146-152.

380. Otero-Losada, M., et al., *Antioxidants Supplementation in Elderly Cardiovascular Patients %J Oxidative Medicine and Cellular Longevity.* Oxid Med Cell Longev, 2013. 2013: p. 5.

381. Hsu, C.-C., et al., *Role of vitamin B6 status on antioxidant defenses, glutathione, and related enzyme activities in mice with homocysteine-induced oxidative stress.* Food Nutr Res, 2015. 59: p. 25702-25702.

382. Jain, S.K. and G. Lim, *Pyridoxine and pyridoxamine inhibits superoxide radicals and prevents lipid peroxidation, protein glycosylation, and (Na+ + K+)-ATPase activity reduction in high glucose-treated human erythrocytes.* Free Radic Biol Med, 2001. 30(3): p. 232-7.

383. Mahfouz, M.M. and F.A. Kummerow, *Vitamin C or Vitamin B6 supplementation prevent the oxidative stress and decrease of prostacyclin generation in homocysteinemic rats.* Int J Biochem Cell Biol, 2004. 36(10): p. 1919-32.

384. Anand, S.S., *Pyridoxine attenuates chromium-induced oxidative stress in rat kidney.* Basic Clin Pharmacol Toxicol, 2005. 97(1): p. 58-60.

385. Anand, S.S., *Protective effect of vitamin B6 in chromium-induced oxidative stress in liver.* J Appl Toxicol, 2005. 25(5): p. 440-443.

386. Tas, S., E. Sarandol, and M. Dirican, *Vitamin B6 Supplementation Improves Oxidative Stress and Enhances Serum Paraoxonase/Arylesterase Activities in Streptozotocin-Induced Diabetic Rats.* Sci World J, 2014. 2014: p. 7.

387. Cheng, S.-B., et al., *Vitamin B-6 Supplementation Could Mediate Antioxidant Capacity by Reducing Plasma Homocysteine Concentration in Patients with Hepatocellular Carcinoma after Tumor Resection.* Biomed Res Int, 2016. 2016: p. 7658981-7658981.

388. DiFrancisco-Donoghue, J., et al., *Effects of exercise and B vitamins on homocysteine and glutathione in Parkinson's disease: a randomized trial.* Neurodegener Dis, 2012. 10(1-4): p. 127-34.

389. Suliman, M.E., et al., *Effects of High-Dose Folic Acid and Pyridoxine on Plasma and Erythrocyte Sulfur Amino Acids in Hemodialysis Patients.* JASN, 1999. 10(6): p. 1287.

390. Winkler, B.S., S.M. Orselli, and T.S. Rex, *The redox couple between glutathione and ascorbic acid: a chemical and physiological perspective.* Free Radic Biol Med, 1994. 17(4): p. 333-49.

391. Meister, A., *Glutathione-ascorbic acid antioxidant system in animals.* J Biol Chem, 1994. 269(13): p. 9397-400.

392. Meister, A., *The Antioxidant Effects of Glutathione and Ascorbic Acid*, in *Oxidative Stress, Cell Activation and Viral Infection*, C. Pasquier, et al., Editors. 1994, Birkhäuser Basel: Basel. p. 101-111.

393. Lal, H., et al., *Effect of methionine and vitamin C supplementation on pulmonary glutathione-s-transferase and glutathione levels in ageing rats.* Indian J Clin Biochem, 1993. 8(1): p. 33-35.

394. Chen, L.H. and R.R. Thacker, *An increase in glutathione peroxidase activity induced by high supplementation of vitamin C in rats.* Nutr Res, 1984. 4(4): p. 657-664.

395. Rojas, C., et al., *Effect of vitamin C on antioxidants, lipid peroxidation, and GSH system in the normal guinea pig heart.* J Nutr Sci Vitaminol, 1994. 40(5): p. 411-20.

396. Johnston, C.S., C.G. Meyer, and J.C. Srilakshmi, *Vitamin C elevates red blood cell glutathione in healthy adults.* Am J Clin Nutr, 1993. 58(1): p. 103-5.

397. Lenton, K.J., et al., *Vitamin C augments lymphocyte glutathione in subjects with ascorbate deficiency.* Am J Clin Nutr, 2003. 77(1): p. 189-95.

398. Karajibani, M., et al., *Effect of Vitamin E and C Supplements on Antioxidant Defense System in Cardiovascular Disease Patients in Zahedan, Southeast Iran.* J Nutr Sci Vitaminol (Tokyo), 2010. 56(6): p. 436-440.

399. Zal, F., et al., *Effect of vitamin E and C supplements on lipid peroxidation and GSH-dependent antioxidant enzyme status in the blood of women consuming oral contraceptives.* Contraception, 2012. 86(1): p. 62-66.

400. Al-Taie, O.H., et al., *Selenium supplementation enhances low selenium levels and stimulates glutathione peroxidase activity in peripheral blood and distal colon mucosa in past and present carriers of colon adenomas.* Nutr Cancer, 2003. 46(2): p. 125-30.

401. Lubos, E., J. Loscalzo, and D.E. Handy, *Glutathione peroxidase-1 in health and disease: from molecular mechanisms to therapeutic opportunities.* Antioxid Redox Signal, 2011. 15(7): p. 1957-1997.

402. Venardos, K., et al., *Effects of dietary selenium on glutathione peroxidase and thioredoxin reductase activity and recovery from cardiac ischemia-reperfusion.* J Trace Elem Med Biol, 2004. 18(1): p. 81-8.

403. Chow, C.K. and A.L. Tappel, *Response of glutathione peroxidase to dietary selenium in rats.* J Nutr, 1974. 104(4): p. 444-51.

404. Wortzman, M.S., H.J. Besbris, and A.M. Cohen, *Effect of Dietary Selenium on the Interaction between 2-Acetylaminofluorene and Rat Liver DNA in VIvo.* Cancer Res, 1980. 40(8 Part 1): p. 2670.

405. van Rij, A.M., et al., *Selenium and vitamin E supplementation: activities of glutathione peroxidase in human tissues.* Am J Clin Nutr, 1988. 48(2): p. 316-323.

406. Sedighi, O., M. Zargari, and G. Varshi, *Effect of selenium supplementation on glutathione peroxidase enzyme activity in patients with chronic kidney disease: a randomized clinical trial.* Nephrourol Mon, 2014. 6(3): p. e17945-e17945.

407. Zachara, B.A., et al., *Selenium supplementation on plasma glutathione peroxidase activity in patients with end-stage chronic renal failure.* Biol Trace Elem Res, 2004. 97(1): p. 15-30.

408. Zachara, B.A., et al., *Selenium and glutathione levels, and glutathione peroxidase activities in blood components of uremic patients on hemodialysis supplemented with selenium and treated with erythropoietin.* J Trace Elem Med Biol, 2001. 15(4): p. 201-8.

409. Wang Y.X. and K. J., *Effect of Selenium Supplementation on Platelet Selenium, Glutathione Peroxidase, and Aggregation.* Biol Trace Elem Res, 1988. 15(15): p. 89-96.

410. Nève, J., *Human Selenium Supplementation as Assessed by Changes in Blood Selenium Concentration and Glutathione Peroxidase Activity.* J Trace Elem Med Biol, 1995. 9(2): p. 65-73.

411. Steiner, G., et al., *Plasma glutathione peroxidase after selenium supplementation in patients with reduced selenium state.* Eur J Pediatr, 1982. 138(2): p. 138-140.

412. Oliveira-Silva, J.A.d., et al., *Oxidative stress assessment by glutathione peroxidase activity and glutathione levels in response to selenium supplementation in patients with Mucopolysaccharidosis I, II and VI.* Genet Mol Biol, 2019. 42: p. 1-8.

413. Jiang, X., et al., *Effects of organic selenium supplement on glutathione peroxidase activities: a meta-analysis of randomized controlled trials.* Wei Sheng Yan Jiu, 2012. 41(1): p. 120-3.

414. Jamba, L., B. Nehru, and M.P. Bansal, *Effect of selenium supplementation on the influence of cadmium on glutathione and glutathione peroxidase system in mouse liver.* 2000. 13: p. 299-304.

415. Tarp, U., et al., *Glutathione redox cycle enzymes and selenium in severe rheumatoid arthritis: lack of antioxidative response to selenium supplementation in polymorphonuclear leucocytes.* Ann Rheum Dis, 1992. 51(9): p. 1044-9.

416. Vertongen, F., J. Nève, and P. Capel, *Selenium supplementation in healthy Belgian adults: response in platelet glutathione peroxidase activity and other blood indices.* Am J Clin Nutr, 1988. 48(1): p. 139-143.

417. Hsu, J.M., B. Rubenstein, and A.G. Paleker, *Role of magnesium in glutathione metabolism of rat erythrocytes.* J Nutr, 1982. 112(3): p. 488-96.

418. Ige, A.O., E.O. Adewoye, and E.O. Makinde, *Oral Magnesium Potentiates Glutathione Activity in Experimental Diabetic Rats.* Int J Diabetes Res, 2016. 5(2): p. 21-25.

419. Howard, J.M., S. Davies, and A. Hunnisett, *Red cell magnesium and glutathione peroxidase in infertile women--effects of oral supplementation with magnesium and selenium.* Magnes Res, 1994. 7(1): p. 49-57.

420. Bede, O., et al., *Effects of magnesium supplementation on the glutathione redox system in atopic asthmatic children.* Inflamm Res, 2008. 57(6): p. 279-86.

421. Bahmani, F., et al., *Magnesium supplementation affects metabolic status and pregnancy outcomes in gestational diabetes: a randomized, double-blind, placebo-controlled trial.* Am J Clin Nutr, 2015. 102(1): p. 222-229.

422. Davis, C., et al., *Definition of the Mediterranean Diet; a Literature Review.* Nutrients, 2015. 7(11): p. 9139-9153.

423. Simopoulos, A.P., *The Mediterranean Diets: What Is So Special about the Diet of Greece? The Scientific Evidence.* J Nutr, 2001. 131(11): p. 3065S-3073S.

424. Dai, J., et al., *Association between adherence to the Mediterranean diet and oxidative stress.* Am J Clin Nutr, 2008. 88(5): p. 1364-1370.

425. Pastori, D., et al., *Is There an Interplay Between Adherence to Mediterranean Diet, Antioxidant Status, and Vascular Disease in Atrial Fibrillation Patients?* Antioxid Redox Signal, 2016. 25(14): p. 751-755.

426. Shively, C.A., et al., *Consumption of Mediterranean versus Western Diet Leads to Distinct Mammary Gland Microbiome Populations.* Cell Rep, 2018. 25(1): p. 47-56.e3.

427. Bettermann, E.L., et al., *Higher Mediterranean Diet Quality Scores and Lower Body Mass Index Are Associated with a Less-Oxidized Plasma Glutathione and Cysteine Redox Status in Adults.* J Nutr, 2018. 148(2): p. 245-253.

428. Furukawa, S., et al., *Increased oxidative stress in obesity and its impact on metabolic syndrome.* J Clin Invest, 2004. 114(12): p. 1752-1761.

429. Challa, H.J. and K.R. Uppaluri, *DASH Diet (Dietary Approaches to Stop Hypertension)*, in *StatPearls [Internet]*. 2019, StatPearls Publishing: Treasure Island (FL).

430. Asemi, Z., et al., *A randomized controlled clinical trial investigating the effect of DASH diet on insulin resistance, inflammation, and oxidative stress in gestational diabetes.* Nutrition, 2013. 29(4): p. 619-24.

431. Lang, C.A., et al., *Blood glutathione decreases in chronic diseases.* J Lab Clin Med, 2000. 135(5): p. 402-5.

432. Razavi Zade, M., et al., *The effects of DASH diet on weight loss and metabolic status in adults with non-alcoholic fatty liver disease: a randomized clinical trial.* Liver Int, 2016. 36(4): p. 563-71.

433. Asemi, Z., et al., *Effects of DASH diet on lipid profiles and biomarkers of oxidative stress in overweight and obese women with polycystic ovary syndrome: a randomized clinical trial.* Nutrition, 2014. 30(11-12): p. 1287-93.

434. Krajcovicova-Kudlackova, M., et al., *[Alternative nutrition and glutathione levels].* Cas Lek Cesk, 1999. 138(17): p. 528-31.

435. Poornima, K., et al., *Oxidant and antioxidant status in vegetarians and fish eaters.* Indian J Clin Biochem, 2003. 18(2): p. 197-205.

436. Rauma, A.L., et al., *Antioxidant status in long-term adherents to a strict uncooked vegan diet.* Am J Clin Nutr, 1995. 62(6): p. 1221-7.

437. Appleby, P.N. and T.J. Key, *The long-term health of vegetarians and vegans.* Proc Nutr Soc, 2016. 75(3): p. 287-93.

438. Kahleova, H., et al., *Vegetarian diet improves insulin resistance and oxidative stress markers more than conventional diet in subjects with Type 2 diabetes.* Diabet Med, 2011. 28(5): p. 549-559.

439. Haldar, S., et al., *Influence of habitual diet on antioxidant status: a study in a population of vegetarians and omnivores.* Eur J Clin Nutr, 2007. 61(8): p. 1011-22.

440. Kim, M.K., S.W. Cho, and Y.K. Park, *Long-term vegetarians have low oxidative stress, body fat, and cholesterol levels.* Nutr Res Pract, 2012. 6(2): p. 155-161.

441. Statovci, D., et al., *The Impact of Western Diet and Nutrients on the Microbiota and Immune Response at Mucosal Interfaces.* Front Immunol, 2017. 8: p. 838-838.

442. Vuković, R., et al., *Impact of ovariectomy, high fat diet, and lifestyle modifications on oxidative/antioxidative status in the rat liver.* Croat Med J, 2014. 55(3): p. 218-227.

443. Li, L., et al., *A Western diet induced NAFLD in LDLR(-/)(-) mice is associated with reduced hepatic glutathione synthesis.* Free Radic Biol Med, 2016. 96: p. 13-21.

444. Erdelyi, I., et al., *Western-style diets induce oxidative stress and dysregulate immune responses in the colon in a mouse model of sporadic colon cancer.* J Nutr, 2009. 139(11): p. 2072-2078.

445. Xiao, Y., et al., *Dietary protein and plasma total homocysteine, cysteine concentrations in coronary angiographic subjects.* Nutr J, 2013. 12(1): p. 144-144.

446. Olsen, T., et al., *Combining Dietary Sulfur Amino Acid Restriction with Polyunsaturated Fatty Acid Intake in Humans: A Randomized Controlled Pilot Trial.* Nutrients, 2018. 10(12).

447. Okreglicka, K., *Health effects of changes in the structure of dietary macronutrients intake in western societies.* Rocz Panstw Zakl Hig, 2015. 66(2): p. 97-105.

448. Piccolomini, A.F., et al., *High hydrostatic pressure pre-treatment of whey proteins enhances whey protein hydrolysate inhibition of oxidative stress and IL-8 secretion in intestinal epithelial cells.* Food Nutr Res, 2012. 56.

449. Grey, V., et al., *Improved glutathione status in young adult patients with cystic fibrosis supplemented with whey protein.* J Cyst Fibros, 2003. 2(4): p. 195-8.

450. Zeevalk, G.D., L.P. Bernard, and F.T. Guilford, *Liposomal-glutathione provides maintenance of intracellular glutathione and neuroprotection in mesencephalic neuronal cells.* Neurochem Res, 2010. 35(10): p. 1575-87.

451. Ly, J., et al., *Liposomal Glutathione Supplementation Restores TH1 Cytokine Response to Mycobacterium tuberculosis Infection in HIV-Infected Individuals.* J Interferon Cytokine Res, 2015. 35(11): p. 875-887.

452. Lauver, D.A., N.M. Kaissarian, and B.R. Lucchesi, *Oral pretreatment with liposomal glutathione attenuates reperfusion injury in rabbit isolated hearts.* J Cardiovasc Pharmacol, 2013. 61(3): p. 233-9.

453. Rahman, I., A. Kode, and S.K. Biswas, *Assay for quantitative determination of glutathione and glutathione disulfide levels using enzymatic recycling method.* Nat Protoc, 2006. 1(6): p. 3159-65.

454. Park HJ, M.E., Bruno RS, *Validation of high-performance liquid chromatographyboron-doped diamond detection for assessing hepatic glutathione redox status.* Anal Biochem, 2010. 407: p. 151-159.

455. Camera, E., et al., *Simultaneous determination of reduced and oxidized glutathione in peripheral blood mononuclear cells by liquid chromatography-electrospray mass spectrometry.* J Chromatogr B Biomed Sci Appl, 2001. 757(1): p. 69-78.

456. Sen, C.K., *Glutathione homeostasis in response to exercise training and nutritional supplements.* Mol Cell Biochem, 1999. 196(1-2): p. 31-42.

457. Davies, K.J.A., et al., *Free radicals and tissue damage produced by exercise.* Biochem Biophys Res Commun, 1982. 107(4): p. 1198-1205.

458. Nyberg, M., et al., *Roles of sedentary aging and lifelong physical activity in exchange of glutathione across exercising human skeletal muscle.* Free Radic Biol Med, 2014. 73: p. 166-173.

459. Powers, S.K., et al., *Exercise-induced oxidative stress: Friend or foe?* J Sport Health Sci, 2020. 9(5): p. 415-425.

460. Sastre, J., et al., *Exhaustive physical exercise causes oxidation of glutathione status in blood: prevention by antioxidant administration.* Am J Physiol Regul Integr Comp Physiol, 1992. 263(5): p. R992-R995.

461. Elokda, A.S. and D.H. Nielsen, *Effects of exercise training on the glutathione antioxidant system.* Eur J Cardiovasc Prev Rehabil, 2007. 14(5): p. 630-637.

462. Austin, C.P., et al., *The knockout mouse project.* Nat Genet, 2004. 36(9): p. 921-924.

463. Winkler, A., et al., *Glutathione is essential for early embryogenesis--analysis of a glutathione synthetase knockout mouse.* Biochem Biophys Res Commun, 2011. 412(1): p. 121-6.

464. Esworthy, R.S., et al., *Mice with combined disruption of Gpx1 and Gpx2 genes have colitis.* Am J Physiol Gastrointest Liver Physiol, 2001. 281(3): p. G848-55.

465. Chabory, E., et al., *Epididymis seleno-independent glutathione peroxidase 5 maintains sperm DNA integrity in mice.* JCI, 2009. 119(7): p. 2074-2085.

466. McConnachie, L.A., et al., *Glutamate cysteine ligase modifier subunit deficiency and gender as determinants of acetaminophen-induced hepatotoxicity in mice.* Toxicol Sci, 2007. 99(2): p. 628-36.

467. Yang, Y., et al., *Initial characterization of the glutamate-cysteine ligase modifier subunit Gclm(-/-) knockout mouse. Novel model system for a severely compromised oxidative stress response.* J Biol Chem, 2002. 277(51): p. 49446-52.

468. Dalton, T.P., et al., *Knockout of the mouse glutamate cysteine ligase catalytic subunit (Gclc) gene: embryonic lethal when homozygous, and proposed model for moderate glutathione deficiency when heterozygous.* Biochem Biophys Res Commun, 2000. 279(2): p. 324-9.

469. Feng, W., et al., *Gclc deficiency in mouse CNS causes mitochondrial damage and neurodegeneration.* Hum Mol Genet, 2017. 26(7): p. 1376-1390.

470. Han, C., et al., *GSR is not essential for the maintenance of antioxidant defenses in mouse cochlea: Possible role of the thioredoxin system as a functional backup for GSR.* PLoS One, 2017. 12(7): p. e0180817.

471. Fujii, J., et al., *Unveiling the roles of the glutathione redox system in vivo by analyzing genetically modified mice.* J Clin Biochem Nutr, 2011. 49(2): p. 70-78.

472. Kwon, J.M. and A.M. Goate, *The candidate gene approach.* Alcohol Res Health, 2000. 24(3): p. 164-168.

473. Méplan, C., et al., *Association between polymorphisms in glutathione peroxidase and selenoprotein P genes, glutathione peroxidase activity, HRT use and breast cancer risk.* PloS one, 2013. 8(9): p. e73316.

474. Udler, M., et al., *Common germline genetic variation in antioxidant defense genes and survival after diagnosis of breast cancer.* J Clin Oncol, 2007. 25(21): p. 3015-23.

475. Corredor, Z., et al., *Genetic Variants Associated with Chronic Kidney Disease in a Spanish Population.* Sci Rep, 2020. 10(1): p. 144.

476. Arsova-Sarafinovska, Z., et al., *Glutathione peroxidase 1 (GPX1) genetic polymorphism, erythrocyte GPX activity, and prostate cancer risk.* Int Urol Nephrol, 2009. 41(1): p. 63-70.

477. Bănescu, C., et al., *From Six Gene Polymorphisms of the Antioxidant System, Only GPX Pro198Leu and GSTP1 Ile105Val Modulate the Risk of Acute Myeloid Leukemia.* Oxid Med Cell Longev, 2016. 2016: p. 2536705.

478. Mohammedi, K., et al., *Glutathione peroxidase-1 gene (GPX1) variants, oxidative stress and risk of kidney complications in people with type 1 diabetes.* Metabolism, 2016. 65(2): p. 12-9.

479. Voetsch, B., et al., *Promoter polymorphisms in the plasma glutathione peroxidase (GPx-3) gene: a novel risk factor for arterial ischemic stroke among young adults and children.* Stroke, 2007. 38(1): p. 41-9.

480. Rupérez, A.I., et al., *Association of Genetic Polymorphisms for Glutathione Peroxidase Genes with Obesity in Spanish Children.* Lifestyle Genom, 2014. 7(3): p. 130-142.

481. Ahn, J., et al., *No association between glutathione peroxidase Pro198Leu polymorphism and breast cancer risk.* Cancer Epidemiol Biomarkers Prev, 2005. 14(10): p. 2459-61.

482. Aydin, A., et al., *Oxidative stress and antioxidant status in non-metastatic prostate cancer and benign prostatic hyperplasia.* Clin Biochem, 2006. 39(2): p. 176-9.

483. Dursun, H., et al., *Antioxidant enzyme activities and lipid peroxidation levels in erythrocytes of patients with oesophageal and gastric cancer.* J Int Med Res, 2006. 34(2): p. 193-9.

484. Pawłowicz, Z., et al., *Blood selenium concentrations and glutathione peroxidase activities in patients with breast cancer and with advanced gastrointestinal cancer.* J Trace Elem Electrolytes Health Dis, 1991. 5(4): p. 275-7.

485. Ravn-Haren, G., et al., *Associations between GPX1 Pro198Leu polymorphism, erythrocyte GPX activity, alcohol consumption and breast cancer risk in a prospective cohort study.* Carcinogenesis, 2006. 27(4): p. 820-5.

486. Saygili, E.I., et al., *Glutathione and glutathione-related enzymes in colorectal cancer patients.* J Toxicol Environ Health A, 2003. 66(5): p. 411-5.

487. Ristoff, E. and A. Larsson, *Patients with genetic defects in the gamma-glutamyl cycle.* Chem Biol Interact, 1998. 111-112: p. 113-21.

488. McKone, E.F., et al., *Variants in the Glutamate-Cysteine-Ligase Gene Are Associated with Cystic Fibrosis Lung Disease.* Am J Respir Crit Care Med, 2006. 174(4): p. 415-419.

489. Bentley, A.R., P. Emrani, and P.A. Cassano, *Genetic variation and gene expression in antioxidant related enzymes and risk of COPD: a systematic review.* Thorax, 2008. 63(11): p. 956-61.

490. Wang, D., et al., *Polymorphism in glutamate cysteine ligase catalytic subunit (GCLC) is associated with sulfamethoxazole-induced hypersensitivity in HIV/AIDS patients.* BMC Med Genom, 2012. 5(1): p. 32.

491. T, M. and Y. E, *A Combination Polymorphism of the Glutathione Synthesis Genes Can Be a Predictive Biomarker for Anti-Tuberculosis Drug-Induced Hepatotoxicity in Japanese Patients with Pulmonary Tuberculosis.* J Lung Dis Treat, 2016. 02.

492. Kishi, T., et al., *Glutamate Cysteine Ligase Modifier (GCLM) Subunit Gene Is Not Associated with Methamphetamine-Use Disorder or Schizophrenia in the Japanese Population.* Ann N Y Acad Sci, 2008. 1139: p. 63-9.

493. Hanzawa, R., et al., *No association between glutathione-synthesis-related genes and Japanese schizophrenia.* Psych Clin Neurosci, 2011. 65(1): p. 39-46.

494. Bowers, K., et al., *Glutathione pathway gene variation and risk of autism spectrum disorders.* J Neurodev Dis, 2011. 3(2): p. 132-143.

495. Breton, C.V., et al., *Genetic variation in the glutathione synthesis pathway, air pollution, and children's lung function growth.* Am J Respir Crit Care Med, 2011. 183(2): p. 243-248.

496. Agrawal, S., et al., *Relationship between GSTs gene polymorphism and susceptibility to end stage renal disease among North Indians.* Ren Fail, 2007. 29(8): p. 947-53.

497. Li, Y.-J., et al., *Glutathione S-transferase omega-1 modifies age-at-onset of Alzheimer disease and Parkinson disease.* Hum Mol Genet, 2003. 12(24): p. 3259-3267.

498. Katoh, T., et al., *Genetic polymorphisms of human cytosol glutathione S-transferases and prostate cancer.* Pharmacogenomics, 2007. 9(1): p. 93-104.

499. Koh, W.P., et al., *Glutathione S-transferase (GST) gene polymorphisms, cigarette smoking and colorectal cancer risk among Chinese in Singapore.* Carcinogenesis, 2011. 32(10): p. 1507-11.

500. Mandic-Maravic, V., et al., *Interaction of glutathione S-transferase polymorphisms and tobacco smoking during pregnancy in susceptibility to autism spectrum disorders.* Sci Rep, 2019. 9(1): p. 3206.

501. Rodríguez-Santiago, B., et al., *Association of common copy number variants at the glutathione S-transferase genes and rare novel genomic changes with schizophrenia.* Mol Psych, 2010. 15(10): p. 1023-1033.

502. White, D.L., et al., *Genetic Variants of Glutathione S-Transferase as Possible Risk Factors for Hepatocellular Carcinoma: A HuGE Systematic Review and Meta-Analysis.* Am J Epidemiol, 2008. 167(4): p. 377-389.

503. Cao, T., et al., *Effects of Glutathione S-Transferase Gene Polymorphisms and Antioxidant Capacity per Unit Albumin on the Pathogenesis of Chronic Obstructive Pulmonary Disease.* Oxid Med Cell Longev, 2017. 2017: p. 6232397.

504. Beutler, E. and F. Matsumoto, *Ethnic variation in red cell glutathione peroxidase activity.* Blood, 1975. 46(1): p. 103-10.

505. Necheles, T.F., et al., *Hemozygous Erythrocyte Glutathione-Peroxidase Deficiency: Clinical and Biochemical Studies.* Blood, 1969. 33(2): p. 164-169.

506. Necheles, T.F., M.H. Steinberg, and D. Cameron, *Erythrocyte Glutathione-Peroxidase Deficiency.* British J Haematol, 1970. 19(5): p. 605-612.

507. Perona, G., et al., *Neonatal Erythrocyte Glutathione Peroxidase Deficiency as a Consequence of Selenium Imbalance during Pregnancy.* British J Haematol, 1979. 42(4): p. 567-574.

508. Steinberg, M., M.J. Brauer, and T.F. Necheles, *Acute Hemolytic Anemia Associated With Erythrocyte Glutathione-Peroxidase Deficiency.* Arch Intern Med, 1970. 125(2): p. 302-303.

509. Freedman, J.E., et al., *Decreased platelet inhibition by nitric oxide in two brothers with a history of arterial thrombosis.* J Clin Invest, 1996. 97(4): p. 979-87.

510. Kenet, G., et al., *Plasma glutathione peroxidase deficiency and platelet insensitivity to nitric oxide in children with familial stroke.* Arterioscler Thromb Vasc Biol, 1999. 19(8): p. 2017-23.

511. Willis, M.N., et al., *Enzymatic defects underlying hereditary glutamate cysteine ligase deficiency are mitigated by association of the catalytic and regulatory subunits.* Biochemistry, 2011. 50(29): p. 6508-6517.

512. Mañú Pereira, M., et al., *Chronic non-spherocytic hemolytic anemia associated with severe neurological disease due to gamma-glutamylcysteine synthetase deficiency in a patient of Moroccan origin.* Haematologica, 2007. 92(11): p. e102-5.

513. Hamilton, D., et al., *A novel missense mutation in the gamma-glutamylcysteine synthetase catalytic subunit gene causes both decreased enzymatic activity and glutathione production.* Blood, 2003. 102(2): p. 725-30.

514. Ristoff, E., et al., *A missense mutation in the heavy subunit of gamma-glutamylcysteine synthetase gene causes hemolytic anemia.* Blood, 2000. 95(7): p. 2193-6.

515. Beutler, E., et al., *The molecular basis of a case of gamma-glutamylcysteine synthetase deficiency.* Blood, 1999. 94(8): p. 2890-4.

516. Hirono, A., et al., *Three cases of hereditary nonspherocytic hemolytic anemia associated with red blood cell glutathione deficiency.* Blood, 1996. 87(5): p. 2071-4.

517. Goebel, K.M., L. Hausmann, and H. Kaffarnik, *Pancytopenia with Hemolytic Anemia in Glutathione Reductase Deficiency.* Enzyme, 1971. 12: p. 375-381.

518. El-Hazmi, M.A.F. and A.S. Warsy, *Glutathione Reductase Deficiency in Association with Sickle Cell and Thalassaemia Genes in Saudi Populations.* Human Heredity, 1985. 35(5): p. 326-332.

519. Kamerbeek, N.M., et al., *Molecular basis of glutathione reductase deficiency in human blood cells.* Blood, 2007. 109(8): p. 3560-6.

520. Borroz KI, R.H., Eaton DL, *Mouse strain differences in glutathione S-transferase activity and aflatoxin B1 biotransformation.* Toxicol Lett, 1991. 58(1): p. 97-105.

521. Egaas E, F.J., Dauterman WC, *A study of gender, strain and age differences in mouse liver glutathione-S-transferase.* Comp Biochem Physiol C Pharmacol Toxicol Endocrinol, 1995. 110(1): p. 35-40.

522. Rebrin I, F.M., Sohal RS, *Effects of age and caloric intake on glutathione redox state in different brain regions of C57BL/6 and DBA/2 mice.* Brain Res, 2007. 1127(1): p. 10-18.

523. Rebrin I, F.M., Sohal RS, *Association between life-span extension by caloric restriction and thiol redox state in two different strains of mice.* Free Radic Biol Med, 2011. 51(1): p. 225-233.

524. Ferguson M, R.I., Forster M, Sohal R, *Comparison of metabolic rate and oxidative stress between two different strains of mice with varying response to caloric restriction.* Exp Gerontol, 2008. 43(8): p. 757-763.

525. Tsuchiya, M., et al., *Interstrain differences in liver injury and one-carbon metabolism in alcohol-fed mice.* Hepatology, 2012. 56(1): p. 130-139.

526. Zhou Y, H.D., Love-Myers K, Chen Y, Grider A, Wickwire K, Burgess JR, Stochelski MA, Pazdro R, *Genetic analysis of tissue glutathione concentrations and redox balance.* Free Radic Biol Med, 2014. 71: p. 157-164.

527. van 't Erve, T.J., et al., *The concentration of glutathione in human erythrocytes is a heritable trait.* Free Radic Biol Med, 2013. 65: p. 742-9.

528. Norris, K.M., et al., *The anthocyanin cyanidin-3-O-β-glucoside modulates murine glutathione homeostasis in a manner dependent on genetic background.* Redox Biol, 2016: p. 254-263.

529. Norris KM, O.W., Kim WK, Adhikari R, Yoo S, King S, Pazdro R, *A high-fat diet differentially regulates glutathione phenotypes in the obesity-prone mouse strains DBA/2J, C57BL/6J, and AKR/J.* Nutr Res, 2016. 36(12): p. 1316-1324.

530. Tong, J., et al., *Do glutathione levels decline in aging human brain?* Free Radic Biol Med, 2016. 93: p. 110-117.

531. Grunwell, J.R., et al., *Comparison of Glutathione, Cysteine, and Their Redox Potentials in the Plasma of Critically Ill and Healthy Children.* Front Ped, 2015. 3: p. 46-46.

532. Berndt, C., C.H. Lillig, and A. Holmgren, *Thioredoxins and glutaredoxins as facilitators of protein folding.* Biochim Biophys Acta Mol Cell Res, 2008. 1783(4): p. 641-650.

533. Gawlik, K., et al., *Markers of Antioxidant Defense in Patients with Type 2 Diabetes.* Oxid Med Cell Longev, 2016. 2016: p. 2352361.

534. Hakki Kalkan, I. and M. Suher, *The relationship between the level of glutathione, impairment of glucose metabolism and complications of diabetes mellitus.* Pak J Biol Sci, 2013. 29(4): p. 938-942.

535. Calabrese, V., et al., *Oxidative stress, glutathione status, sirtuin and cellular stress response in type 2 diabetes.* Biochim Biophys Acta, 2012. 1822(5): p. 729-736.

536. Yuniastuti, A., R. Susanti, and D. Mustikaningtyas, *Polymorphism of Glutamate-Cysteine Ligase Subunit Catalytic (GCLC) Gene in Pulmonary Tuberculosis Patients.* Pak J Biol Sci, 2017. 20(8): p. 397-402.

537. Walsh, A.C., J.A. Feulner, and A. Reilly, *Evidence for Functionally Significant Polymorphism of Human Glutamate Cysteine Ligase Catalytic Subunit: Association with Glutathione Levels and Drug Resistance in the National Cancer Institute Tumor Cell Line Panel.* Toxicol Sci, 2001. 61(2): p. 218-223.

538. Custodio, H.M., et al., *Polymorphisms in glutathione-related genes affect methylmercury retention.* Arch Environ Health, 2004. 59(11): p. 588-95.

539. Koide, S., et al., *Association of polymorphism in glutamate-cysteine ligase catalytic subunit gene with coronary vasomotor dysfunction and myocardial infarction.* J Am Coll Cardiol, 2003. 41(4): p. 539-45.

540. Skvortsova, L., et al., *Association of GCLM -588C/T and GCLC -129T/C Promoter Polymorphisms of Genes Coding the Subunits of Glutamate Cysteine Ligase with Ischemic Heart Disease Development in Kazakhstan Population.* Disease Markers, 2017. 2017: p. 4209257.

541. Nakamura, S.-i., et al., *Polymorphism in Glutamate-Cysteine Ligase Modifier Subunit Gene Is Associated With Impairment of Nitric Oxide–Mediated Coronary Vasomotor Function.* Circulation, 2003. 108(12): p. 1425-1427.

542. Sun, Z., et al., *Genetic variation in glutathione metabolism and DNA repair genes predicts survival of small-cell lung cancer patients.* Ann Oncol, 2010. 21(10): p. 2011-2016.

543. Dahl, N., et al., *Missense Mutations in the Human Glutathione Synthetase Gene Result in Severe Metabolic Acidosis, 5-Oxoprolinuria, Hemolytic Anemia and Neurological Dysfunction.* Hum Mol Genet, 1997. 6(7): p. 1147-1152.

544. Ristoff, E. and A. Larsson, *Inborn errors in the metabolism of glutathione.* Orphanet J Rare Dis, 2007. 2: p. 16-16.

545. Chesler, E.J., S.L. Rodriguez-Zas, and J.S. Mogil, *In Silico Mapping of Mouse Quantitative Trait Loci.* Science, 2001. 294(5551): p. 2423.

546. Smith Jonathan, D., et al., *In Silico Quantitative Trait Locus Map for Atherosclerosis Susceptibility in Apolipoprotein E–Deficient Mice.* Arterioscler Thromb Vasc Biol, 2003. 23(1): p. 117-122.

547. Burgess-Herbert, S.L., et al., *An experimental assessment of in silico haplotype association mapping in laboratory mice.* BMC Genet, 2009. 10(1): p. 81.

548. Churchill, G.A., et al., *The Diversity Outbred mouse population.* Mamm Genome, 2012. 23(9-10): p. 713-8.

549. Broman, K.W., et al., *R/qtl2: software for mapping quantitative trait loci with high dimensional data and multi-parent populations.* Genetics, 2019. 211(2): p. 495.

550. Jones, D.P. and H. Sies, *The Redox Code.* Antioxid Redox Signal, 2015. 23(9): p. 734-746.

551. Khazim, K., et al., *Glutathione redox potential is low and glutathionylated and cysteinylated hemoglobin levels are elevated in maintenance hemodialysis patients.* Trans Res, 2013. 162(1): p. 16-25.

552. Wang, X., et al., *Intramucosal pH and oxygen extraction in the gastrointestinal tract after major liver resection in rats.* Eur J Surg, 1993. 159(2): p. 81-7.

553. Ziegler, T.R., et al., *Regulation of glutathione redox status in lung and liver by conditioning regimens and keratinocyte frowth factor in murine allogeneic bone marrow transplantation.* Transplantation, 2001. 72(8).

554. Rost, J. and S. Rapoport, *Reduction potential of glutathione.* Nature, 1964. 201: p. 185.

555. Rebrin, I., S. Kamzalov, and R.S. Sohal, *Effects of age and caloric restriction on glutathione redox state in mice.* Free Radic Biol Med, 2003. 35(6): p. 626-635.

556. García-de-la-Asunción, J., et al., *Glutathione oxidation correlates with one-lung ventilation time and PO2/FiO2 ratio during pulmonary lobectomy.* Redox Rep, 2016. 21(5): p. 219-226.

557. Morgan, A.P., et al., *The Mouse Universal Genotyping Array: From Substrains to Subspecies.* G3, 2016. 6(2): p. 263.

558. Svenson, K.L., et al., *High-Resolution Genetic Mapping Using the Mouse Diversity Outbred Population.* Genetics, 2012. 190(2): p. 437.

559. Yang, J., et al., *Advantages and pitfalls in the application of mixed-model association methods.* Nature Genet, 2014. 46(2): p. 100-106.

560. Sen, S. and G.A. Churchill, *A statistical framework for quantitative trait mapping.* Genetics, 2001. 159(1): p. 371-387.

561. Churchill, G.A. and R.W. Doerge, *Empirical threshold values for quantitative trait mapping.* Genetics, 1994. 138(3): p. 963-71.

562. Recla, J.M., et al., *Precise genetic mapping and integrative bioinformatics in Diversity Outbred mice reveals Hydin as a novel pain gene.* Mamm Genome, 2014. 25(5-6): p. 211-22.

563. Recla, J.M., et al., *Genetic mapping in Diversity Outbred mice identifies a Trpa1 variant influencing late-phase formalin response.* Pain, 2019. 160(8): p. 1740-1753.

564. Petryszak, R., et al., *Expression Atlas update--an integrated database of gene and protein expression in humans, animals and plants.* Nucleic Acids Res, 2016. 44(D1): p. D746-52.

565. Finger, J.H., et al., *The mouse Gene Expression Database (GXD): 2017 update.* Nucleic Acids Res, 2017. 45(D1): p. D730-d736.

566. Blake, J.A., et al., *Mouse Genome Database (MGD)-2017: community knowledge resource for the laboratory mouse.* Nucleic Acids Res, 2017. 45(D1): p. D723-d729.

567. Finn, R.D., et al., *InterPro in 2017-beyond protein family and domain annotations.* Nucleic Acids Res, 2017. 45(D1): p. D190-d199.

568. Ashburner, M., et al., *Gene ontology: tool for the unification of biology. The Gene Ontology Consortium.* Nat Genet, 2000. 25(1): p. 25-9.

569. *Expansion of the Gene Ontology knowledgebase and resources.* Nucleic Acids Res, 2017. 45(D1): p. D331-d338.

570. Gagliano Taliun, S.A., et al., *Exploring and visualizing large-scale genetic associations by using PheWeb.* Nat Genet, 2020. 52(6): p. 550-552.

571. Kinsella, R.J., et al., *Ensembl BioMarts: a hub for data retrieval across taxonomic space.* Database, 2011. 2011.

572. Davey, G.M., W.R. Heath, and R. Starr, *SOCS1: a potent and multifaceted regulator of cytokines and cell-mediated inflammation.* Tissue Antigens, 2006. 67(1): p. 1-9.

573. Saint-Germain, E., et al., *SOCS1 regulates senescence and ferroptosis by modulating the expression of p53 target genes.* Aging, 2017. 9(10): p. 2137-2162.

574. Lim, J.K.M., et al., *Cystine/glutamate antiporter xCT (SLC7A11) facilitates oncogenic RAS transformation by preserving intracellular redox balance.* Proc Natl Acad Sci, 2019. 116(19): p. 9433.

575. Ryo, A., et al., *Regulation of NF-kappaB signaling by Pin1-dependent prolyl isomerization and ubiquitin-mediated proteolysis of p65/RelA.* Mol Cell, 2003. 12(6): p. 1413-26.

576. Peng, Z., et al., *Inhibitor of kappaB kinase beta regulates redox homeostasis by controlling the constitutive levels of glutathione.* Mol Pharmacol, 2010. 77(5): p. 784-92.

577. Meng, Q., et al., *Nuclear Factor-κB modulates cellular glutathione and prevents oxidative stress in cancer cells.* Cancer letters, 2010. 299(1): p. 45-53.

578. Ulc, A., et al., *The guanine nucleotide exchange factor Vav3 modulates oligodendrocyte precursor differentiation and supports remyelination in white matter lesions.* Glia, 2019. 67(2): p. 376-392.

579. Roth, S., et al., *Vav Proteins Are Key Regulators of Card9 Signaling for Innate Antifungal Immunity.* Cell Rep, 2016. 17(10): p. 2572-2583.

580. Marui, N., et al., *Vascular cell adhesion molecule-1 (VCAM-1) gene transcription and expression are regulated through an antioxidant-sensitive mechanism in human vascular endothelial cells.* J Clin Invest, 1993. 92(4): p. 1866-1874.

581. Astarci, E., et al., *The NF-κB target genes ICAM-1 and VCAM-1 are differentially regulated during spontaneous differentiation of Caco-2 cells.* FEBS J, 2012. 279(16): p. 2966-86.

582. Deem, T.L. and J.M. Cook-Mills, *Vascular cell adhesion molecule 1 (VCAM-1) activation of endothelial cell matrix metalloproteinases: role of reactive oxygen species.* Blood, 2004. 104(8): p. 2385-93.

583. Li, L., et al., *A family of putative tumor suppressors is structurally and functionally conserved in humans and yeast.* J Biol Chem, 1997. 272(47): p. 29403-6.

584. Li, L., M. Ljungman, and J.E. Dixon, *The human Cdc14 phosphatases interact with and dephosphorylate the tumor suppressor protein p53.* J Biol Chem, 2000. 275(4): p. 2410-4.

585. Paulsen, M.T., et al., *The p53-targeting human phosphatase hCdc14A interacts with the Cdk1/cyclin B complex and is differentially expressed in human cancers.* Mol Cancer, 2006. 5(1): p. 25.

586. Lacroix, M., et al., *Metabolic functions of the tumor suppressor p53: Implications in normal physiology, metabolic disorders, and cancer.* Mol Metab, 2020. 33: p. 2-22.

587. Jiang, P., et al., *p53 regulates biosynthesis through direct inactivation of glucose-6-phosphate dehydrogenase.* Nat Cell Biol, 2011. 13(3): p. 310-316.

588. Han, D., et al., *Mechanisms of Liver Injury. III. Role of glutathione redox status in liver injury.* Am J Physiol Gastrointest Liver Physiol, 2006. 291(1): p. G1-G7.

589. Kim, K.M. and S.H. Ki, *Chapter 28 - Nrf2: A Key Regulator of Redox Signaling in Liver Diseases*, in *Liver Pathophysiol*, P. Muriel, Editor. 2017, Academic Press: Boston. p. 355-374.

590. Habib, E., et al., *Expression of xCT and activity of system xc− are regulated by NRF2 in human breast cancer cells in response to oxidative stress.* Redox Biol, 2015. 5: p. 33-42.

591. Koppula, P., et al., *Amino acid transporter SLC7A11/xCT at the crossroads of regulating redox homeostasis and nutrient dependency of cancer.* Cancer Commun, 2018. 38(1): p. 12.

592. Sasaki, H., et al., *Electrophile response element-mediated induction of the cystine/glutamate exchange transporter gene expression.* J Biol Chem, 2002. 277(47): p. 44765-71.

593. Conrad, M. and H. Sato, *The oxidative stress-inducible cystine/glutamate antiporter, system x (c) (-) : cystine supplier and beyond.* J Amino Acids, 2012. 42(1): p. 231-46.

594. Chia, A.J.L., et al., *Differential effect of covalent protein modification and glutathione depletion on the transcriptional response of Nrf2 and NF-κB.* Biochem Pharmacol, 2010. 80(3): p. 410-421.

595. Fujimoto, M. and T. Naka, *SOCS1, a Negative Regulator of Cytokine Signals and TLR Responses, in Human Liver Diseases.* Gastroenterol Res Pract, 2010: p. 470468.

596. The Jackson Laboratory. *Mouse Genome Database (MGD) at the Mouse Genome Informatics website*. 2020.

597. Marine, J.C., et al., *SOCS1 deficiency causes a lymphocyte-dependent perinatal lethality.* Cell, 1999. 98(5): p. 609-16.

598. Kempinska-Podhorodecka, A., et al., *The Association between SOCS1-1656G>A Polymorphism, Insulin Resistance and Obesity in Nonalcoholic Fatty Liver Disease (NAFLD) Patients.* J Clin Med, 2019. 8(11): p. 1912.

599. Meakin, L.B., et al., *Male mice housed in groups engage in frequent fighting and show a lower response to additional bone loading than females or individually housed males that do not fight.* Bone, 2013. 54(1): p. 113-117.

600. Moreno-Sánchez, R., et al., *Control of the NADPH supply and GSH recycling for oxidative stress management in hepatoma and liver mitochondria.* Biochim Biophys Acta, 2018. 1859(10): p. 1138-1150.

601. Yuan, L. and N. Kaplowitz, *Glutathione in liver diseases and hepatotoxicity.* Mol Aspects Med, 2009. 30(1-2): p. 29-41.

602. Guanliang, C., et al., *Micronutrient Antioxidants and Nonalcoholic Fatty Liver Disease.* Int J Mol Sci, 2016. 17(9): p. 1379.

603. Liu, W., et al., *Antioxidant Mechanisms in Nonalcoholic Fatty Liver Disease.* Curr Drug Targets, 2015. 16(12): p. 1301-14.

604. Fabbrini, E., S. Sullivan, and S. Klein, *Obesity and nonalcoholic fatty liver disease: biochemical, metabolic, and clinical implications.* Hepatology, 2010. 51(2): p. 679-689.

605. Dharmalingam, M. and P.G. Yamasandhi, *Nonalcoholic Fatty Liver Disease and Type 2 Diabetes Mellitus.* Indian J Endocrinol Metab, 2018. 22(3): p. 421-428.

606. Amor, A.J. and V. Perea, *Dyslipidemia in nonalcoholic fatty liver disease.* Curr Opin Endocrinol Diabetes Obes, 2019. 26(2): p. 103-108.

607. Yki-Järvinen, H., *Non-alcoholic fatty liver disease as a cause and a consequence of metabolic syndrome.* Lancet Diabet Endocrinol, 2014. 2(11): p. 901-910.

608. Kudaravalli, P. and S. John, *Nonalcoholic Fatty Liver*, in *StatPearls*. 2020: Treasure Island (FL).

609. Lash, L.H., *Role of glutathione transport processes in kidney function.* Toxicol Appl Pharmacol, 2005. 204(3): p. 329-342.

610. Chen, Y., et al., *Glutathione defense mechanism in liver injury: insights from animal models.* Food Chem Toxicol, 2013. 60: p. 38-44.

611. Rom, O., et al., *Glycine-based treatment ameliorates NAFLD by modulating fatty acid oxidation, glutathione synthesis, and the gut microbiome.* Sci Transl Med, 2020. 12(572).

612. Gaggini, M., et al., *Altered amino acid concentrations in NAFLD: Impact of obesity and insulin resistance.* Hepatology, 2018. 67(1): p. 145-158.

613. Brial, F., et al., *Systems Genetics of Hepatic Metabolome Reveals Octopamine as a Target for Non-Alcoholic Fatty Liver Disease Treatment.* Sci Rep, 2019. 9(1): p. 3656.

614. Brown, G.T. and D.E. Kleiner, *Histopathology of nonalcoholic fatty liver disease and nonalcoholic steatohepatitis.* Metab Clin Exp, 2016. 65(8): p. 1080-1086.

615. Liang, W., et al., *Establishment of a general NAFLD scoring system for rodent models and comparison to human liver pathology.* PloS one, 2014. 9(12): p. e115922-e115922.

616. Ryu, J.-E., et al., *Evaluation of Nonalcoholic Fatty Liver Disease in C57BL/6J Mice by Using MRI and Histopathologic Analyses.* Compar Med, 2015. 65(5): p. 409-415.

617. Bedossa, P. and T. Poynard, *An algorithm for the grading of activity in chronic hepatitis C. The METAVIR Cooperative Study Group.* Hepatology, 1996. 24(2): p. 289-93.

618. Calès, P., et al., *Diagnosis of different liver fibrosis characteristics by blood tests in non-alcoholic fatty liver disease.* Liver Int, 2010. 30(9): p. 1346-54.

619. Almpanis, Z., M. Demonakou, and D. Tiniakos, *Evaluation of liver fibrosis: "Something old, something new…".* Ann Gastroenterol, 2016. 29(4): p. 445-453.

620. Williams, A.L. and J.H. Hoofnagle, *Ratio of serum aspartate to alanine aminotransferase in chronic hepatitis. Relationship to cirrhosis.* Gastroenterology, 1988. 95(3): p. 734-9.

621. De Ritis, F., M. Coltorti, and G. Giusti, *An enzymic test for the diagnosis of viral hepatitis; the transaminase serum activities.* Clin Chim Acta, 1957. 2(1): p. 70-4.

622. Wroblewski, F., *The clinical significance of alterations in transaminase activities of serum and other body fluids.* Adv Clin Chem, 1958. Vol. 1(2): p. 313-51.

623. Vroon, D.H. and Z. Israili, *Aminotransferases*, in *Clinical Methods: The History, Physical, and Laboratory Examinations*. Butterworths: Boston.

624. Kadowaki, M., et al., *N-cadherin mediates cortical organization in the mouse brain.* Dev Biol, 2007. 304(1): p. 22-33.

625. Mohammed, F.F., et al., *Metalloproteinase inhibitor TIMP-1 affects hepatocyte cell cycle via HGF activation in murine liver regeneration.* Hepatology, 2005. 41(4): p. 857-67.

626. Toita, R., et al., *Increased hepatic inflammation in a normal-weight mouse after long-term high-fat diet feeding.* J Toxicol Pathol, 2018. 31(1): p. 43-47.

627. Omagari, K., et al., *Fatty liver in non-alcoholic non-overweight Japanese adults: incidence and clinical characteristics.* J Gastroenterol Hepatol, 2002. 17(10): p. 1098-105.

628. Sattar, N., E. Forrest, and D. Preiss, *Non-alcoholic fatty liver disease.* BMJ, 2014. 349: p. g4596.

629. Sanyal, D., et al., *Profile of liver enzymes in non-alcoholic fatty liver disease in patients with impaired glucose tolerance and newly detected untreated type 2 diabetes.* Indian J Endocrinol Metab, 2015. 19(5): p. 597-601.

630. VanSaun, M.N., et al., *High fat diet induced hepatic steatosis establishes a permissive microenvironment for colorectal metastases and promotes primary dysplasia in a murine model.* Am J Pathol, 2009. 175(1): p. 355-364.

631. Lau, J.K.C., X. Zhang, and J. Yu, *Animal models of non-alcoholic fatty liver disease: current perspectives and recent advances.* J Pathol, 2017. 241(1): p. 36-44.

632. Lauschke, V.M., S. Mkrtchian, and M. Ingelman-Sundberg, *The role of microRNAs in liver injury at the crossroad between hepatic cell death and regeneration.* Biochem Biophys Res Commun, 2017. 482(3): p. 399-407.

633. Meng, Z., et al., *miR-194 is a marker of hepatic epithelial cells and suppresses metastasis of liver cancer cells in mice.* Hepatology, 2010. 52(6): p. 2148-2157.

634. Fourman, L.T., et al., *Effects of tesamorelin on hepatic transcriptomic signatures in HIV-associated NAFLD.* JCI Insight, 2020. 5(16).

635. Gawrieh, S., et al., *A Pilot Genome-Wide Analysis Study Identifies Loci Associated With Response to Obeticholic Acid in Patients With NASH.* Hepatol Commun, 2019. 3(12): p. 1571-1584.

636. Yang, C., et al., *Cadherins Associate with Distinct Stem Cell-Related Transcription Factors to Coordinate the Maintenance of Stemness in Triple-Negative Breast Cancer.* Stem Cells Int, 2017. 2017: p. 5091541-5091541.

637. Loh, C.-Y., et al., *The E-Cadherin and N-Cadherin Switch in Epithelial-to-Mesenchymal Transition: Signaling, Therapeutic Implications, and Challenges.* Cells, 2019. 8(10): p. 1118.

638. Chen, P.-Y., M.A. Schwartz, and M. Simons, *Endothelial-to-Mesenchymal Transition, Vascular Inflammation, and Atherosclerosis.* Front Cardiovasc Med, 2020. 7(53).

639. Zhao, Y.-L., R.-T. Zhu, and Y.-L. Sun, *Epithelial-mesenchymal transition in liver fibrosis.* Biomed Rep, 2016. 4(3): p. 269-274.

640. Sun, X. and E.N. Harris, *New aspects of hepatic endothelial cells in physiology and nonalcoholic fatty liver disease.* Am J Physiol Cell Physiol, 2020. 318(6): p. C1200-c1213.

641. Syn, W.-K., et al., *Hedgehog-mediated epithelial-to-mesenchymal transition and fibrogenic repair in nonalcoholic fatty liver disease.* Gastroenterology, 2009. 137(4): p. 1478-1488.e8.

642. Sharma, D., et al., *Regulation of the hedgehog pathway by the ketogenic diet with radiation exposure.* FASEB J, 2019. 33(S1): p. 795.18-795.18.

643. Rouillard, A.D., et al., *The harmonizome: a collection of processed datasets gathered to serve and mine knowledge about genes and proteins.* Database, 2016. 2016.

644. Balsano, C., et al., *Fat and hepatocellular carcinoma.* Hepatoma Res, 2018. 4: p. 38.

645. Kim, G.-H., et al., *Proteomic and bioinformatic analysis of membrane proteome in type 2 diabetic mouse liver.* PROTEOMICS, 2013. 13(7): p. 1164-1179.

646. Sies, H., *Glutathione and its role in cellular functions.* Free Radic Biol Med, 1999. 27(9-10): p. 916-21.

647. Purucker, E., et al., *Differences in glutathione status and lipid peroxidation of red and white muscles: alterations following ischemia and reperfusion.* Res Exp Med, 1991. 191(3): p. 209-17.

648. Deneke, S.M., *Thiol-based antioxidants.* Curr Top Cell Regul, 2000. 36: p. 151-80.

649. Lash, L.H., *Renal Membrane Transport of Glutathione in Toxicology and Disease.* Vet Pathol, 2010. 48(2): p. 408-419.

650. McIntyre, T.M. and N.P. Curthoys, *The interorgan metabolism of glutathione.* Int J Biochem, 1980. 12(4): p. 545-51.

651. Potter, D.W. and T.B. Tran, *Apparent rates of glutathione turnover in rat tissues.* Toxicol Appl Pharmacol, 1993. 120(2): p. 186-92.

652. Himmelfarb, J., et al., *The elephant in uremia: oxidant stress as a unifying concept of cardiovascular disease in uremia.* Kidney Int, 2002. 62(5): p. 1524-38.

653. Hagen, T.M., T.Y. Aw, and D.P. Jones, *Glutathione uptake and protection against oxidative injury in isolated kidney cells.* Kidney Int, 1988. 34(1): p. 74-81.

654. Witko-Sarsat, V., et al., *Advanced oxidation protein products as novel mediators of inflammation and monocyte activation in chronic renal failure.* J Immunol, 1998. 161(5): p. 2524-32.

655. Signorini, L., et al., *Naturally Occurring Compounds: New Potential Weapons against Oxidative Stress in Chronic Kidney Disease.* Int J Mol Sci, 2017. 18(7).

656. Chao, C.-T., et al., *Interplay between Superoxide Dismutase, Glutathione Peroxidase, and Peroxisome Proliferator Activated Receptor Gamma Polymorphisms on the Risk of End-Stage Renal Disease among Han Chinese Patients.* Oxid Med Cell Longev, 2016. 2016: p. 8516748.

657. dos Anjos, L.R.B., et al., *Impact of Oxidative Changes and Possible Effects of Genetics Polymorphisms of Glutathione S-Transferase in Diabetics Patients with Complications*. Vol. Glutathione in Health and Diseases. 2018.

658. Shang, Y., et al., *Downregulation of Glutathione Biosynthesis Contributes to Oxidative Stress and Liver Dysfunction in Acute Kidney Injury.* Oxid Med Cell Longev, 2016. 2016: p. 9707292.

659. Purucker, E., et al., *Increase in renal glutathione in cholestatic liver disease is due to a direct effect of bile acids.* Am J Physiol Renal Physiol, 2002. 283(6): p. F1281-F1289.

660. Sevrioukova, I.F., *Redox-linked conformational dynamics in apoptosis-inducing factor.* J Mol Biol, 2009. 390(5): p. 924-38.

661. Turgeon, M.O., et al., *TRH Action Is Impaired in Pituitaries of Male IGSF1-Deficient Mice.* Endocrinology, 2017. 158(4): p. 815-830.

662. Cano-Gauci, D.F., et al., *Glypican-3-deficient mice exhibit developmental overgrowth and some of the abnormalities typical of Simpson-Golabi-Behmel syndrome.* J Cell Biol, 1999. 146(1): p. 255-264.

663. Sajorda, B.J., et al., *Simpson-Golabi-Behmel syndrome type 1*. 2006, University of Washington, Seattle: Seattle (WA).

664. Grisaru, S., et al., *Glypican-3 modulates BMP- and FGF-mediated effects during renal branching morphogenesis.* Dev Biol, 2001. 231(1): p. 31-46.

665. Valsechi, M.C., et al., *GPC3 reduces cell proliferation in renal carcinoma cell lines.* BMC cancer, 2014. 14: p. 631-631.

666. Miramar, M.D., et al., *NADH oxidase activity of mitochondrial apoptosis-inducing factor.* J Biol Chem, 2001. 276(19): p. 16391-8.

667. Morton, S.U., et al., *AIFM1 mutation presenting with fatal encephalomyopathy and mitochondrial disease in an infant.* Cold Spring Harb Mol Case Stud, 2017. 3(2): p. a001560-a001560.

668. Bano, D. and J.H.M. Prehn, *Apoptosis-Inducing Factor (AIF) in Physiology and Disease: The Tale of a Repented Natural Born Killer.* EBioMedicine, 2018. 30: p. 29-37.

669. Daugas, E., et al., *Mitochondrio-nuclear translocation of AIF in apoptosis and necrosis.* Faseb j, 2000. 14(5): p. 729-39.

670. Yuste, V., H.-K. Lorenzo, and S.A. Susin, *AIFM1 (apoptosis-inducing factor, mitochondrion-associated, 1).* Atlas Genet Cytogenet Oncol Haematol, 2008. 12: p. 190-194.

671. Garrido, C., et al., *Mechanisms of cytochrome c release from mitochondria.* Cell Death Differ, 2006. 13(9): p. 1423-1433.

672. Kesavardhana, S. and T.-D. Kanneganti, *Stressed-out ROS take a silent death route.* Nat Immunol, 2018. 19(2): p. 103-105.

673. Lo, S.-C. and M. Hannink, *PGAM5 tethers a ternary complex containing Keap1 and Nrf2 to mitochondria.* Exp Cell Res, 2008. 314(8): p. 1789-1803.

674. Vahsen, N., et al., *AIF deficiency compromises oxidative phosphorylation.* EMBO J, 2004. 23(23): p. 4679-4689.

675. Bénit, P., et al., *The variability of the harlequin mouse phenotype resembles that of human mitochondrial-complex I-deficiency syndromes.* PLoS One, 2008. 3(9): p. e3208.

676. Coughlan, M.T., et al., *Deficiency in Apoptosis-Inducing Factor Recapitulates Chronic Kidney Disease via Aberrant Mitochondrial Homeostasis.* Diabetes, 2016. 65(4): p. 1085-98.

677. Cañadas-Garre, M., et al., *Genetic Susceptibility to Chronic Kidney Disease – Some More Pieces for the Heritability Puzzle.* Front Genet, 2019. 10(453).

678. Montalbano, M., et al., *Biology and function of glypican-3 as a candidate for early cancerous transformation of hepatocytes in hepatocellular carcinoma (Review).* Oncol Rep, 2017. 37(3): p. 1291-1300.

679. Borroz KI, Ramsdell HS, and Eaton DL, *Mouse strain differences in glutathione S-transferase activity and aflatoxin B1 biotransformation.* Toxicol Lett, 1991. 58(1): p. 97-105.

680. Rebrin I, Forster MJ, and S. RS, *Effects of age and caloric intake on glutathione redox state in different brain regions of C57BL/6 and DBA/2 mice.* Brain Res, 2007. 1127(1): p. 10-18.

681. Churchill, G.A., et al., *The Diversity Outbred mouse population.* Mamm Genome, 2012. 23(9-10): p. 713-718.

682. Collaborative Cross Consortium, *The genome architecture of the Collaborative Cross mouse genetic reference population.* Genetics, 2012. 190(2): p. 389-401.

683. Svenson, K.L., et al., *High-resolution genetic mapping using the Mouse Diversity outbred population.* Genetics, 2012. 190(2): p. 437-447.

684. Saul, M.C., et al., *High-Diversity Mouse Populations for Complex Traits.* Trends Genet, 2019. 35(7): p. 501-514.

685. Civelek, M. and A.J. Lusis, *Systems genetics approaches to understand complex traits.* Nat Rev Genet, 2014. 15(1): p. 34-48.

686. Amos, W., E. Driscoll, and J.I. Hoffman, *Candidate genes versus genome-wide associations: which are better for detecting genetic susceptibility to infectious disease?* Proc Biol Sci, 2011. 278(1709): p. 1183-1188.

687. Bogue, M.A., G.A. Churchill, and E.J. Chesler, *Collaborative Cross and Diversity Outbred data resources in the Mouse Phenome Database.* Mamm Genome, 2015. 26(9): p. 511-520.

688. Flurkey, K., J.M. Currer, and D.E. Harrison, *Mouse models in aging research*, in *2000-2009*. 2007, The Mouseion *at* the JAXlibrary. p. 1685.

689. Wang, H., H. Liu, and R.M. Liu, *Gender difference in glutathione metabolism during aging in mice.* Exp Gerontol, 2003. 38(5): p. 507-17.

690. Liu, H., et al., *Gender differences in glutathione metabolism in Alzheimer's disease.* J Neurosci Res, 2005. 79(6): p. 861-7.

691. Liang, Q., et al., *The gender-dependent difference of liver GSH antioxidant system in mice and its influence on isoline-induced liver injury.* Toxicology, 2011. 280(1-2): p. 61-9.

692. Tietze, F., *Enzymic method for quantitative determination of nanogram amounts of total and oxidized glutathione: applications to mammalian blood and other tissues.* Anal Biochem, 1969. 27(3): p. 502-22.

693. Griffith, O.W., *Determination of glutathione and glutathione disulfide using glutathione reductase and 2-vinylpyridine.* Anal Biochem, 1980. 106(1): p. 207-12.

694. Norris, R.L., et al., *A sensitive and specific assay for glutathione with potential application to glutathione disulphide, using high-performance liquid chromatography-tandem mass spectrometry.* J Chromatogr B Biomed Sci Appl, 2001. 762(1): p. 17-23.

695. Fariss, M.W. and D.J. Reed, *High-performance liquid chromatography of thiols and disulfides: dinitrophenol derivatives.* Methods Enzymol, 1987. 143: p. 101-9.

696. Jones, D.P., et al., *Glutathione measurement in human plasma. Evaluation of sample collection, storage and derivatization conditions for analysis of dansyl derivatives by HPLC.* Clin Chim Acta, 1998. 275(2): p. 175-84.

APPENDIX A

METHOD DEVELOPMENT

The Diversity Outbred (DO) mouse stock

Rodent models are useful in addressing the tissue-specific variation of glutathione concentrations, however current research on glutathione variability in rodents is limited to inbred strains [175, 203, 521, 523-526, 679, 680]. Though this gives insight into whether or not variation exists, the homozygous backgrounds between strain lines do not address the genetic diversity seen in the human model. The Diversity Outbred (DO) mouse stock (J:DO) was developed by the Jackson Laboratory as a method of modeling the high levels of genetic diversity found in humans to advance our understanding of complex medical traits [681]. It is a multiparental heterogenous stock developed using the eight founder strains of the Collaborative Cross (CC), another multiparental recombinant inbred mouse panel [681]. Because the genetic structure of each of the CC lines is known [682], 144 independent lineages from the CC mouse stock were used to create a mating scheme that allowed for a large population size but also minimized drift and allele frequency selection (Figure A1) [681].

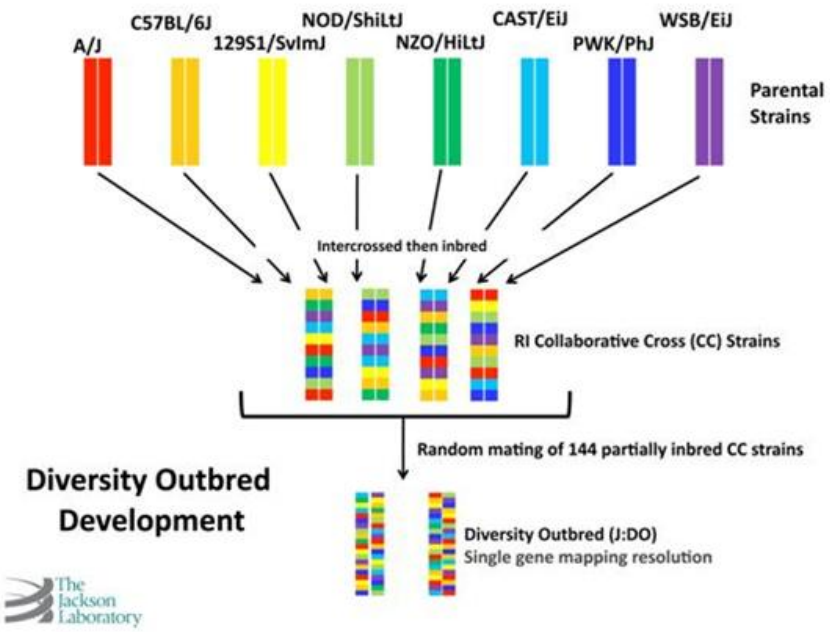

Figure A1. J:DO mice: novel tools for high-resolution genetic mapping. Figure from The Jackson Laboratory [596].

Though the CC model gives insight into whether or not variation exists, the homozygous backgrounds between strain lines do not address the genetic diversity seen in the human model. The DO stock is considered a novel resource because each mouse has a high level of allelic heterozygosity modeling the human condition [681]. Furthermore, this high level of genetic diversity from randomized outcrossing allows us to investigate medical traits that are genetically complex [683]. Liver and kidney GSH/GSSG were previously measured in the eight founder strains of the DO and concluded that glutathione redox status varies by strain (Figure A2) [526], suggesting that glutathione phenotypes will likewise vary in the DO animals.

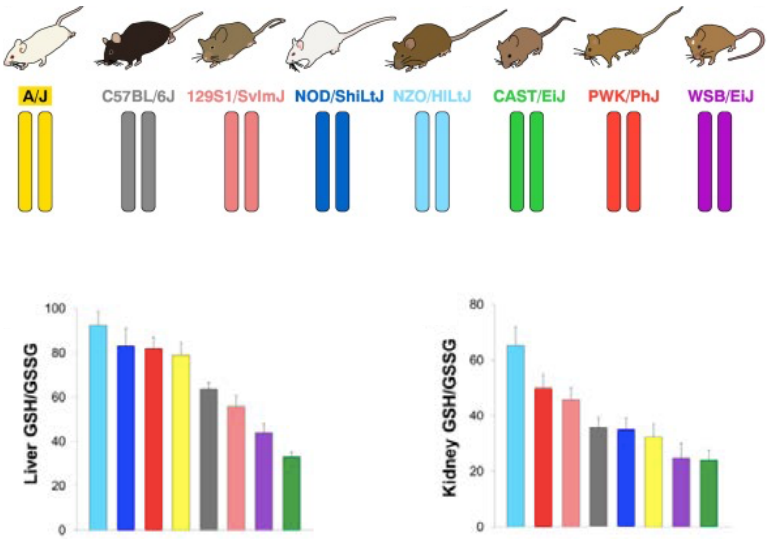

Figure A2. Variation in liver and kidney GSH/GSSG by DO founder strain. Adapted from Zhou et al. (2014) and Saul et al. (2019) [526, 684].

Genetic mapping

To better understand the complex glutathione redox system, we turned to a systems genetics model which examines intermediate molecular phenotypes, such as GSH, to understand the impact of DNA variation on its concentrations [685]. This approach utilizes genome-wide association studies (GWAS) which scan the genome to find genetic variations associated with phenotypes of interest [686]. Previously, inbred strain backcrosses and intercrosses were used for association mapping, but those techniques have limited mapping resolution [681]. Through the use of heterogeneous stocks, high-resolution mapping can be accomplished [681]. Using the hidden Markov model, binary single nucleotide polymorphism (SNP) data can be used to reconstruct founder haplotypes (Figure A3) [681]. The Mouse Universal Genotyping Array (MUGA) was originally used to assay SNPs in the DO [681]. A higher density SNP platform, the Giga-MUGA, was created to account for the recombination events that have accumulated [681]. Ultimately, the DO serve as a "hypothesis generator," allowing for phenotypic effects to be established and further evaluated using the associated genetic loci in the CC founder strains [681]. The R/qtl2 interactive

software allows for linkage mapping to occur by regressing each phenotype on haplotype probabilities at each marker and was developed to perform mapping of quantitative trait loci (QTL) from multi-parent populations such as the CC and DO mice [549]. Significance thresholds are calculated through permutation tests and mapping of the permuted trait can be conducted [549]. Through all of this, loci and high-priority candidate genes can be identified for further analysis to ultimately establish a more defined regulatory network for phenotypes in tissue [549].

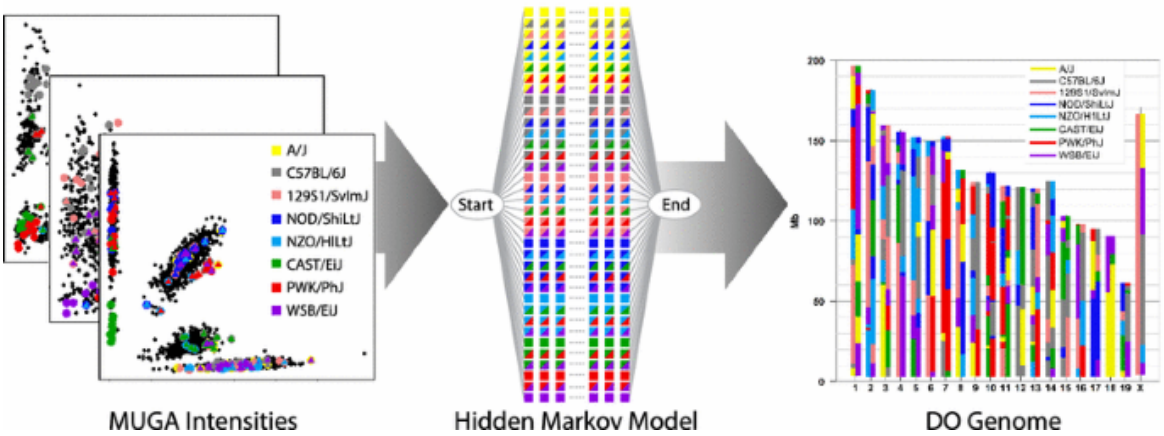

Figure A3. DO genotyping. Figure from Bogue, Churchill, and Chesler (2015) [687].

Mouse characteristics

Life stages in mice have been compared to human beings [688]. Between birth and 1 month, mice age 150 times faster than humans, and between 1-6 months, 45 times faster [688]. After 6 months, mice age 25 times faster than humans [688]. Between 3 to 6 months, mice are considered equivalent in age to mature adults, and between 10-14 months, mice are considered middle-aged [688]. To understand natural glutathione variation without any additional stressors, including advanced age, this study investigated glutathione status of mice at 5-6 months which are comparable to healthy, young-adult humans. Glutathione metabolism appears to be regulated differently based on gender in both rodents [689] and humans [690], with males exhibiting

markedly lower GSH levels. There is evidence that there is lower activity of glutathione-related enzymes in males compared to females, which may put them at further risk of both developing a disease and expediting its progression [691]. To further investigate the sex effect on glutathione metabolism, both male and female mice will be included in equal numbers in this dissertation research.

Tissue selection

Due to the tissue-specificity of glutathione heritability and overall variation, it is important to assess glutathione concentrations across a panel of tissues. The liver and kidney are vital metabolic organs that have significant levels of GSH [204]. To investigate the natural variation of glutathione in these metabolic tissues, glutathione phenotypes were quantified in the liver and kidney.

Assessment of glutathione phenotypes

To use the genetic mapping techniques, precise quantification of glutathione concentrations in individual tissues must be used to ensure accurate phenotypic data. Previous approaches to measuring GSH and GSSG have relied on spectrophotometric analysis [692, 693], mass-spectrometry [455, 694], and HPLC [695, 696]. Spectrophotometric approaches are reliable but are limited in use because concentrations are not measured directly [454]. Mass spectrometry allows for quantification without derivatization, but is not available in all laboratories [454]. HPLC offers a greater specificity and sensitivity to measuring GSH and GSSG status directly and simultaneously [454]. Various forms of HPLC have been developed and used for measuring GSH redox status given the poor absorptive nature of thiols [454]. HPLC-ultraviolet (HPLC-UV) and HPLC-fluorescence (HPLC-FL) approaches have been used to effectively measure GSH and GSSG, however, sample preparation and instrument use is labor intensive and time consuming

[454]. HPLC analysis using electrochemical detection is an efficient and cost-effective method of directly measuring GSH and GSSG [454]. HPLC with a boron-doped diamond electrode (HPLC-BDD) allows for high oxidation potentials to be used which is necessary given the high voltages needed for GSH and GSSG detection and is less labor-intensive than HPLC-UV detection [454]. Park et al. validated GSH and GSSG measurements using HPLC-BDD compared to HPLC-UV and found that there were no significant differences in findings between the two HPLC methods [454]. Furthermore, they determined the optimal voltage, injection volumes, and column temperature for measuring both GSH and GSSG using HPLC-BDD [454]. A potential of 1475 for the analytical cell, 500 mV for the conditioning cell, and 30 degrees C column temperature with a clean cell command (1900 mV, 0.5 min) following each run were deemed the best conditions to quantify GSH and GSSG [454]. Our lab further tested these HPLC-BDD methods and based on our results, we agreed with Park et al. that the reported conditions were appropriate but that they could be slightly modified for our instrument to achieve greater separation between peaks (unpublished data). We found the optimal conditions to achieve proper peak separation was using a lower flow rate at 0.220 mL/min (compared to the reported 0.6 mL/min) and a mobile phase composition of 4% acetonitrile, 0.1% pentafluoropropionic acid, and 0.02% ammonium hydroxide (compared to the reported 6% acetonitrile mobile phase). Chromatograms displaying peaks for hepatic GSH and GSSG and renal GSH and GSSG are in Figures A4 and A5, respectively.

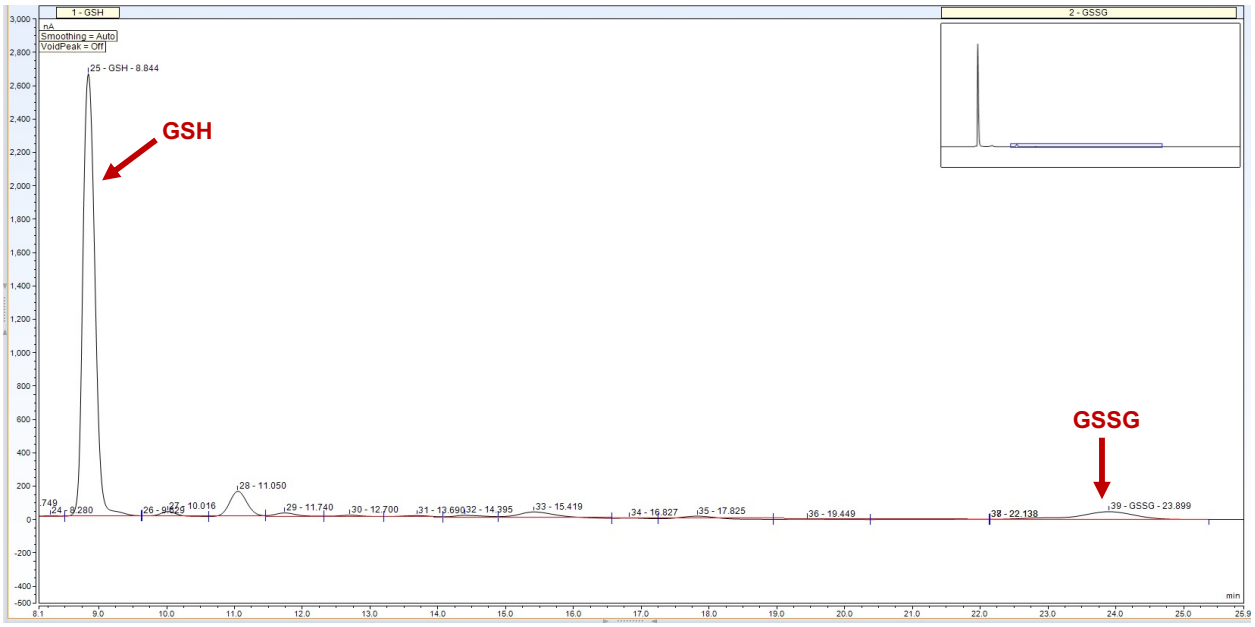

Figure A4. Chromatogram of hepatic GSH and GSSG in DO mouse obtained by HPLC-BDD.

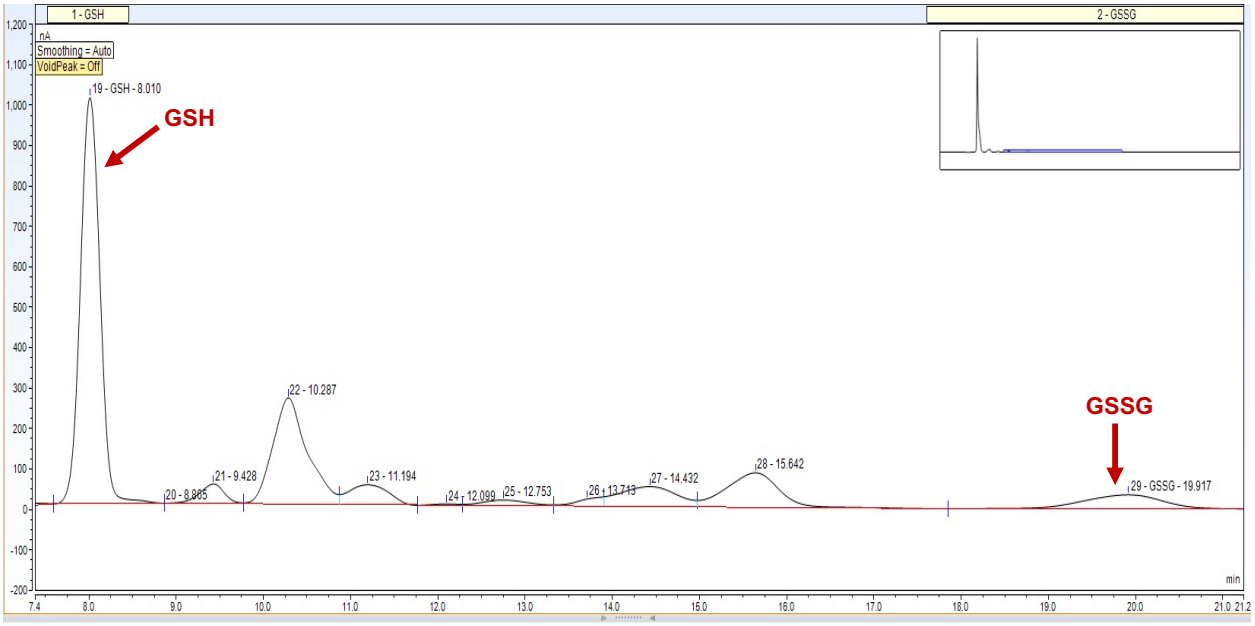

Figure A5. Chromatogram of renal GSH and GSSG in DO mouse obtained by HPLC-BDD.